POWER SYSTEM STATE ESTIMATION AND PROBABILISTIC LOADFLOW ANALYSIS

A thesis

presented for the degree of

Doctor of Philosophy in Electrical Engineering

in the

University of Canterbury,

Christchurch, New Zealand

by

E.P.M. BROWN B.E. (HONS), M.E.

1981

"Never take anything for granted"

Benjamin Disraeli
1804-1881

Speech at Salthall
5th October 1864

CONTENTS

Page

Page

CHAPTER 10 HIERARCHICAL STATE ESTIMATION OF A COMBINED ELECTRICAL-HYDROTURBINE AND OPEN CHANNEL HYDROCANAL SYSTEM - FEASIBILITY INVESTIGATIONS

APPENDICES

LIST OF ILLUSTRATIONS

LIST OF TABLES

LIST OF PRINCIPAL SYMBOLS

The majority of symbols are defined in the text, but for convenience the principal symbols are redefined below. Some symbols have more than one meaning. However, the context in which the symbol is used should clarify any ambiguities.

a	-	transformer ratio
a.c.	-	alternating current
A	-	cross-sectional area of flow (m^2/sec)
A_I	-	availability of device i
$\bar{A}_I$	-	unavailability of device i ($= 1 - A_I$)
B	-	susceptance
C_i	-	cost of data acquisition system measurement i
C_m	-	flow constant (= 1.0)
cov(A,B)	-	co-variance between dependent events A and B
d.c.	-	direct current
D	-	"self regulation effect" gain
D.L.F.	-	deterministic loadflow
e_f	-	frequency residual (p.u.)
E	-	expectation operator
E_r	-	error in gaussian sum-moment approximation
E'	-	transient voltage of the hydrogenerator (p.u.)
$\|E\|$	-	convertor alternating voltage (p.u.)
f	-	frequency deviation of the generating unit (p.u.)
f_o	-	nominal frequency (50 Hz)
f_{ref}	-	frequency deviation of the reference generator (p.u.)
g	-	gravitational constant (= 9.806)
	-	non-linear transformation

G - conductance

$G(x)$ - R.H.S. matrix of the general state estimator

$\underline{h}$ - non-linear measurement function vector $\{h_p : h_q : h_{dc}\}$ $(m \times 1)$

h.v.d.c. - high voltage direct current

$\underline{H}$ - Jacobian matrix $(m \times n)$

$\underline{H}_k$ - inertia constant of the rotor

I - current (p.u.)

$\underline{I}$ - identity matrix

$\underline{I}(\underline{x})$ - information matrix

j - denotes an imaginary number $j = \sqrt{-1}$

J - residual

$\underline{K}$ - Kalman gain matrix

K_0 - derivative control constant

K_I - integral control constant

K_p - proportional control constant

K_1 - $3\sqrt{2/\pi}$

K_2 - $3/\pi$

$\underline{L}(\underline{x})$ - L.H.S. (information) matrix of the general state estimator

m - level of variance conditioning

- number of measurements

m_i - number of nodally dependent gaussian components at node i

m_{NG_j} - non-gaussian moment of order j

m_{GA_j} - gaussian sum approximation moment of order j

n - number of busbars in the power system

- Manning roughness factor

$N(0,R)$ - normal distribution with zero mean and variance R

N_G - normal distribution with variance σ

p_i - probability of event i occurring

p_n - non-gaussian probability density function

p.d.f. - probability density function

P - active power (p.u.)

- wetted perimeter of a trapezoidal canal

P.L.F. - probabilistic loadflow

$P_e(t)$ - incremental electric power demand with time

q - lateral inflow per unit length of channel

- level of variance conditioning

q_i - number of lines attached to bus i

- probability of event i not occurring ($= 1 - p_i$)

- number of reactive power or voltage gaussian sum components

Q - flow of water in a canal (m^3/sec)

- reactive power (p.u.)

$\underline{r}$ - measurement residual $(\underline{z} - \underline{h}(\underline{x}))$

r_i - number of active power gaussian sum components

r_m - normalised residual

r_w - weighted residual

R - resistance

- measurement noise co-variance matrix ($m \times m$)

- hydraulic radius (m)

R_{dc} - d.c. line resistance

R_N - random number (normalised gaussian)

s - friction term per unit length

s_o - channel slope per unit length

S - complex power P + jQ

S.L.F. - stochastic loadflow

t,T - transformer ratio (% off nominal)

- time (seconds)

T_p - time constant of the pilot servo

T_v - time constant of the distributing valve

T_{wk} - time constant of the hydraulic turbine

u - commutation overlap angle ($= \delta - \alpha$)

V - instantaneous velocity of the fluid (m/sec)

$V \angle \theta$ - nodal voltage (phase angle referred to slack node)

$V \angle \psi$ - nodal voltage (phase angle referred to convertor current)

V_f - observation error

$w_r(t)$ - frequency deviation

$\underline{W}$ - residual sensitivity matrix

$x, \underline{x}$ - state vector = $\{\underline{\theta}, \underline{v}, \underline{a}, \underline{x}_{dc}\}$ (n×1)

X - random variable

- reactance

X_d' - transient reactance of the generator unit

X_{fm}, X_{fn} - filter reactance of rectifier and inverter

X_m, X_n - commutation reactances at rectifier and inverter

y - height of water in hydrocanal (m)

Y - admittance ($Y = \frac{1}{z} = R + j\,B$)

z - measurement vector $\{\underline{z}_q, \underline{z}_p, z_{dc}\}$ (m×1)

- impedance ($z = R + jX$)

z' - measurement transformation (pseudo line-flow)

α - rate of change between successive measurement scans

- channel slope

- convertor control angle

α_i - weighting factor for gaussian sum component

$\{\alpha_i\}$ - set of all transmission lines connected to bus i

ρ - weighting factor

- mass density

$\underline{\eta}$ - measurement noise vector (m×1)

δ - extinction angle of the convertor

$\delta(t)$ - internal rotor angle w.r.t the frequency generator

δ_i - probability of no failure or repair, between measurement scans, of plant i

δ_x - estimation error

λ - eigenvalue

λ_i - mean time to failure (MTBF)

$\underline{\Sigma}$ - network structure vector

$\underline{\Sigma}_r$ - residual co-variance matrix

$\underline{\Sigma}_x$ - estimation co-variance matrix

μ - mean value

μ_i - mean time to repair device i

σ_i - standard deviation of the i^{th} measurement error

$\omega(t)$ - model inaccuracies and system noise

ν - unit weight of fluid

τ_o - shear stress

θ - voltage phase angle referred to slack node

ψ - voltage phase angle referred to convertor current

ϕ - phase angle of convertor alternating voltage

Subscripts and superscripts

dc - h.v.d.c. link pseudomeasurement

I - imaginary part of a complex variable

k - iteration number

m - rectifier side of the h.v.d.c. link

- number of measurements

n - inverter side of the h.v.d.c. link

- number of states in the state vector

p - active power measurement partition

pr - primary side of transformer

q'	-	reactive power measurement partition
r	-	real part of a complex variable
s	-	h.v.d.c. link pseudomeasurement
sec	-	secondary side of transformer
x^{-1}	-	inverse of a matrix x
x^{T}	-	transpose of matrix x
$\dot{x}$	-	time derivative of x
x_t	-	value of x at time t
x_{ij}	-	general element of matrix x
x^j	-	j^{th} estimate of x

ABSTRACT

This thesis investigates the treatment of aposteriori and apriori uncertainties in power system planning and operation.

Aposteriori uncertainty is treated by power system state estimators. A survey of existing techniques and their limitations is described. A method is presented that improves the speed of weighted least squares state estimation by modifying the structure of injection measurements to give a very sparse information matrix, the matrix to be inverted. Used with fast decoupling, this approach yields a very fast on-line state estimator, capable of handling all types of measurements.

Bad data detection and identification techniques are reviewed and an improvement based on "mathematical" bad data removal is presented.

The inclusion of h.v.d.c. links into a.c. state estimation is considered. Decoupling and geographic partitioning of the multi a.c.-h.v.d.c. state estimator are shown to cause little degradation in the estimates, and a method of accurately representing commutation overlap angle is outlined.

Availability analysis in state estimator operation and design is considered, and applied to optimal meter placement design.

The feasibility of hierarchical central-electrical, local-dynamic hydroturbine and canal state estimation, based on a linearized Kalman filter, is investigated.

Apriori uncertainty in long-term future planning studies involving expected nodal generation and loads can be included in stochastic load-flows. A method is presented which enables the stochastic loadflow, which handles only gaussian statistics, to handle non-gaussian probability distributions via gaussian sum approximations. H.v.d.c. links are also included in a.c. stochastic loadflows, using both correlated and uncorrelated data.

ACKNOWLEDGEMENTS

I especially wish to thank my supervisor, Dr H.R. Sirisena, for his enthusiasm and guidance throughout this research.

Acknowledgements are also due to Professor J. Arrillaga, Professor I.R. Wood and Dr A.J. Sutherland for answering my queries, and to my postgraduate colleages; in particular Messrs B.J. Harker, M.D. Heffernan and K.S. Turner, for many valuable discussions.

I wish also to thank New Zealand Electricity and the State Services Commission for their financial assistance and granting of leave for this study. I also wish to thank Mr C.V. Currie, Mr W. Wilson, Mr B. Thompson, and the staff of the Christchurch District Draughting Section of New Zealand Electricity for draughting all the many figures in this text.

The staff of the Computer Centre of the University of Canterbury are also to be thanked for their invaluable help, and Mrs A.J. Dellow for typing this thesis.

Last, but not least, I am indebted to my wife, Lesley, for her continued patience and encouragement throughout this research and for proofreading my manuscripts.

CHAPTER 1

INTRODUCTION

The proliferation of computerised power system control centres which monitor large sets of measurements by remote data acquisition from around the power system is in response to the need for fast, accurate control and restorative procedures. Control centre design is becoming extremely complicated; on-line programs are now available which give updated security analysis, economic dispatch and fault analysis. These programs guide the operator in the choice of restorative action, maximize the security and economy of generation, and minimize damage and down time caused by a fault. All programs rely on having a clean data base available within the computer from which they can derive decisions. The data base within the computer is regularly updated by new measurement "snapshot" scans of the power system every few minutes. This measurement data updating procedure is intended to continue, on-line, indefinitely without failure. Each snapshot scan may contain 1000 or more individual measurements, and it is likely that, at some time, the raw measurement data arriving at the system control centre may contain bad data; metering errors that result from excessive drift or failure, or failure of communication equipment within the data acquisition system. The presence of such errors in the data base may produce the wrong control or alarm action (Schweppe *et al.*, 1970; Schweppe and Handschin, 1974; Handschin and Bongers, 1975).

State estimation algorithms have been proposed for use in power systems to buffer the data base of the control centre from raw

measurement errors (see Figure 1.1).

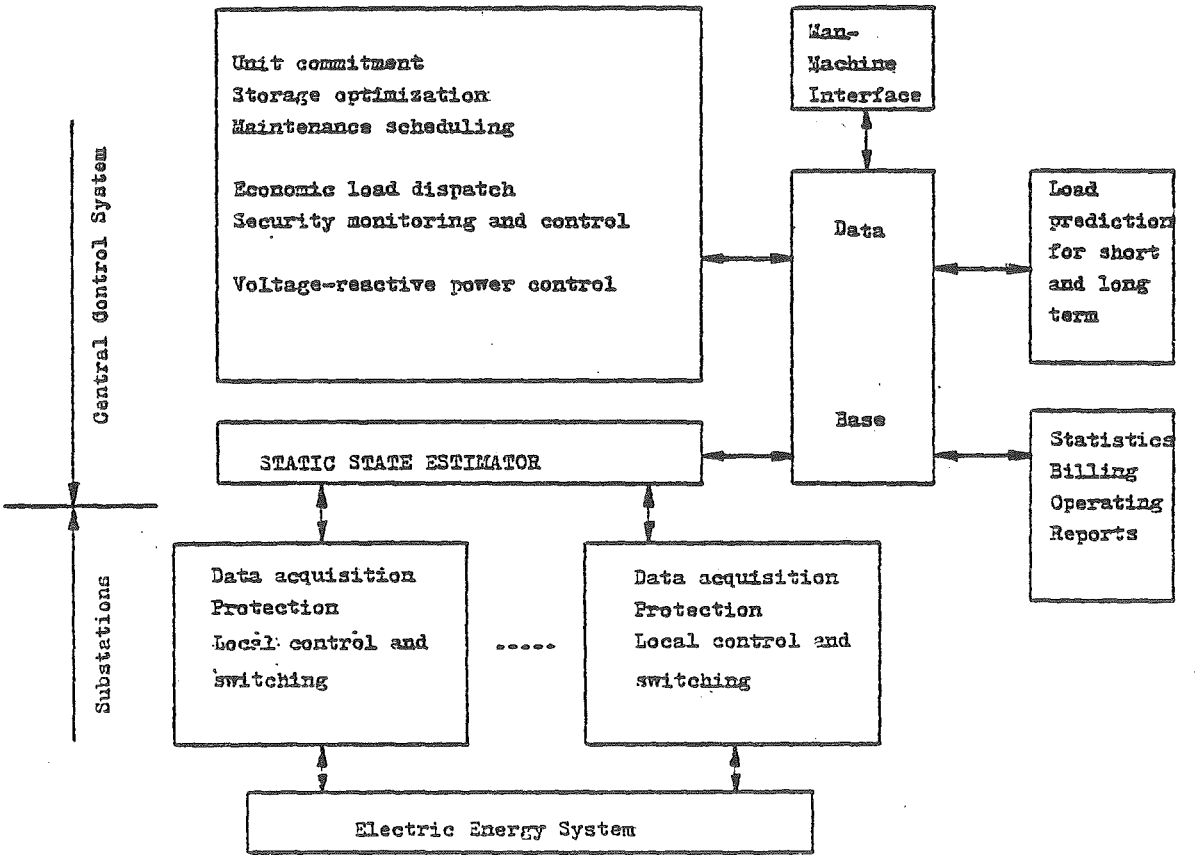

Figure 1.1 Typical control centre operation. Schweppe and Handschin, 1974.)

Such buffering action is achieved by processing a redundant set of data; having more measurements present than is needed to completely specify the states (see Figure 1.2).

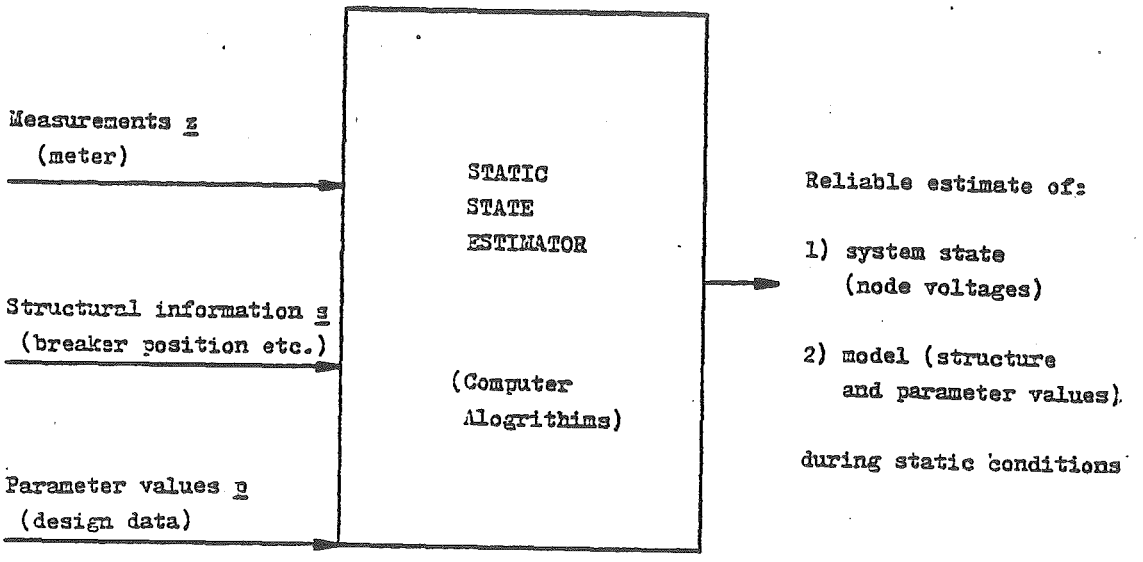

Figure 1.2 The static state estimator as a buffer.
(Schweppe and Handschin, 1974.)

For the purpose of state estimation, states are taken to be the voltage magnitude and phase angle at nodes around the power system, together with any transformer taps or line parameters that may need estimating. Measurements may include real and reactive injected power, real and reactive line-flow power, current flow and nodal voltage magnitudes, as well as isolator and circuit breaker status information (see Figure 1.3).

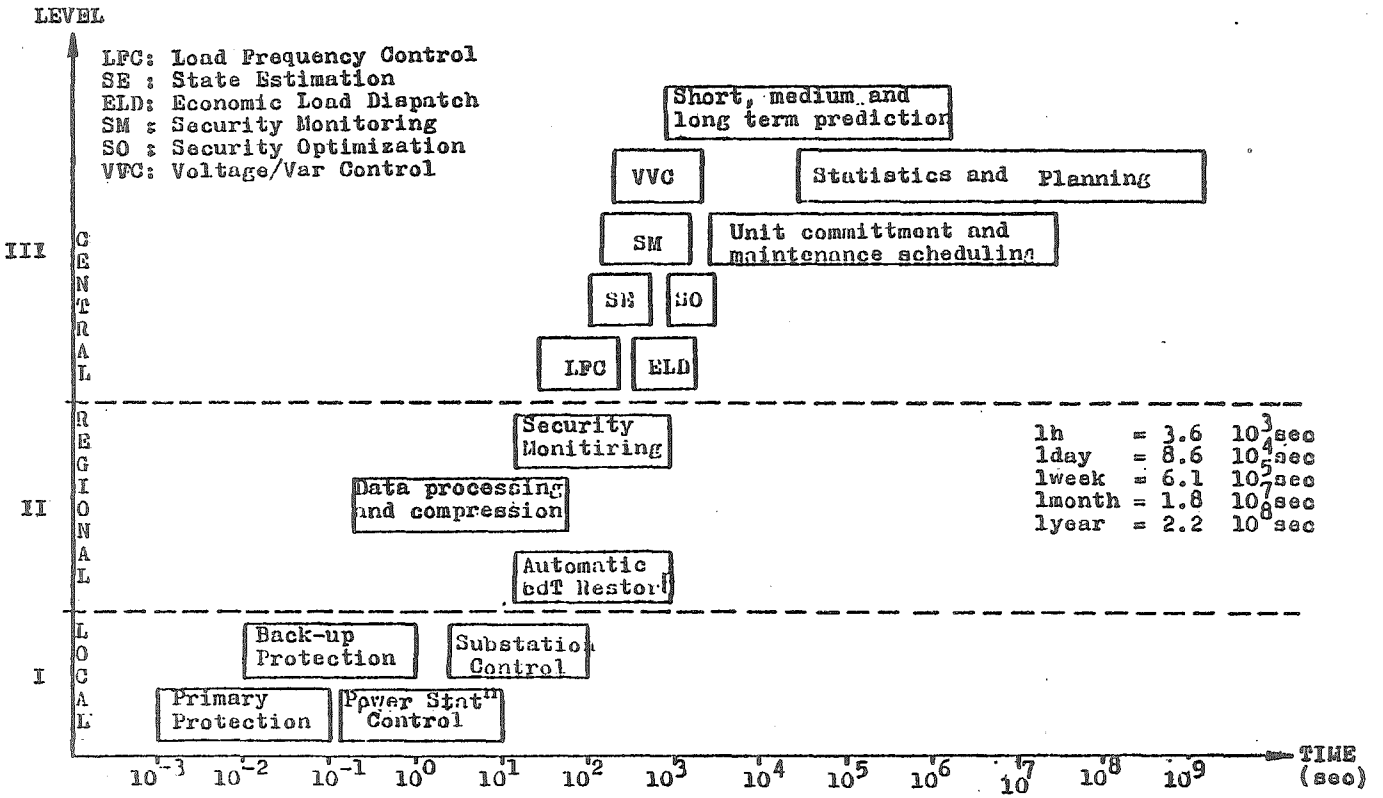

Figure 1.3 Time interval in which monitoring and control functions must be performed. (Handschin and Bongers, 1975.)

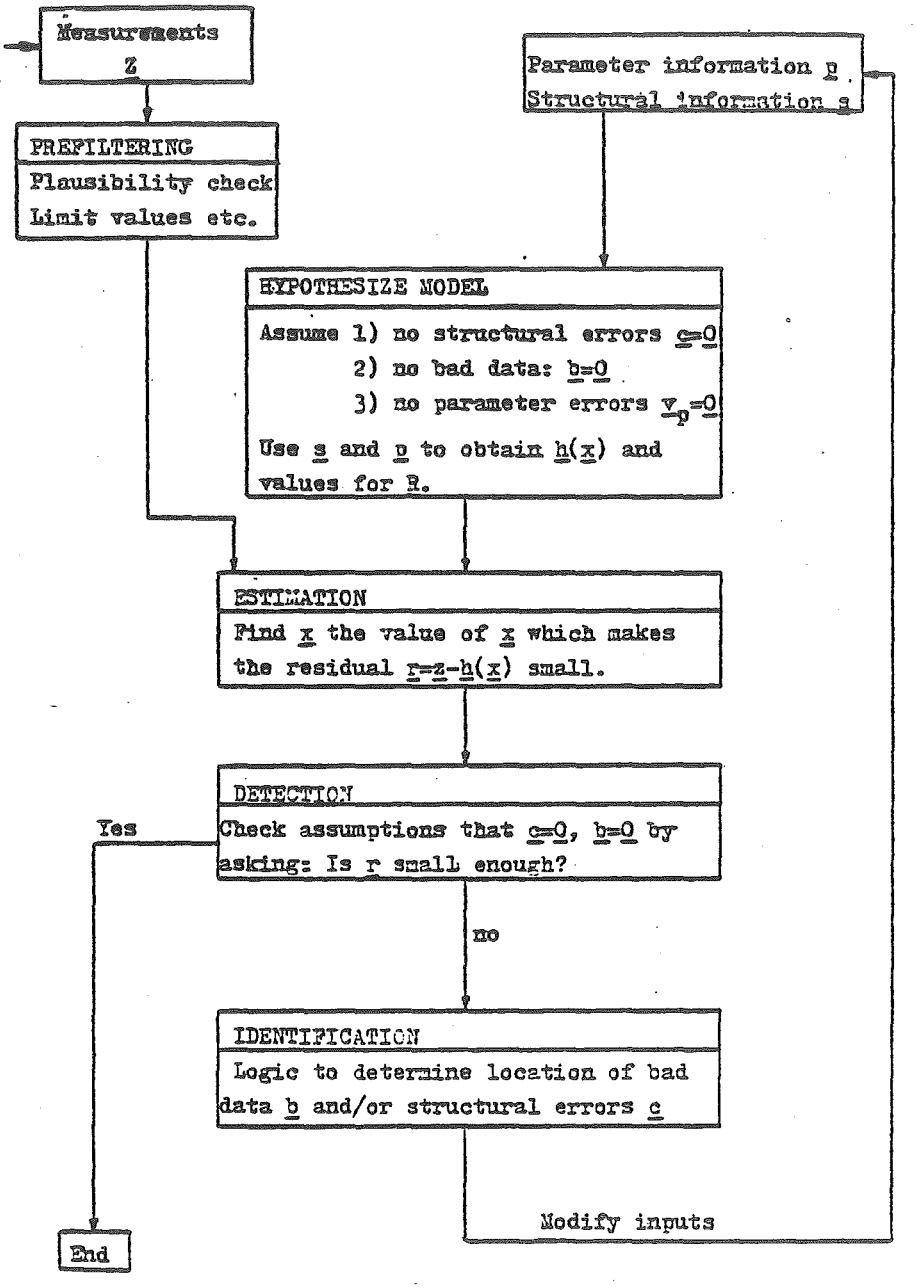

Figure 1.4 Basic operation of the state estimator. (Schweppe and Handschin, 1974.)

Processing a redundant set of measurement data allows bad data detection and identification schemes to be included in the state estimator algorithm, to locate and remove any faulty measurement data or circuit disconnect status information (see Figure 1.4) (Schweppe and Handschin, 1974).

The concept of state estimation was first used by Gauss (1777-1855) to process data on the orbits of planetary bodies. Since the late 1950s, with the beginning of aerospace exploration, state estimators have become more sophisticated in order to dynamically monitor noisy measurement data from outer space. The "small-scale" nature of the aerospace problem has allowed complex state estimation techniques to be used. The power system's application, on the other hand, produces an extremely large scale problem. Some power systems may contain 500 busbars or more. Fortunately, however, power systems usually are weakly intercoupled and as a result most matrix manipulation in power system problems involves sparse matrices. Sparsity techniques can be used to handle these matrices, storing only their non-zero values and location addresses. Sparsity techniques, and the quantum leap in computing speed and power of commercial computers over the last decade, have made power system state estimation a reality (Sugarmann, 1980). However only the simple, static state estimation algorithms which process the current measurement snapshot, taking no account of any dynamics, have achieved any success in the power system's applications. The problem of regularly producing reliable power system state estimates from noisy on-line data acquisition system measurements is not trivial (Brown and Sirisena, 1981). The "noise" usually is measurement accuracy noise, but occasionally this metering noise will contain bad data. The state estimation algorithm required to process these measurements must do so rapidly, detecting and identifying any bad data present before the next scan of measurements arrives to be processed.

Power system state estimation was first seriously suggested twelve years ago by Schweppe *et al.* (1970), and since then a large body of work has been published on various aspects of the topic (Schweppe and Handschin, 1974; Ariatti, 1976; Dy Liacco, 1978). However the emphasis

in most early papers on state estimation was concerned with generating minimum variance, optimally filtered estimates from the noisy measurement data available. Only recently has there been an awareness that the maintenance of a "reliable" data base, free from bad data (errors which are not necessarily measurement-accuracy noise), which can rapidly change with the changing state of the power system and allow the identification of any bad data before the next measurement scan, is as important as the generation of optimally filtered estimates. More important, however, is to consider the characteristics of the power system to which the proposed state estimator is to be applied. The characteristics of the New Zealand electricity system, the power system of concern in this study, can be summarized as follows:

- A computerized data acquisition system control centre has been installed in the North Island of New Zealand, at Whakamaru; and in the South Island of New Zealand, at Islington, another centre is nearing completion. Both monitor large a.c. power systems.
- The North and South Island a.c. power systems are linked by an h.v.d.c. submarine cable. Over half of the electricity generated in the South Island is rectified, either at Tiwai Point Aluminium Smelter or at Benmore, for transmission to the North Island.
- Monitoring equipment of varying vintages may be present in the data acquisition system. This is a result of the data acquisition system being "added to" over the years. Hence the accuracy and availability of monitoring equipment may vary quite markedly.
- Some regional area-control centres, such as Twizel, have local computers that monitor water levels and the flow in hydro canals feeding hydraulic turbines, as well as the measurements on the electrical systems.

As a result of the above considerations, the specifications for building a state estimation algorithm(s) applicable to the New Zealand power system would be as follows:

(i) The state estimator should rapidly process all measurement data available, regardless of its type, accuracy and availability, and thus maintain a reliable data base, free from bad data. The presence of the h.v.d.c. link must also be modelled in the state estimator.

(ii) Any optimal meter placement design should include measurement availability aspects. Optimal meter placement design involves the selection of the "best" set of measurements to acquire from the power system, with regard to their individual cost, placement and type, in order to get the best coverage for the data acquisition system capital resource available.

(iii) Establish whether "local area" power system state estimators which include hydro canal as well as hydro turbine dynamics are feasible in a real time sense.

The areas of research carried out in this study have been in response to the above three factors. The material is presented in self-contained chapters. Only brief discussions on computational details will appear in the text. This is because the use of efficient, sparsely orientated programming of storage and solution has been extensively studied and any further advances are unlikely to dramatically reduce computation times. The use of such procedures is now "standard" power systems programming practice.

Chapter 2 reviews advances and concepts in the state estimation of power systems. The necessary mathematical background to understand Weighted Least Squares (W.L.S.) state estimation is presented.

W.L.S. state estimation is the technique originally advocated by Schweppe *et al.* (1970) and generates minimum variance estimates. Reasons for choosing the W.L.S. state estimation method are also outlined.

Chapter 3 investigates ways of reducing the speed limitations of W.L.S. state estimation when processing injection measurements. When injection measurements are included in the W.L.S. state estimation, the density of non-zero elements in the "information" matrix, the matrix to be reduced in the solution by sparsity techniques, rise dramatically. As a result the solution time increases. By "creating" pseudo line-flow measurements from the injection measurements the density of non-zero elements in the information matrix remains constant. A technique is outlined which retains the optimality of W.L.S., after the pseudo line-flow creation, yet has significant speed advantages over conventional W.L.S. state estimation when processing moderate density injection measurement sets.

Another speed limiting factor of W.L.S. state estimation is that all matrix quantiles require recalculation at each iteration. Many authors have suggested P-θ, Q-v decoupling and fast decoupling techniques to overcome these speed limitations by reducing the number of non-zero matrix elements requiring re-evaluation and/or to make these values constant. Chapter 4 summarizes the suggested decoupling techniques and investigates their performance by theoretically evaluating their convergence-eigenvalues and comparing the analytic results with practical test simulations. The aim of the tests and analysis is to identify stable decoupled and fast decoupled state estimation schemes whose convergence and accuracy are unaffected by the transmission line R/X ratio of the test a.c. system or by the relative values of the real and reactive power variance weightings.

Chapter 5 discusses and tests a modified W.L.S. algorithm that is extremely fast yet generates near optimal estimates. Pseudo line-flow creation, from injection measurement data, is included in a fast decoupled W.L.S. state estimation algorithm selected from the tests carried out in Chapter 4.

In Chapter 6, methods for detecting and identifying bad data in on-line state estimation are reviewed. A major limitation of most bad data detection and identification schemes is that they require a large amount of computation, usually involving the removal of suspect measurements, recalculation and re-ordering of all matrices within the state estimation, and re-estimation to check whether the measurement data is indeed corrupt. This removal process is usually repeated until the bad data is located. A technique which mathematically removes the presence of suspect bad data is presented. The technique is identical to the physical removal of suspect bad data, however as re-ordering or re-calculation of gain matrix quantiles are necessary and rapid detection and identification, essential for maintaining the integrity of the on-line data-base, follows. Where measurement redundancies are such that removal of suspect bad data would cause a loss of observability, "replacement" of the suspect bad data by previous scan measurement can be used to aid the identification process.

Chapter 7 considers the inclusion of h.v.d.c. links into a.c. power systems state estimation. Measurement equations that describe h.v.d.c. link conditions in and around the convertor terminals are presented. A method of geographical decoupling of the h.v.d.c. link into separate convertor terminal blocks is also considered and the inclusion of h.v.d.c. links into fast P-θ, Q-v decoupled a.c. power system state estimators is discussed and tested.

In Chapter 8, a more exact representation for the h.v.d.c. link is proposed and tested. This model includes the effect of the commutation overlap angle after the firing of the convertor. It is also shown that the approximate h.v.d.c. link representation, discussed in Chapter 7, can be modified to generate exact h.v.d.c. link model estimates if the residuals in the "approximate" algorithm are made exact.

The use of availability data in the design and operation of state estimators is considered in Chapter 9. Most optimal meter placement design techniques that have been advocated assume that the measurements present at commissioning will always be present. However all measurements have a possibility of failure at some stage and thus membership of the measurement set is dynamic. A technique is advocated to include the effect that likely failure has on the observability of the state estimator measurement set in the optimal meter placement design process. Application of availability analysis to large scale systems is shown to be straightforward and for most purposes does not require the use of a computer. The suggested, availability based optimal meter placement design technique augments optimal meter placement design techniques which optimize the bad data detection capability.

Chapter 10 considers the problem of locally estimating the states of a hydro turbine and canal structure. A dynamic state estimation algorithm based on a linearized Kalman filter is used to monitor the behaviour of the canal and hydro turbine, and this state estimator is co-ordinated to a higher level, static state estimator which is estimating the states of the power system in a hierarchical manner.

All of the preceding discussion has applied to state estimation. However, with little or no modification the state estimation algorithm used to account for "aposteriori", past or present measurement data uncertainties, can be made to perform a stochastic load flow and account for apriori or future prediction uncertainties. In long-term planning or design of new transmission lines, a large number of deterministic load flows may be required to test the effect that different generation-load levels at nodes around the system during future operation will have on the loading of the proposed new transmission line. Stochastic load flows process the expected generation or load data at each bus together with its Gaussian variance or spread, to give the expected power flow, and its spread or variance, down each transmission line. Thus the long-term, expected maximum power flow, required during the design for circuit breaker ratings, can be found. One stochastic load flow can replace the large number of conventional load flows required in the planning of a new transmission line (Dopazo *et al.*, 1975). The concepts of the stochastic load flow and the probabilistic load flow are summarized in Chapter 11. Probabilistic load flows can process any type of nodal probability distribution - Gaussian, discrete or binomial, while the stochastic load flow handles only Gaussian probability distribution statistics (Borkowska, 1973; Allan and Al-Shakarchi, 1976).

A technique for representing non-Gaussian probability distributions in the stochastic load flow, by means of Gaussian sum approximations, is discussed in Chapter 12. Thus the stochastic load flow, which is easily made from an existing state estimation algorithm, can be made to perform probabilistic load flows; accurately modelling the available nodal data.

Chapter 13 discusses the inclusion of an h.v.d.c. link into a.c. stochastic load flow studies. The representation of the h.v.d.c. link

follows from Chapter 7. Multi a.c. h.v.d.c. stochastic load flows can be used in long-term planning or in the design of a new h.v.d.c. link or a new transmission line in the vicinity of an existing h.v.d.c. link. Both uncorrelated and correlated load flow data are included in the study.

CHAPTER 2

REVIEW OF TRANSMISSION LINE MODELLING AND WEIGHTED LEAST SQUARES STATE ESTIMATION CONCEPTS

2.1 INTRODUCTION

In this chapter the mathematical principles of power system analysis are reviewed. The π-equivalent lumped parameter model for a transmission line is presented, and equations relating to the measurement of active and reactive line flow and nodal power are defined. A derivation of the W.L.S. state estimation algorithm for use in power systems analysis is also presented. Other possible state estimation methods which also have been advocated are reviewed and reasons why W.L.S. state estimation has been chosen are given.

2.2 TRANSMISSION LINE MODEL AND POWER SYSTEM MEASUREMENT EQUATIONS

The lumped parameter π-equivalent circuit for a transmission line connecting two busbars i and j is shown in Figure 2.1.

For a transmission line, $\bar{Y}_{ij}$ represents the transfer impedance and $\bar{Y}_{ii}$ the shunt susceptance

$$\bar{Y}_{ij} = \frac{1}{R_{ij} + jX_{ij}} \tag{2.1}$$

$$\bar{Y}_{ii} = \bar{Y}_{jj} = -j\left(\frac{B_{ish}}{2}\right) \tag{2.2}$$

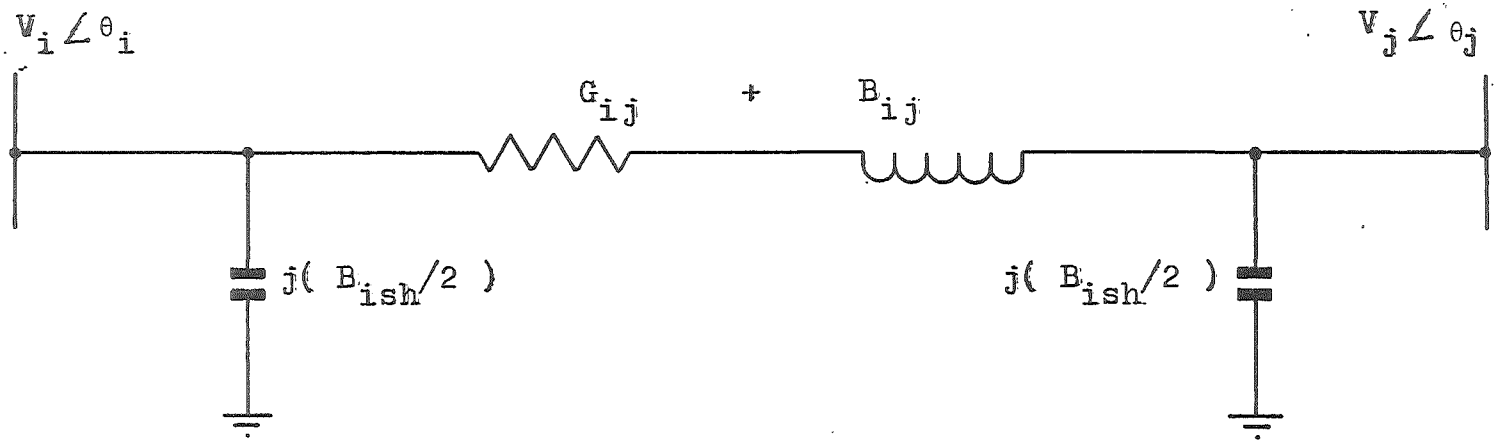

Figure 2.1 π-equivalent model of a transmission line.

For an off-nominal tap transformer the elements defined above are modified by the tap position. If the tap position, T, is given in per cent, off-nominal, then

$$a_{ij} = 1 + 0.01T \tag{2.3}$$

and

$$\bar{Y}_{ij_t} = a_{ij}\ \bar{Y}_{ij} \tag{2.4}$$

$$\bar{Y}_{ii_t} = (a_{ij}^2 - a_{ij})\ \bar{Y}_{ij} \tag{2.5}$$

$$\bar{Y}_{jj_t} = (1 - a_{ij})\ \bar{Y}_{ij} \tag{2.6}$$

A suitable state vector to describe conditions on the power system is

$$\underline{x} = \{v_k \angle \theta_k \ k=1...N, a_{ij}\} = [v_1, \theta_2, v_2, \ldots \theta_N, v_N, a_{ij}]^T \tag{2.7}$$

where N is the number of busbars in the power system, and

$v_i \angle \theta_i$ is the nodal voltage at each node i.

In terms of the $2N - 1$ system states, the relationships between measurements and states can be written (Aschmoneit, 1975):

Nodal voltage magnitude measurement, v_i

$$v_i = v_i \tag{2.8}$$

Active power line-flow measurement, P_{ij}

$$P_{ij} = G_{ij}\ v_i^2 + c_{ij} \tag{2.9}$$

where $c_{ij} = - v_i\ v_j\ (G_{ij} \cos(\theta_i - \theta_j) + B_{ij} \sin(\theta_i - \theta_j)$

Reactive power line-flow measurement, Q_{ij}

$$Q_{ij} = - B_{ii}\ v_i^2 + d_{ij} \tag{2.10}$$

where $d_{ij} = v_i\ v_j\ (- G_{ij} \sin(\theta_i - \theta_j) + B_{ij} \cos(\theta_i - \theta_j))$

Active injected power measurement, P_i

$$P_i = \sum_{j\varepsilon\{\alpha\}} P_{ij} \tag{2.11}$$

Reactive injected power measurement, Q_i

$$Q_i = \sum_{j\varepsilon\{\alpha\}} Q_{ij} \tag{2.12}$$

where $\{\alpha\}$ is the set of transmission lines connected to bus i,

G_{ij} is the transmission line admittance between nodes i and j,

B_{ij} is the transmission line susceptance between nodes i and j, and

B_{ish} is the transmission line shunt susceptance between nodes i and j.

$$B_{ii} = B_{ij} + \frac{B_{ish}}{2} \tag{2.13}$$

Thus any measurement made on the power system can be described by one of the above equations.

2.3 MEASUREMENT NOISE

Consider a measurement, z_ρ, made with metering equipment having an accuracy, η_ρ (Schweppe and Handschin, 1974).

$$z_\rho = h_\rho (\underline{x}, \underline{\Sigma}, \underline{p}) + \eta_\rho \tag{2.14}$$

where $\underline{\Sigma}$ is a vector representing the network structure, the manner in which the network is connected together to form a single line diagram, and

$\underline{p}$ is a vector representing the network parameters.

When m measurements are made simultaneously, the measurement set can be written as, (Schweppe and Handschin, 1974):

$$\underline{z} = \underline{h} (\underline{x}, \underline{\Sigma}, \underline{p}) + \underline{\eta} \tag{2.15}$$

where $\underline{\eta}$ is a random vector representing measurement errors, parameter errors, structural errors, uncertainty due to communication link failure and transients. Parameter errors are caused by an insufficient knowledge of G_{ij}, B_{ij} and/or B_{ish}. Tables of line parameters are usually only accurate to within a few percent. Parameter values can be included as states within the state estimator, and estimated (Debs, 1974; Clements and Ringlee, 1974; Allam and Laughton, 1974). Structural errors result from faulty circuit breaker or isolator switch status information being telemetered to the systems control centre. This can result in the computer constructing a faulty single line diagram of the network topology (Sasson *et al.*, 1973; Couch and Morrison, 1974; Kato and Hammerlund, 1977). Lines or circuit elements may be assumed to be connected when in practice they are not, or vice-versa. Structural errors and communication link failure cause very large errors but rarely occur.

The measurement noise vector, $\underline{\eta}$ in (2.15), is modelled as a normally distributed random vector.

$$\underline{\eta} \sim N(\underline{0}, \underline{R}) \tag{2.16}$$

with zero mean; having no bias component, and a diagonal variance matrix $\underline{R}$:

$$\underline{R} = \text{diag}\,(\sigma_i^2)_{i=1,\ldots m} \tag{2.17}$$

Any bias effects present can be removed by subtracting the bias, b_ρ, from the measurement, z_ρ. Modelling the random measurement noise by a normal distribution appears to be satisfactory for most cases (Discussion, Dopazo *et al.*, 1970).

2.4 WEIGHTED LEAST SQUARES STATIC STATE ESTIMATION

Weighted Least Squares (W.L.S.) state estimation was the first technique to be advocated for the state estimation of power systems (Schweppe *et al.*, 1970). Although W.L.S. state estimation is not the only method to be applied to the power system problem, it is the most general, in terms of the range of measurement data that it can handle.

When measurements are non-linearly related to the state of the power system, the W.L.S. criterion is to minimize (Schweppe and Handschin, 1974):

$$J(\underline{x}) = (\underline{z} - \underline{h}(\underline{x}))^T \quad \underline{R}^{-1}(\underline{z} - \underline{h}(\underline{x})) \tag{2.18}$$

Differentiating (2.18) with respect to $\underline{x}$ leads to the following optimality condition:

$$\left.\frac{dJ}{d\underline{x}}\right|_{\underline{x}=\hat{\underline{x}}} = \underline{H}^T(\hat{\underline{x}})\ \underline{R}^{-1}(\underline{z} - \underline{h}(\hat{\underline{x}})) = \underline{0} \tag{2.19}$$

where $\hat{\underline{x}}$ is defined to be the value of $\underline{x}$ which minimizes (2.18), and $\underline{H}(\underline{x})$ is the Jacobian matrix,

$$\underline{H}(\underline{x}) = \frac{\partial \underline{h}(\underline{x})}{\partial(\underline{x})} \quad , \quad \text{of order } (m \times n) \tag{2.20}$$

Linearization with a Taylor series expansion of $\underline{h}(\hat{\underline{x}})$ about $\underline{x}_i$, the i^{th} iterated value, gives

$$\underline{h}(\hat{\underline{x}}) \simeq \underline{h}(\underline{x}_i) + \underline{H}(\underline{x}_i)\ (\hat{\underline{x}} - \underline{x}_i) + \ldots. \tag{2.21}$$

and substitution into (2.19), assuming $\underline{H}(\underline{x}_i) = \underline{H}(\hat{\underline{x}})$, gives

$$(\underline{H}^T(\underline{x}_i)\ \underline{R}^{-1}\underline{H}(\underline{x}_i))\ \Delta\underline{x}_{i+1} = \underline{H}^T(\underline{x}_i)\ \underline{R}^{-1}(\underline{z} - \underline{h}(\underline{x}_i)) \tag{2.22}$$

where $$\Delta\underline{x}_{i+1} = \hat{\underline{x}} - \underline{x}_i \tag{2.23}$$

That is, $$\Delta\underline{x}_{i+1} \simeq \underline{x}_{i+1} - \underline{x}_i.$$

The optimal, minimum variance estimate for $\underline{x}$, $\hat{\underline{x}}$, is found by iteratively solving (2.22) until convergence. Because the R.H.S. of (2.22) is identical with the R.H.S. of (2.19), the L.H.S. of (2.22), i.e. the information matrix

$$\underline{I}(\underline{x}_i) = \underline{H}^T(\underline{x}_i)\ \underline{R}^{-1}\ \underline{H}(\underline{x}_i) \tag{2.24}$$

acts only as a gain matrice influencing convergence and not the final estimate (Schweppe *et al.*, 1970).

The measurement system is considered redundant when more measurements are present than states, $m > 2N - 1$, and all states are observable. When as many measurements as states are present, $m = 2N - 1$, and provided the states are observable, equation (2.22) degenerates to the load flow equation

$$\underline{H}(\underline{x}_i)\ \Delta\underline{x}_{i+1} = \Delta\underline{z} \tag{2.25}$$

where

$$\Delta\underline{z} = \underline{z} - \underline{h}(\underline{x}_i) \tag{2.26}$$

When sufficient measurement redundancy is present, filtering of the estimates occurs and detection and identification of bad data becomes possible. Bad data detection and identification techniques are discussed in Chapter 5.

2.5 OTHER METHODS OF STATE ESTIMATION

Other possible methods of state estimation include the following.

2.5.1 Dynamic tracking state estimators

The Bonneville Power Administration (BPA) state estimation algorithm is the first and only attempt to implement a dynamic Kalman-Bucy Filter on a large scale power system (Larson *et al.*, 1970; Debs and Larson, 1970; Debs and Litzenberger, 1971; Debs and Litzenberger, 1975).

The method developed by Debs *et al.* uses a diagonalized co-variance matrix to reduce the computational burden and has been commissioned and tested on the B.P.A. power system, sequentially processing the measurement data. Since the B.P.A. dynamic state estimation algorithm is not optimal, it requires regular recalculation of the Kalman gain matrices. Other dynamic state estimation algorithms have been proposed but remain untried on large scale power systems (Banerjee and Rajamani, 1977; Mahalanabis *et al.*, 1978). Bad data detection and identification properties of dynamic state estimators are not well defined.

2.5.2 Transformation-based state estimators

These state estimation algorithms include the American Electric Power (A.E.P.) "line-only" algorithm and the Johnsson current transformation algorithm (Dopazo *et al.*, 1972; Dopazo *et al.*, 1976; Johnsson, 1973). Transformational methods for state estimation will be discussed in more detail in Chapter 3. However it is sufficient to say that the measurement transformations are performed on the non-linear measurement equations (2.9) - (2.12), which result in new equations which are state independent. As a result the Jacobian elements in the transformed state estimator are constant and do not require re-evaluation. In the case of the A.E.P. "line-only" algorithm, apart from monitoring a reference voltage, only real and reactive line-flow measurements are processed, giving the matrices a sparse, admittance matrix-like structure. As a result the A.E.P. state estimator is extremely rapid (Dopazo *et al.*, 1972). The Johnsson "current" transformation state estimator is not restricted in the type of measurements it can process; however it does require the monitoring of real and reactive measurement pairs (Johnsson, 1973). A disadvantage of transformational algorithms is that they do not generate optimal solutions (Handschin and Schweppe,

1974). Bad data detection and identification properties may be complicated by the transformation.

2.5.3 Linear programming - state estimation

Irving (1978) advocated using linear programming for processing state estimation data, particularly when the measurements are affected by gross bad data. However the method has limited application because sparsity and decoupling cannot be easily included to reduce the computation required by the linear programming (Brameller *et al.*, 1979).

2.5.4 Sequential state estimation

Measurements are processed one at a time in sequential state estimation. This reduces the computational storage burden of state estimation. The B.P.A. algorithm proposed by Debs and Larson (1970) is a cyclic dynamic state estimator, as is the scheme proposed by Banerjee and Rajamani (1977). Lu and Rao (1978) propose a sequential method which uses the Square Root Information Filter (S.R.I.F.) approach together with Householder Transformations to perform estimation and detection of bad data, a function normally carried out by W.L.S.

2.6 COMPARISON OF OTHER METHODS OF STATE ESTIMATION WITH W.L.S.

W.L.S. state estimation was chosen for further study in this thesis because:

(1) W.L.S. state estimations can handle all measurement types; voltage magnitude, real and reactive power flow and injections as well as current measurements and zero injection pseudo-measurements (Schweppe *et al.*, 1970; Aschmoneit, 1975).

(2) W.L.S. generates optimal, minimum variance estimates. Thus the properties of the estimator are well defined, particularly

during bad data detection and identification (Schweppe and Handschin, 1974).

(3) Dynamic state estimation of large scale power systems requires Kalman gain matrices to be diagonalised, etc. (Debs and Larson, 1970).

(4) W.L.S. state estimation has been vigorously tested and numerous techniques of P-θ, Q-v decoupling and fast decoupling have been suggested to improve its performance (Schweppe and Handschin, 1974).

2.7 CONCLUSION

The mathematical foundations underlying W.L.S. state estimation have been reviewed and the properties of W.L.S. compared with other methods. W.L.S. state estimation will be the subject of further study in this thesis, to improve both its performance and speed.

CHAPTER 3

FAST, OPTIMAL STATE ESTIMATION WITH PSEUDO LINE-FLOW CREATION FROM INJECTION MEASUREMENTS

3.1 INTRODUCTION

The two main state estimation techniques advocated for Power Systems are the Schweppe *et al.* (1970) Weighted Least Squares (W.L.S.) and the American Electric Power (A.E.P.) "line-only" transformation (Dopazo *et al.*, 1972).

W.L.S. produces optimal minimum variance estimates from combined "line flow-injection" measurement sets. The form of the algorithm is, from Chapter 2,

$$(H^T(\underline{x}_i)\underline{R}^{-1}\ \underline{H}(\underline{x}_i))\ \Delta\underline{x}_{i+1} = \underline{H}^T(\underline{x}_i)\underline{R}^{-1}\ (\underline{z}_i - \underline{h}(\underline{x}_i)) \qquad (3.1)$$

Transformation techniques act on a measurement set $\underline{z}$, to produce a state invariant linear estimator (Handschin and Schweppe, 1974), i.e.

$$\underline{z}' = \underline{g}(\underline{z}, \underline{x}) = \underline{M} \cdot \underline{x} + \underline{\varepsilon} \qquad (3.2)$$

where $\underline{\varepsilon}$ is the "noise" vector associated with the measurement,

$\underline{M}$ is a matrix linearly relating the transformed measurements, $\underline{z}'$ to states $\underline{x}$, and

$\underline{g}$ is a non-linear transformation.

Non-linear transformations cannot produce matrices that are state independent. The A.E.P. transformation produces optimal estimates only when all lines have similar parameters. The A.E.P. algorithm, in addition to a voltage reference, processes only line-flow measurements.

This gives an estimator of the form (Dopazo et al., 1972):

$$(\underline{B}^T \underline{D} \underline{B}) \underline{E} = \underline{B}^T \underline{D} (\underline{v}_m - \underline{A}_g \underline{E}_g) \qquad (3.3)$$

This algorithm has the same form as W.L.S., but $\underline{B}$ and $\underline{B}^T \underline{D} \underline{B}$ are constant matrices with the same structure as the admittance matrix of the Power System. The admittance matrix structure is very sparse and the resulting A.E.P. algorithm is extremely fast. Basic W.L.S. in comparison is very slow. Speed disadvantages result from:

(1) The Jacobian matrices in (3.1) require repeat evaluation at each iteration. Fast decoupling the Jacobian matrix overcomes this limitation.

(2) Use of injection measurements in the estimator degrades sparsity. Injection measurements produce large numbers of off-diagonal terms in $\underline{H}(\underline{x}_i)$. Formation of the L.H.S. of (3.1) results in "secondary fill-in" effects as the off diagonal terms in $\underline{H}(\underline{x}_i)$ mesh together. Typically a fourfold degradation in sparsity can result when all injection measurements are used. This disadvantages the speed of W.L.S. and fast decoupled W.L.S. over the A.E.P. "line-only" algorithm.

The inclusion of injection measurements in power system state estimation is of great importance from an economic point of view. More than 40% of the injection measurements possible on a power system may be considered to be zero (Mafaakher *et al.*, 1979). These are zero-injection pseudomeasurements that do not require monitoring, having both a high availability and high accuracy. Injection measurements also enhance filtering of the estimates. The inability of the A.E.P. algorithm to include injection measurements is its major disadvantage, and a number of "modifications" were proposed to overcome this limitation. These include:

(1) Extending the A.E.P. "line-only" formulation to include injection pairs (Dopazo *et al.*, 1976; Van Meeteren *et al.*, 1975; Stadlin, 1976; Ionescu and Radu, 1974). Complicated expressions result and the admittance-like sparsity of the original algorithm is lost as summation terms appear.

(2) Augmenting the A.E.P. algorithm by "equality-constrained" minimizations (Ionescu and Radu, 1974; Srinvasan, 1976). Injections are used as constraints. Complexity and loss of sparsity result. Srinvasan's (1976) method, with only 10 out of 80 possible injection measurements present, increases the C.P.U. time from 0.6 seconds to 0.67 seconds, or 10%.

Methods (1) and (2) increase complexity and decrease sparsity. Fast state estimation will only result when a small percentage of injection measurements are included. Injection measurements also must be included as pairs, each pair having the same variance. The following methods do not decrease sparsity or require injection measurement pairs to be monitored, i.e.

(3) Pseudo line-flow measurements are created from injection measurements if at least $(m - 1)$ line flows are measured at the same node (Srinvasan and Robichaud, 1974). The requirement of measuring at least all but one of the line flows at the same node where the injection is monitored seems to limit the application of this method.

(4) Methods of transformation other than the A.E.P. algorithm. Johnsson (1973) proposes a current transformation that includes line-flow and injection measurement pairs. Duran (1977) evolves a Linear Complex Model that can incorporate line and injection pairs with the possibility of different weightings. The inclusion of injection measurements by both methods, however,

involves summations and decreased sparsity.

In this chapter, techniques to enhance the sparsity of "line-flow injection" measurement sets by creating pseudo line flows from injection measurements or by modifying the structure of the information matrix, are outlined. The techniques proposed do not require the monitoring of measurement pairs, have "admittance-like" sparsity and when used with W.L.S., optimal estimates can result. These methods are equally applicable to W.L.S. or to the A.E.P. "line-only" algorithm. In this chapter only the methods of application to W.L.S. are investigated. In sections 3.2 and 3.3, four methods are outlined which give the information matrix "admittance-like" sparsity and in sections 3.4 - 3.6 the properties of the estimates and the rate of convergence of the proposed schemes are analytically evaluated, and tested in section 3.7. The method which shows the most promise is selected and a two stage state estimation algorithm using this method is outlined in sections 3.8 - 3.9 which generate rapid, optimal W.L.S.-like state estimates, and is tested in section 3.10.

3.2 CREATION OF PSEUDO LINE-FLOWS FROM INJECTION MEASUREMENTS

Consider z_{p_i}, a measurement of the active or reactive power injected at node i

$$z_{p_i} = h(\underline{x})_{p_i} + \eta_{z_{p_i}} \tag{3.4}$$

This injected power must also equal the sum of the power flowing through the transmission lines, (j,ℓ,...k), connected to bus i, i.e.

$$h(\underline{x})_{p_i} = h(\underline{x})_{p_{ij}} + h(\underline{x})_{p_{i\ell}} + \ldots + h(\underline{x})_{p_{ik}} \tag{3.5}$$

Pseudo line-flow measurements may be created from the injection measurement, z_{p_i}, in at least two different ways.

3.2.1 Method 1

$$\begin{aligned} z_{p_{ij}}' &= z_{p_i} - (h(\underline{x})_{p_i} - h(\underline{x})_{p_{ij}}) \\ z_{p_{i\ell}}' &= z_{p_i} - (h(\underline{x})_{p_i} - h(\underline{x})_{p_{i\ell}}) \\ &\vdots \qquad\quad \vdots \qquad\quad \vdots \qquad\quad \vdots \\ z_{p_{ik}}' &= z_{p_i} - (h(\underline{x})_{p_i} - h(\underline{x})_{p_{ik}}) \end{aligned} \tag{3.6}$$

3.2.2 Method 2

$$\begin{aligned} z_{p_{ij}}' &= z_{p_i} \times \frac{h(\underline{x})_{p_{ij}}}{h(\underline{x})_{p_i}} \\ z_{p_{i\ell}}' &= z_{p_i} \times \frac{h(\underline{x})_{p_{i\ell}}}{h(\underline{x})_{p_i}} \\ &\vdots \qquad\quad \vdots \qquad\quad \vdots \\ z_{p_{ik}}' &= z_{p_i} \times \frac{h(\underline{x})_{p_{ik}}}{h(\underline{x})_{p_i}} \end{aligned} \tag{3.7}$$

These pseudo line-flow measurements created by either method 1 or 2, are related to the power system states, by

$$\begin{aligned} z_{p_{ij}}' &= h(\underline{x})_{p_{ij}} + \eta_{z_{p_{ij}}}' \\ z_{p_{i\ell}}' &= h(\underline{x})_{p_{i\ell}} + \eta_{z_{p_{i\ell}}}' \\ &\vdots \qquad\quad \vdots \qquad\quad \vdots \\ z_{p_{ik}}' &= h(\underline{x})_{p_{ik}} + \eta_{z_{p_{ik}}}' \end{aligned} \tag{3.8}$$

The creation of pseudo line flows has expanded the measurement set. Each injection measurement is replaced by q_i pseudo line-flows, where q_i is the number of connected lines to bus i. Pseudo line-flow

creation increases the dimensionality of m to m', where

$$m' = m - N_i + \sum_{\substack{i=1 \\ i\varepsilon\{N_i\}}}^{N_i} q_i \tag{3.9}$$

where N_i is the number of injection measurements and $\{N_i\}$ is the set of injection measurements. The optimal estimate $\hat{\underline{x}}$ is now found by iteratively solving

$$\left(\underline{H}_a^T(\underline{x}_k)\, R_a^{-1}\, \underline{H}_a(\underline{x}_k)\right) \Delta\underline{x}_{k+1} = \underline{H}_a^T(\underline{x}_k)\, \underline{R}^{-1}\, \left(\underline{z}_a - \underline{h}_a(\underline{x}_k)\right) \tag{3.10}$$

where

$$\underline{z}_a = \begin{vmatrix} \underline{z}_{LF} \\ \hline z'_{ij} \\ z'_{i\ell} \\ \vdots \\ z'_{ik} \\ \hline \end{vmatrix} \quad \underline{R}_a = \begin{vmatrix} \underline{R}_{LF} \\ \hline R_{z_{ij}} \\ R_{z_{i\ell}} \\ \vdots \\ R_{z_{ik}} \\ \hline \end{vmatrix} \quad \underline{h}_a(\underline{x}) = \begin{vmatrix} \underline{h}(\underline{x})_{LF} \\ \hline h(\underline{x})_{z_{ij}} \\ h(\underline{x})_{z_{i\ell}} \\ \vdots \\ h(\underline{x})_{z_{ik}} \\ \hline \end{vmatrix} \quad \underline{H}_a(\underline{x}) = \begin{vmatrix} \underline{H}_{LF}(\underline{x}) \\ \hline \partial h(\underline{x})_{z_{ij}}/\partial(\underline{x}) \\ \partial h(\underline{x})_{z_{i\ell}}/\partial(\underline{x}) \\ \vdots \\ \partial h(\underline{x})_{z_{ik}}/\partial(\underline{x}) \\ \hline \end{vmatrix}$$

LF refers to the subset of any line-flow measurements present.

In matrix notation method 1, (3.6) becomes:

$$\underline{z}_a = \underline{z}' - \underline{h}_a(\underline{x}_k) + \underline{h}_p(\underline{x}_k) \tag{3.11}$$

where

$$\underline{z}' = \begin{vmatrix} \underline{z}_{LF} \\ \hline z_i \\ z_i \\ \vdots \\ z_i \\ \hline \end{vmatrix} \quad \underline{h}_p(\underline{x}) = \begin{vmatrix} \underline{h}_{LF}(\underline{x}) \\ \hline h_{z_i}(\underline{x}) \\ h_{z_i}(\underline{x}) \\ \vdots \\ h_{z_i}(\underline{x}) \\ \hline \end{vmatrix} \quad \underline{H}_p(\underline{x}) = \begin{vmatrix} \underline{H}_{LF}(\underline{x}) \\ \hline \partial h(\underline{x})_{z_i}/\partial(\underline{x}) \\ \partial h(\underline{x})_{z_i}/\partial(\underline{x}) \\ \vdots \\ \partial h(\underline{x})_{z_i}/\partial(\underline{x}) \\ \hline \end{vmatrix}$$

and $$\underline{H}_p(\underline{x}) = \partial \underline{h}_p(\underline{x})/\partial \underline{x} \tag{3.12}$$

And in matrix notation method 2, (3.7) becomes

$$\underline{z}_a = \underline{z}' \; \underline{h}_p^{-1}(\underline{x}_k)\underline{h}_a(\underline{x}_k) \tag{3.13}$$

3.3 MODIFICATIONS TO THE INFORMATION MATRIX TO GIVE SPARSE STRUCTURES

Methods 1 and 2 are pseudo line-flow creations applied to the injection measurement set. Modifications can be made solely to the information matrix, on the L.H.S. of equation (2.22), to give the necessary sparse, "line-flow"-like non-zero structure from mixed "line-flow and injection" measurement sets.

3.3.1 Method 3

Compute $\underline{H}(\underline{x})$, $\underline{R}$, $\underline{H}_a(\underline{x})$ and $\underline{R}_a$ for the injection line-flow measurement mix. The L.H.S. of (3.10) can be combined with the R.H.S. of the W.L.S. state estimator algorithm (2.22) to give

$$(\underline{H}_a^T(\underline{x}_k)\underline{R}_a^{-1}\underline{H}_a(\underline{x}_k))\,\Delta\underline{x}_{k+1} = \underline{H}^T(\underline{x}_k)\underline{R}^{-1}(\underline{z} - \underline{h}(\underline{x}_k)) \tag{3.14}$$

Admittance matrix sparsity in the information matrix results.

3.3.2 Method 4

Compute all the matrices involved in the W.L.S. state estimation algorithm, given by (2.22). After forming the information matrix, apply a sparsity operator that sets elements to zero which do not correspond to non-zero admittance matrix locations

$$(\underline{H}^T(\underline{x}_k)\underline{R}^{-1}\underline{H}(\underline{x}_k))^{op}\,\Delta\underline{x}_{k+1} = \underline{H}^T(\underline{x}_k)\underline{R}^{-1}(\underline{z} - \underline{h}(\underline{x}_k)) \tag{3.15}$$

where $$(\underline{H}^T(\underline{x}_k)\underline{R}^{-1}\underline{H}(\underline{x}_k))^{op}_{ij} = \begin{cases} (\underline{H}^T(\underline{x}_k)\underline{R}^{-1}\underline{H}(\underline{x}_k))_{ij} & \text{if } Y_{ij} \neq 0 \\ 0 & \text{otherwise} \end{cases}$$

"Admittance-like" sparsity of the information matrix follows.

3.4 OPTIMALITY OF THE ESTIMATES OBTAINED FROM PSEUDO LINE-FLOW CREATION OR FROM MODIFICATIONS TO THE INFORMATION MATRIX

Provided the noise in the created pseudo line-flow measurements is taken to have the same variance as the noise in the original injection measurement, i.e.

$$\sigma_{z_{p_{ij}}}' = \sigma_{z_{p_{i\ell}}}' = \ldots = \sigma_{z_{p_{ik}}}' = \sigma_{z_{p_i}} \tag{3.16}$$

the W.L.S. estimates using pseudo line-flow creation via method 1 are identical to the W.L.S. estimates obtained using injection measurements, z_{p_i}. A proof is given in Appendix A1. The estimate properties of pseudo line-flow creation using method 2 are more complex and "biased" to the value of the states (see Appendix A2).

Methods 3 and 4, which only modify the values and structure of the information matrix, yield optimal solutions since the R.H.S. of (3.9) and (3.10) are identical to the R.H.S. of the W.L.S. state estimation algorithm, (2.22). This is because the information matrix acts only as a gain matrix, influencing the convergence and not the final estimate. Optimal W.L.S. type estimation results (Schweppe *et al.*, 1970).

3.5 CONVERGENCE PROPERTIES OF W.L.S. WITH AND WITHOUT PSEUDO LINE-FLOW CREATION OR MODIFICATION TO THE INFORMATION MATRIX

Consider the general form of state estimation:

$$\underline{L}(\underline{x}_k) \cdot (\underline{x}_{k+1} - \underline{x}_k) = \underline{G}(\underline{x}_k)\ (\underline{z} - \underline{h}(\underline{x}_k)) \tag{3.17}$$

All state estimation algorithms have this form. Depending on the nature of the algorithm, $\underline{L}(\underline{x}_k)$ and $\underline{G}(\underline{x}_k)$ may be constant or state dependent matrices. It is shown in Appendix A3 that the rate of convergence depends on the eigenvalues of

$$[\ \underline{I} - \underline{L}^{-1}(\underline{x}_k)\ \underline{G}(\underline{x}_k)\ \underline{H}(\underline{x}_k)\ ] \tag{3.18}$$

where $\underline{H}(\underline{x}_k)$ is the Jacobian matrix

$$\underline{H}(\underline{x}_k) = \left.\frac{\partial \underline{h}(\underline{x}_k)}{\partial \underline{x}}\right|_{\underline{x}=\underline{x}_k} \tag{3.19}$$

Using (3.18), a convergence analysis for W.L.S. state estimation with and without pseudo line-flow creation is given in Appendix A4. W.L.S. state estimation without pseudo line-flow creation is known to have a very fast convergence, usually taking only 3-4 iterations to converge to within 0.00001 p.u. In the "linearized" analysis in Appendix A4, zero eigenvalues were predicted (i.e., one-step convergence). However the non-linear nature of the W.L.S. state estimation algorithm means that, in practice, a few "extra" iterations are required.

3.5.1 Method (1)

When pseudo line-flow creation via method 1 is used, convergence depends on the eigenvalues of

$$[\ \underline{I} - (\underline{H}_a^T(\underline{x}_k)\underline{R}_{a_L}^{-1}\ \underline{H}_a(\underline{x}_k))^{-1}(\underline{H}_a^T(\underline{x}_k)\underline{R}_{a_R}^{-1}\ \underline{H}_p(\underline{x}_k))\ ] \tag{3.20}$$

Fast convergence will occur when $(\underline{H}_a^T(\underline{x}_k)\underline{R}_{a_L}^{-1}\underline{H}_a(\underline{x}_k))^{-1}(\underline{H}_a^T(x_k)\underline{R}_{a_R}^{-}\ \underline{H}_p(\underline{x}_k))\to\underline{I}$. The amount of degradation in convergence when pseudo line-flow creation via method (1) is used will depend on how different $\underline{H}_p(\underline{x})$ is from $\underline{H}_a(\underline{x})$. This difference will depend on the ratio of the number of line-flow measurements, p, present to the number of pseudo line-flow measurements

created, k. When a large number of line-flow measurements are present and only a small number of injection measurements are available, the ratio p:k will be large and $\underline{H}_a(\underline{x}) \rightarrow \underline{H}(\underline{x})$. When no injection measurements are available, $\underline{H}_p(\underline{x}) = \underline{H}_a(\underline{x})$ and "typical", fast, W.L.S.-like convergence results. When a large number of injection measurements, and very few line-flow measurements are present, the differences between $\underline{H}_a(\underline{x})$ and $\underline{H}_p(\underline{x})$ will become large and convergence will degenerate as the ratio p:k becomes small. Convergence may also depend on whether the line-flow measurement base is observable before the pseudo line-flows are added via method (1).

3.5.2 Method (2)

When pseudo line-flow creation via method (2) is used, convergence, from Appendix A4, depends on the eigenvalues of a very complex expression (see Appendix A4). Fast convergence will occur when these eigenvalues tend $\rightarrow \underline{0}$. However the eigenvalues are complicated and depend on the measurements, $\underline{z}$, as well as on the state of the system. Simulation is needed to find out more about the convergence properties of method (2).

3.5.3 Method (3)

When the information matrix of the W.L.S. state estimator algorithm is computed using method (3), convergence, from Appendix A4, depends on the eigenvalues of

$$- \left(\underline{H}_a^T(\underline{x}_k)\ \underline{R}_a^{-1}\underline{H}_a(\underline{x}_k)\right)^{-1} \left[\left(\underline{H}^T(\underline{x}_k)\ \underline{R}^{-1}\ \underline{H}(\underline{x}_k)\right) - \left(\underline{H}_a^T(\underline{x}_k)\ \underline{R}_a^{-1}\underline{H}_a(\underline{x}_k)\right)\right] \quad (3.21)$$

The two terms within the brackets are computed using the Jacobian's $\underline{H}(\underline{x})$ and $\underline{H}_a(\underline{x})$. Most of the non-zero elements within $\underline{H}_a^T(\underline{x})\ \underline{R}_a^{-1}\underline{H}_a(\underline{x})$ are only slightly different from the same non-zero elements in $\underline{H}^T(\underline{x})\ \underline{R}^{-1}\ \underline{H}(\underline{x})$. As a result when these two information

matrices are subtracted, all non-zero elements not common to both $\underline{H}_a^T(\underline{x})\ \underline{R}_a^{-1}\underline{H}_a(\underline{x})$ and $\underline{H}^T(\underline{x})\ \underline{R}^{-1}\underline{H}(\underline{x})$ will remain present in the difference, while the non-zero elements corresponding to non-zero admittance matrix elements will become small when the two information matrices are subtracted. The structure of the difference matrix,

$$[(\underline{H}^T(\underline{x}_k)\ \underline{R}^{-1}\ \underline{H}(\underline{x}_k)) - (\underline{H}_a^T(\underline{x}_k)\ \underline{R}_a^{-1}\ \underline{H}_a(\underline{x}_k))]$$

is shown in Figure 3.1. Because of the non-zero element value structure, and from (3.13), factors which improve the convergence of method (1) should also improve the convergence of method (3).

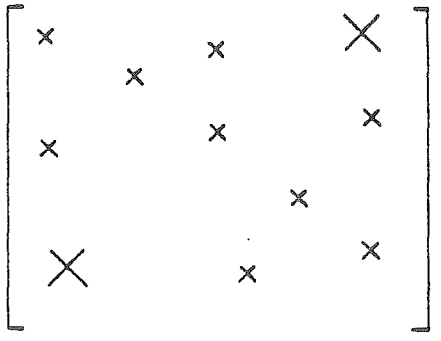

X - denotes small non-zero term (at admittance matrix locations)

X - denotes large non-zero term caused by Secondary fill in.

Figure 3.1 Structure of the difference matrix for method (3).

3.5.4 Method (4)

When the information matrix of the W.L.S. state estimation algorithm is modified using method (4), convergence, from Appendix A[4], depends on the eigenvalues of:

$$- (\underline{H}^T(\underline{x}_k)\underline{R}^{-1}\underline{H}(\underline{x}_k))^{op} \left[(\underline{H}^T(\underline{x}_k)\underline{R}^{-1}\underline{H}(\underline{x}_k)) - (\underline{H}^T(\underline{x}_k)\underline{R}^{-1}H(\underline{x}_k))^{op}\right] \qquad (3.22)$$

When the difference is computed using the information matrices within the brackets, the only non-zero elements that will remain are those off-diagonal elements which do not correspond to admittance matrix type locations and which are caused by the 2nd order meshing fill-in of the unmodified information matrix. The structure of the difference matrix,

$$\left[(\underline{H}^T(x_k)\ \underline{R}^{-1}\ \underline{H}(\underline{x}_k)) - (\underline{H}^T(\underline{x}_k)\ \underline{R}^{-1}\ \underline{H}(\underline{x}_k))^{op}\right] \qquad (3.23)$$

is shown in Figure 3.2. This difference matrix has zero diagonal values and large non-zero off-diagonal values, and as a result convergence will probably be poor.

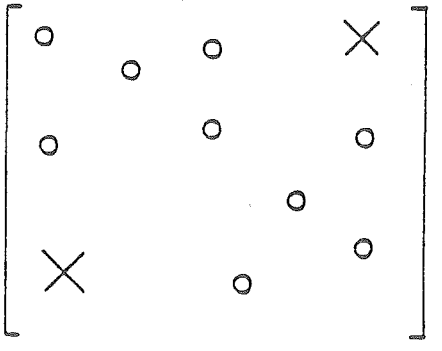

O-denotes zero term (at admittance matrix locations)

X-denotes large non-zero term caused by Secondary fill in.

Figure 3.2 Structure of the "difference" matrix for method (4).

3.6 METHODS OF IMPROVING THE CONVERGENCE OF W.L.S. WHEN PSEUDO LINE-FLOW CREATION AND INFORMATION MATRIX MODIFICATIONS ARE USED

Pseudo line-flows created, and information matrix modifications, can be de-sensitized by variance conditioning until they have little effect on convergence. That is, for method (1), the convergence eigenvalue components become equal, when

$$||(\underline{H}_a^T(\underline{x}_k)\underline{R}_{a_L}^{-1}\underline{H}_a(\underline{x}_k))|| \simeq ||(\underline{H}_a^T(\underline{x}_k)\underline{R}_{a_R}^{-1}\underline{H}_a(\underline{x}_k))|| \qquad (3.24)$$

Variance conditioning occurs when

$$\sigma_{z'_{p_{ij}}} = \sigma_{z'_{p_{il}}} = \ldots = \sigma_{z'_{p_{ik}}} = m\sigma_{z_{p_i}} \qquad (3.25)$$

where $m > 1$.

When $m \gg 1$, W.L.S. convergence with pseudo line-flow creation, and modification to the information matrix, depend entirely on the line-flow measurements, $\underline{z}_{LF}$. Convergence in 3-4 iterations occurs to within 0.0001 p.u. However, desensitizing the pseudo line-flows, or modifying the information matrix by variance conditioning, produces sub-optimal estimates. The W.L.S. estimates that result from using variance conditioned pseudo line-flows or modified information matrices are the same as the W.L.S. estimates that result from using variance conditioned injection measurements, $\underline{z}_{p_i}$. Information has been discarded in order to obtain faster convergence. The effect this has on the quality of the estimates will later be investigated by carrying out a series of simulations.

3.7 TEST RESULTS

The performance of both small and large scale systems was investigated. The 5 bus 7 line system from Stagg and El-Abiad (1968),

shown in Figure 3.3, was used to test the effect of variance conditioning different measurement sets having different levels of redundancy and different p:k ratios.

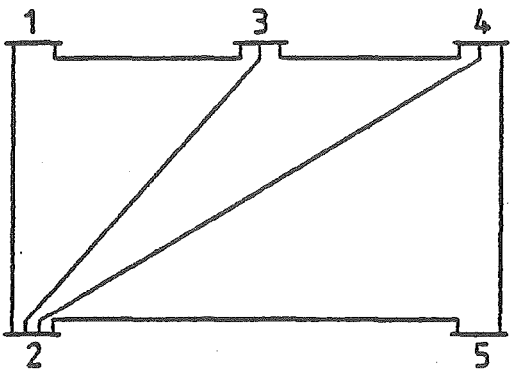

Figure 3.3 5 bus a.c. test system.
(Stagg and El-Abiad, 1968.)

In all tests, unless otherwise stated in tables, etc., the injection and line-flow measurements are assumed to have the same variance, $\sigma_{z_i} = \sigma_{z_{LF}}$ and the pseudo line-flows and modified information matrices are variance conditioned to $R_{z_{ij}}' = (m\sigma_{z_i})^2 q_i$ where q_i is the number of lines attached to node i where the injection is measured. It was originally felt that since q_i pseudo line-flow measurements were being created from each injection measurement, at node i, and used as q_i independent measurements in the state estimator, then to preserve the information content of the original injection measurement, the variance of each pseudo line-flow should be at least q_i times the variance of the original injection measurement. It was later realized that the first method advocated for pseudo line-flow creation, was in fact optimal and variance conditioning $R_{z_{ij}}'$ to $(m\sigma_{z_i})^2$ is all that is required. The performance of variance

conditioned pseudo line-flow creation is shown in Table 3.1. When variance conditioning, $R_{z_{ij}} > (3\sigma_{z_i})q_i$, is used, state estimation involving pseudo line-flow creation converges in three iterations to within 0.0001 p.u. Altering the number of voltage measurements present, or the ratio of p:k, by altering the number of line-flow measurements present, has little effect on convergence provided the line-flow measurement base is observable. When an unobservable line-flow measurement base is used, convergence degrades slightly and a higher level of variance conditioning, $(4\sigma_{z_i})^2 q_i$ is required, for method (1); while method (2) requires variance conditioning to $(30\ \sigma_{z_i})^2 q_i$ or more before the method will converge. Generally method (1) requires less variance conditioning than method (2) to converge. However method (2) did converge for extreme p:k ratios, 2:5, when $2v_i + 2P_{ij} + 2Q_{ij} + 2P_i + 2Q_i$ are used to monitor the 5 bus test system. For this case the line-flow measurement base is unobservable and method (1) failed to converge. This test case is an extreme example, however, that is unlikely to be encountered in a practical situation.

When method (3) is used to compute the information matrix, variance conditioning of $R_a > (10\sigma_{z_i})q_i$ must be used for convergence to within 0.00001 p.u. in four iterations (see Table 3.2). Altering the number of voltage measurement percent or the ratio of p:k, by altering the number of line-flow measurements present, only has a slight effect on convergence, provided the line-flow measurement base is observable. When an unobservable line-flow measurement base was used, method (3) diverges, even when an extremely high level of variance conditioning, $(30\sigma_{z_i})q_i$, was used.

Using method (4) to modify the information matrix proved very unstable. Variance conditioning of $R_a \geq (30\sigma_{z_i})q_i$ was needed for convergence. When only a small proportion of the total possible number

Table 3.1 Effect of different measurement configurations (p:k ratio) on the performance of W.L.S. with pseudo line-flow creation.

CASE		METHOD (1) NUMBER OF ITERATIONS <0.001 p.u.	METHOD (1) NUMBER OF ITERATIONS <0.00001 p.u.	METHOD (1) VARIANCE CONDITIONING	METHOD (2) NUMBER OF ITERATIONS <0.001 p.u.	METHOD (2) NUMBER OF ITERATIONS <0.00001 p.u.	METHOD (2) VARIANCE CONDITIONING	RATIO m:k
Effect of varying # of v		4	7	$\sigma^2_{z_i}\cdot q_i$				14:14
$14P_{ij} + 14Q_{ij} + 5P_i + 5Q_i +$	$5v_i$	3	4	$(3\sigma_{z_i})^2\cdot q_i$	3	5	$(3\sigma_{z_i})^2\cdot q_i$	
Ratio m:k = 14:14	$4v_i$	4	7	$\sigma^2_{z_i}\cdot q_i$	3	5	$(3\sigma_{z_i})^2\cdot q_i$	14:14
Fully observable line-flow base	$3v_i$	4	7	$\sigma_{z_i}\cdot q_i$	3	5	$(3\sigma_{z_i})^2\cdot q_i$	14:14
	$2v_i$	4	7	$\sigma^2_{z_i}\cdot q_i$	3	4	$(3\sigma_{z_i})^2\cdot q_i$	14:14
	$1v_i$	5	8	$\sigma^2_{z_i}\cdot q_i$				14:14
		3	4	$(3\sigma_{z_i})^2\cdot q_i$	3	4	$(3\sigma_{z_i})^2\cdot q_i$	14:14
Effect of varying the # of injection in a fully observable set		4	7	$\sigma^2_{z_i}\cdot q_i$				14:14
$14P_{ij} + 14Q_{ij} +$	$5v+5P_i+5Q_i$	3	4	$(3\sigma_{z_i})^2\cdot q_i$	3	5	$(3\sigma_{z_i})^2\cdot q_i$	14:14
Ratio m:k varies	$1v+5P_i+5Q_i$	5	8	$\sigma^2_{z_i}\cdot q_i$			$(3\sigma_{z_i})^2\cdot q_i$	14:14
Fully observable line-flow base	$5v_i+4P_i+4Q_i$	4	8	$\sigma^2_{z_i}\cdot q_i$	3	4	$(3\sigma_{z_i})^2\cdot q_i$	14:12
	$5v_i+3P_i+3Q_i$	4	9	$\sigma^2_{z_i}\cdot q_i$	3	4	$(3\sigma_{z_i})^2\cdot q_i$	14:10
	$5v_i+2P_i+2Q_i$	5	9	$\sigma^2_{z_i}\cdot q_i$	3	4	$(3\sigma_{z_i})^2\cdot q_i$	14:7
	$5v_i+P_i+Q_i$	5	9	$\sigma^2_{z_i}\cdot q_i$				14:4
	$1v_i+P_i+Q_i$	6	10	$\sigma^2_{z_i}\cdot q_i$				14:4
		3	4	$(3\sigma_{z_i})^2\cdot q_i$				14:4
Effect of varying the # of injections in a minimally observable line-flow base set		5	10	$\sigma^2_{z_i}\cdot q_i$				7:14
$7P_{ij} + 7Q_{ij} +$	$5v_i+5P_i+5Q_i$	3	4	$(3\sigma_{z_i})^2\cdot q_i$	4	5	$(3\sigma_{z_i})^2\cdot q_i$	7:14
Minimally observable line-flow base	$1v_i+5P_i+5Q_i$	6	11	$\sigma^2_{z_i}\cdot q_i$				7:14
	$5v_i+4P_i+4Q_i$	6	11	$\sigma^2_{z_i}\cdot q_i$	4	5	$(3\sigma_{z_i})^2\cdot q_i$	7:12
	$5v_i+3P_i+3Q_i$	7	>15	$\sigma^2_{z_i}\cdot q_i$	4	5	$(3\sigma_{z_i})^2\cdot q_i$	7:10
	$5v_i+2P_i+2P_i$	8	>15	$\sigma^2_{z_i}\cdot q_i$	4	5	$(3\sigma_{z_i})^2\cdot q_i$	7:7
	$5v_i+P_i+Q_i$	7	>15	$\sigma^2_{z_i}\cdot q_i$				7:4
		3	4	$(3\sigma_{z_i})^2\cdot q_i$				7:4
	$1v_i+P_i+Q_i$	10	>15	$\sigma^2_{z_i}\cdot q_i$				7:4
		3	5	$(3\sigma_{z_i})^2\cdot q_i$				7:4
Effect of varying the # of injections on an unobservable line-flow base		9	18	$\sigma^2_{z_i}\cdot q_i$	15	21	$(3\sigma_{z_i})^2\cdot q_i$	7:14
$7P_{ij} + 7Q_{ij} +$	$5v_i+5P_i+5Q_i$	6	3	$(3\sigma_{z_i})^2\cdot q_i$	7	12	$(30\sigma_{z_i})^2\cdot q_i$	7:14
Ratio m:k varies		11	20	$\sigma^2_{z_i}\cdot q_i$	10	15	$(3\sigma_{z_i})^2\cdot q_i$	7:14
Unobservable line-flow base	$1v_i+5P_i+5Q_i$	8	14	$(3\sigma_{z_i})^2\cdot q_i$	8	14	$(30\sigma_{z_i})^2\cdot q_i$	7:14
	$5v_i+4P_i+4Q_i$	8	17	$\sigma^2_{z_i}\cdot q_i$	8	13	$(30\sigma_{z_i})^2\cdot q_i$	7:12
	$5v_i+3P_i+3Q_i$	12	23	$\sigma^2_{z_i}\cdot q_i$	† 10	13	$(30\sigma_{z_i})^2\cdot q_i$	7:10
	$5v_i+2P_i+2Q_i$	11	25	$\sigma^2_{z_i}\cdot q_i$	† 8	13	$(30\sigma_{z_i})^2\cdot q_i$	7:7
	$5v_i+P_i+Q_i$	19	>25	$\sigma^2_{z_i}\cdot q_i$	>15	>15	$(3\sigma_{z_i})^2\cdot q_i$	7:4
		5	9	$(3\sigma_{z_i})^2\cdot q_i$	† 9	18	$(30\sigma_{z_i})^2\cdot q_i$	7:4
	$1v_i+P_i+Q_i$	>25	>25	$\sigma^2_{z_i}\cdot q_i$				7:4
		5	9	$(3\sigma_{z_i})^2\cdot q_i$				7:4

† Value converged to wrong solution.

of voltage measurements possible were present, method (4) diverged whether the line-flow measurement base was observable or not (see Table 3.2).

Tests were also carried out on a 29 bus system which contains 37 transmission lines, and forms the 220 kV system of the South Island of New Zealand. The performance of the state estimator at tracking five measurement cycles from a near flat start was investigated with different levels of variance conditioned pseudo line-flow creation or information matrix modification. These results are compared with the performance of conventional W.L.S. with and without variance conditioning. The results are shown in Table 3.3. Two different measurement systems were used in the tests; the first contained 62% of all possible injection measurements while the second contained all possible injection measurements. Execution times shown in Table 3.3 include time spent reading data, building up pointers and initialization as well as the time required to track the five measurement cycles. The program was run on a Burroughs B6700 computer operating on a time-shared basis. Execution times would improve dramatically if the program was run on a dedicated machine or on a more powerful computer. The time per iteration to track the 213 measurements and 57 states is 2 seconds for W.L.S with pseudo line-flow creation via method (1) and variance conditioning, and 2.5 seconds for conventional W.L.S. Variance conditioning merely reduces the total number of iterations from 16 to 11. When all injection measurements are included, the time per iteration to track the 235 measurements and 57 states is still 2 seconds while the time per iteration for conventional W.L.S. is about 7 seconds. When all injection measurements are present, W.L.S. with variance conditioned pseudo line-flow creation via method (1), is four times as fast as conventional W.L.S. without variance conditioning.

Table 3.2 Effect of different measurement configurations (p:k ratio) on the performance of W.L.S. with measurement modifications.

CASE		METHOD (3) NUMBER OF ITERATIONS <0.001 p.u.	METHOD (3) NUMBER OF ITERATIONS <0.00001 p.u.	METHOD (3) VARIANCE CONDITIONING	METHOD 4) NUMBER OF ITERATIONS <0.001 p.u.	METHOD 4) NUMBER OF ITERATIONS <0.00001 p.u.	METHOD 4) VARIANCE CONDITIONING	RATIO m:k
Effect of varying # of v		4	7	$(3\sigma_{z_i})^2 \cdot q_i$	3	7	$(30\sigma_{z_i})^2 \cdot q_i$	14:14
$14P_{ij} + 14Q_{ij} + 5P_i + 5Q_i +$	$5v_i$	3	4	$(10\sigma_{z_i})^2 \cdot q_i$	3	5	$(50\sigma_{z_i})^2 \cdot q_i$	
Ratio m:k = 14:14	$4v_i$	3	7	$(3\sigma_{z_i})^2 \cdot q_i$	3	9	$(30\sigma_{z_i})^2 \cdot q_i$	14:14
Fully observable line-flow base	$3v_i$	4	7	$(3\sigma_{z_i})^2 \cdot q_i$	4	15	$(30\sigma_{z_i})^2 \cdot q_i$	14:14
	$2v_i$	4	7	$(3\sigma_{z_i})^2 \cdot q_i$	Diverge	Diverge	$(30\sigma_{z_i})^2 \cdot q_i$	14:14
	$1v_i$	4	7	$(3\sigma_{z_i})^2 \cdot q_i$	Diverge	Diverge	$(30\sigma_{z_i})^2 \cdot q_i$	14:14
		3	4	$(10\sigma_{z_i})^2 \cdot q_i$				14:14
Effect of varying the # of injections in a fully observable set		4	7	$(3\sigma_{z_i})^2 \cdot q_i$	3	7	$(30\sigma_{z_i})^2 \cdot q_i$	14:14
$14P_{ij} + 14Q_{ij} +$	$5v+5P_i+5Q_i$	3	4	$(10\sigma_{z_i})^2 \cdot q_i$	3	5	$(50\sigma_{z_i})^2 \cdot q_i$	14:14
Ratio m:k varies	$1v+5P_i+5Q_i$	4	7	$(3\sigma_{z_i})^2 \cdot q_i$			$(30\sigma_{z_i})^2 \cdot q_i$	14:14
Fully observable line-flow base	$5v_i+4P_i+4Q_i$	4	7	$(3\sigma_{z_i})^2 \cdot q_i$	7	3	$(30\sigma_{z_i})^2 \cdot q_i$	14:12
	$5v_i+3P_i+3Q_i$	3	7	$(3\sigma_{z_i})^2 \cdot q_i$	7	3	$(30\sigma_{z_i})^2 \cdot q_i$	14:10
	$5v_i+2P_i+2Q_i$	4	7	$(3\sigma_{z_i})^2 \cdot q_i$	6	3	$(30\sigma_{z_i})^2 \cdot q_i$	14:7
	$5v_i+P_i+Q_i$	4	7	$(3\sigma_{z_i})^2 \cdot q_i$	3	3	$(30\sigma_{z_i})^2 \cdot q_i$	14:4
	$1v_i+P_i+Q_i$			$(3\sigma_{z_i})^2 \cdot q_i$			$(30\sigma_{z_i})^2 \cdot q_i$	14:4
				$(10\sigma_{z_i})^2 \cdot q_i$			$(50\sigma_{z_i})^2 \cdot q_i$	14:4
Effect of varying the # of injections in a minimally observable line-flow base set		5	10	$(3\sigma_{z_i})^2 \cdot q_i$	3	8	$(30\sigma_{z_i})^2 \cdot q_i$	7:14
$7P_{ij} + 7Q_{ij} +$	$5v_i+5P_i+5Q_i$	3	4	$(10\sigma_{z_i})^2 \cdot q_i$			$(50\sigma_{z_i})^2 \cdot q_i$	7:14
Minimally observable line-flow base	$1v_i+5P_i+5Q_i$	6	12	$(3\sigma_{z_i})^2 \cdot q_i$	Diverge	Diverge	$(30\sigma_{z_i})^2 \cdot q_i$	7:14
	$5v_i+4P_i+4Q_i$	5	10	$(3\sigma_{z_i})^2 \cdot q_i$	4	8	$(30\sigma_{z_i})^2 \cdot q_i$	7:12
	$5v_i+3P_i+3Q_i$	5	11	$(3\sigma_{z_i})^2 \cdot q_i$	4	8	$(30\sigma_{z_i})^2 \cdot q_i$	7:10
	$5v_i+2P_i+2P_i$	5	11	$(3\sigma_{z_i})^2 \cdot q_i$	3	4	$(30\sigma_{z_i})^2 \cdot q_i$	7:7
	$5v_i+P_i+Q_i$	5	10	$(3\sigma_{z_i})^2 \cdot q_i$	3	5	$(30\sigma z_i)^2 \cdot q_i$	7:4
				$(10\sigma_{z_i})^2 \cdot q_i$			$(50\sigma_{z_i})^2 \cdot q_i$	7:4
	$1v_i+P_i+Q_i$	5	11	$(3\sigma_{z_i})^2 \cdot q_i$	Diverge	Diverge	$(30\sigma_{z_i})^2 \cdot q_i$	7:4
				$(10\sigma_{z_i})^2 \cdot q_i$			$(50\sigma_{z_i})^2 \cdot q_i$	7:4
Effect of varying the # of injections on an unobservable line-flow base				$(3\sigma_{z_i})^2 \cdot q_i$	4	8	$(30\sigma_{z_i})^2 \cdot q_i$	7:14
$7P_{ij} + 7Q_{ij} +$	$5v_i+5P_i+5Q_i$	Diverge	Diverge	$(30\sigma_{z_i})^2 \cdot q_i$			$(50\sigma_{z_i})^2 \cdot q_i$	7:14
Ratio m:k varies				$(3\sigma_{z_i})^2 \cdot q_i$	Diverge	Diverge	$(30\sigma_{z_i})^2 \cdot q_i$	7:14
Unobservable line-flow base	$1v_i+5P_i+5Q_i$	Diverge	Diverge	$(30\sigma_{z_i})^2 \cdot q_i$			$(50\sigma_{z_i})^2 \cdot q_i$	7:14
	$5v_i+4P_i+4Q_i$	Diverge	Diverge	$(30\sigma_{z_i})^2 \cdot q_i$	7	11	$(30\sigma_{z_i})^2 \cdot q_i$	7:12
	$5v_i+3P_i+3Q_i$	Diverge	Diverge	$(30\sigma_{z_i})^2 \cdot q_i$	7	11	$(30\sigma_{z_i})^2 \cdot q_i$	7:10
	$5v_i+2P_i+2Q_i$	Diverge	Diverge	$(30\sigma_{z_i})^2 \cdot q_i$	6	10	$(30\sigma_{z_i})^2 \cdot q_i$	7:7
	$5v_i+P_i+Q_i$	Diverge	Diverge	$(3\sigma_{z_i})^2 \cdot q_i$	3	6	$(30\sigma_{z_i})^2 \cdot q_i$	7:4
		Diverge	Diverge	$(30\sigma_{z_i})^2 \cdot q_i$			$(50\sigma_{z_i})^2 \cdot q_i$	7:4
	$1v_i+P_i+Q_i$	Diverge	Diverge	$(3\sigma_{z_i})^2 \cdot q_i$	Diverge	Diverge	$(30\sigma_{z_i})^2 \cdot q_i$	7:4
		Diverge	Diverge	$(30\sigma_{z_i})^2 \cdot q_i$			$(50\sigma_{z_i})^2 \cdot q_i$	7:4

Table 3.3 Large scale performance of W.L.S. with and without pseudo line-flow creation and measurement modification.

VARIANCE CONDITIONING (INJECTIONS)	W.L.S. WITHOUT PSEUDO LINE-FLOW CREATION		VARIANCE CONDITIONING (PSEUDO LINE-FLOWS)	METHOD (1) W.L.S. WITH PSEUDO LINE-FLOW CREATION		VARIANCE CONDITIONING (PSEUDO LINE-FLOWS)	METHOD (2) W.L.S. WITH PSEUDO LINE-FLOW CREATION		VARIANCE CONDITIONING	METHOD (3) W.L.S. WITH MODIFIED INFORMATION MATRIX		VARIANCE CONDITIONING	METHOD (4) W.L.S. WITH MODIFIED INFORMATION MATRIX	
	NO. OF ITER. REQUIRED TO TRACK 5 CYCLES	EXECUTION TIME		NO. OF ITER. REQUIRED TO TRACK 5 CYCLES	EXECUTION TIME		NO. OF ITER. REQUIRED TO TRACK 5 CYCLES	EXECUTION TIME		NO. OF ITER. REQUIRED TO TRACK 5 CYCLES	EXECUTION TIME		NO. OF ITER. REQUIRED TO TRACK 5 CYCLES	EXECUTION TIME
(1) 213 measurements/57 states (63% of all injections) $29v_i+74P_{ij}+74Q_{ij}+18P_i+18Q_i$														
$\sigma^2_{z_i}$	16 iterations	51.5 secs	$\sigma^2_{z_i}\cdot q_i$	25 iterations	56 secs	$\sigma^2_{z_i}\cdot q_i$	>30 iterations	69 secs						
			$(3\sigma_{z_i})^2\cdot q_i$	16 iterations	38 secs	$(3\sigma_{z_i})^2\cdot q_i$	19 iterations	41 secs	$(3\sigma_{z_i})^2\cdot q_i$	22 iterations	51 secs	$(30\sigma_{z_i})^2\cdot q_i$	UNSTABLE	
						$(5\sigma_{z_i})^2\cdot q_i$	15 iterations	38 secs	$(10\sigma_{z_i})^2\cdot q_i$	15 iterations	39 secs	$(50\sigma_{z_i})^2\cdot q_i$	UNSTABLE	
$(10\sigma_{z_i})^2$	11 iterations	39 secs	$(10\sigma_{z_i})^2\cdot q_i$	11 iterations	28 secs	$(10\sigma_{z_i})^2\cdot q_i$	13 iterations	28 secs	$(50\sigma_{z_i})^2\cdot q_i$	11 iterations	36 secs	$(90\sigma_{z_i})^2\cdot q_i$	UNSTABLE	
						$(30\sigma_{z_i})^2\cdot q_i$	12 iterations	29 secs						
(2) 235 measurements/57 states (100% of all injections) $29v_i+74P_{ij}+74Q_{ij}+29P_i+29Q_i$														
$\sigma^2_{z_i}$	16 iterations	124 secs				NOT APPLICABLE			$(20\sigma_{z_i})^2\cdot q_i$	14 iterations	40 secs	$(90\sigma_{z_i})^2\cdot q_i$	UNSTABLE	
$(10\sigma_{z_i})^2$	11 iterations	91 secs	$(10\sigma_{z_i})^2\cdot q_i$	13 iterations	37 secs	METHOD (2) CANNOT HANDLE			$(30\sigma_{z_i})^2\cdot q_i$	12 iterations	38 secs			
$(20\sigma_{z_i})^2$	11 iterations	91 secs	$(20\sigma_{z_i})^2\cdot q_i$	11 iterations	33 secs	ZERO INJECTION PSEUDOMEASUREMENTS			$(50\sigma_{z_i})^2\cdot q_i$	11 iterations	38 secs			

Note: (i) results are accurate to within 2-4 seconds. This is due to the "time-shared" nature of the B6700 computer used.
(ii) convergence tolerance for the track was 0.001 p.u.
(iii) 11 iterations is the fastest one can track the 5 cycles from initialization.

Pseudo line-flow creation using method (2) and variance conditioning had a similar speed improvement as method (1) over conventional W.L.S., with and without variance conditioning, when all 62% of all possible injection measurements were present. However method (2) is not applicable when zero injection pseudo measurements are included in the state estimator. This is because some of the measurements, $\underline{z}$, are now zero and no information can be obtained about the likely magnitude of the pseudo line-flows using method (2).

The use of method (3) to compute the information matrix in the W.L.S. state estimation algorithm converged for high levels of variance conditioning, both with and without the zero injection pseudomeasurements present. Method (4) proved unstable for all test cases shown in Table 3.3.

3.7.1 Discussion of results and selection of the best method for further testing

Clearly, from Tables 3.1 - 3.3, the best method for reducing the number of non-zero terms in the information matrix is the pseudo line-flow creation method (1). Simulation has shown this method to have the best convergence properties and thus require the least variance conditioning to achieve fast convergence in 3-4 iterations, for both observable and unobservable line-flow measurement bases. Method (1) can also handle zero injection pseudomeasurements, which is a distinct advantage over method (2). The expansion of injection measurements by pseudo line-flow creation, now taken to mean method (1) in the following sections, can preserve the minimum variance, unbiased optimality of W.L.S. The expanded Jacobian, $\underline{\underline{H}}_a(\underline{x}_k)$, has a line-flow type structure and when squared to form the information matrix, $\underline{\underline{H}}_a^T(\underline{x}_k)\underline{\underline{R}}_a^{-1}\underline{\underline{H}}_a(\underline{x}_k)$, an "admittance-like" sparsity results. The information matrix now has a

similar structure to the $\underline{B}^T \underline{D} \underline{B}$ matrix on the L.H.S. of the A.E.P. algorithm, given by (3.3), yet results from a mixed "line-flow injection" measurement set.

3.7.2 Reasons for the dramatic speed improvement when pseudo line-flow creation is used

Increasing the number of injection measurements in the "line-flow injection" measurement mix from 63% to 100% caused a 2½ fold increase in the execution time of conventional W.L.S. state estimation. The number of multiply-add operations, M-A, to be performed in the factorization of a symmetric matrix is given by (Aschmoneit et al., 1977)

$$M\text{-}A = \sum_{i=1}^{m'} (r_i^2 + r_i)/2 \qquad (3.26)$$

where m' is the dimension of the information matrix (number of states), and r_i is the number of terms to the right of the diagonal of the factorized i^{th} row. This relationship is linear with system size, and second order with matrix density. As the number of injection measurements present increases, the density of the conventional W.L.S. information matrix increases and the factorization time increases by the square of the relative density increase. Figure 3.4 shows the non-zero element density for the 29 bus test system when all injection measurements are present. Including injection measurements by pseudo line-flow creation expands the Jacobian matrix from $\underline{H}(\underline{x})$ to $\underline{H}_a(\underline{x})$. This increase in dimensionality does not affect the size or density of the information matrix. Figure 3.5 shows the non-zero element density when all line-flow measurements are present. The non-zero structure is the same when all injection measurements are handled by pseudo line-flow creation. Aschmoneit et al. (1977) proposed a method to handle zero injections as equality constraints and thus increases

estimate accuracy while avoiding second order fill-in effects in the information matrix. Only a 10% improvement in speed was noted when 61% of all possible injections were handled by equality constrained W.L.S. state estimation, while above a 50% speed improvement was noted when W.L.S. with pseudo line-flow creation and variance conditioning was used to process 63% of all possible injection measurements present.

3.8 FURTHER REFINEMENTS TO METHOD (1) WHICH DO NOT DEGRADE OPTIMALITY

Equation (3.19) implies that for $(\underline{H}_a^T(\underline{x})\ \underline{R}_{a_L}^{-1}\ \underline{H}_a(\underline{x}))^{-1}$ $(\underline{H}_a^T(\underline{x})\ \underline{R}_{a_R}^{-1}\ \underline{H}_p(\underline{x})) \to \underline{I}$, then

$$\underline{R}_{a_L}^{-1}\ \underline{H}_a(\underline{x}) = \underline{R}_{a_R}^{-1}\ \underline{H}_p(\underline{x}) \tag{3.27}$$

If no variance conditioning is used on the R.H.S. of (3.10), the estimate will be given by

$$(\underline{H}_a^T(\underline{x})\ \underline{R}_{a_L}^{-1}\ \underline{H}_a(\underline{x}))\ \Delta\underline{x} = \underline{H}_a^T(\underline{x})\ \underline{R}_{a_R}^{-1}\ (\underline{z}_a - \underline{h}_a(\underline{x})) \tag{3.28}$$

This estimate will be optimal, even though the L.H.S. of the equation has been "variance-conditioned". The L.H.S. of the W.L.S. equation contains only gain matrices that affect convergence, not the optimality of the solution. By satisfying (3.27), zero eigenvalues and convergence in 3-4 iterations should be obtained. However (3.27) would need recomputing at each iteration, and although $\underline{R}_{a_R}$ is a diagonal matrix, $\underline{R}_{a_L}$ would be full (m×m). It is not feasible to use (3.27); instead use

$$||\underline{R}_{a_L}^{-1}\ \underline{H}_a(\underline{x})|| \simeq ||\underline{R}_{a_R}^{-1}\ \underline{H}_p(\underline{x})|| \tag{3.29}$$

since $\underline{R}_{a_L}$ and $\underline{R}_{a_R}$ are positive definite,

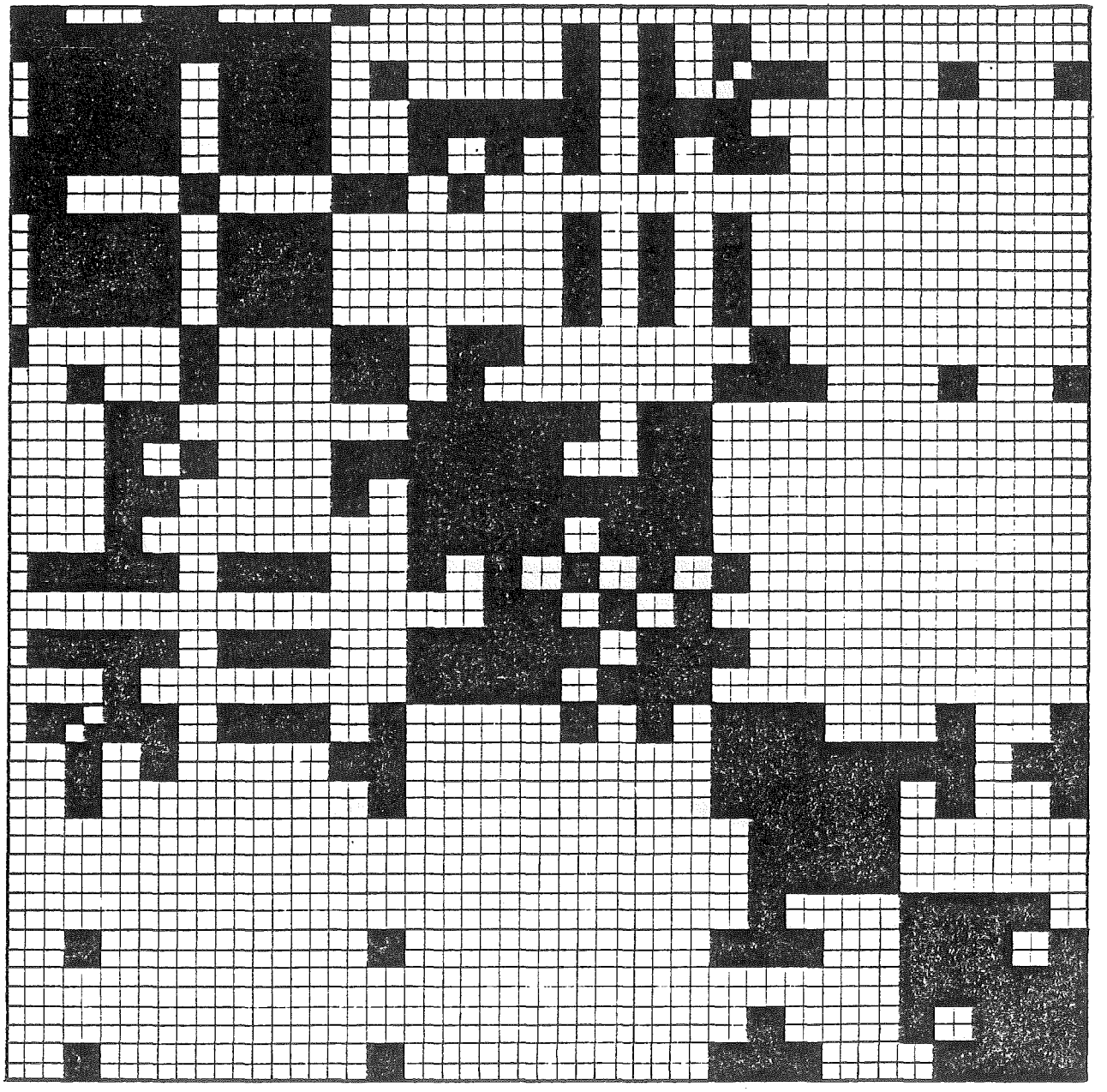

Figure 3.4 Information matrix when 29 $(P_i + Q_i)$ injection measurements are present.

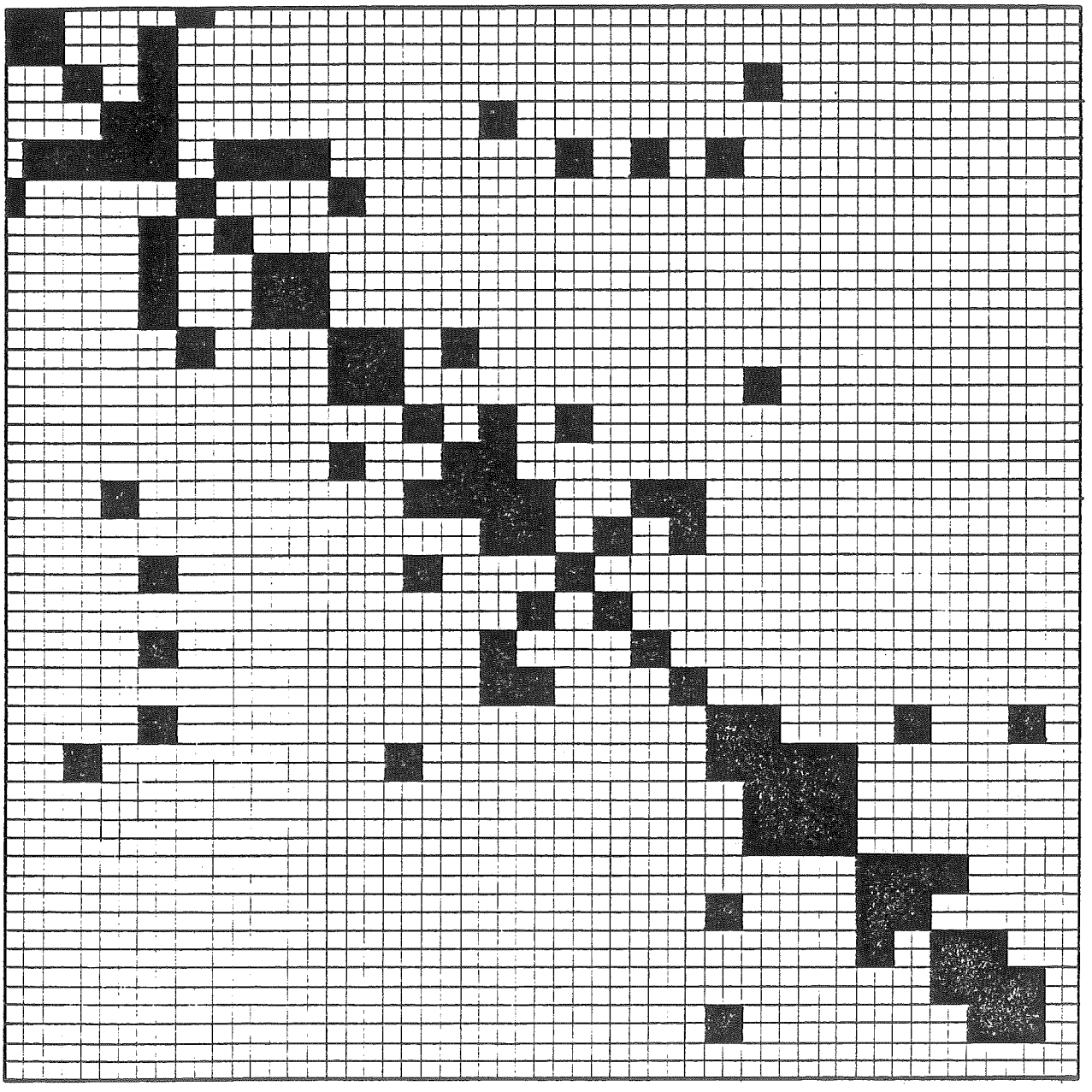

Figure 3.5 Information matrix when 74 ($P_i + Q_i$) line-flow measurements are present.

$$\underline{R}_{a_L}^{-1} \, ||\underline{H}_a(\underline{x})|| \simeq \underline{R}_{a_R}^{-1} \, ||\underline{H}_p(\underline{x})|| \qquad (3.30)$$

This relationship will be satisfied, for line-flow and voltage measurements, when $\underline{R}_{a_L} = \underline{R}_{a_R}$ and for injection measurements when $R_{a_L} = R_{a_R}/q_i$. This is because $||\underline{H}_p(\underline{x})|| \simeq q_i ||\underline{H}_a(\underline{x})||$ for each injection measurement expansion; from

$$||\underline{H}_p(\underline{x})|| \simeq q_i \, ||\underline{H}_a(\underline{x})||,$$

equation (3.11), and noting that

$$\partial h(\underline{x})_{z_i}/\partial x = \partial h(\underline{x})_{z_{ij}}/\partial \underline{x} + \partial h(\underline{x})_{z_{i\ell}}/\partial \underline{x} + \ldots + \partial h(\underline{x})_{z_{ik}}/\partial \underline{x}$$

Thus convergence of W.L.S. with pseudo line-flow creation can be improved if each injection measurement expansion is also made to satisfy (3.30) by setting $R_{a_L} = R_{a_R}/q_i$. Because (3.30) is an approximation to (3.27), a combination of variance conditioning the pseudo line-flows to a level $R_{a_R} = m\sigma_{p_{z_i}}$ and then setting $R_{a_L} = (m\sigma_{p_{z_i}})^2/q_i$ may be needed to get fast convergence in 3-4 iterations.

3.9 TWO STAGE OPTIMAL W.L.S. ESTIMATION WITH PSEUDO LINE-FLOW CREATION

The technique outlined in section 3.8 involves variance-conditioning the pseudo line-flows to obtain a fast W.L.S.-like convergence. Estimates, however, are suboptimal because less confidence is given to the injection measurements. However, when identifying bad data or dispatching or billing applications, optimal estimates may be necessary. A two-stage W.L.S. state estimation technique based on pseudo line-flow creation can generate optimal estimates (see Fig. 3.6). In the first stage the pseudo line-flows are variance conditioned to obtain fast convergence to a suboptimal solution in three iterations.

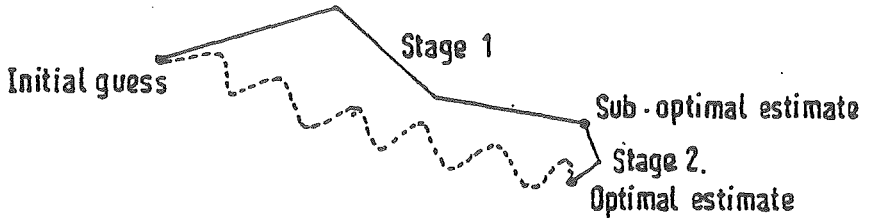

Figure 3.6 Optimal estimation using two-stage W.L.S. with pseudo line-flow creation.

This solution point is close to the optimal solution that results when no various conditioning is used. After convergence, all variance conditioning on the R.H.S. of (3.28) is removed and a further iteration, or iterations, are carried out until sufficiently accurate optimal estimates are obtained.

3.10 TESTING THE REFINEMENTS TO METHOD (1)

3.10.1 Performance of methods of improving convergence without degrading optimality

In section 3.8 it was proposed that variance conditioning the L.H.S. of equation (3.28) differently to the R.H.S., for pseudo line-flow creation, by setting $\underline{R}_{\underline{a}_L} = \rho \underline{R}_{\underline{a}_R}/q_i$ should improve convergence. When $\sigma_{R_a} = \sigma_{z_i}$, optimal estimates should result. ρ is a number that is used to tune the convergence of the estimator without affecting $\underline{R}_{\underline{a}_R}$ and thus without affecting the optimality of the estimates. The choice of ρ is arbitrary. "Good choices" of ρ differ from different test systems but can easily be found by simulation. Table 3.4 shows the convergence properties of the pseudo line-flow creation for the 5 bus

Table 3.4 Effect of altering $\underline{R}_{a_L}$ and $\underline{R}_{a_R}$ by different amounts when variance conditioning pseudo line-flows (p:k) = 14.14: present.

VARIANCE CONDITIONING (PSEUDO LINE FLOWS)		CONVERGENCE	
$\underline{R}_{a_L}$	$\underline{R}_{a_R}$	TOL <0.001 p.u.	TOL <0.00001 p.u.
(1) Optimal estimation $\underline{R}_{a_R} = \sigma_{z_i}$			
$\sigma^2_{z_i}$	$\sigma^2_{z_i}$	>35 iterations	>35 iterations
$\sigma^2_{z_i}.q_i$	$\sigma^2_{z_i}$	Diverge	Diverge
$(3\sigma_{z_i})^2.q_i$	$\sigma^2_{z_i}$	Diverge	Diverge
$(0.3\sigma_{z_i})^2 q_i$	$\sigma^2_{z_i}$	6 iterations	14 iterations
$(0.1\sigma_{z_i})^2 q_i$	$\sigma^2_{z_i}$	Diverge	Diverge
$\sigma^2_{z_i}/q_i$	$\sigma^2_{z_i}$	7 iterations	19 iterations
$(0.4\sigma_{z_i})^2/q_i$	$\sigma^2_{z_i}$	9 iterations	>25 iterations
$(0.8\sigma_{z_i})^2/q_i$	$\sigma^2_{z_i}$	8 iterations	>25 iterations
$(1.20\sigma_{z_i})^2/q_i$	$\sigma^2_{z_i}$	6 iterations	14 iterations
$(1.25\sigma_{z_i})^2/q_i$	$\sigma^2_{z_i}$	6 iterations	12 iterations
$(1.30\sigma_{z_i})^2/q_i$	$\sigma^2_{z_i}$	6 iterations	13 iterations
$(1.50\sigma_{z_i})^2/q_i$	$\sigma^2_{z_i}$	8 iterations	15 iterations
(2) Variance conditioning + refinement			
$(2\sigma_{z_i})^2/q_i$	$(2\sigma_{z_i})^2$	5 iterations	11 iterations
(3) Variance conditioning only			
$(\sigma_{z_i})^2.q_i$	$(\sigma_{z_i})^2.q_i$	5 iterations	8 iterations
$(3\sigma_{z_i})^2$	$(3\sigma_{z_i})^2$	4 iterations	7 iterations
$(3\sigma_{z_i})^2.q_i$	$(3\sigma_{z_i})^2 q_i$	3 iterations	4 iterations

test system when $\underline{R}_{\underline{a}_L}$ and $\underline{R}_{\underline{a}_R}$ are not equal. When $\underline{R}_{\underline{a}_L} = \underline{R}_{\underline{a}_R} = \sigma_{z_i}^2$, the state estimator does not converge within 35 iterations. However, if the pseudo line-flow creation is tuned with ρ between 1.2 and 1.3, and $\underline{R}_{\underline{a}_R} = \sigma_{z_i}^2$, optimal estimates can be generated in six iterations to within 0.001 p.u. A combination of variance conditioning, $\underline{R}_{\underline{a}_R} = (m\sigma_{z_i})^2$, and use of the refinement $\underline{R}_{\underline{a}_L} = \rho \underline{R}_{\underline{a}_R}/q_i$, can be used to improve convergence further. Acceleration factors may also be used to improve convergence. Figure 3.7 shows the state estimator has monotonic convergence when $\rho = 1.25$ and $\underline{R}_{\underline{a}_R} = \sigma_{z_i}$. Acceleration factors, α, that have the form $\alpha(\underline{x}_{i+1} - \underline{x}_i)$, where $\alpha > 1$, can be applied after the second iteration of the state estimator. Convergence results are shown in Table 3.5. Simple forms of α do not significantly improve convergence, and more complicated acceleration schemes may be required (Rao and Tripathy, 1978).

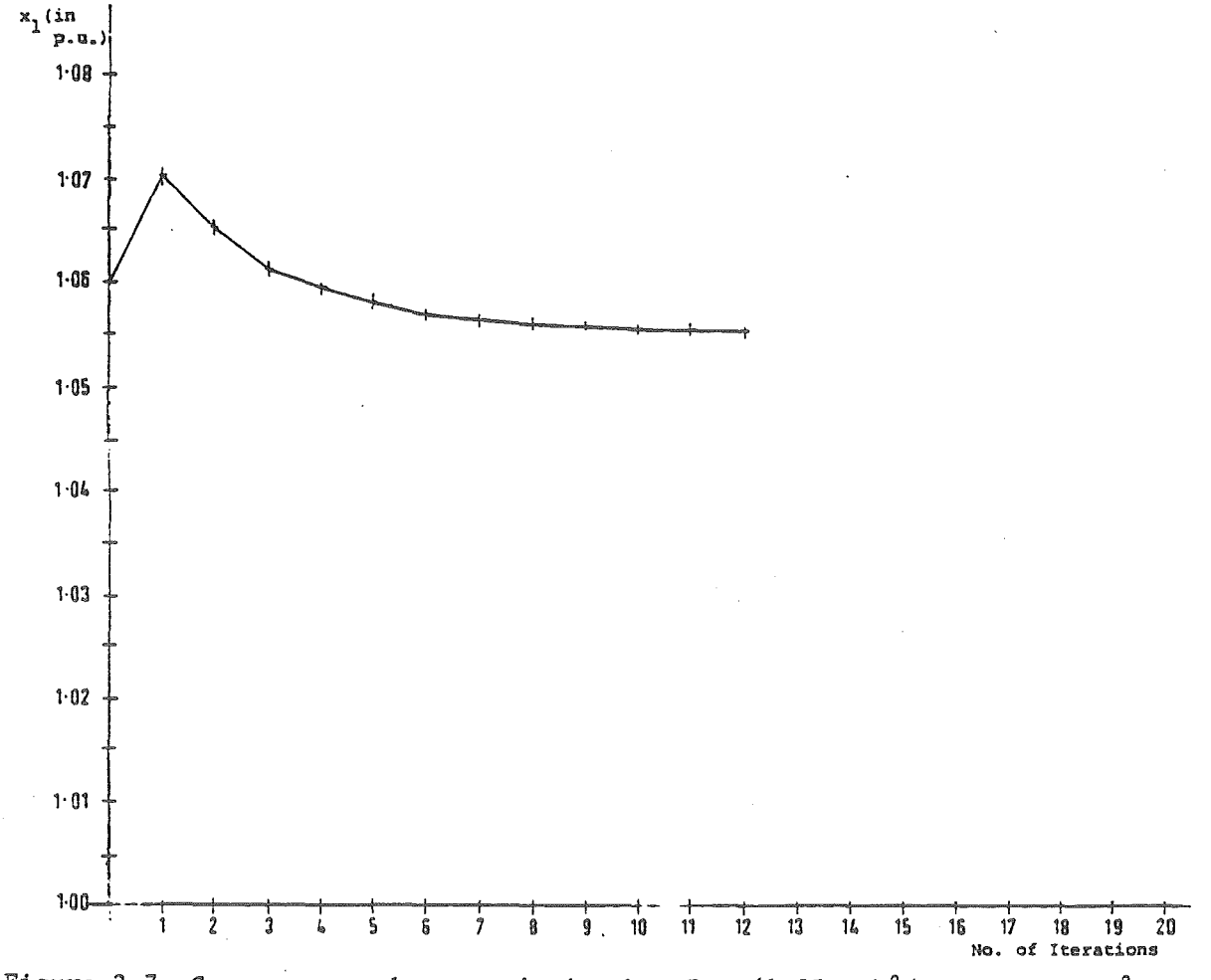

Figure 3.7 Convergence characteristic when $\underline{R}_{\underline{a}_L} = (1.25\sigma_{z_i})^2/q_i$ and $\underline{R}_{\underline{a}_R} = \sigma_i^2$.

Table 3.5 Effect of acceleration factors on convergence of pseudo line-flow creation when $\underline{R}_{a_L} = (1.25\sigma_{z_i})/q_i$ and $\underline{R}_{a_R} = \sigma_{z_i}$.

ACCELERATION FACTOR α	CONVERGENCE		
	<0.001 p.u.	<0.0001 p.u.	<0.00001 p.u.
1	6 iterations	9 iterations	12 iterations
1.05	6 iterations	9 iterations	12 iterations
1.10	6 iterations	8 iterations	11 iterations
1.15	6 iterations	8 iterations	10 iterations
1.20	6 iterations	10 iterations	12 iterations
1.25	9 iterations	11 iterations	>12 iterations
2.00	>12 iterations	>12 iterations	>12 iterations

3.10.2 Fast, optimal two stage W.L.S. state estimation with pseudo line-flow creation

Test results in section 3.10.1 showed that optimal state estimation requires at least six iterations to converge to within 0.001 p.u. for the 5 bus test system. The concept of two stage optimal state estimation was outlined in section 3.9. Measurements to the state estimator are corrupted by nominal measurement noise $<3\sigma_i$. During the first stage, variance conditioning is used to achieve rapid convergence with $m > 3$ in $\underline{R}_{\underline{a}_R} = (m\sigma_{z_i})^2$ and $\underline{R}_{\underline{a}_L} = \rho\, \underline{R}_{\underline{a}_R}/q_i$. When the p:k ratio of the measurement system is 14:14, the first stage converges in three iterations to within 0.001 p.u., and after m is reset to unity the second stage converges in three iterations to the optimal solution to within 0.0001 p.u. This performance is better than the optimal estimation technique advocated in section 3.8. When the p:k ratio of the measurement system is 7:14 the first stage takes four iterations to converge to within 0.001 p.u. and after m is reset to unity, the second stage takes five iterations to converge to within 0.0001 p.u. of the optimal solution.

The two stage optimal state estimator with pseudo line-flow creation was tested on the 235 measurement/57 state system outlined in section 3.7. The p:k ratio of the system is 74:74. Measurements were corrupted by normal measurement noise $<3\sigma_i$. During the first stage, variance conditioning of $m = 10$ was used to ensure that the state estimator converged in three iterations to within 0.001 p.u. m was then reset to unity and the second stage converged in five iterations to within 0.0001 p.u. of the optimal solution (and one iteration to within 0.001 p.u. of the optimal solution). Conventional optimal W.L.S. requires four iterations to converge to within 0.0001 p.u. of the optimal solution, with a time per iteration of 7 seconds. Total

execution time is hence 28 seconds. Two stage, optimal W.L.S. with variance conditioned pseudo line-flow creation took eight iterations, at 2 seconds per iteration, for a total execution time of 16 seconds. This is nearly twice as fast as conventional W.L.S.

All tests carried out have assumed that $\sigma_{z_i} = \sigma_{z_{ij}}$, i.e., all measurements have the same uncertainty. Sometimes injection measurements may be more accurate than the line-flow measurements, especially when zero injection pseudo measurements are used. When $\sigma_{z_i} = 0.1\ \sigma_{z_{LF}}$ and $m = 100$, the first stage of the state estimator converges in three iterations <0.001. m is then reset to unity and a further seven iterations are required to converge to within 0.0001 p.u. of the optimal solution. Total execution time was 20 seconds, nearly a third faster than conventional W.L.S.

3.10.3 Effect of variance conditioning on estimate accuracy when measurement noise is present

3.10.3.1 Nominal measurement noise (<3σ)

Variance conditioned pseudo line-flow creation degrades state estimator optimality because less regard is taken of the injection measurement data. The degradation that occurs in the estimates for different metering patterns, p:k ratios, and level of variance conditioning is shown in Table 3.6. The amount of degradation in estimate accuracy in the presence of nominal measurement noise clearly depends on the proportion of measurements in the state estimator that are not variance conditioned, i.e. on the p:k ratio and on the number of voltage measurements present. For p:k ratios greater or equal to 1:1, variance conditioned pseudo line-flow creation does not affect estimate quality, from an on-line tracking point of view where 0.001 p.u. is a sufficiently accurate tolerance to maintain a reliable data

Table 3.6 Estimate degradation due to variance conditioning in the presence of noisy measurements ($\leq 3\sigma$) (in p,u,).

DIFFERENCE BETWEEN ESTIMATES WITH $\sigma_{ij}'^2 = (6\sigma_{z_i})^2$ and $\sigma_{ij}'^2 = \sigma_{z_i}^2$				
	$5v + 14P_{ij} + 14Q_{ij} + 5P_i + 5Q_i$	$1v + 14P_{ij} + 14Q_{ij} + 2P_i + 2Q_i$	$1v + 7P_{ij} + 7Q_{ij} + 5P_i + 5Q_i$	$1v + 7P_{ij} + 7Q_{ij} + 5P_i + 5Q_i$
	p:k = 14:14	p:k = 14:7	p:k = 7:14	p:k = 7:14
	OBSERVABLE LINE FLOW BASE	OBSERVABLE LINE FLOW BASE	OBSERVABLE LINE FLOW BASE	UNOBSERVABLE LINE FLOW BASE
Q_1	0.0	0.0	0.0	0.0
V_1	0.00103	0.00095	0.00523	0.00637
Q_2	-0.00004	0.00016	0.00031	0.00036
V_2	0.00095	0.00080	0.00350	0.00627
Q_3	-0.00048	-0.00061	0.00046	0.00064
V_3	0.00137	0.00114	0.00663	0.00766
Q_4	-0.00094	-0.00093	0.00013	0.00038
V_4	0.00134.	0.00111	0.00646	0.00753
Q_5	-0.00014	0.00048	0.00111	0.00066
V_5	0.00063	0.00121	0.00584	0.00617

5 bus test system used.

base, free from bad data. If more accurate estimates are required, the two stage optimal W.L.S. technique with pseudo line-flow creation can be used instead. In all cases shown in Table 3.6, the maximum error caused by the variance conditioning is much less than the measurement accuracy of 0.01 p.u.

3.10.3.2 Bad data ($>3\sigma_i$) present

For a variance conditioned state estimator, bad data in line-flow measurements will be "seen" when the error in the measurement exceeds $3\sigma_{z_{LF}}$. Errors in the injection measurements will not "appear" as bad data in the variance-conditioned pseudo line-flows until the size of the error exceeds $3\sigma_{z_{ij}}'$ where $\sigma_{z_{ij}}' = m\sigma_{z_i}$. When this occurs, the error can be detected and identified. Injection measurement error lying between $3\sigma_{z_i}$ and $3m\sigma_{z_i}$ will go undetected until the variance conditioning is removed or reduced. Errors lying within this range will not affect the quality of the variance conditioned state estimates. However, during detection and identification of bad data, the two stage optimal estimation algorithm should be used. Removal of all variance conditioning during the second stage allows all the information present to be brought to bear in identifying bad data. Removal of variance conditioning is also important in generating accurate estimates for economic dispatch, etc. Injection measurement meter faults causing bad data lying within the range $3\sigma_{z_i}$ to $3m\sigma_{z_i}$ may accumulate after a variance conditioned on-line state estimator has been operating for some time. Failure to periodically check and remove these errors, using the two stage optimal estimator, means that when significant bad data appears, requiring two stage optimal estimation and the removal of variance conditioning, all accumulated faulty meters producing errors within $3\sigma_{z_i}$ to $3m\sigma_{z_i}$ now appear as bad data and complicate the identification process.

Table 3.7 Detection and modification of bad data when variance conditioned pseudo line-flow creation is used.

WEIGHTED RESIDUAL LOCATION (r_u)	WEIGHTED RESIDUALS WHEN MEASUREMENT NOISE <3σ PRESENT AND VARIANCE CONDITIONING $\sigma_{ij}'^2=(1.25\sigma_{z_i})^2$	WEIGHTED RESIDUALS WHEN MEASUREMENT NOISE <3σ PRESENT AND VARIANCE CONDITIONING $\sigma_{ij}'^2=(6\sigma_{z_i})^2$	WEIGHTED RESIDUALS WHEN MEASUREMENT NOISE <3σ AND BAD DATA OF 20σ IN P_{2-4}, P_4, V_4. VARIANCE CONDITIONING $\sigma_{ij}'^2=(1.25\sigma_{z_i})^2$	WEIGHTED RESIDUALS WHEN MEASUREMENT NOISE <3σ AND BAD DATA OF 20σ IN V_4, P_{2-4} AND P_4. VARIANCE CONDITIONING $\sigma_{ij}'^2=(6\sigma_{z_i})^2$	2 STAGE ALGORITHM WEIGHTED RESIDUALS MEASUREMENT NOISE <3σ AND BAD DATA OF 20σ IN V_4, P_{2-4}, P_4. ONE ITERATION OF 2nd STAGE WITH $\sigma_{ij}'^2=(1.25\sigma_{z_i})^2$
V_1	-0.7830	-0.7189	-4.5744	-4.6536	-4.5891
V_2	-1.1794	-1.1233	-5.0211	-5.1176	-5.0115
V_3	-0.6139	-0.5228	-4.5454	-5.4791	-4.6125
B.D.P. → V_4	0.3494	0.4396	16.3835 *	16.4807 *	16.3087 *
V_5	2.1531	2.1864	-1.7336	-1.8614	-1.7700
P_{1-2}	0.5086	0.6969	0.6116	1.2349	-0.3182
P_{1-3}	-0.1718	0.0177	-0.2679	-2.1199	0.2815
P_{2-3}	1.8761	2.0501	1.7214	-0.9395	2.7627
P_{2-5}	0.1779	0.3330	-0.8454	-0.6829	-0.2355
P_{3-4}	-0.1549	1.0526	3.0202	0.5595	3.6044
P_{4-2}	0.4589	0.0875	-0.0856	3.1098	-0.9951
P_{5-4}	-1.5368	-1.3506	-0.7143	-3.0802	-0.1969
B.D.P. → P_{2-4}	0.8595	0.2987	19.6821 *	16.5666 *	20.7931 *
P_{4-3}	2.2148	1.0116	-1.1307	1.5053	-1.5312
P_{4-5}	0.1927	0.0047	-0.6361	1.7499	-1.1589
P_{2-1}	0.7739	0.5897	0.7669	0.1633	1.6702
P_{3-1}	1.2090	1.0279	1.3798	3.1313	0.8602
P_{3-2}	0.2823	0.1109	0.4576	3.0483	-0.5575
P_{5-2}	1.1844	1.0353	2.2455	2.0919	1.6592
Q_{1-2}	0.8263	0.9219	1.2932	1.4226	1.1116
Q_{1-3}	1.1226	0.9595	1.5457	1.3413	1.6432
Q_{2-3}	0.2435	-0.0118	0.5437	0.3398	0.6959
Q_{2-5}	0.0601	0.7586	0.5854	0.8035	0.8304
Q_{3-4}	-0.4676	-0.7933	-0.3026	-0.5327	-0.1594
Q_{4-2}	-0.3783	-0.0551	-0.2622	-0.2654	-0.3495
Q_{5-4}	0.4347	0.1269	0.8095	0.6409	0.3020
Q_{3-2}	-1.0318	-0.7744	-0.9414	-0.9468	-0.1012
Q_{3-1}	0.0086	0.1890	0.2210	0.1249	0.2175
Q_{2-4}	1.1515	1.0607	1.4654	1.4065	1.5679
Q_{4-3}	-1.4114	-1.0762	-1.3738	-1.1699	-1.5120
Q_{4-5}	0.1494	0.4458	0.1673	0.3979	0.1645
Q_{2-1}	-0.6691	-0.9704	-0.3280	-0.5982	-0.1457
Q_{5-2}	0.3992	0.7560	1.2719	1.0887	1.0996
P_1	0.9133	0.2533	0.9188	0.0133	0.6145
P_2	0.2414	0.1385	0.3667	1.1125	2.5657
P_3	0.9961	0.3051	3.9588	1.1081	3.0524
B.D.P. → P_4	1.9697	0.7044	10.3897 *	3.5048	8.7817 *
P_5	0.6742	0.1343	0.8329	0.2464	0.7777
Q_1	0.6095	0.1383	0.1024	0.0088	0.0350
Q_2	0.7919	0.2466	0.0464	0.0608	0.0505
Q_3	0.4438	0.0737	0.0696	0.0697	0.0141
Q_4	0.3413	0.2302	0.4785	0.1715	0.2959
Q_5	0.9870	0.2807	0.3892	0.1397	0.5330
$J(x)$ test $= \sum_{i=1}^{m} (Z_i - r_i)/\sigma_i)^2$	39.879	26.93	887.86	699.28	908.69

The effect of bad data on the weighted residuals of variance conditioned pseudo line-flow creation in W.L.S. is shown in Table 3.7. A weighted residual is defined as

$$r_{W_i} = (z_i - h_i(\underline{x}))/\sigma_i \qquad (3.31)$$

When nominal measurement noise $<3\sigma$ is present, all weighted residuals are less than 3 and the value of $J(\underline{x})$ is less than 40. When nominal measurement noise $<3\sigma$ + multiple bad data, size 20σ, is present in P_{2-4}, P_4 and v_4 and when $m = 1.25$, the $J(\underline{x})$ test detects the presence of bad data, $(J(\underline{x})>887)$, and the $\underline{r}_W$ test identifies the location of the bad data since r_W at P_{2-4}, P_4 and v_4 is much greater than elsewhere. However when $m = 6$ and the same multiple bad data is present, $J(\underline{x})$ still detects bad data, $(J(\underline{x})>699)$, but the $\underline{r}_W$ test only identifies bad data at v_4 and P_{2-4}. This is to be expected since bad data of size $20\sigma_{z_i}$, when used in variance conditioned pseudo line-flow creation with $m = 6$, appears to be only of size $r_W = (20/6)$ or 3.3. However, if after the detection of bad data using the $J(\underline{x})$ test, the two stage estimation is invoked, and m is reset to 1.25 for the second stage and the state estimator allowed only ONE further iteration, all bad data is easily identified.

3.11 CONCLUSIONS

Four methods of modifying the structure of the information matrix of W.L.S. to have an admittance-like sparsity have been presented and tested. A pseudo line-flow creation technique, which can generate optimal estimates at the expense of convergence, gave the best performance. Variance conditioning these pseudo line-flows results in convergence in three iterations to within 0.001 p.u. but optimality is lost.

However the degradation in the accuracy of the estimates is less than 0.0015 p.u. for a 5 bus test system when a similar number of line-flow measurements and pseudomeasurements, corrupted by nominal measurement noise $<3\sigma$, are present. This accuracy is sufficient for most on-line tracking state estimators where the emphasis is on maintaining a reliable data base, free from bad data (Koenig and O'Malley, 1972). The fast nature of the pseudo line creation technique, particularly when applied to high density injection measurement systems means that estimation is completed in a quarter to a third of the time taken by conventional W.L.S. The data base can be updated more regularly. Pseudo line-flow creation makes fast state estimation more economical because all zero injection pseudomeasurements, which cost nothing to monitor and are highly accurate and highly available, can be included in algorithms. Optimal estimates may be required, either for tracking, economic dispatch, billing, or for detection and identification of bad data. These can easily be generated by a two stage pseudo creation technique where the variance conditioning is removed during the second stage, after convergence of the first stage to a close suboptimal solution. Convergence to the optimal solution, close by, follows. This technique can generate optimal estimates to an accuracy of 0.0001 p.u. at nearly twice the speed of conventional W.L.S., in high density injection measurement mixes. It can be used in on-line tracking but if inaccuracies caused by variance conditioning are tolerable, then sub-optimal estimation involving the first part of the stage can be used to give even better speed advantages over conventional W.L.S.

Recently a pseudo creation technique has been advocated by Aboyles and Molina (1979). This method involves further transformations to "linearize" the pseudomeasurement and make it suitable for use in the A.E.P. "line-only" algorithm. Aboyles and Molina do not show the

technique to be optimal.

CHAPTER 4

REVIEW AND CONVERGENCE ANALYSIS OF DECOUPLED AND FAST DECOUPLED STATE ESTIMATION TECHNIQUES

4.1 INTRODUCTION

The Scheweppe Weighted Least Squares state estimation algorithm has the advantage of generating optimal minimum variance estimates from mixed "line-flow injection" measurement sets. However, speed disadvantages result from (Schweppe and Handschin, 1974) the following:

(1) the gain matrices require repeat evaluation at every iteration; and

(2) the use of injection measurements in the state estimator degrades the sparsity of the information matrix.

As a result, modifications to the form of the W.L.S. algorithm have been proposed. The information matrix on the L.H.S. can be bandwidth limited to reduce storage, or tuned to provide a better rate of convergence. Constant gain matrices can be used whereby the information matrix remains at its initial value. P-θ, Q-v decoupling can also be used to reduce the number of non-zero elements in the gain matrix by a factor of two. In general, for most operating conditions, the active power is highly dependent only on the voltage phase angle at nodes throughout the power system while the reactive power is closely coupled only with the voltage magnitudes. Cross coupling effects are small and their presence in the information matrix can be neglected. Schweppe et al. (1970) first suggested using P-θ, Q-v decoupling in state estimation

and a similar technique was later advocated by Uemura (1972) and Couch et al. (1974). Couch et al. (1975) advocated decoupling the Jacobian matrix on both sides of the W.L.S. state estimation algorithm and using constant gain matrices. Couch (1976) also advocated a transformation scheme to remove the voltage dependence of the reactive power expressions in the Jacobian by division by the voltage magnitude at the node at which the measurement occurred. Aschmoneit (1976) later implemented a modal fast decoupled state estimation scheme based on Couch's method. Because P-θ, Q-v decoupling is involved on both sides of the W.L.S. state estimation algorithm, equation (2.22), the modal-decoupling technique generates suboptimal estimates. Horisberger et al. (1976) and Masiello and Horton (1977) advocate P-θ, Q-v decoupling schemes that only affect the information matrix. As a result, these algorithm-decoupled schemes generate optimal estimates. Garcia et al. (1978) suggested an algorithm decoupled scheme which affects the matrices on both sides of the W.L.S. algorithm. Singh et al. (1976) and Singh et al. (1978) advocated a completely decomposed P-θ, Q-v decoupled state estimator whereby the P-θ partition of the state estimator is iterated to convergence, treating v as a parameter and then the Q-v partition is iterated, treating Q as a constant until convergence. Wognar (1977), Bermundez and Brameller (1978), Mafaakher et al. (1979), Bermundez (1977), Rao and Tripathy (1978), Tripathy et al. (1979), Van Meeteren et al. (1978) and Van Meeteren (1979) have advocated using fast decoupling to make the Jacobian completely state independent, and dependent only on the line parameters of the power system.

In this chapter the convergence properties of decoupled and fast decoupled state estimation are established from both simulation and analytical calculation under conditions where the ratio of the resistance to reactance, (R/X) ratio, is varied and where the weightings

($\underline{R}_p$:$\underline{R}_q$) given to the real and reactive power measurements is also varied. From these tests and calculations, stable decoupling or fast decoupling schemes are identified.

4.2 P-θ, Q-v PARTITIONING

The measurement vector $\underline{z}$ can be partitioned into real power line-flow and injection measurements, $\underline{z}_p$, and voltage magnitudes and reactive line-flow and injection measurements, $\underline{z}_q$.

$$\begin{aligned} \underline{z}_p &= \underline{h}_p(\underline{x}) + \underline{\eta}_p \\ \underline{z}_q &= \underline{h}_q(\underline{x}) + \underline{\eta}_q \end{aligned} \tag{4.1}$$

where

$$\underline{z} = \begin{bmatrix} \underline{z}_p \\ \underline{z}_q \end{bmatrix} \quad \underline{h}(\underline{x}) = \begin{bmatrix} \underline{h}_p(\underline{x}) \\ \underline{h}_q(\underline{x}) \end{bmatrix} \quad \text{and} \quad \underline{\eta} = \begin{bmatrix} \underline{\eta}_p \\ \underline{\eta}_q \end{bmatrix} \tag{4.2}$$

The Jacobian matrix non-zero terms, for $\underline{H}(\underline{x})$, are shown in Table 7.1. The partitioned Jacobian is:

$$\underline{H}(\underline{x}) = \frac{\partial \underline{h}(\underline{x})}{\partial \underline{x}} = \begin{bmatrix} \dfrac{\partial \underline{h}_p(\underline{x})}{\partial \underline{\theta}} & \dfrac{\partial \underline{h}_p(\underline{x})}{\partial \underline{v}} \\ \dfrac{\partial \underline{h}_q(\underline{x})}{\partial \underline{\theta}} & \dfrac{\partial \underline{h}_q(\underline{x})}{\partial \underline{v}} \end{bmatrix} \tag{4.3}$$

where $$\underline{x} = (\underline{\theta}, \underline{v}) \tag{4.4}$$

In terms of the real and reactive partitioned components, the W.L.S. state estimation algorithm given by (2.22) becomes:

$$\begin{bmatrix} \frac{\partial \underline{h}_p^T(\underline{x})}{\partial \underline{\theta}} \underline{R}_p^{-1} \frac{\partial \underline{h}_p(\underline{x})}{\partial \underline{\theta}} + \frac{\partial \underline{h}_q^T(\underline{x})}{\partial \underline{\theta}} \underline{R}_q^{-1} \frac{\partial \underline{h}_q(\underline{x})}{\partial \underline{\theta}} & \frac{\partial \underline{h}_p^T(\underline{x})}{\partial \underline{\theta}} \underline{R}_p^{-1} \frac{\partial \underline{h}_p(\underline{x})}{\partial \underline{v}} + \frac{\partial \underline{h}_q^T(\underline{x})}{\partial \underline{\theta}} \underline{R}_q^{-1} \frac{\partial \underline{h}_q(\underline{x})}{\partial \underline{v}} \\ \frac{\partial \underline{h}_p^T(\underline{x})}{\partial \underline{v}} \underline{R}_p^{-1} \frac{\partial \underline{h}_p(\underline{x})}{\partial \underline{\theta}} + \frac{\partial \underline{h}_q^T(\underline{x})}{\partial \underline{v}} \underline{R}_q^{-1} \frac{\partial \underline{h}_q(\underline{x})}{\partial \underline{\theta}} & \frac{\partial \underline{h}_p^T(\underline{x})}{\partial \underline{v}} \underline{R}_p^{-1} \frac{\partial \underline{h}_p(\underline{x})}{\partial \underline{v}} + \frac{\partial \underline{h}_q^T(\underline{x})}{\partial \underline{v}} \underline{R}_q^{-1} \frac{\partial \underline{h}_q(\underline{x})}{\partial \underline{v}} \end{bmatrix} \cdot \begin{bmatrix} \Delta\underline{\theta} \\ \Delta\underline{v} \end{bmatrix}$$

$$= \begin{bmatrix} \frac{\partial \underline{h}_p(\underline{x})}{\partial \underline{\theta}} & \frac{\partial \underline{h}_p(\underline{x})}{\partial \underline{v}} \\ \frac{\partial \underline{h}_q(\underline{x})}{\partial \underline{\theta}} & \frac{\partial \underline{h}_q(\underline{x})}{\partial \underline{v}} \end{bmatrix}^T \begin{bmatrix} \underline{R}_p^{-1} & \underline{0} \\ \underline{0} & \underline{R}_q^{-1} \end{bmatrix} \begin{bmatrix} \underline{z}_p - \underline{h}_p(\underline{\theta},\underline{v}) \\ \underline{z}_q - \underline{h}_q(\underline{\theta},\underline{v}) \end{bmatrix} \qquad (4.5)$$

where $$\underline{R}_p = E\{\underline{\eta}_p \underline{\eta}_p^T\}$$

and $$\underline{R}_q = E\{\underline{\eta}_q \underline{\eta}_q^T\} \qquad (4.6)$$

4.3 CONVERGENCE ANALYSIS FOR STATE ESTIMATION

Convergence analysis can be employed to establish the convergence properties of W.L.S. type state estimation. In this chapter the convergence analysis outlined in section 3.5 will be used to highlight the likely convergence properties of state estimator algorithms.

Consider the convergence properties of exact W.L.S. state estimation. According to the analysis in section 3.5, exact W.L.S. state estimation has zero convergence eigenvalues, i.e.

$$\lambda_1, \lambda_2 \ldots \lambda_N = 0, 0, \ldots 0$$

As a result convergence is rapid, theoretically occurring in one step according to the "linearized" analysis. In practice, the state estimator is not linear and takes in 3-4 iterations to converge within 0.00001 p.u. First iteration values, however, are accurate to within

0.002 p.u. Thus the first iteration brings the estimate quite close to the true solution from a flat start. Note also that the convergence analysis neglects higher order terms. As a result, convergence is strongly influenced by the degree of "linearity" of the measurement set equations and the resulting Jacobian elements. The influence of measurement "linearity" on the rate of convergence is present because the derivation of the W.L.S. state estimation algorithm involves a Taylor series linearization about the solution point. The more linear the measurement set equations and Jacobian elements, the less number of iterations will be required for convergence. Couch (1976) proposes a transformation to "linearize" the reactive power measurement equations and partial derivatives, and remove their dependence on the nodal voltage magnitudes, as seen in Table 4.1. Each reactive power measurement is divided by the nodal voltage magnitude at the point of measurement. Thus

$$Q_{ij}' = \frac{Q_{ij}}{v_i} = - B_{ii} v_i + v_j(- G_{ij}\sin(\theta_i - \theta_j) + B_{ij}\cos(\theta_i - \theta_j))$$

$$Q_i' = \frac{Q_i}{v_i} = \sum_{j\varepsilon\{\alpha\}} Q_{ij}'$$

and thus the Jacobian elements become

$$\frac{\partial Q_{ij}'}{\partial v_i} = - B_{ii} \tag{4.7}$$

$$\frac{\partial Q_{ij}'}{\partial v_j} = - G_{ij} \sin(\theta_i - \theta_j) + B_{ij} \cos(\theta_i - \theta_j) \tag{4.8}$$

$$\frac{\partial Q_i'}{\partial v_i} = - \sum_{j\varepsilon\{\alpha\}} B_{ii} \tag{4.9}$$

and

$$\frac{\partial Q_i'}{\partial v_j} = \sum_{j\varepsilon\{\alpha\}} (- G_{ij} \sin(\theta_i - \theta_j) + B_{ij} \cos(\theta_i - \theta_j)) \tag{4.10}$$

Table 4.1 Non-zero Jacobian partial derivatives

MEASUREMENT	$\frac{\partial}{\partial \theta_i}$	$V_i \frac{\partial}{\partial V_i}$
V_i	0	V_i
P_{ij}	$-d_{ij}$	$2 V_i^2 G_{ii} - c_{ij}$
P_{ji}	d_{ij}	$-c_{ij}$
Q_{ij}	$-c_{ij}$	$-2 V_i^2 B_{ii} + d_{ij}$
Q_{ji}	c_{ij}	d_{ij}
P_i	$-\sum_{j\varepsilon\{\alpha\}} d_{ij}$	$2 V_i^2 \sum_{j\varepsilon\{\alpha\}} G_{ii} - \sum_{j\varepsilon\{\alpha\}} c_{ij}$
P_j	d_{ij}	$-c_{ij}$
Q_i	$-\sum_{j\varepsilon\{\alpha\}} c_{ij}$	$-2 V_i^2 \sum_{j\varepsilon\{\alpha\}} B_{ii} + \sum_{j\varepsilon\{\alpha\}} d_{ij}$
Q_j	c_{ij}	d_{ij}

As a result of the transformation, gain matrices are used in the state estimator whose values are insensitive to variations in the power system - voltage operating point. The Jacobian terms given by (4.10) and (4.12) depend on the voltage angle difference $(\theta_i - \theta_j)$. However, $B_{ij} \cos(\theta_i - \theta_j) >> G_{ij} \sin(\theta_i - \theta_j)$, and $\cos(\theta_i - \theta_j)$ is rather insensitive to changes in $(\theta_i - \theta_j) < 20^o$.

More recently, Reichert and Sullivan (1977) advocated using a "voltage squared" transformation to linearize the reactive power Jacobian elements and measurement equations. However its advantages have not been clearly established.

Linearization of the measurement set aids convergence by making the linearized convergence analysis results (which for W.L.S., predicts one step convergence) more applicable.

4.4 SUMMARY OF POSSIBLE P-θ, Q-v DECOUPLED AND FAST DECOUPLED SCHEMES

Different possibilities of P-θ, Q-v decoupling or fast decoupling and their convergent properties, are summarized.

4.4.1 Algorithm P-θ, Q-v decoupling

4.4.1.1 Horisberger et al. (1976) advocated decoupling the Jacobian matrix, $\underline{H}(\underline{\theta},\underline{v})$ only in the computation of the information matrix on the L.H.S. of (2.22). Thus the information matrix in (2.22) becomes

$$\begin{bmatrix} \frac{\partial \underline{h}_p^T(\underline{\theta},\underline{v})}{\partial \underline{\theta}} & \underline{0} \\ \underline{0} & \frac{\partial \underline{h}_q^T(\underline{\theta},\underline{v})}{\partial \underline{v}} \end{bmatrix} \begin{bmatrix} \underline{R}_p^{-1} & \underline{0} \\ \underline{0} & \underline{R}_q^{-1} \end{bmatrix} \begin{bmatrix} \frac{\partial \underline{h}_p(\underline{\theta},\underline{v})}{\partial \underline{\theta}} & \underline{0} \\ \underline{0} & \frac{\partial \underline{h}_q(\underline{\theta},\underline{v})}{\partial \underline{v}} \end{bmatrix}$$

$$= \begin{bmatrix} \frac{\partial \underline{h}_p^T(\underline{\theta},\underline{v})}{\partial \underline{\theta}} \underline{R}_p^{-1} \frac{\partial \underline{h}_p(\underline{\theta},\underline{v})}{\partial \underline{\theta}} & \underline{0} \\ \underline{0} & \frac{\partial \underline{h}_q^T(\underline{\theta},\underline{v})}{\partial \underline{v}} \underline{R}_q^{-1} \frac{\partial \underline{h}_q(\underline{\theta},\underline{v})}{\partial \underline{v}} \end{bmatrix}$$

which results in two state estimator equations

$$\left(\frac{\partial \underline{h}_p^T(\underline{\theta}_k,\underline{v}_k)}{\partial \underline{\theta}} \underline{R}_p^{-1} \frac{\partial \underline{h}_p(\underline{\theta}_k,\underline{v}_k)}{\partial \underline{\theta}}\right)\Delta\underline{\theta}_{k+1} = \left[\frac{\partial \underline{h}_p^T(\underline{\theta}_k,\underline{v}_k)}{\partial \underline{\theta}}, \frac{\partial \underline{h}_q^T(\underline{\theta}_k,\underline{v}_k)}{\partial \underline{\theta}}\right][R]^{-1}[\underline{z}-\underline{h}(\underline{\theta}_k,\underline{v}_k)]\Big|_{\substack{\underline{v}=\underline{v}_k \\ \underline{\theta}=\underline{\theta}_k}}$$

$$\left(\frac{\partial \underline{h}_q^T(\underline{\theta}_k,\underline{v}_k)}{\partial \underline{v}} \underline{R}_q^{-1} \frac{\partial \underline{h}_q(\underline{\theta}_k,\underline{v}_k)}{\partial \underline{v}}\right)\Delta\underline{v}_{k+1} = \left[\frac{\partial \underline{h}_p^T(\underline{\theta}_k,\underline{v}_k)}{\partial \underline{v}}, \frac{\partial \underline{h}_q^T(\underline{\theta}_k,\underline{v}_k)}{\partial \underline{v}}\right][R]^{-1}[\underline{z}-\underline{h}(\underline{\theta}_k,\underline{v}_k)]\Big|_{\substack{\underline{v}=\underline{v}_k \\ \underline{\theta}=\underline{\theta}_k}} \quad (4.11)$$

which:

(1.1.1) can be solved simultaneously

(1.1.2) solved sequentially

(1.1.3) solved simultaneously with constant gain matrices on the L.H.S. of (4.11)

(1.1.4) solved sequentially with constant gain matrices on the L.H.S. of (4.11). This was the form suggested by Horisberger et al. (1976).

Alternatively, the equations can be decomposed and the P-θ partition of the state estimator iterated for $\underline{\theta}$, treating $\underline{v}$ as a constant. Then the Q-v partition can be iterated, treating $\underline{\theta}$ as a constant until convergence with:

(1.1.5) the gain matrices on the L.H.S. of (4.11) updated at each iteration, or

(1.1.6) the gain matrices on the L.H.S. constant at their initial values.

The six different P-θ, Q-v decoupling possibilities are shown in Table 4.2. Note that (1.1.1) - (1.1.4) are algorithm decoupled and guarantee exact optimal W.L.S. solutions. The sequential processes are exact, in the sense that each sub P-θ, Q-v sub estimator is exact, and on convergence the sequential realization gives the exact solution.

Table 4.2 Different Horisberger type P-θ, Q-v decoupling possibilities and their convergence.

HORISBERGER TYPE P-θ, Q-v DECOUPLING SCHEMES	CONVERGENT EIGENVALUE EXPRESSIONS
1.1.1 Simultaneous formulation	
$\left[(\underline{h}_{11}^T \underline{R}_p^{-1} \underline{h}_{11})\Delta\underline{\theta}_{k+1} = [\underline{h}_{11}^T, \underline{h}_{21}^T]\ [\underline{R}]^{-1}\ [\underline{z} - \underline{h}(\underline{\theta}_k, \underline{v}_k)]\right]\Big\|_{\substack{v=v_k \\ \theta=\theta_k^k}}$ $\left[(\underline{h}_{22}^T \underline{R}_q^{-1} \underline{h}_{22})\Delta\underline{v}_{k+1} = [\underline{h}_{12}^T, \underline{h}_{22}^T]\ [\underline{R}]^{-1}\ [\underline{z} - \underline{h}(\underline{\theta}_k, \underline{v}_k)]\right]\Big\|_{\substack{v=v_k \\ \theta=\theta_k^k}}$	$\begin{bmatrix} -(\underline{h}_{11}^T \underline{R}_p^{-1} \underline{h}_{11})^{-1}(\underline{h}_{21}^T \underline{R}_q^{-1} \underline{h}_{21}) & -(\underline{h}_{11}^T \underline{R}_p^{-1} \underline{h}_{11})^{-1}(\underline{h}_{11}^T \underline{R}_p^{-1} \underline{h}_{12} + \underline{h}_{21}^T \underline{R}_q^{-1} \underline{h}_{22}) \\ -(\underline{h}_{22}^T \underline{R}_q^{-1} \underline{h}_{22})^{-1}(\underline{h}_{12}^T \underline{R}_p^{-1} \underline{h}_{11} + \underline{h}_{12}^T \underline{R}_q^{-1} \underline{h}_{21}) & -(\underline{h}_{22}^T \underline{R}_q^{-1} \underline{h}_{22})^{-1}(\underline{h}_{12}^T \underline{R}_p^{-1} \underline{h}_{12}) \end{bmatrix}$
1.1.2 Sequential formulation	
$\left[(\underline{h}_{11}^T \underline{R}_p^{-1} \underline{h}_{11})\Delta\underline{\theta}_{k+1} = [\underline{h}_{11}^T, \underline{h}_{21}^T]\ [\underline{R}]^{-1}\ [\underline{z} - \underline{h}(\underline{\theta}_k, \underline{v}_k)]\right]\Big\|_{\substack{v=v_k \\ \theta=\theta_k^k}}$ $\left[(\underline{h}_{22}^T \underline{R}_q^{-1} \underline{h}_{22})\Delta\underline{v}_{k+1} = [\underline{h}_{12}^T, \underline{h}_{22}^T]\ [\underline{R}]^{-1}\ [\underline{z} - \underline{h}(\underline{\theta}_{k+1}, \underline{v}_k)]\right]\Big\|_{\substack{v=v_k \\ \theta=\theta_{k+1}^k}}$	$\begin{bmatrix} [\underline{I} - (\underline{h}_{11}^T\underline{R}_p^{-1}\underline{h}_{11})_0^{-1}(\underline{h}_{11}^T\underline{R}_p^{-1}\underline{h}_{11} + \underline{h}_{21}^T\underline{R}_q^{-1}\underline{h}_{21})_0] & -[(\underline{h}_{11}^T \underline{R}_p^{-1} \underline{h}_{11})_0^{-1}(\underline{h}_{11}^T \underline{R}_p^{-1} \underline{h}_{12} + \underline{h}_{21}^T \underline{R}_q^{-1} \underline{h}_{22})_0] \\ -[(\underline{h}_{22}^T\underline{R}_q^{-1}\underline{h}_{22})_1^{-1}(\underline{h}_{22}^T\underline{R}_p^{-1}\underline{h}_{11} + \underline{h}_{22}^T\underline{R}_q^{-1}\underline{h}_{21})_1 & [\underline{I} - (\underline{h}_{22}^T\underline{R}_q^{-1}\underline{h}_{22})_1^{-1}(\underline{h}_{12}^T\underline{R}_p^{-1}\underline{h}_{12} + \underline{h}_{22}^T\underline{R}_q^{-1}\underline{h}_{22})_1 - (\underline{h}_{12}^T\underline{R}_p^{-1}\underline{h}_{11} \\ [\underline{I} - (\underline{h}_{11}^T\underline{R}_p^{-1}\underline{h}_{11})_0^{-1}(\underline{h}_{11}^T\underline{R}_p^{-1}\underline{h}_{11} + \underline{h}_{21}^T\underline{R}_q^{-1}\underline{h}_{21})_0] & + \underline{h}_{22}^T \underline{R}_q^{-1}\underline{h}_{21})_1(\underline{h}_{11}^T\underline{R}_p^{-1}\underline{h}_{11})_0^{-1}(\underline{h}_{11}^T\underline{R}_p^{-1}\underline{h}_{12} + \underline{h}_{21}^T\underline{R}_q^{-1}\underline{h}_{22})_0] \end{bmatrix}$
1.1.3 Simultaneous update with constant gain matrices	
$[(\underline{h}_{11}^T \underline{R}_p^{-1} \underline{h}_{11})]\Big|_{\substack{\theta_o=0^\circ \\ v_o=1_{p.u.}}} \Delta\underline{\theta}_{k+1} = \left[[\underline{h}_{11}^T, \underline{h}_{21}^T]\ [\underline{R}]^{-1}\ [\underline{z} - \underline{h}(\underline{\theta}_k, \underline{v}_k)]\right]\Big|_{\substack{v=v_k \\ \theta=\theta_k^k}}$ $[(\underline{h}_{22}^T \underline{R}_q^{-1} \underline{h}_{22})]\Big|_{\substack{\theta_o=0^\circ \\ v_o=1_{p.u.}}} \Delta\underline{v}_{k+1} = \left[[\underline{h}_{12}^T, \underline{h}_{22}^T]\ [\underline{R}]^{-1}\ [\underline{z} - \underline{h}(\underline{\theta}_k, \underline{v}_k)]\right]\Big|_{\substack{v=v_k \\ \theta=\theta_k^k}}$	$\begin{bmatrix} \underline{I} - (\underline{h}_{11_o}^T \underline{R}_p^{-1} \underline{h}_{11_o})^{-1}(\underline{h}_{11}^T \underline{R}_p^{-1} \underline{h}_{11} + \underline{h}_{21}^T \underline{R}_q^{-1} \underline{h}_{21}) & -(\underline{h}_{11_o}^T \underline{R}_p^{-1} \underline{h}_{11_o})^{-1}(\underline{h}_{11}^T \underline{R}_p^{-1} \underline{h}_{12} + \underline{h}_{21}^T \underline{R}_q^{-1} \underline{h}_{22}) \\ -(\underline{h}_{22_o}^T \underline{R}_q^{-1} \underline{h}_{22_o})^{-1}(\underline{h}_{12}^T \underline{R}_p^{-1} \underline{h}_{11} + \underline{h}_{12}^T \underline{R}_q^{-1} \underline{h}_{21}) & \underline{I} - (\underline{h}_{22_o}^T \underline{R}_q^{-1} \underline{h}_{22_o})^{-1}(\underline{h}_{12}^T \underline{R}_p^{-1} \underline{h}_{12} + \underline{h}_{22}^T \underline{R}_q^{-1} \underline{h}_{22}) \end{bmatrix}$
1.1.4 Sequential update with constant gain matrices	
$[(\underline{h}_{11}^T \underline{R}_p^{-1} \underline{h}_{11})]\Big|_{\substack{\theta_o=0^\circ \\ v_o=1_{p.u.}}} \Delta\underline{\theta}_{k+1} = \left[[\underline{h}_{11}^T, \underline{h}_{21}^T]\ [\underline{R}]^{-1}\ [\underline{z} - \underline{h}(\underline{\theta}_k, \underline{v}_k)]\right]\Big|_{\substack{v=v_k \\ \theta=\theta_k^k}}$ $[(\underline{h}_{22}^T \underline{R}_q^{-1} \underline{h}_{22})]\Big|_{\substack{\theta_o=0^\circ \\ v_o=1_{p.u.}}} \Delta\underline{v}_{k+1} = \left[[\underline{h}_{12}^T, \underline{h}_{22}^T]\ [\underline{R}]^{-1}\ [\underline{z} - \underline{h}(\underline{\theta}_{k+1}, \underline{v}_k)]\right]\Big|_{\substack{v=v_k \\ \theta=\theta_{k+1}^k}}$	$\begin{bmatrix} [\underline{I} - (\underline{h}_{11_o}^T\underline{R}_p^{-1}\underline{h}_{11_o})^{-1}(\underline{h}_{11}^T\underline{R}_p^{-1}\underline{h}_{11} + \underline{h}_{21}^T\underline{R}_q^{-1}\underline{h}_{21})_0] & -[(\underline{h}_{11_o}^T \underline{R}_p^{-1} \underline{h}_{11_o})^{-1}(\underline{h}_{11}^T \underline{R}_p^{-1} \underline{h}_{12} + \underline{h}_{21}^T \underline{R}_q^{-1} \underline{h}_{22})_0] \\ -[(\underline{h}_{22_o}^T\underline{R}_p^{-1}\underline{h}_{22_o})^{-1}(\underline{h}_{12}^T\underline{R}_p^{-1}\underline{h}_{11} + \underline{h}_{22}^T\underline{R}_q^{-1}\underline{h}_{21})_1 & [\underline{I} - (\underline{h}_{22_o}^T\underline{R}_q^{-1}\underline{h}_{22_o})^{-1}(\underline{h}_{12}^T\underline{R}_p^{-1}\underline{h}_{12} + \underline{h}_{22}^T\underline{R}_q^{-1}\underline{h}_{22})_1 - (\underline{h}_{12}^T\underline{R}_p^{-1}\underline{h}_{11} \\ [\underline{I} - (\underline{h}_{11_o}^T\underline{R}_p^{-1}\underline{h}_{11_o})^{-1}(\underline{h}_{11}^T\underline{R}_p^{-1}\underline{h}_{21} + \underline{h}_{21}^T\underline{R}_q^{-1}\underline{h}_{21})_0] & + \underline{h}_{22}^T\underline{R}_q^{-1}\underline{h}_{21})]_1(\underline{h}_{11_o}^T\underline{R}_p^{-1}\underline{h}_{11_o})^{-1}(\underline{h}_{11}^T\underline{R}_p^{-1}\underline{h}_{12} + \underline{h}_{21}^T\underline{R}_q^{-1}\underline{h}_{22})_0] \end{bmatrix}$
1.1.5 Decomposed decoupling	
$\left[(\underline{h}_{11}^T \underline{R}_p^{-1} \underline{h}_{11})\Delta\underline{\theta}_{k+1} = [\underline{h}_{11}^T, \underline{h}_{21}^T]\ [\underline{R}]^{-1}\ [\underline{z} - \underline{h}(\underline{\theta}_k, \underline{v}_o)]\right]\Big|_{\substack{\theta=\theta_k \\ v=v_o^k}}$ $\left[(\underline{h}_{22}^T \underline{R}_q^{-1} \underline{h}_{22})\Delta\underline{v}_{k+1} = [\underline{h}_{12}^T, \underline{h}_{22}^T]\ [\underline{R}]^{-1}\ [\underline{z} - \underline{h}(\hat{\underline{\theta}}, \underline{v}_k)]\right]\Big|_{\substack{\theta=\hat{\theta} \\ v=v_k}}$	For $\underline{\theta}_{k+1}$ $\quad ([\underline{I} - (\underline{h}_{11}^T \underline{R}_p^{-1} \underline{h}_{11})^{-1}\ [\underline{h}_{11}^T \underline{R}_p^{-1} \underline{h}_{11} + \underline{h}_{21}^T \underline{R}_q^{-1} \underline{h}_{21}])_2$ For $\underline{v}_{k+1}$ $\quad ([\underline{I} - (\underline{h}_{22}^T \underline{R}_q^{-1} \underline{h}_{22})^{-1}\ [\underline{h}_{12}^T \underline{R}_p^{-1} \underline{h}_{12} + \underline{h}_{22}^T \underline{R}_q^{-1} \underline{h}_{22}])_3$
1.1.6 Decomposed decoupling with constant gain matrices	
$[(\underline{h}_{11}^T \underline{R}_p^{-1} \underline{h}_{11})]\Big|_{\substack{\theta_o=0^\circ \\ v_o=1_{p.u.}}} \Delta\underline{\theta}_{k+1} = \left[[\underline{h}_{11}^T, \underline{h}_{21}^T]\ [\underline{R}]^{-1}\ [\underline{z} - \underline{h}(\underline{\theta}_k, \underline{v}_o)]\right]\Big|_{\substack{\theta=\theta \\ v=v_o}}$ $[(\underline{h}_{22}^T \underline{R}_q^{-1} \underline{h}_{22})]\Big|_{\substack{\theta_o=0^\circ \\ v_o=1_{p.u.}}} \Delta\underline{v}_{k+1} = \left[[\underline{h}_{12}^T, \underline{h}_{22}^T]\ [\underline{R}]^{-1}\ [\underline{z} - \underline{h}(\hat{\underline{\theta}}, \underline{v}_k)]\right]\Big|_{\substack{\theta=\hat{\theta} \\ v=v_k}}$	For $\underline{\theta}_{k+1}$ $\quad [\underline{I} - (\underline{h}_{11_o}^T \underline{R}_p^{-1} \underline{h}_{11_o})^{-1}\ (\underline{h}_{11}^T \underline{R}_p^{-1} \underline{h}_{11} + \underline{h}_{21}^T \underline{R}_q^{-1} \underline{h}_{21})_2]$ For $\underline{v}_{k+1}$ $\quad [\underline{I} - (\underline{h}_{22_o}^T \underline{R}_q^{-1} \underline{h}_{22_o})^{-1}\ (\underline{h}_{12}^T \underline{R}_p^{-1} \underline{h}_{12} + \underline{h}_{22}^T \underline{R}_q^{-1} \underline{h}_{22})_3]$

The decomposed algorithms are not exact and do not give exact solutions.

The convergence properties of the Horisberger type decoupling schemes can also be found using an analysis similar to that carried out in section 3.5 and Appendix A3. Thus for the simultaneous update Horisberger type algorithm, (1.1.1), the convergence eigenvalues are those of the matrix

$$\left[\begin{bmatrix} \underline{I} & \underline{0} \\ \underline{0} & \underline{I} \end{bmatrix} - \begin{bmatrix} (\underline{h}_{11}^T \underline{R}_p^{-1} \underline{h}_{11})^{-1} & \underline{0} \\ \underline{0} & (\underline{h}_{22}^T \underline{R}_q^{-1} \underline{h}_{22})^{-1} \end{bmatrix} \begin{bmatrix} \underline{h}_{11}^T & \underline{h}_{21}^T \\ \underline{h}_{12}^T & \underline{h}_{22}^T \end{bmatrix} \begin{bmatrix} \underline{R}_p^{-1} & \underline{0} \\ \underline{0} & \underline{R}_q^{-1} \end{bmatrix} \begin{bmatrix} \underline{h}_{11} & \underline{h}_{12} \\ \underline{h}_{21} & \underline{h}_{22} \end{bmatrix}\right] \quad (4.12)$$

which simplifies to

$$\left[\begin{array}{c|c} -(\underline{h}_{11}^T \underline{R}_p^{-1} \underline{h}_{11})^{-1}(\underline{h}_{21}^T \underline{R}_q^{-1} \underline{h}_{21}) & -(\underline{h}_{11}^T \underline{R}_p^{-1} \underline{h}_{11})^{-1}(\underline{h}_{11}^T \underline{R}_p^{-1} \underline{h}_{12} + \underline{h}_{21}^T \underline{R}_q^{-1} \underline{h}_{22}) \\ \hline -(\underline{h}_{22}^T \underline{R}_q^{-1} \underline{h}_{22})^{-1}(\underline{h}_{12}^T \underline{R}_p^{-1} \underline{h}_{12} + \underline{h}_{22}^T \underline{R}_q^{-1} \underline{h}_{21}) & -(\underline{h}_{22}^T \underline{R}_q^{-1} \underline{h}_{22})^{-1}(\underline{h}_{12}^T \underline{R}_p^{-1} \underline{h}_{12}) \end{array}\right] \quad (4.13)$$

where

$$\underline{h}_{11} = \partial \underline{h}_p(\underline{\theta}_k, \underline{v}_k)/\partial \underline{\theta}_k \quad (4.14)$$

$$\underline{h}_{12} = \partial \underline{h}_p(\underline{\theta}_k, \underline{v}_k)/\partial \underline{v}_k \quad (4.15)$$

$$\underline{h}_{21} = \partial \underline{h}_q(\underline{\theta}_k, \underline{v}_k)/\partial \underline{\theta}_k \quad (4.16)$$

and

$$\underline{h}_{22} = \partial \underline{h}_q(\underline{\theta}_k, \underline{v}_k)/\partial \underline{v}_k \quad (4.17)$$

Convergence depends on the relative values of $\underline{h}_{11}$, $\underline{h}_{12}$, $\underline{h}_{21}$ and $\underline{h}_{22}$ as well as on $\underline{R}_p$ and $\underline{R}_q$. Tests carried out on the 5 bus test system, shown in Figure 3.3, show that the convergence is not stable, with the rate of convergence varying when the R/X ratio of the test system is altered or when the ratio $\underline{R}_p : \underline{R}_q$ is varied (see Figure 4.1).

The variation of convergence with the R/X ratio of the power system can be explained as follows. When the R/X ratio is small, $<<1$,

$$G_{ij} << B_{ij}$$

and as a result the value of $\underline{h}_{12} << \underline{h}_{11}$ and $\underline{h}_{21} << \underline{h}_{22}$, since the terms for $\underline{h}_{11}$ or $\underline{h}_{22}$ involve expressions

$$(- G_{ij} \sin (\theta_i - \theta_j) + B_{ij} \cos (\theta_i - \theta_j))$$

whereas terms for $\underline{h}_{12}$ or $\underline{h}_{21}$ have expressions

$$(G_{ij} \cos (\theta_i - \theta_j) + B_{ij} \sin (\theta_i - \theta_j))$$

as can be seen from Table 4.1. Thus for small R/X ratios, the decoupling assumption of neglecting off diagonal element effects $\underline{h}_{12}$ and $\underline{h}_{21}$ on the L.H.S., or the L.H.S. and R.H.S. of the W.L.S. state estimator equation have little effect.

The theoretical convergence properties for Horisberger et al. simultaneous update with constant gain matrices on the L.H.S., (1.1.3), is shown in Table 4.2, where

$$\underline{h}_{11_0}^T = \underline{h}_{11}^T\Big|_{k=0} \tag{4.18}$$

$$\underline{h}_{12_0}^T = \underline{h}_{12}^T\Big|_{k=0} \tag{4.19}$$

$$\underline{h}_{21_0}^T = \underline{h}_{21}^T\Big|_{k=0} \tag{4.20}$$

$$\underline{h}_{22_0}^T = \underline{h}_{22}^T\Big|_{k=0} \tag{4.21}$$

Convergence for "simultaneous update Horisberger-type" P-θ, Q-v decoupling with constant gain matrices is more unstable than without the use of constant gain matrices. The convergence eigenvalues show convergence depends on the R/X ratio of the test system and on the ratio of $\underline{R}_p : \underline{R}_q$. These dependencies were verified by simulation (see Figure 4.2). Convergence is so unstable that integer overflow occurs in the Burroughs B6700 48-bit word length after five or six iterations.

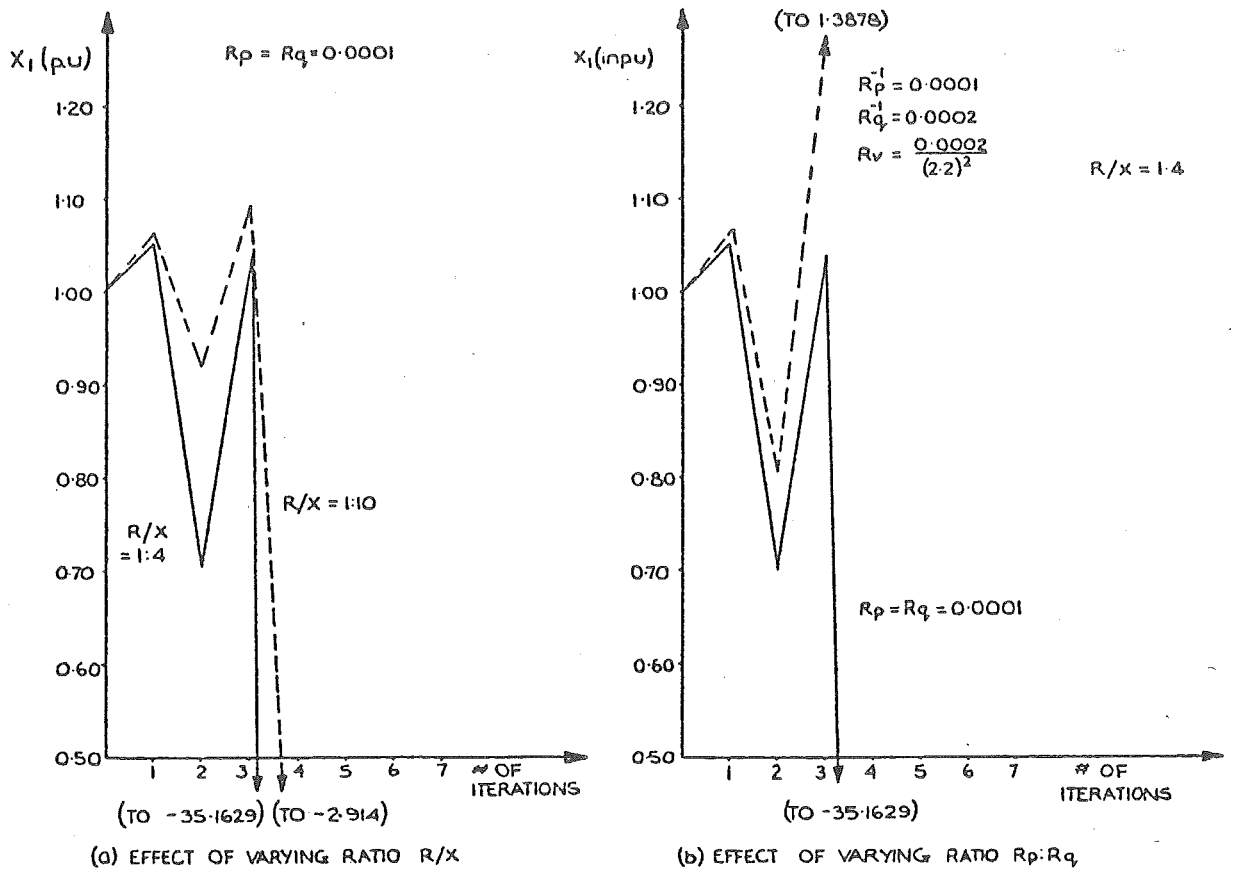

Figure 4.1 Horisberger type decoupling (1.1.1).

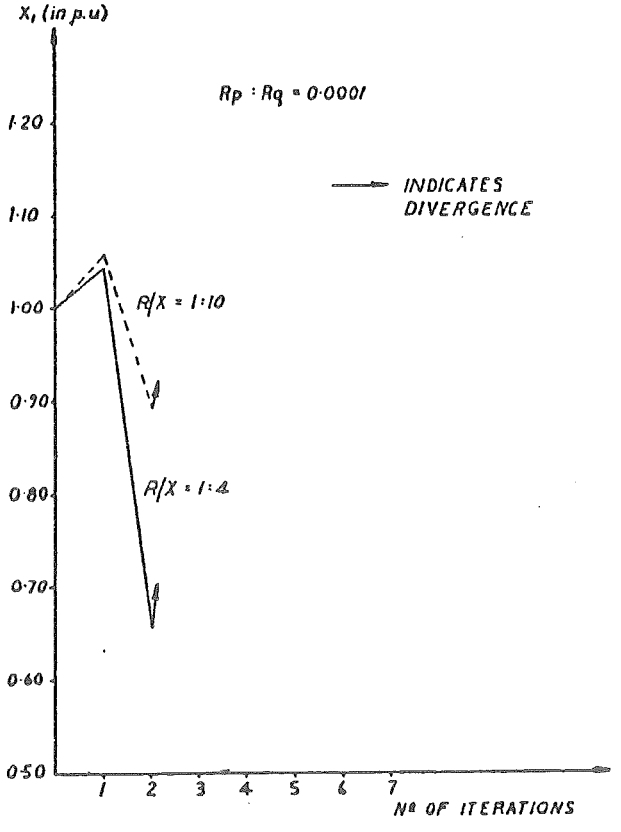

Figure 4.2 Horisberger type decoupling: unified with constant gain. (1.1.3).

Consider the sequential P-θ, Q-v decoupled Horisberger-type algorithm summarized in (1.1.2). From (1.1.2) the eigenvalues determining the convergence, given by (4.11), are found, firstly for the P-θ iteration

$$(\underline{h}_{11}^{T}\,\underline{R}_{p}^{-1}\,\underline{h}_{11})\,(\underline{\theta}_{k+1}-\underline{\theta}_{k}) = [\underline{h}_{11}^{T},\,\underline{h}_{21}^{T}]\begin{bmatrix}\underline{R}_{p}^{-1} & \underline{0}\\ \underline{0} & \underline{R}_{q}^{-1}\end{bmatrix}\begin{bmatrix}\underline{z}_{p}-\underline{h}_{p}(\underline{\theta}_{k},\underline{v}_{k})\\ \underline{z}_{q}-\underline{h}_{q}(\underline{\theta}_{k},\underline{v}_{k})\end{bmatrix} \tag{4.22}$$

$\underline{h}_{p}(\underline{\theta}_{k},\underline{v}_{k})$ and $\underline{h}_{q}(\underline{\theta}_{k},\underline{v}_{k})$ can be expressed in terms of their partial derivatives

$$\begin{aligned}\underline{h}_{p}(\underline{\theta}_{k},\,\underline{v}_{k}) &= \underline{h}_{11}\,\underline{\theta}_{k}+\underline{h}_{12}\,\underline{v}_{k}+\text{constant}\\ \underline{h}_{q}(\underline{\theta}_{k},\,\underline{v}_{k}) &= \underline{h}_{21}\,\underline{\theta}_{k}+\underline{h}_{22}\,\underline{v}_{k}+\text{constant}\end{aligned} \tag{4.23}$$

Since the constant term in (4.23) does not influence the convergence,

$$\begin{aligned}\underline{h}_{p}(\underline{\theta}_{k},\,\underline{v}_{k}) &\longrightarrow \underline{h}_{11}\,\underline{\theta}_{k}+\underline{h}_{12}\,\underline{v}_{k}\\ \underline{h}_{q}(\underline{\theta}_{k},\,\underline{v}_{k}) &\longrightarrow \underline{h}_{21}\,\underline{\theta}_{k}+\underline{h}_{22}\,\underline{v}_{k}\end{aligned} \tag{4.24}$$

and thus the P-θ iteration becomes

$$\underline{\theta}_{k+1} = \underline{\theta}_{k}+(\underline{h}_{11}^{T}\,\underline{R}_{p}^{-1}\,\underline{h}_{11})^{-1}[\underline{h}_{11}^{T},\underline{h}_{21}^{T}]\begin{bmatrix}\underline{R}_{p}^{-1} & \underline{0}\\ \underline{0} & \underline{R}_{q}^{-1}\end{bmatrix}\begin{bmatrix}\underline{z}_{p}-\underline{h}_{11}\,\underline{\theta}_{k}-\underline{h}_{12}\,\underline{v}_{k}\\ \underline{z}_{q}-\underline{h}_{21}\,\underline{\theta}_{k}-\underline{h}_{22}\,\underline{v}_{k}\end{bmatrix} \tag{4.25}$$

which simplifies to

$$\begin{aligned}\underline{\theta}_{k+1} = &\left[\underline{I}-(\underline{h}_{11}^{T}\,\underline{R}_{p}^{-1}\,\underline{h}_{11})^{-1}\,[\underline{h}_{11}^{T}\,\underline{R}_{p}^{-1}\,\underline{h}_{11}+\underline{h}_{21}^{T}\,\underline{R}_{q}^{-1}\,\underline{h}_{21}]\right]\underline{\theta}_{k}\\ &-(\underline{h}_{11}^{T}\,\underline{R}_{p}^{-1}\,\underline{h}_{11})^{-1}\,[\underline{h}_{11}^{T}\,\underline{R}_{p}^{-1}\,\underline{h}_{12}+\underline{h}_{21}^{T}\,\underline{R}_{q}^{-1}\,\underline{h}_{22}]\,\underline{v}_{k}\\ &+(\underline{h}_{11}^{T}\,\underline{R}_{p}^{-1}\,\underline{h}_{11})^{-1}\,[\underline{h}_{11}^{T}\,\underline{R}_{p}^{-1}\,\underline{z}_{p}+\underline{h}_{21}^{T}\,\underline{R}_{q}^{-1}\,\underline{z}_{q}]\end{aligned} \tag{4.26}$$

Now analyse the Q-v iteration,

$$(\underline{h}_{22}\ \underline{R}_q^{-1}\ \underline{h}_{22})^{-1}(\underline{v}_{k+1} - \underline{v}_k) = \begin{bmatrix} \underline{h}_{12}^T, & \underline{h}_{22}^T \end{bmatrix} \begin{bmatrix} \underline{R}_p^{-1} & \underline{0} \\ \underline{0} & \underline{R}_q^{-1} \end{bmatrix} \begin{bmatrix} \underline{z}_p - \underline{h}_p(\underline{\theta}_{k+1},\ \underline{v}_k) \\ \underline{z}_q - \underline{h}_q(\underline{\theta}_{k+1},\ \underline{v}_k) \end{bmatrix} \quad (4.27)$$

$\underline{h}_p(\underline{\theta}_{k+1},\ \underline{v}_k)$ and $\underline{h}_q(\underline{\theta}_{k+1},\underline{v}_k)$ can be expressed in terms of their partial derivatives

$$\underline{h}_p(\underline{\theta}_{k+1},\ \underline{v}_k) \rightarrow \underline{h}_{11}\ \underline{\theta}_{k+1} + \underline{h}_{12}\ \underline{v}_k \quad (4.28)$$

$$\underline{h}_q(\underline{\theta}_{k+1},\ \underline{v}_k) \rightarrow \underline{h}_{21}\ \underline{\theta}_{k+1} + \underline{h}_{22}\ \underline{v}_k \quad (4.29)$$

and thus the Q-v iteration becomes

$$\underline{v}_{k+1} = \underline{v}_k + (\underline{h}_{22}^T\ \underline{R}_q^{-1}\ \underline{h}_{22})^{-1} \begin{bmatrix} \underline{h}_{12}^T, & \underline{h}_{22}^T \end{bmatrix} \begin{bmatrix} \underline{R}_p^{-1} & \underline{0} \\ \underline{0} & \underline{R}_q^{-1} \end{bmatrix} \begin{bmatrix} \underline{z}_p - \underline{h}_{11}\ \underline{\theta}_{k+1} - \underline{h}_{12}\ \underline{v}_k \\ \underline{z}_q - \underline{h}_{21}\ \underline{\theta}_{k+1} - \underline{h}_{22}\ \underline{v}_k \end{bmatrix} \quad (4.30)$$

which simplifies to

$$\begin{aligned} \underline{v}_{k+1} = \Big[\underline{I} &- (\underline{h}_{22}^T\ \underline{R}_q^{-1}\ \underline{h}_{22})^{-1} [\underline{h}_{12}^T\ \underline{R}_p^{-1}\ \underline{h}_{12} + \underline{h}_{22}^T\ \underline{R}_q^{-1}\ \underline{h}_{22}]\ \underline{v}_k \\ &- (\underline{h}_{22}^T\ \underline{R}_q^{-1}\ \underline{h}_{22})^{-1} [\underline{h}_{12}^T\ \underline{R}_p^{-1}\ \underline{h}_{11} + \underline{h}_{22}^T\ \underline{R}_q^{-1}\ \underline{h}_{21}]\ \underline{\theta}_{k+1} \\ &- (\underline{h}_{22}^T\ \underline{R}_q^{-1}\ \underline{h}_{22})^{-1} [\underline{h}_{12}^T\ \underline{R}_p^{-1}\ \underline{z}_p + \underline{h}_{22}^T\ \underline{R}_q^{-1}\ \underline{z}_q] \Big] \end{aligned} \quad (4.31)$$

Substitution of (4.26) into (4.31) gives

$$\begin{aligned} \underline{v}_{k+1} = \Big[\underline{I} &- (\underline{h}_{22}^T\underline{R}_q^{-1}\underline{h}_{22})_1^{-1} [(\underline{h}_{12}^T\underline{R}_p^{-1}\underline{h}_{12} + \underline{h}_{22}^T\underline{R}_q^{-1}\underline{h}_{22})_1 - (\underline{h}_{12}^T\underline{R}_p^{-1}\underline{h}_{11} + \underline{h}_{22}^T\underline{R}_q^{-1}\underline{h}_{21})_1 \\ &(\underline{h}_{11}^T\underline{R}_p^{-1}\underline{h}_{11})_0^{-1} (\underline{h}_{11}^T\underline{R}_p^{-1}\underline{h}_{12} + \underline{h}_{21}^T\underline{R}_q^{-1}\underline{h}_{22})_0] \Big] \underline{v}_k - \Big[(\underline{h}_{22}^T\underline{R}_q^{-1}\underline{h}_{22})_1^{-1} \\ &[(\underline{h}_{12}^T\underline{R}_p^{-1}\underline{h}_{12} + \underline{h}_{22}^T\underline{R}_q^{-1}\underline{h}_{21})_1] [\underline{I} - (\underline{h}_{11}^T\underline{R}_p^{-1}\underline{h}_{11})_0^{-1} (\underline{h}_{11}^T\underline{R}_p^{-1}\underline{h}_{11} \\ &+ \underline{h}_{21}^T\underline{R}_q^{-1}\underline{h}_{21})_0] \Big] \underline{\theta}_k + \Big[(\underline{h}_{22}^T\underline{R}_q^{-1}\underline{h}_{22})_1^{-1} [(\underline{h}_{12}^T\underline{R}_p^{-1}\underline{z}_p + \underline{h}_{22}^T\underline{R}_q^{-1}\underline{z}_q)_1 \\ &- (\underline{h}_{12}^T\underline{R}_p^{-1}\underline{h}_{11} + \underline{h}_{22}^T\underline{R}_q^{-1}\underline{h}_{21})_1] (\underline{h}_{11}^T\underline{R}_p^{-1}\underline{h}_{11})_0^{-1} (\underline{h}_{11}^T\underline{R}_p^{-1}\underline{z}_p + \underline{h}_{21}^T\underline{R}_q^{-1}\underline{z}_q)_0 \Big] \end{aligned} \quad (4.32)$$

Thus convergence for the sequentially P-θ, Q-v decoupled Horisberger algorithm depends on the eigenvalues of the matrix:

$$\begin{bmatrix} [\underline{I} - (\underline{h}_{11}^T \underline{R}_p^{-1} \underline{h}_{11})^{-1}]_0 & -[(\underline{h}_{11}^T \underline{R}_p^{-1} \underline{h}_{11})^{-1}]_0 \\ (\underline{h}_{11}^T \underline{R}_p^{-1} \underline{h}_{11} + \underline{h}_{21}^T \underline{R}_q^{-1} \underline{h}_{21})_0 & (\underline{h}_{11}^T \underline{R}_p^{-1} \underline{h}_{12} + \underline{h}_{21}^T \underline{R}_q^{-1} \underline{h}_{22})_0 \\ \hline -\Big[(\underline{h}_{22}^T \underline{R}_q^{-1} \underline{h}_{22})^{-1}_1 (\underline{h}_{12}^T \underline{R}_p^{-1} \underline{h}_{11} & \Big[\underline{I} - (\underline{h}_{22}^T \underline{R}_q^{-1} \underline{h}_{22})^{-1}_1 [(\underline{h}_{12}^T \underline{R}_p^{-1} \underline{h}_{12} + \underline{h}_{22}^T \underline{R}_q^{-1} \underline{h}_{22})_1 \\ + \underline{h}_{22}^T \underline{R}_q^{-1} \underline{h}_{21})_1 [\underline{I} - (\underline{h}_{11}^T \underline{R}_p^{-1} \underline{h}_{11})^{-1}_0 & - (\underline{h}_{12}^T \underline{R}_p^{-1} \underline{h}_{11} + \underline{h}_{22}^T \underline{R}_q^{-1} \underline{h}_{21})_1 (\underline{h}_{11}^T \underline{R}_p^{-1} \underline{h}_{11})^{-1}_0 \\ [(\underline{h}_{11}^T \underline{R}_p^{-1} \underline{h}_{11} + \underline{h}_{21}^T \underline{R}_q^{-1} \underline{h}_{21})_0]\Big] & (\underline{h}_{11}^T \underline{R}_p^{-1} \underline{h}_{12} + \underline{h}_{21}^T \underline{R}_q^{-1} \underline{h}_{22})_0\Big] \end{bmatrix} \tag{4.33}$$

where a bracket with a prefix "0" denotes that the Jacobian elements within are evaluated at $(\underline{v}_k, \underline{\theta}_k)$ while a prefix "1" denotes that the Jacobian elements within are evaluated at $(\underline{v}_k, \underline{\theta}_{k+1})$. These expressions for the eigenvalues are also summarized in Table 4.2.

Convergence depends on the R/X ratio of the power system and on the relative values of $\underline{R}_p$ and $\underline{R}_q$. The eigenvalue expressions all contain terms similar to

$$[\underline{I} - (\underline{h}_{22}^T \underline{R}_q^{-1} \underline{h}_{22})^{-1} (\underline{h}_{12}^T \underline{R}_p^{-1} \underline{h}_{12} + \underline{h}_{22}^T \underline{R}_q^{-1} \underline{h}_{22})] \tag{4.34}$$

$$\equiv [- (\underline{h}_{22} \underline{R}_q^{-1} \underline{h}_{22})^{-1} (\underline{h}_{12}^T \underline{R}_p^{-1} \underline{h}_{12})]$$

When the system R/X ratio is low, with $\underline{R}_p = \underline{R}_q$, $\underline{h}_{12} << \underline{h}_{22}$, expression (4.34) tends to zero. Thus better convergence is expected for test systems having a low R/X ratio. Simulations verify this analysis, as shown in Figure 4.3. Altering the ratio of $\underline{R}_p : \underline{R}_q$ causes the state estimation algorithm to diverge.

The theoretical convergence properties for sequential P-θ, Q-v Horisberger type decoupling with constant gain matrix are shown in Table 4.2. Again terms appear in the eigenvalue expressions determining the convergence of (1.1.4) which are similar to

$$\begin{aligned}&[\ \underline{I} - (\underline{h}_{22_0}^T\ \underline{R}_q^{-1}\ \underline{h}_{22_0})^{-1}\ (\underline{h}_{12}^T\ \underline{R}_p^{-1}\ \underline{h}_{12} + \underline{h}_{22}^T\ \underline{R}_q^{-1}\ \underline{h}_{22})\ ] \\ &\quad \simeq\ -\ [(\underline{h}_{22_0}^T\ \underline{R}_q^{-1} \underline{h}_{22_0})^{-1}\ (\underline{h}_{12}^T\ \underline{R}_p^{-1}\ \underline{h}_{12})]\end{aligned} \tag{4.35}$$

if $\underline{h}_{22_0} \simeq \underline{h}_{22}$.

Thus sequential P-θ, Q-v Horisberger type decoupling with constant gain matrices has similar convergent properties to (1.1.2). Better convergence occurs at low R/X ratios, and convergence depends on the ratio of $\underline{R}_p : \underline{R}_q$. Simulation results are shown in Figure 4.4.

Consider the decomposed P-θ, Q-v Horisberger-type decoupled algorithm given by (1.1.5). The eigenvalues determining convergence can be found, firstly, for the P-θ sub estimator. $\underline{v}$ is treated as a parameter in $\underline{h}_p(\underline{\theta},\underline{v})$.

$$(\underline{h}_{11}^T\ \underline{R}_p^{-1} \underline{h}_{11})(\underline{\theta}_{k+1} - \underline{\theta}_k) = \begin{bmatrix}\underline{h}_{11}^T, & \underline{h}_{21}^T\end{bmatrix} \begin{bmatrix}\underline{R}_p^{-1} & \underline{0} \\ \underline{0} & \underline{R}_q^{-1}\end{bmatrix} \begin{bmatrix}\underline{z}_p - \underline{h}_p(\underline{\theta}_k,\ \underline{v}_k) \\ \underline{z}_q - \underline{h}_q(\underline{\theta}_k,\ \underline{v}_k)\end{bmatrix} \tag{4.36}$$

$\underline{h}_p(\underline{\theta}_k,\underline{v}_k)$ and $\underline{h}_q(\underline{\theta}_k,\underline{v}_k)$ can be expressed in terms of their partial derivatives, i.e.

$$\underline{h}_p(\underline{\theta}_k,\ \underline{v}_k),\ \text{treating } \underline{v}_k \text{ as a parameter} \rightarrow \underline{h}_{11}\ \underline{\theta}_k \tag{4.37}$$

$$\underline{h}_q(\underline{\theta}_k,\ \underline{v}_k),\ \text{treating } \underline{v}_k \text{ as a parameter} \rightarrow \underline{h}_{21}\ \underline{\theta}_k \tag{4.38}$$

Thus (4.36) becomes:

$$\underline{\theta}_{k+1} = \underline{\theta}_k + (\underline{h}_{11}^T\ \underline{R}_p^{-1}\ \underline{h}_{11})^{-1} \begin{bmatrix}\underline{h}_{11}^T, & \underline{h}_{21}^T\end{bmatrix} \begin{bmatrix}\underline{R}_p^{-1} & \underline{0} \\ \underline{0} & \underline{R}_q^{-1}\end{bmatrix} \begin{bmatrix}\underline{z}_p - \underline{h}_{11}\ \underline{\theta}_k \\ \underline{z}_q - \underline{h}_{21}\ \underline{\theta}_k\end{bmatrix} \tag{4.39}$$

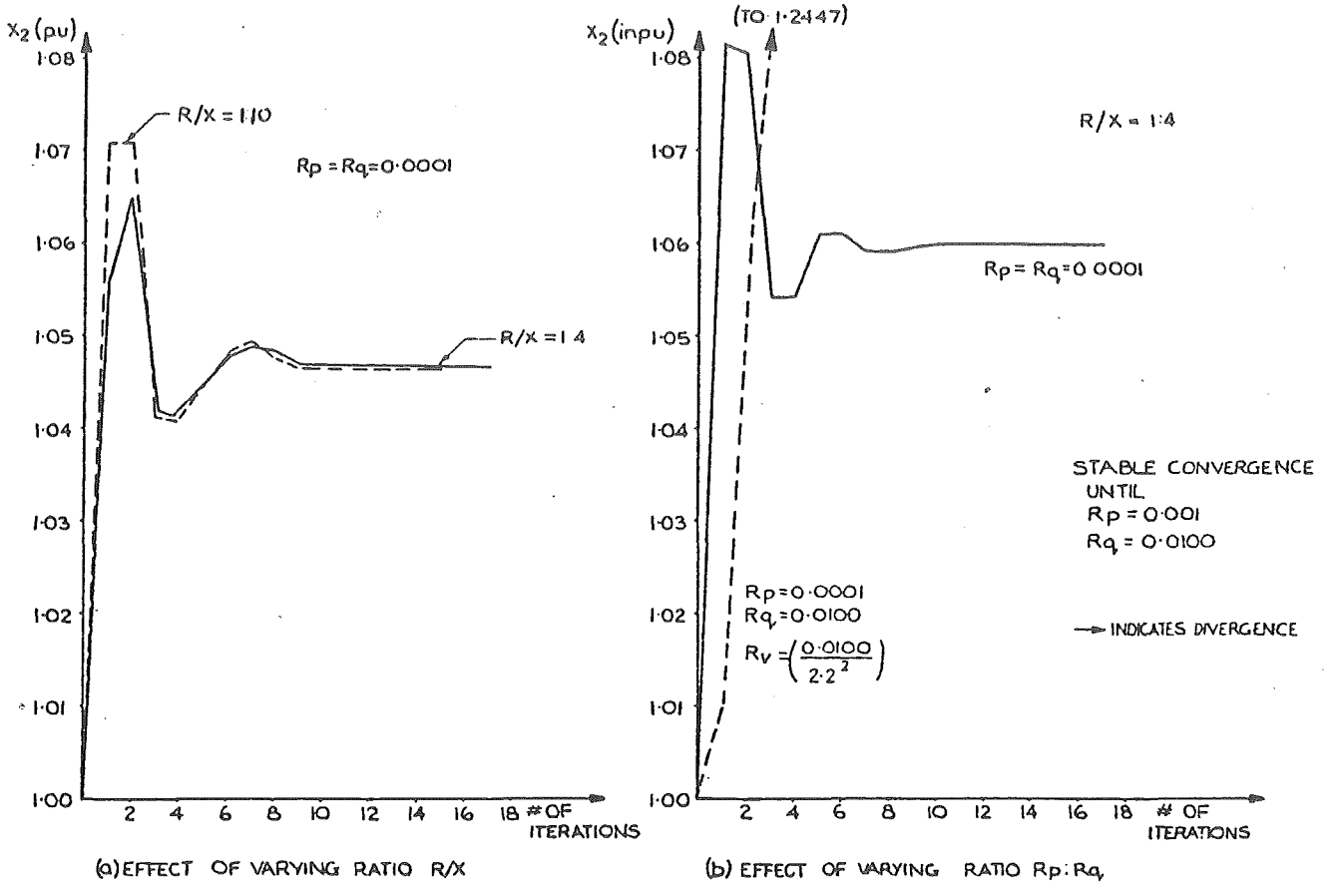

Figure 4.3 Horisberger type decoupling: sequential (1.1.2).

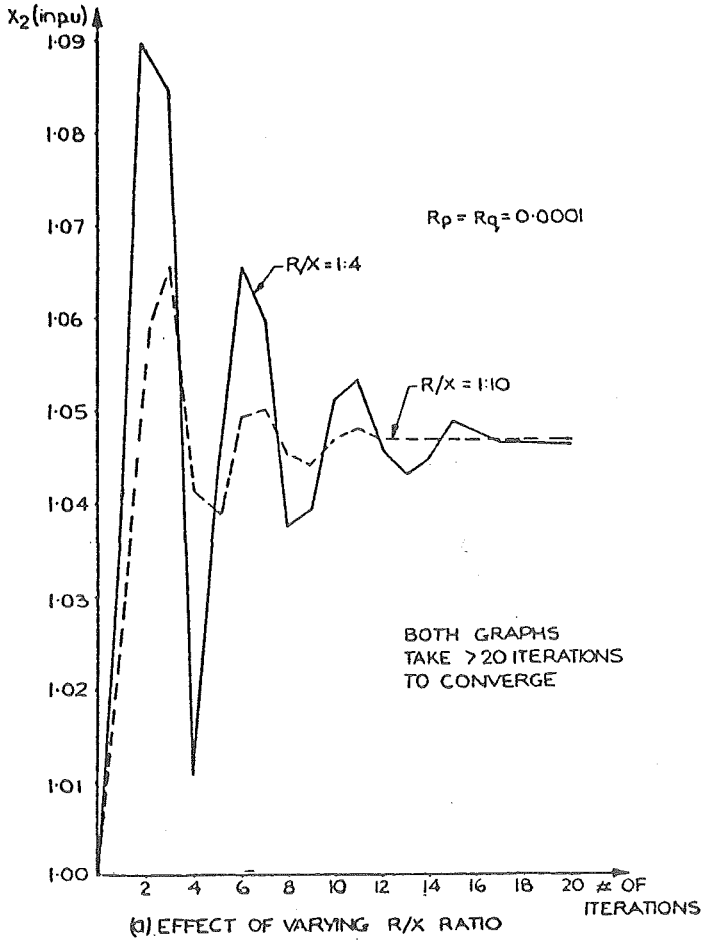

Figure 4.4 Horisberger type decoupling: sequential with constant gain (1.1.4).

which simplifies to

$$\underline{\theta}_{k+1} = \left(\left[\underline{I} - (\underline{h}_{11}^T \underline{R}_p^{-1} \underline{h}_{11})^{-1} [\underline{h}_{11}^T \underline{R}_p^{-1} \underline{h}_{11} + \underline{h}_{21}^T \underline{R}_q^{-1} \underline{h}_{21}] \right] \hat{\underline{\theta}}_k + (\underline{h}_{11}^T \underline{R}_p^{-1} \underline{h}_{11})^{-1} (\underline{h}_{11}^T \underline{R}_p^{-1} \underline{z}_p + \underline{h}_{21}^T \underline{R}_q^{-1} \underline{z}_q) \right)_2 \tag{4.40}$$

Similarly for the Q-v sub estimator, $\underline{\theta}_k$ is treated as a parameter in

$$(\underline{h}_{22}^T \underline{R}_q^{-1} \underline{h}_{22}) (\underline{v}_{k+1} - \underline{v}_k) = \left[\underline{h}_{12}^T, \underline{h}_{22}^T \right] \begin{bmatrix} \underline{R}_p^{-1} & \underline{0} \\ \underline{0} & \underline{R}_q^{-1} \end{bmatrix} \begin{bmatrix} \underline{z}_p - \underline{h}_p(\underline{\theta}_k, \underline{v}_k) \\ \underline{z}_q - \underline{h}_q(\underline{\theta}_k, \underline{v}_k) \end{bmatrix} \tag{4.41}$$

$\underline{h}_p(\underline{\theta}_k, \underline{v}_k)$ and $\underline{h}_q(\underline{\theta}_k, \underline{v}_k)$ can be expressed in terms of their partial derivatives, i.e.

$$\underline{h}_p(\underline{\theta}_k, \underline{v}_k), \text{ treating } \underline{\theta}_k \text{ as a parameter} \rightarrow \underline{h}_{12}\, \underline{v}_k \tag{4.42}$$

$$\underline{h}_q(\underline{\theta}_k, \underline{v}_k), \text{ treating } \underline{\theta}_k \text{ as a parameter} \rightarrow \underline{h}_{22}\, \underline{v}_k \tag{4.43}$$

Thus (4.41) becomes

$$\underline{v}_{k+1} = \underline{v}_k + (\underline{h}_{22}^T \underline{R}_q^{-1} \underline{h}_{22})^{-1} \left[\underline{h}_{12}^T, \underline{h}_{22}^T \right] \begin{bmatrix} \underline{R}_p^{-1} & \underline{0} \\ \underline{0} & \underline{R}_q^{-1} \end{bmatrix} \begin{bmatrix} \underline{z}_p - \underline{h}_{12}\, \underline{v}_k \\ \underline{z}_q - \underline{h}_{22}\, \underline{v}_k \end{bmatrix} \tag{4.44}$$

which simplifies to

$$\underline{v}_{k+1} = \left(\left[\underline{I} - (\underline{h}_{22}^T \underline{R}_q^{-1} \underline{h}_{22})^{-1} [\underline{h}_{12}^T \underline{R}_p^{-1} \underline{h}_{12} + \underline{h}_{22}^T \underline{R}_q^{-1} \underline{h}_{22}] \right] \underline{v}_k + (\underline{h}_{22}^T \underline{R}_q^{-1} \underline{h}_{22})^{-1} (\underline{h}_{12}^T \underline{R}_p^{-1} \underline{z}_p + \underline{h}_{22}^T \underline{R}_q^{-1} \underline{z}_q) \right)_3 \tag{4.45}$$

The eigenvalues for convergence of the $\hat{\underline{\theta}}_{k+1}$ sub estimator are given by

$$[\underline{I} - (\underline{I} + (\underline{h}_{11}^T \underline{R}_p^{-1} \underline{h}_{11})_2^{-1} (\underline{h}_{21}^T \underline{R}_q^{-1} \underline{h}_{21})_2] \tag{4.46}$$

and the eigenvalues for convergence of the $\hat{v}_{k+1}$ sub estimator are given by

$$[\underline{I} - (\underline{I} + (\underline{h}_{22}^T \underline{R}_q^{-1} \underline{h}_{22})_3^{-1} (\underline{h}_{12}^T \underline{R}_p^{-1} \underline{h}_{12})_3] \qquad (4.47)$$

These expressions are also summarized in Table 4.2. A bracket with a prefix "2" indicates that the Jacobian elements within are evaluated at $(\underline{v}_o, \underline{\theta}_k)$ while a prefix "3" denotes that the Jacobian elements within are evaluated at $(\underline{v}_k, \hat{\underline{\theta}})$.

Convergence depends on the R/X ratio of the power system and on the relative values of $\underline{R}_p$ and $\underline{R}_q$. When the system R/X ratio is low and $\underline{R}_p \simeq \underline{R}_q$, expressions (4.46) and (4.47) tend to zero since $\underline{h}_{12} \ll \underline{h}_{22}$, $\underline{h}_{21} \ll \underline{h}_{11}$. Better convergence is expected for test systems having a low R/X ratio. Test simulations highlight this trend, as shown in Figure 4.5. The convergence is very unstable.

The theoretical convergence properties for decomposed P-θ, Q-v Horisberger-type decoupling with constant gain matrices are shown in Table 4.2. Terms appearing in the eigenvalue convergence expression for (1.1.6) tend to zero when $\underline{h}_{11_o} \simeq \underline{h}_{11}$, $\underline{h}_{22_o} = \underline{h}_{22}$, $\underline{R}_p \simeq \underline{R}_q$, and when the R/X ratio of the test system is low so that $\underline{h}_{12} \ll \underline{h}_{22}$ and $\underline{h}_{21} \ll \underline{h}_{11}$. Thus convergence is best at low R/X ratios, and varies with the ratio of R/X and of $\underline{R}_p$ to $\underline{R}_q$, as shown in Figure 4.6. Convergence is extremely unstable.

4.4.1.2 Masiello and Horton (1979) advocate decoupling the information matrix by setting the off-diagonal submatrices to zero, i.e.

$$\begin{bmatrix} \frac{\partial \underline{h}_p^T(\underline{\theta},\underline{v})}{\partial \underline{\theta}} \underline{R}_p^{-1} \frac{\partial \underline{h}_p(\underline{\theta},\underline{v})}{\partial \underline{\theta}} + \frac{\partial \underline{h}_q^T(\underline{\theta},\underline{v})}{\partial \underline{\theta}} \underline{R}_q^{-1} \frac{\partial \underline{h}_q(\underline{\theta},\underline{v})}{\partial \underline{\theta}} & \underline{0} \\ \underline{0} & \frac{\partial \underline{h}_p^T(\underline{\theta},\underline{v})}{\underline{v}} \underline{R}_p^{-1} \frac{\partial \underline{h}_p(\underline{\theta},\underline{v})}{\underline{v}} + \frac{\partial \underline{h}_q^T(\underline{\theta},\underline{v})}{\underline{v}} \underline{R}_q^{-1} \frac{\partial \underline{h}_q(\underline{\theta},\underline{v})}{\underline{v}} \end{bmatrix}$$

(4.48)

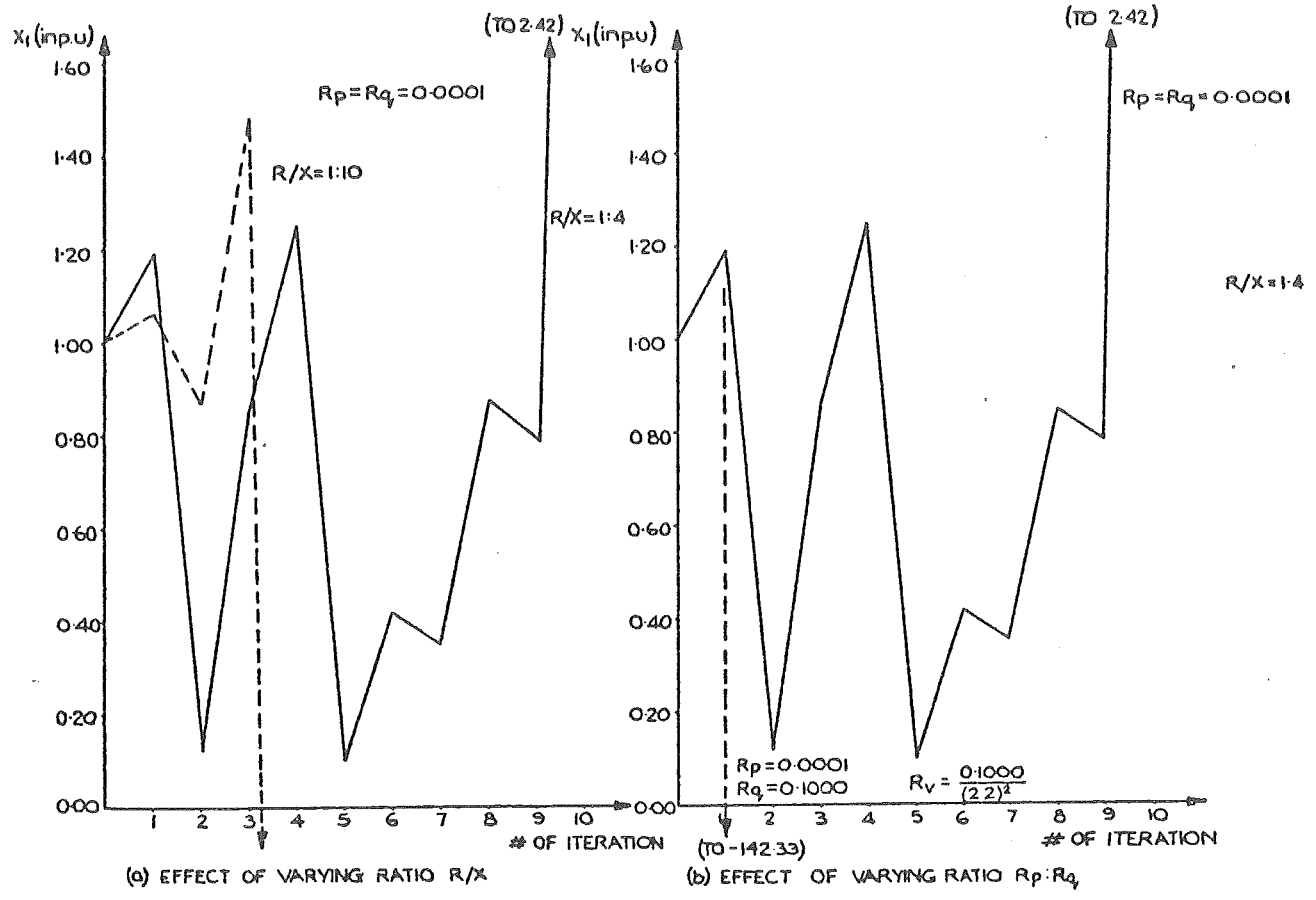

Figure 4.5 Horisberger type decoupling: decomposed (1.1.5).

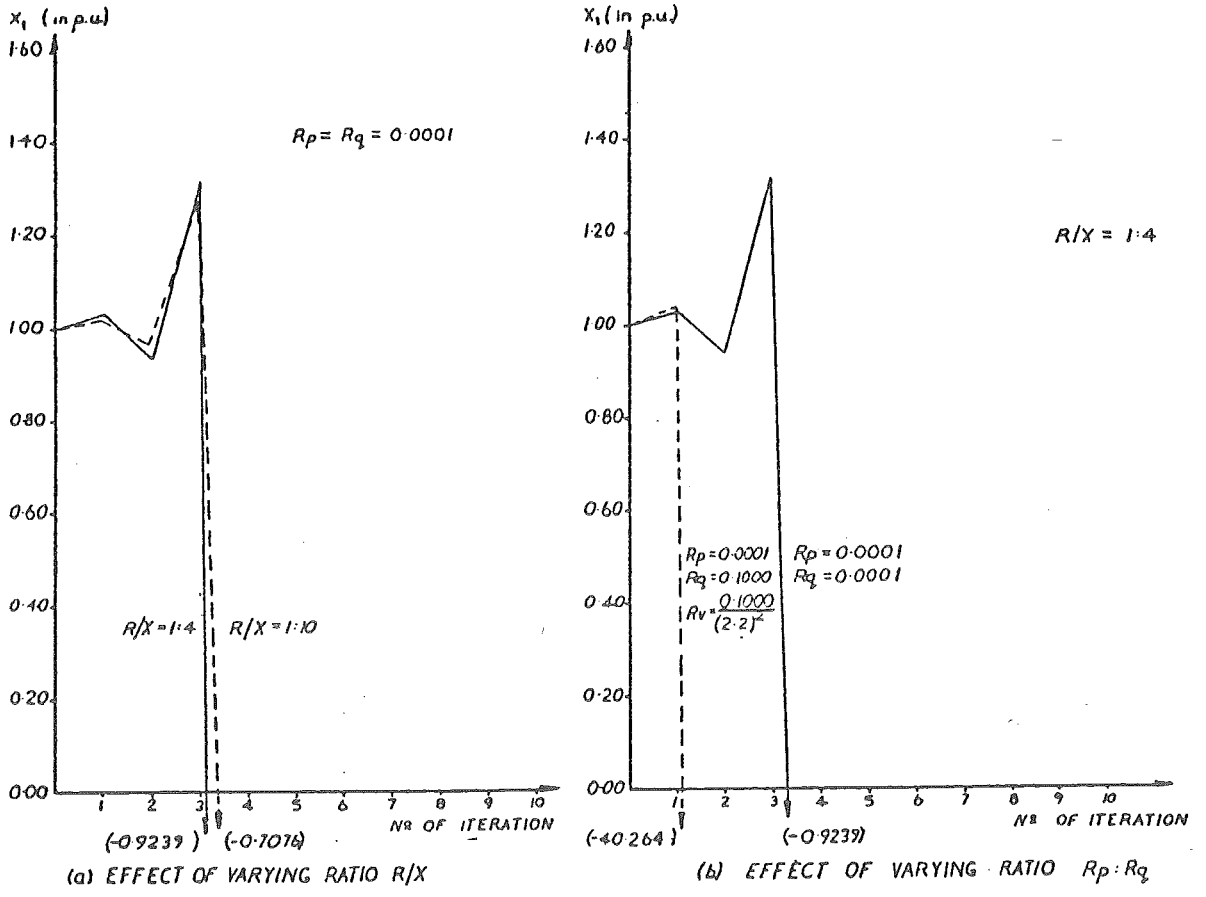

Figure 4.6 Horisberger type decoupling: decomposed with constant gain (1.1.6).

which results in the two state estimator equations

$$\left(\frac{\partial \underline{h}_p^T(\underline{\theta}_k,\underline{v}_k)}{\partial \underline{\theta}}\ \underline{R}_p^{-1}\ \frac{\partial \underline{h}_p(\underline{\theta}_k,\underline{v}_k)}{\partial \underline{\theta}} + \frac{\partial \underline{h}_q^T(\underline{\theta}_k,\underline{v}_k)}{\partial \underline{\theta}}\ \underline{R}_q^{-1}\ \frac{\partial \underline{h}_q(\underline{\theta}_k,\underline{v}_k)}{\partial \underline{\theta}}\right)\Delta\underline{\theta}_{k+1}$$

$$= \left[\frac{\partial \underline{h}_p^T(\underline{\theta}_k,\underline{v}_k)}{\partial \underline{\theta}}\ ,\ \frac{\partial \underline{h}_q^T(\underline{\theta}_k,\underline{v}_k)}{\partial \underline{\theta}}\right]\ [\underline{R}]^{-1}\ [\underline{z} - \underline{h}(\underline{\theta}_k,\underline{v}_k)]\Big|_{\substack{\underline{v}=\underline{v}_k \\ \underline{\theta}=\underline{\theta}_k}}$$

(4.49)

$$\left(\frac{\partial \underline{h}_p^T(\underline{\theta}_k,\underline{v}_k)}{\partial \underline{v}}\ \underline{R}_p^{-1}\ \frac{\partial \underline{h}_p(\underline{\theta}_k,\underline{v}_k)}{\partial \underline{v}} + \frac{\partial \underline{h}_q^T(\underline{\theta}_k,\underline{v}_k)}{\partial \underline{v}}\ \underline{R}_q^{-1}\ \frac{\partial \underline{h}_q(\underline{\theta}_k,\underline{v}_k)}{\partial \underline{v}}\right)\Delta\underline{v}_{k+1}$$

$$= \left[\frac{\partial \underline{h}_p^T(\underline{\theta}_k,\underline{v}_k)}{\partial \underline{v}}\ ,\ \frac{\partial \underline{h}_q^T(\underline{\theta}_k,\underline{v}_k)}{\partial \underline{v}}\right]\ [\underline{R}]^{-1}\ [\underline{z} - \underline{h}(\underline{\theta}_k,\underline{v}_k)]\Big|_{\substack{\underline{v}=\underline{v}_k \\ \underline{\theta}=\underline{\theta}_k}}$$

which

(1.2.1) can be solved simultaneously

(1.2.2) solved sequentially

(1.2.3) solved simultaneously with constant gain matrices on the L.H.S. of (4.49)

(1.2.4) solved sequentially with constant gain matrices on the L.H.S. of (4.49).

Alternatively the equation can be decomposed and the P-θ portion of the state estimator iterated, for $\underline{\theta}$, treating $\underline{v}$ as a constant. Then the Q-$\underline{v}$ partition can be iterated, treating $\underline{\theta}$ as a constant until convergence with

(1.2.5) the gain matrices on the L.H.S. of (4.49) updated at each iteration, or

(1.2.6) the gain matrices on the L.H.S. constant at their initial values.

The six different P-θ, Q-v decoupling possibilities are shown in Table 4.3. (1.2.1) - (1.2.4) are algorithm decoupled, guaranteeing exact optimal W.L.S. solutions.

The convergence-eigenvalue properties for (1.2.1) - (1.2.6) can also be found using a similar analysis to that used to find the eigenvalues for (1.1.1) - (1.1.6). The resulting convergence eigenvalue expressions for the Masiello and Horton decoupling are shown in Table 4.3.

When simultaneous-update P-θ, Q-v Masiello and Horton-type decoupling is used the convergence, as expressed by (1.2.1), depends on the ratio of $\underline{R}_p$ to $\underline{R}_q$ and on the test system R/X ratio. Tests show the convergence to be slightly dependent on the R/X ratio (Figure 4.7) and the convergence is unstable. When constant gain matrices are used and the Masiello and Horton-type decoupling simultaneously updated, the convergence as expressed by (1.2.3) depends on the ratio of $\underline{R}_p$ to $\underline{R}_q$ and on the test system R/X ratio. Simulations show that the convergence improves slightly as the R/X ratio of the test power system is decreased (see Figure 4.8). Convergence however is still slow, but stable.

Sequential update P-θ, Q-v Masiello and Horton decoupling convergence eigenvalue properties are given by (1.2.2). Convergence is dependent, both on the R/X ratio of the test power system and on the relative values of $\underline{R}_p$ and $\underline{R}_q$. The eigenvalue expression for (1.2.2) contains terms similar to

$$- (\underline{h}_{11}^T \underline{R}_p^{-1} \underline{h}_{11} + \underline{h}_{21}^T \underline{R}_q^{-1} \underline{h}_{21})^{-1} (\underline{h}_{11}^T \underline{R}_p^{-1} \underline{h}_{12} + \underline{h}_{21}^T \underline{R}_q^{-1} \underline{h}_{22}) \qquad (4.50)$$

Clearly when the R/X ratio is small, $\underline{h}_{12} \ll \underline{h}_{11}$ and $\underline{h}_{21} \ll \underline{h}_{22}$, and the term given by (4.50) tends to zero, thus improving the convergence.

Table 4.3 Different Masiello and Horton type P-θ, Q-v decoupling possibilities and their convergence.

MASIELLO AND HORTON TYPE P-θ, Q-v DECOUPLING SCHEMES	CONVERGENT EIGENVALUE EXPRESSIONS
1.2.1 Simultaneous formulation	
$\left[(\underline{h}_{11}^T \underline{R}_p^{-1} \underline{h}_{11} + \underline{h}_{21}^T \underline{R}_q^{-1} \underline{h}_{21})\Delta\underline{\theta}_{k+1} = [\underline{h}_{11}^f, \underline{h}_{21}^T]\ [\underline{R}^{-1}]\ [\underline{z} - \underline{h}(\underline{\theta}_k, \underline{v}_k)]\right]\Big\|_{\substack{v=v_k \\ \theta=\theta_k}}$ $\left[(\underline{h}_{12}^T \underline{R}_p^{-1} \underline{h}_{12} + \underline{h}_{22}^T \underline{R}_q^{-1} \underline{h}_{22})\Delta\underline{v}_{k+1} = [\underline{h}_{12}^T, \underline{h}_{22}^T]\ [\underline{R}^{-1}]\ [\underline{z} - \underline{h}(\underline{\theta}_k, \underline{v}_k)]\right]\Big\|_{\substack{v=v_k \\ \theta=\theta_k}}$	$\begin{bmatrix} \underline{0} & -(\underline{h}_{11}^T\underline{R}_p^{-1}\underline{h}_{11} + \underline{h}_{21}^T\underline{R}_q^{-1}\underline{h}_{21})^{-1}(\underline{h}_{11}^T\underline{R}_p^{-1}\underline{h}_{12} + \underline{h}_{21}^T\underline{R}_q^{-1}\underline{h}_{22}) \\ -(\underline{h}_{12}^T\underline{R}_p^{-1}\underline{h}_{12} + \underline{h}_{22}^T\underline{R}_q^{-1}\underline{h}_{22})^{-1}(\underline{h}_{12}^T\underline{R}_p^{-1}\underline{h}_{11} + \underline{h}_{22}^T\underline{R}_q^{-1}\underline{h}_{21}) & \underline{0} \end{bmatrix}$
1.2.2 Sequential formulation	
$\left[(\underline{h}_{11}^T \underline{R}_p^{-1} \underline{h}_{11} + \underline{h}_{21}^T \underline{R}_q^{-1} \underline{h}_{21})\Delta\underline{\theta}_{k+1} = [\underline{h}_{11}^T, \underline{h}_{21}^T]\ [\underline{R}^{-1}]\ [\underline{z} - \underline{h}(\underline{\theta}_k, \underline{v}_k)]\right]\Big\|_{\substack{v=v_k \\ \theta=\theta_k}}$ $\left[(\underline{h}_{12}^T \underline{R}_p^{-1} \underline{h}_{12} + \underline{h}_{22}^T \underline{R}_q^{-1} \underline{h}_{22})\Delta\underline{v}_{k+1} = [\underline{h}_{12}^T, \underline{h}_{22}^T]\ [\underline{R}^{-1}]\ [\underline{z} - \underline{h}(\underline{\theta}_{k+1}, \underline{v}_k)]\right]\Big\|_{\substack{v=v_k \\ \theta=\theta_{k+1}}}$	$\begin{bmatrix} [-(\underline{h}_{11}^T\underline{R}_p^{-1}\underline{h}_{11} + \underline{h}_{21}^T\underline{R}_q^{-1}\underline{h}_{21})_0^{-1}(\underline{h}_{11}^T\underline{R}_p^{-1}\underline{h}_{12} + \underline{h}_{21}^T\underline{R}_q^{-1}\underline{h}_{22})_0] & \underline{0} \\ \underline{0} & -[(\underline{h}_{12}^T\underline{R}_p^{-1}\underline{h}_{12} + \underline{h}_{22}^T\underline{R}_q^{-1}\underline{h}_{22})_1^{-1}(\underline{h}_{12}^T\underline{R}_p^{-1}\underline{h}_{11} + \underline{h}_{22}^T\underline{R}_q^{-1}\underline{h}_{21})_1 \\ & (\underline{h}_{11}^T\underline{R}_p^{-1}\underline{h}_{11} + \underline{h}_{21}^T\underline{R}_q^{-1}\underline{h}_{21})_0^{-1}\ (\underline{h}_{11}^T\underline{R}_p^{-1}\underline{h}_{12} + \underline{h}_{21}^T\underline{R}_q^{-1}\underline{h}_{22})_0] \end{bmatrix}$
1.2.3 Simultaneous update with constant gain matrices	
$[(\underline{h}_{11_o}^T \underline{R}_p^{-1} \underline{h}_{11_o} + \underline{h}_{21_o}^T \underline{R}_q^{-1} \underline{h}_{21_o})]\Big\|_{\substack{\theta_o=0 \\ v_o=1 \text{ p.u.}}} \Delta\underline{\theta}_{k+1} = \left[[\underline{h}_{11}^T, \underline{h}_{21}^T][\underline{R}^{-1}][\underline{z} - \underline{h}(\underline{\theta}_k, \underline{v}_k)]\right]\Big\|_{\substack{v=v_k \\ \theta=\theta_k}}$ $[(\underline{h}_{12_o}^T \underline{R}_p^{-1} \underline{h}_{12_o} + \underline{h}_{22_o}^T \underline{R}_q^{-1} \underline{h}_{22_o})]\Big\|_{\substack{\theta_o=0 \\ v_o=1 \text{ p.u.}}} \Delta\underline{v}_{k+1} = \left[[\underline{h}_{12}^T, \underline{h}_{22}^T][\underline{R}^{-1}][\underline{z} - \underline{h}(\underline{\theta}_k, \underline{v}_k)]\right]\Big\|_{\substack{v=v_k \\ \theta=\theta_k}}$	$\begin{bmatrix} \underline{I} - (\underline{h}_{11_o}^T\underline{R}_p^{-1}\underline{h}_{11_o} + \underline{h}_{21_o}^T\underline{R}_q^{-1}\underline{h}_{21_o})^{-1}(\underline{h}_{11}^T\underline{R}_p^{-1}\underline{h}_{11} + \underline{h}_{21}^T\underline{R}_q^{-1}\underline{h}_{21}) & -(\underline{h}_{11_o}^T\underline{R}_p^{-1}\underline{h}_{11_o} + \underline{h}_{21_o}^T\underline{R}_q^{-1}\underline{h}_{21_o})^{-1}(\underline{h}_{11}^T\underline{R}_p^{-1}\underline{h}_{12} + \underline{h}_{21}^T\underline{R}_q^{-1}\underline{h}_{22}) \\ -(\underline{h}_{12_o}^T\underline{R}_p^{-1}\underline{h}_{12_o} + \underline{h}_{22_o}^T\underline{R}_q^{-1}\underline{h}_{22_o})^{-1}(\underline{h}_{12}^T\underline{R}_p^{-1}\underline{h}_{11} + \underline{h}_{22}^T\underline{R}_q^{-1}\underline{h}_{21}) & \underline{I} - (\underline{h}_{12_o}^T\underline{R}_p^{-1}\underline{h}_{12_o} + \underline{h}_{22_o}^T\underline{R}_q^{-1}\underline{h}_{22_o})^{-1}(\underline{h}_{12}^T\underline{R}_p^{-1}\underline{h}_{12} + \underline{h}_{22}^T\underline{R}_q^{-1}\underline{h}_{22}) \end{bmatrix}$
1.2.4 Sequential formulation with constant gain matrices	
$[(\underline{h}_{11_o}^T \underline{R}_p^{-1} \underline{h}_{11_o} + \underline{h}_{21_o}^T \underline{R}_q^{-1} \underline{h}_{21_o})]\Big\|_{\substack{\theta_o=0 \\ v_o=1 \text{ p.u.}}} \Delta\underline{\theta}_{k+1} = \left[[\underline{h}_{11}^T, \underline{h}_{21}^T]\ [\underline{R}^{-1}][\underline{z} - \underline{h}(\underline{\theta}_k, \underline{v}_k)]\right]\Big\|_{\substack{v=v_k \\ \theta=\theta_k}}$ $[(\underline{h}_{12_o}^T \underline{R}_p^{-1} \underline{h}_{12_o} + \underline{h}_{22_o}^T \underline{R}_q^{-1} \underline{h}_{22_o})]\Big\|_{\substack{\theta_o=0 \\ v_o=1 \text{ p.u.}}} \Delta\underline{v}_{k+1} = \left[[\underline{h}_{12}^T, \underline{h}_{22}^T]\ [\underline{R}^{-1}][\underline{z} - \underline{h}(\underline{\theta}_{k+1}, \underline{v}_k)]\right]\Big\|_{\substack{v=v_k \\ \theta=\theta_{k+1}}}$	$\begin{bmatrix} [\underline{I} - (\underline{h}_{11_o}^T\underline{R}_p^{-1}\underline{h}_{11_o} + \underline{h}_{21_o}^T\underline{R}_q^{-1}\underline{h}_{21_o})^{-1}(\underline{h}_{11}^T\underline{R}_p^{-1}\underline{h}_{11} + \underline{h}_{21}^T\underline{R}_q^{-1}\underline{h}_{21})_0] & -[(\underline{h}_{11_o}^T\underline{R}_p^{-1}\underline{h}_{11_o} + \underline{h}_{21_o}^T\underline{R}_q^{-1}\underline{h}_{21_o})_0^{-1}(\underline{h}_{11}^T\underline{R}_p^{-1}\underline{h}_{12} + \underline{h}_{21}^T\underline{R}_q^{-1}\underline{h}_{22})_0] \\ -[(\underline{h}_{12_o}^T\underline{R}_p^{-1}\underline{h}_{12_o} + \underline{h}_{22_o}^T\underline{R}_q^{-1}\underline{h}_{22_o})_1^{-1}(\underline{h}_{12}^T\underline{R}_p^{-1}\underline{h}_{11} + \underline{h}_{22}^T\underline{R}_q^{-1}\underline{h}_{21})_1 & [\underline{I} - (\underline{h}_{12_o}^T\underline{R}_p^{-1}\underline{h}_{12_o} + \underline{h}_{22_o}^T\underline{R}_q^{-1}\underline{h}_{22_o})_1^{-1}[(\underline{h}_{12}^T\underline{R}_p^{-1}\underline{h}_{12} + \underline{h}_{22}^T\underline{R}_q^{-1}\underline{h}_{22})_1 \\ (\underline{h}_{11_o}^T\underline{R}_p^{-1}\underline{h}_{11_o} + \underline{h}_{21_o}^T\underline{R}_q^{-1}\underline{h}_{21_o})_0^{-1}(\underline{h}_{11}^T\underline{R}_p^{-1}\underline{h}_{12} + \underline{h}_{21}^T\underline{R}_q^{-1}\underline{h}_{22})_0] & -(\underline{h}_{12}^T\underline{R}_p^{-1}\underline{h}_{11} + \underline{h}_{22}^T\underline{R}_q^{-1}\underline{h}_{21})_1(\underline{h}_{11_o}^T\underline{R}_p^{-1}\underline{h}_{11_o} + \underline{h}_{21_o}^T\underline{R}_q^{-1}\underline{h}_{21_o})_0 \\ & (\underline{h}_{11}^T\underline{R}_p^{-1}\underline{h}_{12} + \underline{h}_{21}^T\underline{R}_q^{-1}\underline{h}_{22})_0] \end{bmatrix}$
1.2.5 Decomposed decoupling	
$\left[(\underline{h}_{11}^T \underline{R}_p^{-1} \underline{h}_{11} + \underline{h}_{21}^T \underline{R}_q^{-1} \underline{h}_{21})\Delta\underline{\theta}_{k+1} = [\underline{h}_{11}^T, \underline{h}_{21}^T]\ [\underline{R}^{-1}][\underline{z} - \underline{h}(\underline{\theta}_k, \underline{v}_o)]\right]\Big\|_{\substack{v=v_o \\ \theta=\theta_k^o}}$ $\left[(\underline{h}_{12}^T \underline{R}_p^{-1} \underline{h}_{12} + \underline{h}_{22}^T \underline{R}_q^{-1} \underline{h}_{22})\Delta\underline{v}_{k+1} = [\underline{h}_{12}^T, \underline{h}_{22}^T]\ [\underline{R}^{-1}][\underline{z} - \underline{h}(\hat{\underline{\theta}}, \underline{v}_k)]\right]\Big\|_{\substack{v=v_k \\ \theta=\hat{\theta}}}$	For $\underline{\theta}_{k+1}$ [0] thus eigenvalues are zero and the algorithm has a stable, rapid convergence For $\underline{v}_{k+1}$ [0] thus eigenvalues are zero and the algorithm has a stable, rapid convergence
1.2.6 Decomposed decoupling with constant gain matrices	
$[(\underline{h}_{11_o}^T \underline{R}_p^{-1} \underline{h}_{11_o} + \underline{h}_{21_o}^T \underline{R}_q^{-1} \underline{h}_{21_o})]\Big\|_{\substack{\theta_o=0 \\ v_o=1 \text{ p.u.}}} \Delta\underline{\theta}_{k+1} = \left[[\underline{h}_{11}^T, \underline{h}_{21}^T]\ [\underline{R}^{-1}]\ [\underline{z} - \underline{h}(\underline{\theta}_k, \underline{v}_o)]\right]\Big\|_{\substack{v=v_o \\ \theta=\theta_k^o}}$ $[(\underline{h}_{12_o}^T \underline{R}_p^{-1} \underline{h}_{12_o} + \underline{h}_{22_o}^T \underline{R}_q^{-1} \underline{h}_{22_o})]\Big\|_{\substack{\theta_o=0 \\ v_o=1 \text{ p.u.}}} \Delta\underline{v}_{k+1} = \left[[\underline{h}_{12}^T, \underline{h}_{22}^T]\ [\underline{R}^{-1}]\ [\underline{z} - \underline{h}(\hat{\underline{\theta}}, \underline{v}_k)]\right]\Big\|_{\substack{v=v_k \\ \theta=\hat{\theta}}}$	For $\underline{\theta}_{k+1}$ $[\underline{I} - (\underline{h}_{11_o}^T \underline{R}_p^{-1} \underline{h}_{11_o} + \underline{h}_{21_o}^T \underline{R}_q^{-1} \underline{h}_{21_o})^{-1}(\underline{h}_{11}^T \underline{R}_p^{-1} \underline{h}_{11} + \underline{h}_{21}^T \underline{R}_q^{-1} \underline{h}_{21})_2]$ For $\underline{v}_{k+1}$ $[\underline{I} - (\underline{h}_{12_o}^T \underline{R}_p^{-1} \underline{h}_{12_o} + \underline{h}_{22_o}^T \underline{R}_q^{-1} \underline{h}_{22_o})^{-1}(\underline{h}_{12}^T \underline{R}_p^{-1} \underline{h}_{12} + \underline{h}_{22}^T \underline{R}_2^{-1} \underline{h}_{22})_3]$

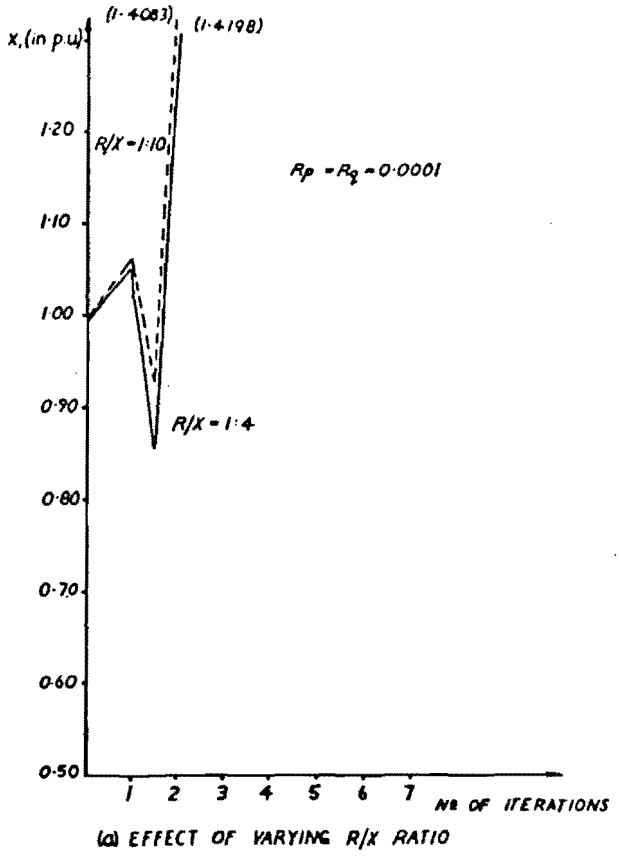

Figure 4.7 Masiello-type decoupling: unified (1.2.1).

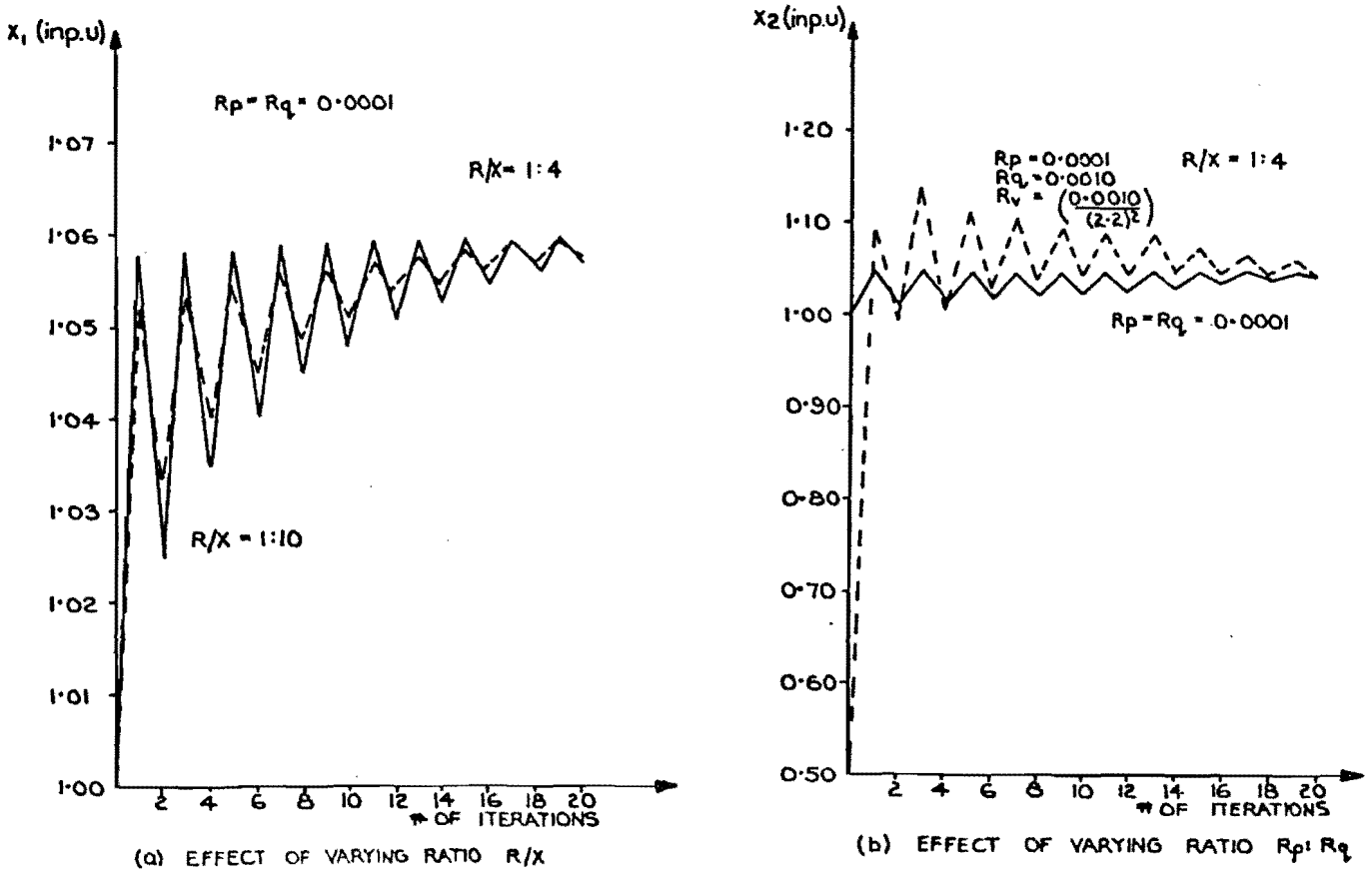

Figure 4.8 Masiello-type decoupling: unified with constant gain (1.2.3).

Simulation shows that convergence only improves slightly as the R/X ratio of the test power system was decreased (see Figure 4.9). Convergence is very dependent on the ratio of $\underline{R}_p$ to $\underline{R}_q$. For extreme ratios of $\underline{R}_p$ to $\underline{R}_q$, the algorithm given by (1.2.2) converges to the wrong solution. When constant gain matrices are used on the L.H.S. of the sequentially decoupled algorithm, the eigenvalue convergence properties are expressed by (1.2.4). Simulation shows the convergence to be only slightly dependent on the R/X ratio, but very dependent on the relative values of $\underline{R}_p$ to $\underline{R}_q$. Extreme values of $\underline{R}_p$ to $\underline{R}_q$ can cause divergence (see Figure 4.10).

The theoretical convergence properties for "decomposed" P-θ, Q-v Masiello and Horton-type decoupling is shown in (1.2.5) of Table 4.3 to have zero eigenvalues. Convergence is thus rapid, invariant to changes in the R/X ratio of the power system and to changes in the relative values of $\underline{R}_p$ and $\underline{R}_q$. Simulations carried out verify this analysis (see Figure 4.11). When constant gain matrices are used in the "decomposed" P-θ, Q-v Masiello and Horton-decoupled algorithm, the convergence properties change, as shown by the eigenvalue expression in (1.2.6). If $\underline{h}_{11_o} \neq \underline{h}_{11}$, $\underline{h}_{12_o} \neq \underline{h}_{12}$, $\underline{h}_{21_o} \neq \underline{h}_{21}$ and $\underline{h}_{22_o} \neq \underline{h}_{22}$, convergence will depend on the R/X ratio and on the relative values of $\underline{R}_p$ to $\underline{R}_q$. Simulation shows the algorithm to be unstable and the convergence to be dependent, both on the ratio of $\underline{R}_p$:$\underline{R}_q$ and on the R/X ratio of the test power system (see Figure 4.12).

4.4.2 Modal P-θ, Q-v decoupling

4.4.2.1. Garcia et al. (1978) decouple the information matrix on the L.H.S. of (2.22) in the same manner as Masiello and Horton, i.e. equation (4.48). The R.H.S. of (2.22) is decoupled in the following manner:

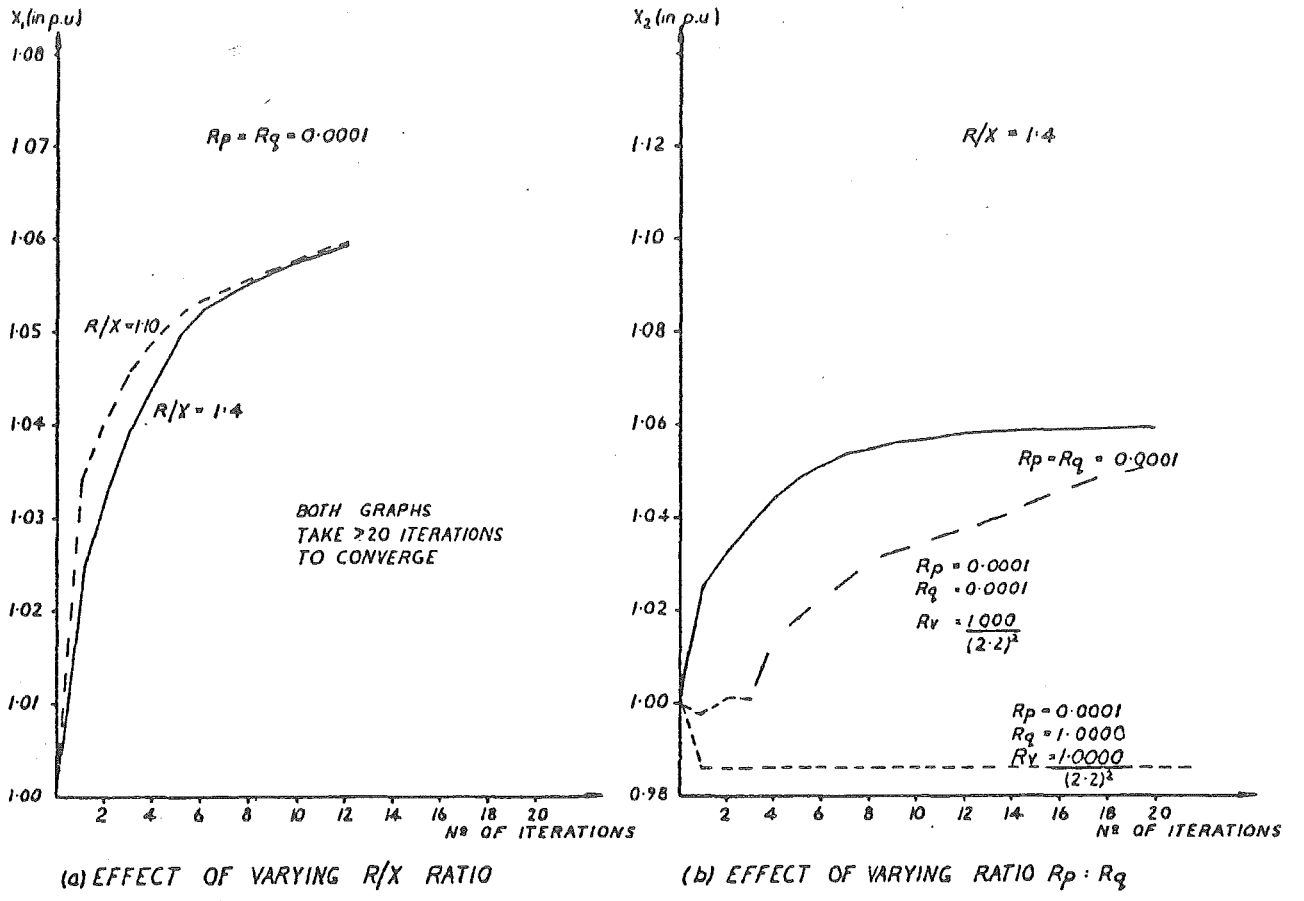

Figure 4.9 Masiello and Horton type decoupling: sequential (1.2.2).

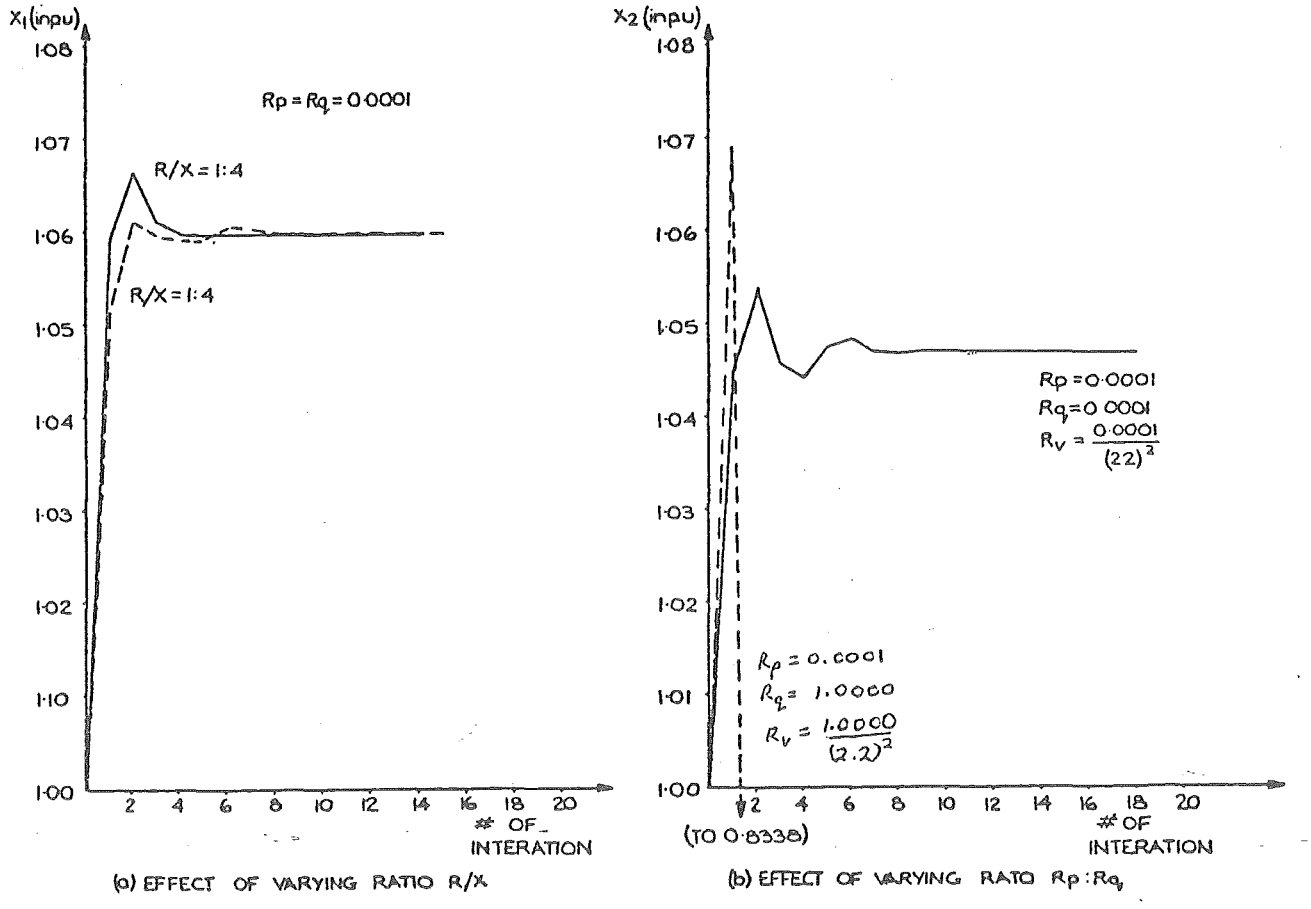

Figure 4.10 Masiello and Horton type decoupling: sequential with constant gain (1.2.4).

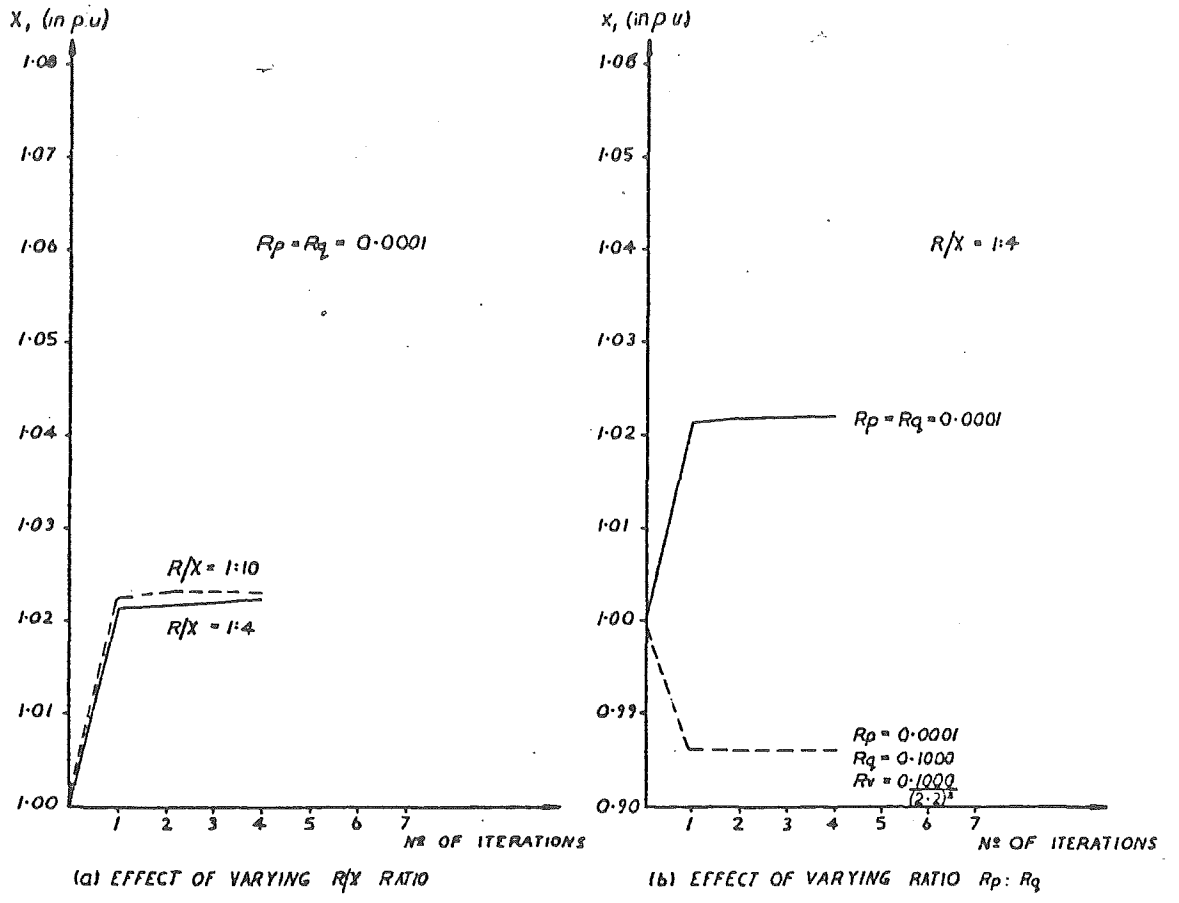

Figure 4.11 Masiello type decoupling: decomposed (1.2.5).

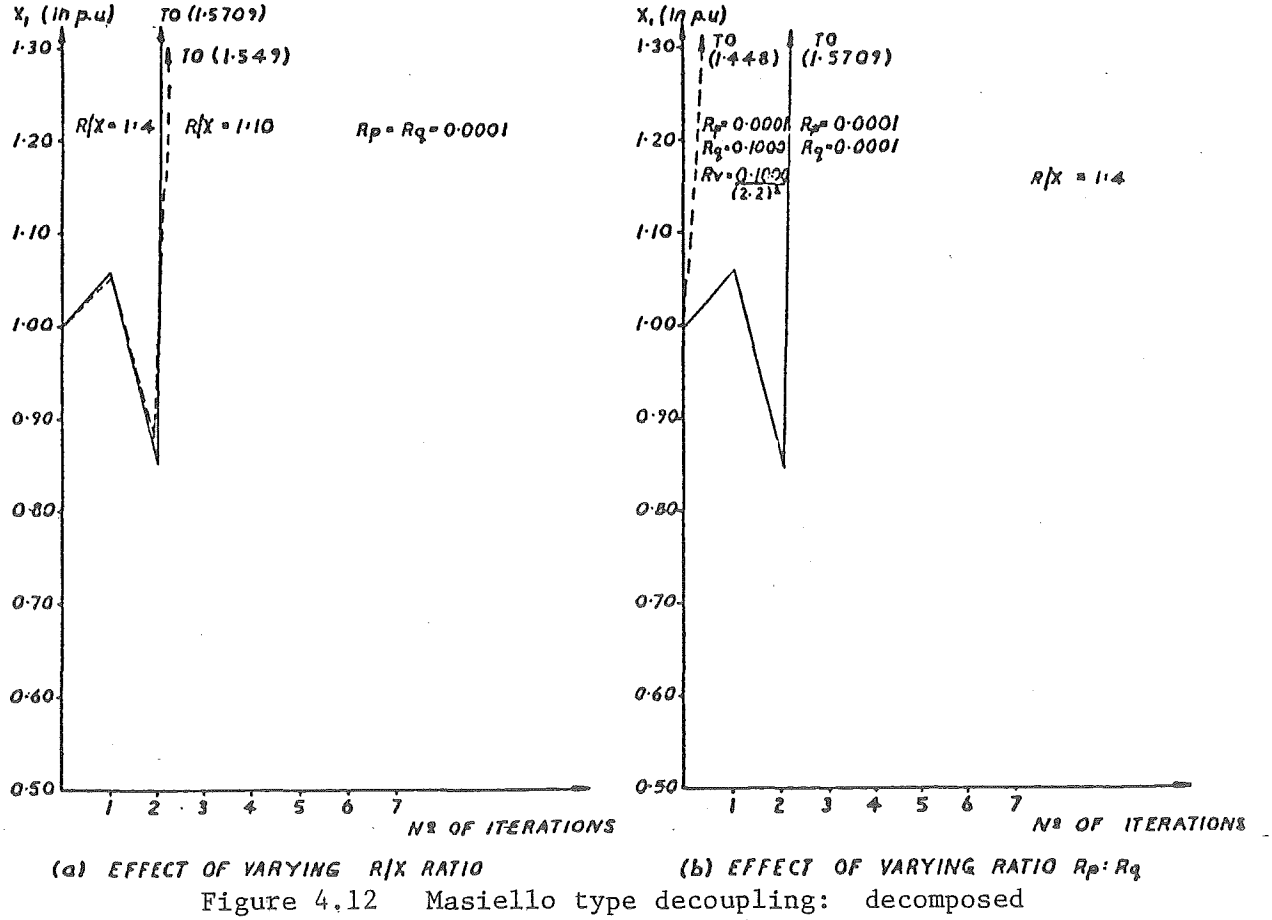

Figure 4.12 Masiello type decoupling: decomposed with constant gain (1.2.6).

$$\begin{bmatrix} \frac{\partial \underline{h}_p^T(\underline{\theta},\underline{v})}{\partial \underline{\theta}} & \underline{0} \\ \underline{0} & \frac{\partial \underline{h}_q^T(\underline{\theta},\underline{v})}{\partial \underline{v}} \end{bmatrix} \begin{bmatrix} \underline{R}_p^{-1} & \underline{0} \\ \underline{0} & \underline{R}_q^{-1} \end{bmatrix} \begin{bmatrix} \underline{z}_p - \underline{h}_p(\underline{\theta},\underline{v}) \\ \underline{z}_q - \underline{h}_q(\underline{\theta},\underline{v}) \end{bmatrix} \tag{4.51}$$

which results in two state estimator equations

$$\left(\frac{\partial \underline{h}_p^T(\underline{\theta}_k,\underline{v}_k)}{\partial \underline{\theta}} \underline{R}_p^{-1} \frac{\partial \underline{h}_p(\underline{\theta}_k,\underline{v}_k)}{\partial \underline{\theta}} + \frac{\partial \underline{h}_q^T(\underline{\theta}_k,\underline{v}_k)}{\partial \underline{\theta}} \underline{R}_q^{-1} \frac{\partial \underline{h}_q(\underline{\theta}_k,\underline{v}_k)}{\partial \underline{\theta}} \right) \Delta\underline{\theta}_{k+1}$$

$$= \left(\frac{\partial \underline{h}_p^T(\underline{\theta}_k,\underline{v}_k)}{\partial \underline{\theta}} \right) \underline{R}_p^{-1} \left[\underline{z}_p - \underline{h}_p(\underline{\theta}_k,\underline{v}_k) \right] \Big|_{\substack{\underline{v}=\underline{v}_k \\ \underline{\theta}=\underline{\theta}_k}} \tag{4.52}$$

$$\left(\frac{\partial \underline{h}_p^T(\underline{\theta}_k,\underline{v}_k)}{\partial \underline{v}} \underline{R}_p^{-1} \frac{\partial \underline{h}_p(\underline{\theta}_k,\underline{v}_k)}{\partial \underline{v}} + \frac{\partial \underline{h}_q^T(\underline{\theta}_k,\underline{v}_k)}{\partial \underline{v}} \underline{R}_q^{-1} \frac{\partial \underline{h}_q(\underline{\theta}_k,\underline{v}_k)}{\partial \underline{v}} \right) \Delta\underline{v}_{k+1}$$

$$\left(\frac{\partial \underline{h}_q^T(\underline{\theta}_k,\underline{v}_k)}{\partial \underline{v}} \right) \underline{R}_q^{-1} \left[\underline{z}_q - \underline{h}_q(\underline{\theta}_k,\underline{v}_k) \right] \Big|_{\substack{\underline{v}=\underline{v}_k \\ \underline{\theta}=\underline{\theta}_k}}$$

which

(1.3.1) can be solved simultaneously

(1.3.2) solved sequentially

(1.3.3) solved simultaneously with constant gain matrices on the L.H.S. of (4.52)

(1.3.4) solved sequentially with constant gain matrices on the L.H.S. of (4.52).

Alternatively the equations can be decomposed and the $\underline{P}$-$\underline{\theta}$ partition of the state estimator iterated for $\underline{\theta}$, treating $\underline{v}$ as a constant. Then the $\underline{Q}$-$\underline{v}$ portion can be iterated, treating $\underline{\theta}$ as a constant until convergence with

(1.3.5) the gain matrices on the L.H.S. of (4.52) updated at each iteration, or

Table 4.4 Different Garcia et al. type P-θ, Q-v decoupling possibilities and their convergence properties.

GARCIA ET AL. TYPE P-θ, Q-v DECOUPLING SCHEMES	CONVERGENT EIGENVALUE EXPRESSIONS
1.3.1 Simultaneous formulation	
$\left[(\underline{h}_{11}^T \underline{R}_p^{-1} \underline{h}_{11} + \underline{h}_{21}^T \underline{R}_q^{-1} \underline{h}_{21})\Delta\underline{\theta}_{k+1} = \underline{h}_{11}^T \underline{R}_p^{-1} [\underline{z}_p - \underline{h}_p(\underline{\theta}_k, \underline{v}_k)]\right]\Big\|_{\substack{v=v_k \\ \theta=\theta_k}}$ $\left[(\underline{h}_{12}^T \underline{R}_p^{-1} \underline{h}_{22} + \underline{h}_{22}^T \underline{R}_q^{-1} \underline{h}_{12})\Delta\underline{v}_{k+1} = \underline{h}_{22}^T \underline{R}_q^{-1} [\underline{z}_q - \underline{h}_q(\underline{\theta}_k, \underline{v}_k)]\right]\Big\|_{\substack{v=v_k \\ \theta=\theta_k}}$	$\begin{bmatrix} \underline{I} - (\underline{h}_{11}^T \underline{R}_p^{-1} \underline{h}_{11} + \underline{h}_{21}^T \underline{R}_q^{-1} \underline{h}_{21})^{-1} \underline{h}_{11}^T \underline{R}_p^{-1} \underline{h}_{11} & -(\underline{h}_{11}^T \underline{R}_p^{-1} \underline{h}_{11} + \underline{h}_{21}^T \underline{R}_q^{-1} \underline{h}_{21})^{-1} \underline{h}_{11}^T \underline{R}_p^{-1} \underline{h}_{12} \\ -(\underline{h}_{12}^T \underline{R}_p^{-1} \underline{h}_{12} + \underline{h}_{22}^T \underline{R}_q^{-1} \underline{h}_{22})^{-1} \underline{h}_{22}^T \underline{R}_q^{-1} \underline{h}_{21} & \underline{I} - (\underline{h}_{12}^T \underline{R}_p^{-1} \underline{h}_{12} + \underline{h}_{22}^T \underline{R}_q^{-1} \underline{h}_{22})^{-1} \underline{h}_{22}^T \underline{R}_q^{-1} \underline{h}_{22} \end{bmatrix}$
1.3.2 Sequential formulation	
$\left[(\underline{h}_{11}^T \underline{R}_p^{-1} \underline{h}_{11} + \underline{h}_{21}^T \underline{R}_q^{-1} \underline{h}_{21})\Delta\underline{\theta}_{k+1} = \underline{h}_{11}^T \underline{R}_p^{-1} [\underline{z}_p - \underline{h}_p(\underline{\theta}_k, \underline{v}_k)]\right]\Big\|_{\substack{v=v_k \\ \theta=\theta_k}}$ $\left[(\underline{h}_{12}^T \underline{R}_p^{-1} \underline{h}_{12} + \underline{h}_{22}^T \underline{R}_q^{-1} \underline{h}_{22})\Delta\underline{v}_{k+1} = \underline{h}_{22}^T \underline{R}_q^{-1} [\underline{z}_q - \underline{h}_q(\underline{\theta}_{k+1}, \underline{v}_k)]\right]\Big\|_{\substack{v=v_k \\ \theta=\theta_k}}$	$\begin{bmatrix} [\underline{I} - (\underline{h}_{11}^T \underline{R}_p^{-1} \underline{h}_{11} + \underline{h}_{21}^T \underline{R}_q^{-1} \underline{h}_{21})_0^{-1} (\underline{h}_{11}^T \underline{R}_p^{-1} \underline{h}_{11})_0] & -[(\underline{h}_{11}^T \underline{R}_p^{-1} \underline{h}_{11} + \underline{h}_{21}^T \underline{R}_q^{-1} \underline{h}_{21})_0^{-1} (\underline{h}_{11}^T \underline{R}_p^{-1} \underline{h}_{12})_0] \\ -[(\underline{h}_{12}^T \underline{R}_p^{-1} \underline{h}_{12} + \underline{h}_{22}^T \underline{R}_q^{-1} \underline{h}_{22})_1^{-1} (\underline{h}_{22}^T \underline{R}_q^{-1} \underline{h}_{22})_1 & [\underline{I} - (\underline{h}_{12}^T \underline{R}_p^{-1} \underline{h}_{12} + \underline{h}_{22}^T \underline{R}_q^{-1} \underline{h}_{22})_1^{-1} [(\underline{h}_{22}^T \underline{R}_q^{-1} \underline{h}_{22})_1 - (\underline{h}_{22}^T \underline{R}_q^{-1} \underline{h}_{21})_1 \\ [\underline{I} - (\underline{h}_{11}^T \underline{R}_p^{-1} \underline{h}_{11} + \underline{h}_{21}^T \underline{R}_q^{-1} \underline{h}_{21})_0^{-1} (\underline{h}_{11}^T \underline{R}_p^{-1} \underline{h}_{11})_0] & (\underline{h}_{11}^T \underline{R}_p^{-1} \underline{h}_{11} + \underline{h}_{21}^T \underline{R}_q^{-1} \underline{h}_{21})_0^{-1} (\underline{h}_{11}^T \underline{R}_p^{-1} \underline{h}_{12})_0] \end{bmatrix}$
1.3.3 Simultaneous update with constant gain matrices	
$[(\underline{h}_{11_o}^T \underline{R}_p^{-1} \underline{h}_{11_o} + \underline{h}_{21_o}^T \underline{R}_q^{-1} \underline{h}_{21_o})]\Big\|_{\substack{v_o=1 \text{ p.u.} \\ \theta_o=0}} \Delta\underline{\theta}_{k+1} = \left[\underline{h}_{11}^T \underline{R}_p^{-1} [\underline{z}_p - \underline{h}_p(\underline{\theta}_k, \underline{v}_k)]\right]\Big\|_{\substack{v=v_k \\ \theta=\theta_k}}$ $[(\underline{h}_{12_o}^T \underline{R}_p^{-1} \underline{h}_{12_o} + \underline{h}_{22_o}^T \underline{R}_q^{-1} \underline{h}_{22_o})]\Big\|_{\substack{v_o=1 \text{ p.u.} \\ \theta_o=0}} \Delta\underline{v}_{k+1} = \left[\underline{h}_{22}^T \underline{R}_q^{-1} [\underline{z}_q - \underline{h}_q(\underline{\theta}_k, \underline{v}_k)]\right]\Big\|_{\substack{v=v_k \\ \theta=\theta_k}}$	$\begin{bmatrix} \underline{I} - (\underline{h}_{11_o}^T \underline{R}_p^{-1} \underline{h}_{11_o} + \underline{h}_{21_o}^T \underline{R}_q^{-1} \underline{h}_{21_o})^{-1} \underline{h}_{11}^T \underline{R}_p^{-1} \underline{h}_{11} & -(\underline{h}_{11_o}^T \underline{R}_p^{-1} \underline{h}_{11_o} + \underline{h}_{21_o}^T \underline{R}_q^{-1} \underline{h}_{21_o})^{-1} \underline{h}_{11}^T \underline{R}_p^{-1} \underline{h}_{12} \\ -(\underline{h}_{12_o}^T \underline{R}_p^{-1} \underline{h}_{12_o} + \underline{h}_{22_o}^T \underline{R}_q^{-1} \underline{h}_{22_o})^{-1} \underline{h}_{22_o}^T \underline{R}_q^{-1} \underline{h}_{21} & \underline{I} - (\underline{h}_{12_o}^T \underline{R}_p^{-1} \underline{h}_{12_o} + \underline{h}_{22_o}^T \underline{R}_q^{-1} \underline{h}_{22_o})^{-1} \underline{h}_{22}^T \underline{R}_q^{-1} \underline{h}_{22} \end{bmatrix}$
1.3.4 Sequential update with constant gain matrices	
$[(\underline{h}_{11_o}^T \underline{R}_p^{-1} \underline{h}_{11_o} + \underline{h}_{21_o}^T \underline{R}_q^{-1} \underline{h}_{21_o})]\Big\|_{\substack{v_o=1 \text{ p.u.} \\ \theta_o=0}} \Delta\underline{\theta}_{k+1} = \left[\underline{h}_{11}^T \underline{R}_p^{-1} [\underline{z}_p - \underline{h}_p(\underline{\theta}_k, \underline{v}_k)]\right]\Big\|_{\substack{v=v_k \\ \theta=\theta_k}}$ $[(\underline{h}_{12_o}^T \underline{R}_p^{-1} \underline{h}_{12_o} + \underline{h}_{22_o}^T \underline{R}_q^{-1} \underline{h}_{22_o})]\Big\|_{\substack{v_o=1 \text{ p.u.} \\ \theta_o=0}} \Delta\underline{v}_{k+1} = \left[\underline{h}_{22}^T \underline{R}_q^{-1} [\underline{z}_q - \underline{h}_q(\underline{\theta}_{k+1}, \underline{v}_k)]\right]\Big\|_{\substack{v=v_k \\ \theta=\theta_{k+1}}}$	$\begin{bmatrix} [\underline{I} - (\underline{h}_{11_o}^T \underline{R}_p^{-1} \underline{h}_{11_o} + \underline{h}_{21_o}^T \underline{R}_q^{-1} \underline{h}_{21_o})_0^{-1} (\underline{h}_{11}^T \underline{R}_p^{-1} \underline{h}_{11})_0] & -[(\underline{h}_{11_o}^T \underline{R}_p^{-1} \underline{h}_{11_o} + \underline{h}_{21_o}^T \underline{R}_q^{-1} \underline{h}_{21_o})_0^{-1} (\underline{h}_{11}^T \underline{R}_p^{-1} \underline{h}_{12})_0] \\ -[(\underline{h}_{12_o}^T \underline{R}_p^{-1} \underline{h}_{12_o} + \underline{h}_{22_o}^T \underline{R}_q^{-1} \underline{h}_{22_o})_1^{-1} (\underline{h}_{22}^T \underline{R}_q^{-1} \underline{h}_{22})_1 & [\underline{I} - (\underline{h}_{12_o}^T \underline{R}_p^{-1} \underline{h}_{12_o} + \underline{h}_{22_o}^T \underline{R}_q^{-1} \underline{h}_{22_o})_1^{-1} (\underline{h}_{22}^T \underline{R}_q^{-1} \underline{h}_{22})_1 - \\ [\underline{I} - (\underline{h}_{11_o}^T \underline{R}_p^{-1} \underline{h}_{11_o} + \underline{h}_{21_o}^T \underline{R}_q^{-1} \underline{h}_{21_o})_0^{-1} (\underline{h}_{11}^T \underline{R}_p^{-1} \underline{h}_{11})_0] & (\underline{h}_{22}^T \underline{R}_q^{-1} \underline{h}_{21})_1 (\underline{h}_{11_o}^T \underline{R}_p^{-1} \underline{h}_{11_o} + \underline{h}_{21_o}^T \underline{R}_q^{-1} \underline{h}_{21_o})_0^{-1} (\underline{h}_{11}^T \underline{R}_p^{-1} \underline{h}_{12})_0] \end{bmatrix}$
1.3.5 Decomposed decoupling	
$\left[(\underline{h}_{11}^T \underline{R}_p^{-1} \underline{h}_{11} + \underline{h}_{21}^T \underline{R}_q^{-1} \underline{h}_{21})\Delta\underline{\theta}_{k+1} = \underline{h}_{11}^T \underline{R}_p^{-1} [\underline{z}_p - \underline{h}_p(\underline{\theta}_k, \underline{v}_o)]\right]\Big\|_{\substack{v=v \\ \theta=\theta_k^o}}$ $\left[(\underline{h}_{12}^T \underline{R}_p^{-1} \underline{h}_{12} + \underline{h}_{22}^T \underline{R}_q^{-1} \underline{h}_{22})\Delta\underline{v}_{k+1} = \underline{h}_{22}^T \underline{R}_q^{-1} [\underline{z}_q - \underline{h}_q(\hat{\underline{\theta}}, \underline{v}_k)]\right]\Big\|_{\substack{v=v_k \\ \theta=\hat{\theta}}}$	For $\underline{\theta}_{k+1}$ $\quad [\underline{I} - (\underline{h}_{11}^T \underline{R}_p^{-1} \underline{h}_{11} + \underline{h}_{21}^T \underline{R}_q^{-1} \underline{h}_{21})^{-1} \underline{h}_{11}^T \underline{R}_p^{-1} \underline{h}_{11}]$ For $\underline{v}_{k+1}$ $\quad [\underline{I} - (\underline{h}_{12}^T \underline{R}_p^{-1} \underline{h}_{12} + \underline{h}_{22}^T \underline{R}_q^{-1} \underline{h}_{22})^{-1} \underline{h}_{22}^T \underline{R}_q^{-1} \underline{h}_{22}]$
1.3.6 Decomposed decoupling with constant gain	
$[(\underline{h}_{11_o}^T \underline{R}_p^{-1} \underline{h}_{11_o} + \underline{h}_{21_o}^T \underline{R}_q^{-1} \underline{h}_{21_o})]\Big\|_{\substack{v_o=1 \text{ p.u.} \\ \theta_o^o=0}} \Delta\underline{\theta}_{k+1} = \left[\underline{h}_{11}^T \underline{R}_p^{-1} [\underline{z}_p - \underline{h}_p(\underline{\theta}_k, \underline{v}_o)]\right]\Big\|_{\substack{v=v_o \\ \theta=\theta_k}}$ $[(\underline{h}_{12_o}^T \underline{R}_p^{-1} \underline{h}_{12_o} + \underline{h}_{22_o}^T \underline{R}_q^{-1} \underline{h}_{22_o})]\Big\|_{\substack{v_o=1 \text{ p.u.} \\ \theta_o^o=0}} \Delta\underline{v}_{k+1} = \left[\underline{h}_{22}^T \underline{R}_q^{-1} [\underline{z}_q - \underline{h}_q(\hat{\underline{\theta}}, \underline{v}_k)]\right]\Big\|_{\substack{v=v_k \\ \theta=\hat{\theta}}}$	For $\underline{\theta}_{k+1}$ $\quad [\underline{I} - (\underline{h}_{11_o}^T \underline{R}_p^{-1} \underline{h}_{11_o} + \underline{h}_{21_o}^T \underline{R}_q^{-1} \underline{h}_{21_o})^{-1} \underline{h}_{11}^T \underline{R}_p^{-1} \underline{h}_{11}]$ For $\underline{v}_{k+1}$ $\quad [\underline{I} - (\underline{h}_{12_o}^T \underline{R}_p^{-1} \underline{h}_{12_o} + \underline{h}_{22_o}^T \underline{R}_q^{-1} \underline{h}_{22_o})^{-1} \underline{h}_{22}^T \underline{R}_q^{-1} \underline{h}_{22}]$

(1.3.6) the gain matrices on the L.H.S. constant at their initial values. The six different P-θ, Q-v decoupling possibilities are shown in Table 4.4. All are modal decoupled and converge to near optimal solutions.

The convergent properties of the eigenvalues of (1.3.1) - (1.3.6) can also be found using a similar analysis to that used for finding the convergence eigenvalue for (1.1.1) - (1.1.6). The convergence eigenvalue expressions for Garcia et al. modal P-θ, Q-v decoupling are shown in Table 4.4.

When simultaneous update P-θ, Q-v Garcia et al. type decoupling is used, the convergence given by (1.3.1) depends on the ratio of $\underline{R}_p$ to $\underline{R}_q$ and on the test system R/X ratio. Convergence is best at low R/X ratios. When X >> R and $\underline{R}_p^{-1} \simeq \underline{R}_q^{-1}$, $\underline{h}_{11} >> \underline{h}_{21}$ and (1.3.1) tends $\rightarrow \underline{0}$. This is because the significance of the $\underline{h}_{21}^T \underline{R}_q^{-1} \underline{h}_{21}$ term and the $\underline{h}_{12}^T \underline{R}_p^{-1} \underline{h}_{12}$ term disappears in relation to $\underline{h}_{11}^T \underline{R}_p^{-1} \underline{h}_{11}$ and $\underline{h}_{22}^T \underline{R}_q^{-1} \underline{h}_{22}$ terms. Note also that Garcia et al.'s P-θ, Q-v decoupling technique is a modal decoupling technique which produces sub-optimal estimates. The estimate changes drastically when $\underline{R}_p >> \underline{R}_q$ (see Figure 4.13). When constant gain matrices are used in Garcia et al.-type simultaneous update decoupling, the convergence properties, as expressed by (1.3.3), depend on the ratio of $\underline{R}_p$ to $\underline{R}_q$ and on the test system R/X ratio. Convergence profiles are shown in Figure 4.14. The tests show that convergence improves slightly as the R/X ratio is decreased.

Sequential update P-θ, Q-v Garcia et al. decoupling covergent-eigenvalue expressions are shown in (1.3.2). Convergence is both dependent on the R/X ratio of the test system and on the relative values of $\underline{R}_p$ and $\underline{R}_q$. The eigenvalue expressions for (1.3.2) contain terms similar to

$$[\underline{I} - (\underline{h}_{11}^T \underline{R}_p^{-1} \underline{h}_{11} + \underline{h}_{21}^T \underline{R}_q^{-1} \underline{h}_{21})^{-1} (\underline{h}_{11}^T \underline{R}_p^{-1} \underline{h}_{11})] \qquad (4.53)$$

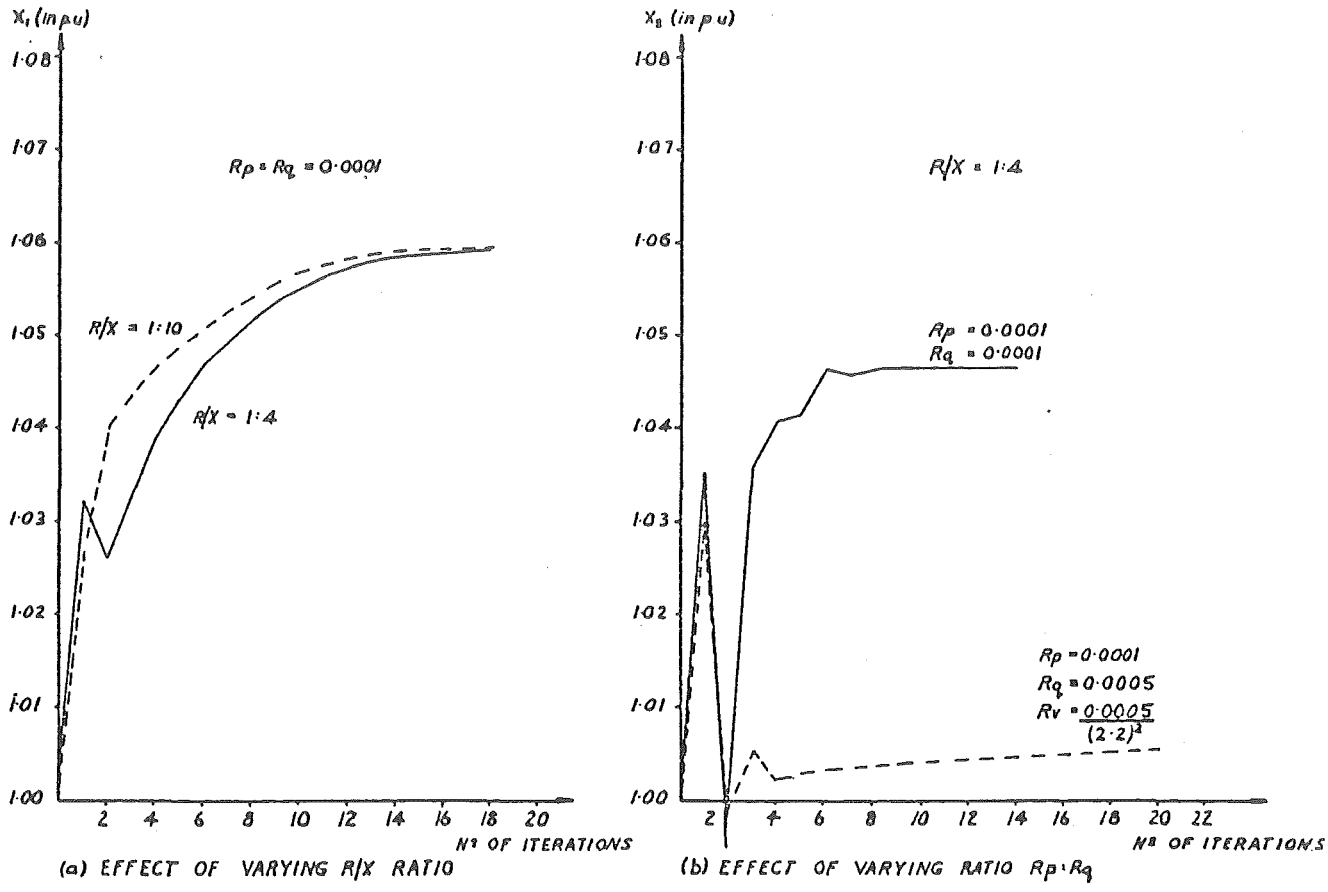

Figure 4.13 Garcia *et al.* type decoupling: unified (1.3.1).

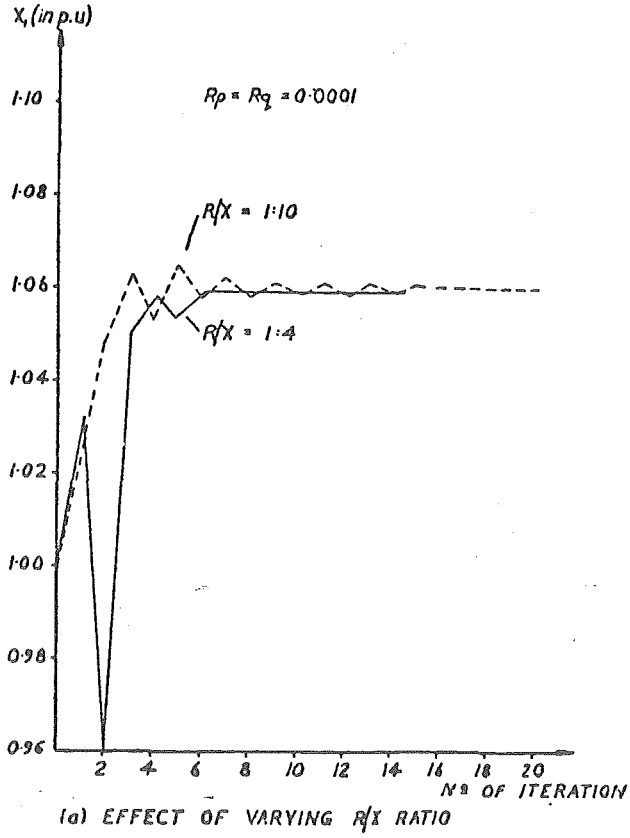

Figure 4.14 Garcia *et al.* type decoupling: unified with constant gain (1.3.3).

When the test system R/X ratio is low, $\underline{h}_{21} << \underline{h}_{11}$ and $\underline{h}_{12} << \underline{h}_{22}$ and the eigenvalue expressions tend to zero. However the term

$$- [(\underline{h}_{11}^T \underline{R}_p^{-1} \underline{h}_{11} + \underline{h}_{21}^T \underline{R}_q^{-1} \underline{h}_{21})^{-1} (\underline{h}_{11}^T \underline{R}_p^{-1} \underline{h}_{12})] \tag{4.54}$$

does not disappear, and the convergence properties may not improve as the test system R/X ratio is decreased. Figure 4.15 shows that convergence depends only slightly on the R/X ratio of the test system. Convergence, however, is slow. When constant gain matrices are used with the sequentially decoupled modal algorithm, the eigenvalue-properties are expressed by (1.3.4). Simulation shows convergence to be rapid and only slightly dependent on the R/X ratio of the power system and very dependent on the relative value of $\underline{R}_p^{-1}$ and $\underline{R}_q^{-1}$ (see Figure 4.16). For extreme ratios of $\underline{R}_p : \underline{R}_q$ the modally decoupled algorithm given by (1.3.4) converges to a different solution.

The theoretical convergence properties for "decomposed" P-θ, Q-v Garcia et al.-type decoupling is shown in (1.3.5). Clearly when the R/X of the test system is low, $\underline{h}_{11} >> \underline{h}_{21}$ and $\underline{h}_{22} >> \underline{h}_{12}$, the eigenvalue expressions tend to zero and the convergence properties improve. This is verified by the prcfile in Figure 4.17. Since Garcia et al.'s decomposed decoupling is modally decoupled, convergence and the solution point depend upon the relative values of $\underline{R}_p^{-1}$ to $\underline{R}_q^{-1}$ (see Figure 4.17). When constant gain matrices are used in the decomposed P-θ, Q-v Garcia et al.-type decoupled algorithm, the convergence properties change and are given by the eigenvalue-expression in (1.3.6). Convergence still slightly improves with decreasing R/X test system ratio and still depends on the relative value of $\underline{R}_p^{-1}$ and $\underline{R}_q^{-1}$ (see Figure 4.18). For extreme ratios of $\underline{R}_p^{-1}$ to $\underline{R}_q^{-1}$ the modally decoupled algorithm converges to a different solution.

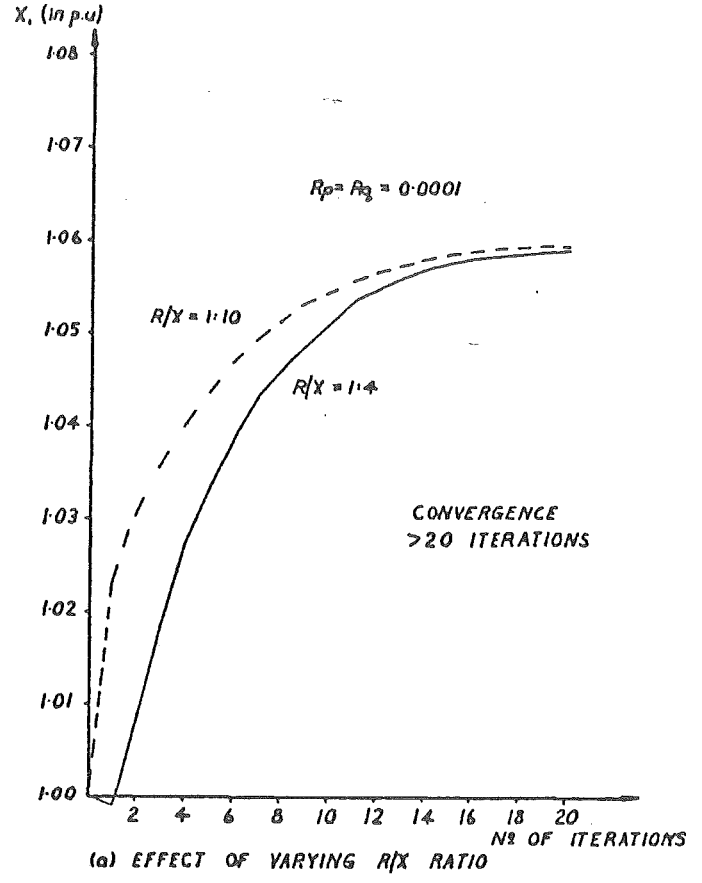

Figure 4.15 Garcia *et al.* type decoupling: sequential (1.3.2).

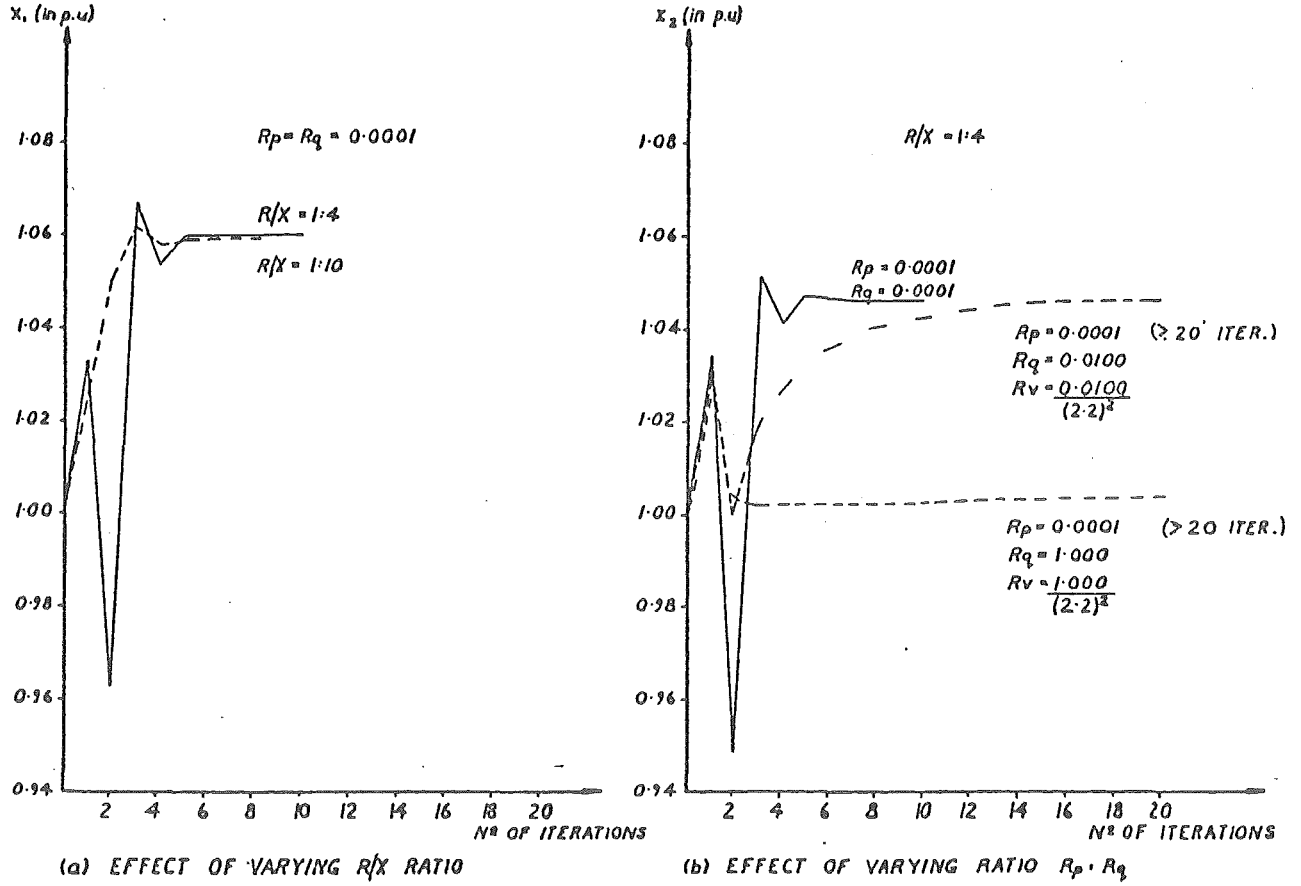

Figure 4.16 Garcia *et al.* type decoupling: sequential with constant gain (1.3.4).

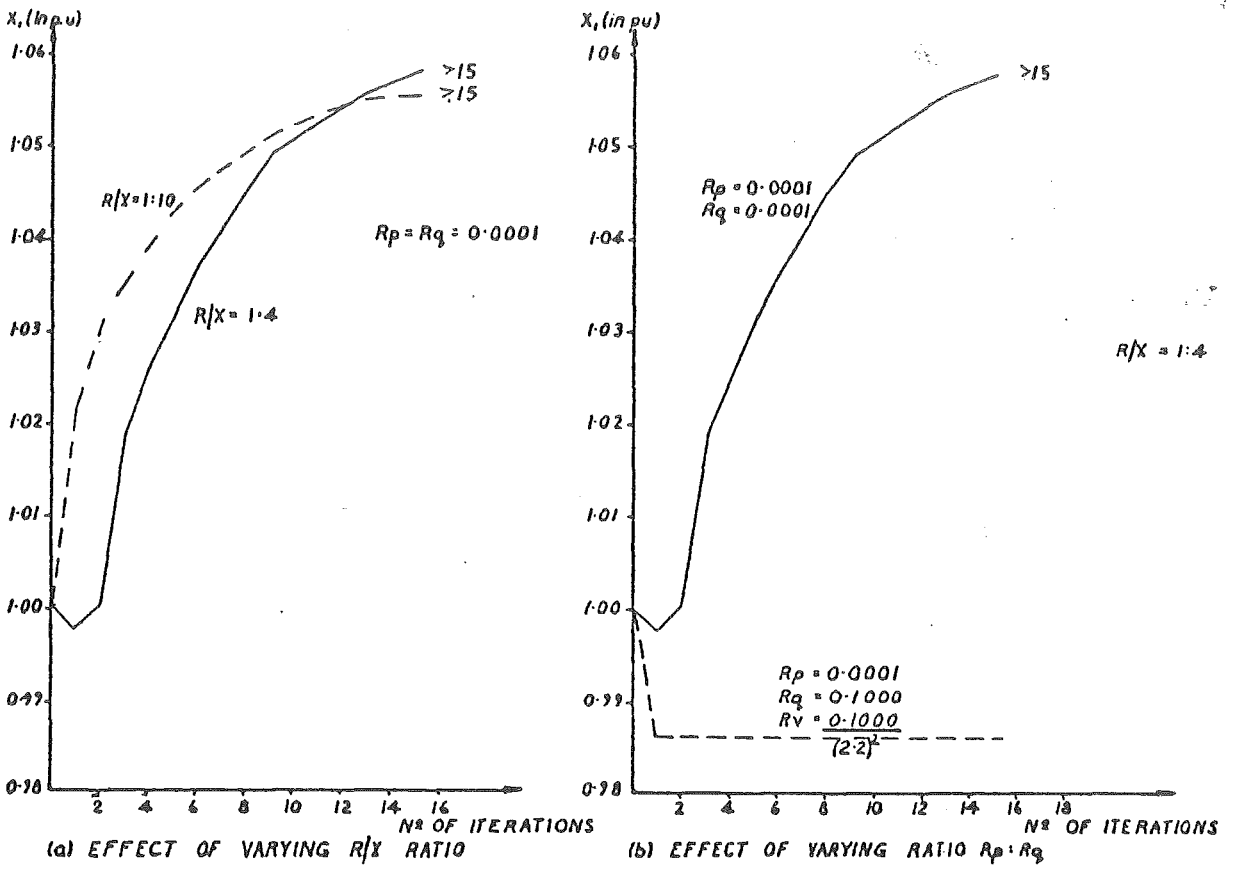

Figure 4.17 Garcia *et al.* type decoupling: decomposed (1.3.5).

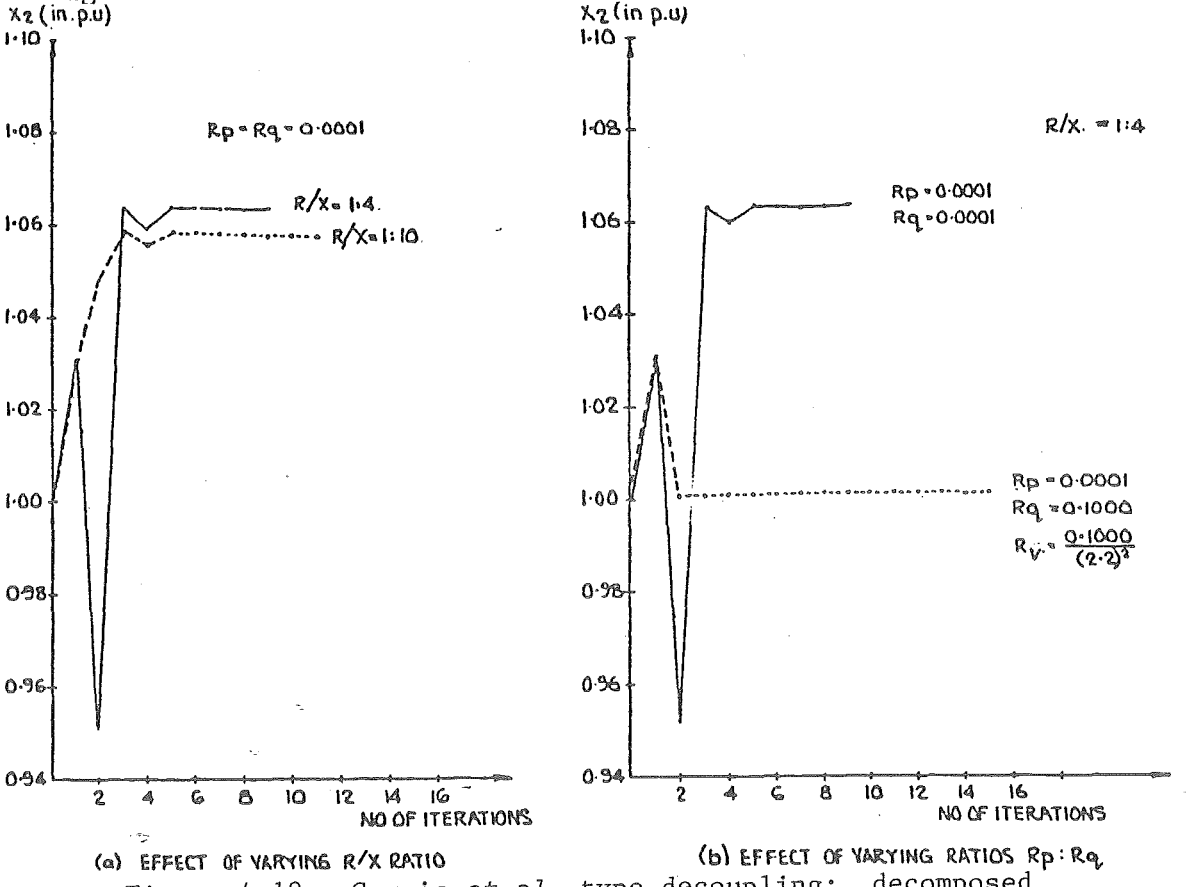

Figure 4.18 Garcia *et al.* type decoupling: decomposed with constant gain (1.3.6).

4.4.4.2 Couch et al. (1974) decouples the Jacobian matrix, $\underline{H}(\underline{\theta},\underline{v})$, on both sides of (2.22). Couch's suggested algorithm has a L.H.S. as given by Horisberger et. al., (4.10), and the R.H.S. as given by Garcia et al., (4.51). As a result the decoupling technique is modally decoupled and if it converges, will converge to the same suboptimal solution as Garcia et al.'s P-θ, Q-v decoupled algorithm. Two state estimator equations result from Couch et al.-type modal decoupling

$$\left(\frac{\partial \underline{h}_p^T(\underline{\theta}_k,\underline{v}_k)}{\partial \underline{\theta}} \underline{R}_p^{-1} \frac{\partial \underline{h}_p(\underline{\theta}_k,\underline{v}_k)}{\partial \underline{\theta}}\right)\Delta\underline{\theta}_{k+1} = \left(\frac{\partial \underline{h}_p^T(\underline{\theta}_k,\underline{v}_k)}{\partial \underline{\theta}}\right)\underline{R}_p^{-1}[\underline{z}_p - \underline{h}_p(\underline{\theta}_k,\underline{v}_k)]\Big|_{\substack{v=v_k \\ \theta=\theta_k}}$$

$$\left(\frac{\partial \underline{h}_q'^T(\underline{\theta}_k,\underline{v}_k)}{\partial \underline{v}} \underline{R}_q'^{-1} \frac{\partial \underline{h}_q'(\underline{\theta}_k,\underline{v}_k)}{\partial \underline{v}}\right)\Delta\underline{v}_{k+1} = \left(\frac{\partial \underline{h}_q'^T(\underline{\theta}_k,\underline{v}_k)}{\partial \underline{v}}\right)\underline{R}_q'^{-1}[\underline{z}_q' - \underline{h}_q'(\underline{\theta}_k,\underline{v}_k)]\Big|_{\substack{v=v_k \\ \theta=\theta_k}} \quad (4.55)$$

which:

(1.4.1) can be solved simultaneously

(1.4.2) solved sequentially

(1.4.3) solved simultaneously with constant gain matrices on the L.H.S. of (4.55)

(1.4.4) solved sequentially with constant gain matrices on the L.H.S. of (4.55).

Alternatively the equations can be decomposed and the P-θ portion of the state estimator iterated for $\underline{\theta}$, treating $\underline{v}$ as a constant. Then the Q-$\underline{v}$ portion can be iterated, treating $\underline{\theta}$ as a constant until convergence with

(1.4.5) the gain matrices on the L.H.S. of (4.55) updated at each iteration, or

(1.4.6) the gain matrices on the L.H.S. constant at their initial

values.

The six different P-θ, Q-v decoupling possibilities are shown in Table 4.5. All are modal decoupled and thus converge to suboptimal estimates. The convergent properties of the eigenvalues of (1.3.1) - (1.3.6) can be found using a similar analysis to that used to find the convergence eigenvalues for (1.1.1) - (1.1.6). The convergene eigenvalues for Couch et al.-type modal P-θ, Q-v decoupling are shown in Table 4.5.

When simultaneous update P-θ, Q-v Couch et al. decoupling is used, the convergence, given by (1.4.1), depends on the R/X ratio of the power system. This is because $\underline{h}_{11} >> \underline{h}_{12}$ and $\underline{h}'_{22} >> \underline{h}'_{12}$ at low R/X ratios, and as a result the eigenvalue expression, (1.4.1), tends to zero, thus improving the convergence properties (see Figure 4.19). Convergence is invariant to changes in the relative values of $\underline{R}_p^{-1}$ and $\underline{R}_q^{-1}$ (see Figure 4.19). This can be explained by the fact that when the R/X ratios of all lines within the test system are identical, say equal to α, then from Appendix A5,

$$\underline{h}_{11} \simeq \alpha \, \underline{h}_{21} \tag{4.56}$$

and

$$\underline{h}_{22} \simeq \alpha \, \underline{h}_{12} \tag{4.57}$$

and thus the eigenvalue expression given by (1.4.1) becomes:

$$\begin{bmatrix} \underline{0} & -\frac{1}{\alpha}\left(\underline{h}_{11}^T \underline{R}_p^{-1} \underline{h}_{11}\right)^{-1}\left(\underline{h}_{11}^T \underline{R}_p^{-1} \underline{h}_{11}\right) \\ -\frac{1}{\alpha}\left(\underline{h}_{22}^T \underline{R}_q^{-1} \underline{h}_{22}\right)^{-1}\left(\underline{h}_{22}^T \underline{R}_q^{-1} \underline{h}_{22}\right) & \underline{0} \end{bmatrix} \tag{4.58}$$

$$= \begin{bmatrix} \underline{0} & -\frac{1}{\alpha} \\ -\frac{1}{\alpha} & \underline{0} \end{bmatrix} \tag{4.59}$$

Table 4.5 Different Couch *et al.* type P-θ, Q-v decoupling possibilities and their convergence properties.

COUCH ET AL. TYPE P-θ, Q-v DECOUPLING SCHEMES	CONVERGENT EIGENVALUE EXPRESSIONS
1.4.1 Simultaneous formulation	
$\left[(\underline{h}_{11}^T \underline{R}_p^{-1} \underline{h}_{11})\Delta\underline{\theta}_{k+1} = \underline{h}_{11}^T \underline{R}_p^{-1} [\underline{z}_p - \underline{h}_p(\underline{\theta}_k, \underline{v}_k)]\right]\Big\|_{\substack{v=v_k \\ \theta=\theta_k^k}}$ $\left[(\underline{h}'^T_{22} \underline{R}_q^{-1} \underline{h}'_{22})\Delta\underline{v}_{k+1} = \underline{h}'^T_{22} \underline{R}_q^{-1} [\underline{z}'_q - \underline{h}'_q(\underline{\theta}_k, \underline{v}_k)]\right]\Big\|_{\substack{v=v_k \\ \theta=\theta_k^k}}$	$\left[\begin{array}{c\|c} \underline{0} & -(\underline{h}_{11}^T \underline{R}_p^{-1} \underline{h}_{11})^{-1}(\underline{h}_{11}^T \underline{R}_p^{-1} \underline{h}_{21}) \\ \hline -(\underline{h}_{22}'^T \underline{R}_q^{-1} \underline{h}'_{22})^{-1}(\underline{h}_{22}'^T \underline{R}_q^{-1} \underline{h}_{12}) & \underline{0} \end{array}\right]$
1.4.2 Sequential formulation	
$\left[(\underline{h}_{11}^T \underline{R}_p^{-1} \underline{h}_{11})\Delta\underline{\theta}_{k+1} = \underline{h}_{11}^T \underline{R}_p^{-1} [\underline{z}_p - \underline{h}_p(\underline{\theta}_k, \underline{v}_k)]\right]\Big\|_{\substack{v=v_k \\ \theta=\theta_k^k}}$ $\left[(\underline{h}'^T_{22} \underline{R}_q^{-1} \underline{h}'_{22})\Delta\underline{v}_{k+1} = \underline{h}'^T_{22} \underline{R}_q^{-1} [\underline{z}'_q - \underline{h}'_q(\underline{\theta}_{k+1}, \underline{v}_k)]\right]\Big\|_{\substack{v=v_k \\ \theta=\theta_{k+1}^k}}$	$\left[\begin{array}{c\|c} \underline{0} & [-(\underline{h}_{11}^T \underline{R}_p^{-1} \underline{h}_{11})^{-1} \underline{h}_{11}^T \underline{R}_p^{-1} \underline{h}_{12}]_0 \\ \hline -[(\underline{h}_{22}'^T \underline{R}_q^{-1} \underline{h}'_{22})^{-1} \underline{h}_{22}'^T \underline{R}_q^{-1} \underline{h}'_{21}(\underline{h}_{11}^T \underline{R}_p^{-1} \underline{h}_{11})^{-1} (\underline{h}_{11}^T \underline{R}_p^{-1} \underline{h}_{12})] & \underline{0} \end{array}\right]$
1.4.3 Simultaneous update with constant gain matrices	
$[(\underline{h}_{11}^T \underline{R}_p^{-1} \underline{h}_{11})]\Big\|_{\substack{v=1 \\ \theta_o^o=\hat{0}^{p.u.}}} \Delta\underline{\theta}_{k+1} = \left[\underline{h}_{11}^T \underline{R}_p^{-1} [\underline{z}_p - \underline{h}_p(\underline{\theta}_k, \underline{v}_k)]\right]\Big\|_{\substack{v=v_k \\ \theta=\theta_k^k}}$ $[(\underline{h}'^T_{22} \underline{R}_q^{-1} \underline{h}'_{22})]\Big\|_{\substack{v=1 \\ \theta_o^o=\hat{0}^{p.u.}}} \Delta\underline{v}_{k+1} = \left[\underline{h}'^T_{22} \underline{R}_q^{-1} [\underline{z}'_q - \underline{h}'_q(\underline{\theta}_{k+1}, \underline{v}_k)]\right]\Big\|_{\substack{v=v_k \\ \theta=\theta_{k+1}^k}}$	$\left[\begin{array}{c\|c} \underline{I} - (\underline{h}_{11_o}^T \underline{R}_p^{-1} \underline{h}_{11_o})^{-1}(\underline{h}_{11}^T \underline{R}_p^{-1} \underline{h}_{11}) & -(\underline{h}_{11_o}^T \underline{R}_p^{-1} \underline{h}_{11_o})^{-1}(\underline{h}_{11}^T \underline{R}_p^{-1} \underline{h}_{21}) \\ \hline -(\underline{h}_{22_o}'^T \underline{R}_q^{-1} \underline{h}'_{22_o})^{-1}(\underline{h}_{22}'^T \underline{R}_q^{-1} \underline{h}_{12}) & \underline{I} - (\underline{h}_{22_o}'^T \underline{R}_q^{-1} \underline{h}'_{22_o})^{-1}(\underline{h}_{22}'^T \underline{R}_q^{-1} \underline{h}'_{22}) \end{array}\right]$
1.4.4 Sequential update with constant gain matrices	
$[(\underline{h}_{11}^T \underline{R}_p^{-1} \underline{h}_{11})]\Big\|_{\substack{v=1 \\ \theta_o^o=\hat{0}^{p.u.}}} \Delta\underline{\theta}_{k+1} = \left[\underline{h}_{11}^T \underline{R}_p^{-1} [\underline{z}_p - \underline{h}_p(\underline{\theta}_k, \underline{v}_k)]\right]\Big\|_{\substack{v=v_k \\ \theta=\theta_k^k}}$ $[(\underline{h}'^T_{22} \underline{R}_q^{-1} \underline{h}'_{22})]\Big\|_{\substack{v=1 \\ \theta_o^o=\hat{0}^{p.u.}}} \Delta\underline{v}_{k+1} = \left[\underline{h}'^T_{22} \underline{R}_q^{-1} [\underline{z}'_q - \underline{h}'_q(\underline{\theta}_{k+1}, \underline{v}_k)]\right]\Big\|_{\substack{v=v_k \\ \theta=\theta_{k+1}^k}}$	$\left[\begin{array}{c\|c} [\underline{I} - (\underline{h}_{11_o}^T \underline{R}_p^{-1} \underline{h}_{11_o})^{-1}(\underline{h}_{11}^T \underline{R}_p^{-1} \underline{h}_{11})]_0 & -[(\underline{h}_{11_o}^T \underline{R}_p^{-1} \underline{h}_{11_o})^{-1} \underline{h}_{11}^T \underline{R}_p^{-1} \underline{h}_{12}]_0 \\ \hline -[(\underline{h}_{22_o}'^T \underline{R}_q^{-1} \underline{h}'_{22_o})_1^{-1}(\underline{h}_{22}'^T \underline{R}_q^{-1} \underline{h}'_{21})_1 (\underline{h}_{11_o}^T \underline{R}_p^{-1} \underline{h}_{11_o})_0^{-1} & [\underline{I} - [(\underline{h}_{22_o}'^T \underline{R}_q^{-1} \underline{h}'_{22_o})_1^{-1}[(\underline{h}_{22}'^T \underline{R}_q^{-1} \underline{h}'_{22})_1 - \underline{h}_{22}'^T \underline{R}_q^{-1} \underline{h}'_{21})_1 \\ (\underline{h}_{11}^T \underline{R}_p^{-1} \underline{h}_{12})_0] & (\underline{h}_{11_o}^T \underline{R}_p^{-1} \underline{h}_{11_o})_0^{-1}(\underline{h}_{11}^T \underline{R}_p^{-1} \underline{h}_{12})_0] \end{array}\right]$
1.4.5 Decomposed decoupling	
$\left[(\underline{h}_{11}^T \underline{R}_p^{-1} \underline{h}_{11})\Delta\underline{\theta}_{k+1} = \underline{h}_{11}^T \underline{R}_p^{-1} [\underline{z}_p - \underline{h}_p(\underline{\theta}_k, \underline{v}_k)]\right]\Big\|_{\substack{v=v \\ \theta=\theta_k^o}}$ $\left[(\underline{h}'^T_{22} \underline{R}_q^{-1} \underline{h}'_{22})\Delta\underline{v}_{k+1} = \underline{h}'^T_{22} \underline{R}_2^{-1} [\underline{z}'_q - \underline{h}'_q(\hat{\underline{\theta}}, \underline{v}_k)]\right]\Big\|_{\substack{v=v_k \\ \theta=\hat{\theta}}}$	For $\underline{\theta}_{k+1}$ $[\underline{0}]$ thus eigenvalues are zero and the algorithm has a rapid, stable convergence For $\underline{v}_{k+1}$ $[\underline{0}]$ thus eigenvalues are zero and the algorithm has a rapid, stable convergence
1.4.6 Decomposed decoupling with constant gain matrices	
$[(\underline{h}_{11_o}^T \underline{R}_p^{-1} \underline{h}_{11_o})]\Big\|_{\substack{v=1 \\ \theta_o^o=\hat{0}^{p.u.}}} \Delta\underline{\theta}_{k+1} = \left[\underline{h}_{11}^T \underline{R}_p^{-1} [\underline{z}_p - \underline{h}_p(\underline{\theta}_k, \underline{v}_o)]\right]\Big\|_{\substack{v=v \\ \theta=\theta_k^o}}$ $[(\underline{h}'^T_{22_o} \underline{R}_q^{-1} \underline{h}'_{22_o})]\Big\|_{\substack{v=1 \\ \theta_o^o=\hat{0}^{p.u.}}} \Delta\underline{v}_{k+1} = \left[\underline{h}'^T_{22} \underline{R}_q^{-1} [\underline{z}'_q - \underline{h}'_q(\hat{\underline{\theta}}, \underline{v}_k)]\right]\Big\|_{\substack{v=v_k \\ \theta=\hat{\theta}}}$	For $\underline{\theta}_{k+1}$ $[\underline{I} - (\underline{h}_{11_o}^T \underline{R}_p^{-1} \underline{h}_{11_o})^{-1} (\underline{h}_{11}^T \underline{R}_p^{-1} \underline{h}_{11})_2]$ For $\underline{V}_{k+1}$ $[\underline{I} - (\underline{h}_{22_o}'^T \underline{R}_q^{-1} \underline{h}'_{22_o})^{-1} (\underline{h}_{22}'^T \underline{R}_q^{-1} \underline{h}'_{22})_3]$

' Denotes Couch et al. transformation is used.

which is invariant to changes in the ratio of $\underline{R}_p$ and $\underline{R}_q$. Where R/X ratios of lines differ:

$$\alpha_{min}\ \underline{h}_{21} \leq \underline{h}_{11}$$

and (4.60)

$$\alpha_{min}\ \underline{h}_{12} \leq \underline{h}_{22}$$

where α_{min} is the smallest R/X ratio in the test power system.

Thus the convergence is bounded by:

$$\begin{bmatrix} \underline{0} & -\frac{1}{\alpha_{min}} \\ -\frac{1}{\alpha_{min}} & \underline{0} \end{bmatrix} \tag{4.61}$$

When constant gain matrices are used on Couch et al.-type simultaneous update decoupling, the convergence properties are given by (1.4.3). Convergence now depends on the R/X ratio of the test system and on the relative weightings $\underline{R}_p^{-1}$ and $\underline{R}_q^{-1}$. Convergence will only be invariant of the weightings $\underline{R}_p^{-1}$ and $\underline{R}_q^{-1}$ if $\underline{h}_{11_0} \simeq \underline{h}_{11}$ and $\underline{h}'_{22_0} \simeq \underline{h}'_{22}$. Convergence profiles are shown in Figure 4.20.

Sequential update P-θ, Q-v Couch et al. decoupling convergence eigenvalue-expressions are given by (1.4.2). Convergence is both dependent on the R/X ratio of the test system and on the relative values of $\underline{R}_p^{-1}$ and $\underline{R}_q^{-1}$. When R/X ratio of the test system is small

$$\underline{h}_{22} \leq \alpha\ \underline{h}_{21}$$

and (4.62)

$$\underline{h}_{11} \leq \alpha\ \underline{h}_{12}$$

and thus the convergence eigenvalue expression in (1.4.2) tends to $\frac{1}{\alpha^2}\ \underline{I}$ and $\frac{1}{\alpha}\ \underline{I}$. Thus as the R/X ratio decreases, the eigenvalue expression (1.4.2) gradually tends to zero and convergence improves. Again, from (1.4.2), convergence tends to be invariant of the relative weightings

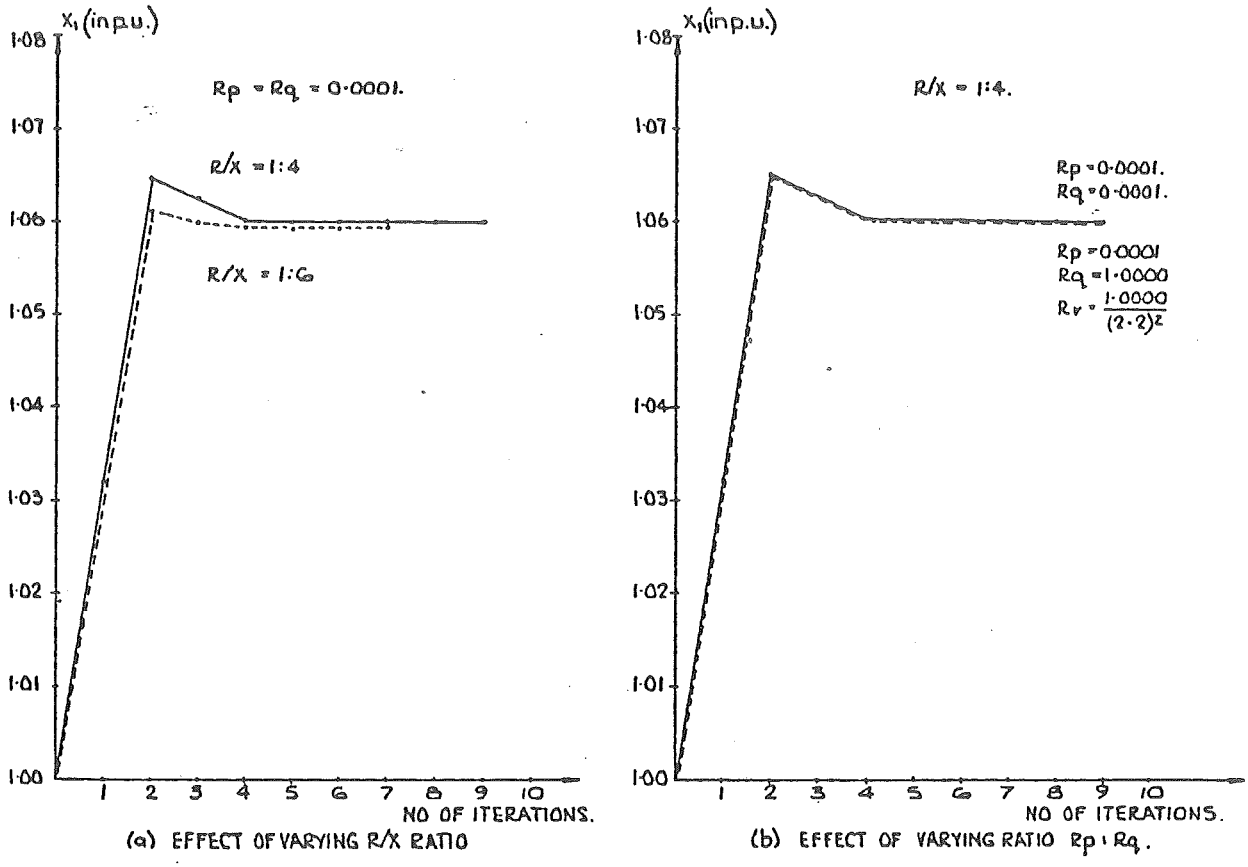

Figure 4.19 Couch *et al.* type decoupling: unified (1.4.1).

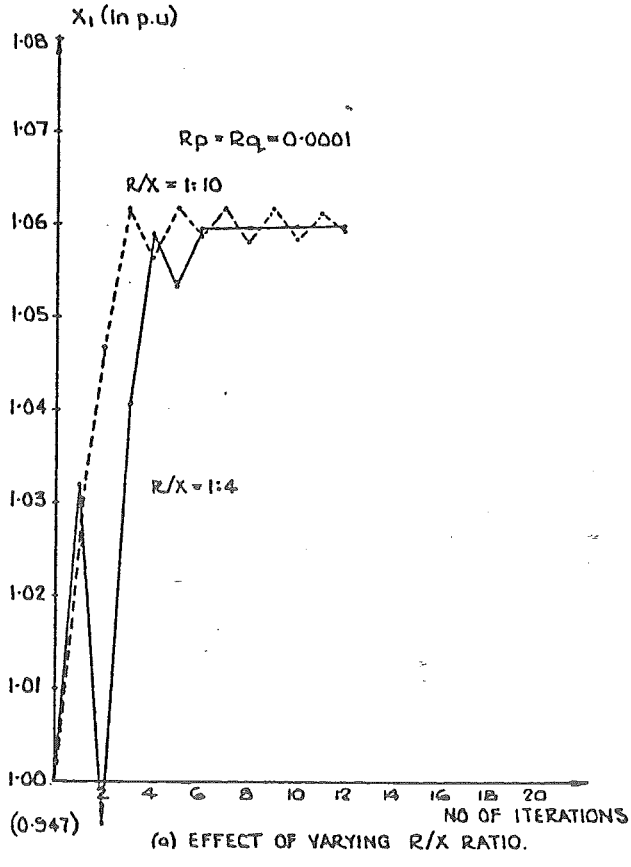

Figure 4.20 Couch *et al.* type decoupling: unified with constant gain (1.4.3).

of $\underline{R}_p^{-1}$ to $\underline{R}_q^{-1}$. This is because the convergence is bounded by α_{min}, the smallest R/X ratio in the test power system. Convergence profiles are shown in Figure 4.21. When constant gain matrices are used in the sequentially decoupled modal algorithm, the eigenvalue properties are expressed by (1.4.4). Simulation shows convergence to be heavily dependent on the R/X ratio of the test system and very dependent on the relative values of $\underline{R}_p^{-1}$ and $\underline{R}_q^{-1}$ if $\underline{h}_{11_0} \neq \underline{h}_{11}$ and $\underline{h}'_{22_0} \neq \underline{h}'_{22}$ (see Figure 4.22). For large R/X ratios divergence occurs.

The theoretical convergence properties for "decomposed P-θ, Q-v Couch et al.-type decoupling", originally proposed by Singh et al., are shown in (1.4.5) as having zero eigenvalues, the same convergence properties as exact W.L.S. Convergence is thus rapid and invariant of both the R/X ratio of the test power system and of the relative weightings, $\underline{R}_p^{-1}$ and $\underline{R}_q^{-1}$. Simulations verify this analysis (see Figure 4.23). When constant gain matrices are used in the Couch et al. decomposed decoupled algorithm, the convergence properties change, as shown by (1.4.6). If $\underline{h}_{11_0} \neq \underline{h}_{11}$ and $\underline{h}'_{22_0} \neq \underline{h}'_{22}$, convergence will become dependent on both the R/X ratio of the test system and on the relative values of $\underline{R}_p^{-1}$ and $\underline{R}_q^{-1}$ (see Figure 4.24). Convergence is definitely dependent on the R/X ratio of the power system.

4.4.3 Other fast decoupled schemes

The Jacobian matrix in (2.22) was decoupled on both sides of the state estimator algorithm by setting:

$$\frac{\partial \underline{h}_p(\underline{\theta},\underline{v})}{\partial \underline{v}} = \underline{0} \quad \text{and} \quad \frac{\partial \underline{h}_q(\underline{\theta},\underline{v})}{\partial \underline{\theta}} = \underline{0} \tag{4.63}$$

and leaving the expressions for

$$\frac{\partial \underline{h}_p(\underline{\theta},\underline{v})}{\partial \underline{\theta}} \quad \text{and} \quad \frac{\partial \underline{h}_q(\underline{\theta},\underline{v})}{\partial \underline{v}}$$

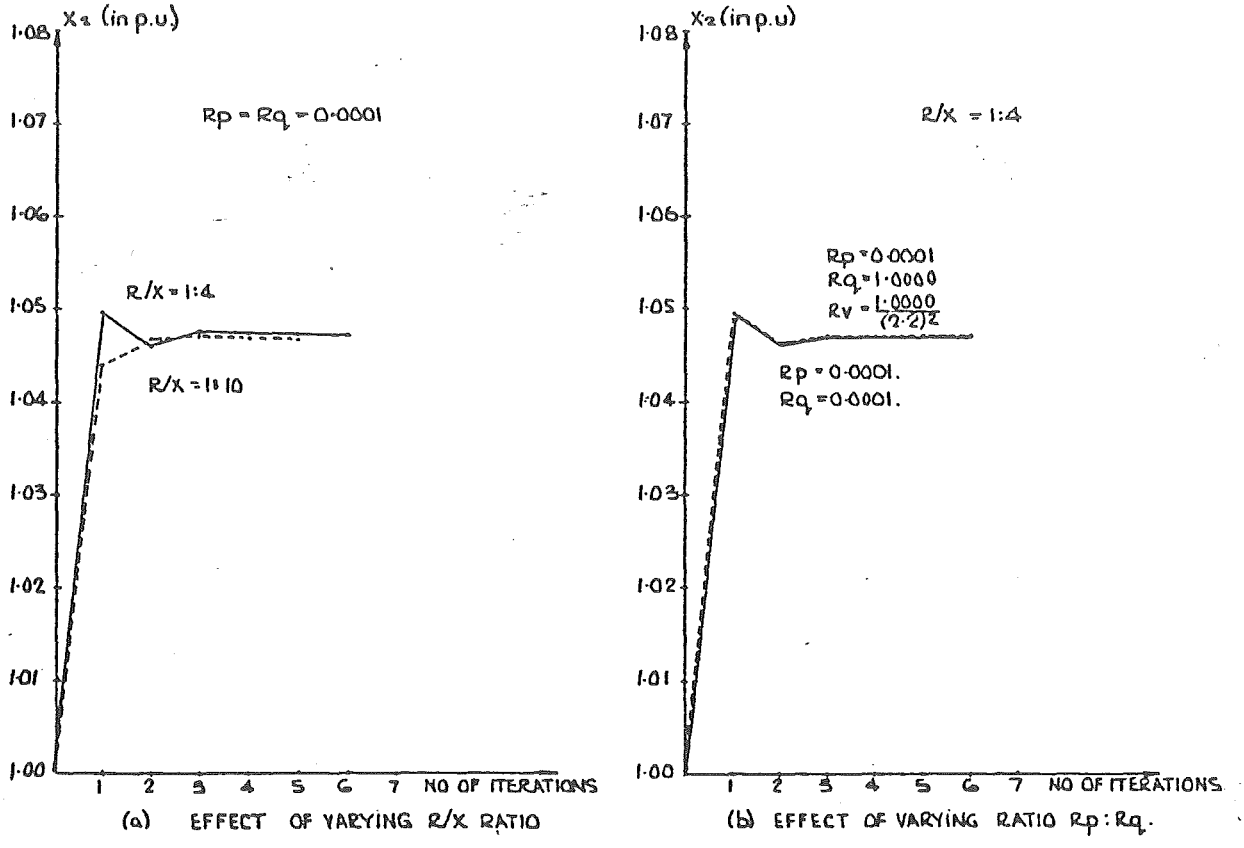

Figure 4.21 Couch *et al.* decoupling: sequential (1.4.2).

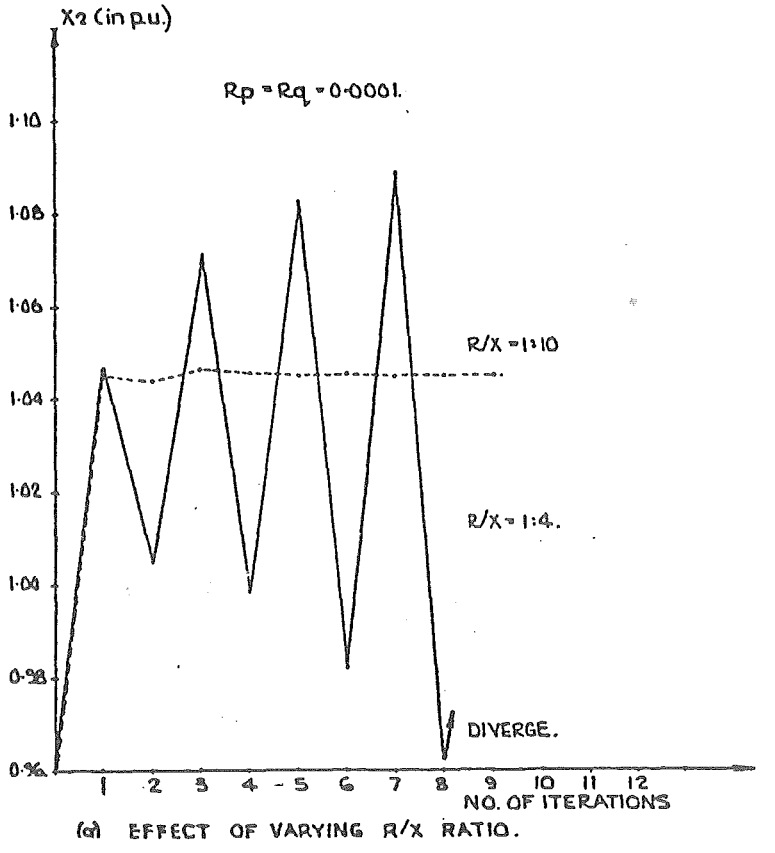

Figure 4.22 Couch *et al.* decoupling: sequential with constant gain (1.4.4).

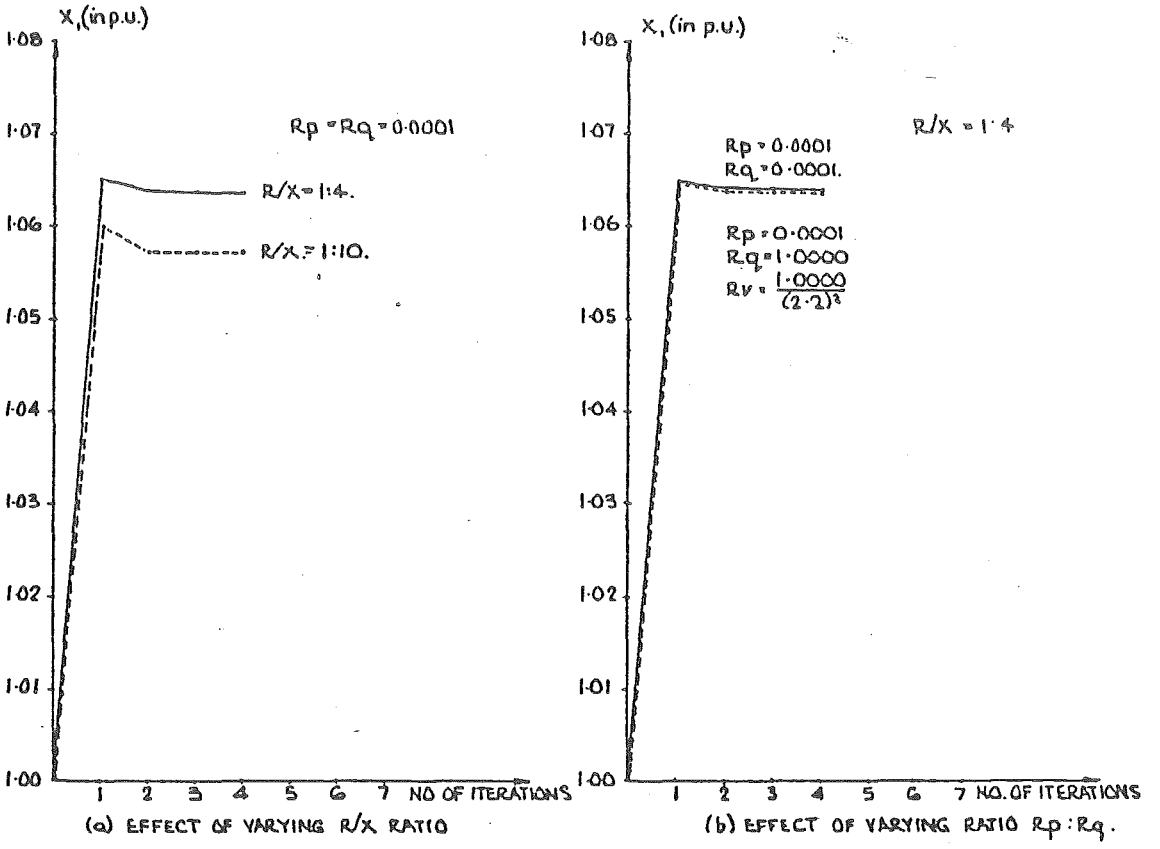

Figure 4.23 Couch *et al.* decoupling: decomposed (1.4.5).

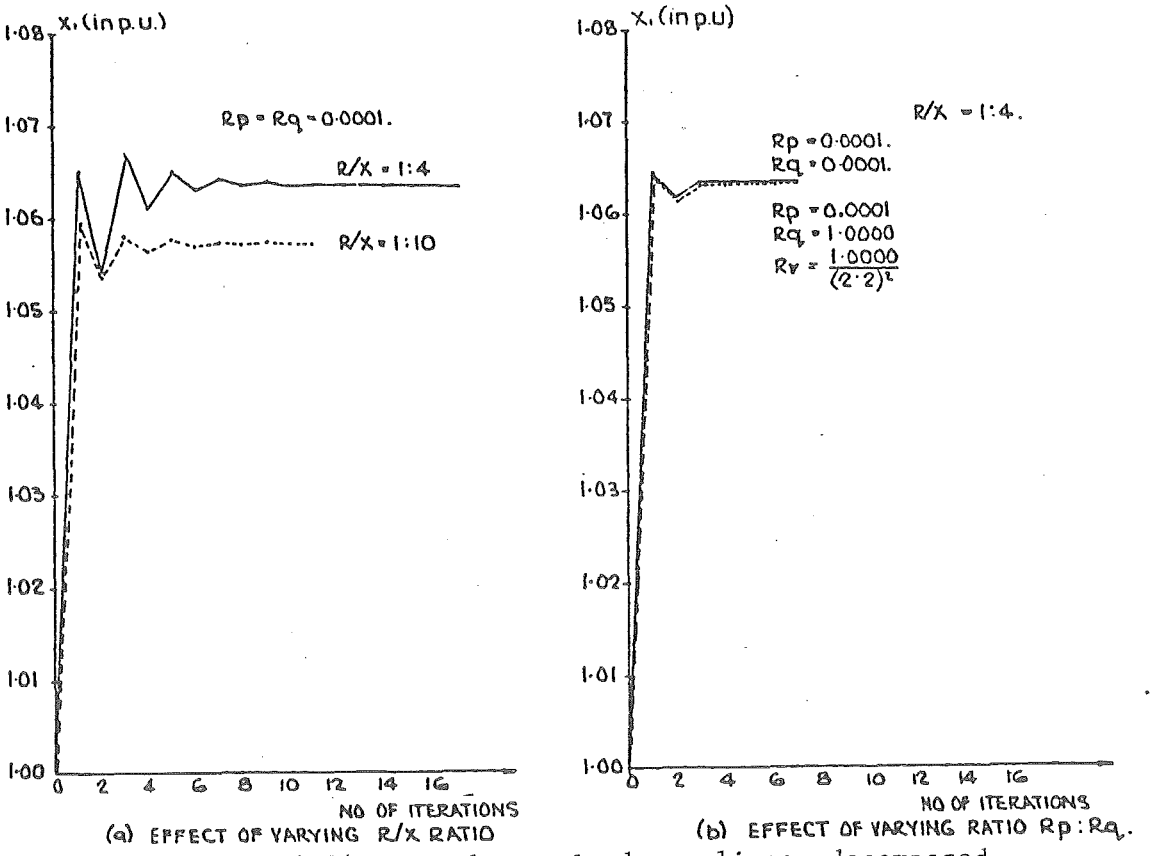

Figure 4.24 Couch *et al.* decoupling: decomposed with constant gain (1.4.6).

unchanged. Reichert and Sullivan (1977) suggest using approximate coefficients to simplify $\partial \underline{h}_p(\underline{\theta},\underline{v})/\partial\underline{\theta}$ and $\partial \underline{h}_q(\underline{\theta},\underline{v})/\partial\underline{v}$ by assuming

$$G_{ii} = G_{ij} = 0,\ \cos(\theta_i - \theta_j) \simeq 1 \quad \text{and} \quad \sin(\theta_i - \theta_j) \simeq (\theta_i - \theta_j) \tag{4.64}$$

and thus, from (2.9) and (2.10);

$$c_{ij} = v_i\, v_j\, B_{ij}\, (\theta_i - \theta_j) \tag{4.65}$$

and

$$d_{ij} = v_i\, v_j\, B_{ij} \tag{4.66}$$

can be used to represent $\partial \underline{h}_p(\underline{\theta},\underline{v})/\partial\underline{\theta}$ and $\partial \underline{h}_q(\underline{\theta},\underline{v})/\partial\underline{v}$ in the Jacobian on both sides of (2.22). However these Jacobian non-zero partial derivatives still have to be updated at each iteration.

The decoupling process can further be extended to fast decouple the Jacobian matrix on both sides of (2.22) in a manner similar to Stott and Alsac's (1974) fast decoupled loadflow. Bermundez (1977), Bermundez and Brameller (1978), Wognar (1977), Rao and Tripathy (1978), Tripathy et al. (1979), Van Meeteren et al. (1978) and Van Meeteren (1979) have all advocated methods for fast decoupling the Jacobian matrix. Since their properties are similar, Bermundez and Brameller's method of fast decoupling the Jacobian will be outlined.

Bermundez and Brameller (1978) use Couch's transformation, outlined in section 4.3, to linearize the reactive power measurement equations. Thus

$$\underline{z}_q' = \underline{h}_q'(\underline{x}) + \underline{\eta}_q' \tag{4.67}$$

where

$$z_{q_m}' = \frac{z_q}{v_m}, \quad h_{q_m}'(\underline{x}) = \frac{h_q(\underline{x})}{v_m} \quad \text{and} \quad \eta_{q_m} = \frac{\eta_q}{v_m} \tag{4.68}$$

where v_m is the magnitude of the nodal voltage at the node, m, at which the measurement, z_{q_m}', is being made. Since $v_m \simeq 1.0$ p.u.

$$\underline{R}_q' \simeq \underline{R}_q \tag{4.69}$$

Bermundez and Brameller then fast decouple by assuming

$$\begin{aligned} &\cos(\theta_i - \theta_j) \simeq 0 \\ &v_i,\ v_j \simeq 1.0 \\ &G_{ij} \sin(\theta_i - \theta_j) \ll B_{ij} \cos(\theta_i - \theta_j) \end{aligned} \tag{4.70}$$

and the components of the Jacobian matrix become state independent. Table 4.1 becomes Table 4.6. Note that G_{ij} is approximated to zero in the calculation of the active power partial derivatives. This is shown to improve convergence substantially. The fast decoupled technique is a modal scheme and as such produces suboptimal estimates. In summary, the algorithm is:

$$\begin{aligned} \left(\frac{\partial \tilde{\underline{h}}_p}{\partial \underline{\theta}}^T \underline{R}_p^{-1} \frac{\partial \tilde{\underline{h}}_p}{\partial \underline{\theta}}\right) \Delta\underline{\theta}_{k+1} &= \left(\frac{\partial \tilde{\underline{h}}_p}{\partial \underline{\theta}}^T\right) \underline{R}_p^{-1} \left[\underline{z}_p - \tilde{\underline{h}}_p(\underline{\theta}_k, \underline{v}_k)\right]\Big|_{\substack{v = v_k \\ \theta = \theta_k}} \\ \left(\frac{\partial \tilde{\underline{h}}_q}{\partial \underline{v}}^T \underline{R}_q^{-1} \frac{\partial \tilde{\underline{h}}_q}{\partial \underline{v}}\right) \Delta\underline{v}_{k+1} &= \left(\frac{\partial \tilde{\underline{h}}_q}{\partial \underline{v}}^T\right) \underline{R}_q^{-1} \left[\underline{z}_q' - \tilde{\underline{h}}_q'(\theta_{k+1}, v_k)\right]\Big|_{\substack{v = v_k \\ \theta = \theta_{k+1}}} \end{aligned} \tag{4.71}$$

where $\partial \tilde{\underline{h}}_p / \partial \underline{\theta}$ and $\partial \tilde{\underline{h}}_q / \partial \underline{v}$ are the modified Jacobian elements corresponding to $\partial \underline{h}_p(\underline{\theta}_k, \underline{v}_k)/\partial \underline{\theta}$ and $\partial \underline{h}_q(\underline{\theta}_k, \underline{v}_k)/\partial \underline{v}$. The scheme is:

(1.5.1) solved sequentially, as advocated by Bermundez and Brameller, or alternatively

(1.5.2) the equations can be decomposed and the $\underline{P}$-$\underline{\theta}$ portion of the state estimator iterated for $\underline{\theta}$, treating $\underline{v}$ as a constant. Then the $\underline{Q}$-$\underline{v}$ portion can be iterated, treating $\underline{\theta}$ as a constant until convergence.

Table 4.6 Non-zero Jacobian partial derivatives for Bermundez and Brameller's fast decoupling

MEASUREMENT	$\frac{\partial}{\partial \theta_i}$	$\frac{\partial}{\partial V_i}$
V_i	0	1
P_{ij}	B_{ij}	0
P_{ji}	B_{ij}	0
Q_{ij}	0	B_{ii}
Q_{ji}	0	$-B_{ij}$
P_i	$-\sum_{j\varepsilon\{\alpha\}} B_{ij}$	0
P_j	$-B_{ij}$	0
Q_i	0	$-\sum_{j\varepsilon\{\alpha\}} B_{ii}$
Q_j	0	$-B_{ij}$

The two different possibilities are summarized in Table 4.7. The convergence eigenvalues for Bermundez and Brameller type modal fast decoupling are also shown in Table 4.7. When sequential modal fast decoupling is used, the convergence given by (1.5.1) depends on the R/X ratio of the power system and on the ratio of $\underline{R}_p^{-1}$ to $\underline{R}_q^{-1}$. However, extensive simulation shows the convergence to be invariant of either the R/X ratio of the test system or the ratio of $\underline{R}_p^{-1}$ to $\underline{R}_q^{-1}$ (see Figure 4.25). Note that the expression, $\tilde{\underline{h}}_{11}$ and $\tilde{\underline{h}}_{22}$, in (1.5.1) has been linearized and is now state independent. This linearization, by using Couch's transformation and fast decoupling, appears to have stabilized the convergence of Bermundez and Brameller's fast decoupled scheme.

The theoretical convergence properties of decomposed Bermundez and Brameller-type modal fast decoupling is shown in (1.5.2). It appears that convergence will depend on the R/X ratio of the test system and on the relative values of $\underline{R}_p^{-1}$ to $\underline{R}_q^{-1}$. However simulation shows, in Figure 4.26, that the convergence is invariant with the R/X ratio of the test system and is invariant of the ratio of $\underline{R}_p^{-1}$ to $\underline{R}_q^{-1}$.

Note also that the theoretical convergence analysis for Bermundez and Brameller fast decoupling gives the same result or "form" as that for Couch et al.'s sequential decoupling. The only difference is that in Bermundez and Brameller's case a $\tilde{\underline{h}}$ is used instead of $\underline{h}$. Thus it would appear the two have similar properties, due to having similar algorithm structures, although simulation has shown this is not the case. What is different between the two methods of state estimation, which cannot be accounted for in the analysis, is that the measurement equations and Jacobian elements in Bermundez and Brameller's case have been linearized by fast decoupling and by use of Couch et al.'s transformation.

Table 4.7 Different Bermundez and Brameller type P-θ, Q-v decoupling possibilities and their convergence.

BERMUNDEZ AND BREMELLER P-θ, Q-v DECOUPLING SCHEMES	CONVERGENT EIGENVALUE EXPRESSIONS
1.5.1 Sequential formulation	
$[(\tilde{\underline{h}}_{11}^{T}\underline{R}_{p}^{-1}\tilde{\underline{h}}_{11})]\Delta\underline{\theta}_{k+1} = \tilde{\underline{h}}_{11}^{T}\underline{R}_{p}^{-1}[\underline{z}_{p} - \underline{h}_{p}(\underline{\theta}_{k},\underline{v}_{k})]\Big\|_{\substack{v=v_k \\ \theta=\theta_k}}$ $[(\tilde{\underline{h}}_{22}^{T}\underline{R}_{q}^{-1}\tilde{\underline{h}}_{22})]\Delta\underline{v}_{k+1} = \tilde{\underline{h}}_{22}^{T}\underline{R}_{q}^{-1}[\underline{z}_{q}' - \underline{h}_{q}'(\underline{\theta}_{k+1},\underline{v}_{k})]\Big\|_{\substack{v=v_k \\ \theta=\theta_{k+1}}}$	$\left[\begin{array}{c\|c} [\underline{I} - (\tilde{\underline{h}}_{11}^{T}\underline{R}_{p}^{-1}\tilde{\underline{h}}_{11})^{-1}(\tilde{\underline{h}}_{11}^{T}\underline{R}_{p}^{-1}\underline{h}_{11})]_{0} & -[(\tilde{\underline{h}}_{11}^{T}\underline{R}_{p}^{-1}\tilde{\underline{h}}_{11})^{-1}] \\ \hline -[(\tilde{\underline{h}}_{22}^{T}\underline{R}_{q}^{-1}\underline{h}_{22}')^{-1}(\underline{h}_{22}^{T}\underline{R}_{q}^{-1}\underline{h}_{21}')_{1} & [\underline{I} - (\tilde{\underline{h}}_{22}^{T}\underline{R}_{q}^{-1}\tilde{\underline{h}}_{22}')^{-1}[(\tilde{\underline{h}}_{22}^{T}\underline{R}_{q}^{-1}\underline{h}_{21}')_{1} - (\tilde{\underline{h}}_{22}^{T}\underline{R}_{q}^{-1}\tilde{\underline{h}}_{21}')_{1} \\ (\tilde{\underline{h}}_{11}^{T}\underline{R}_{p}^{-1}\tilde{\underline{h}}_{11})_{0}^{-1}(\tilde{\underline{h}}_{11}^{T}\underline{R}_{p}^{-1}\underline{h}_{12})_{0}] & (\tilde{\underline{h}}_{11}^{T}\underline{R}_{p}^{-1}\tilde{\underline{h}}_{11})_{0}^{-1}(\tilde{\underline{h}}_{11}^{T}\underline{R}_{p}^{-1}\underline{h}_{12})_{0}]] \end{array}\right]$
$[(\tilde{\underline{h}}_{11}^{T}\underline{R}_{p}^{-1}\tilde{\underline{h}}_{11})\ \Delta\underline{\theta}_{k+1} = \tilde{\underline{h}}_{11}^{T}\underline{R}_{p}^{-1}[\underline{z}_{p} - \underline{h}_{p}(\underline{\theta}_{k},\underline{v}_{o})]\Big\|_{\substack{v=v_o \\ \theta=\theta_k}}$ $[(\tilde{\underline{h}}_{22}^{T}\underline{R}_{q}^{-1}\tilde{\underline{h}}_{22})\ \Delta\underline{v}_{k+1} = \tilde{\underline{h}}_{22}^{T}\underline{R}_{q}^{-1}[\underline{z}_{q}' - \underline{h}_{q}'(\hat{\underline{\theta}},\underline{v}_{k})]\Big\|_{\substack{v=v_k \\ \theta\ \hat{\theta}}}$	For $\underline{\theta}_{k+1}$ $\quad [\underline{I} - (\tilde{\underline{h}}_{11}^{T}\underline{R}_{p}^{-1}\tilde{\underline{h}}_{11})^{-1}(\tilde{\underline{h}}_{11}^{T}\underline{R}_{p}^{-1}\underline{h}_{11})_{2}]$ For $\underline{v}_{k+1}$ $\quad [\underline{I} - (\tilde{\underline{h}}_{22}^{T}\underline{R}_{q}^{-1}\tilde{\underline{h}}_{22}')^{-1}(\tilde{\underline{h}}_{22}^{T}\underline{R}_{q}^{-1}\underline{h}_{22}')_{3}]$

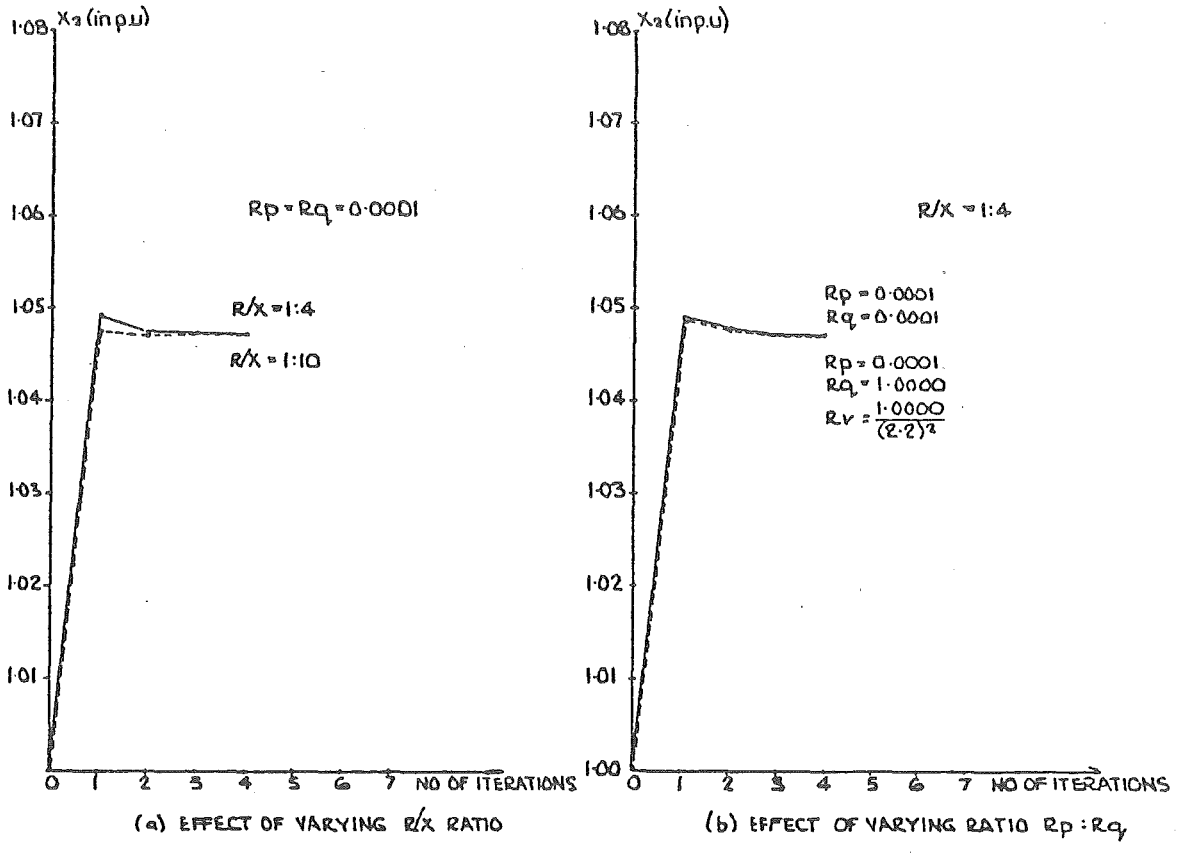

Figure 4.25 Bermundez and Brameller fast decoupling (1.5.1).

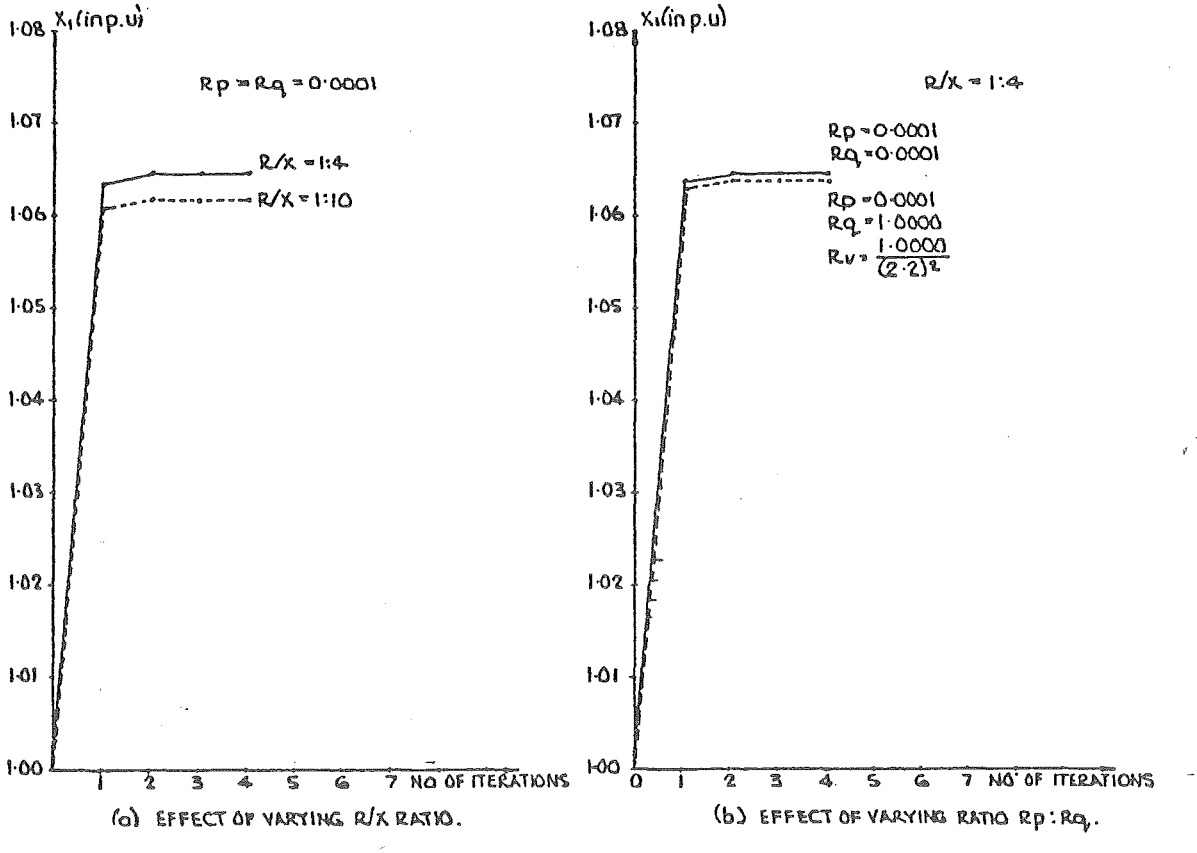

Figure 4.26 Bermundez and Brameller fast decoupling: decomposed (1.5.2).

4.5 ASSUMPTIONS INHERENT IN THE METHODS OF DECOUPLING PRESENTED

The significance of the departure of the P-θ, Q-v decoupling algorithm forms, presented in section 4.4 from exact W.L.S., depends on how well the following inherent assumption, made in the derivation of these algorithms, holds. The L.H.S. of Masiello and Horton and Garcia et al.-type decoupling algorithms will agree closely with the L.H.S. of the W.L.S. state estimation algorithm if, in practice,

$$\underline{h}_{11}^{T}\,\underline{R}_{p}^{-1}\,\underline{h}_{11} + \underline{h}_{21}^{T}\,\underline{R}_{q}^{-1}\,\underline{h}_{21} \gg \underline{h}_{11}^{T}\,\underline{R}_{p}^{-1}\,\underline{h}_{12} + \underline{h}_{21}^{T}\,\underline{R}_{q}^{-1}\,\underline{h}_{22}$$

and (4.72)

$$\underline{h}_{12}^{T}\,\underline{R}_{p}^{-1}\,\underline{h}_{12} + \underline{h}_{22}^{T}\,\underline{R}_{q}^{-1}\,\underline{h}_{22} \gg \underline{h}_{12}^{T}\,\underline{R}_{p}^{-1}\,\underline{h}_{11} + \underline{h}_{22}^{T}\,\underline{R}_{q}^{-1}\,\underline{h}_{21}$$

The L.H.S. and R.H.S. of Horisberger et al. and the R.H.S. of Garcia et al., and subsequently Bermundez and Brameller, will closely agree with the L.H.S. and R.H.S., and the R.H.S. respectively of the W.L.S. algorithm, if

$$\underline{h}_{11} \gg \underline{h}_{21}$$

and $\underline{h}_{22} \gg \underline{h}_{12}$ (4.73)

and $\underline{R}_{p} \simeq \underline{R}_{q}$

Thus the decoupling assumes that the relative weightings, given to the real and reactive measurements, are of a similar order of magnitude and the R/X ratio of the power system is small so that (4.73) holds. Fast decoupled expressions like Bermundez and Brameller also rely on the nodal voltages, v, being approximately 1 p.u. and on the angle difference, $(\theta_i - \theta_j)$, being approximately zero.

4.6 ACCURACY OF THE P-θ, Q-v DECOUPLING SCHEMES

In section 4.4 it was noted that the P-θ, Q-v decoupling schemes given by (1.1.1) - (1.1.4) and (1.2.1) - (1.2.4) converge to the same optimal solution as that given by W.L.S. The remaining schemes converge to suboptimal estimates. In this section the accuracy of these sub-optimal algorithms, with and without nominal measurement noise $<3\sigma$ present, will be considered. The suboptimal estimates, presented in Table 4.8, result from the convergence of stable P-θ, Q-v algorithm decoupled schemes when all voltage magnitude and real and reactive injection and line-flow power measurements taken around the 5-bus test system are present. Decoupling schemes not shown in Table 4.8 are unstable and do not, in fact, converge. Exact estimates are given by the convergence of Horisberger et al. sequential decoupling (1.1.2) and Masiello and Horton sequential decoupling (1.2.2). Algorithm type P-θ, Q-v decoupling (Couch et al., Garcia et al., and Bermundez and Brameller) causes only a slight loss of optimality in the estimates. The degree of suboptimality proves independent of the ratio of $\underline{R}_{p}^{-1}$ to $\underline{R}_{q}^{-1}$ and only slightly dependent on the R/X ratio of the test system.

Decomposed P-θ, Q-v decoupling causes a marked loss of optimality, however, and excludes its implementation, with the possible exception of the Garcia et al. decomposed decoupling technique, (1.4.5) or (1.4.6), when processing only "injection and voltage" measurements sets. The Results in Table 4.8 show a degradation in the optimality of the decomposed estimates when line-flow measurements are included in the decomposed estimator, as noted by Singh et al.

Note that loss of optimality for the algorithm-decoupled schemes depends on how well the decoupling assumptions outlined in section 4.5 are satisfied. This is because, for the optimal schemes where decoupling

Table 4.8 Accuracy of stable suboptimal estimation schemes.

		EXACT SEQUENTIAL METHODS		SUBOPTIMAL SEQUENTIAL			SUBOPTIMAL UNIFIED			SUBOPTIMAL DECOMPOSED DECOUPLING				
		MASIELLO AND HORTON (CONST. GAIN) (1.2.4)	HORISBERGER ET AL. (1.1.2)	GARCIA ET AL. (CONST. GAIN) (1.3.4)	COUCH ET AL. (1.4.2)	BERMUNDEZ AND BRAMELLER (1.5.1)	COUCH ET AL. (1.4.1)			MASIELLO AND HORTON (1.2.5)	GARCIA ET AL. (CONST. GAIN) (1.3.6)	COUCH ET AL. (1.4.5)	COUCH ET AL. (CONST. GAIN) (1.4.6)	BERMUNDEZ AND BRAMELLER (1.5.3)
R/X = 1:10 $\underline{R}_p^{-1}:\underline{R}_q^{-1}$ = 1:1 NO MEASUREMENT NOISE $\begin{bmatrix} 5V_1 \\ 5(P_i+Q_i) \\ 14(P_{ij}+Q_{ij}) \end{bmatrix}$	θ_1	0.0	0.0	0.0	0.0	0.0	0.0	R/X = 1:10 $\underline{R}_p^{-1}:\underline{R}_q^{-1}$ = 1:1 NO MEASUREMENT NOISE $\begin{bmatrix} 5V_1 \\ 5(P_i+Q_i) \\ 14(P_{ij}+Q_{ij}) \end{bmatrix}$	θ_1	0.0	0.0	0.0	0.0	0.0
	θ_2	-0.16179	-0.16179	-0.16179	-0.16192	-0.16183	-0.16180		θ_2	-0.18209	-0.18005	-0.18005	-0.18005	-0.18004
	θ_3	-0.30192	-0.30192	-0.30193	-0.30213	-0.30197	-0.30193		θ_3	-0.32769	-0.33029	-0.33029	-0.33029	-0.33025
	θ_4	-0.32121	-0.32122	-0.32123	-0.32141	-0.32126	-0.32123		θ_4	-0.34709	-0.34918	-0.34918	-0.34918	-0.34915
	θ_5	-0.37156	-0.37156	-0.37157	-0.37180	-0.37159	-0.37157		θ_5	-0.39907	-0.40111	-0.40111	-0.40111	-0.40112
	V_1	1.05989	1.05987	1.05986	1.05946	1.05973	1.05987		V_1	1.02329	1.05737	1.05728	1.05729	1.06178
	V_2	1.04689	1.04687	1.04686	1.04649	1.04676	1.04687		V_2	1.01245	1.04308	1.04293	1.04294	1.04730
	V_3	0.98481	0.98480	0.98478	0.98471	0.98499	0.98479		V_3	0.95226	0.98189	0.98176	0.98176	0.98628
	V_4	0.98735	0.98734	0.98732	0.98729	0.98757	0.98733		V_4	0.95538	0.98483	0.98473	0.98474	0.98922
	V_5	0.97814	0.97813	0.97812	0.97816	0.97845	0.97812		V_5	0.94710	0.97515	0.97514	0.97514	0.97962
R/X = 1:4 $\underline{R}_p^{-1}:\underline{R}_q^{-1}$ = 1:1 NO MEASUREMENT NOISE $\begin{bmatrix} 5V_1 \\ 5(P_i+Q_i) \\ 14(P_{ij}+Q_{ij}) \end{bmatrix}$	θ_1	0.0	0.0	0.0	0.0	0.0	0.0	R/X = 1:4 $\underline{R}_p^{-1}:\underline{R}_q^{-1}$ = 1:1 NO MEASUREMENT NOISE $\begin{bmatrix} 5V_1 \\ 5(P_i+Q_i) \\ 14(P_{ij}+Q_{ij}) \end{bmatrix}$	θ_1	0.0	0.0	0.0	0.0	0.0
	θ_2	-0.06454	-0.06454	-0.06454	-0.06453	-0.06453	-0.06454		θ_2	-0.07226	-0.07493	-0.07493	-0.07493	-0.07493
	θ_3	-0.11664	-0.11664	-0.11664	-0.11666	-0.11666	-0.11664		θ_3	-0.12822	-0.13740	-0.13740	-0.13740	-0.13741
	θ_4	-0.12427	-0.12427	-0.12426	-0.12428	-0.12428	-0.12426		θ_4	-0.13623	-0.14544	-0.14544	-0.14544	-0.14544
	θ_5	-0.14348	-0.14348	-0.14348	-0.14350	-0.14350	-0.14348		θ_5	-0.15632	-0.16718	-0.16718	-0.16718	-0.16719
	V_1	1.06005	1.06004	1.06005	1.06002	1.06003	1.06005		V_1	1.02206	1.06388	1.06389	1.06390	1.06477
	V_2	1.04705	1.04705	1.04706	1.04696	1.04696	1.04705		V_2	1.00885	1.04814	1.04806	1.04806	1.04891
	V_3	1.02017	1.02017	1.02017	1.02019	1.02019	1.02017		V_3	0.98153	1.01918	1.01916	1.01917	1.02002
	V_4	1.01992	1.01992	1.01992	1.01993	1.01993	1.01992		V_4	0.98134	1.01892	1.01889	1.01890	1.01974
	V_5	1.01379	1.01379	1.01380	1.01380	1.01381	1.01380		V_5	0.97510	1.01198	1.01195	1.01196	1.01280
R/X = 1:4 $\underline{R}_p^{-1}:\underline{R}_q^{-1}$ = 1:1000 NO MEASUREMENT NOISE $\begin{bmatrix} 5V_1 \\ 5(P_i+Q_i) \\ 14(P_{ij}+Q_{ij}) \end{bmatrix}$	θ_1	DIVERGE	DIVERGE	NO CONVERGENCE IN 20 ITER.	0.0	0.0	0.0	R/X = 1:4 $\underline{R}_p^{-1}:\underline{R}_q^{-1}$ 1:1000 NO MEASUREMENT NOISE $\begin{bmatrix} 5V_1 \\ 5(P_i+Q_i) \\ 14(P_{ij}+Q_{ij}) \end{bmatrix}$	θ_1	0.0	NO CONVERGENCE IN 15 ITER.	0.0	0.0	0.0
	θ_2				-0.06452	-0.06453	-0.06453		θ_2	-0.07493		-0.07493	-0.07493	-0.07493
	θ_3				-0.11666	-0.11666	-0.11664		θ_3	-0.13740		-0.13740	-0.13740	-0.13741
	θ_4				-0.12428	-0.12428	-0.12426		θ_4	-0.14543		-0.14538	-0.14544	-0.14544
	θ_5				-0.14350	-0.14350	-0.14348		θ_5	-0.16717		-1.16718	-0.16718	-0.16719
	V_1				1.06002	1.06004	1.06005		V_1	0.98667		1.06370	1.06370	1.06388
	V_2				1.04697	1.04698	1.04705		V_2	0.97464		1.04790	1.04791	1.04807
	V_3				1.02020	1.02020	1.02017		V_3	0.95604		1.01904	1.01904	1.01920
	V_4				1.01994	1.01994	1.01992		V_4	0.95315		1.01877	1.01878	1.01893
	V_5				1.01382	1.01383	1.01380		V_5	0.94397		1.01185	1.01185	1.01201
R/X = 1:4 $\underline{R}_p^{-1}=\underline{R}_q^{-1}$ = 1:1 NOMINAL MEASUREMENT NOISE <3σ $\begin{bmatrix} 5V_1 \\ 5(P_i+Q_i) \\ 14(P_{ij}+Q_{ij}) \end{bmatrix}$	θ_1	0.0	0.0	0.0	0.0	0.0	0.0	R/X = 1:4 $\underline{R}_p^{-1}:\underline{R}_q^{-1}$ = 1:1 NO MEASUREMENT NOISE $\begin{bmatrix} 5V_1 \\ 5(P_i+Q_i) \end{bmatrix}$	θ_1	0.0	0.0	0.0	0.0	0.0
	θ_2	-0.06420	-0.06419	-0.06420	-0.06419	-0.06420	-0.06420		θ_2	-0.07306	-0.07484	-0.05448	-0.05448	-0.07485
	θ_3	-0.11594	-0.11593	-0.11596	-0.11598	-0.11599	-0.11596		θ_3	-0.12933	-0.13726	-0.10756	-0.10756	-0.13727
	θ_4	-0.12326	-0.12325	-0.12328	-0.12329	-0.12330	-0.12328		θ_4	-0.13749	-0.14530	-0.11384	-0.11384	-0.14531
	θ_5	-0.14112	-0.14112	-0.14108	-0.14111	-0.14112	-0.14107		θ_5	-0.15783	-0.16700	-0.13371	-0.13371	-0.16701
	V_1	1.06303	1.06304	1.06306	1.06303	1.06297	1.06314		V_1	1.02603	1.06365	1.05833	1.05833	1.06406
	V_2	1.05067	1.05068	1.05071	1.05059	1.05052	1.05079		V_2	1.01325	1.04814	1.04761	1.04761	1.04849
	V_3	1.02384	1.02385	1.02387	1.02385	1.02379	1.02396		V_3	0.98626	1.01944	1.02008	1.02009	1.01975
	V_4	1.02397	1.02398	1.02400	1.02397	1.02390	1.02409		V_4	0.98620	1.01930	1.02006	1.02006	1.01960
	V_5	1.01888	1.01890	1.01894	1.01893	1.01886	1.01901		V_5	0.98035	1.01245	1.01358	1.01358	1.01273

only affects the information matrix on the L.H.S. of (2.22), the condition for a minimum is given by

$$\left.\frac{\partial J(\underline{x})}{\partial \underline{x}}\right|_{\underline{x}=\hat{\underline{x}}} = \underline{H}^T(\hat{\underline{x}})\ \underline{R}^{-1}\ (\underline{z} - \underline{h}(\hat{\underline{x}})) = 0 \qquad (4.74)$$

whereas for the suboptimal, algorithm decoupled schemes this minimum is observed to be

$$\left.\frac{\partial J(\underline{x})}{\partial \underline{x}}\right|_{\underline{x}=\hat{\underline{x}}} = \underline{H}^T(\hat{\underline{x}})\ \underline{R}^{-1}\ (\underline{z}' - \underline{h}'(\hat{\underline{x}})) = 0 \qquad (4.75)$$

Clearly the distance between the true minimum and the suboptimal minimum depends on how closely $\underline{H}^T(\hat{\underline{x}})$ resembles $\underline{H}^T(\underline{x})$ and on how closely $\underline{h}'(\underline{x})$ and $\underline{z}'$ are to $\underline{h}(\underline{x})$ and $\underline{z}$.

4.7 CONCLUSION

Numerous P-θ, Q-v decoupling techniques have been suggested in the literature to be applied to power system state estimation in order to reduce the computational burden associated with W.L.S. No attempt has been made, however, to analyse the convergence and degree of optimality of these possible decoupling schemes and test their performance using a standard problem. Most P-θ, Q-v decoupling techniques assume that the R/X ratio of the test power system is small and that the relative weighting, or variance, of the real and reactive power and voltage measurements are similar. However, in practice, the data acquisition system serving the state estimator may have evolved over a number of years and have monitoring equipment of varying accuracy present. It is also likely that the R/X ratio of transmission line within the power system will vary, and thus it is important to establish how the proposed P-θ, Q-v decoupling schemes fare under such conditions. Simulations showed some of the possible decoupling schemes to be stable

while others diverged as the R/X ratio of the test power system and the relative values of $\underline{R}_p^{-1}$ and $\underline{R}_q^{-1}$ were varied. Tests also indicate that the most suitable method for implementation in power systems is the fast P-θ, Q-v decoupled-type decoupling technique proposed by Bermundez and Brameller (1978). The "inherent" stability of this decoupling method appears to result from the "linearization" of the reactive power measurement equations and their Jacobian elements by applying Couch's (1976) transformation. The fast decoupling is also carried out in a manner akin to Stott's fast decoupled load flow and the resulting algorithm, having constant matrices that do not require updating, has a stable convergence, unaffected by either changes in the ratio of $\underline{R}_p^{-1}$ to $\underline{R}_q^{-1}$ or the R/X ratio of the test system. Although the technique is suboptimal, the loss of optimality is insignificant, being typically <0.001 p.u.

The method of examining the eigenvalue expressions determining convergence has been shown to be very useful for establishing dependence in the different structured P-θ, Q-v decoupled state estimation schemes. The method, however, cannot differentiate subtleties within each structure caused by differences in linearity of the measurement set.

Bermundez and Brammeler's fast decoupled state estimation technique (1.5.1) has the same structure as Couch et al.'s (1974) method of decoupling (1.4.2). Yet without going into the actual Jacobian elemental values, the eigenvalue-convergence property method would predict similar convergent properties for both schemes. Eigenvalue based convergence analysis can highlight decoupling schemes whose convergence is very dependent on either the $\underline{R}_p^{-1}$ to $\underline{R}_q^{-1}$ ratio for the R/X ratio of the power system, eliminating the need for simulation in such cases.

CHAPTER 5

FAST DECOUPLED STATE ESTIMATION WITH PSEUDO LINE-FLOW CREATION FROM INJECTION MEASUREMENTS

5.1 INTRODUCTION

In Chapter 3 the A.E.P. "line-only" algorithm was compared with the more versatile W.L.S. algorithm. W.L.S. was found to be very slow, with speed disadvantages resulting from the following:

(1) The use of injection measurements in the state estimator degrades sparsity. This problem can be overcome by using the pseudo line-flow creation technique outlined in Chapter 3 to provide a sparse, "admittance-like" information matrix structure.

(2) The Jacobian matrices in the state estimator require repeat evaluation at each iteration. In Chapter 4, decoupling and fast decoupling schemes were reviewed and "stable" methods identified. Fast decoupling the Jacobian matrix along the lines of Bermundez and Brameller (1978) produces constant Jacobian matrices containing only half the original, non-zero values. While estimates are suboptimal, in practice they are very close to the true solution. If optimality is required, the fast decoupling techniques of Horisberger *et al.* (1976) or Masiello and Horton (1977) can be used to give constant gain matrices in the information matrix, and retain optimality.

In this chapter the pseudo line-flow creation technique is applied to Bermundez and Brameller's fast decoupled state estimator. The resulting

constant gain algorithm has the same structure and properties as the A.E.P. "line-only"algorithm (see Table 5.1).

Table 5.1 Comparison of W.L.S. and A.E.P. "line-only" method when pseudo line-flow creation is used.

	LINEAR (no repeat evaluation of gain matrices)	NON-LINEAR (repeat evaluation of gain matrices)
Sparse "admittance matrix" like information Matrix structure	(i) A.E.P. (ii) A.E.P. with injections handled by pseudo lineflow creation. (iii) Fast Decoupled W.L.S. with injections handled by Pseudo line flow creation.	W.L.S. with injections handled by pseudo line flow creation.
Variable Information matrix structure. Depends on the # of injections.	(i) A.E.P. with injections handled by other methods. (ii) Fast Decoupled W.L.S.	W.L.S.

5.2 PERFORMANCE OF FAST DECOUPLED W.L.S. STATE ESTIMATION WITH PSEUDO LINE-FLOW CREATION

The performance of fast decoupled W.L.S. state estimation with variance conditioned pseudo line-flow creation is summarised in Table 5.2. The five bus test system used in Section 3.7 was used in the tests. Fast decoupling assumes the power system R/X ratio to be small; however convergence is only slightly affected as the R/X ratio is varied. Convergence is affected by the p:k ratio of the measurement system. Estimates in the table resulting from fast decoupled W.L.S. with variance conditioned pseudo line-flows closely agree with the load flow estimates.

The performance of the fast decoupled variance conditioned pseudo line-flow W.L.S. state estimation scheme was also investigated using Irvings' (1978) 30 bus - 40 line test system. Two hundred and fifty measurements and 59 states were present. The R/X ratio of the lines

Table 5.2 Performance of fast decoupled W.L.S. with pseudo line-flow creation (measurement noise-free).

		FAST DECOUPLED W.L.S. WITH VARIANCE CONDITIONED PSEUDO LINE FLOW CREATION						LOAD FLOW ESTIMATES (THAT PROVIDE INITIAL S.E. DATA)		
	SYSTEM R/X RATIO	1:4	1:4	1:4	1:4	1:10	1:3	1:4	1:10	1:3
	PSEUDO LINE FLOW VARIANCE CONDITIONING	$\sigma^{2,2}_{z_{ij}}=(2\sigma_{z_i})^2$	$\sigma^{2,}_{z_{ij}}=(3\sigma_{z_i})^2$	$\sigma^{2,}_{z_{ij}}=(4\sigma_{z_i})^2$	$\sigma^{2,}_{z_{ij}}=(3\sigma_{z_i})^2$	$\sigma^{2,}_{z_{ij}}=(3\sigma_{z_i})^2$	$\sigma^{2,}_{z_{ij}}=(3\sigma_{z_i})^2$	NONE USED	NONE USED	NONE USED
	MEASUREMENT CONFIGURATION (m:k)	$5v_i$ $14P_{ij}+14Q_{ij}$ $5P_i+5Q_i$	$5v_i$ $14P_{ij}+14Q_{ij}$ $5P_i+5Q_i$	$5v_i$ $14P_{ij}+14Q_{ij}$ $5P_i+5Q_i$	$5v_i$ $7P_{ij}+7Q_{ij}$ $5P_i+5Q_i$	$5v_i$ $14P_{ij}+14Q_{ij}$ $5P_i+5Q_i$	$5v_i$ $14P_{ij}+14Q_{ij}$ $5P_i+5Q_i$			
NO. OF ITERATIONS TO CONVERGE	< 0.001 p.u.	13v + 13θ	8v + 8θ	6v + 6θ	11v + 11θ	6v + 6θ	8v + 8θ			
	< 0.0001 p.u.	9v + 10θ	6v + 6θ	5v + 5θ	8v + 9θ	5v + 5θ	6v + 6θ			
	< 0.00001 p.u.	5v + 6θ	4v + 4θ	4v + 3θ	5v + 6θ	4v + 4θ	4v + 4θ			
ESTIMATE	θ_1	0.0	0.0	0.0	0.0	0.0	0.0	0.0	0.0	0.0
	θ_2	-0.06451	-0.06451	-0.06451	-0.06451	-0.16189	-0.04880	-0.06434	-0.16175	-0.04895
	θ_3	-0.11668	-0.11669	-0.11669	-0.11669	-0.30208	-0.08716	-0.11665	-0.30185	-0.08714
	θ_4	-0.12430	-0.12430	-0.12431	-0.12431	-0.32137	-0.09294	-0.12426	-0.32114	-0.09293
	θ_5	-0.14352	-0.14353	-0.14353	-0.14355	-0.31171	-0.10728	-0.14350	-0.37147	-0.10726
	V_1	1.06001	1.06000	1.05999	1.05999	1.05953	1.06007	1.060	1.060	1.060
	V_2	1.04688	1.04684	1.04682	1.04684	1.04647	1.04691	1.047	1.047	1.047
	V_3	1.02024	1.02027	1.02028	1.02023	0.98517	1.02397	1.020	0.989	1.024
	V_4	1.01997	1.01999	1.02000	1.01995	0.98775	1.02331	1.020	0.987	1.023
	V_5	1.01385	1.01387	1.01388	1.01397	0.97861	1.01763	1.014	0.978	1.018

5 bus test system used.

within the test system varied from 1:2.5 to 1:12. Table 5.3 summarises the test results. A speed advantage of more than 2:1 occurs when variance conditioned pseudo line-flow creations are used to represent injection measurements in fast decoupled W.L.S. and when all injection measurements possible are present. Bermundez and Brameller (1978) report that when 10% of all possible injection measurements are added to a "line-only" set, the time per iterations to execute their fast decoupling technique increases by 58%. Without pseudo line-flow creation to handle injection measurements, Bermundez and Brameller's technique, like all P-θ Q-v decoupling techniques, suffers from the increased information matrix density effect outlined in Section 3.7, as injection measurements are added.

5.3 CONCLUSION

Pseudo line-flow creation can be included in the Fast P-θ, Q-v Decoupled W.L.S. to make an extremely fast state estimator, particularly when significant numbers of injection measurement are included. Fast decoupled W.L.S. with pseudo line-flow creation is similar to the A.E.P. "line-only" algorithm. Both have sparse constant gain matrices. Yet fast decoupled W.L.S. with pseudo line-flow creation can handle injection measurements without losing sparsity. The pseudo line-flow creation technique outlined could also be applied to the A.E.P. method to preserve sparsity when handling injection measurement mixes.

Table 5.3 30 bus test system performance of fast decoupled W.L.S. with pseudo line-flow creation.

	250 measurements/59 states : $30v_i + 80P_{ij} + 80Q_{ij} + 30P_i + 3Q_i$		
	W.L.S. WITH INJECTION MEASUREMENTS WITH VARIANCE CONDITIONING $\sigma'^2_{ij} = (10\sigma_{z_i})^2$	FAST DECOUPLED W.L.S. WITH VARIANCE CONDITIONED INJECTION MEASUREMENTS $\sigma'^2_{ij} = (10\sigma_{z_i})^2$	FAST DECOUPLED W.L.S. WITH VARIANCE CONDITIONED PSEUDO LINE FLOW CREATION $\sigma'^2_{ij} = (10\sigma_z)^2$
CONVERGENCE	4 iterations <0.00001 p.u. 3 iterations <0.0001 p.u. 3 iterations <0.001 p.u.	12θ+12v <0.00001 p.u. 7θ+7v <0.0001 p.u. 5θ+5v <0.001 p.u.	12θ+12v <0.00001 p.u. 7θ+7v <0.0001 p.u. 5θ+5v <0.001 p.u.
TIME PER ITERATION	9.6 seconds per iteration	5.6 seconds per θ+v iteration	2.3 seconds per θ+v iteration

Time per iteration figures also include a small % of the time spent reading pointers in.

CHAPTER 6

FAST IDENTIFICATION OF BAD DATA IN POWER SYSTEM TRACKING STATE ESTIMATION

6.1 INTRODUCTION

State estimators are used to provide a reliable data base, free from bad data that can be used for dispatching, monitoring or control on the power system. Bad data detection, identification and treatment of the bad data points after identification are an important aspect of the "on-line" state estimator. Garcia *et al.* (1979) note that a monitoring system of 500 measurements or more, each measurement having a 0.1 per cent probability of bad data occurrence, implies an average of one gross error will occur for every state estimator run. It becomes important to detect efficiently, identify and suppress the bad data. Simple techniques that do this are outlined in this paper. These bad data detection and identification techniques do not involve re-calculation of gain matrices in the state estimator equation. The performance of the suggested technique is evaluated on a test system having varying degrees of observability when single and multiple bad data are present.

Bad data suppression based on the use of non-quadratic criteria (Merrill and Schweppe, 1971) is not investigated. Such suppression techniques may generate many local minima. Potential difficulties can also arise when constant gain-matrices are used in state estimators having bad data suppression facilities.

6.2 BAD DATA DETECTION AND IDENTIFICATION

After each measurement scan the estimates from an "on-line" state estimator are checked for bad data (Handschin *et al.*, 1975; Schweppe *et al.*, 1970; Schweppe and Handschin, 1974).

6.2.1 $J(\underline{x})$ test - evaluate the scalar quantity:

$$J = (\underline{z} - \underline{h}(\underline{x}))^T \underline{R}^{-1} (\underline{z} - \underline{h}(\underline{x})) = \sum_{L=1}^{M} (r_i/\sigma_i)^2 \qquad (6.1)$$

where $r_i = z_i - h_i(\underline{x})$ (6.2)

6.2.2 Weighted residual test, $\underline{r}_w$

$$\underline{r}_w = \sqrt{\underline{R}^{-1}}\, \underline{r}(\underline{x}) \qquad (6.3)$$

where $\underline{r}(\underline{x}) = \underline{z} - \underline{h}(\underline{x})$ (6.4)

6.2.3 Normalised residual test, $\underline{r}_N$

$$\underline{r}_N = \sqrt{\underline{D}^{-1}(\underline{x})}\, \underline{r} \qquad (6.5)$$

where $\underline{D}(\underline{x}) = \text{diag}\, \underline{\Sigma}_r(\underline{x})$ (6.6)

$\underline{\Sigma}_r(\underline{x})$ is the residual co-variance matrix,

$$\underline{\Sigma}_r(\underline{x}) = \underline{W}(\underline{x})\, \underline{r}(\underline{x}) \qquad (6.7)$$

and $\underline{W}(\underline{x})$ is the residual sensitivity matrix,

$$\underline{W}(\underline{x}) = \underline{I} - \underline{H}(\underline{x})\, \underline{\Sigma}_x(\underline{x})\, \underline{H}^T(\underline{x})\, \underline{R}^{-1} \qquad (6.8)$$

where $\underline{\Sigma}_x(\underline{x})$ is the estimation co-variance matrix,

$$\underline{\Sigma}_x(\underline{x}) = (\underline{H}^T(\underline{x})\, \underline{R}^{-1}\, \underline{H}(\underline{x}))^{-1} \quad . \qquad (6.9)$$

Handschin *et al.* (1975) found the $\underline{r}_N$ test to be more effective than the $\underline{r}_w$ test in all cases. The $\underline{r}_w$ test also identifies single bad data points and is more effective than the $J(\underline{x})$ when single bad data is present. However, the $J(\underline{x})$ test was found to be sometimes better than the $\underline{r}_N$ test when multiple interacting or non-interacting bad data is present. Appendix A.6 outlines an example that contains multiple interacting bad data. Handschin *et al.* (1975) recommend using either the "$J(\underline{x})$ test and the $\underline{r}_w$ test" or the "$J(\underline{x})$ test and the $\underline{r}_N$ test" for detection. Detection occurs if either test of a pair fails. Identification simply involves removing suspect measurements and re-estimating. Using the ordered residual search, suspect measurements are arranged in order of their decreasing weighted residuals $\underline{r}_w$ or normalised residuals $\underline{r}_N$. A measurement or a block of measurements having the largest residuals $\underline{r}_w^{max}$ or $\underline{r}_N^{max}$ is removed first. If only one bad data point is present, r_N^{max} identifies the bad data location. The removal and re-estimation procedure must be repeated until the bad data is identified.

Removal of suspect measurements and re-estimation during the identification of bad data involves re-evaluating all matrices in the W.L.S. state estimation algorithm. Merlin and Broussolle (1977) advocated using the Sherman-Morrisson formulae to "update" the matrices involved in the calculation of the residual error co-variance, $\underline{\Sigma}_r(\underline{x})$, given by equation (6.7).

Updating $\underline{\Sigma}_r(\underline{x})$ takes less time than the complete re-evaluation of $\underline{\Sigma}_r(\underline{x})$ during the identification. Sparse matrix inversion techniques (Broussolle, 1977) were also used to calculate the error co-variance matrix, $\underline{\Sigma}_x(\underline{x})$, used in the calculation of $\underline{\Sigma}_r(\underline{x})$.

An identification method that does not require the re-evaluation of matrices each time a suspect measurement is removed has recently been

suggested by Duran (1977). He advocates a Linear Complex Model as the basis for state estimation. "Surrogate" measurements can then be used to represent the removal of suspect measurements. No re-triangularization of gain matrices is necessary. However transformations are required to express the non-linear measurements, shown in equation (2.15), in linear complex form. If estimate optimality is to be retained, state-dependent transformations that require re-evaluation at each iteration must be used.

For fast detection and identification of bad data, the "$J(\underline{x}) + \underline{r}_w$" test pair should be used rather than the $\underline{r}_N$ and $\underline{\Sigma}_r(\underline{x})$ pair. In addition a mathematical "removal" technique, outlined below, can be used to remove the effect of suspect bad data. The mathematical "removal" does not reduce the dimension of matrices in the W.L.S. state estimation algorithm and thus no re-ordering and re-evaluation of lists and pointers is necessary. The mathematical removal technique is precisely equivalent to physical removal of suspect bad data (see Appendix A.7). The technique simply involves setting

$$(z_i^{bad} - h_i(\underline{x}^k)) = 0 \quad \text{at each iteration, } k, \tag{6.10}$$

at the suspect bad data location z_i^{bad}, in the R.H.S. of equation (2.22). This is equivalent to replacing

$$z_i^{bad} \xrightarrow{\text{replace}} h_i(\underline{x}^k)$$

and updating the relationship at each iteration, k.

No notice is now taken of the suspect measurement, z_i^{bad}, when computing state estimates. During bad data identification, only constant gain matrices on the left-hand side of equation (2.22) are required. The mathematical "removal" technique does not affect the gain matrices and so no re-triangularization of the left-hand side of equation

(2.22) is necessary when identifying bad data. After identification of the bad data, the relationship given by equation (6.10) can be enforced at the bad data locations until the faulty measurements are repaired or recommissioned. Re-ordering of lists due to a change in the dimension of equation (2.22), caused by a change in the number of measurements present in the state estimator, is no longer necessary.

In some circumstances "removal" of suspect bad data may cause loss of observability to the state estimator. In these "marginal-observability" situations "replacement" of suspect bad data by a pseudo-measurement must be used instead. Simple techniques based on information from the previous scan can be used. Methods include replacing

$$z_i^{bad} \xrightarrow{\text{replace}} z_{i_{previous}} \tag{6.11}$$

$$z_i^{bad} \xrightarrow{\text{replace}} h_i(\underline{x}_{previous}) \tag{6.12}$$

where $z_{i_{previous}}$ is the measurement of z_i, taken at the previous scan; and $\underline{z}_{previous}$ is the estimate resulting from processing measurements, at the previous scan. Provided the power system is not rapidly changing, between measurement scans, simple "replacement" methods can be used to identify bad data.

Garcia *et al.* (1979) proposed a technique to "replace" bad data after identification. The normalised residual test, $\underline{r}_N$, is used to identify the bad data by "removal" of suspect bad data. The bad data z_i^{bad} is then "replaced" by a pseudomeasurement, z_i^{new}, where

$$z_i^{new} = z_i^{bad} - \sigma_i^2/\ell_{ii}(z_i^{bad} - z_i^{estimate}) \tag{6.13}$$

and

$$\ell_{ii} = (\underline{\Sigma}_r(\underline{x}))_{ii} \tag{6.14}$$

$$\sigma_i^2 = \underline{R}_{ii} \tag{6.15}$$

Only "replacement" of bad data is necessary when "removal" would cause a loss of observability to the state estimates. Garcia *et al.*'s (1979) technique also involves evaluating $\underline{\Sigma}_r(\underline{x})_{ii}$.

6.3 TEST RESULTS

The 5 bus-7 line test system shown in Figure 3.3, taken from Stagg and El-Abiad (1968), is used in the tests. Each state estimator run comprises two measurement scans. Measurements are initially formed by perturbing load flow results by normal measurement noise ($<3\sigma_i$). These measurements are then processed to generate state estimates, $\underline{x}_{s1}$. Estimates are then modified to represent the state of the system at the next scan, $\underline{x}_{s2}$. The modification reflects random power system dynamics, which causes states to change between successive measurement scans, and is made by adding a fraction, αR_N, of a uniformly-distributed random number R_N, where $|R_N|<3$. Measurements for the second scan are formed by computing $\underline{h}(\underline{x}_{s2})$, "noise free" measurements similar to a load flow, and then adding uniformly-distributed noise $<3\sigma_i$. Adding measurement noise $>>3\sigma_i$ to selected measurements in $h_i(\underline{x}_{s2})$ simulates the effects of bad data. The noisy measurements are then processed to generate state estimates for the second scan, $\underline{x}_{s2}$. $J(\underline{x}_{s2})$ and $\underline{r}_w$ are also evaluated.

Two different measurement sets were used for the tests:

(1) A "strong", highly redundant set where all measurements possible are used, i.e.

5 voltage magnitudes

14 real and reactive line flows

5 real and reactive injections.

(2) A "weaker", moderately redundant set containing:

1 voltage magnitude

7 real and reactive line flows

5 real and reactive injections.

6.3.1 Verification of the "mathematical removal" technique for handling suspect bad data.

Measurement system 1 was used with bad data, size 20σ, present in the measurement of P_{2-4} and P_4. After estimation, with the bad data present, $z_{p_i}^{BAD} - h_{p_i}(\underline{x}_k)$ was set to zero and the state estimator further iterated. The resulting estimates, together with the estimates that result when P_{2-4} and P_4 are "physically" removed and re-estimation occurs, are shown in Table 6.1. Both estimates are the same. Moreover, no degradation in convergence occurs when the "mathematical removal" technique is used.

6.3.2 Performance of bad data handling techniques.

The performance of the bad data handling techniques outlined in equations (6.10), (6.11) and (6.12) is compared for different random rates of change in states between successive measurement scans; $\alpha = 0.005$ and $\alpha = 0.001$ are used. The resulting change in states, αR_N, between successive measurement scans is shown in Table 6.2. Changes in power of 0.400 MW p.u. and 0.080 MVAR p.u. for $\alpha = 0.005$ and 0.001 occur as a result of these changes in state.

During the second measurement scan, gross errors of 20σ are present in the measurement of P_{2-4} and P_4 for measurement system 1, and a gross error of 10σ is present in the measurement of P_1 for measurement system 2. The performance of the bad data handling techniques after detection is shown in Table 6.3. The estimates shown

Table 6.1 Comparison between estimates after mathematical and physical bad data removal.

	ESTIMATE (MATHEMATICAL BAD DATA) REMOVAL	ESTIMATE (PHYSICAL BAD DATA) REMOVAL
δ_1	0.0	0.0
v_1	1.0634366	1.0634376
δ_2	-0.0479648	-0.0479654
v_2	1.0584563	1.0584560
δ_3	-0.0699121	-0.0699095
v_3	1.0322575	1.0322613
δ_4	-0.0903039	-0.0903015
v_4	1.0404151	1.0404186
δ_5	-0.1030138	-0.1030123
v_5	1.0232142	1.0232169

Table 6.2 Change in power system states between successive measurement scans.

	(X_2-X_1) p.u. α=0.005	(X_2-X_1) p.u. α=0.001
$\Delta\delta_1$	-0.0019230	-0.0003846
Δv_1	-0.0038852	-0.0007767
$\Delta\delta_2$	-0.0019339	-0.0004849
Δv_2	0.0042091	0.0008459
$\Delta\delta_3$	0.0149348	0.0025870
Δv_3	-0.0006046	-0.0001430
$\Delta\delta_4$	-0.0024196	-0.0004839
Δv_4	0.0082540	0.0016508
$\Delta\delta_5$	-0.0014271	-0.0002855
Δv_5	-0.0022981	-0.0004596

Table 6.3 Comparison of bad data handling methods for different measurement configurations and power system dynamics.

	ESTIMATE WITH BAD DATA PRESENT	ESTIMATE AFTER BAD DATA MATHEMATICALLY "REMOVED" (CORRECT ESTIMATES)	ESTIMATE AFTER BAD DATA "REPLACED" BY $z_{i_{PREVIOUS}}$	ESTIMATE AFTER BAD DATA "REPLACED" BY $h_i(\underline{x}_{PREVIOUS})$
(1)	Strong measurement system (1) with α=0.005 and gross error, 10σ in P_{2-4} and P_4			
δ_1	0.0	0.0	0.0	0.0
V_1	1.0630431	1.0634376	1.0622756	1.0622039
δ_2	-0.0479772	-0.0479654	-0.0479249	-0.0479226
V_2	1.0580639	1.0584560	1.0573297	1.0572600
δ_3	-0.0705549	-0.0699095	-0.0663190	-0.0661394
V_3	1.0316780	1.0322613	1.0324818	1.0324808
δ_4	-0.0901422	-0.0963015	-0.0848748	-0.0845675
V_4	1.0401343	1.0404186	1.0412518	1.0413027
δ_5	-0.1041128	-0.1030123	-0.1044441	-0.1045583
V_5	1.0224013	1.0232169	1.0214844	1.0213677
(2)	Strong measurement system (1) with α=0.001 and gross error, 10σ in P_{2-4} and P_4			
δ_1	0.0	0.0	0.0	0.0
V_1	1.0663031	1.0664932	1.0663841	1.0663153
δ_2	-0.0475651	-0.0475731	-0.0475674	-0.0475649
V_2	1.0548521	1.0550385	1.0549304	1.0548632
δ_3	-0.0823287	-0.0817139	-0.0813661	-0.0811875
V_3	1.0323129	1.0326864	1.0327120	1.0327117
δ_4	-0.0897058	-0.0899181	-0.0893919	-0.0890847
V_4	1.0337063	1.0337831	1.0338705	1.0339140
δ_5	-0.1044693	-0.1034149	-0.1035536	-0.1036666
V_5	1.0244041	1.0250002	1.0248382	1.0247247
(3)	Weaker measurement system (2) with α=0.005 and gross error, 10σ in P_1			
δ_1	0.0	0.0	0.0	0.0
V_1	1.0750636	1.0746617	1.0747397	1.0747364
δ_2	-0.0477421	-0.0468178	-0.0469973	-0.0469897
V_2	1.0697722	1.0696642	1.0696851	1.0696842
δ_3	-0.0712176	-0.0698055	-0.0700796	-0.0700680
V_3	1.0422372	1.0422605	1.0422558	1.0422560
δ_4	-0.0922477	-0.0908488	-0.0911203	-0.0911089
V_4	1.0509841	1.0510042	1.0510001	1.0510003
δ_5	-0.1056707	-0.1046309	-0.1048328	-0.1048243
V_5	1.0347522	1.0346861	1.0346861	1.0346854
(4)	Weaker measurement system (2) with α=0.001 and gross error, 10σ in P_1			
δ_1	0.0	0.0	0.0	0.0
V_1	1.0781306	1.0777848	1.0778034	1.0778010
δ_2	-0.0473404	-0.0464107	-0.0464618	-0.0464542
V_2	1.0663078	1.0662537	1.0662567	1.0662562
δ_3	-0.0832762	-0.0818510	-0.0819295	-0.0819177
V_3	1.0426901	1.0427664	1.0427622	1.0427629
δ_4	-0.0918766	-0.0904643	-0.0905419	-0.0905303
V_4	1.0445033	1.0443766	1.0443726	1.0443732
δ_5	-0.1060929	-0.1050417	-0.1050994	-0.1050908
V_5	1.0365508	1.0365237	1.0365253	1.0365250

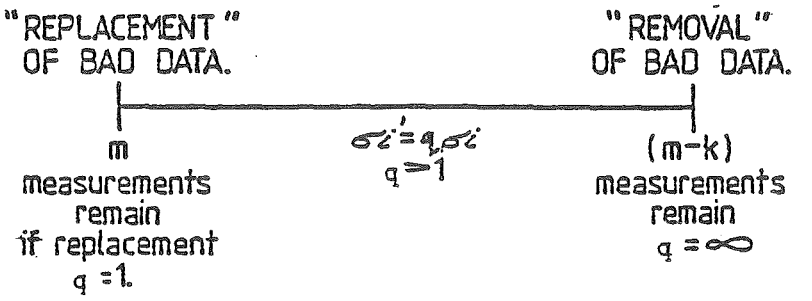

m = no. of measurements

q = level of variance conditioning

σ = standard deviation.

Figure 6.1 Effect of variance conditioned bad data "replacement" techniques.

result after removal or replacement of the bad data points by the methods outlined in equations (6.10), (6.11) and (6.12).

When redundancy permits, the "mathematical removal" given by equation (6.10) will give the best results. The "replacement" techniques that substitute $z_{i_{previous}}$ or $h_i(\underline{x}_{previous})$ for z_i^{BAD} work well provided the rate of change in states between measurement scans is low (e.g. $\alpha = 0.001$). "Replacement" of bad data in the strong system undergoing a high rate of change in power system states, between measurement scans ($\alpha = 0.005$), degrades the estimates more than the presence of the bad data, whereas the "weaker" measurement system has less resistance to distortion caused by bad data and the "replacement" techniques give better estimates than "no removal of bad data" for both $\alpha = 0.005$ and $\alpha = 0.001$.

6.3.3 Effect of modifying the variance when treating bad data.

In Section 6.3.2 "replacement" techniques where $z_i^{BAD} \longrightarrow z_{i_{PREVIOUS}}$ or $h_i(\underline{x}_{previous})$ or "no removal of bad data" left the variance of z_i^{BAD} unchanged. However, the variance can be increased at the suspect bad data point to desensitize the error caused by pseudomeasurement "replacement" of, or "leaving-in", the bad data. Variance σ_{z_i} is increased to $q\sigma_{z_i}$ where $q>1$. Pseudomeasurement replacement with variance conditioning is an intermediate stage between replacement and removal, as shown in Figure 6.1. In the limit, as $q\to\infty$ "variance conditioned" bad data "replacement" becomes "removal". Variance conditioned "replacement" of bad data is useful in situations where the measurement system has insufficient measurements to allow removal and the power system states are changing rapidly between measurement scans. Tests are carried out on measurement system 1. During the second scan, gross errors of 20σ are present in the

measurement of P_{2-4} and P_4. Table 6.4 shows the effect of variance conditioning the bad data location (q=1→q=6) when either pseudo-"replacement" techniques are used to treat the bad data or when the bad data is left, $\alpha = 0.005$. Desensitizing the bad data location gives improved estimates when the bad data is left and when pseudomeasurement replacement is used. This can be seen from the estimates and location of weighted residuals exceeding 3, shown in Table 6.4.

6.3.4 Performance of bad data "replacement" techniques under conditions where "removal" cannot be attempted.

Mathematical "removal" of bad data cannot be attempted where a removal would cause loss of observability to the remaining measurements. Replacement techniques must be used instead, or the bad data left untreated. Measurement system 1 becomes unobservable on "removal", when gross bad data of size 20σ appears in the measurement of P_{2-4}, P_4, P_{3-4}, P_{4-2}, P_{5-4}, P_{4-3} and P_{4-5}, during the second measurement scan. Measurement system 2 becomes unobservable, on "removal" of bad data, when bad data of size 10σ appears in the measurement of P_1 and P_{1-2}, during measurement scan 2. Estimates are evaluated under these conditions, for $\alpha = 0.005$ and 0.001 when bad data replacement, using equations (6.11) and (6.12), is used. The estimates that result when the bad data is untreated are also shown. In all these tests no "variance conditioning" of the suspect bad data location is used. The estimates, and size and location of weighted residuals that exceed 3, that result, are shown in Tables 6.5 and 6.6. When a strong measurement system is used, undergoing a rapid rate of change in power system states between measurement scans, the best policy is not to replace the bad data at all. However when a weak measurement system is used and/or a moderate rate of change in power system states between measurement scans is present, pseudo-

Table 6.4 Comparison of variance conditioned bad data handling "replacement" methods when measurement system 1 is used. (Bad data is present in the measurement of P_{2-4} and P_4.)

	INCREASE IN VARIANCE OF THE MEASUREMENT AT BAD DATA LOCATION				TRUE ESTIMATE
	$\sigma_{z_i}=\sigma^{BAD}_{z_i}$ $\phi_i=1$	$\sigma_{z_i}=2\sigma^{BAD}_{z_i}$ $\phi_i=2$	$\sigma_{z_i}=3\sigma^{BAD}_{z_i}$ $\phi_i=2$	$\sigma_{z_i}=6\sigma^{BAD}_{z_i}$ $\phi_i=6$	
(1) Estimate after bad data variance conditioned but not replaced (measurement system 1)					
δ_1	0.0	0.0	0.0	0.0	0.0
V_1	1.0630431	1.0631407	1.0633125	1.0634032	1.0634376
δ_2	-0.0479772	-0.0479647	-0.0479635	-0.0479663	-0.0479654
V_2	1.0580639	1.0582145	1.0583351	1.0584227	1.0584560
δ_3	-0.0705549	-0.0695923	-0.0697256	-0.0698514	-0.0699095
V_3	1.0316788	1.0321491	1.0323222	1.0322491	1.0322613
δ_4	-0.0901422	-0.0895611	-0.0887981	-0.0901881	-0.0903015
V_4	1.0401343	1.0404557	1.0406507	1.0404258	1.0404186
δ_5	-0.0104112	-0.1034501	-0.1033675	-0.1030656	-0.1030123
V_5	1.0224013	1.0227981	1.0227526	1.0231604	1.0232169
$r_w>3\sigma$					
P_{2-4}	20.7238	10.5302	6.9164	3.4441	
P_4	11.5600	7.7914	5.6087	-	
P_{3-4}	3.8959*	-	-	-	
P_3	3.3750*	-	-	-	
(2) Estimate after bad data replaced with $z_{i_{previous}}$ and variance conditioned (measurement System 1)					
δ_1	0.0	0.0	0.0	0.0	
V_1	1.0622756	1.0628101	1.0631174	1.0633490	
δ_2	-0.0479249	-0.0479433	-0.0479539	-0.0479638	
V_2	1.0573297	1.0578494	1.0581472	1.0583711	SAME
δ_3	-0.0663190	-0.0678946	-0.0688848	-0.0096253	AS
V_3	1.0324818	1.0324048	1.0323222	1.0322801	ABOVE
δ_4	-0.0848748	-0.0873342	-0.0887981	-0.0898878	IN (1)
V_4	1.0412598	1.0408827	1.0406507	1.0404814	
δ_5	-0.1044441	-0.1037231	-0.1033675	-0.1031060	
V_5	1.0214842	1.0223039	1.0227526	1.0230899	
$r_w>3\sigma$					
P_{2-3}	4.1932*	3.2256*	-	-	
P_{3-4}	7.4655*	4.3144*	-	-	
P_{4-2}	3.1138*	-	-	-	
P_{2-4}	13.6804	-	-	-	
P_{4-3}	5.3161*	-	-	-	
P_2	3.4356*	-	-	-	
P_4	16.9707	13.6251	10.2049	5.5173	
P_5	4.0807*	-	-	-	
(3) Estimate after bad data replaced with $h_i(x_{previous})$ and variance conditioned (measurement system 1)					
δ_1	0.0	0.0	0.0	0.0	
V_1	1.0622039	1.0627688	1.0630961	1.0633435	
δ_2	-0.0479226	-0.0479419	-0.0479532	-0.0479370	
V_2	1.0572600	1.0578093	1.0587265	1.0583651	SAME
δ_3	-0.0661394	-0.0677725	-0.0688219	-0.0696079	AS
V_3	1.0324808	1.0324107	1.0323352	1.0322812	ABOVE
δ_4	-0.0845675	-0.0871458	-0.0887020	-0.0898615	IN (1)
V_4	1.0413027	1.0409111	1.0406649	1.0404852	
δ_5	-0.1045583	-0.1037765	-0.1033938	-0.1031130	
V_5	1.0213673	1.0222404	1.0227208	1.0230812	
$r_w>3\sigma$					
P_{2-3}	4.3035*	3.3006*	-	-	
P_{3-4}	7.9224*	4.5408*	3.3500*	-	
P_{4-2}	3.2994*	-	-	-	
P_{2-4}	4.5503	-	-	-	
P_{4-3}	5.7687*	-	-	-	
P_{4-5}	3.0637*	-	-	-	
P_2	3.5888*	-	-	-	
P_4	18.2793	14.6285	10.9493	5.9175	
P_5	4.3060*	-	-	-	

- indicates $r_w<3\sigma$ at the measurement location

* indicates measurement has no bad data although $r_w>3$

Table 6.5 Comparison of bad data handling "replacement" methods when measurement system 1 would be unobservable if "removal" of bad data was attempted. (Bad data, size 20σ, is present on the measurement of P_{2-4}, P_4, P_{3-4}, P_{4-2}, P_{5-4}, P_{4-3} and P_{4-5}.)

	ESTIMATE WITH BAD DATA PRESENT	ESTIMATE AFTER BAD DATA "REPLACED" BY $z_{i_{PREVIOUS}}$	ESTIMATE AFTER BAD DATA "REPLACED" BY $h_i(x_{PREVIOUS})$	TRUE VALUE OF $\underline{x}$
(1) Strong measurement system (1) with α=0.005				
δ_1	0.0	0.0	0.0	0.0
V_1	1.0622516	1.0611037	1.0610991	1.0634376
δ_2	-0.0480283	-0.0470752	-0.0470835	-0.0479654
V_2	1.0572744	1.0565328	1.0565249	1.0584566
δ_3	-0.0683251	-0.0683867	-0.0683265	-0.0699053
V_3	1.0317044	1.0304395	1.0304579	1.0322613
δ_4	-0.0880276	-0.0809174	-0.0809148	-0.0903015
V_4	1.0401224	1.0413492	1.0413467	1.0404180
δ_5	-0.1038928	-0.1016455	-0.1016614	-0.1030123
V_5	1.0216959	1.0214230	1.0214106	1.0232169
$r_w > 3\sigma$				
P_{2-3}	3.0300*	-	-	
P_{3-4}	23.9431	10.7616	10.8144	
P_{4-2}	17.9742	5.6223	6.0844	
P_{5-4}	21.3748	-	4.4906	
P_{2-4}	22.0873	-	6.2676	
P_{4-3}	16.1069	12.5685	10.5599	
P_{4-1}	18.6069	4.3654	4.5669	
P_4	10.1504	-	-	
P_1	-	3.2358*	3.2460*	
P_2	-	3.5983*	3.6443*	
P_3	-	22.2032*	21.9828*	
(2) Strong measurement system (1) with α=0.001				
δ_1	0.0	0.0	0.0	0.0
V_1	1.0658526	1.0663331	1.0663207	1.0664932
δ_2	-0.0476701	-0.0474571	-0.0474612	-0.0475731
V_2	1.0543425	1.0549248	1.0549089	1:0550385
δ_3	-0.0799595	-0.0816792	-0.0816223	-0.0817139
V_3	1.0326964	1.0325308	1.0325395	1.0326864
δ_4	-0.0874578	-0.0885524	-0.0885532	-0.0899181
V_4	1.0340336	1.0340928	1.0340808	1.0337851
δ_5	-0.1053061	-0.1038829	-0.1039000	-0.1034149
V_5	1.0236368	1.0246904	1.0246711	1.0250022
$r_w > 3\sigma$				
P_{2-3}	3.1495*	-	-	
P_{3-4}	23.8888	-	-	
P_{4-2}	17.8905	-	-	
P_{5-4}	21.8951	-	-	
P_{2-4}	22.1751	-	-	
P_{4-3}	16.1311	-	-	
P_{4-5}	18.0832	4.0513	-	
P_4	9.6843	-	-	
P_3	-	4.3179*	4.0991*	

\- indicates $r_w < 3\sigma$ at the measurement location

* indicates measurement is not actually bad data although $r_w > 3$

Table 6.6 Comparison of bad data handling "replacement" methods when measurement system 2 would be unobservable if "removal" of bad data was attempted. (Bad data, size 20σ, is present in the measurement of P_1 and P_{1-2}.)

	ESTIMATE WITH BAD DATA PRESENT	ESTIMATE AFTER BAD DATA "REPLACED" BY $z_{i_{PREVIOUS}}$	ESTIMATE AFTER BAD DATA "REPLACED" BY $h_i(\underline{x}_{PREVIOUS})$	TRUE VALUE of $\underline{x}$
(1) Weak, measurement system (2) with α=0.005				
δ_1	0.0	0.0	0.0	0.0
V_1	1.0763455	1.0752686	1.0752550	1.0746617
δ_2	-0.0527031	-0.0490044	-0.0489587	-0.0468178
V_2	1.0695470	1.0695989	1.0696000	1.0696642
δ_3	-0.0753930	-0.0717693	-0.0717257	-0.0698055
V_3	1.0422657	1.0422727	1.0422731	1.0422605
δ_4	-0.0964856	-0.0928351	-0.0927911	-0.0908488
V_4	1.0509977	1.0510109	1.0510110	1.0510042
δ_5	-0.1107460	-0.1068850	-0.1068382	-0.1046309
V_5	1.0345195	1.0345966	1.0345977	1.0346861
$r_w > 3\sigma$				
P_{1-2}	0.27000	-	-	
P_{1-3}	3.58839*	-	-	
P_1	7.77108	-	-	
(2) Weak, measurement system (2) with α=0.001				
δ_1	0.0	0.0	0.0	0.0
V_1	1.0795574	1.0780148	1.0780009	1.0777848
δ_2	-0.0522862	-0.0471793	-0.0471337	-0.0464107
V_2	1.0662437	1.0662488	1.0662488	1.0662537
δ_3	-0.0874071	-0.0825288	-0.0824854	-0.0818510
V_3	1.0428450	1.0427938	1.0427928	1.0427614
δ_4	-0.0960684	-0.0911502	-0.0911064	-0.0904643
V_4	1.0444923	1.0444019	1.0444011	1.0443766
δ_5	-0.1111334	-0.1058305	-0.1057831	-0.1050417
V_5	1.0364838	1.0365171	1.0365173	1.0365237
$r_w > 3\sigma$				
P_{1-2}	0.26008	-	-	
P_{1-3}	3.60897*	-	-	
P_1	7.76931	-	-	

\- indicates $R_w < 3\sigma$ at the measurement location

* indicates measurement is not actually bad data although $r_w > 3$

measurement replacement of bad data gives the best suppression and identification results.

6.4 CONCLUSION

Simple methods that allow rapid detection, identification and treatment of both single and multiple bad data have been suggested and investigated. The use of the "$J(\underline{x}) + \underline{r}_{\underline{w}}$" test is preferred for detection and identification of bad data. A mathematical "removal" technique that deletes the effect of suspect bad data, without the need to re-order lists or re-evaluate gain matrices, as with the "physical" removal of suspect bad data, has been presented. This technique is simple and fast, and generates estimates that are identical to estimates obtained after the physical removal of bad data. Mathematical removal should be used whenever observability permits. Measurement observability is simply evaluated by using the "tracing" techniques of Clements and Wollenberg (1975) and, more recently, Masiello and Horton (1977). Where measurement "removal" causes loss of observability to the remaining measurements, pseudomeasurement "replacement" of suspect bad data must be used instead. Two simple techniques were outlined, either to replace z_i^{BAD} by $z_{i_{previous}}$ or $h_i(\underline{x}_{previous})$. When a high rate of change in power system states between successive measurement scans is present, "variance conditioning" the pseudomeasurement "replacement" from σz_i to $q\sigma z_i$ $(q>1)$ is necessary to avoid degradation in the estimates. The rate of change in power system states between measurement scans can be evaluated by summing the

$$\left(\frac{\sum_{i=1}^{N} z_{v_i}{}_{present} - \sum_{i=1}^{N} z_{v_i}{}_{previous}}{N} \right) \qquad (6.16)$$

previous and present voltage measurements and finding the difference. When this difference exceeds a threshold level, variance conditioned pseudo "replacement" is used. Replacement of suspect bad data by $h_i(\underline{x}_{previous})$ is preferred to $z_{i_{previous}}$. Only $\underline{x}_{previous}$ need be stored, not $\underline{z}_{i_{previous}}$. Statistically, due to the filtering of the state estimator, $h_i(\underline{x}_{previous})$ will be closer to $h_i(\underline{x}_{true\ previous})$ than $z_{i_{previous}}$. After measurement, z_i^{BAD} is removed and the measurement set becomes marginally unobservable; $h_i(\underline{x}_{k_{previous}})$ can be used with successive values of $\underline{x}_k$, to give observability, until measurement z_i is restored.

CHAPTER 7

INCLUSION OF H.V.D.C. LINKS INTO A.C. POWER SYSTEM STATE ESTIMATION

7.1 INTRODUCTION

A large amount of work has been published on a.c. power system state estimation (Aschmoneit, 1975; Schweppe *et al.*, 1970; Schweppe and Handschin, 1974). However no attempt has been made to include h.v.d.c. links into state estimation. H.v.d.c. links have been incorporated into load flow calculations by Stott and Arrillaga (Stott, 1971; Arrillaga and Bodger, 1977; Arrillaga *et al.*, 1978; Arrillaga *et al.*, 1980). The same basic representation used in the load flow (see Figure 7.1) can be used to incorporate h.v.d.c. links into a.c. power system state estimation. The model is completely general, not being restricted to any mode of h.v.d.c. operation.

The extension of a.c. power system state estimation to include h.v.d.c. links is becoming increasingly important. New h.v.d.c. links are being commissioned all the time. By the end of 1980, 16 000 MW will be capable of being transmitted by h.v.d.c. schemes in thirteen different countries (El-Amin *et al.*, 1979). The bulk transfer of power is not the sole benefit that results from the introduction of h.v.d.c. links. The performance of connected a.c. systems during voltage dips, loss of transmission capacity and loss of Var compensation, can be enhanced by the presence of h.v.d.c. links. The interconnected h.v.d.c. link helps control the change of frequency, improve dynamic stability, damp the connected a.c. systems, and provide tie-line power control (El-Amin *et al.*, 1979).

In this chapter a model or state space for the h.v.d.c. link is selected which is stable, but is not a minimal "number of states" realization. The resulting multi a.c. -h.v.d.c. state estimator algorithm, based on this model, is tested and evaluated. A method for geographically partitioning the h.v.d.c. link to allow estimation within the separate a.c. systems is presented and tested, and methods of fast decoupling the multi a.c. -h.v.d.c. state estimator are outlined and their performances evaluated.

7.2 H.V.D.C. LINK MODEL

7.2.1 Selection of a suitable h.v.d.c. link state space

The selection of a suitable h.v.d.c. link state space is of the utmost importance from the standpoint of speed and accuracy of the estimation process. Arrillaga *et al.* (1980) use a non-minimal set of variables in defining the state vector in the h.v.d.c. load flow formulation. All variables which are influenced by control action are retained in the model. In theory, four independent variables are sufficient to model an h.v.d.c. link, operating under balanced conditions from a known terminal voltage source. However if such a minimum number of variables are used then the control specifications must be translated into equations in terms of these variables. These equations will often contain complex non-linearities.

The same argument applies to the inclusion of h.v.d.c. links into a.c. power system state estimation.

Consider firstly a non-minimal realization. A suitable set of state variables that describe conditions on the h.v.d.c. link, shown in Figure 7.1, are:

$$\underline{x}_{h.v.d.c.} = \left\{ \begin{matrix} \psi_m, I_{1-2}, V_{dm}, a_m, \cos\alpha_m \\ \psi_n, I_{5-6}, V_{dn}, a_n, \cos\delta_n \end{matrix} \right\} I_{dc}$$

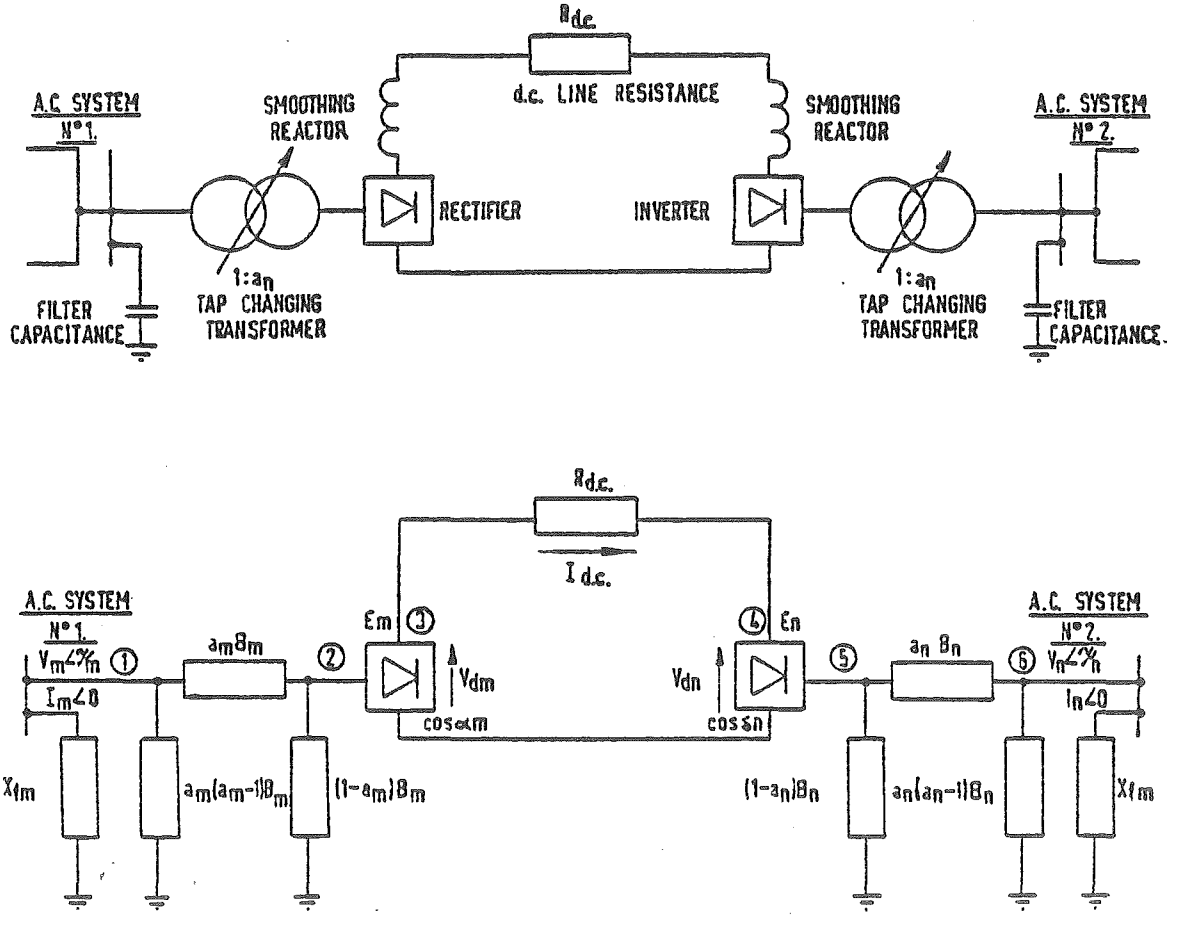

Figure 7.1 H.v.d.c. link and equivalent circuit.

These are in addition to the a.c. terminal voltages, V_m and V_n, which are already part of the a.c. state space. The 11 states are not independent because they are related by the following six equations that are derived from a consideration of rectifier and inverter operation (Kimbark, 1971). For the rectifier:

$$s_1 \; : \; 0 = I_{1-2} - a_m K_1 I_{dc} \tag{7.1}$$

$$s_2 \; : \; 0 = V_{dm} - a_m K_1 V_m \cos\psi_m \tag{7.2}$$

$$s_3 \; : \; 0 = V_{dm} - a_m K_1 \cos\alpha_m - K_2 X_m I_{dc} \tag{7.3}$$

and for the inverter:

$$s_4 \; : \; 0 = I_{5-6} - a_n K_1 I_{dc} \tag{7.4}$$

$$s_5 \; : \; 0 = V_{dn} - a_n K_1 V_n \cos\psi_n \tag{7.5}$$

$$s_6 \; : \; 0 = V_{dn} - a_n K_1 \cos\delta_n + K_2 X_n I_{dc} \tag{7.6}$$

When used with the non-minimal h.v.d.c. link state space, the six equations (7.1) - (7.6), together with

$$s_7 \; : \; 0 = V_{dm} - V_{dn} + R_{dc} I_{dc} \tag{7.7}$$

are treated as pseudomeasurements. An alternative approach, which has not been explored, is to treat the pseudomeasurements as equality constraints, along the lines of Aschmoneit *et al.* (1977). However the pseudomeasurement equations (7.1) - (7.7) are valid only when the overlap angle, u, of the convertor is less than 60^o. Under some fault conditions u may become greater than 60^o. Treating equations (7.1) - (7.7) as pseudomeasurements allows modification of their "variance" weightings within the state estimator. Provided suitable logic can detect when a fault occurs, the variance of-equations (7.1) - (7.7) can be increased and the effect of possible inaccuracies suppressed. Alternatively, a sufficiently large variance can initially be allotted to pseudo-

measurements (7.1) - (7.7), to encompass possible "inaccuracies" when faults occur.

7.2.2 H.v.d.c. link measurement equations.

Twenty-five different measurements that describe conditions around the rectifier and inverter terminals are possible. These are in addition to the a.c. terminal measurements of V_m, P_m and Q_m (V_n, P_n and Q_n):

$$\underline{Z}_{h.v.d.c.} = \begin{bmatrix} Q_{fm}, P_{1-2}, Q_{1-2}, |I|_{1-2}, E_m, P_{2-3}, Q_{2-3}, |I|_{2-3}, a_m, \cos\alpha_m, P_{dm}, V_{dm}, \\ Q_{fn}, P_{5-6}, Q_{5-6}, |I|_{5-6}, E_n, P_{4-5}, Q_{4-5}, |I|_{4-5}, a_n, \cos\delta_n, P_{dn}, V_{dn}, \end{bmatrix} I_{dc}$$

The h.v.d.c. link measurement equations for the rectifier side of the link are:

$$Q_{fm} = \frac{-V_m^2}{X_{fm}} \tag{7.8}$$

$$P_{1-2} = \sqrt{3}\, V_{m_r}\, I_{1-2} \tag{7.9}$$

However, since I_{1-2} has a phase angle arbitrarily defined to be zero, $I_{1-2} \angle 0$, then

$$P_{1-2} = \sqrt{3}\, V_m\, I_{1-2} \cos\psi_m \tag{7.10}$$

Similarly,

$$Q_{1-2} = \sqrt{3}\, V_{m_I}\, I_{1-2} \tag{7.11}$$

$$= \sqrt{3}\, V_m\, I_{1-2} \sin\psi_m \tag{7.12}$$

$$E_m = \left[\frac{a_m^4 B_m^2 V_m^2 + I_{1-2}^2 + 2a_m^2 B_m I_{1-2} V_m \sin\psi_m}{a_m^2 B_m^2} \right]^{\frac{1}{2}} \tag{7.13}$$

$$P_{2-3} = \sqrt{3}\, I_{1-2}\, V_m \cos\psi_m \tag{7.14}$$

$$P_{2-3} = \sqrt{3}\, I_{1-2}\, V_m \cos\psi_m \tag{7.14}$$

$$Q_{2-3} = \sqrt{3} \left[\frac{I_{1-2}^2 + a_m^2 I_{1-2} B_m V_m \sin\psi_m}{a_m^2 B_m^2} \right] \tag{7.15}$$

$$I_{2-3} = \frac{I_{1-2}}{a_m} \tag{7.16}$$

$$P_{dm} = I_{dc} V_{dm} \tag{7.17}$$

For a derivation of equations (7.13) - (7.16), see Appendix A.8. Identical equations can be derived for the inverter side of the h.v.d.c. link by replacing prefixes m by n, 1-2 by 5-6, 2-3 by 4-5 and $\cos\alpha_m$ by $\cos\delta_n$. I_{dc} remains unchanged. Many different types of h.v.d.c. link measurements are possible and little sparsity results. Non-zero partial derivative Jacobian elements for the measurement equations and pseudomeasurements are shown in Tables 7.1 and 7.2.

The measurement equations for the h.v.d.c. link have been derived on the assumption that sinusoidal waveforms exist at all "a.c." nodes of the link. This assumption does not hold at nodes (2) and (5) for the link shown in Figure 7.1. Distorted waveforms of voltage and current result from the convertor switching. However the measurement equations (7.13) - (7.16) can be used, provided their "variance" is increased to account for inaccuracy in the equations that result from the sinusoidal assumptions. Filters at the terminal buses (1) and (6), in Figure 7.1, ensure near-sinusoidal waveforms exist. Thus all other equations, (7.8) - (7.12) and (7.17), correctly model h.v.d.c. link operations.

Measurement equations that describe a.c. terminal injected active and reactive power must be modified to include the h.v.d.c. link,

$$\text{i.e.} \quad P_m = P_{m_{a.c.}} + P_{m_{h.v.d.c.}} = \sum_{j\varepsilon\{\alpha\}} P_{mj} + \sqrt{3}\, V_m\, I_{1-2} \cos\psi_m \tag{7.18}$$

Table 7.1 Pseudomeasurement non-zero Jacobian terms for the rectifier side

S_1	$\partial S_1/\partial I_{1-2} = 1$ $\partial S_1/\partial a_m = -K_1 I_{dc}$ $\partial S_1/\partial I_{dc} = -K_1 a_m$
S_2	$\partial S_2/\partial V_m = -a_m K_1 \cos\psi_m$ $\partial S_2/\partial \psi_m = a_m K_1 V_m \sin\psi_m$ $\partial S_2/\partial a_m = -K_1 V_m \cos\psi_m$ $\partial S_2/\partial V_{dm} = 1$
S_3	$\partial S_3/\partial V_m = -K_1 a_m \cos\alpha_m$ $\partial S_3/\partial a_m = -K_1 V_m \cos\alpha_m$ $\partial S_3/\partial V_{dm} = 1$ $\partial S_3/\partial \cos\alpha_m = -K_1 V_m a_m$ $\partial S_3/\partial I_{dc} = K_2 X_m$
Jacobian partial derivatives for the inverter side are identical in form and are found by replacing m by n, 1-2 by 5-6, 2-3 by 4-5 and $\cos\alpha_m$ by $\cos\delta_n$. Equation S_4 above, however, becomes $-K_2X_m$ rather than K_2X_m. Non-zero Jacobian elements for the remaining pseudomeasurement, S_7, are	
S_7	$\partial S_7/\partial V_{dm} = 1$ $\partial S_7/\partial V_{dn} = -1$ $\partial S_7/\partial I_{dc} = -R_{dc}$

Table 7.2 Jacobian elements for the h.v.d.c. link measurement equations.

Jacobian elements are defined as $\underline{H}(\underline{x}) = \frac{\partial \underline{h}(\underline{x})}{\partial \underline{x}}$

For the rectifier side of the h.v.d.c. link, non zero Jacobian terms are:-

(1)	Q_{fm}	$\partial Q_{fm}/\partial V_m = -\frac{2V_m}{X_{fm}}$
(2)	P_{1-2}	$\partial P_{1-2}/\partial V_m = \sqrt{3}\, I_{1-2} \cos\psi_m$ $\partial P_{1-2}/\partial I_{1-2} = \sqrt{3}\, V_m \cos\psi_m$ $\partial P_{1-2}/\partial \psi_m = -\sqrt{3}\, V_m\, I_{1-2} \sin\psi_m$
(3)	Q_{1-2}	$\partial Q_{1-2}/\partial V_m = \sqrt{3}\, I_{1-2} \sin\psi_m$ $\partial Q_{1-2}/\partial I_{1-2} = \sqrt{3}\, V_m \sin\psi_m$ $\partial Q_{1-2}/\partial \psi_m = \sqrt{3}\, V_m\, I_{1-2} \cos\psi_m$
(4)	I_{1-2}	$\partial I_{1-2}/\partial I_{1-2} = 1$
(5)	E_m	$\partial E_m/\partial V_m = \frac{(E_m^2)^{-\frac{1}{2}}}{2(a_m^2 B_m^2)} (2V_m a_m^4 B_m^2 + 2a_m^2 B_m I_{1-2} \sin\psi_m)$ $\partial E_m/\partial I_{1-2} = \frac{(E_m^2)^{-\frac{1}{2}}}{2(a_m^2 B_m^2)} (2I_{1-2} + 2a_m^2 B_m V_m \sin\psi_m)$ $\partial E_m/\partial \psi_m = \frac{(E_m^2)^{-\frac{1}{2}}}{2(a_m^2 B_m^2)} (2a_m^2 B_m I_{1-2} V_m \cos\psi_m)$ $\partial E_m/\partial a_m = \frac{(E_m^2)^{-\frac{1}{2}}}{2(a_m^2 B_m^2)}$ $\left(\frac{a_m^2 B_m^2 (4a_m^3 V_m^3 B_m^2 + 4a_m B_m I_{1-2} V_m \sin\psi_m) - 2a_m B_m^2 (a_m^4 V_m^2 B_m^2 + I_{1-2}^2 + 2a_m^2 B_m I_{1-2} V_m \sin\psi_m)}{a_m^4 B_m^4} \right)$
(6)	P_{2-3}	$\partial P_{2-3}/\partial V_m = \sqrt{3}\, I_{1-2} \cos\psi_m$ $\partial P_{2-3}/\partial I_{1-2} = \sqrt{3}\, V_m \cos\psi_m$ $\partial P_{2-3}/\partial \psi_m = -\sqrt{3}\, V_m\, I_{1-2} \sin\psi_m$
(7)	Q_{2-3}	$\partial Q_{2-3}/\partial V_m = \sqrt{3}\, I_{1-2} \sin\psi_m$ $\partial Q_{2-3}/\partial I_{1-2} = \sqrt{3}\, V_m \sin\psi_m$ $\partial Q_{2-3}/\partial \psi_m = \sqrt{3}\, V_m\, I_{1-2} \cos\psi_m$
(8)	I_{2-3}	$\partial I_{2-3}/\partial I_{1-2} = \frac{1}{a_m}$ $\partial I_{2-3}/\partial a_m = \frac{-I_{1-2}}{a_m^2}$
(9)	a_m	$\partial a_m/\partial a_m = 1$
(10)	$\cos\alpha_m$	$\partial \cos\alpha_m/\partial \cos\alpha_m = 1$
(11)	V_{dm}	$\partial \bar{V}_{dm}/\partial V_{dm} = 1$
(12)	I_{dc}	$\partial I_{dc}/\partial I_{dc} = 1$
(13)	P_{dc}	$\partial P_{dc}/\partial V_{dc} = I_{dc}$ $\partial P_{dc}/\partial I_{dc} = V_{dc}$

$$Q_m = Q_{m_{a.c.}} + Q_{m_{h.v.d.c.}} = \sum_{j\in\{\alpha\}} Q_{mj} - \frac{V_m^2}{X_{fm}} + \sqrt{3}\, V_m\, I_{1-2}\, \sin\psi_m \qquad (7.19)$$

7.2.3 Effect of approximation error present in the h.v.d.c. link model

The h.v.d.c. link model, described by convertor relationships $s_1 - s_7$, is an approximate h.v.d.c. link model. No account is taken of the commutation overlap angle, u, in the convertor switching. In the derivation of equations (7.1), (7.2), (7.4) and (7.5) a simplifying assumption made by Kimbark (1971) is used. This assumption is that, for the rectifier side,

$$\cos\psi_m = \frac{(\cos\alpha_m + \cos\delta_m)}{2} \qquad (7.20)$$

Commutation from one valve to the next is assumed instantaneous and the inductance of the power system is assumed to be zero. This approximation is valid when the overlap angle $u = 0$. At $u = 30^o$ the maximum approximation error is 1.1% while at $u = 60^o$ the maximum error is 4.3% (Kimbark, 1971).

Using the non-minimal - 11 h.v.d.c. state space outlined in Section 7.2.1 - gives the most accurate realization because the approximation error occurs only explicitly four times, in equations (7.1), (7.2), (7.4) and (7.5). The non-zero structure of the h.v.d.c. Jacobian for the minimum approximation error h.v.d.c. link realization is shown in Figure 7.2. Seventy-eight non-zero Jacobian elements are present when all h.v.d.c. link measurements possible are monitored.

7.2.4 "Minimal-state" h.v.d.c. link state vector realization

A minimal state h.v.d.c. link realization is possible, with four h.v.d.c. link states, in addition to terminal a.c. states V_m and V_n, when the state vector chosen is

$$\underset{\sim}{x}_{h.v.d.c.} = [\psi_m,\ a_m,\ \psi_n,\ a_n]$$

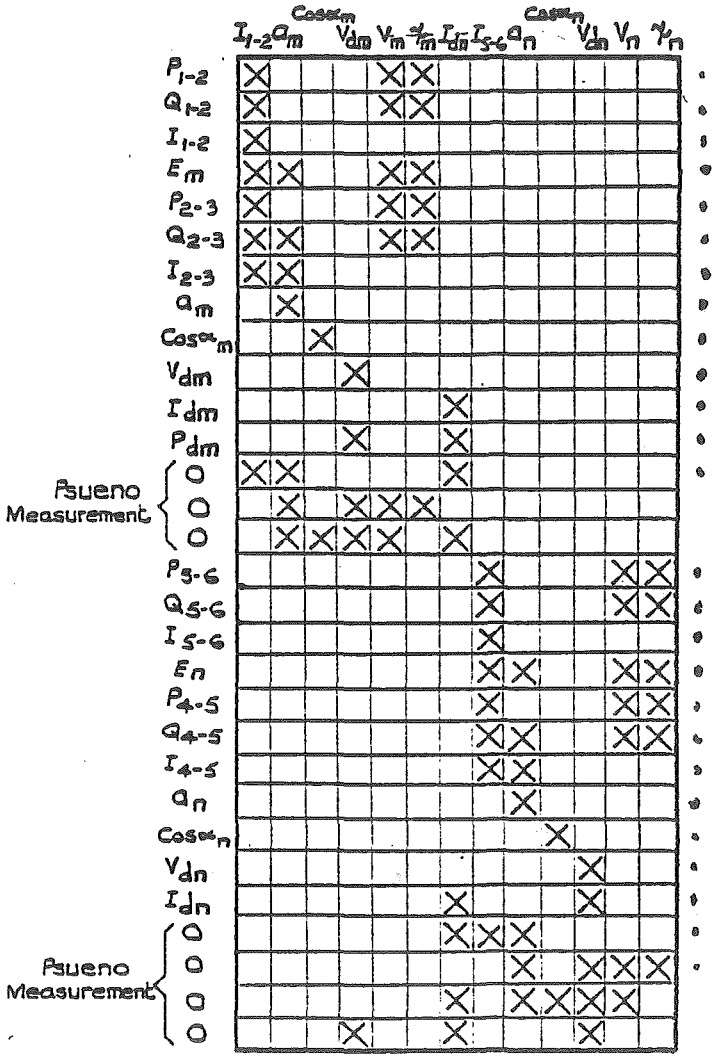

• Denotes measurement equation contains no approximation error.

Figure 7.2 H.v.d.c. Jacobian structure for minimal error realization (78 non-zero elements).

Measurement equations are shown in Table 7.3 and derived in Appendix A.9. All convertor pseudomeasurement relationships have been treated as exact expressions, and "eliminated" by row reduction to reduce the size of the h.v.d.c. link state space by seven states. However, equations (7.1), (7.2), (7.4) and (7.5) contain approximation error, and in the "elimination" process this error has smeared all but two of the measurement equations. In the derivation of some of the measurement equations the approximation error may have "combined" from three or four sources containing the error.

Figure 7.3 shows the non-zero structure of the h.v.d.c. Jacobian for the minimal state realization. One hundred and thirty-eight non-zero elements are present when all h.v.d.c. link measurements possible are monitored.

7.2.5 Comparison of minimal approximation error and minimal state h.v.d.c. link state vector realizations

No advantages can be gained from using the minimal state realization. The "minimal state" state space produces nearly twice as many non-zero Jacobian elements as the "minimum error" realization and most of these elements will be tainted with approximation error effects.

The complicated smearing of all but two "minimal state" measurement equations by approximation error makes the "minimal state" state estimator potentially unreliable. Minimal state measurement equations are also complex and highly non-linear when compared with the "minimal approximation error" realization. As a result, since the state estimation algorithm is derived using a Taylor series linearization, the "minimal state" realization is likely to have poor convergence as well as poor accuracy. The minimal approximation error

Table 7.3 Measurement equations for "minimal-state" h.v.d.c. link realization

For the rectifier side of the h.v.d.c. link, measurement equations are:

(1) $Q_{fm} = Q_{fm}$
(2) $P_{1-2} = \sqrt{3}\, a_m V_m K_1^2 (a_m V_m \cos\psi_m^2 + a_n V_n \cos\psi_n \cos\psi_m)/R_{dc}$
(3) $Q_{1-2} = \sqrt{3}\, a_m V_m K_1^2 (a_m V_m \cos\psi_m + a_n V_n \cos\psi_n) \sin\psi_m/R_{dc}$
(4) $I_{1-2} = a_m K_1^2 (a_m V_m \cos\psi_m + a_n V_n \cos\psi_n)/R_{dc}$
(5) $E_m = (R_{dc}^2 a_m^4 B_m^2 V_m^2 + a_m^2 K_1^4 (a_m V_m \cos\psi_m + a_n V_n \cos\psi_n)^2 + 2 a_m R_{dc} B_m K_1^2 V_m (a_m V_m \cos\psi_m + a_n v_n \cos\psi_n))/ (R_{dc}^2 a_m^2 B_m^2)$
(6) $P_{2-3} = \sqrt{3}\, a_m V_m K_1^2 (a_m V_m \cos\psi_m^2 + a_n V_n \cos\psi_n \cos\psi_m)/R_{dc}$
(7) $Q_{2-3} = \sqrt{3}\, (a_m^2 K_1^2 (a_m V_m \cos\psi_m + a_n V_n \cos\psi_n) + R_{dc}^2 a_m^3 K_1^2 B_m V_m (a_m V_m \cos\psi_m + a_n V_n \cos\psi_n) \sin\psi_m) / a_m^2 B_m R_{dc}^2$
(8) $I_{2-3} = K_1^2 (a_m V_m \cos\psi_m + a_n V_n \cos\psi_n)/R_{dc}$
(9) $a_m = a_m$
(10) $\cos\alpha_m = (R_{dc} a_m V_m \cos\psi_m + K_2 X_m (a_m V_m \cos\psi_m + a_n V_n \cos\psi_n))/a_n V_n$
(11) $V_{dm} = K_1 a_m V_m \cos\psi_m$
(12) $I_{dc} = K_1 (a_m V_m \cos\psi_m + a_n V_n \cos\psi_n)/R_{dc}$
(13) $P_{dc} = K_1^2 (a_m^2 V_m^2 \cos^2\psi_m + a_m a_n V_m V_n \cos\psi_m \cos\psi_n)/R_{dc}$

Measurement equations for the inverter side are identical, and are found by replacing m by n, 1-2 by 5-6, 2-3 by 4-5 and $\cos\alpha_m$ by $\cos\delta_n$.

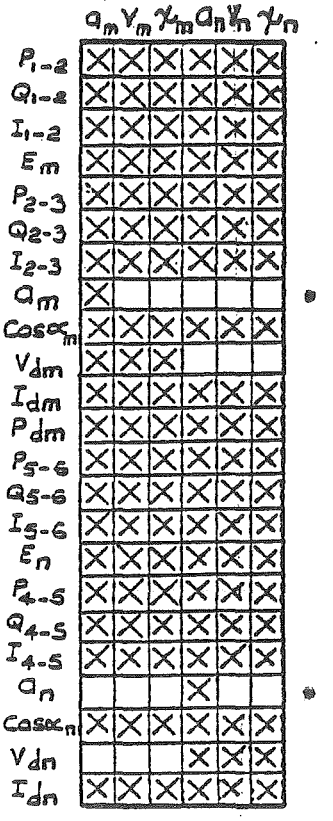

• Denotes measurement equation contains no approximation error

Figure 7.3 H.v.d.c. link Jacobian structure for minimal state realization (122 non-zero elements).

-11 h.v.d.c. link state state realization will be used to model the h.v.d.c. link in the multi a.c.-h.v.d.c. state estimator. This realization also allows geographic partitioning of I_{dc} into I_{dm} and I_{dn} and allows separate estimation of each a.c. system and its associated converter terminal.

7.3 PERFORMANCE OF THE COMBINED MULTI "A.C. H.V.D.C." STATE ESTIMATOR

The multi a.c.-h.v.d.c. power system used in the following tests is shown in Figure 7.4. It consists of two identical 5 bus a.c. systems that are connected by an h.v.d.c. link. Parameters for the a.c. and h.v.d.c. systems are given in Table 7.4. Measurement data for the multi a.c.-h.v.d.c. test system is listed in Table 7.5.

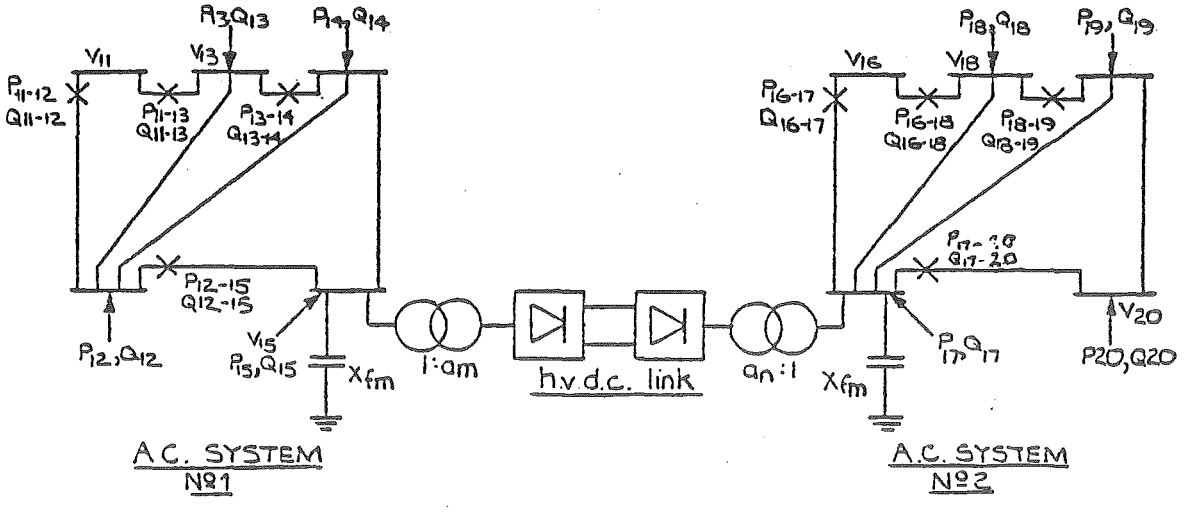

Figure 7.4 Multi a.c.-h.v.d.c. test system.

Table 7.4 A.c. and h.v.d.c. link parameters.

A.C. SYSTEM PARAMETER			D.C. LINK PARAMETERS		
BUSBAR(p-q)	IMPEDANCE $G_{ij}+jB_{ij}$	LINE CHANGING ($B_{ish}/2$)	PARAMETER	RECTIFIER	INVERTER
11-12 16-17	0.02+j0.06	j0.030	Filter reactance X_{fm} (p.u.)	2.100	1.590
11-13 16-18	0.08+j0.24	j0.025	Transformer Reactance X_m (p.u.)	0.126	0.0728
12-13 17-18	0.06+j0.18	j0.020			
12-14 17-19	0.06+j0.18	j0.020	D.C. Link Resistance R_{dc}	0.0033 ohms	
12-15 17-20	0.04+j0.12	j0.015			
13-14 17-19	0.01+j0.03	j0.010			
14-15 19-20	0.08+j0.24	j0.025			

Line parameters for a.c. systems 1 & 2 are identical

Table 7.5 A.c.-h.v.d.c. measurement data.

A.C. SYSTEM 1		A.C. SYSTEM 2		H.V.D.C. LINK 1 (RECTIFIER SIDE)		H.V.D.C. LINK 1 (INVERTER SIDE)	
LOCATION	VALUE (P.U.)	LOCATION	VALUE (P.U.)	LOCATION	VALUE (P.U.)	LOCATION	VALUE (P.U.)
V_{11}	1.060	V_{16}	1.060	P_{1-2}	0.586	P_{5-6}	-0.5853
P_{11-12}	1.38647	P_{16-17}	0.38308	Q_{1-2}	0.189504	Q_{5-6}	0.1688
Q_{11-12}	-0.20966	Q_{16-17}	0.07154	I_{1-2}	0.60188	I_{5-6}	0.5818
P_{11-13}	0.54120	P_{16-18}	0.31410	E_m	0.97358	E_n	0.97238
Q_{11-13}	-0.01517	Q_{16-18}	0.03514	I_{2-3}	0.61909	I_{4-6}	0.61914
P_{12}	0.2000	P_{17}	0.2000	Q_{2-3}	0.141206	Q_{4-6}	0.14093
Q_{12}	0.22080	Q_{17}	-0.54150	a_m	0.9722	a_n	0.93974
P_{12-15}	0.97251	P_{17-20}	0.56466	V_{dm}	1.2782	V_{dn}	-1.27668
Q_{12-15}	-0.07758	Q_{17-20}	0.06883	$\cos\alpha_m$	0.9926	$\cos\delta_n$	-0.98481
V_{13}	1.02300	V_{18}	1.02400	P_{dm}	0.5860	P_{dn}	-0.58526
P_{13}	-0.4500	P_{18}	-0.4500	I_{dc} = 0.4585			
Q_{13}	-0.1500	Q_{18}	-0.1500				
P_{13-14}	0.32776	P_{18-19}	0.14055				
Q_{13-14}	-0.10954	Q_{18-19}	-0.03226				
P_{14}	-0.4000	P_{19}	-0.4000				
Q_{14}	-0.0500	Q_{19}	-0.0500				
V_{15}	1.02300	V_{20}	1.01800				
P_{15}	-0.58600	P_{20}	-0.6000				
Q_{15}	-0.10000	Q_{20}	-0.1000				

7.3.1 Effect of retaining a.c. system slack (reference) buses

Measurement and pseudomeasurement equations in Section 7.2 are derived on the assumption that the phase angle of the h.v.d.c. link convertor terminal current is zero. This assumption results in simpler h.v.d.c. equations. It also results in an a.c. terminal bus voltage phase angle, ψ_m, referred to the convertor current of the h.v.d.c. link. All voltage phase angles in the a.c. systems can be referred to the convertor current and any a.c. system reference (slack) bus bars eliminated. When all a.c. voltage phase angles are referred to the convertor current, the multi a.c.-h.v.d.c. state estimator converges in 12-13 iterations to a tolerance <0.00001 p.u.

Alternatively the a.c. system reference bus bars can be retained. Two a.c. terminal voltage phase angles result at each a.c. terminal bus. One angle, ψ_m, is the a.c. terminal voltage phase angle referred to the convertor current and the other, θ_m, is the a.c. terminal voltage phase angle referred to the a.c. system reference bus, $V_i\angle 0$. Convergence of the multi a.c.-h.v.d.c. state estimator improves to 4-5 iterations to a tolerance of 0.00001 p.u. This is roughly the same number of iterations that is required for a.c. state estimation. Similar improvements were noted in multi a.c.-h.v.d.c. load flow studies (Arrillaga and Bodger, 1977).

The resulting a.c. voltage phase angle estimates can be converted from the a.c. reference to the convertor current reference by using

$$\psi_{i_{a.c.}} = (\theta_{i_{a.c.}} - \theta_m) + \psi_m \qquad (7.21)$$

7.3.2 Minimum h.v.d.c. link observability conditions

If the a.c. terminal active and reactive injected power is measured and sufficient redundancy is present in the a.c. system to observe V_m (V_n) then the h.v.d.c. link is fully observable. H.v.d.c.

link states I_{1-2}, ψ_m, (I_{5-6},ψ_n) are observable from the a.c. system measurements of P_m and Q_m, given by equations (7.18) and (7.19) respectively. $V_m(V_n)$ and the a.c. states in $\sum_{j\varepsilon\{\alpha\}} P_{mj}$ and $\sum_{j\varepsilon\{\alpha\}} Q_{mj}$ are "fixed" by the a.c. system's redundancy. Thus the above expressions for (7.18) and (7.19) contain only two unknowns: I_{1-2} and ψ_m (I_{5-6} and ψ_n). Seven states remain unobserved:

$$\{ V_{dm}, a_m, \cos\alpha_m, I_{dc}, V_{dn}, a_n, \cos\alpha_n \}$$

However, seven pseudomeasurements, given by equations (7.1)-(7.7), are present. Thus it appears that all 11 h.v.d.c. link states may be observable even in the absence of "physical" h.v.d.c. link measurements. This was verified using the test system shown in Figure 7.4. However the presence of bad data in the a.c. terminal injection measurements, P_m or Q_m, can adversely affect the quality of the h.v.d.c. link estimates. Table 7.6 shows the estimates that result when bad data of various size is present in the a.c. terminal measurement of P_m, i.e. P_{15}. It is thus unlikely, however, that a utility could operate a multi a.c.-h.v.d.c. link state estimator with a minimal observability measurement set.

7.3.3 Additional pseudomeasurements

Usually h.v.d.c. links are operated under constant d.c. power control, constant current, or constant extinction angle control. Operators could "feed" these control specifications into the state estimator as pseudomeasurements if actual measurements are not present.

7.3.4 Geographic partitioning of the h.v.d.c. link

Multi a.c.-h.v.d.c. state estimation with two or more separate a.c. systems, as in Figure 7.4, requires all measurements to be co-ordinated to a central location to allow state estimation.

Table 7.6 Effect of bad data in a.c. terminal measurement, P_{15}, on the quality of the approximate model h.v.d.c. link estimates at minimal observability conditions.

	NO BAD DATA IN P_{15}	BAD DATA SIZE 1σ IN P_{15}	BAD DATA SIZE 2.5σ IN P_{15}	BAD DATA SIZE 5σ IN P_{15}	BAD DATA SIZE 10σ IN P_{15}	BAD DATA SIZE 20σ IN P_{15}
ESTIMATES (p.u.)						
I_{5-6}	0.60190	0.61121	0.62520	0.64859	0.69558	0.79024
I_{dc}	0.44898	1.79774	2.78878	3.91830	5.52309	7.79792
V_{dm}	1.30507	0.33150	0.21907	0.16230	0.12419	0.10079
a_m	0.99267	0.25175	0.16600	0.12257	0.09325	0.07504
$\cos\alpha_m$	0.99103	-1.57506	2.41836	3.74268	6.12213	10.02269
ψ_m	0.31225	0.30734	0.30024	0.28910	0.26906	0.23617
I_{5-6}	0.58181	0.58181	0.58181	0.58181	0.58181	0.58181
V_{dn}	-1.30359	-0.32557	-0.20987	-0.14937	-0.10597	-0.07505
a_n	0.95954	0.23964	0.15448	0.10995	0.07800	0.05524
$\cos\delta_n$	-0.98371	-1.32950	-1.84817	-2.71263	-4.44155	-7.89939
ψ_n	2.86035	2.86035	2.86035	2.86035	2.86035	2.86035
θ_{15}	-0.18973	-0.18973	-0.18973	-0.18973	-0.18973	-0.18973
V_{15}	1.02298	1.02298	1.02298	1.02298	1.02298	1.02298
θ_2	-0.01881	-0.01881	-0.01881	-0.01881	-0.01881	-0.01881
V_2	1.04711	1.04711	1.04711	1.04711	1.04711	1.04711
CONVERGENCE						
NO. OF ITER. TO CONVERGE WITHIN						
0.00001 p.u.	9	12	12	10	12	12
0.0001 p.u.	9	12	11	10	12	12
0.001 p.u.	8	12	11	10	11	11

In New Zealand, the h.v.d.c. submarine link interconnects a.c. systems in separate Islands. Each Island has its own a.c. system's control centre. Geographic partitioning of the h.v.d.c. link would allow simpler implementation and reduce the number of measurements required at each regional state estimator, as shown in Figure 7.5.

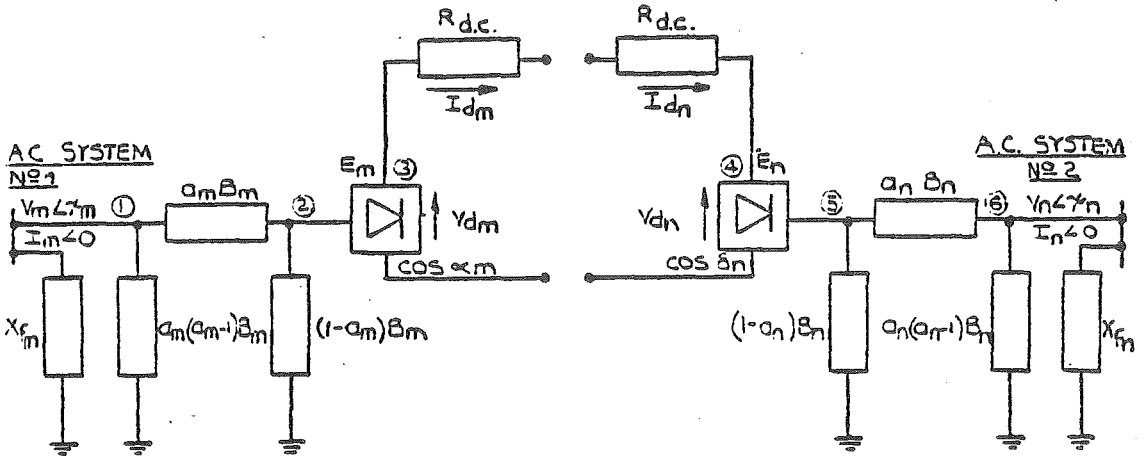

Figure 7.5 Partitioned h.v.d.c. link equivalent circuit.

The h.v.d.c. link can be partitioned by splitting the link down the middle. The only h.v.d.c. state that is common to the rectifier and inverter side of the h.v.d.c. link, I_{dc}, is partitioned into two states: I_{dc_m} and I_{dc_n}. Pseudomeasurement s_7 given by equation (7.7) is no longer applicable since it requires a knowledge of both V_{dm} and V_{dn}. The loss of one pseudomeasurement and the creation of two new states from I_{dc} means that at least one "physical" h.v.d.c. link measurement per side must be present to allow the h.v.d.c. link state estimates observability. The geographically partitioned estimator is

sub-optimal.

However, the effect of this on a "full" h.v.d.c. link measurement set is negligible as shown in Table 7.7. Estimates with and without geographic partitioning are shown. For the "exact" measurement set that is noise-free, given by Table 7.5, estimates are identical. However, when these measurements are corrupted by random measurement noise $<3\sigma$ (<0.03), the estimates still agree to within 0.001 p.u. for a convergence tolerance of less than 0.00001 p.u. These results appear quite acceptable. When no bad data is present in the h.v.d.c. link measurements, I_{dm} should be approximately equal to I_{dn}. If not, bad data should be suspected.

The basic convertor terminal representation can be used as a building block when modelling multi terminal h.v.d.c. links that have convertor terminals connected in series or parallel.

7.3.5 Performance results

The performance of the multi a.c. - h.v.d.c. state estimator on the test system, shown in Figure 7.6, comprising three a.c. systems and two h.v.d.c. links is now investigated. Three hundred and sixty-nine measurements and 92 states are present.

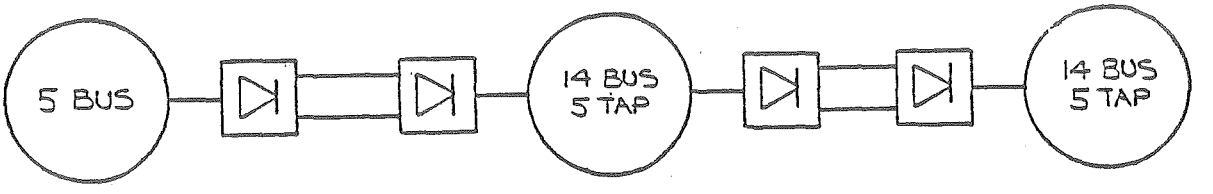

Figure 7.6 3 a.c. - 2 h.v.d.c. link test system.

Table 7.7 Comparison of h.v.d.c. link estimates with and without geographic partitioning.

	NOISE FREE MEASUREMENTS		MEASUREMENTS WITH NOISE <3σ	
	WITHOUT PARTITIONING	WITH PARTITIONING	WITHOUT PARTITIONING	WITH PARTITIONING
V_m †	1.02305	1.02305	1.02614	1.02597
θ_m †	-0.18970	-0.18970	-0.18883	-0.18884
I_{1-2}	0.60194	0.60194	0.60478	0.60403
V_{dm}	1.27818	1.27818	1.28172	1.28021
a_m	0.97228	0.97228	0.97066	0.97048
$\cos\alpha_m$	0.99257	0.99256	0.99189	0.99126
ψ_m	0.31270	0.31270	0.32461	0.32506
I_{5-6}	0.58179	0.58179	0.57724	0.57800
V_{dn}	-1.27668	-1.27669	-1.28479	-1.28628
a_n	0.93968	0.93969	0.94736	0.94754
$\cos\delta_n$	-0.98479	-0.98479	-0.98285	-0.98342
ψ_n	2.86071	2.86071	2.85224	2.85273
I_{dc_m})	I_{dc}=0.45845	0.45845)	I_{dc}=0.45736	0.45486
I_{dc_n})		0.45844)		0.45991
V_n *	1.04707	1.04707	1.05091	1.05107
θ_n *	-0.01881	-0.01881	-0.01935	-0.01933

† Rectifier a.c. terminal bus estimates.

* Inverter a.c. terminal bus estimates.

A breakdown of states and measurements present is shown in Table 7.8. The state estimator converted in five iterations to a tolerance less than 0.00001 p.u. from the flat start described in Table 7.9. This state estimation took 40 seconds on a Burroughs B6700 time-shared computer. The execution time includes time spent in reading-in measurement data, power system structure and parameters, storing pointers, building up graphs and other housekeeping tasks. In comparison, estimation of the three separate a.c. systems without h.v.d.c. links takes 32.5 seconds. Two hundred and ninety-seven measurements and 63 states are present. Thus the extra time spent in computing additonal h.v.d.c. link states is small. If a convergence tolerance of 0.00002 p.u. is acceptable, the multi a.c. - h.v.d.c. state estimator converges in four iterations. This would reduce the 40 second execution time quoted above, further.

7.4 FAST DECOUPLED MULTI "A.C. - H.V.D.C." STATE ESTIMATION

Techniques for P-θ, Q-V fast decoupling a.c. measurement Jacobian elements have been widely used to halve the number of non-zero elements in the Jacobian and make the remaining elements state independent (constant) (Schweppe and Handschin, 1974; Bermundez and Brameller, 1978). A review of such techniques was made in Chapter 4 and the stable, modal P-θ,Q-V sequential fast decoupling technique developed by Bermundez and Brameller (1978), Mafaakher *et al.* (1979) and Bermundez (1977), which fast decouples a.c. Jacobian elements on both sides of the W.L.S. state estimation algorithm, will be used in the tests.

The measurement set $\underline{Z}$ can be partitioned into active line flow and injection power measurements, $\underline{Z}_p$, reactive line flow, injected power and voltage magnitude measurements, $\underline{Z}_q$', and h.v.d.c. link measurements

Table 7.8 Measurement breakdown for a.c.-h.v.d.c. system.

MEASUREMENT TYPE	A.C. SYSTEM 1	A.C. SYSTEM 2	A.C. SYSTEM 3	H.V.D.C. LINK 1 H.V.D.C. LINK 2
$\|V_i\|$	5	14	14	12 h.v.d.c. link measurements/ side + 3 pseudomeasurements/side = total of 48 h.v.d.c. link measurements plus 12 pseudo-measurements.
P_{ij}	14	40	40	
Q_{ij}	14	40	40	
P_i	5	14	14	
Q_i	5	14	14	
a_{ij}	-	5	5	
NUMBER OF STATES	9	27*	27*	6 h.v.d.c. link states/side = Total of 24 h.v.d.c. link states

* Includes 5 transformer taps.

Table 7.9 A.c.-h.v.d.c. flat start "conditions".

STATES	A.C. SYSTEM 1 A.C. SYSTEM 2 A.C. SYSTEM 3	H.V.D.C. LINKS 1 & 2 RECTIFIER (p.u.) INVERTER
States as shown	Voltage magnitudes = 1 p.u. Voltage phase angles = 0^o	$I_{1-2} = 1$ $I_{5-6} = 1$ $I_{dm} = 0$ $I_{dm} = 0$ $V_{dm} = 1$ $V_{dn} = -1$ $a_m = 1$ $a_n = 1$ $\cos\alpha_m = 1$ $\cos\alpha_n = -1$ $\psi_m = 0$ $\psi_n = 3.0$ (rad)

$\underline{Z}_{d.c.}$. Similar partitioning of $\underline{h}$, $\underline{\eta}$ and $\underline{R}$, discussed in Chapter 2, follows. The state vector $\underline{x}$ can be partitioned into a.c. voltage phase angles, $\underline{\theta}$, a.c. voltage magnitudes, $\underline{V}$, and h.v.d.c. link states, $\underline{x}_{dc}$. The observation equation (2.14) becomes:

$$\begin{vmatrix} \underline{Z}_p \\ \underline{Z}_q' \\ \underline{Z}_{dc} \end{vmatrix} = \begin{vmatrix} \underline{h}_p\ (\underline{\theta},\ \underline{V},\ \underline{x}_{dc}) \\ \underline{h}_q'(\underline{\theta},\ \underline{V},\ \underline{x}_{dc}) \\ \underline{h}_{dc}(\underline{\theta},\ \underline{V},\ \underline{x}_{dc}) \end{vmatrix} + \begin{vmatrix} \underline{\eta}_p \\ \underline{\eta}_q' \\ \underline{\eta}_{dc} \end{vmatrix} \tag{7.22}$$

Thus

$$\underline{H}(\underline{x}) = \frac{\partial \underline{h}(\underline{\theta},\underline{V},\underline{x}_{dc})}{\partial(\underline{\theta},\underline{V},\underline{x}_{dc})} = \begin{vmatrix} \frac{\partial \underline{h}_p(\underline{x})}{\partial \underline{\theta}}, & \frac{\partial \underline{h}_p(\underline{x})}{\partial \underline{V}}, & \frac{\partial \underline{h}_p(\underline{x})}{\partial \underline{x}_{dc}} \\ \frac{\partial \underline{h}_q'(\underline{x})}{\partial \underline{\theta}}, & \frac{\partial \underline{h}_q'(\underline{x})}{\partial \underline{V}}, & \frac{\partial \underline{h}_q'(\underline{x})}{\partial \underline{x}_{dc}} \\ \frac{\partial \underline{h}_{dc}(\underline{x})}{\partial \underline{\theta}}, & \frac{\partial \underline{h}_{dc}(\underline{x})}{\partial \underline{V}}, & \frac{\partial \underline{h}_{dc}(\underline{x})}{\partial \underline{x}_{dc}} \end{vmatrix}, \quad \underline{R}^{-1} = \begin{vmatrix} \underline{R}_p^{-1} & \underline{0} & \underline{0} \\ \underline{0} & \underline{R}_q^{-1} & \underline{0} \\ \underline{0} & \underline{0} & \underline{R}_{dc}^{-1} \end{vmatrix} \tag{7.23}$$

where $$\underline{x} = (\underline{\theta},\ \underline{V},\ \underline{x}_{dc}) \tag{7.24}$$

Since $\underline{\theta}$ does not appear in the h.v.d.c. measurement and pseudomeasurement equations:

$$\frac{\partial \underline{h}_{dc}(\underline{x})}{\partial \underline{\theta}} = \underline{0} \tag{7.25}$$

P-θ, Q-V decoupling assumes that

$$\frac{\partial \underline{h}_p(\underline{x})}{\partial \underline{V}} = \underline{0} \tag{7.26}$$

and

$$\frac{\partial \underline{h}_q'(\underline{x})}{\partial \underline{\theta}} = \underline{0} \tag{7.27}$$

Fast P-θ, Q-V decoupling assumes that:

$$\underline{H}_p = \frac{\partial \underline{h}_p(\underline{x})}{\partial \underline{\theta}} \simeq \frac{\partial \underline{h}_p(\underline{x})}{\partial \underline{\theta}}\Bigg|_{\underline{V}=1 \text{ p.u.}, \ \underline{\theta}=0^o}$$

and

$$\underline{H}_q' = \frac{\partial \underline{h}_q'(\underline{x})}{\partial \underline{V}} \simeq \frac{\partial \underline{h}_q'(\underline{x})}{\partial \underline{V}}\Bigg|_{\underline{V}=1 \text{ p.u.}, \ \underline{\theta}=0^o}$$

and

$$\underline{H}(\underline{x}) = \begin{bmatrix} \underline{H}_p & \underline{0} & \dfrac{\partial \underline{h}_p(\underline{x})}{\partial \underline{x}_{dc}} \\ \underline{0} & \underline{H}_q' & \dfrac{\partial \underline{h}_q'(\underline{x})}{\partial \underline{x}_{dc}} \\ \underline{0} & \dfrac{\partial \underline{h}_{dc}(\underline{x})}{\partial \underline{V}} & \dfrac{\partial \underline{h}_{dc}(\underline{x})}{\partial \underline{x}_{dc}} \end{bmatrix} \qquad (7.28)$$

A unified fast decoupled multi a.c. -h.v.d.c. state estimator, using Jacobian $\underline{H}(\underline{x})$ in (7.28) in the algorithm given by (2.22) is quite complex. All state dependent derivatives in the Jacobian, (7.28), require re-evaluation at each iteration. However the Jacobian can be simplified to make the off-diagonal block elements, $\partial \underline{h}_p(\underline{x})/\partial \underline{x}_{dc}$, $\partial \underline{h}_q'(\underline{x})/\partial \underline{x}_{dc}$, and $\partial \underline{h}_{dc}(\underline{x})/\partial \underline{V}$ become equal to zero. The terminal a.c. voltage magnitudes, V_m and V_n, can be treated as parameters, not states, when evaluating h.v.d.c. link measurement equations. This results in $\partial \underline{h}_{dc}(\underline{x}) / \partial \underline{V}$ becoming equal to zero. A.c. terminal, real and reactive power measurements (7.18) and (7.19) are the only measurements that have non-zero partial derivatives with respect to $\underline{x}_{dc}$. These measurements can be modified to remove the effect of the h.v.d.c. states I_{1-2} and ψ_m. Thus for the rectifier side:

$$P_m \rightarrow P_m' = \sum_{j \in \{\alpha\}} P_{mj} \qquad (7.29)$$

$$Q_m \rightarrow Q_m' = \sum_{j\varepsilon\{\alpha\}} Q_{mj} - \frac{V_m^2}{X_{fm}} \tag{7.30}$$

and

$$\frac{\partial \underline{h}_p(\underline{x})}{\partial \underline{x}_{dc}} = \underline{0} \quad \text{and} \quad \frac{\partial \underline{h}_q'(\underline{x})}{\partial \underline{x}_{dc}} = \underline{0} \tag{7.31}$$

P_m and Q_m can be modified to P_m' and Q_m' in three different ways.

7.4.1 Method 1

Monitor measurement pairs (P_m and P_{1-2}) and (Q_m and Q_{1-2}), then form pseudomeasurements:

$$P_m' = P_m - P_{1-2} \tag{7.32}$$

$$Q_m' = Q_m - Q_{1-2} \tag{7.33}$$

7.4.2 Method 2

Monitor only P_m and Q_m and transform these measurements using:

$$P_m' = P_m - \sqrt{3}\, V_{m_k} I_{1-2_k} \cos\psi_{m_k} \tag{7.34}$$

$$Q_m' = Q_m - \sqrt{3}\, V_{m_k} I_{1-2_k} \sin\psi_{m_k} \tag{7.35}$$

These equations (7.34) and (7.35) must be updated at each iteration.

7.4.3 Method 3

Monitor only P_m and Q_m, and treat the h.v.d.c. link states in equations (7.18) and (7.19) as parameters:

$$\frac{\partial P_m}{\partial \psi_m} = \frac{\partial P_m}{\partial I_{1-2}} = \frac{\partial Q_m}{\partial \psi_m} = \frac{\partial Q_m}{\partial I_{1-2}} = 0 \tag{7.36}$$

Fast decouple by setting

$$\frac{\partial P_m}{\partial V_m} = 0 \quad \text{and} \quad \frac{\partial Q_m}{\partial V_m} = \frac{\partial Q_m}{\partial V_m}\bigg|_{\underline{V}=1 \text{ p.u.},\ \underline{\theta}=0^\circ,\ \underline{x}_{dc}=\underline{x}_{dc}^{\circ}} \tag{7.37}$$

In each case, the Jacobian $\underline{H}(\underline{x})$ in (7.28) has zero off diagonal elements, and the W.L.S. state estimation algorithm becomes:

$$\begin{bmatrix} \underline{H}_p^T \underline{R}_p^{-1} \underline{H}_p & \underline{0} & \underline{0} \\ \underline{0} & \underline{H}_q'^T \underline{R}_q'^{-1} \underline{H}_q' & \underline{0} \\ \underline{0} & \underline{0} & \underline{H}_{dc}^T(\underline{x}) \underline{R}_{dc}^{-1} \underline{H}_{dc}(\underline{x}) \end{bmatrix} \begin{bmatrix} \Delta\underline{\theta} \\ \Delta\underline{V} \\ \Delta\underline{x}_{dc} \end{bmatrix} = \begin{bmatrix} \underline{H}_p^T & \underline{0} & \underline{0} \\ \underline{0} & \underline{H}_q'^T & \underline{0} \\ \underline{0} & \underline{0} & \underline{H}_{dc}^T(\underline{x}) \end{bmatrix} \begin{bmatrix} \underline{R}_p^{-1} & \underline{0} & \underline{0} \\ \underline{0} & \underline{R}_q'^{-1} & \underline{0} \\ \underline{0} & \underline{0} & \underline{R}_{dc}^{-1} \end{bmatrix} \begin{bmatrix} \underline{Z}_p - \underline{h}_p(\underline{x}) \\ \underline{Z}_q' - \underline{h}_q'(\underline{x}) \\ \underline{Z}_{dc} - \underline{h}_{dc}(\underline{x}) \end{bmatrix} \tag{7.38}$$

This algorithm can be solved sequentially as follows:

$$\underline{\theta}_{k+1} = \underline{\theta}_k + (\underline{H}_p^T \underline{R}_p^{-1} \underline{H}_p)^{-1} \underline{H}_p^T \underline{R}_p^{-1} (\underline{Z}_p - \underline{h}_p(\underline{\theta}_k, \underline{V}_k, \underline{x}_{dc_k}))$$

$$\underline{V}_{k+1} = \underline{V}_k + (\underline{H}_q'^T \underline{R}_q'^{-1} \underline{H}_q')^{-1} \underline{H}_q'^T \underline{R}_q^{-1} (\underline{Z}_q' - \underline{h}_q'(\underline{\theta}_{k+1}, \underline{V}_k, \underline{x}_{dc_k})) \tag{7.39}$$

$$\underline{x}_{dc_{k+1}} = \underline{x}_{dc_k} + (\underline{H}_{dc}^T(\underline{x}_k) \underline{R}_{dc}^{-1} \underline{H}_{dc}(\underline{x}_k))^{-1} \underline{H}_{dc}^T(\underline{x}_k) \underline{R}_{dc}^{-1} (\underline{Z}_{dc} - \underline{h}_{dc}(\underline{\theta}_{k+1}, \underline{V}_{k+1}, \underline{x}_{dc_k}))$$

where
$$(\underline{x}_k) = (\underline{\theta}_{k+1}, \underline{V}_{k+1}, \underline{x}_{dc_k}) \tag{7.40}$$

and
$$\underline{H}_{dc}(\underline{x}) = \frac{\partial \underline{h}_{dc}(\underline{x})}{\partial \underline{x}_{dc}} \tag{7.41}$$

All a.c. matrices are now fast decoupled. In effect, equation (7.39) is an extension of the sequential fast decoupling technique of Bermundez and Bramellar (1978) to a.c.-h.v.d.c. state estimation.

The three suggested methods for modifying the a.c. terminal injections were tested using the multi a.c.-h.v.d.c. power system shown in Figure 7.4. The performance of each of the schemes proved equally acceptable (see Table 7.10). Of course, method 1 can be used only when P_{1-2} and Q_{1-2} are measured. As expected, a.c. fast decoupling affects only the quality of the a.c. estimates, which are accurate to within

Table 7.10 Comparison of various fast decoupled a.c.-h.v.d.c. state estimation schemes.

	SEQUENTIAL FAST DECOUPLED A.C.-H.V.D.C. SOLUTION			EXACT W.L.S. A.C.-H.V.D.C. SOLUTION (NO DECOUPLING)
	TERMINAL INJECTIONS TREATED VIA METHOD(1)	TERMINAL INJECTIONS TREATED VIA METHOD(2)	TERMINAL INJECTIONS TREATED VIA METHOD(3)	
θ_m†	-0.18954	-0.18954	-0.18941	-0.18970
V_m†	1.02240	1.02241	1.02241	1.02305
I_{1-2}	0.60217	0.60217	0.60217	0.60194
V_{dm}	1.27808	1.27808	1.27808	1.27818
a_m	0.97271	0.97271	0.97270	0.97228
$\cos\alpha_m$	0.99264	0.99264	0.99264	0.99257
ψ_m	0.31269	0.31269	0.31270	0.31270
I_{5-6}	0.58175	0.58175	0.58180	0.58179
V_{dn}	-1.27666	-1.27666	-1.27664	-1.27668
a_n	0.93960	0.93960	0.93969	0.93968
$\cos\delta_n$	-0.98477	-0.98477	-0.98479	-0.98479
ψ_n	2.86072	2.86072	2.86073	2.86071
I_{dc}	0.45845	0.45845	0.45845	0.45845
θ_n*	-0.01887	-0.01887	-0.01883	-0.01881
V_n*	1.04718	1.04718	1.04763	1.04707
Number of Iterations Required	6θ-5v-5 dc<0.00001 5θ-4v-4 dc<0.0001 3θ-3v-3 dc<0.001	5θ-5v-5 dc<0.00001 4θ-5v-4 dc<0.0001 3θ-4v-4 dc<0.001	6θ-6v-6 dc<0.00001 5θ-4v-4 dc<0.0001 4θ-4v-4 dc<0.001	4 iterations<0.00001 4 iterations<0.0001 3 iterations<0.001
Total Execution Time $	5.387 sec.	5.144 sec.	5.443 sec.	7.444 sec.

† Rectifier a.c. terminal bus estimates

* Inverter a.c. terminal bus estimates

$ Total execution time includes time spent storing pointers and compiling graphs on a "time-shared" Burroughs B6700 computer.

0.001 p.u. anyway. Fast decoupled multi a.c. - h.v.d.c. state estimation has speed advantages over the undecoupled version even for the small 2×5 bus a.c. test system shown. Greater speed advantages are likely with much larger systems.

7.5 CONCLUSION

A method for including h.v.d.c. links in a.c. power system state estimation has been presented and tested. Both the multi a.c. - h.v.d.c. and the a.c. state estimators have similar convergence properties. Both require 4-5 iterations to converge to a tolerance of 0.00001 p.u. The introduction of h.v.d.c. links causes only a slight increase in state estimator execution time. Minimum observability requires only measurement of the a.c. terminal injected power at both ends of the h.v.d.c. link.

A method of geographically partitioning the h.v.d.c. link has been outlined and tested. Although the method is suboptimal, the degradation in the estimates is less than 0.001 p.u. in the presence of measurement noise ($<3\sigma$). Partitioning allows separate state estimation to be carried out in each a.c. system. All measurements no longer need focussing to one central state estimator.

Sequential "fast decoupled a.c." - h.v.d.c. state estimation is possible without any degradation in convergence occurring, when compared to a.c. sequential fast decoupled state estimation. Both require 5-6 iterations to converge to a tolerance of 0.00001 p.u. No degradation of the h.v.d.c. estimates occurs. Fast decoupled a.c. state estimates agree with the undecoupled values to within 0.001 p.u.

CHAPTER 8

ACCURATE REPRESENTATION OF COMMUTATION OVERLAP IN A.C. - H.V.D.C. STATE ESTIMATION AND LOAD FLOWS

8.1 INTRODUCTION

In the previous chapter the "standard" model for the h.v.d.c. link representation was outlined and tested. However in this "approximate" model for the h.v.d.c. link only the firing angle, α_m, and the extinction angle δ_m are used to describe convertor switching. The model assumes the convertor switching to be instantaneous. In practice, however, sufficient reactance is present in the a.c. power system to limit the rate of change of current from one valve to another and delay the commutation. This delay in switching of current from one valve to another, after firing, is called the commutation overlap angle, u. Four independent variables: α_m, δ_m, α_n and δ_n, are thus required to model converter switching accurately.

In this chapter an accurate, "exact" h.v.d.c. link model is included in a.c. power system state estimation and load flow analysis, and ways of improving stability and convergence discussed.

8.2 ASSUMPTIONS MADE IN THE DERIVATION OF THE APPROXIMATE H.V.D.C. LINK MODEL

The exact h.v.d.c. link model equations derived by Kimbark (1971) to describe convertor operation are, for the rectifier side:

$$s_1' \qquad 0 = I_{1-2} - a_m K_1 I_{dc}\left(\frac{\cos\alpha_m + \cos\delta_m}{2\cos\psi_m}\right) \tag{8.1}$$

$$s_2' \qquad 0 = V_{dm} - a_m K_1 V_m \left(\frac{\cos\alpha_m + \cos\delta_m}{2}\right) \tag{8.2}$$

$$s_3 \qquad 0 = V_{dm} - a_m K_1 \cos\alpha_m - K_2 X_m I_{dc} \tag{8.3}$$

Kimbark then makes the approximation that

$$\cos\psi_m \simeq \frac{\cos\alpha_m + \cos\delta_m}{2} \tag{8.4}$$

and as a result s_1' and s_2' become

$$s_1 \qquad 0 = I_{1-2} - a_m K_1 I_{dc} \tag{8.5}$$

$$s_2 \qquad 0 = V_{dm} - a_m K_1 V_m \cos\psi_m \tag{8.6}$$

Similar expressions hold for inverter operation

$$s_4' \qquad 0 = I_{5-6} - a_n K_1 I_{dc}\left[\frac{\cos\alpha_n + \cos\delta_n}{2\cos\psi_n}\right] \tag{8.7}$$

$$s_5' \qquad 0 = V_{dn} - a_n K_1 V_n \left[\frac{\cos\alpha_n + \cos\delta_n}{2}\right] \tag{8.8}$$

$$s_6 \qquad 0 = V_{dn} - a_n K_1 \cos\delta_n + K_2 X_n I_{dc} \tag{8.9}$$

Approximate

$$\cos\psi_n \simeq \frac{\cos\alpha_n + \cos\delta_n}{2} \tag{8.10}$$

results in s_4' and s_5' becoming

$$s_4 \qquad 0 = I_{5-6} - a_n K_1 I_{dc} \tag{8.11}$$

$$s_5 \qquad 0 = V_{dn} - a_n K_1 V_n \cos\psi_n \tag{8.12}$$

Together with the relationship that

$$s_7 \qquad 0 = V_{dm} - V_{dn} + R_{dc}\, I_{dc} \tag{8.13}$$

$s_1 - s_7$ completely describes convertor operation in the approximate h.v.d.c. link model, being identical to (7.1) - (7.7) in Chapter 7. Note that the approximate h.v.d.c. link model expressions, s_1, s_2, s_4 and s_5, are more linear than their exact forms s_1', s_2', s_4' and s_5'. As a result the approximate h.v.d.c. link model Jacobian elements will be more linear, and convergence will be more stable. This is because a Taylor series linearization is used in deriving the W.L.S. state estimation algorithm in Chapter 2.

Because δ_m and α_n do not appear in the approximate h.v.d.c. link model state space,

$$\underline{x}_{h.v.d.c.} = \begin{bmatrix} \psi_m, & I_{1-2}, & V_{dm}, & a_m, & \cos\alpha_m & \\ \psi_n, & I_{5-6}, & V_{dn}, & a_n, & \cos\delta_n & I_{dc} \end{bmatrix}$$

Ad-hoc techniques involving (8.4) and (8.10) are usually used to find "roughly" the value of δ_m and α_n from the estimates of $\cos\alpha_m$, ψ_m, $\cos\delta_n$ and ψ_n.

8.3 ERROR EFFECTS IN THE APPROXIMATE MODEL H.V.D.C. LINK REPRESENTATION

The approximation given by (8.4) and (8.10) is only valid when the commutation overlap angle, u, = 0°. According to Kimbark, when $u = 30^\circ$ the maximum approximation error is 1.1% and when $u = 60^\circ$ the maximum error increases to 4.3%. Figure 8.1 shows in more detail the approximation error in ψ_m, due to (8.4), for normal rectifier steady state operating conditions. Normal steady state operating conditions for the rectifier correspond to having $0^\circ < \alpha_m < 90^\circ$ and $0^\circ < u_m < 60^\circ$.

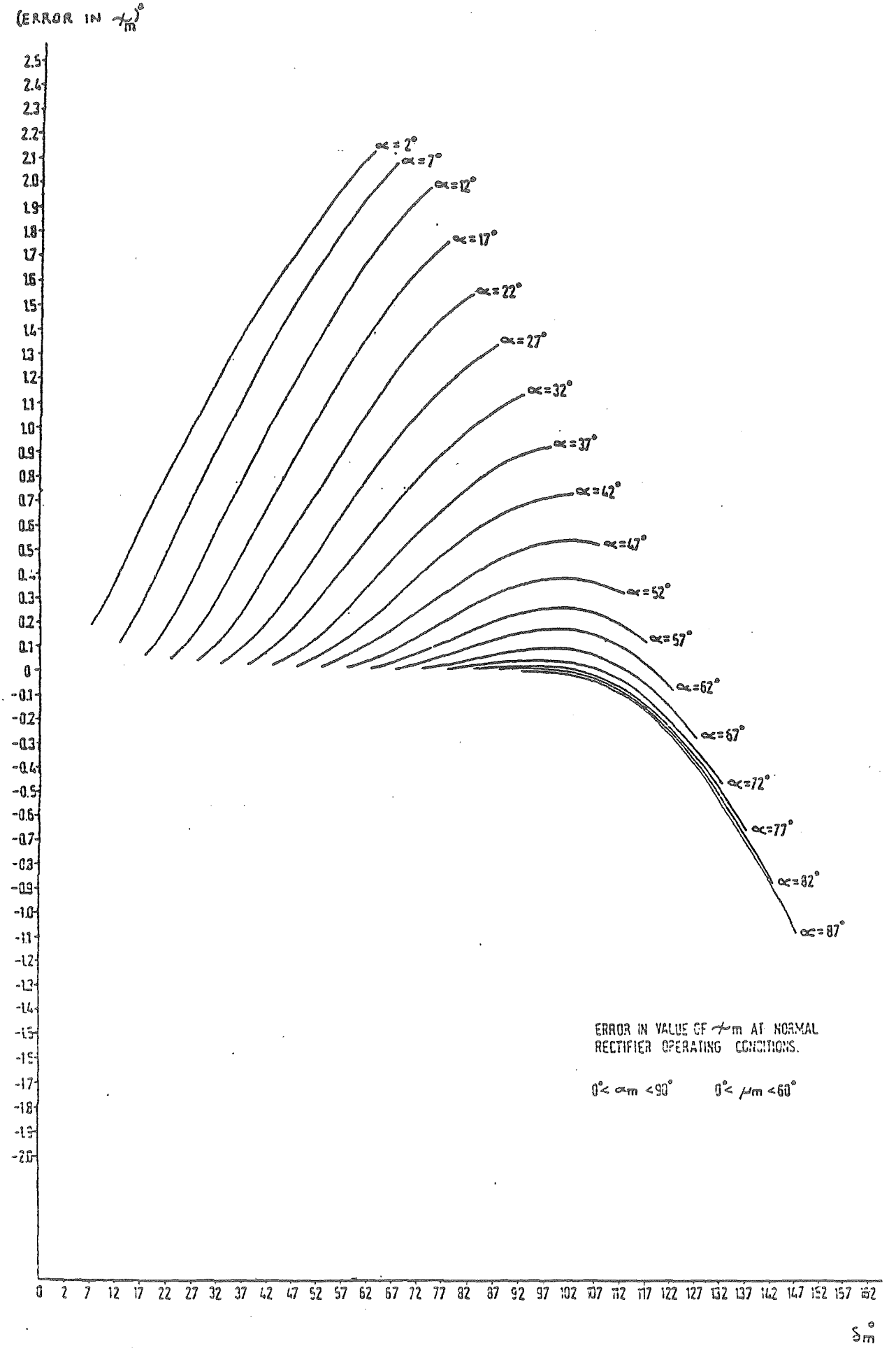

Figure 8.1 Error in value of ψ_m at normal rectifier operating conditions.

The approximation error was found by comparing the estimates of ψ_m, given by the "approximate" expression (8.4) above, with the estimate of ψ_m given by the following expression which describes the true interaction between α_m, δ_m and ψ_m, i.e. (Kimbark, 1971).

$$s_8 \qquad 0 = -\tan\psi_m + \frac{2\delta_m - 2\alpha_m + \sin 2\alpha_m - \sin 2\delta_n}{\cos 2\alpha_m - \cos 2\delta_m} \tag{8.14}$$

A similar expression holds for the inverter side of the h.v.d.c. link.

$$s_9 \qquad 0 = -\tan\psi_n + \frac{2\alpha_n - 2\delta_n + \sin 2\delta_n - \sin 2\alpha_n}{\cos 2\delta_n - \cos 2\alpha_n} \tag{8.15}$$

The commutation process from one phase to another is shown in Figure 8.2. The commutation area, δA, is fixed by the power system reactance, X_c. This area, δA, remains the same at any operating point of the convertor. Thus when the firing angle, α_m, is small, the overlap angle u becomes large to accommodate the area δA in the commutation process. However when the firing angle α_m is large, say, greater than 60°, the overlap angle, u, required to accommodate the same area, δA, is much smaller. It can be seen from Figure 8.1 that errors of more than 2° can occur in the evaluation of ψ_m, using (8.4), when α is small and u is large, while errors of less than 0.5° will occur when α is large and u is small.

Note that Figure 8.1 can also be used to find the approximation error in ψ_n due to (8.10), under normal inverter operating conditions, if ψ_m is replaced by $(180^\circ - \psi_n)$, δ_m by $(180^\circ - \alpha_n)$, and α_m by $(180^\circ - \delta_n)$. Normal steady state operating conditions for the inverter correspond to having $90^\circ < \alpha_n < 180^\circ$ and $\delta_n < 180^\circ$, where $\delta_n = u_n + \alpha_n$. For instance, when $\psi_n = 148^\circ$ and $\delta_n = 158^\circ$, according to (8.10) $\psi_n = 152.58^\circ$ and the error in this approximate value of ψ_n is 0.139°.

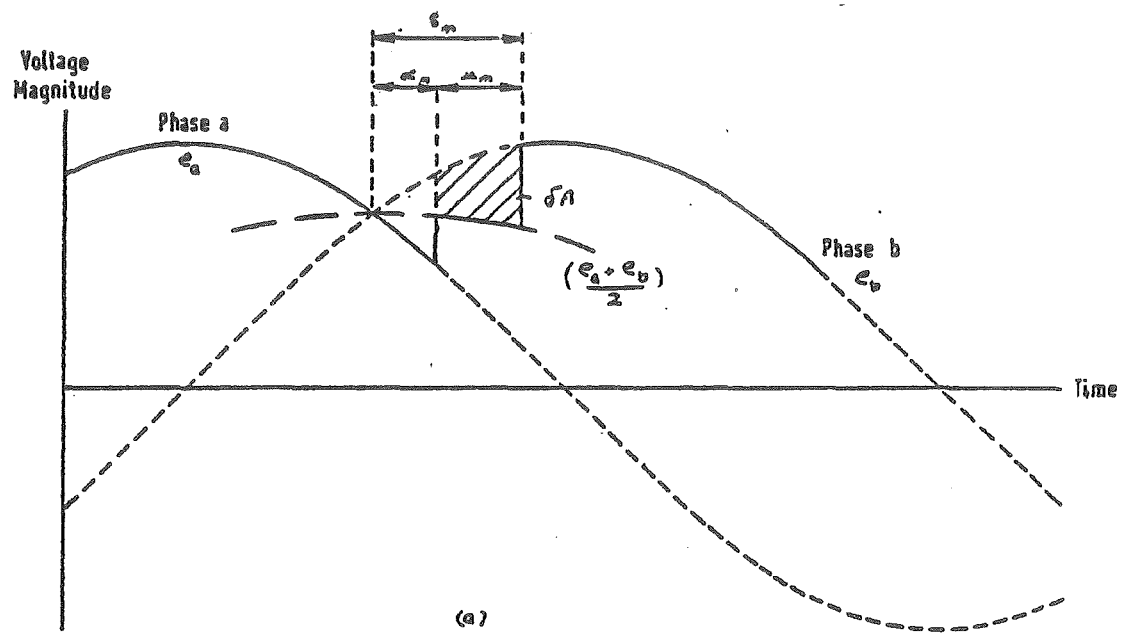

α small

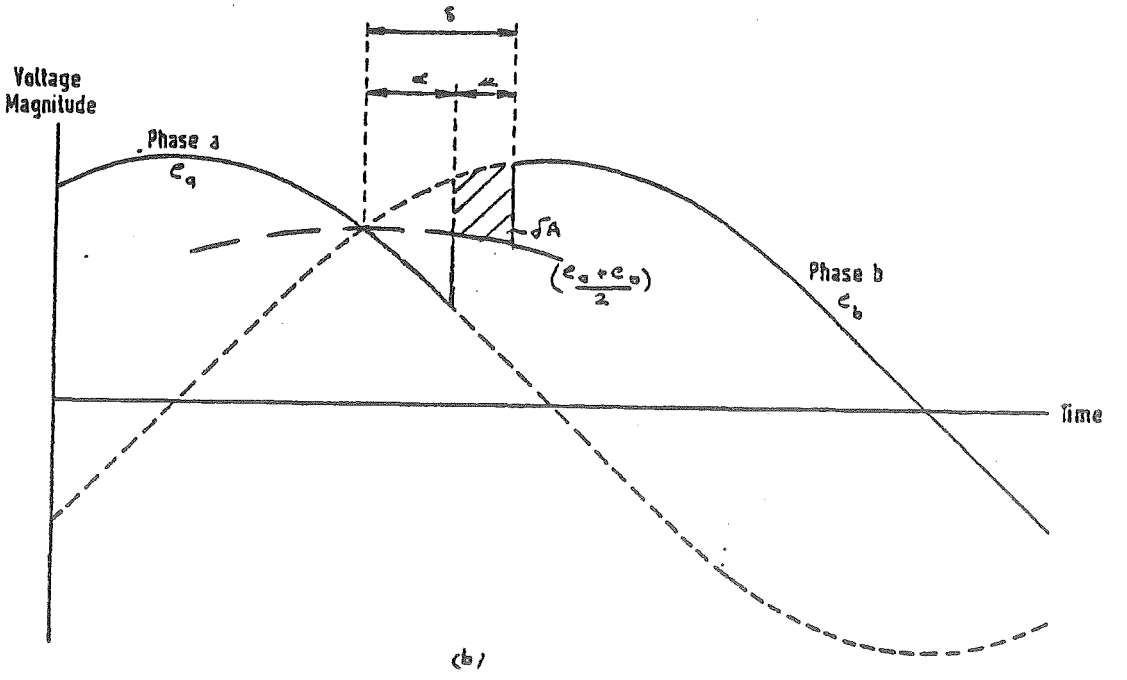

α large

Figure 8.2 Rectifier commutation.

8.4 INCLUSION OF EXACT H.V.D.C. LINK MODELS IN A.C. POWER SYSTEM STATE ESTIMATION

In Section 8.3 the approximation error due to the assumption implicit in (8.4) and (8.10) was evaluated at a large number of possible operating conditions. The two variables, α_m and δ_m, were specified and the third, ψ_m, was computed approximately and exactly, and the results compared. In state estimation, however, depending on measurement redundancies present, only one variable may be fixed and the approximation error may affect the two other variables. The approximation given by (8.4) and (8.10) was used four times in deriving the approximate h.v.d.c. link model equations, s_1, s_2, s_4 and s_5. The resulting approximation error present in the state estimator may combine additively or tend to cancel, and the true method of gauging the effect of approximation error on state estimates is to compare the results of an "a.c. - exact h.v.d.c. link model" state estimator with the results of an "a.c. - approximate h.v.d.c. link model" state estimator. The analysis of approximation error, in Section 8.3, can only serve as a guide to the possible effect the error has on state estimates.

A suitable state vector to describe the exact h.v.d.c. link model is to augment the approximate h.v.d.c. link state space, by including δ_m and α_n, i.e.

$$\underline{x}_{h.v.d.c.} = \begin{bmatrix} \psi_m, & I_{1-2}, & V_{dm}, & a_m, & \cos\alpha_m, & \delta_m, & \\ \psi_n, & I_{5-6}, & V_{dn}, & a_n, & \cos\delta_n, & \alpha_n, & I_{dc} \end{bmatrix}$$

The same h.v.d.c. link measurement equations, on and about the convertor terminals, presented in Section 7.2 still apply. The only difference in the convertor pseudomeasurement relationships used are those of s_1', s_2', s_4' and s_5' instead of s_1, s_2, s_4 and s_5. Equations s_8 and s_9 are

included to represent accurately the interaction between ψ_m, α_m and δ_m, and ψ_n, α_n and δ_n. Non-zero partial derivative Jacobian elements for these exact h.v.d.c. link model convertor relationships are presented in Table 8.1.

8.4.1 Performance results

The 5 bus a.c. - h.v.d.c. link - 5 bus a.c. test system presented earlier in Section 7.3 was used in tests to compare the performance of both the exact and approximate h.v.d.c. link model in multi a.c. - h.v.d.c. state estimation. A total of 69 measurements, in addition to pseudomeasurements, were present to estimate 31 states. A description of the measurements and their locations is given in Table 7.5. Estimates resulting from the exact and approximate h.v.d.c. link model state estimation are shown in Table 8.2. Differences in the estimates resulting from these exact and approximate h.v.d.c. link model based a.c. - h.v.d.c. state estimators are noticeable; particularly in the estimates for α_m, δ_m, α_n and δ_n. These differences are caused by the approximation error.

Consider the rectifier side of the h.v.d.c. link. When $\psi_m = 17.82^o$, the error between the exact and approximate state estimates for α_m is 1.11^o or 14%. Similarly, for the inverter side of the h.v.d.c. link, when $\psi_n = 163.93^o$ the error between the exact and approximate h.v.d.c. link estimates, for α_n, is -0.362^o or 0.22%.

Convergence is not degraded when exact h.v.d.c. link models are included in a.c. power system state estimation, provided moderate measurement redundancy is present.

8.4.2 Minimum h.v.d.c. link observability conditions

Minimum observability conditions for the approximate h.v.d.c. link model correspond to monitoring only the terminal a.c. power

Table 8.1 Non-zero Jacobian elements for exact h.v.d.c. link model convertor pseudomeasurement relationships.

(1) S_1'	$\partial S_1'/\partial I_{1-2} = 1$ $\partial S_1'/\partial a_m = -K_1 I_{dc}\left(\frac{\cos\alpha_m + \cos\delta_m}{2\cos\psi_m}\right)$ $\partial S_1'/\partial I_{dc} = -a_m K_1\left(\frac{\cos\alpha_m + \cos\delta_m}{2\cos\psi_m}\right)$ $\partial S_1'/\partial \cos\alpha_m = \frac{-a_m K_1 I_{dc}}{2\cos\psi_m}$ $\partial S_1'/\partial \psi_m = \frac{-a_m K_1 I_{dc}(\cos\psi_m + \cos\delta_m)\sin\psi_m}{2\cos^2\psi_m}$
(2) S_2'	$\partial S_2'/\partial V_{dm} = 1$ $\partial S_2'/\partial a_m = -K_1 V_m\left(\frac{\cos\alpha_m + \cos\delta_m}{2}\right)$ $\partial S_2'/\partial V_m = -a_m K_1\left(\frac{\cos\alpha_m + \cos\delta_m}{2}\right)$ $\partial S_2'/\partial \cos\alpha_m = \frac{-a_m K_1 V_m}{2}$ $\partial S_2'/\partial \delta_m = \frac{a_m K_1 V_m \sin\delta_m}{2}$
(3) S_3	$\partial S_3/\partial V_m = -K_1 a_m \cos\alpha_m$ $\partial S_3/\partial a_m = -K_1 V_m \cos\alpha_m$ $\partial S_3/\partial V_{dm} = 1$ $\partial S_3/\partial \cos\alpha_m = -K_1 V_m a_m$ $\partial S_3/\partial I_d = K_2 X_m$
(4) S_8	$\partial S_8/\partial \psi_m = \frac{-1}{\cos^2\psi_m}$ $\partial S_8/\partial \delta_m = \frac{(\cos2\alpha_m - \cos2\delta_m)(2-2\cos2\delta_m) - (2\delta_m - 2\alpha_m + \sin2\alpha_m - \sin2\delta_m)(2\sin2\delta_m)}{(\cos2\alpha_m - \cos2\delta_m)^2}$ $\partial S_8/\partial \cos\alpha_m = \frac{2((\cos2\alpha_m - \cos2\delta_m)(1-\cos2\alpha_m) - (2\delta_m - 2\alpha_m + \sin2\alpha_m - \sin2\delta_m)\sin2\alpha_m)}{\sin\alpha_m(\cos2\alpha_m - \cos2\delta_m)^2}$
Jacobian partial derivatives for the invertor side can be found by replacing m by n, 1-2 by 5-6, $\cos\alpha_m$ by $\cos\delta_n$, δ_m by α_n and X_m by $-X_n$ and re-evaluating (1)-(4) to find S_4', S_5', S_6 and S_9.	
(5) S_7	$\partial S_7/\partial V_{dm} = 1$ $\partial S_7/\partial V_{dn} = 1$ $\partial S_7/\partial I_{dc} = -R_{dc}$

Table 8.2 Comparison of exact model h.v.d.c. link and approximate model h.v.d.c. link estimates with and without exact residuals, with moderate measurement redundancy present.

	LOADFLOW USING APPROXIMATE HVDC LINK MODEL	STATE ESTIMATES WITH APPROXIMATE MODEL HVDC LINK $\sigma_{MEAS}=\sigma_{PSEUDO}=0.01$	STATE ESTIMATES FROM EXACT MODEL HVDC LINK $\sigma_{MEAS}=0.01$ $\sigma_{PSEUDO}=0.001$	STATE ESTIMATES WITH EXACT RESIDUALS AND APPROXIMATE HVDC LINK MODEL $\sigma_{MEAS}=0.01$ $\sigma_{PSEUDO}=0.001$
ESTIMATES (p.u.)				
I_{1-2}		0.60194	0.60176	0.60177
I_{dc}		0.45845	0.45911	0.45917
V_{dm}		1.27818	1.27684	1.27685
a_m		0.97228	0.97368	0.97367
$\cos\alpha_m$		0.99257	0.99003	0.99008
ψ_m	-	0.31270	0.31103	0.31108
δ_m		-	0.43266	0.43264
I_{5-6}		0.58179	0.58191	0.58192
V_{dn}		-1.27668	-1.27534	-1.27535
a_n		0.93968	0.93977	0.93977
$\cos\delta_n$		-0.98479	-0.98372	-0.98373
ψ_n		2.86017	2.86119	2.86121
α_n		-	2.78093	2.78094
SPECIFIC ESTIMATES				
ψ_m	17.92°	17.92°	17.82°	17.81°
α_m	7.00°	6.99°	8.10°	8.80°
δ_m	24.44°*	-	24.79°	24.79°
ψ_n	163.91°	163.91°	163.93°	163.94°
α_n	160.00°	-	159.34°	159.34°
δ_n	170.00°	170.00°	169.65°	169.65°
CONVERGENCE				
NO. OF ITERATIONS TO CONVERGE		5	4	6
WITHIN 0.00001 p.u.	-	4	4	5
0.0001 p.u.		3	3	4
0.001 p.u.				

* Load flow values of δ_m and α_n evaluated after load flow converged by using $\cos\delta_m = 2\cos\psi_m - \cos\alpha_m$ and $\cos\alpha_n = 2\cos\psi_n - \cos\delta_n$.

injections P_m, Q_m, P_n and Q_n; provided sufficient a.c. measurement system redundancy is already present. Monitoring P_m, Q_m, P_n and Q_n observes I_{1-2}, ψ_m, I_{5-6} and ψ_n, i.e.

$$P_m = P_{m_{a.c.}} + P_{m_{h.v.d.c.}} = \sum_{j\epsilon\{\alpha\}} P_{mj} + \sqrt{3}\, V_m\, I_{1-2} \cos\psi_m \qquad (8.16)$$

$$Q_m = Q_{m_{a.c.}} + Q_{m_{h.v.d.c.}} = \sum_{j\epsilon\{\alpha\}} Q_{mj} - \frac{V_m^2}{X_{fm}} + \sqrt{3}\, V_m\, I_{1-2} \sin\psi_m \qquad (8.17)$$

Similar relationships hold for the inverter side.

Seven states, $\{V_{dm}, a_m, \cos\alpha_m, I_{dc}, V_{dm}, a_n, \cos\delta_n\}$ remain unobservable, but seven pseudomeasurements, $s_1 - s_7$, are all present in the approximate h.v.d.c. link model based state estimator. Thus the measurement set is minimally observable.

The same conditions apply for the minimal observability of the exact h.v.d.c. link model state estimator. After monitoring P_m, Q_m, P_n and Q_n, nine states, $\{V_{dn}, a_m, \cos\alpha_m, \delta_m, I_{dc}, V_{dn}, a_n, \cos\delta_n, \alpha_n\}$, remain unobserved, but nine pseudomeasurements, s_1', s_2', s_3, s_4', s_5', s_6, s_7, s_8 and s_9, are present in the exact h.v.d.c. link model state estimator. Minimal observability follows.

8.4.2.1 Performance results.

Table 8.3 shows the estimates that result from approximate and exact h.v.d.c. link model representation in a.c. - h.v.d.c. state estimation, at minimum h.v.d.c. link observability conditions. The approximate h.v.d.c. link model state estimator converges in nine iterations to within 0.00001 p.u., whereas the exact h.v.d.c. link model is unstable, oscillating wildly about suspect values after the tenth iteration. The wild oscillations are caused by the extremely non-linear exact model h.v.d.c. link pseudomeasurement equations s_1', s_2', s_4', s_5', s_8 and s_9 and their associated Jacobian elements. Such extreme

Table 8.3 Comparison of exact h.v.d.c. link and approximate model h.v.d.c. link estimates with and without exact residuals at minimum observability conditions.

	STATE ESTIMATES FROM APPROXIMATE MODEL HVDC LINK $\sigma_{MEAS}=\sigma_{PSEUDO}=0.01$	STATE ESTIMATES FROM EXACT MODEL HVDC LINK $\sigma_{MEAS}=0.01$ $\sigma_{PSEUDO}=0.001$		STATE ESTIMATES WITH EXACT RESIDUALS WITH APPROXIMATE HVDC LINK MODEL $\sigma_{MEAS}=0.01$ $\sigma_{PSEUDO}=0.001$
ESTIMATES (p.u.)	$\underline{x}$	$\underline{x}$	$\Delta\underline{x}$ (10th iteration)	$\underline{x}$
I_{1-2}	0.60190	0.60190	-0.00000*	0.60190
I_{dc}	0.44898	-1.33623	-0.01707	0.44899
V_{dm}	1.30507	-0.44131	0.00402	1.30507
a_m	0.99267	0.68382	-0.35184	0.99557
$\cos\alpha_m$	0.99103	-0.61523	-0.04291	0.98816
ψ_m	0.31225	0.31225	-0.00000*	0.31225
δ_m	-	-4.59476	0.38145	0.42848
I_{5-6}	0.58181	0.58181	-0.00000*	0.58182
V_{dn}	-1.30359	0.43690	-0.00407	-1.30359
a_n	0.95954	-0.43475	-6.07626	0.96068
$\cos\delta_n$	-0.98371	1.14336	0.14346	-0.98256
ψ_n	2.86035	2.86035	0.00000*	2.86036
α_n	-	-71.78571	-0.04798	2.78361
SPECIFIC ESTIMATES				
ψ_m	17.89^o			17.89^o
α_m	7.68^o			8.83^o
δ_m	-			24.55^o
ψ_n	163.91^o			163.89^o
α_n	-			159.49^o
δ_n	163.99^o			169.28^o
CONVERGENCE				
NO. OF ITERATIONS TO CONVERGE WITHIN				
0.00001 p.u.	9	>10		17
0.0001 p.u.	9	>10		14
0.001 p.u.	8	>10		11

10TH ITERATION VALUES

NO CONVERGENCE IN 10 ITERATIONS

* h.v.d.c. link states estimated by the a.c. system redundancy

non-linearities degrade convergence.

8.5 EXACT H.V.D.C. LINK ESTIMATES FROM APPROXIMATE H.V.D.C. LINK MODEL STATE ESTIMATION

The approximate model h.v.d.c. link representation has the advantage of having a stable convergence because non-linearities in the Jacobian elements are not extreme. A simple modification can be made to the approximate h.v.d.c. link model state estimation algorithm to yield exact model h.v.d.c. link estimates. In essence, exact h.v.d.c. link model residuals, s_1', s_2', s_4' and s_5' are computed and used in place of the approximate h.v.d.c. link model residuals s_1, s_2, s_4 and s_5. After each iteration, k, of the approximate h.v.d.c. link model state estimator, estimates of δ_m^k and α_n^k, the two states that do not form part of the approximate h.v.d.c. link space are found as follows. The approximate model h.v.d.c. link estimates for $\cos\alpha_m^k$, ψ_m^k, $\cos\delta_n^k$ and ψ_n^k are treated as parameters, and δ_m^k and α_n^k are estimated by solving relations s_8 and s_9 using an iterative Newton Ralphson technique. The Newton Ralphson formulation is

$$x^{(i)} = x^{(i-1)} - \frac{f(x^{(i-1)})}{f'(x^{(i-1)})} \tag{8.18}$$

and when $|x^{(i)} - x^{(i-1)}|$ is less than a specified tolerance, the estimator has converged and $x^{(i)} = x^k$.

For the rectifier side of the h.v.d.c. link

$$x = \delta_m^k \Big|_{\psi_m^k, \cos\alpha_m^k} \quad \text{treated as parameters} \tag{8.19}$$

and

$$f(x) = 0 = -\tan\psi_m^k + \frac{2x - 2\alpha_m^k + \sin 2\alpha_m^k - \sin 2x}{\cos 2\alpha_m^k - \cos 2x} \tag{8.20}$$

f(x) is easily shown to be a smooth, monotonically increasing function in the interval $\alpha_m^k < \pi$ (see Appendix A.10). Hence (8.20) has at most one root in this interval. It is found that convergence to within 10^{-5} rad of this root generally occurs after two iterations if the initial guess x^o is chosen to be

$$x^o = \cos^{-1}(2\cos\psi_m - \cos\alpha_m)$$

where $x^o = \delta_m$.

A similar formulation can be found for the inverter side if $\cos\alpha_m^k$ is replaced by $\cos\delta_n^k$, ψ_m^k by ψ_n^k, and δ_m by α_n.

Residuals corresponding to s_1', s_2', s_4' and s_5' are then evaluated using estimates of δ_m^k, $\cos\alpha_m^k$, ψ_m^k and α_n^k, $\cos\delta_n^k$ and ψ_n^k. The partial derivatives in the approximate h.v.d.c. link model state estimator Jacobian remain unchanged, corresponding to those of s_1, s_2, s_4 and s_5.

The procedure outlined is repeated after each iteration until the hybrid-approximate h.v.d.c. link model state estimation algorithm with exact residuals converges (see the flow diagram in Fig. 8.3). Convergence to the optimum exact h.v.d.c. link estimates is not guaranteed however. The exact h.v.d.c. link model state estimator can be written as

$$(\underline{H}_E^T(\underline{x}_k)\underline{R}^{-1}\ \underline{H}_E(\underline{x}_k))\Delta\underline{x}_{k+1} = \underline{H}_E^T(\underline{x}_k)\underline{R}^{-1}(\underline{Z} - \underline{h}(\underline{x}_k)) \qquad (8.21)$$

where $\underline{H}_E(\underline{x}_k)$ represents the exact h.v.d.c. link model Jacobian. The hybrid approximate h.v.d.c. link model state estimator with exact residuals amounts to modally modifying the exact h.v.d.c. link model Jacobian on both sides of (8.21) to become

$$(\underline{H}_A^T(\underline{x}_k)\underline{R}^{-1}\ \underline{H}_A(\underline{x}_k))\Delta\underline{x}_{k+1} = \underline{H}_A^T(\underline{x}_k)\underline{R}^{-1}(\underline{Z} - \underline{h}(\underline{x}_k)) \qquad (8.22)$$

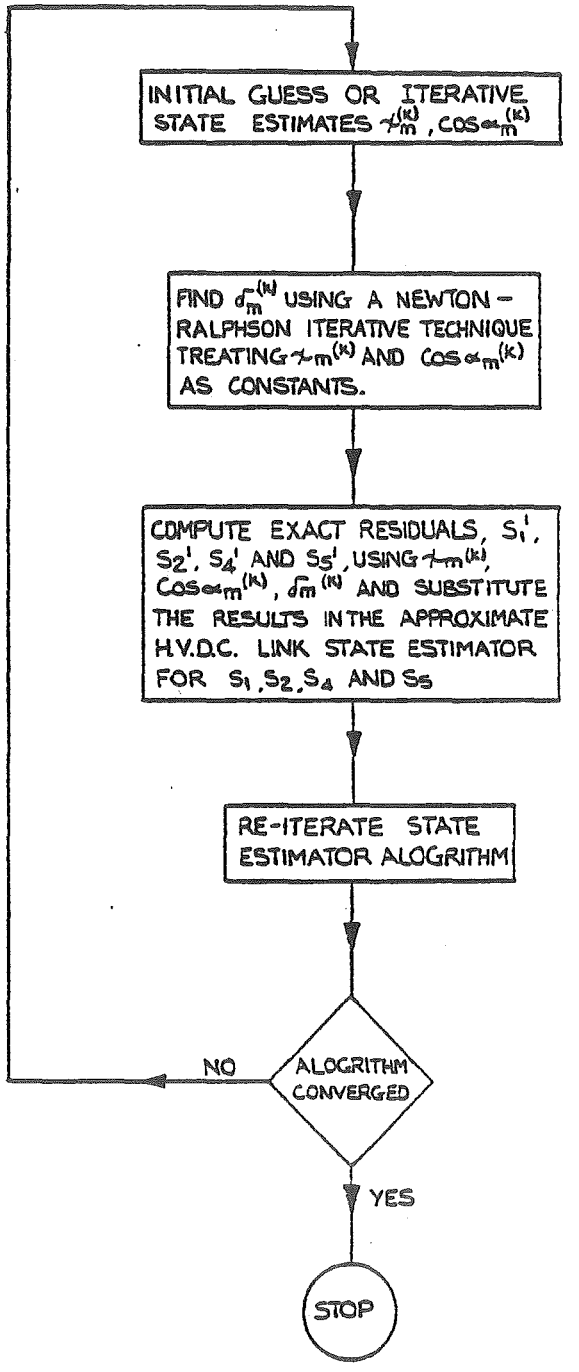

Figure 8.3 Flow diagram for approximate h.v.d.c. link model a.c.-h.v.d.c. state estimation algorithm with exact residuals.

where $\underline{H}_A(\underline{x}_k)$ is the approximate h.v.d.c. link model Jacobian.

However, modal P-θ, Q-V decoupling applied to the Jacobian matrix on both sides of (2.22) has been shown in Chapter 4 to produce stable, near-optimal estimates. It can be expected that similar near-optimal estimates will result from modally modifying (8.21) to give the hybrid approximate h.v.d.c. link model state estimator with exact residuals, as summarised by (8.22). This is confirmed by the computational results presented below.

8.5.1 Performance results

8.5.1.1 Redundant measurement conditions.

Table 8.2 shows estimates resulting from approximate h.v.d.c. link model state estimation with exact model h.v.d.c. link residuals when 69 measurements are processed to estimate 31 states. The hybrid state estimation technique with exact residuals generates similar estimates to the exact h.v.d.c. link model a.c. - h.v.d.c. state estimation algorithm outlined in Section 8.4. No degradation in convergence occurs as a result of enforcing exact residuals in the approximate h.v.d.c. link model state estimator algorithm.

8.5.1.2 Minimum h.v.d.c. link measurement observability conditions.

Thirty-eight a.c. measurements including P_m, Q_m, P_n and Q_n are monitored. Seven h.v.d.c. link pseudomeasurement relationships are present in the state estimator. Estimates are shown in Table 8.3. The hybrid a.c. - h.v.d.c. state estimation technique with exact residuals is stable and converges to the correct estimates at minimum observability conditions.

8.5.1.3 Multi a.c. - h.v.d.c. load flow conditions.

Minimum h.v.d.c. link observability conditions rely on redundancy being present in the a.c. system. A.c. - h.v.d.c. load flow analysis

requires no a.c. system redundancy. As many a.c. measurements as a.c. system states must be present. Thus, four h.v.d.c. link control specifications (measurements to the state estimator) are required to formulate the non-redundant load flow (Arrillaga and Bodger, 1977; Arrillaga *et al.*, 1980). For the 5 bus a.c. -h.v.d.c. link - 5 bus a.c. test system, nine a.c. states are present for each a.c. system. The following a.c. measurement data is used in the multi a.c. -h.v.d.c. load flow:

2 voltage magnitudes
3 reactive power injections
4 active power injections

and specified in each a.c. system. Seven pseudomeasurements are present to describe the 11 approximate h.v.d.c. link model states, and the four control specifications included are:

$$\cos\alpha_m^{spec} = \cos\alpha_m$$

$$\cos\delta_n^{spec} = \cos\delta_n$$

$$P_{dm}^{spec} = P_{dm}$$

$$P_{dn}^{spec} = P_{dn}$$

Load flow estimates based on the approximate h.v.d.c. link model, with and without exact residuals, are shown in Table 8.4. A slight improvement in convergence occurs when exact residuals are incorporated in the approximate h.v.d.c. link model state estimation. Significant differences appear in the estimates of ψ_m and ψ_n. These differences are due to approximation error.

For the rectifier side of the h.v.d.c. link, the error between the exact and approximate state estimates of ψ_m is 0.66^o or 3.6%. The discrepancy in estimates of ψ_m are shown in Table 8.4. Similarly, the error between the exact and approximate state estimates of ψ_n is 0.29^o

Table 8.4 Comparison of exact model h.v.d.c. link Newton Ralphson representation in approximate h.v.d.c. link state estimation algorithm and approximate h.v.d.c. link state estimation for a loadflow measurement set.

	STATE ESTIMATES WITH APPROXIMATE MODEL HVDC LINK	STATE ESTIMATES FROM EXACT RESIDUALS IN APPROXIMATE HVDC LINK ALGORITHM
ESTIMATES (p.u.)		
AC_1 Θ_{11}	0.0	0.0
V_{11}	1.06000	1.06000
Θ_{12}	-0.07812	-0.07818
V_{12}	1.04665	1.04685
Θ_{13}	-0.11896	-0.11894
V_{13}	1.02300	1.02300
Θ_{14}	-0.12929	-0.12931
V_{14}	1.02273	1.02283
Θ_{15}	-0.18953	-0.18969
V_{15}	1.02229	1.02311
AC_2 Θ_1	0.0	0.0
V_1	1.06000	1.06000
Θ_2	-0.01876	-0.01879
V_2	1.04682	1.04693
Θ_3	-0.06480	-0.06479
V_3	1.02400	1.02400
Θ_4	-0.06903	-0.06903
V_4	1.02326	1.02329
Θ_5	-0.07922	-0.07924
V_5	1.01734	1.01742
I_{1-2}	0.60411	0.60138
I_{dc}	0.47354	0.47354
V_{dm}	1.23748	1.23748
a_m	0.94465	0.94391
$\cos\alpha_m$	0.99255	0.99255
ψ_m	0.31211	0.30969
δ_m	-	0.43901
I_{5-6}	0.58283	0.58191
V_{dn}	-1.23591	-1.23592
a_n	0.91137	0.91127
$\cos\delta_n$	-0.98481	-0.98481
ψ_n	2.85516	2.86019
α_n	-	2.77543
SPECIFIC ESTIMATES		
ψ_m	17.74^o	18.40^o
α_m	7.00^o†	7.00^o†
δ_m	25.15^o	25.15^o
ψ_n	163.87^o	163.59^o
α_n	159.02^o*	159.02^o
δ_n	170.00^o†	170.00^o†
CONVERGENCE		
NO. OF ITERATIONS TO CONVERGENCE TO WITHIN		
0.00001 p.u.	10	9
0.0001 p.u.	9	8
0.001 p.u.	9	7

* Approximate values of δ_m and α_n evaluated after load flow converged by using $\cos\delta_m = 2\cos\psi_m - \cos\alpha_m$ and $\cos\alpha_m = 2\cos\psi_n - \cos\delta_n$

† Load flow control specifications.

or 0.18%.

Note that for the non-redundant load flow, the technique presented, having exact h.v.d.c. link model residuals in approximate h.v.d.c. link model state estimation, gives precisely the same estimates as exact h.v.d.c. link model state estimation. This is because at the solution, $\Delta\underline{x}_{k+1} \rightarrow \underline{0}$ and (8.21) and (8.22) become

$$\underline{0} = \underline{H}_E^T(\underline{x}_k)\ \underline{R}^{-1}(\underline{Z} - \underline{h}(\underline{x}_k)) \tag{8.23}$$

and

$$\underline{0} = \underline{H}_A^T(\underline{x}_k)\ \underline{R}^{-1}(\underline{Z} - \underline{h}(\underline{x}_k)) \tag{8.24}$$

Since the Jacobians $\underline{H}_E(\underline{x}_k)$ and $\underline{H}_A(\underline{x}_k)$ are both square and non-singular, in both cases $(\underline{Z} - \underline{h}(\underline{x}_k)) \rightarrow \underline{0}$, which implies convergence to the same value of $\underline{x}$.

8.6 VALIDITY OF CONVERTOR RELATIONSHIPS UNDER FAULT CONDITIONS WHEN $u > 60^o$

The convertor relationships described in the previous section are only valid when the overlap angle u is less than 60^o. Under some fault conditions u may become greater than 60^o. Measurements may be taken at the instant of a fault, for which the convertor pseudomeasurements may be invalid. Faults are cleared on the h.v.d.c. link by pumping the power in the h.v.d.c. link out to the neighbouring a.c. system by changing the firing angle from rectification to inversion. The h.v.d.c. link is then slowly re-energized after the fault is cleared. The time for the h.v.d.c. link to re-attain normal operation is usually less than 400 milliseconds (Arrillaga and Heffernan *et al.*, 1980; Heffernan *et al.*, 1980; Heffernan, 1980). This time interval is much less than the cycle time between successive measurement scans of the on-line state estimator. In the

unlikely event of monitoring measurements made during a fault, when $u > 60^{o}$, the best policy, if a fault is suspected, is to wait for the next measurement scan to arrive before processing the h.v.d.c. link measurements. The a.c. measurements obtained during the fault can still be processed to yield accurate a.c. state estimates.

8.7 CONCLUSIONS

Multi a.c.-h.v.d.c. state estimation will possibly be required to track a wide range of operating conditions. The "approximated" h.v.d.c. link model, which removes the effect of commutation overlap angle, will hold with varying accuracy at the different operating points. The largest errors result when the firing angle is small and the commutation overlap angle is large. Tests carried out showed that the error in the state estimate of α exceeded 1^{o} (or 14%). Thus for accurate a.c.-h.v.d.c. state estimation, the h.v.d.c. link without any approximations should be used. However the exact representation for the h.v.d.c. link proves potentially unstable in practice when little measurement redundancy is present. The lack of stability of the exact-model h.v.d.c. link representation's convergence is due to extreme non-linearities in unapproximated convertor relationships and their associated Jacobian values. A modification to the approximate h.v.d.c. link model a.c.-h.v.d.c. state estimator algorithm, enforcing exact h.v.d.c. link model residuals at each iteration without changing the approximate h.v.d.c. link model Jacobian structure, was tested, which generated stable, near exact estimates. The technique was also tested with a minimum observability measurement set and with a load flow configuration, and the method proved to be stable. The technique can easily be incorporated in existing a.c.-h.v.d.c. load flow programs to generate exact h.v.d.c. link estimates.

CHAPTER 9

USE OF AVAILABILITY DATA IN STATE ESTIMATOR OPERATION AND OPTIMAL METER PLACEMENT DESIGN

9.1 INTRODUCTION

The purpose of a real-time, on-line state estimator is to provide reliable estimates of power system states from noisy redundant measurement data. These estimates must be free from bad data rather than necessarily optimally filtered. Corruption of the data base, buffered by the state estimator, can occur when measurements containing noise $>3\sigma$, bad data, are processed by the estimator. Bad data "detection" tests on the estimates are performed after each estimation. Identification tests can then be used to isolate and remove the suspect bad data. In this way a reliable data base is maintained and faulty metering and communication equipment can be isolated and repaired after failure or drift occurs.

Metering and communication equipment will randomly fail and after certain failure combinations, certain nodes within the power system will be unobservable to the state estimator. The expected outage time per year which individual nodal estimates will be unavailable depends on the data acquisition system availability and on the metering configuration chosen.

Availability is defined by Shooman (1968) to be

$$A_I = \frac{\mu_i}{\lambda_i + \mu_i} \tag{9.1}$$

where μ_i is the mean time to repair, and λ_i is the mean time to failure.

Few authors account for the time varying nature of the measurement system when considering state estimation or designing for optimal meter placement. Rather, they assume that what equipment is present when the state estimator is commissioned will always be available. Methods that do include availability and equipment outage rates do so through simulations. Ariatti *et al.* (1975) studied the effect random loss of communication and metering equipment has on the observability and filtering properties of state estimates. Le Roy and Villard (1975) employ a similar technique. Masiello and Horton (1979) simulate the effect that loss of communication links has on estimate observability. Phua and Dillon (1977) use a similar technique to evaluate the effect that loss of communication links has on estimation error. However, simulation methods are time-consuming, cannot guarantee to check the effect of all possible combinations of measurement outages, particularly adverse ones since they have a low probability of occurrences, and are usually only used to check the validity of a chosen measurement set. With the exception of Ariatti *et al.* (1975), none of the meter placement methods generates quantitative availability data that describes the probability of nodes being unobservable.

In this chapter, a simple analytical method for evaluating the probability (availability) of generating observable nodal estimates and the probability of retaining the observable nodal estimates after the loss or removal of suspect measurements, when identifying bad data, is considered. The use of Markov chain probability theory allows one to determine what effect maintenance policies, influencing the mean time to repair, for individual measurement and communication link equipment, have on the availability of the observable nodal estimates. Optimal meter placement design techniques which choose the "best" set of measurements to make on the power system with regard to their individual

cost, placement and type, are reviewed and their shortcomings considered. An optimal meter design technique, based on availability analysis concepts, is proposed and its advantages and disadvantages with regard to other methods later examined.

9.2 REVIEW OF MINIMUM OBSERVABILITY CRITERIA FOR POWER SYSTEM STATE ESTIMATION

The probability (availability) of observing state estimates depends on the availability of the measurement and communication equipment of the data acquisition system and on the observability of the measurement data that reaches the state estimator. When insufficient measurements reach the state estimator to allow estimation of all or a portion of the states, the measurement set is said to be unobservable.

For a measurement set or subset to be observable, at least one nodal voltage magnitude must be monitored, and the real and reactive line-flow and injection power measurements must span the network tree or subtree of the monitored power system. The observability of combined "line-flow and injection" measurement sets can be checked by grouping the "line-flow plus voltage" measurements into a subportion of the network tree. If this subportion does not span the network tree, the estimator is only partially observable in each "line-flow plus voltage" subset. For the injection measurements now "added", to be observable, they should:

(i) Completely span any unobservable islands, meshing these islands with the observable "line-flow plus voltage" subportions. Note that an injection measurement "spans" all nodes connected by lines to that node at which the injection measurement is made.

(ii) There should be at least as many injection measurements as unobservable states.

Consider the 5 bus system shown in Figure 9.1a. Ten measurements are present. The "line-flow plus voltage" subtree is shown in Figure 9.1b. This observable island observes 5 states at nodes 1, 2 and 3 (v_1, θ_2, v_2, θ_3, v_3). Four states (θ_4, v_4, θ_5 and v_5) remain unobserved. Adding the two injection measurement pairs, s_4 and s_5, makes the measurement set completely observable. Consider the observability of the measurement set shown in Figure 9.2a. The "line-flow plus voltage" subtree observable island is shown in Figure 9.2b. Three nodes (6 states: θ_2, v_2, θ_4, v_4, θ_5, v_5) remain unobserved. Only two injection measurement pairs, s_4 and s_5, are to be added and hence only states v_1, θ_3 and v_3 are observable.

9.3 AVAILABILITY ANALYSIS

For large-scale systems, it is easier to calculate the availability for each node i of generating observable estimates rather than calculating the availability of all or some nodes being observable. Local redundancy effects simplify such nodal availability calculations.

In order to calculate the availability that a given node i will be observable, producing satisfactory estimates;

(i) "Remove" the node and its nearest neighbours from the large scale system. Observability to the node, i, is maintained by any real and reactive line-flow and injection measurements made at node i, any injection measurements made at neighbouring nodes k...ℓ and any line-flow measurements made at neighbouring nodes on lines connected to node i. Simultaneous loss of all these "link" measurements will constitute the smallest loss combination which

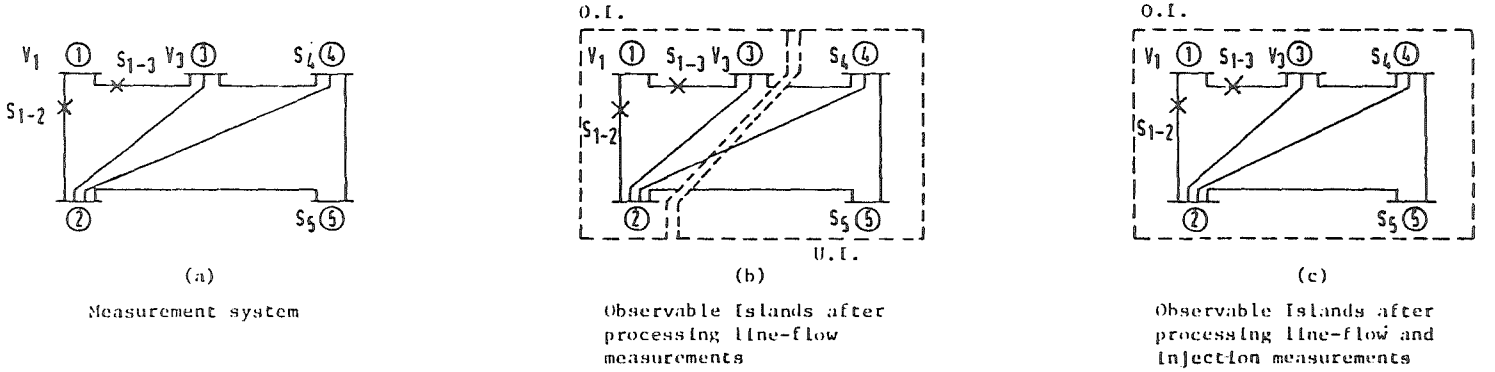

Figure 9.1 Observability of 5 bus test system with an observable measurement set.

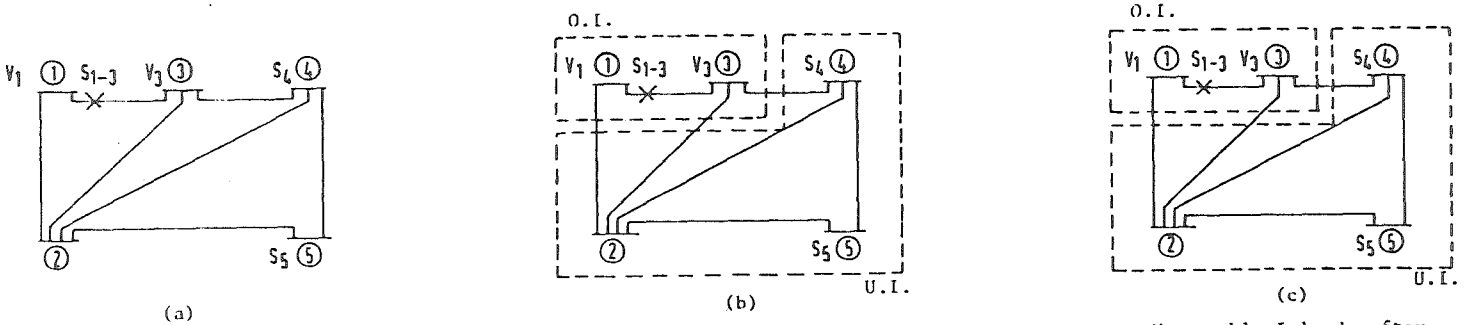

U.I. = Unobservable Island
O.I. = Observable Island

Figure 9.2 Observability of 5 bus test system with an unobservable measurement set.

must occur before node i becomes unobservable.

(ii) As well as maintaining the measurement "link" to node i, a voltage reference measurement must also be maintained. Only one voltage measurement is required when monitoring measurements on a power system. This is because real and reactive injection and line-flow measurements spanning the nodes of the power system "link" the voltage reference (as described in section 9.2). In practice, however, usually more than one nodal voltage measurement is made. Node i will "lose" its voltage reference when all link measurements are lost, as in (i), or when all nodal voltage measurements are simultaneously unavailable. The likelihood of this happening to the I.E.E.E. 14 bus "optimal meter" configuration of Handschin and Bongers (1975), shown in Figure 9.3, is small because such a loss requires simultaneous failure of seven independent communication links, assuming each node in the power system is linked to systems control by its own communication link.

Note: The presence of a voltage measurement at node 9 only guarantees to observe the voltage magnitude, not the phase angle, and thus the arguments in (ii) are still valid.

Consider the availability of node 12 producing observable estimates for the I.E.E.E. 14 bus test system with the "optimal meter" configuration shown in Figure 9.3. Node 12 and its nearest neighbours, isolated from the rest of the system, are shown in Figure 9.4. Link measurement pairs s_{13-12}, s_{13}, s_{6-12} and s_6 are present. The unavailability of node 12 producing observable estimates is, from Appendix A11,

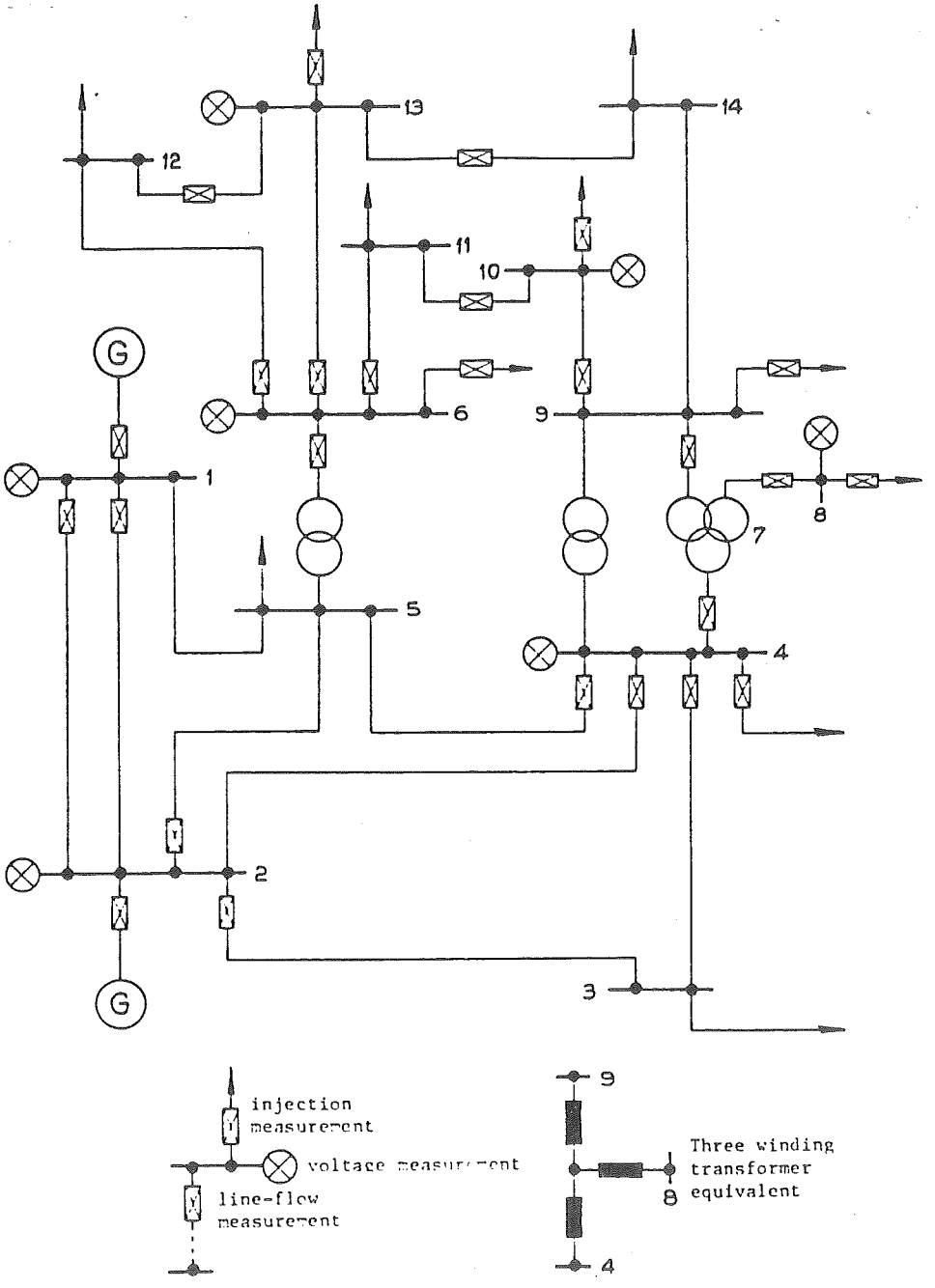

Figure 9.3 I.E.E.E. test network with optimal meter configuration. Handschin and Bongers (1975).

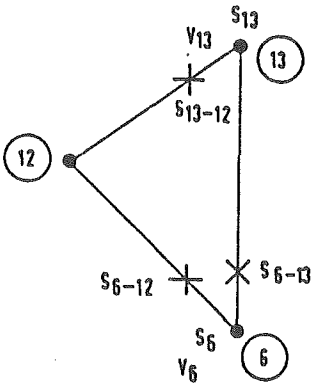

Figure 9.4 Node 12 and its nearest neighbours.

$$\bar{A}(\text{node 12 observable}) = \bar{A}_{s_{13-12}} \bar{A}_{s_{13}} \bar{A}_{s_{6-12}} \bar{A}_{s_6} \tag{9.2}$$

where, for example, $\bar{A}_{s_6}$ denotes the unavailability of the real and reactive injected power measurement at node 6, and A_{s_6} denotes the availability of the real and reactive injected power measurement at node 6, where

$$A_{s_6} = 1 - \bar{A}_{s_6} \tag{9.3}$$

It can be seen from (9.2) that the loss or removal of the four link measurement pairs s_{13-12}, s_{13}, s_{6-12} and s_6 will cause node 12 to become unobservable. Thus node 12 has a non-zero probability (availability) of producing observable nodal estimates after the simultaneous removal of any three measurement pairs. Node 12 has a

non-zero possibility of identifying any three multiple bad data points and thus has an identification capability of three.

In general, if a node is attached to other nodes by n link measurement pairs, the multiple bad data identification capability of that node is (n - 1).

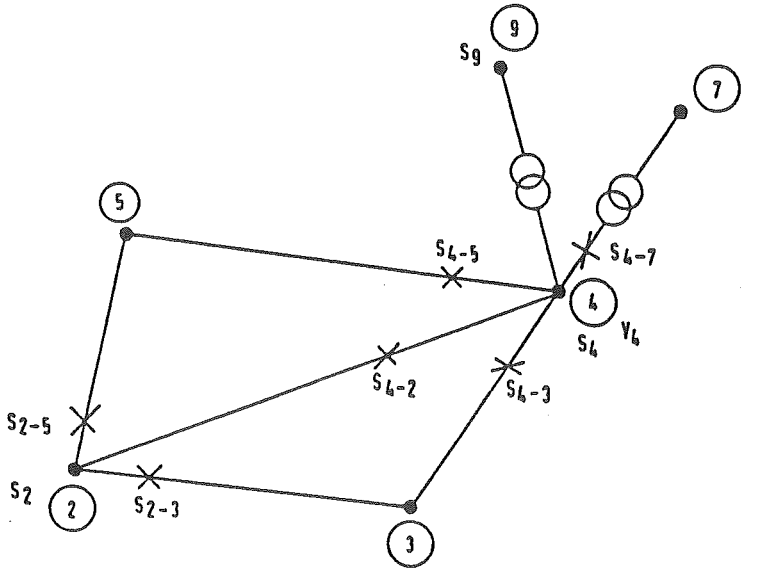

Figure 9.5 Node 4 and its nearest neighbours.

Consider node 4 and its nearest neighbours, shown in Figure 9.5. Seven link measurement pairs are attached to node 4. Thus the unavailability of node 4 producing observable estimates is

$$\bar{A}\ (\text{node 4 observable}) = \bar{A}_{s_9}\,\bar{A}_{s_4}\,\bar{A}_{s_{4-7}}\,\bar{A}_{s_{4-3}}\,\bar{A}_{s_{4-2}}\,\bar{A}_{s_2}\,\bar{A}_{s_{4-5}}\,\bar{A}_I \qquad (9.4)$$

using the arguments in Appendix A11. However the voltage reference is lost when all seven voltage measurements present in the metering configuration are simultaneously lost. Thus

$$\bar{A}\ (\text{node 4 observable}) \simeq \left[\bar{A}_{s_9}\bar{A}_{s_4}\bar{A}_{s_{4-7}}\bar{A}_{s_{4-3}}\bar{A}_{s_{4-2}}\bar{A}_{s_2}\bar{A}_{s_{4-5}} + \bar{A}_{v_1}\bar{A}_{v_2}\bar{A}_{v_4}\bar{A}_{v_6}\bar{A}_{v_8}\bar{A}_{v_{10}}\bar{A}_{v_{13}}\right] \cdot A_I \tag{9.5}$$

From Appendix A11 it can be shown that $A_I = 1$.

Node 4 has a non-zero probability of being observable after removal or loss of any six measurements, and thus has an identification capability of six.

Table 9.1 summarizes the number of link measurement pairs surrounding each node of Handschin and Bongers "optimal meter" configuration which must be lost before the node becomes unobservable. The multiple bad data "identification capability" which has a non-zero probability of identifying bad data is shown also. The number of measurements about the node which are affected by a communication link failure to the link (which transports all measurements made at the node) is also summarized. Communication link failure constitutes a "worst-case" failure. The nodes at which measurements are made are assumed to have their own independent communication link. With the exception of node 8, all nodes have a non-zero probability of remaining observable after a fault causing the loss of the communication link. Simultaneous, adjacent communication link failure has an extremely low probability of occurrence and is not considered when evaluating Table 9.1.

The effect of communication link outages on measurement data, monitored at two nodes and transmitted in the same communication link, is considered in Table 9.2. All nodal combinations are given. Nearly half of the nodal combinations, particularly when nodes are adjacent,

Table 9.1 Nodal availabilities for "optimal meter configuration", 14 bus I.E.E.E. test system and effect of communication link failure (one link per node).

NODE	NO. OF LINK MEASUREMENTS	MULTIPLE BAD DATA IDENTIFICATION CAPABILITY	COMMON MODE BAD DATA AS A RESULT OF COMMUNICATION LINK FAILURE †	LOCAL REDUNDANCY (Handschin and Bongers, 1975)
1	3	2	2	2.40
2	7	6	3	2.56
3	4	3	0	3.17
4	7	6	5	1.83
5	7	6	0	3.78
6	6	5	5	1.80
7	6	5	0	2.50
8	2	1	2*	1.25
9	5	4	2	2.20
10	4	3	3	1.83
11	4	3	0	3.00
12	4	3	0	3.00
13	5	4	3	2.25
14	3	2	0	1.83

* Denotes multiple bad data identification capability is less than the number of measurements lost as a result of communication link failure.

† Includes only loss of real and reactive injection and line-flow pair terms.

Table 9.2 Effect of communication link failure when measurements from two nodes are transmitted through the same link. "Optimal meter configuration" 14 bus I.E.E.E. test system.

NODES TRANSMITTED THROUGH COMMON COMMUNICATION LINK	EFFECT OF LOSS OF COMMUNICATION LINK
1,2*	Node 1 unobservable, 2 observable
1,4	Nodes 1 and 4 observable
1,8	Node 1 observable, 8 unobservable
1,9	Nodes 1 and 9 observable
1,10	Nodes 1 and 10 observable
1,6	Nodes 1 and 6 observable
1,13	Nodes 1 and 13 observable
2,4*	Nodes 2 and 4 observable, 3 unobservable
2,8	Node 2 observable, 8 unobservable
2,9	Nodes 2 and 9 unobservable
2,10	Nodes 2 and 10 observable
2,6	Nodes 2 and 6 observable
2,13	Nodes 2 and 13 observable
4,8	Node 4 observable, 8 unobservable
4,9*	Nodes 4 and 9 observable
4,10	Nodes 4 and 10 observable
4,6	Nodes 4 and 6 observable
4,13	Nodes 4 and 13 observable
6,8	Node 6 observable, 8 unobservable
6,9	Nodes 6 and 9 observable
6,10	Nodes 6 and 10 observable, 11 unobservable
6,13*	Nodes 13, 12 and 6 unobservable
8,9	Node 8 unobservable, 9 observable
8,10	Node 8 unobservable, 10 observable
8,13	Node 8 unobservable, 13 observable
9,10*	Node 9 observable, 10 unobservable
9,13	Nodes 9 and 13 observable, 14 unobservable
10,13	Nodes 10 and 13 observable

* Denotes adjacent nodes.

result in loss of observability after communication link failure. Without parallel, redundant communication paths, such a scheme is unlikely to be used in practice.

The number of link measurement pairs surrounding each node of Handschin and Bongers' (1975) "first meter" configuration, shown in Figure 9.6, is summarized in Table 9.3. Although eight link measurement pairs surround node 6, only seven voltage magnitude measurements are monitored in the power system, thus limiting the multiple bad data identification capability of node 6 to six. From Table 9.3, it can be seen that three nodes, 8, 10 and 13, will become unobservable after a fault affecting the communication link. The effect of outages on communication links carrying measurement data from two nodes is shown in Table 9.4. Nearly all of the possible nodal combinations, particularly the adjacent nodes, result in loss of observability due to failure of the link.

9.3.1 Inclusion of zero injection pseudomeasurements

Most optimal metering design techniques do not take special account of zero injection pseudomeasurements. Zero injection pseudomeasurements have a high accuracy, unity availability and cost nothing to monitor. In practice, as many as 40% of the injection measurements possible on a power system can be considered as zero injection pseudomeasurements. When included in an availability based optimal metering design, their presence can be relied upon and the capital resource available for the data acquisition system can be spent improving the availability of estimation at nodes which are "less secure" and are not influenced by the zero injection pseudomeasurements. The optimal metering configuration of Handschin and Bongers' (1975) contains a zero injection at node 7 that is not accounted for in their design.

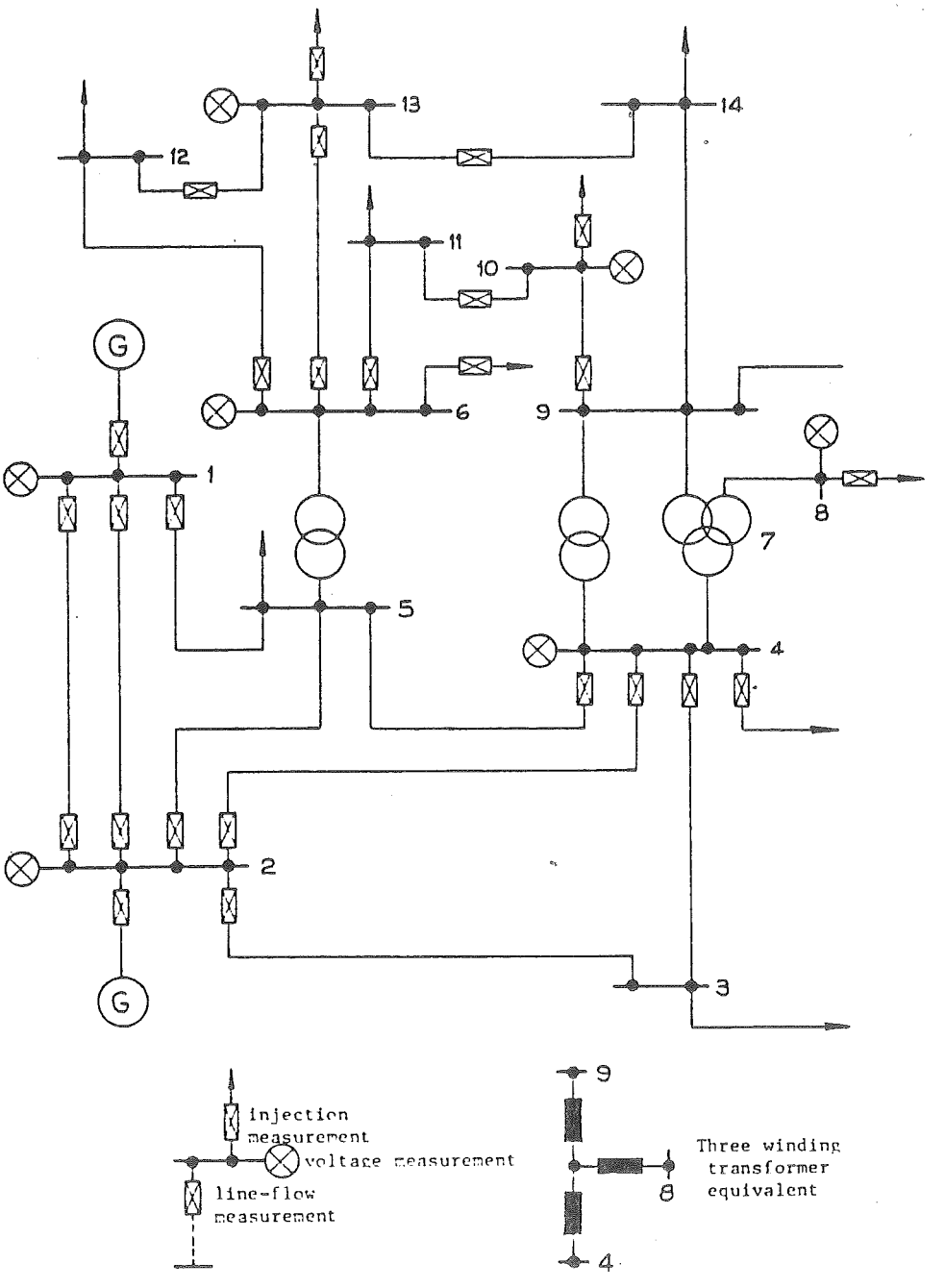

Figure 9.6 I.E.E.E. test network with first meter configuration. Handschin and Bongers (1975).

Table 9.3 Nodal availabilities for "first meter configuration", 14 bus I.E.E.E. test system and effect of communication link failure (one link per node).

NODE	NO. OF LINK MEASUREMENTS	MULTIPLE BAD DATA IDENTIFICATION CAPABILITY	COMMON MODE BAD DATA AS A RESULT OF COMMUNICATION LINK FAILURE†
1	5	4	3
2	9	8	5
3	4	3	0
4	5	4	4
5	7	6	0
6	8	5	4
7	2	1	0
8	1	0	1 *
9	3	2	0
10	3	2	3 *
11	4	3	0
12	4	3	0
13	6	5	4 *
14	2	1	0

* Denotes multiple bad data identification capabilities less than the number of measurements lost as a result of communication link failure.

† Includes only loss of real and reactive injection and line-flow pair terms.

Table 9.4 Effect of communication link failure when measurements from two nodes are transmitted through the same link. "First meter configuration" 14 bus I.E.E.E. test system.

NODES TRANSMITTED THROUGH COMMON COMMUNICATION LINK	EFFECT OF LOSS OF COMMUNICATION LINK
1,2*	Node 1 unobservable, 2 observable
1,4	Nodes 1 and 4 observable
1,8	Node 1 observable, 8 unobservable
1,10	Nodes 1 and 10 observable
1,6	Nodes 1 and 6 observable
1,13	Nodes 1 and 13 observable, 14 unobservable
2,4*	Node 2 observable, 4 and 3 unobservable
2,8	Node 2 observable, 8 unobservable
2,10	Nodes 2 and 10 observable
2,6	Nodes 2 and 6 observable
2,13	Nodes 2 and 13 observable, 14 unobservable
4,8	Node 4 observable, 8 and 7 unobservable
4,10	Node 4 observable, 10 and 9 unobservable
4,6	Nodes 4 and 6 observable
4,13	Nodes 4 and 13 observable, 14 unobservable
6,8	Nodes 6 and 8 unobservable
6,10	Node 6 observable, 11 and 10 unobservable
6,13*	Nodes 6, 12, 13 and 14 unobservable
8,10	Nodes 8 and 10 unobservable
8,13	Nodes 8 and 14 unobservable, 13 observable
10,13	Nodes 10 and 14 unobservable, 13 observable

* Denotes adjacent nodes.

The presence of this zero injection modifies the availability of the estimates at nodes 4, 7, 8 and 9. From Figure 9.1

$$\begin{aligned}
\bar{A}_7 &= \bar{A}_{s_9}\bar{A}_{s_{9-7}}\bar{A}_{s_{8-7}}\bar{A}_{s_8}\bar{A}_{s_{4-7}}\bar{A}_{s_4}\bar{A}_{s_7} + \bar{A}_{v_1}\bar{A}_{v_2}\bar{A}_{v_4}\bar{A}_{v_6}\bar{A}_{v_8}\bar{A}_{v_{10}}\bar{A}_{v_{13}} \\
\bar{A}_9 &= \bar{A}_{s_9}\bar{A}_{s_{9-7}}\bar{A}_{s_7}\bar{A}_{s_{10-9}}\bar{A}_{s_{10}}\bar{A}_{s_4} + \bar{A}_{v_1}\bar{A}_{v_2}\bar{A}_{v_4}\bar{A}_{v_6}\bar{A}_{v_8}\bar{A}_{v_{10}}\bar{A}_{v_{13}} \\
\bar{A}_8 &= \bar{A}_{s_7}\bar{A}_{s_{8-7}}\bar{A}_{s_8} + \bar{A}_{v_1}\bar{A}_{v_2}\bar{A}_{v_4}\bar{A}_{v_6}\bar{A}_{v_8}\bar{A}_{v_{10}}\bar{A}_{v_{13}} \\
\bar{A}_4 &= \bar{A}_{s_9}\bar{A}_{s_4}\bar{A}_{s_{4-7}}\bar{A}_{s_{4-3}}\bar{A}_{s_{4-2}}\bar{A}_{s_2}\bar{A}_{s_{4-5}}\bar{A}_{s_7} + \bar{A}_{v_1}\bar{A}_{v_2}\bar{A}_{v_4}\bar{A}_{v_6}\bar{A}_{v_8}\bar{A}_{v_{10}}\bar{A}_{v_{13}}
\end{aligned} \tag{9.6}$$

However, $\bar{A}_{s_7} = 0$. Thus

$$\begin{aligned}
&\bar{A}(\text{node 7 observable}) = \bar{A}(\text{node 9 observable}) = \bar{A}(\text{node 8 observable}) \\
&= \bar{A}(\text{node 4 observable}) = \bar{A}_{v_1}\bar{A}_{v_2}\bar{A}_{v_4}\bar{A}_{v_6}\bar{A}_{v_8}\bar{A}_{v_{10}}\bar{A}_{v_{13}}
\end{aligned} \tag{9.7}$$

Since the link measurement, A_{s_7}, is always available, loss of observability for estimates of nodes 4, 8, 7 and 9 depends only on losing the voltage reference to the state estimator. The estimates can be generated for nodes 4, 8, 7 and 9 after the removal of any type of bad data in the vicinity of these nodes. However, removal which causes loss of the voltage reference cannot be tolerated. The revised Table 9.1, including the zero injection of node 7, is shown in Table 9.5. All nodal estimates now have a non-zero probability of being observable after communication link failure.

9.3.2 "Local redundancy" versus "no. of link measurements"

The concept of "local redundancy" as a means of determining meter coverage can be useful but misleading. The "local redundancy" about each node is found by summing up the number of measurements made on the node and at adjacent nodes, and dividing by the number of unknowns on and at adjacent nodes. Thus voltage measurements are

Table 9.5 Nodal availability for "optimal meter configuration" 14 bus I.E.E.E. test system and effect of communication link failure (one link per node) when zero injection pseudomeasurement at node 7 is included.

NODE	NO. OF LINK MEASUREMENTS	MULTIPLE BAD DATA IDENTIFICATION CAPABILITY	COMMON MODE BAD DATA AS A RESULT OF COMMUNICATION LINK FAILURE†
1	3	2	2
2	7	6	3
3	4	3	0
4	7	7 *	5
5	7	6	0
6	6	6	5
7	6	6 *	0
8	2	2 *	2
9	5	5 *	2
10	4	3	3
11	4	3	0
12	4	3	0
13	5	4	3
14	3	2	0

* Denotes effects of the zero injection pseudomeasurement at node 7 on the multiple bad data identification capabilities at nodes 4, 7, 8 and 9.

† Includes only loss of real and reactive injection and line-flow pair terms.

included in the figure of merit as well as measurements made at the adjacent nodes, to other nodes which provide no links to the node in question. As an example, the local redundancy for nodes 6 and 12 of the Handschin and Bonger (1975) optimal metering configuration is 1.8 and 3 respectively, whereas the number of link measurements present is 6 and 4 respectively. Node 6 will have a greater nodal estimate availability than node 12, even though the "local redundancy" of node 6 is less than node 12.

9.4 DETAILED NODAL ESTIMATE - AVAILABILITY ANALYSIS

In the previous section, the availability concept of producing observable nodal estimates and bad data identification capability were outlined. A more detailed approach can be taken if Shooman's (1968) definition of availability is used (equation 9.1).

After each state estimation or series of state estimations, the probability of generating observable nodal estimates and the possible level of bad data identification capability can be computed. Depending on the equipment availabilities, the maintenance policies which determine the mean time to repair, μ_i, can be altered to give the best "coverage". If particular nodes have poor probability of bad data identification then the maintenance policy for measurement failures in the vicinity of such nodes can be geared to rapid repair. However, failures at nodes where zero injection pseudomeasurements are made in the vicinity do not need such stringent maintenance policies. Thus a hierarchical repair strategy, based on having observable nodal estimates, can be evolved to handle failure of meter and/or communication links. This repair strategy changes and evolves in time. Figure 9.7 shows possible changes in the probability of generating an observable estimate for node 1, during the change from measurement scan at time k to the measurement

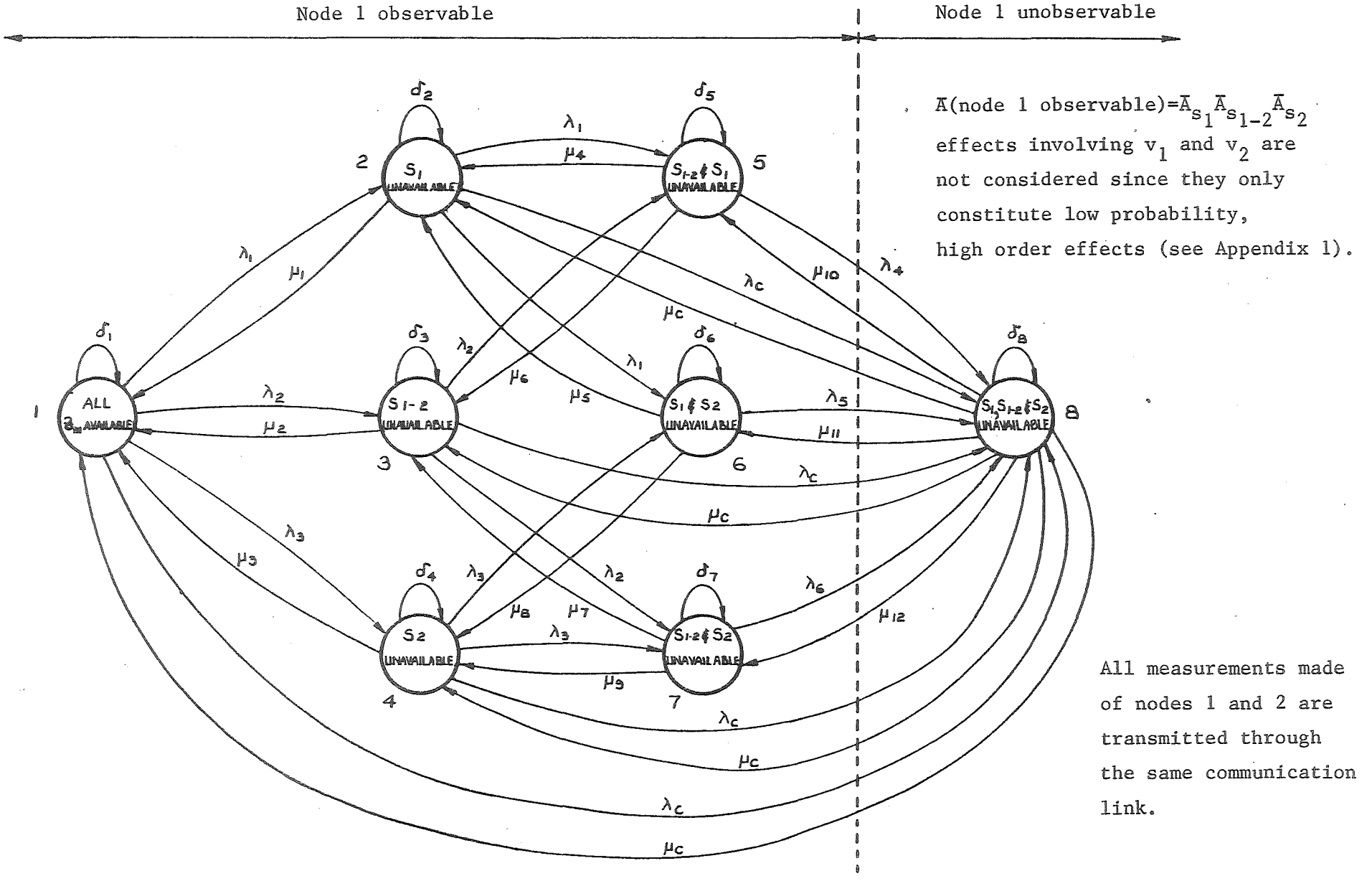

$\bar{A}$(node 1 observable)$=\bar{A}_{s_1}\bar{A}_{s_{1-2}}\bar{A}_{s_2}$ effects involving v_1 and v_2 are not considered since they only constitute low probability, high order effects (see Appendix 1).

All measurements made of nodes 1 and 2 are transmitted through the same communication link.

Figure 9.7 Transition diagram for node 1.

scan at time (k+1). Measurements may remain unrepaired and unavailable for a large number of measurement scans. A definition of probabilities in the Markov transition diagram follows (Lipschutz, 1965).

δ_i = probability that having been present at state i, at time $k\Delta t$, the "probability of generating an observable estimate" for node 1 remains unchanged, remaining at state i, at time $(k+1)\Delta t$

λ_i = probability that having been present at state i, at time $k\Delta t$, an additional measurement is lost and the "probability of generating an observable estimate" for node 1 decreases, to state j, at time $(k+1)\Delta t$.

μ_i = probability that having been present at state i, at time $k\Delta t$, a repaired measurement is re-introduced into service and the "probability of generating an observable estimate" for node 1 increases to state ℓ at time $(k+1)\Delta t$.

Only single measurement or communication link failures are considered in the state transition diagram. Communication link failure causes the simultaneous loss of measurements s_1, s_{1-2} and s_2, taking the estimate "availability" to state 8 at time $(k+1)\Delta t$, from any state i, at time $k\Delta t$. The probability of multiple measurement failure during the time scan from $k\Delta t$ to $(k+1)\Delta t$ is extremely low and can be neglected.

The Markov transition diagram contains no absorbing states (states that can be entered but not left), so long-term expected probabilities can be influenced by suitable choices of λ_i and μ_i. The probability of failure, λ_i, can be reduced by selecting high availability equipment or the use of alternate, redundant communication links during the design of the data acquisition system. The probability of failure, λ_i, thus remains largely fixed. The choice of μ_i, the meant time to repair, can be varied and determined by the operator. If measurement s_1 fails, taking the estimate "availability" for node 1 from state 1 to

state 2, the "availability" of the estimate is still high and the estimate will still be observable after further measurement failures. The mean time to repair the measurement of s_1 is not crucial. However, if failure of measurement s_1 takes the estimate "availability" for node 1 from state 2 to state 5 then the mean time to repair, μ_i, becomes crucial if secure operation is to be maintained. Further measurement failure will cause loss of observability to node 1.

The transition matrix $\underline{P}$ for the Markov chain is shown below. $\underline{P}$ forms a stochastic matrix where the rows are probability vectors; each entry of $\underline{P}$ is non-negative and the sum of the entries in each row is unity. $\underline{P}$ is also in regular matrix because all the entries of $\underline{P}$ are positive.

$$\underline{P} = \begin{array}{c} \begin{matrix} 1 & 2 & 3 & 4 & 5 & 6 & 7 & 8 \end{matrix} \\ \left[\begin{array}{cccccccc} \delta_1 & \lambda_1 & \lambda_2 & \lambda_3 & 0 & 0 & 0 & \lambda_c \\ \mu_1 & \delta_2 & 0 & 0 & \lambda_1 & \lambda_1 & 0 & \lambda_c \\ \mu_2 & 0 & \delta_3 & 0 & \lambda_2 & 0 & \lambda_2 & \lambda_c \\ \mu_3 & 0 & 0 & \delta_4 & 0 & \lambda_3 & \lambda_3 & \lambda_c \\ 0 & \mu_4 & \mu_6 & 0 & \delta_5 & 0 & 0 & \lambda_4 \\ 0 & \mu_5 & 0 & \mu_8 & 0 & \delta_6 & 0 & \lambda_5 \\ 0 & 0 & \mu_7 & \mu_9 & 0 & 0 & \delta_7 & \lambda_6 \\ \mu_c & \mu_c & \mu_c & \mu_c & \mu_{10} & \mu_{11} & \mu_{12} & \delta_8 \end{array}\right] \end{array} \quad \begin{array}{l} \lambda_4 = \lambda_1 + \lambda_c \\ \lambda_5 = \lambda_2 + \lambda_c \\ \lambda_6 = \lambda_3 + \lambda_c \end{array} \qquad (9.8)$$

Let $\underline{p}^{(o)} = \underline{P}_i$ be the initial probability distribution of the system at time $k\Delta t$ or when the state estimator is initialized. The initial probability vector, $\underline{p}^{(o)}$, indicates the availability of measurements to the state estimator when estimation begins. The probability distribution one scan later is given by $\underline{p} \cdot \underline{P}$, and the "n-step" probability distribution, n steps later at time $(k+n)\Delta t$, is given by $\underline{p}^{(n)} = \underline{p}^{(o)} \underline{P}^n$. The unique fixed point long-term probability

vector, $\underline{t}$, can also be found. The sequence, $\underline{p}$, $\underline{p}^2$, $\underline{p}^3$... of powers of $\underline{p}$ approaches the matrix $\underline{T}$ whose rows are each the fixed point vector $\underline{t}$. Also if $\underline{p}$ is any probability vector, then the sequence of vectors $\underline{p}\,\underline{P}$, $\underline{p}\,\underline{P}^2$, $\underline{p}\,\underline{P}^3$ approaches the long-term probability fixed point vector $\underline{t}$, and $\underline{t} = \underline{t}\,\underline{P}$. Thus the expected long-term probability of residing in any one of the Markov states depends only on the transition matrix $\underline{P}$ and not on the initial probability vector $\underline{p}^{(o)}$ at which the state estimator began scanning (Lipschutz, 1965). The long-term probability vector $\underline{t}$, indicating the availability of measurements influencing the state estimation of node 1, needs only evaluation once for a given λ_i, δ_i and μ_i.

If the long-term expected probability of being in Markov state 8 (where node 1 becomes unobservable) is too great, then maintenance policies affecting μ_i and δ_i should be modified and the long-term expected probabilities of generating observable estimates recomputed until a satisfactory result is obtained.

Note that the long-term expected probability of being in Markov state 8 should be numerically the same as the unavailability of node 1 generating observable estimates, found by using the methods of section 9.3. This is because the analysis in section 9.3 is based on long-term availability data while the analysis in this section is based on the availabilities of a measurement between successive scans.

9.5 REVIEW OF OPTIMAL METER PLACEMENT METHODS

Complete optimal filtering in power systems state estimation is not economically feasible since it would require the monitoring of all possible measurements. All nodal voltages, injected powers and line power flows would need monitoring, thus making data acquisition costs prohibitive. Rather, the problem is to choose the best set of

measurements to make on the power system, with regard to their individual cost, placement and type, to give the best coverage for a given capital expenditure. This is called the "optimal meter placement" problem. Coverage is taken to mean, by most authors, the degree of "noise-filtering" that occurs in the estimator as a result of the measurement set present. Most optimal meter placement designs minimize criteria involving the error co-variance matrix or its inverse, the information matrix. Schweppe *et al.* (1971, 1974) suggest using the trace of the error co-variance matrix when determining meter placement. Fetzer and Anderson (1975) apply observability theory to the information matrix in order to select the best "new" measurement to add to an existing measurement set. Edelmann (1975) uses condition numbers to access the degree of noise filtering for different metering configurations. Ogawa (1978) uses a similar criterion to assess the best way of expanding an existing measurement set. Koglin (1975), using a similar criterion to Schweppe, evaluates the degree of filtering of "quantities of interest" rather than the filtering of the estimates themselves. Arriatti *et al.* (1975) simulates the effect of meter and communication link outages by noting how the error co-variance is affected, and when nodes become unobservable due to insufficient measurement data reaching the state estimator. Le Roy and Villard (1975) extensively simulate the effect random metering errors have on the error co-variance matrix, and compare results with theoretical expectations as a way of selecting optimum meter placement. Phua and Dillon (1977) use information theory to validate Schweppe's (1970) idea that the amount of filtering in the estimate given by the trace of the error co-variance matrix. Phua and Dillon then perform an inequality constrained minimization, based on the trace of the co-variance matrix, to select the optimal meter placement. Constraints on the total available capital and lower bounded inequality

constraints on measurement accuracy are also included.

More recently, some authors have realized that the primary role of a power system state estimator is to rapidly update and maintain a reliable data base, free from bad data, rather than necessarily maintaining an optimally filtered one. In such a role, the bad data detection and identification capabilities of the state estimator become more important. Handschin and Bongers (1975) and Mafaakher *et al.* (1979) optimize the "power function of the J(x) test" which relates to the detection of bad data. The method used by these authors only accurately represents the detection of a single bad data point. Multiple common mode bad data can confuse criteria used in determing the "power function of the J(x) test", as shown in Appendix A6.

Bad data detection does not involve the removal of measurement data and hence has the same observability as the state estimation process. Bad data identification, however, involves grouping suspect bad data, removing it, and re-estimating. If insufficient measurement redundancy remains after removal of the suspect bad data, estimates may not be observable and the suspect bad data cannot be identified and the integrity of the data base cannot be maintained. Thus to an on-line state estimator, whose primary function is to maintain a reliable data base, free from bad data, identification is the most important function performed when considering optimal meter placement. The ability of the state estimator to identify bad data, after the suspect measurements have been removed, can be expressed as a probability or availability that sufficient measurements will still be present to generate observable estimates. This probability of bad data identification will depend on the availability of measurement and communication link equipment within the data acquisition system and on the observability of measurements that remain in the state estimator after the suspect

measurements are removed. An optimal meter placement method based on availability analysis is presented in the next section.

9.6 OPTIMUM METER PLACEMENT

Unavailabilities for the nodal estimates of the 14 bus test system are shown in Table 9.6.

9.6.1 Optimization constraints

The availability, A_i, of a measurement or communication link increases with cost. The cost, c_{i_z}, of providing metering equipment with availability A_{i_z} is

$$c_{i_z} = c_{i_1} A_{i_z} \tag{9.9}$$

and the cost, c_{i_c}, of installing a communication link, with availability A_{i_c}, is

$$c_{i_c} = c_{i_2} A_{i_c} \tag{9.10}$$

where c_{i_1} and c_{i_2} are constants of proportionality.

Thus the availability of a measurement arriving at the state estimator, $A_{i_{SE}}$, is

$$A_{i_{SE}} = A_{i_z} \cdot A_{i_c} \tag{9.11}$$

and the cost associated with this measurement, $c_{i_{SE}}$,

$$c_{i_{SE}} = c_{i_z} + c_{i_c} \tag{9.12}$$

Communication links can either be of "single" or parallel redundancy. In the case of two parallel links

$$A_{i_c} = 1 - (1 - A_{i_1})(1 - A_{i_2}) \tag{9.13}$$

Table 9.6 Probability of generating observable estimates for the 14 bus optimal meter configuration.

NODE	PROBABILITY OF HAVING UNOBSERVABLE NODAL ESTIMATES
1	$\bar{A}_{s_{1-2}}$ $\bar{A}_{s_1}$ $\bar{A}_{s_2}$
2	$\bar{A}_{s_2}$ $\bar{A}_{s_{2-5}}$ $\bar{A}_{s_{2-4}}$ $\bar{A}_{s_{2-3}}$ $\bar{A}_{s_1}$ $\bar{A}_{s_{1-2}}$ $\bar{A}_{s_4}$ $\bar{A}_{s_{4-7}}$
3	$\bar{A}_{s_2}$ $\bar{A}_{s_{2-3}}$ $\bar{A}_{s_4}$ $\bar{A}_{s_{4-3}}$
4	$\bar{A}_{s_4}$ $\bar{A}_{s_{4-3}}$ $\bar{A}_{s_{4-2}}$ $\bar{A}_{s_{4-5}}$ $\bar{A}_{s_{4-7}}$ $\bar{A}_{s_9}$ $\bar{A}_{s_2}$ *
5	$\bar{A}_{s_1}$ $\bar{A}_{s_2}$ $\bar{A}_{s_{2-5}}$ $\bar{A}_{s_4}$ $\bar{A}_{s_{4-1}}$ $\bar{A}_{s_6}$ $\bar{A}_{s_{6-5}}$
6	$\bar{A}_{s_6}$ $\bar{A}_{s_{6-5}}$ $\bar{A}_{s_{6-11}}$ $\bar{A}_{s_{6-13}}$ $\bar{A}_{s_{6-12}}$ $\bar{A}_{s_{13}}$
7	$\bar{A}_{s_9}$ $\bar{A}_{s_{9-7}}$ $\bar{A}_{s_4}$ $\bar{A}_{s_{4-7}}$ $\bar{A}_{s_{8-7}}$ $\bar{A}_{s_8}$ *
8	$\bar{A}_{s_8}$ $\bar{A}_{s_{8-7}}$ *
9	$\bar{A}_{s_9}$ $\bar{A}_{s_{9-7}}$ $\bar{A}_{s_{10-9}}$ $\bar{A}_{s_{10}}$ $\bar{A}_{s_4}$ *
10	$\bar{A}_{s_{10}}$ $\bar{A}_{s_{10-11}}$ $\bar{A}_{s_{10-9}}$ $\bar{A}_{s_9}$
11	$\bar{A}_{s_6}$ $\bar{A}_{s_{6-11}}$ $\bar{A}_{s_{10}}$ $\bar{A}_{s_{10-11}}$
12	$\bar{A}_{s_{13}}$ $\bar{A}_{s_{13-12}}$ $\bar{A}_{s_{6-12}}$ $\bar{A}_{s_6}$
13	$\bar{A}_{s_{13}}$ $\bar{A}_{s_{13-12}}$ $\bar{A}_{s_{13-14}}$ $\bar{A}_{s_6}$ $\bar{A}_{s_{6-13}}$
14	$\bar{A}_{s_{13}}$ $\bar{A}_{s_{13-14}}$ $\bar{A}_{s_9}$

* Probability of unobservable nodal estimates at nodes 4, 7, 8 and 9 equals zero when zero injection pseudomeasurement at node 7 is taken into account.

where A_{i_1} is the availability of one of the two links, and

A_{i_2} is the availability of the other link.

For the duplex link

$$c_{i_c} = c_{i_2} A_{i_1} + c_{i_3} A_{i_2} \tag{9.14}$$

where c_{i_3} is a constant of proportionality.

Note that if a zero injection exists at node i

$$A_{i_{SE}} = 1 \quad \text{and} \quad c_{i_{SE}} = 0 \tag{9.15}$$

Consider the availability of observable nodal estimates at node 1 when a duplex link is used. From Table 9.6

$$\bar{A} \text{ (node 1 observable)} = \bar{A}_{s_{1-2_{SE}}} \bar{A}_{s_{1_{SE}}} \bar{A}_{s_{2_{SE}}} \tag{9.16}$$

where $\bar{A}_{s_{1-2_{SE}}} = 1 - A_{s_{1-2_{SE}}} = [1 - A_{s_{1-2_z}} (1 - (1-A_{11})(1-A_{12}))]$

Similar expressions hold for $\bar{A}_{s_1}$ and $\bar{A}_{s_2}$. Thus

$$\bar{A}\text{(node 1 observable)} = [1 - A_{s_{1-2_z}} (1-(1-A_{11})(1-A_{12}))] [1-A_{s_{1_z}} (1-(1-A_{11})(1-A_{12}))] [1-A_{s_{2_z}} (1-(1-A_{21})(1-A_{22}))] \tag{9.17}$$

Note that:

(i) if only one communication path is present, $A_{12} = A_{22} = 0$, and

(ii) if the two communication paths have the same availability,

$A_{11} = A_{12}$, $A_{21} = A_{22}$.

A similar analysis can be used to determine the availability of the observable nodal estimates, at other nodes, based on the individual measurement and communication link availability data.

9.6.2 Statement of the minimization problem

Minimize the total data acquisiton measurement and communication system costs, c_T, subject to minimum observable nodal estimate availability constraints, $A_{i_{min}}$, where

$$A_{i_{SE}} \geq A_{i_{min}} \tag{9.18}$$

and where $A_{i_{min}}$ results from the individual metering and communication link availability data, i.e. equation (9.17).

9.6.3 Steps in the optimum meter placement design

1. Allot minimum permissible nodal estimate occuracies, $r_{i_{min}}$, and availabilities, $A_{i_{min}}$.
2. Postulate a data acqusition measurement system.
3. Modify the accuracy of the metering equipment, r_i, until the accuracy of the nodal estimates is sufficient ($r \geq r_{i_{min}}$).
   The accuracy of the nodal estimates (i.e. the degree of filtering necessary) is given by the trace of the inverse of the information matrix evaluated at the estimate. That is,

$$\sigma_{x_i} = \text{diag}_{ii}[(\underline{H}^T(\hat{\underline{x}})\ \underline{R}^{-1}\ \underline{H}(\hat{\underline{x}}))^{-1}] \tag{9.19}$$

   Compute the cost, c_a, of obtaining metering equipment to give this accuracy.
   (At this stage, if desired, a minimization to work out the individual meter accuracies to give the minimum cost of c_a can be done using any of the optimal meter placement techniques described in section 9.5.)
4. Postulate a communication link metering pattern linking the nodes in the power system to the control centre. Either single or parallel redundant communication paths can be considered in the

analysis.

5. Minimize the total data acquisition system cost, c_T, subject to the minimum nodal estimate availability constraints. (Although stated, the problem was not solved using test examples in this study. Since contraints are linear, the Sequential Linearly Constrained Minimization Technique (SLCMT) used by Phua and Dillon (1979) would be a suitable minimization technique, or, if all the availabilities are similar, an integer programming approach could be used.)

6. Repeat (4)-(5) with different communication link patterns until all "reasonable" possibilities have been tried.

7. Choose the scheme which gives the least data acqusition system availability cost. The total data acquisition system costs include both the availability costs and the accuracy cost.

8. Repeat steps (3)-(7) using different data acquisition measurement systems.

9. Choose the data acquisition system which had the least total cost to satisfy the minimum availabilities and accuracy constraints. Ensure that the total cost is less than the total resource available. If desired, raise or lower the minimum permissible nodal estimate accuracies and availabilities, and repeat (1)-(9).

9.7 COMPARISON BETWEEN "THE POWER OF THE $J(\hat{\underline{x}})$" TEST AND AVAILABILITY-BASED METER PLACEMENT DESIGN

Limitations of the "power of the $J(\hat{\underline{x}})$" test, which aims to optimize the detection capability of a data acquisition system and give an even coverage of detection capability, (Appendix A6), result

because the test only models distortion in $J(\hat{\underline{x}})$ caused by single and multiple non-interacting bad data. It cannot give any information about multiple interacting bad data. Another limitation of the power of the $J(\hat{\underline{x}})$ test is that it does not model the changing membership of the data acquisition system, with time, as meter and/or communication links fail and are repaired.

The availability based meter placement scheme, on the other hand, gives the identification capability of each node, which is the largest number of measurements about the node that can simultaneously be removed without resulting in a "zero-probability" of producing an observable nodal estimate when the remaining measurements are processed. However the availability approach assumes that having an observable estimate is the same as having sufficient bad data detection capability. Some observable estimates may have poor bad data detection capability, thus the availability based approach to meter placement is a "necessary but not sufficient" condition for detecting multiple bad data. It is a "necessary and sufficient" condition for generating observable estimates after the removal of multiple bad data. To relate the observable estimates to bad data detection capability, the power of the $J(\hat{\underline{x}})$ test should be used. Thus both the power of the $J(\hat{\underline{x}})$ test and the availability based meter placement design are complementary and should be used together during optimal meter placement design. No test has yet been found which accurately models distortions caused by multiple interacting bad data and can be used in the design of metering systems.

9.8 CONCLUSION

The primary task of an on-line state estimator is to provide reliable estimates, free from bad data. As a result, the most important

property of the state estimator is its ability to identify single and multiple interacting and non-interacting bad data and thus maintain a "clean" data base for monitoring and control purposes.

Availability aspects of generating observable nodal estimates are more important than optimal filtering of the estimates, particularly for on-line state estimation. Availability aspects can be accounted for by defining the "identification capability" of each node, to be the largest number of measurements about the node that can be simultaneously removed from the state estimator without resulting in a "zero-probability" of producing observable nodal estimates when the remaining measurement set is processed. Meter placement can be decided using "identification capability" and availability aspects. Advantages of the design method include the following:

- Most of the design can be done without recourse to a computer.
- Most data acquisition systems commissioned augment existing data acquisition equipment that may be of a different vintage, and have a lower accuracy and availability. In some cases, measurement C.T's may have been previously used for relays. The meter placement design technique can account for these different availabilities.
- Zero injection pseudomeasurements can be used in the design. Zero injection measurements are highly accurate and highly available (100%) pseudomeasurements that do not require monitoring. Other optimal meter placement designs do not account for the special qualities of the zero injections. Availability based optimal meter placement can pivot other measurements away from the highly available pseudomeasurements to spread the nodal estimation availabilities evenly.

Availability based meter placement design is a "necessary but not sufficient" test of multiple and single bad data detection and identification capability. It is a "sufficient" test of nodal estimate observability. The availability based meter placement design should be used in a "complementary" manner with the power of the $J(\hat{x})$ test optimal meter placement design which accurately models the detection of single and multiple non-interacting bad data, but assumes all measurements present in the data acquisition system will always be present, and cannot handle multiple interacting bad data.

CHAPTER 10

HIERARCHICAL STATE ESTIMATION OF A COMBINED ELECTRICAL HYDROTURBINE AND OPEN CHANNEL HYDROCANAL SYSTEM - FEASIBILITY INVESTIGATIONS

10.1 INTRODUCTION

The concept of "energy-system" state estimation involving the estimation of composite power systems - , hydro, electrical and/or mechanical - was first suggested by Peterson (1977) but as yet no practical large scale applications have appeared.

Consider the role of the area computer located at Twizel, which monitors a portion of the South Island power system. Twizel is the control centre of the Upper Waitaki power development. The quantities monitored are electrical power and voltages at and around nodes within the area, water height and pseudomeasurements of flow within the open channel power canals linking the generating stations, and measurements on the generating units. The data base within the area computer is then used to aid the operator in remotely controlling the power output etc. of the generating stations. A "possible" configuration of high voltage electrical measurements to be made on the Upper Waitaki system is shown in Figure 10.1. Figure 10.2 indicates local 33 kV power board and service supplies. Measurements made on the Tekapo B power canal are shown in Figure 10.3.

The canal as shown is about 25 km long, with only five monitoring points where the depth is measured. At the generating stations at each end of the canal, the flow is computed by interpolating between values in a 9×9 look-up table which describes the station's stored discharge-head relationship.

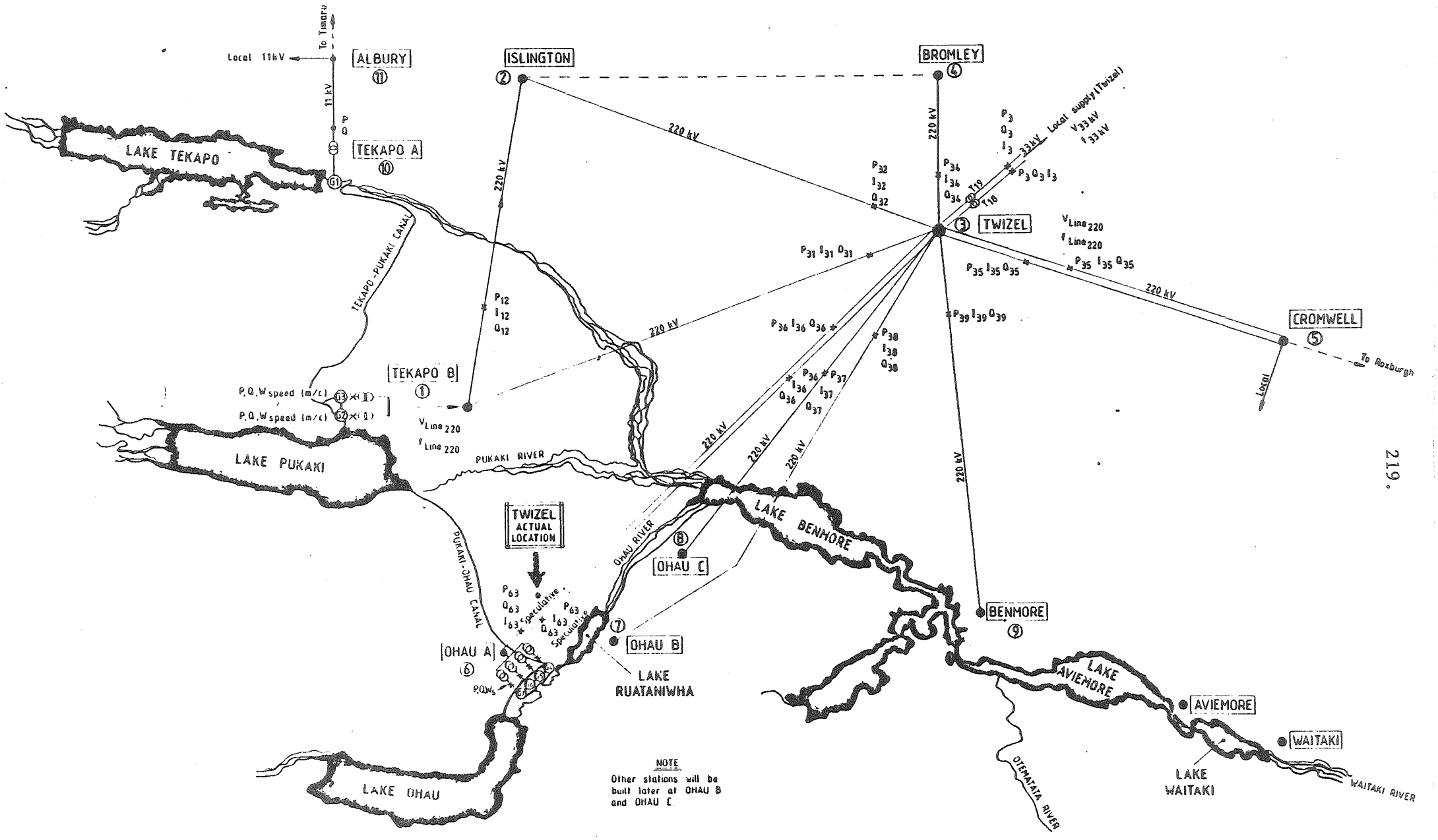

Figure 10.1 "Possible" 220 kJ measurements on the Upper Waitaki system.

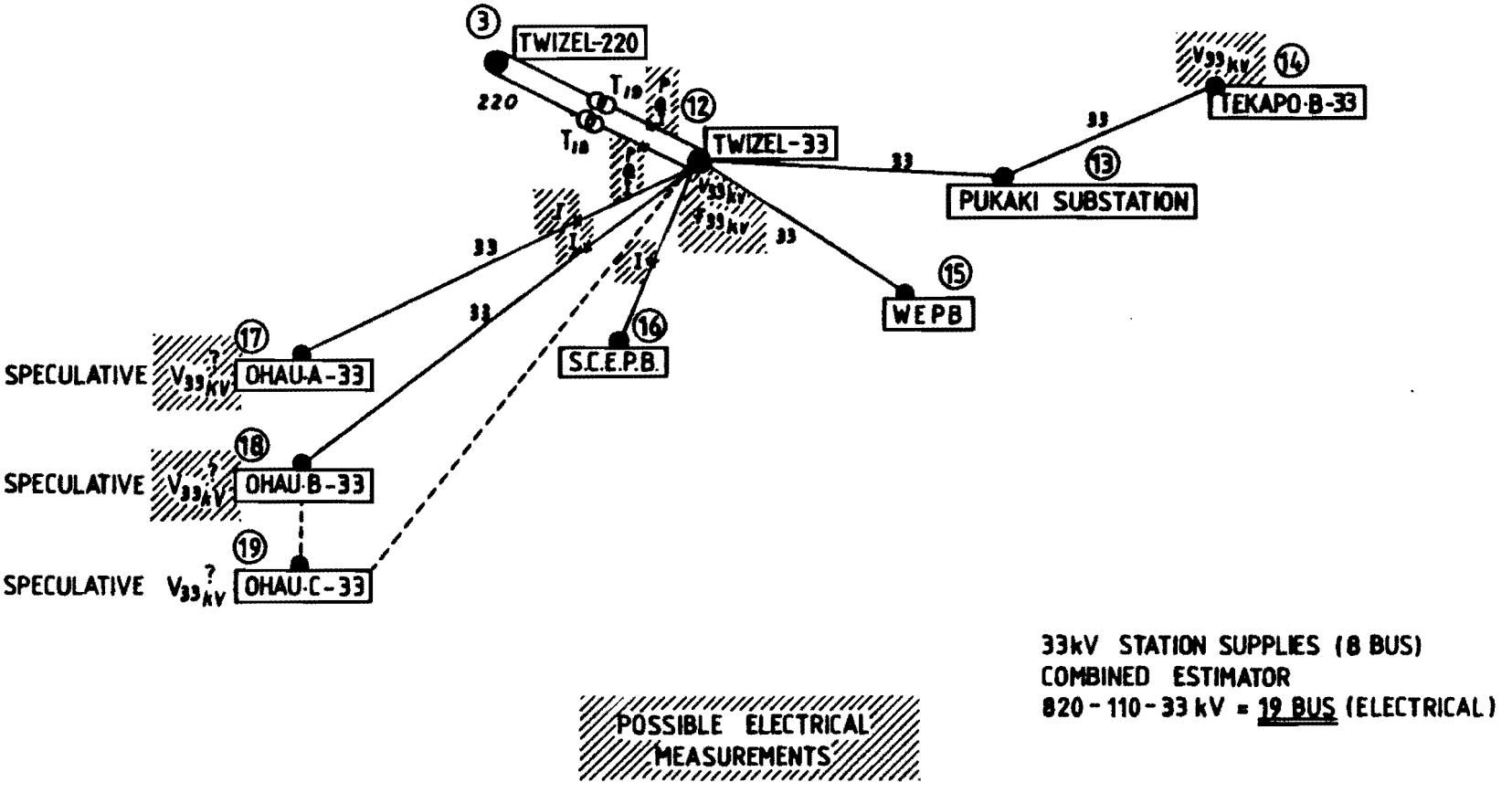

Figure 10.2 "Possible" 33 kV electrical measurements.

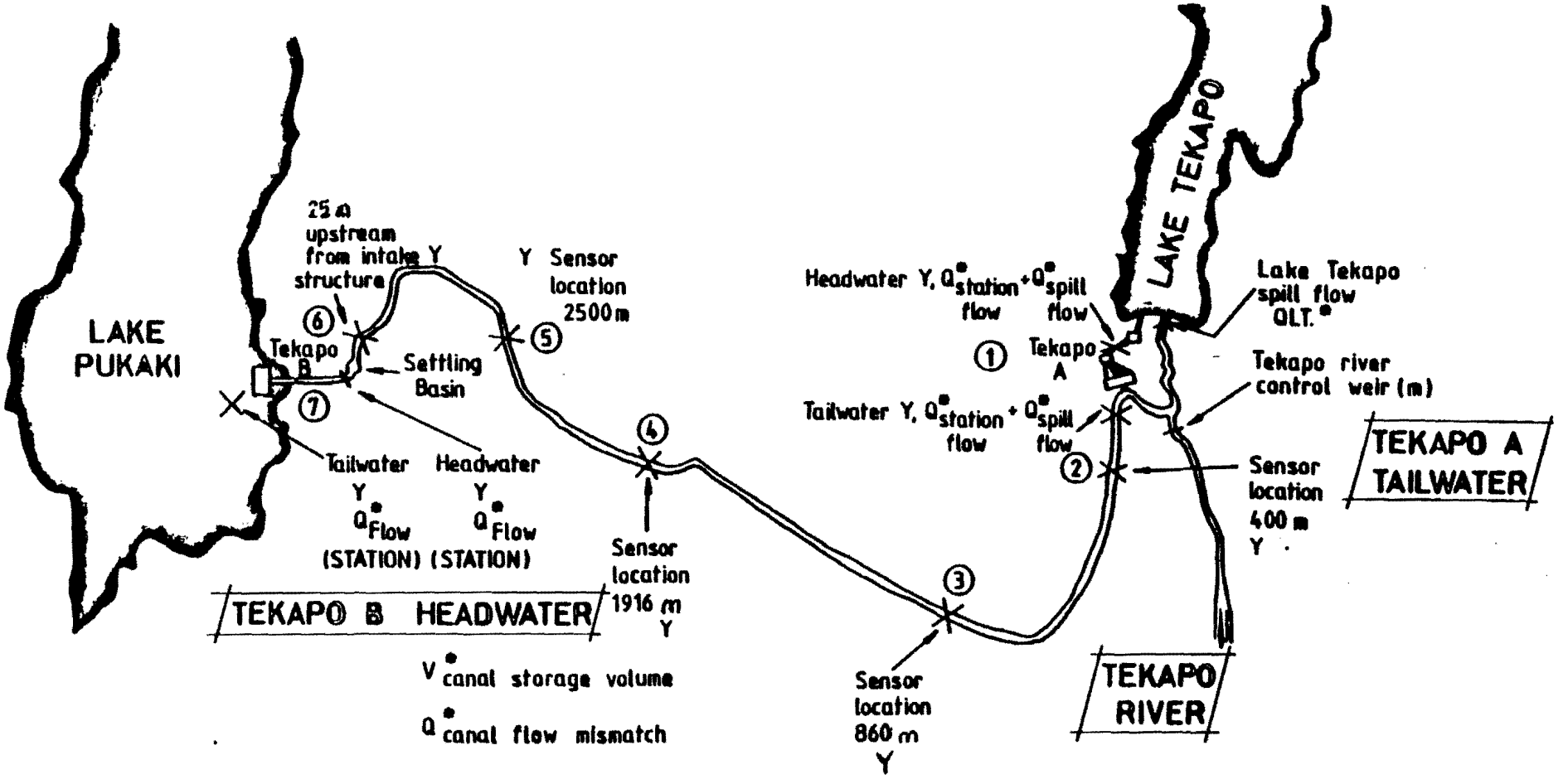

Figure 10.3 Location of Tekapo canal height and flow measurements.

* - Indicates flow psuedomeasurement calculated by the computer

Note the nature of the Tekapo B canal is such that the water in the canal would overflow its banks if both Tekapo A and B generating stations were shut down simultaneously. When shutting down the canal, Tekapo B must pass water (through either a bypass valve or generation) until the settled level of the remaining water is lower than the height of the canal. Thus it would be of some advantage to use a state estimator to check the consistency of the open channel flow and height and the hydrogenerator measurements, as well as those of the electrical systems.

In this chapter, the feasibility and performance of a combined electrical-mechanical-hydraulic, static, dynamic hierarchical state estimator is investigated.

10.2 STRUCTURE OF THE COMBINED ELECTRICAL/HYDRAULIC STATE ESTIMATOR

Because the mathematical equations describing open channel flow and turbine dynamics are time dependent, containing "inertia" effects, any state estimator which is to estimate the hydro or mechanical states must be dynamic. Little published work has appeared involving the estimation of generation units status (Handschin and Galiana, 1973; Galiana and Handschin, 1972; Miller and Lewis, 1971, Ljubojevic, 1979) and no work has appeared concerning the dynamic estimation of hydrocanal states, other than papers reviewing the problem or solving only the open channel flow dynamics (Chiu and Isu, 1978; Moore, 1973; Longham, 1971; Yeh and Becker, 1973). Also, the work published on generating unit estimation only models thermal unit behaviour. Handschin and Galiana (1973) use a linear formulation of the Kalman filter to dynamically estimate the thermal units states. Updated electrical generation measurement data is received from a central, tracking, static W.L.S.

state estimator which estimates the state of the electrical system. The measurement scan rate of this global static state estimator is much slower than that of the local dynamic state estimators. Consequently the local dynamic estimators can detect more precisely and rapidly, anomalous system behaviour in their area before the global tracking state estimator. If a disturbance does occur, more detailed information can be co-ordinated, when required, from the local state estimator to the systems control centre to aid decision making. Transmitting all of the measurements all of the time to the global state estimator would require large, expensive, central computers (Handschin and Galiana, 1973).

Such a hierarchical estimation structure can be applied to the functions of area computers controlling hydrocanals and hydroturbines, as shown in Figure 10.4. Generation busbar states $v(t_k) \angle \theta(t_k)$ are co-ordinated to the local dynamic state estimator after each global tracking state estimation has been completed. Detection and identification of any electrical power system bad data occurs before the busbar state estimates are transmitted, to ensure that $v(t_k) \angle \theta(t_k)$ are free from bad data and can be treated as parameters in the local estimators. Note that if communication between the central control centre and the area computer is unreliable, then the local state estimator can also estimate the electrical states within its "area".

The hierarchical estimation concepts as outlined could also be extended to model large loads or interconnected neighbouring systems, as shown in Figure 10.5 (Handschin and Galiana, 1973). However, in this study only combined estimation of electrical, hydrogenerator and open channel hydro state is considered.

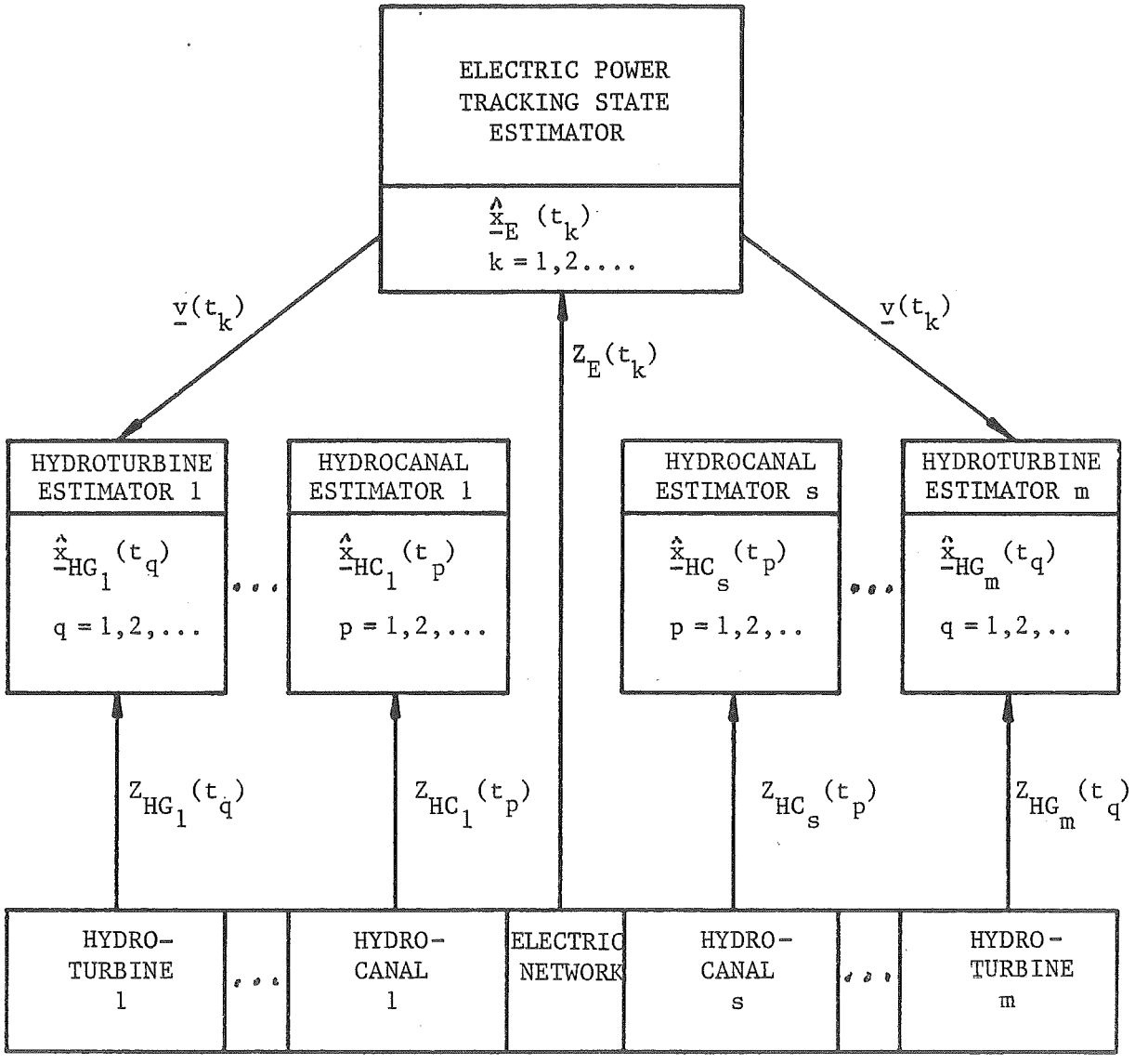

Figure 10.4 Two-level "static-dynamic" state estimator of network, hydrocanal and power plant states, when s hydrocanals and m hydrogenerators are present.

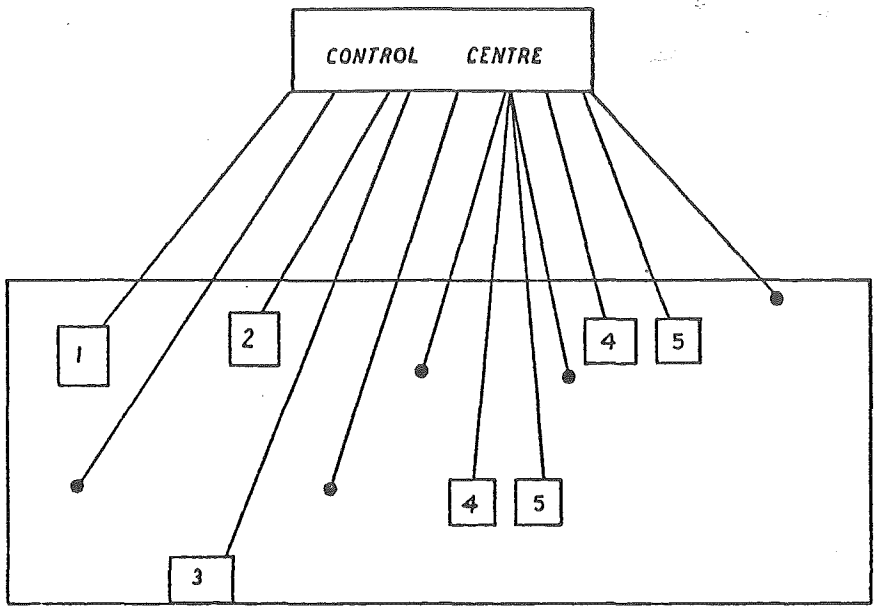

Figure 10.5 Hierarchical estimation scheme with centralized tracking estimator and local dynamic estimators for thermal power plant (1), large loads (2), tie lines (3), hydropower plant (4), and hydro-canal states (5).

10.3 ELECTRIC POWER SYSTEM TRACKING STATE ESTIMATOR

The central electric power system tracking state estimator uses the conventional W.L.S. formulation described in Chapter 2, where equation (2.22) now becomes

$$\hat{\underline{x}}_E(t_{k+1}) = \hat{\underline{x}}_E(t_k) + (\underline{H}^T(\hat{\underline{x}}_E(t_k))\underline{R}^{-1}\underline{H}(\underline{x}_E(t_k)))^{-1}\underline{H}^T(\underline{x}_E(t_k))\ \underline{R}^{-1}(\underline{z}(t_{k+1})-\underline{h}(x_E(t_k)) \tag{10.1}$$

No satisfactory mathematical model is available to predict the change of the electric power state with time, and so the tracking state

estimator always lags behind the actual state of the power system (Handschin and Galiana, 1973). Information about hydrocanal or hydro-turbine states cannot be obtained from a knowledge of $\underline{x}_E(t_{k+1})$.

10.4 MODEL FOR THE HYDROTURBINE PORTION OF A HYDROGENERATING UNIT

Models for thermal turbine units have been suggested by Galiana and Handschin (1972), Handschin and Galiana (1973) and Ljubojevic (1979) and used for state estimation purposes. However, the role of a hydro station in a power system differs somewhat from that of the thermal station. Hydro stations usually follow peak load variations whereas the thermal units usually provide "base load" power. Thus the hydro-generator is more responsive than the thermal unit; more rapidly changing its state between global static state estimate measurement scans. As a result it may be desirable to have local dynamic state estimation of the hydrogenerator. Models for hydroturbine and governor plant have been published in Sterling (1979), Wylie and Streeter (1978), Hovey (1962), Schleif and Wilbur (1966), Thorne and Hill (1975), Dhaliwal and Wichert (1978), Hagihara *et al.* (1979), Ramey and Skooglund (1970), Chaudry (1970), Brekke (1974) and Simpson (1976). The models presented in these references vary in complexity. The papers presented by Brekke (1974), Chaudry (1970) and Streeter and Wylie (1978) contain hydroturbine models which include the effects of water hammer in the penstocks, in addition to modelling the influence of turbine characteristics, the governor, and the influence of the generator and load. Ramey and Skooglund's paper does not model water hammer, however, but includes a penstock-turbine transfer function. If such hydroturbine models which include penstock effects, particularly water hammer, were used, dynamic state estimation of the combined hydro-

canal-turbine would be possible rather than the separate dynamic estimation of the hydrocanal and hydroturbine, as shown in Figure 10.4. For the purposes of this study, however, the separate estimation of canal and turbine "only" will be attempted. The hydroturbine model chosen for the study is taken from the paper of Dhaliwal and Wichert (1978) and actually models the Kettle generating station of the Maintoba hydro system.

The block diagram for the Kettle turbine and governor equipment is shown in Figure 10.6. Included in the model is a load self-regulation factor, α.

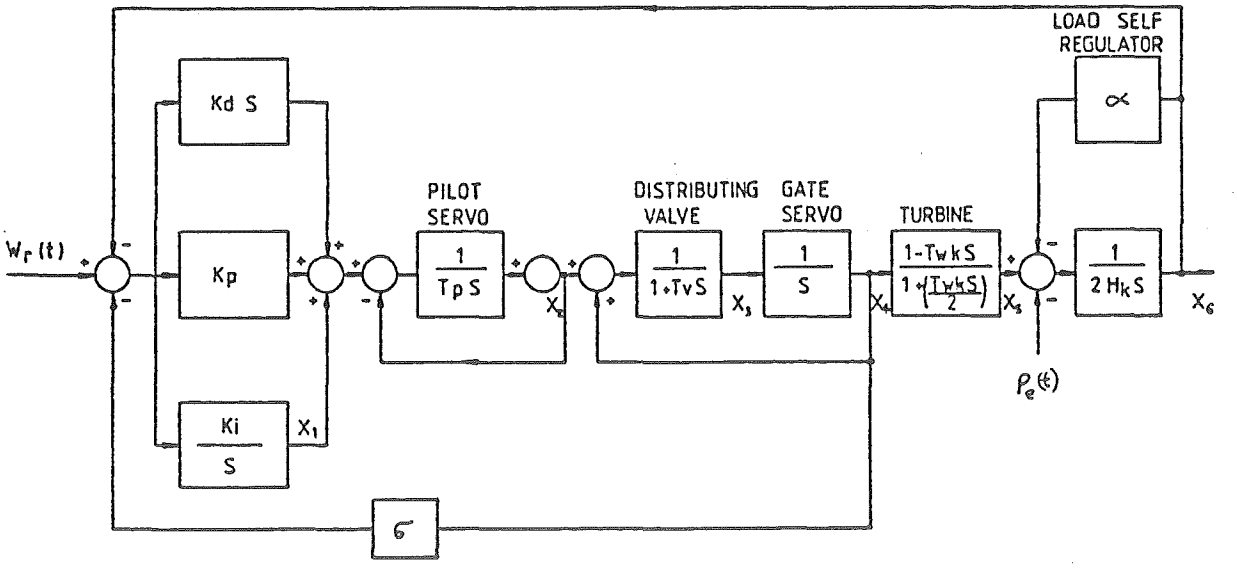

Figure 10.6 "Kettle" hydroturbine and governor.

Assumptions made in deriving the state variable formulation are:

(1) A linear system representation is used. This implies that only small signal disturbances are to be considered.

(2) The relationship between mechanical torque and gate is given by

$$T_{mech} = \frac{1 - T_W \cdot S}{1 + \left(\frac{T_W \cdot S}{2}\right)} \cdot \text{Gate} \qquad (10.2)$$

(3) All damping torques due to the prime mover, generation and load are negligible.

The model of the Kettle turbine and governor includes a proportional, integral and derivative (P.I.D.) control, with gain constraints, K_p, K_i and K_d. The frequency deviation of the hydroturbine generator is summed, together with the reference frequency deviation and the governor steady state spread droop, σ, and the resulting signal is then fed to the P.I.D. controller. The output of the P.I.D. controller drives a pilot servomechanism which operates the distributing valve and the gate servo. The pilot servo and the distributing valve have time constants, T_p and T_v respectively. The gate servo then operates the hydraulic turbine, with time constant, T_{W_k}, and the output of the turbine, summed with the load demand $P_e(t)$ and the load self regulating effect with gain D, induces the rotor to produce the required electrical power. The rotor output is the frequency deviation of the generator, and the inertia constant of the rotor is $2H_K$.

Using the state space representation of Figure 10.6, a linear model of the form

$$\dot{\underline{x}}_{HG}(t) = A\, x_{HG}(t) + \underline{b}\, P_e(t) + \underline{c}\, w_r(t) + d\, \dot{w}_r(t) + \underline{\omega}(t) \qquad (10.3)$$

can be obtained for the hydrogenerator, where $\underline{A}$ represents the natural dynamics of the free system,

$$\underline{A} = \begin{bmatrix} 0 & 0 & 0 & -K_i\sigma & 0 & -K_i \\ \frac{1}{T_p} & \frac{-1}{T_p} & \frac{-K_d\sigma}{T_p} & \frac{-K_p\sigma}{T_p} & \frac{-K_d}{2H_kT_p} & -\left(\frac{K_p}{T_p} - \frac{\alpha K_d}{2H_kT_p}\right) \\ 0 & \frac{1}{T_v} & \frac{-1}{T_v} & \frac{-1}{T_v} & 0 & 0 \\ 0 & 0 & 1 & 0 & 0 & 0 \\ 0 & 0 & -2 & \frac{2}{T_{wk}} & \frac{-2}{T_{wk}} & 0 \\ 0 & 0 & 0 & 0 & \frac{1}{2H_k} & \frac{-\alpha}{2H_k} \end{bmatrix} \tag{10.4}$$

$\underline{x}_{HG}(t)$ is the state vector describing the hydrogenerator

$$\underline{x}_{HG}(t) = [\underline{x}_1(t), \underline{x}_2(t) \ldots . \underline{x}_6(t)]^T \tag{10.5}$$

$$\underline{b} = [0, \frac{K_d}{2H_kT_p}, 0, 0, 0, -\frac{1}{2H_k}]^T \tag{10.6}$$

$$\underline{c} = [K_i, \frac{K_p}{T_p}, 0, 0, 0, 0]^T \tag{10.7}$$

and

$$\underline{d} = [0, \frac{K_d}{T_p}, 0, 0, 0, 0]^T \tag{10.8}$$

where $P_e(t)$ represents the incremental electric power demand with time;

$w_r(t)$ represents a control input, specified in terms of the reference frequency deviation,

$$\dot{w}_r(t) = \frac{\partial}{\partial t} w_r(t) \tag{10.9}$$

and

$\omega(t)$ is a stochastic disturbance describing model inaccuracies and system noise.

The dynamic model in (10.3) describes the power plant variations about a nominal operating point (i.e. incremental changes). Assuming steady state operating conditions at time $t = 0$, the initial condition of (10.3) is $\underline{x}_{HG}(t) = \underline{0}$.

The stochastic disturbance, $\underline{\omega}(t)$, is modelled as a white noise process, with zero mean, i.e.

$$\underline{\omega}(t) \; : \; E\{\underline{\omega}(t)\} = 0 \tag{10.10}$$

and covariance

$$E\{\underline{\omega}(t)\, \underline{\omega}^T(t+\delta)\} = \underline{Q}\, \delta(\tau)$$

where $\delta(\tau)$ is the delta dirac function.

Consider the case when only the frequency deviation is measured:

$$z_f(t) = \underline{H}\, \underline{x}_{HG}(t) + v_f(t) = x_6(t) + v_f(t) \tag{10.11}$$

since $\underline{H} = [0,\ 0,\ 0,\ 0,\ 0,\ 1]^T$.

The observation error, $v_f(t)$ is modelled as a white noise process with zero mean:

$$v_f(t) \; : \; E\{v_f(t)\} = 0 \tag{10.12}$$

and covariance

$$E\{v_f(t)\, v_f^T\, (t+\tau)\} = R\, \delta(\tau)$$

where $R = \sigma_f^2$, (10.13)

and σ_f is the standard deviation of the measurement error.

10.4.1 Local hydroturbine dynamic estimation

The same approach as used by Handschin and Galiana (1973) for thermal turbine dynamic estimation can be used for hydroturbine dynamic estimation. A linear Kalman filter can be derived to estimate the hydrogenerator state, $\underline{x}_{HG}(t)$, based on the dynamic model (10.3), the observation equation (10.11), and on the statistical noise properties of $\omega_f(t)$ and $v_f(t)$, i.e.

$$\dot{\underline{x}}_{HG}(t) = \underline{A}\,\hat{\underline{x}}_{HG}(t) + \underline{b}\,P_e(t) + \underline{c}\,w_r(t) + \underline{d}\,\dot{w}_r(t) + \underline{K}\,[z_f(t) - \underline{H}\,\hat{\underline{x}}_{HG}(t)] \tag{10.14}$$

where $\underline{K}$ is the linear Kalman gain matrix,

$$\underline{K} = \underline{P}\,\underline{H}^T\,\underline{R}^{-1} \tag{10.15}$$

and

$$\frac{\partial P}{\partial t} = \underline{A}\,\underline{P} + \underline{P}\,\underline{A}^T + \underline{Q} - \underline{P}\,\underline{H}^T\,\underline{R}^{-1}\,\underline{H}\,\underline{P} \tag{10.16}$$

where (10.16) is solved using the standard program solutions to the Riccarti equation involving a Kleinmann iterative technique (Kleinmann, 1968; Bartels and Stewart, 1972; Puripanjavanant, 1980; Sandel *et al.*, 1972).

In the local estimation, the electrical power demand, $P_e(t)$, and the control signals which represent the reference frequency deviation, ($w_r(t)$ and $\dot{w}_r(t)$), are treated as known inputs. Their observation errors can be taken into consideration through the random process $\omega(t)$.

10.4.2 Local residual analysis

Again using Handschin and Galiana (1973) results, the filter residual $e_f(t)$ is defined to be the difference between the actual (z_f) and the estimated ($\hat{z}_f$) measurement:

$$e_f(t) = z_f(t) - \hat{z}_f(t) = z_f(t) - \underline{H}\,\hat{\underline{x}}(t) \tag{10.17}$$

Residual analyses are used because their statistical properties are well defined and sensitive to changes. The residual process $e_f(t)$ is a white noise process with zero mean and co-variance

$$E\{e_f(t)\ e_f^T(t+\tau)\} = (\underline{H}^T\,\underline{K}+1)\,\underline{R}\,\delta(\tau) \tag{10.18}$$

Thus the frequency deviation residual can be used to detect on-line plant disturbances, such as changes in mechanical power. Various statistical tests can then be used, based on (10.18), to detect these changes (see Handschin and Galiana, 1973). Network disturbances such as load changes cannot be detected using (10.18), only plant changes.

10.5 MODEL OF THE ELECTRICAL PART OF A HYDROGENERATOR UNIT

A transient electrical model of the hydrogenerating unit is required when studying the behaviour of a generating unit within seconds after a network level disturbance (such as a sudden change in electrical power demand, P_e) or a disturbance on the generating level (such as a sudden change in mechanical power) (Ljubojevic, 1979).

The interaction between the power plant and transmission network is modelled by a transient complex voltage E' behind a transient reactance x_d', as shown in Figure 10.7.

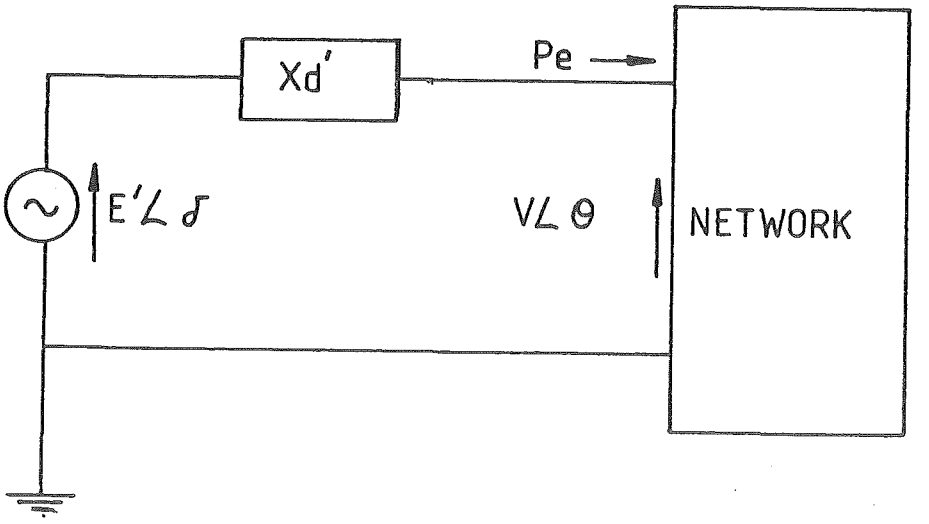

Figure 10.7 Transient model of the electrical part of a generating unit.

The electric power $P_e(t)$ delivered from the generator to the transmission network is

$$P_e(t) = \frac{E'v(t)}{x_d'} \sin [\delta(t) - \theta(t)] \qquad (10.19)$$

where $v(t)\angle\theta(t)$ is the complex voltage of the generator bus;

$\delta(t)$ is the internal rotor angle w.r.t. the reference generator; and

x_d' is the transient reactance of the generating unit.

The rotor angle $\delta(t)$, in radians, is given by

$$\dot{\delta}(t) = 2\pi f_o [f(t) - f_{ref}(t)] \qquad (10.20)$$

where f_o is the nominal frequency (50 Hz);

f is the frequency deviation of the generating unit, $(\underline{x}_{HG}(6))$; and

f_{ref} is the frequency deviation (slip) of the reference generator in per unit:

$$f(t)_{ref} \alpha \frac{1}{W_r(t)}$$

10.5.1 Rotor angle estimation

Using the approach of Handschin and Galiana (1973), under the assumption that the electrical power demand $P_e(t)$ is measured,

$$z_p(t) = P_e(t) + v_p(t) = \frac{E'v(t)}{x_d'} \sin [\delta(t) - \theta(t)] + v_p(t) \qquad (10.21)$$

where $$E\{v_p(t)\} = 0$$

and $$E\{v_p(t)\ v_p^T(t + \tau)\} = \sigma_p^2\ \delta(\tau) \qquad (10.22)$$

An extended Kalman filter approach would generally be required to handle the non-linear dynamic estimation problem given by (10.21) and (10.22). However, Handschin and Galiana use a different approach, using the frequency deviation measurement (see Appendix A13), to derive the

following rotor angle estimator

$$\dot{\hat{\delta}}(t) = 2\pi f_o[\hat{f}(t) - z_f(t)] + K_\delta\left[z_p(t) - \frac{E'v(t_k)}{x_d'}\sin[\hat{\delta}(t) - \hat{\theta}(t_k)]\right] \quad (10.23)$$

where $$K_\delta = \frac{\sigma_{wf}}{\sigma_p} \quad (10.24)$$

$z_f(t)$ = measurement of relative rotor angle $\delta(t)$ of a generator w.r.t. the swing generator;

$$\sigma_{wf}^2 = \sigma_f^2 + \mathrm{cov}(e_f(t)) \quad (10.25)$$

σ_f = standard deviation of the error associated with the measurement of $z_f(t)$; and

where $e_{f_6}(t)$ is the sixth element of the difference vector between the actual $(\underline{x}_{HG}(t))$ and estimated $(\hat{\underline{x}}_{HG}(t))$ state vectors, i.e.

$$\underline{e}(t) = \underline{x}_{HG}(t) - \hat{\underline{x}}_{HG}(t) \quad (10.26)$$

and

$$E[\underline{e}(t)\ \underline{e}^T(t+\tau)] = \underline{\Sigma}\ \delta(\tau) \quad (10.27)$$

The value of (10.27) is found by solving the steady state solution of the Riccarti differential equation (as in section 10.4.1).

Thus measurements of $P_e(t)$ and $f(t)$ are monitored for hydro-turbine estimation. Estimation of the generator internal rotor angle, $\delta(t)$, requires a knowledge of $P_e(t)$, $f(t)$, $\underline{x}_{HG}(6)$ and the centrally estimated nodal voltage $\hat{V}(t_k) \angle \theta(t_k)$.

10.6 TEST SIMULATION RESULTS

The electrical 5 bus test system model of Stagg and El-Abiad (1968) was used in the tests, with generation present at nodes 1 and 2. The generator at bus 1 is the stack generator where the internal rotor angle is arbitrarily zero ($\delta_1(t) = 0$) and where the reference frequency deviation $f_{ref}(t)$ is measured. The test system which includes a hydro-

canal is shown in Figure 10.8.

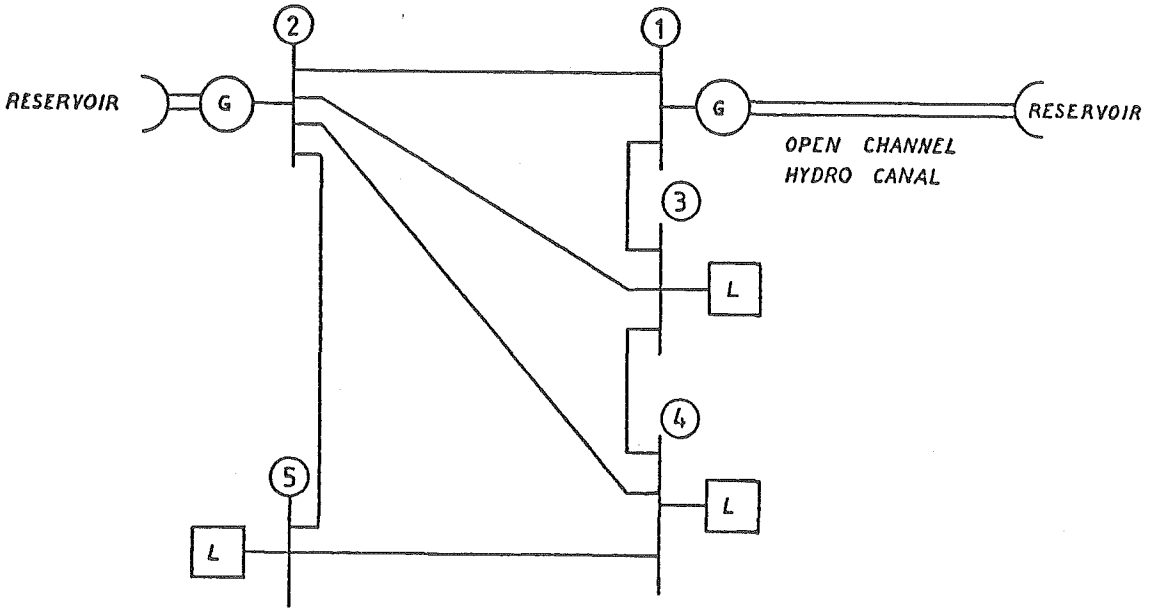

Figure 10.8 Sample network with two hydrogenerators, three loads and one hydrocanal.

Table 10.1 summarises the voltage profile, power infeeds and loads at the beginning of the dynamic simulation. Numerical values for the hydrogenerator parameters are given in Table 10.2. Note also that

$$\text{diag } \underset{\sim}{Q} = 0.00001$$

$$\text{diag } \underset{\sim}{R} = 0.0001$$

Table 10.1 Initial conditions for power system simulation.

Node	Voltage v ∠ θ	Power P + j θ
	p.u. rad.	p.u.
1	1.060 ∠ - 0.1154	1.294 - 0.075
2	1.047 ∠ - 0.1643	0.205 - 0.199
3	1.024 ∠ - 0.2027	-0.452 - 0.145
4	1.024 ∠ - 0.2084	-0.400 - 0.053
5	1.018 ∠ - 0.2228	-0.600 - 0.100

Table 10.2 Power station parameters.

PARAMETER	GENERATORS 1 AND 2
α	0.872
K_i	0.50
T_p	0.20
K_d	0.75
σ	0.03
H_k	4.00
T_v	1.00
T_{wk}	1.00
K_p	2.50

* Note: More typical values of T_p and T_v are 0.04 and 0.2 respectively.

Integration of the dynamic hydroturbine-generator model is based on am implicit trapezoidal integration (Law, 1972). In the simulation, step lengths, TTT, are varied between 0.2 and 0.10 seconds.

Law (1972) showed the trapezoidal method of integration to be, in some cases, more stable than explicit Runga-Kutta methods when solving transient stability problems where the step length is less than 0.02 sec. Since the smallest time constant in the hydrogenerator state estimation problem is much greater than the smallest time constant in a transient stability study, step lengths of TTT > 0.02 should still prove stable. Implicit trapezoidal integration is reviewed in Appendix A14.

Measurements arrive from the centralized tracking, static state estimator at 10 second intervals. Although the tracking state estimator calculates the network states less often in practice, the small time interval is chosen to keep the overall simulation time small.

10.6.1 Example 1

In order to study the local hydrogenerator estimation performance, a change in the electrical power demand, $\Delta P_e(t) = +0.2$ p.u., is simulated, at bus 1, after one second. The control signals $w_r(t)$ and $\dot{w}_r(t)$ are set to zero and the estimator is assumed to have reached stable tracking conditions at $t = 0$. The resulting frequency deviation profile over a 30 second interval is shown in Figure 10.9 for the case where $T_p = 0.2$ and no measurement noise is present. Different numerical integration single step (TTT = 0.02, 0.05 and 0.10 sec) and multi steps (TTT = $0.02 \times 2 = 0.04$, TTT = $0.02 \times 5 = 0.10$ sec) were simulated. In the multi step scheme, where the step length is n = 0.02, the process is repeated m = 5 times before the next measurements arrive, to give an overall integration step length of 0.10 sec. All schemes gave the same numerical accuracy. However it is likely that for TTT > 0.10, "multi-step" numerical integration will prove more accurate.

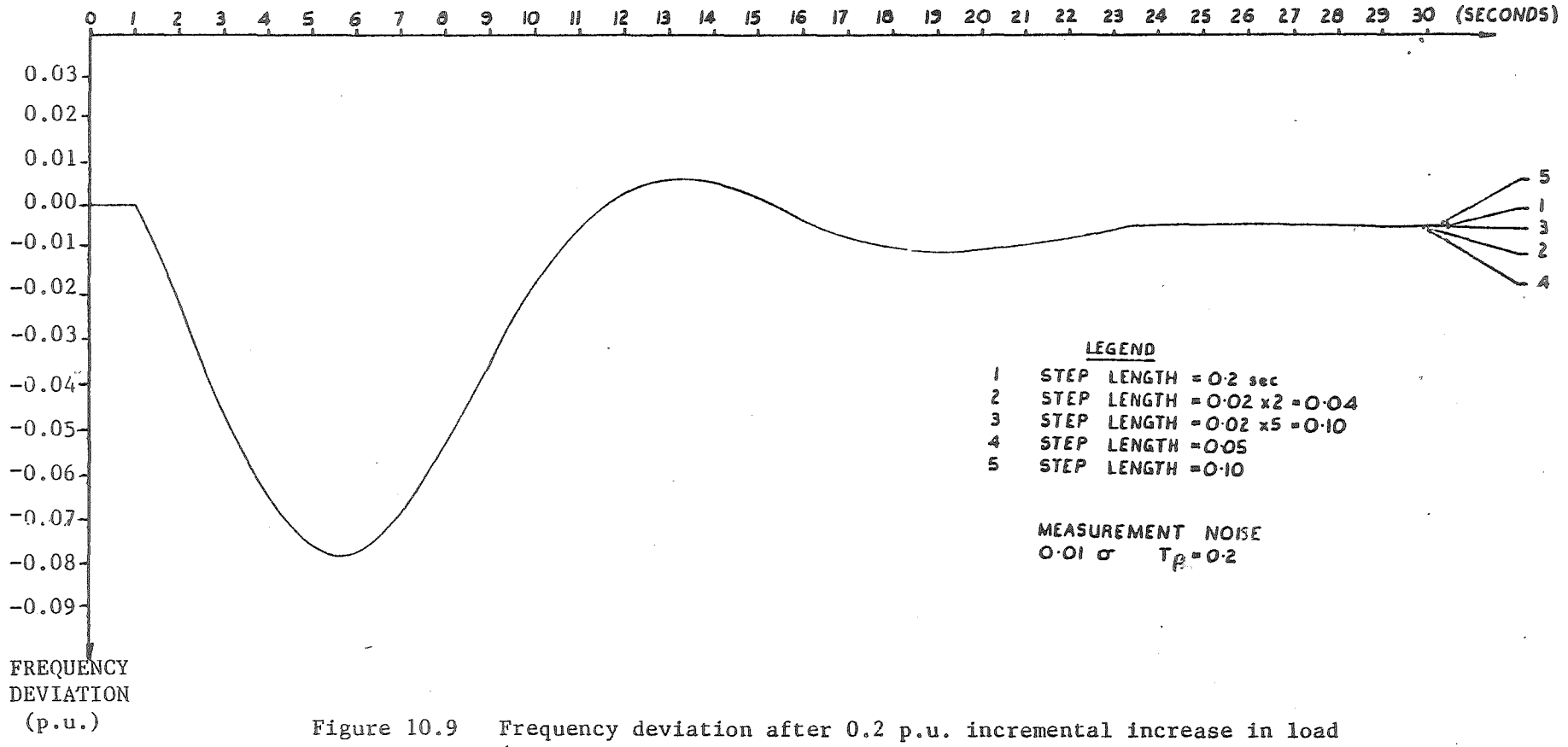

Figure 10.9 Frequency deviation after 0.2 p.u. incremental increase in load (no measurement noise and T_p = 0.2).

When measurement noise is included in the Kalman filter observations, the resulting frequency deviation profile is as shown in Figure 10.10. Note that the accuracy of the simulation is only slightly dependent on the numerical integration step length when the size of the step is less than 0.10 sec.

The same test was repeated with $T_P = 1.0$ and measurement noise present during the Kalman filter observations. The resulting frequency deviation profile is shown in Figure 10.11. The frequency deviation due to the change in load is much greater than in the case where $T_P = 0.02$, and oscillations are still present after 30 seconds. Accuracy is only slightly dependent on the numerical integration step length when the size of the step is less than 0.10 sec. However, multi-step length integration schemes can be expected to give improved accuracy when the step length is larger. Note that Handschin and Galiana (1973) performed the same tests on a thermal turbine generating unit and got a similar shaped frequency deviation profile.

10.6.2 Example 2: Rotor angle estimation.

The relative rotor angle, $\delta_2(t)$, can be estimated, provided the local dynamic estimator obtains an estimate of $\hat{V}(t_k)$ from the tracking estimator, a measurement $z_f(t)$ of the reference frequency deviation $f_{ref}(t)$ at the swing bus, and an estimate $\hat{f}(t)$, the frequency deviation obtained at the local estimator. The control signals $w_r(t)$ and $\dot{w}_r(t)$ are set to zero, and the estimator is assumed to have reached stable conditions at $t = 0$. At $t = 0$, the rotor angle estimator receives the measurement $V_2 \angle \theta_2 = 1.047 \angle -0.18$ radians from the tracking state estimator. At $t = 3$ seconds, the demand at the slack bus suddenly increases ($\Delta P_e(t) = + 0.2$ p.u.), forcing $P_{e_1}(t)$ from 1.291 p.u. to 1.491 p.u. This change in demand causes the frequency deviation of

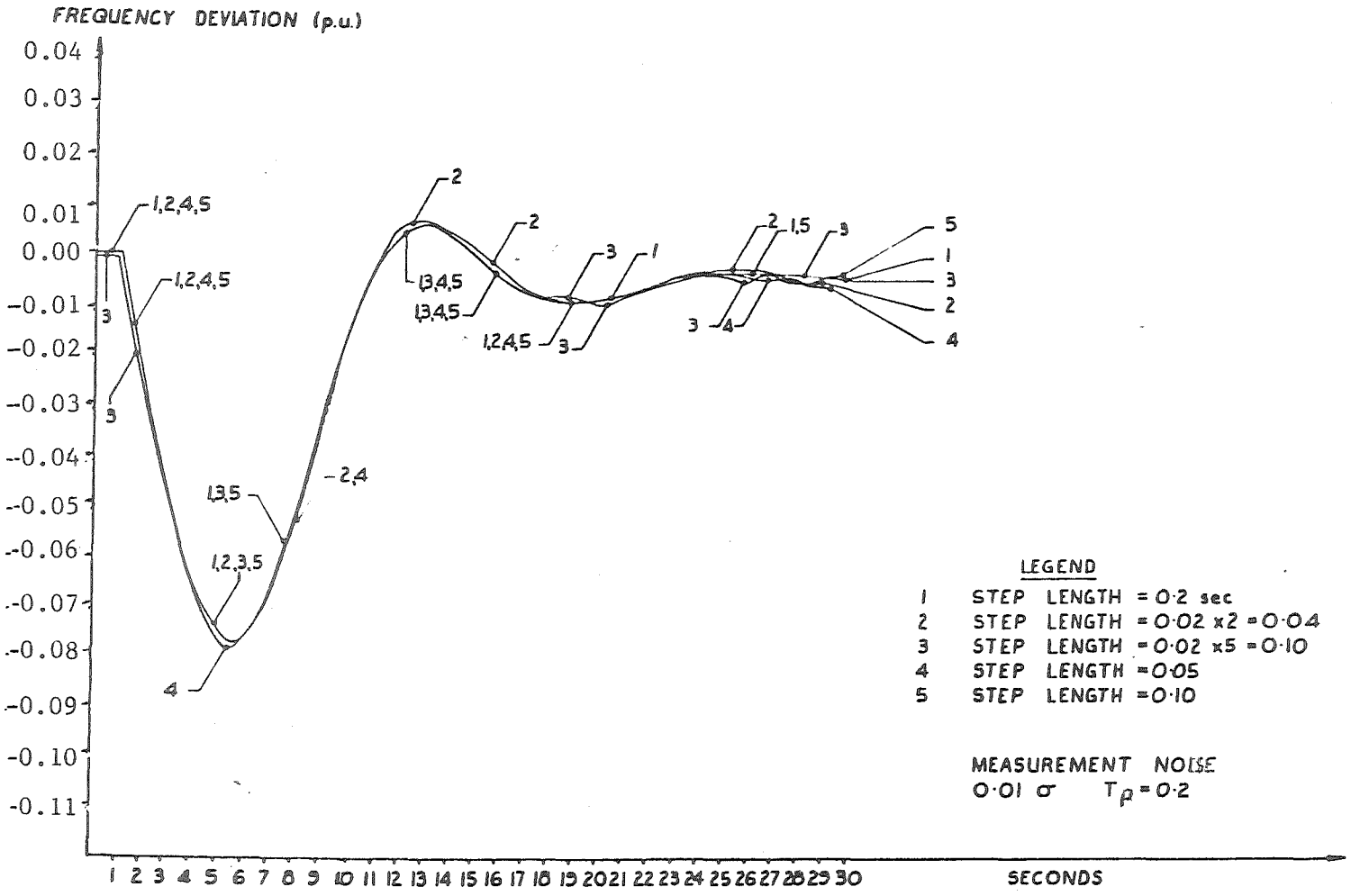

Figure 10.10 Frequency deviation after 0.2 p.u. incremental increase in load (measurement noise and T_p = 0.2).

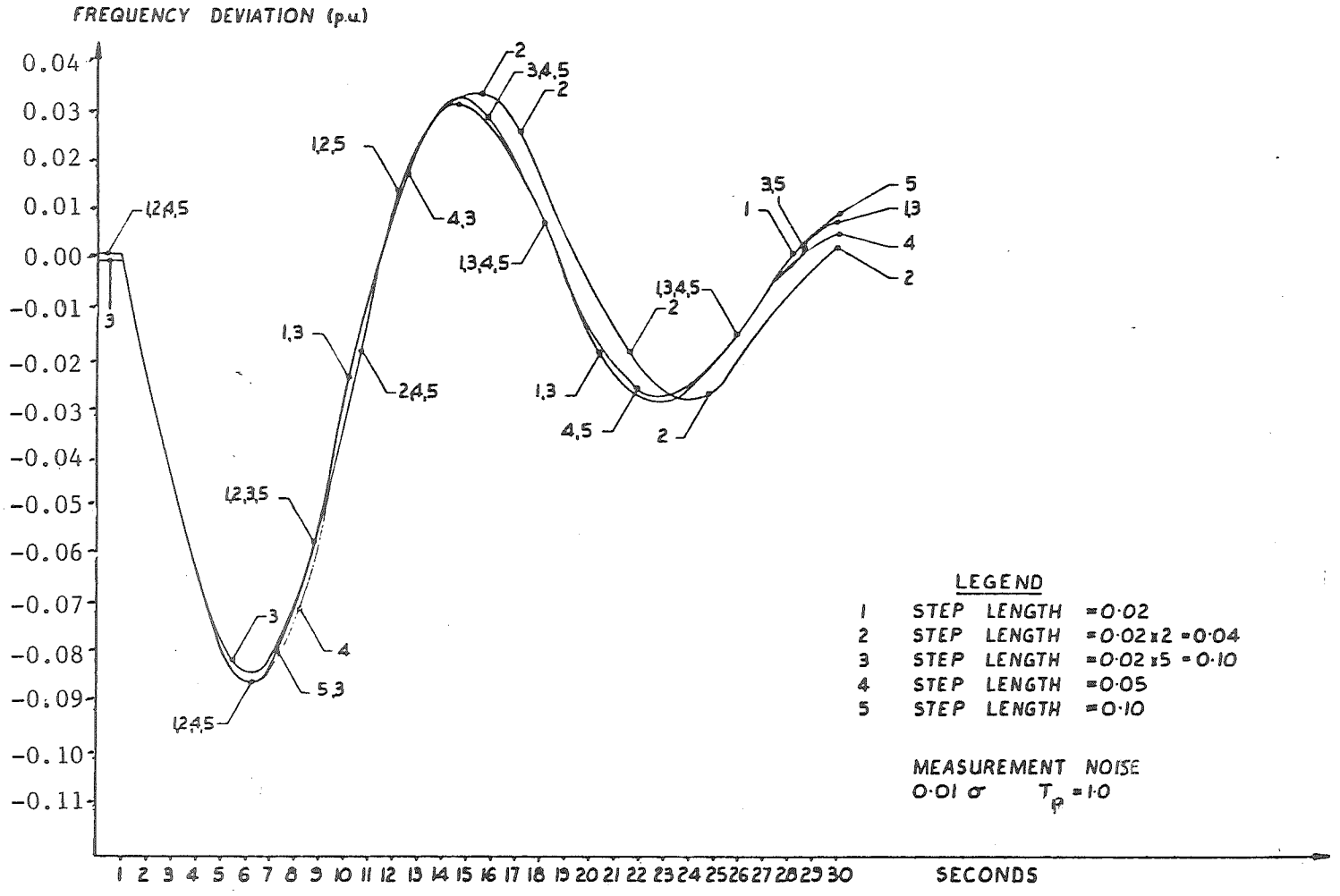

Figure 10.11 Frequency deviation after 0.2 p.u. incremental increase in load (measurement noise and T_p = 1.0).

generator 1 to alter. The next "update" for $V_2 \angle \theta_2$ is received after 10 seconds, and during this time interval other system changes may have occurred. At $t = 10$ seconds, the measurement $V_2 \angle \theta_2 = 1.047 \angle -0.170$ is received from the global static state estimator and this "updated" information used in the rotor angle estimation. The estimated rotor angle deviation is shown in Figure 10.12 and has a similar profile to Handschin and Galiana's results. Accuracy of the rotor angle estimate is only slightly dependent on the size of the numerical integration step when TTT < 0.10 sec.

10.5 MODEL FOR AN OPEN CHANNEL HYDROCANAL

Open channel flow can be complex and have many different modes of propagation. Flow can be uniform, where the slope and cross-section do not vary along the direction of the flow; turbulent, where the frictional characteristics become independent of the Reynolds number and only dependent on the channel roughness; gradually varied (non-uniform) steady flow where the depth, cross-sectional area, bottom slope and roughness change slowly along the channel; gradually varied unsteady flow where the discharge and depth change with time; and rapidly varied unsteady flow. Rapidly varied unsteady flow is caused by abrupt changes in the supply or demand for water. Four types of rapidly varied unsteady flow are possible, as shown in Figure 10.13 (Chow, 1959). The type A surge usually results from a dam break or flood while the type B surge occurs in power channels serving hydraulic turbines. Type B surge is known as a "rejection surge " and this is due to a sudden decrease in power output. Type C flow is generally caused by a sudden decrease in the supply of flow upstream, for example due to a headgate in a channel or at the tailrace of hydroplant, while

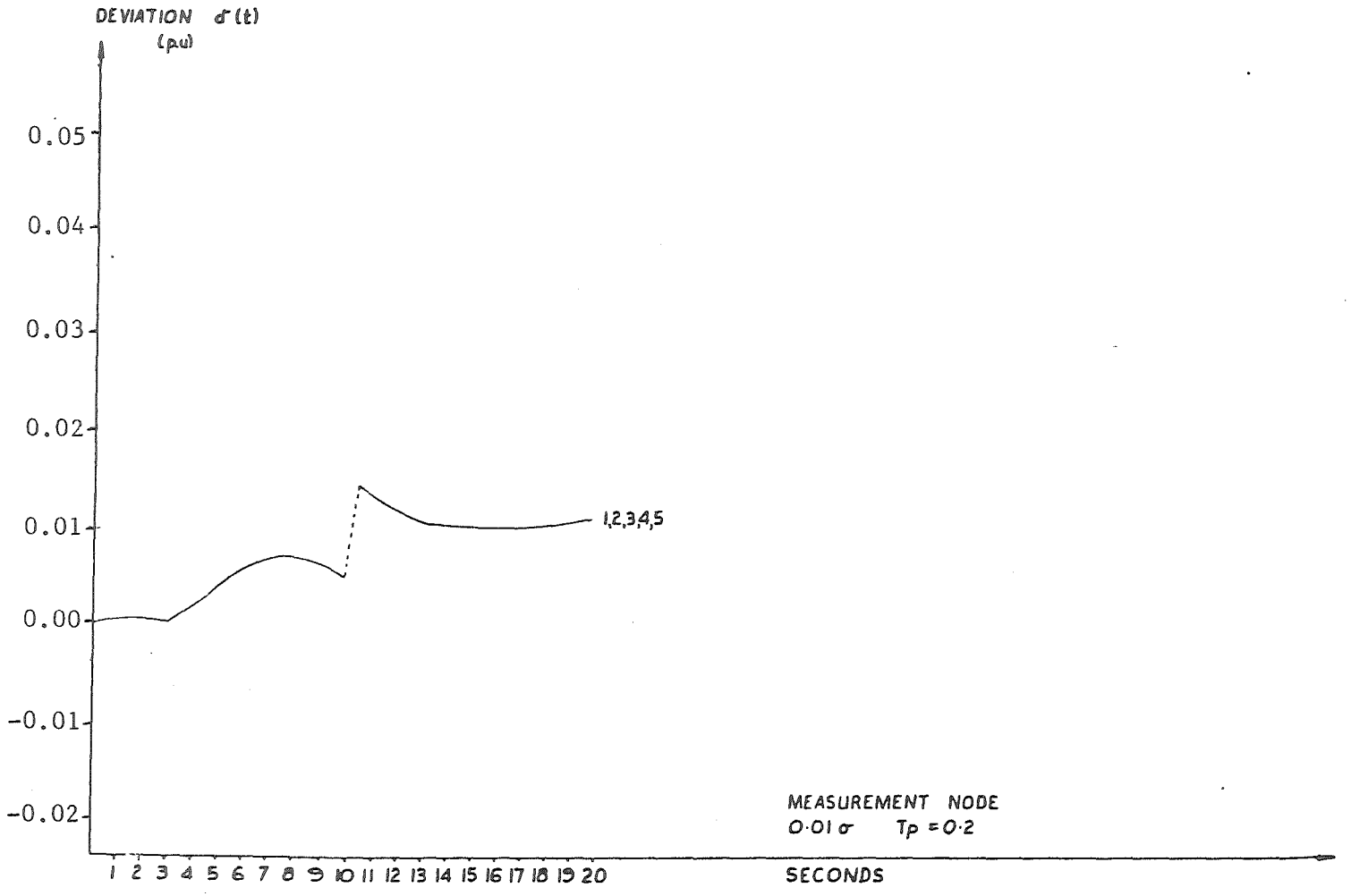

Figure 10.12 Rotor angle estimation (measurement noise and T_p = 0.2).

type D is a demand surge which occurs in power channels serving hydraulic turbines when the demand at the lower end is suddenly increased.(Chow, 1959).

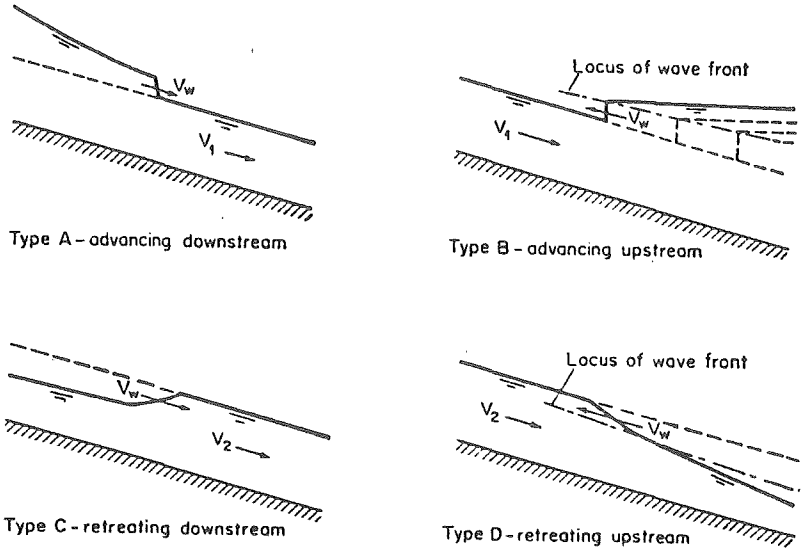

Figure 10.13 Rapidly varied unsteady flow (Chow, 1959).

Note that, when generated, surges have steep wavefronts which, on meeting other surges or channel "open" and "closed" ends, can reflect and sum together to generate large amplitude disturbances. Damping, however, usually ensures the rapid decay of the steep wavefront surges.

In this chapter, only gradually varied unsteady flow is considered when deriving the dynamics for the hydrocanal state estimator. Events causing rapidly varied unsteady flow must occur either at the top or bottom of the open channel and are caused by hydropower station operation. Any sudden lowering or raising of headgates etc. can be noted by the computer, and anomalies between the estimate and the measurements treated with caution for some small period after the event.

However, most operations involving changes in the flow in and out of the hydrocanal will be gradual.

10.7.1 Open channel transient flow

The momentum and continuity equations for gradually varied, unsteady open channel flow, derived in Appendix A12, are:

$$\left(1 - \frac{Q^2 T}{g A^3}\right) \frac{\partial y}{\partial x} + \frac{2Q}{gA^2} \frac{\partial Q}{\partial x} + \frac{1}{gA} \frac{\partial Q}{\partial t} + s - s_o = 0 \qquad (10.28)$$

$$T \frac{\partial y}{\partial t} + \frac{\partial Q}{\partial x} = 0 \qquad (10.29)$$

where Q is the flow rate;

g is the gravitational constant (= 9.806);

A is the cross-sectional area of the water;

T is the width of the canal at the top of the water level;

s is the channel resistance; and

$$s_o = \frac{n^2 P^{4/3}}{c_m^2 A^{10/3}}$$

where n is the manning number (roughness);

c_m is a constant (= 1 for SI units); and

P is the wetted perimeter.

Wylie and Streeter (1978) provide two programs, one based on the method of characteristics and the other based on an implicit Newton method which uses a finite difference formulation to solve (10.28) and (10.29). The method of characteristics gives the more exact result, but allows only the time or distance step, Δt or Δx, to be fixed, while the other's variation is fixed by the characteristics. The implicit method uses a Newton formulation and allows both Δx and Δt to be specified. To give some feel for the treatment of the problem, the implicit method of solving the open channel dynamics will be reviewed.

10.7.2 Implicit method for solving open channel flow dynamics

The partial differential equations (10.28) and (10.29) which describe the unsteady flow dynamics can be placed in finite difference form, for y, if, referring to Figure 10.14, the following substitutions are made (Wylie and Streeter, 1978).

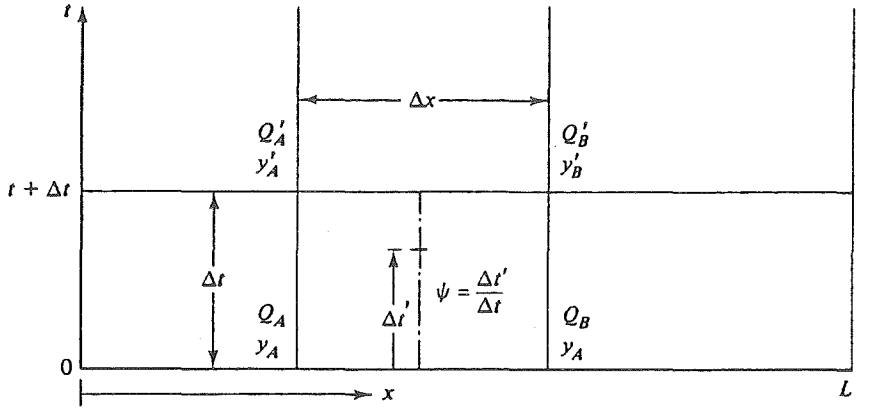

Figure 10.14 Discretization of the open channel (Wylie and Streeter, 1978).

$$\bar{y} = \psi\left[\frac{y_A' + y_B'}{2}\right] + (1 - \psi)\left[\frac{y_A + y_B}{2}\right] \qquad (10.30)$$

$$\frac{\partial y}{\partial x} = \frac{\psi(y_B' - y_A') + (1 - \psi)(y_B - y_A)}{\Delta x} \qquad (10.31)$$

$$\frac{\partial y}{\partial t} = \frac{(y_A' + y_B') - (y_A + y_B)}{2\,\Delta t} \qquad (10.32)$$

where $\psi = \frac{\Delta t'}{\Delta t}$ is a weighting factor. The implicit method of solving the open channel flow is stable provided $0.5 < \psi < 1.0$ and unstable for $\psi < 0.5$.

Similar substitutions can be made for A, T, P and Q.

When the finite difference-equivalents are used to replace all the variables in (10.28) and (10.29), the momentum and continuity

equations become

$$\left(1 - \frac{\bar{Q}^2\ \bar{T}}{g\ \bar{A}^3}\right)[\psi(y_B' - y_A') + (1-\psi)\ (y_B - y_A)]$$

$$+ \frac{2\ \bar{Q}}{g\ \bar{A}^2}\ [\psi(Q_B' - Q_A') + (1-\psi)\ (Q_B - Q_A)] \tag{10.33}$$

$$+ \frac{\Delta x}{\Delta t}\ \frac{1}{g\ \bar{A}}\left[\frac{Q_A' + Q_B'}{2} - \frac{Q_A + Q_B}{2}\right] + \frac{n^2\ \Delta x\ \bar{P}^{4/3}}{c_m^{\,2}\ \bar{A}^{10/3}}\ \bar{Q}|\bar{Q}| - s_o\ \Delta x = 0$$

$$\bar{T}\left[\frac{(y_A' + y_B')}{2} - \frac{(y_A + y_B)}{2}\right] + \frac{\Delta t}{\Delta x}\left[\psi(Q_B' - Q_A') + (1-\psi)(Q_B - Q_A)\right] = 0 \tag{10.34}$$

Equations (10.33) and (10.34) constitute a set of non-linear algebraic equations in four independent unknowns, y_A', y_B', Q_A' and Q_B'. When the channel is partitioned into N cells there are 2N equations and 2(N+1) unknowns. Boundary conditions at each end of the hydrocanal provide the necessary additional equations so that a unique solution can be obtained. A Newton Ralphson procedure is used by Wylie and Streeter (1978) to simultaneously solve the set of non-linear equations.

10.7.3 A dynamic model suitable for a Kalman filter

In the above section it has been shown that the application of finite difference equations results in a "linearized" system difference model if $\bar{Q}$, $\bar{A}$, $\bar{T}$ and $\bar{P}$ are treated as constant parameters during each iteration. However for "real time" implementation, a time dependent form of dynamics must be used, i.e.

$$\dot{\underline{x}}(t) = \underline{A}\ \underline{x}(t) + \underline{B}\ \underline{u}(t) \tag{10.35}$$

The corresponding Kalman filter equation is:

$$\dot{\underline{x}}(t) = \underline{A}\ \underline{x}(t) + \underline{B}\ \underline{u}(t) + \underline{K}(\underline{z} - \underline{h}(\underline{x})) \tag{10.36}$$

A time dependent model can be found by substituting difference

approximations only for $\frac{\partial Q}{\partial x}$ and $\frac{\partial y}{\partial x}$ in the momentum and continuity equations, (10.28) and (10.29). A different "discretization" scheme for the distributed parameter hydrocanal system can be used to realize the Kalman filter (cf. the method outlined in section 10.7.2). This scheme is shown in Figure 10.15.

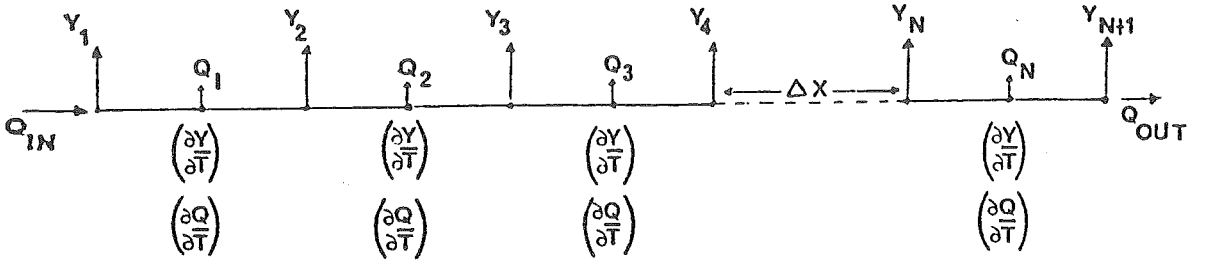

Figure 10.15 Discretization of the open channel for Kalman filter implementation.

States y_i and y_{i+1} are specified at the end of each cell, i, whereas state Q_i is specified at the middle. Input and output flow, Q_{IN} and Q_{OUT}, are treated as "input", $\underline{u}(t)$, to the state estimator and are continually updated. Differential terms describing the open channel flow dynamics now become

$$\left(\frac{\partial Q}{\partial t}\right)_2 = -\frac{g\bar{A}\psi}{\Delta x}\left(1 - \frac{\bar{Q}^2\,\bar{T}}{g\,\bar{A}^3}\right)(y_3' - y_2') - \left(\frac{2\bar{Q}}{2\,\Delta x\,\bar{A}}\right)(Q_3' - Q_1')$$

$$- \psi\, g\bar{A}\left(\frac{n^2\,\bar{P}^{4/3}}{c_m^2\,\bar{A}^{10/3}}|\bar{Q}|\right) Q_2' \qquad (10.37)$$

$$- \left[\left[\frac{(1-\psi)}{\Delta x}\left[g\,\bar{A}\left(1 - \frac{\bar{Q}^2\,\bar{T}}{g\,\bar{A}^3}\right)(y_3 - y_2) + \left(\frac{2\bar{Q}}{2\,\Delta x\,\bar{A}}\right)(Q_3 - Q_1)\right.\right.\right.$$

$$\left.\left.\left. + \Delta x\, g\bar{A}\left(\frac{n^2\,\bar{P}^{4/3}}{c_m^2\,\bar{A}^{10/3}}|\bar{Q}|\right)Q_2\right]\right] - g\,\bar{A}\,s_o\right]$$

where the last term involving y_3, y_2, Q_3, Q_1, Q_2 and s_o forms the driving input, $\underline{u}(t)$, and the first three terms describe the "dynamic" model. Similarly,

$$\left(\frac{\partial y}{\partial t}\right)_2 = -\frac{\psi}{T\Delta x}(Q_2' - Q_1') - \frac{(1-\psi)}{T\,\Delta x}(Q_2 - Q_1) \tag{10.38}$$

where the last term involving Q_2 and Q_1 form the driving input $\underline{u}(t)$, and

$$\begin{aligned} \bar{T} &= b + 2\,z\bar{y} \\ \bar{A} &= \tfrac{1}{2}\,\bar{y}\,(2b + 2\,z\bar{y}) \\ \bar{P} &= b + 2\,\bar{y}\,(\sqrt{1+z^2}) \end{aligned} \tag{10.39}$$

where b is the bottom width of the canal; and

z is the slope.

For the N cell example, shown in Figure 10.15, the dynamic model equations are:

$$\left(\frac{\partial Q_1}{\partial t}\right) = -\frac{g\,\bar{A}_{1-2}\psi}{\Delta x}\left(1 - \frac{\bar{Q}_1^{\,2}\,\bar{T}_{1-2}}{g\,\bar{A}_{1-2}^{\,3}}\right)(y_2' - y_1') - \left(\frac{2\bar{Q}_1\,\psi}{\Delta x\,\bar{A}_{1-2}}\right)\left(\frac{Q_2' - Q_{IN}'}{1.5}\right)$$

$$- g\,\bar{A}_{1-2}\psi\left(\frac{n^2\,\bar{P}_{1-2}^{\,4/3}}{c_m^{\,2}\,\bar{A}_{1-2}^{\,10/3}}\,|\bar{Q}_1|\right)Q_1'$$

$$\left(\frac{\partial Q_2}{\partial t}\right) = -\frac{g\,\bar{A}_{2-3}\psi}{\Delta x}\left(1 - \frac{\bar{Q}_2^{\,2}\,\bar{T}_{2-3}}{g\,\bar{A}_{2-3}^{\,3}}\right)(y_3' - y_2') - \left(\frac{2\bar{Q}_2\,\psi}{\Delta x\,\bar{A}_{2-3}}\right)\left(\frac{Q_3' - Q_1'}{2}\right) \tag{10.34}$$

$$- g\,\bar{A}_{2-3}\,\psi\left(\frac{n^2\,\bar{P}_{2-3}^{\,4/3}}{c_m^{\,2}\,\bar{A}_{2-3}^{\,10/3}}\,|\bar{Q}_2|\right)Q_2'$$

$$\left(\frac{\partial Q_n}{\partial t}\right) = -\frac{g\,\bar{A}_{(n)-(n+1)}\psi}{\Delta x}\left(1 - \frac{\bar{Q}_n\,\bar{T}_{(n)-(n+1)}}{g\,\bar{A}_{(n)-(n+1)}}\right)(y'_{(n+1)} - y'_{(n)}) - \left(\frac{2\,\bar{Q}_n\,\psi}{\Delta x\,\bar{A}_{(n)-(n+1)}}\right)$$

$$\left(\frac{Q_{OUT}' - Q_n'}{1.5}\right) - g\,\bar{A}_{(n)-(n+1)}\psi\left(\frac{n^2\,\bar{P}_{(n)-(n+1)}^{\,4/3}}{c_m^{\,2}\,\bar{A}_{(n)-(n+1)}^{\,10/3}}\,|\bar{\bar{Q}}_n|\right)Q_n'$$

where $$\bar{Q}_1 = \psi Q_1' + (1 - \psi) Q_1$$

and $$\left(\frac{\partial y_1}{\partial t}\right) = -\frac{2\psi}{\bar{T}_1 \Delta x}(Q_1' - Q_{IN}')$$

$$\left(\frac{\partial y_2}{\partial t}\right) = -\frac{2\psi}{\bar{T}_2 \Delta x}(Q_2' - Q_1') \qquad (10.41)$$

$$\vdots \qquad\qquad \vdots$$

$$\left(\frac{\partial y_{n+1}}{\partial t}\right) = -\frac{2\psi}{\bar{T}_{n+1} \Delta x}(Q_{OUT}' - Q_n')$$

These dynamic equations are integrated by using an iterative numerical trapezoidal integration technique (see Appendix A14). During each integration time step, $\bar{y}$, $\bar{A}$, $\bar{P}$, $\bar{Q}$ and $\bar{T}$ are treated as constants, but after the integration-iterative step these parameters are updated using (10.39) and held "constant" for the next integration iterative step. Thus the system dynamic model is linear at each iteration step, but updated between steps. Tests outlined later show the dynamic model to be stable when estimating the 2N+1 hydrocanal states after fixing Q_{IN} and Q_{OUT}. The 2N+1 hydrocanal states are:

$$\underline{x} = \{y_1', y_2' \cdots y_{n+1}, Q_1' \cdots Q_n'\}.$$

10.7.4 Structure of the linearized hydrocanal Kalman filter

A linearized dynamic hydrocanal model and Kalman filter was chosen because, if feasible, it requires the least on-line computation. If the "linearized" approach does not work sufficiently well, extended Kalman filter techniques can be used (Ljubojevic, 1979), but require more storage and regular updating of the Kalman gain.

In the linearized Kalman filter approach, last scan estimates, $\{y_1 \cdots y_{n+1}, Q_1 \cdots Q_n\}$, and last scan data, Q_{IN} and Q_{OUT}, together with the latest data, Q_{IN}' and Q_{OUT}', are treated as inputs, $\underline{u}(t)$, to

the Kalman filter. The model for the "linearized" dynamic Kalman filter is given by (10.36).

10.8 PERFORMANCE RESULTS

10.8.1 Accuracy of the dynamic hydrocanal model

In this section the accuracy of the various schemes (method of characterists, implicit method, and trapezoidal integration) for solving the open channel flow dynamics will be assessed.

The method of characteristics and the Newton Ralphson method for solving the hydrocanal dynamics, outlined in section 10.7.1, agree to within 1% for the hydrocanal problem on page 369 of Wylie and Streeter (1978). Estimates for y are shown in Table 10.3 and represent the estimated water height after 19.168 minutes have elapsed.

Table 10.3 Accuracy of the method of characteristics and the implicit Newton method.

	POSITION ALONG CANAL, X	0 m	300 m	600 m	900 m	1200m	1500m
IMPLICIT	T = 19.167 minutes	2.713	2.705	2.680	2.630	2.594	2.621
CHARACTERISTICS	T = 19.168 minutes	2.714	2.712	2.692	2.642	2.609	2.644

PROBLEM I. Consider the flow situation shown in Figure 10.16. Initially the flow is zero, but after t = 0, the discharge linearly increases according to the relationship

$$Q = Q_I + (Q_F - Q_I)\frac{t}{t_f} \qquad 0 \leq t < t_f$$

$$Q = Q_f \qquad t > t_f$$

and continues until all water has drained out.

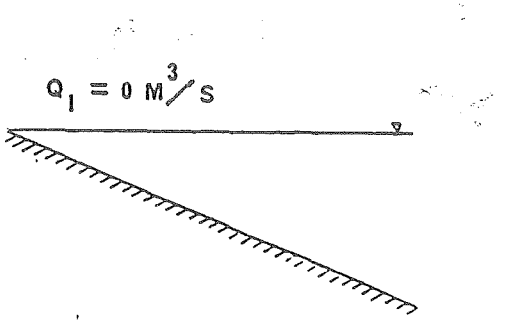

Figure 10.16 Initial flow conditions for problem 1.

In the following example, $Q_1 = 0\ m^3/sec$ and Q_f equals $40\ m^3/sec$ after $t_f = 120$ seconds. The trapezoidal channel has $0X = 150$ m, $b = 10$ m wide side slopes, $z = 0.5$ horizontal to 1 vertical, Manning roughness $n = 0.016$, and bottom slope $s_o = 0.0002$.

When this problem is solved, using the trapezoidal numerical integration technique outlined in section 10.6.3, with the step length equal to 0.1 second, $\psi = 0.6$ and $N = 3$, the results are as shown in Table 10.4.

Table 10.4 Comparison of the accuracy of the method of characteristics with the accuracy of the trapezoidal integration method.

	POSITION ALONG CANAL, X	0 m	150 m	300 m	450 m
TRAPEZOIDAL	T = 600 sec	2.779	2.795	2.728	2.509
CHARACTERISTICS	T = 600 sec	2.782	2.811	2.694	2.519

A comparison with the method of characteristics shows an agreement to within 1.23%. Thus the method involving the trapezoidal numerical integration appears to give acceptable results even for small N.

10.8.2 Dependence of the Kalman filter gain on the flow conditions

In this section the Kalman filter gain for the hydrocanal will be calculated at various flow conditions and an attempt at assessing how dependent the gain is on the flow will be made. Kalman gains were calculated using the iterative Klienman technique described in section 10.4, with

$$\text{diag } \underline{Q} = 0.00001$$

$$\text{diag } \underline{R} = 0.00001$$

in the following calculation of filter gain.

10.8.2.1 Variation of K with measurement set composition ($\psi = 0.6$) for the stable hydrocanal flow condition of the start of problem 1. The canal is divided into three cells, and Kalman gains found for the following measurement combinations:

(i) All measurements possible are monitored (7×7), i.e.

$$\{y_1', y_2', y_3', y_4', Q_1', Q_2', Q_3'\}$$

(ii) Four out of seven measurements are monitored (7×4), i.e.

$$\{y_1', y_2', y_3', y_4'\}$$

(iii) One out of seven measurements are monitored (7×1):

$$\{Q_1'\}$$

The resulting gains are shown in Table 10.5.

PROBLEM 2. Consider the constant flow situation shown in Figure 10.17. Initially the flow is at $Q_I = 40$ m^3/sec, but after $t = 0$ the discharge linearly decreases according to the relationship

$$Q = Q_I + (Q_F - Q_I)\frac{t}{t_f} \qquad 0 \leq t \leq t_f$$

$$Q = Q_F$$

until at $t_f = 120$ sec, $Q_f = 30$ m^3/sec.

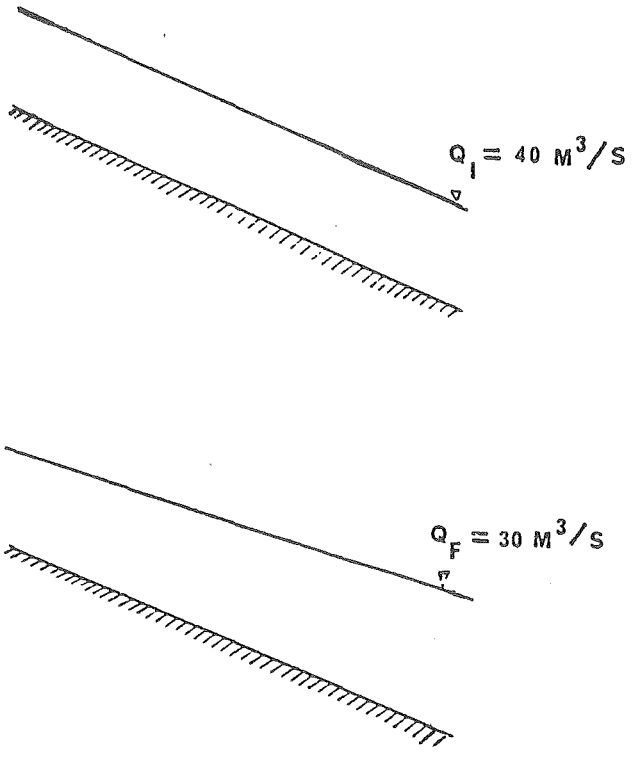

Figure 10.17 Initial and final flow conditions for problem 2.

The canal dimension and parameters are the same as those in problem 1.

10.8.2.2. The variation of K with measurement set composition ($\psi = 0.6$) for the constant flow condition at the start of hydrocanal problem 2. The canal is divided into three cells, and Kalman gains are found for the following measurement combinations:

Table 10.5 Kalman filter gain for the initial conditions of problem 1 ($\psi = 0.6$).

(i) 7×7

0.89894	0.42603	0.07535	0.06001	0.01847	0.01393	0.00720
0.42603	1.61577	-0.36551	-0.22432	-0.04645	-0.03413	-0.01426
0.07535	-0.36551	0.84075	0.38290	0.06458	0.04689	0.01902
0.06001	-0.22432	0.38290	1.59168	-0.38135	-0.22644	-0.06157
0.01847	-0.04645	0.06488	-0.38135	0.83910	0.37051	0.07755
0.01393	-0.03413	0.04689	-0.22644	0.37051	1.63565	-0.43113
0.00720	-0.01426	0.01902	-0.06157	0.07755	-0.43113	0.89619

(ii) 7×4

0.99997	0.01853	0.00017	0.04590	-0.00004	0.09958	0.00009
0.00017	-0.52825	0.99961	0.64930	0.00023	-0.04424	-0.00004
-0.00004	0.03224	0.00023	-0.67728	0.99959	0.64384	0.00024
0.00009	-0.09916	-0.00004	-0.00114	0.00024	-0.22545	0.99985

(iii) 7×1

0.77635	2.12927	-0.64338	35.01063	-0.13710	-3.76615	-0.06456

Table 10.6 Kalman fitter gain for the initial conditions of problem 2 ($\psi = 0.6$).

(i) 7×7

0.91646	0.39069	0.06534	0.04880	0.01368	0.01005	0.00448
0.39069	1.50705	-0.34419	-0.19264	-0.03702	-0.02618	-0.00968
0.06534	-0.34419	0.86483	0.35217	0.05613	0.03883	0.01371
0.04880	-0.19264	0.35217	1.47975	-0.35415	-0.19128	-0.04682
0.01368	-0.03702	0.05613	-0.35415	0.86481	0.34241	0.06538
0.01005	-0.02618	0.03883	-0.19128	0.34241	1.50467	-0.39110
0.00448	-0.00968	0.01371	-0.04682	0.06538	-0.39110	0.91639

(ii) 7×4

1.00031	-0.54840	-0.00002	0.09238	0.00005	0.01983	0.00000
-0.00002	-0.30675	0.99991	-0.18251	-0.00002	0.03793	0.00005
0.00005	-0.03702	-0.00002	0.18063	0.99993	0.31526	-0.00002
0.00000	-0.01918	0.00005	-0.09411	-0.00002	0.54910	1.00038

(iii) 7×1

0.75923	2.02525	-0.99419	46.60576	0.07944	-6.91119	-0.19581

(i) All measurements possible monitored (7×7), i.e.

$$\{y_1', y_2', y_3', y_4', Q_1', Q_2', Q_3'\}$$

(ii) Four out of seven measurements monitored (7×4), i.e.

$$\{y_1', y_2', y_3', y_4'\}$$

(iii) One out of seven measurements monitored (7×1):

$$\{Q_1'\}$$

The resulting gains are shown in Table 10.6.

Table 10.7 Kalman filter gain and co-variance described by problem 3 ($\psi = 0.6$).

OPTIMAL GAINS

0.90279	0.41854	0.07494	0.05631	0.01699	0.01215	0.00523
0.41854	1.59769	-0.36563	-0.20953	-0.04281	-0.02913	-0.01030
0.07494	-0.36563	0.85095	0.36148	0.06030	0.04024	0.01382
0.05631	-0.20953	0.36148	1.52689	-0.37122	-0.19484	-0.04657
0.01699	-0.04281	0.06030	-0.37122	0.86139	0.33200	0.06132
0.01215	-0.02913	0.04024	0.19484	0.33200	1.47916	-0.38419
0.00523	-0.01030	0.01382	-0.04657	0.06132	-0.38419	0.91958

CO-VARIANCES

0.0000090	0.0000042	0.0000007	0.0000006	0.0000002	0.0000001	0.0000001
0.0000042	0.0000160	-0.0000037	-0.0000021	-0.0000004	-0.0000003	-0.0000001
0.0000007	-0.0000037	0.0000085	0.0000036	0.0000006	0.0000004	0.0000001
0.0000006	-0.0000021	0.0000036	0.0000153	-0.0000037	-0.0000019	-0.0000005
0.0000002	-0.0000004	0.0000006	-0.0000037	0.0000086	0.0000033	0.0000006
0.0000001	-0.0000003	0.0000004	-0.0000019	0.0000033	0.0000148	-0.0000038
0.0000001	-0.0000001	0.0000001	-0.0000005	0.0000006	-0.0000038	0.0000092

PROBLEM 3. For this problem, flow conditions at the previous and present scans are:

$$\begin{matrix} y_1' \\ Q_1' \\ y_2' \\ Q_2' \\ y_3' \\ Q_3' \\ y_4' \end{matrix} = \begin{bmatrix} 2.780 \\ 0.095 \\ 2.676 \\ 8.222 \\ 2.533 \\ 17.694 \\ 2.288 \end{bmatrix} \qquad \begin{matrix} y_1 \\ Q_1 \\ y_2 \\ Q_2 \\ y_3 \\ Q_3 \\ y_4 \end{matrix} \begin{bmatrix} 2.782 \\ 0.032 \\ 2.681 \\ 7.935 \\ 2.538 \\ 17.389 \\ 2.297 \end{bmatrix}$$

and $Q_{IN}' \simeq Q_{OUT} = 0.0$, while $Q_{OUT}' \simeq Q_{OUT} = 30.09$.

These conditions are fed to the Kalman gain algorithm and represent a varying flow condition.

10.8.2.3. Varying flow condition. $\psi = 0.6$. The Kalman filter gain and co-variance matrix for the varying flow condition of problem 3 is calculated when all seven measurements are monitored (7×7).

The resulting gain and co-variance matrix are shown in Table 10.7.

10.8.2.4. Effect of varying ψ. In 10.8.2.1 to 10.8.2.3, the value of was maintained at 0.6. Some of the test cases are repeated with $\psi = 1.0$. Cases evaluated include:

(i) The flow conditions present at the start of problem 1 and when all measurements are present (7×7).

(ii) The flow conditions present at the start of problem 2 and when all measurements are present (7×7).

(iii) The flow conditions present at the start of problem 2 and when only four out of seven measurements are present (4×7), i.e.

$$\{y_1', y_3', y_3', y_4'\}$$

The resulting gains are shown in Table 10-8.

Table 10.8 Kalman filter gain for flow conditions described by problems 1, 2 and 3 when $\psi = 1.0$.

(i) 7×7 Problem 1

0.82580	0.53840	0.11050	0.10780	0.04067	0.03212	0.02297
0.53840	2.10604	-0.42972	-0.33863	-0.07617	-0.06349	-0.03289
0.11050	-0.42972	0.75439	0.46557	0.09359	0.07644	0.04154
0.10780	-0.33863	0.46557	2.05751	-0.46348	-0.34068	-0.10989
0.04067	-0.07617	0.09359	-0.46348	0.75275	0.43430	0.11301
0.03212	-0.06349	0.07644	-0.34068	0.43430	2.13543	-0.54248
0.02297	-0.03289	0.04154	-0.10989	0.11301	-0.54248	0.82243

(ii) 7×7 Problem 2

0.84952	0.50600	0.10072	0.09471	0.03299	0.02655	0.01671
0.50600	1.94390	-0.41565	-0.30308	-0.06522	-0.05372	-0.02551
0.10072	-0.41565	0.78180	0.43823	0.08442	0.06848	0.03308
0.09471	-0.30308	0.43823	1.88779	-0.44183	-0.30129	-0.09112
0.03299	-0.06522	0.08442	-0.44183	0.78177	0.41239	0.10084
0.02655	-0.05372	0.06848	-0.30129	0.41239	1.93871	-0.50704
0.01671	-0.02551	0.03308	-0.09112	0.10084	-0.50704	0.84931

(iii) 7×4 Problem 2

1.00018	-0.20195	0.00029	0.13865	-0.00002	0.20037	0.00018
0.00029	-0.73437	0.99908	0.96637	0.00057	-0.07625	-0.00007
-0.00002	0.04062	0.00057	-1.04065	0.99884	1.02577	0.00061
0.00018	-0.19805	-0.00007	-0.02164	0.00061	-0.30980	0.99967

By comparing the results of similar test cases (Tables 10.5 - 10.8), the following observations can be made:

(i) For test cases containing the same number of measurements, the Kalman gain is relatively independent of variations in canal flow or in the value of ψ.

(ii) The Kalman gain is very dependent on the composition of the measurement set.

10.8.2.5. Large scale system Kalman gain. In the cases above, the hydrocanal has only been divided into three units (7 states). However when the canal is discretized into 20 units (or cells), 41 states result. Use of Kleinman's (1968) iterative technique to calculate the gain for a system of this size occasionally proved numerically unstable, especially when less measurements than states were present, and a problem of this size also involves large amounts of computation. The Kalman gain was calculated for the initial flow conditions present at the start of problem 2, when all 41 measurements were present (41×41). The resulting Kalman filter gain has an extremely sparse, band-like structure, with roughly the same sparsity as the "dynamic model", matrix A. In order to lower the burden on computation and storage, the 41×41 Kalman filter gain matrix will be approximated by the sparse band structured matrix shown in Table 10.9.

10.8.3 Kalman filter tracking results

In this section it will be shown that hydrocanal Kalman filtering is possible, and various simulation tests will be carried out to test the sensitivity of the resulting estimates to "approximate" Kalman filter gains (perhaps valid for some other flow condition, or "diagonalised"). The performance of the Kalman filter when less measurements than states are present will also be investigated, as well

Table 10.9 "Approximate" large scale Kalman filter gains for problems 1 and 2.

	APPROXIMATE KALMAN GAIN (41×41)	PROBLEM 1	PROBLEM 2
	K(1,1)	0.9800	0.8988
	K(1,2)	0.3870	0.3600
	K(2,1)	0.3870	0.3600
	K(41,41)	0.9160	0.8712
I = 2,4,...40	K(I,I)	1.4942	1.7955
	K(I,I+1)	-0.3410	-0.3900
	K((+1,I)	-0.3410	-0.3900
I = 3,5,...39	K(I,I)	0.8571	0.8700
	K(I,I+1)	0.3490	0.3600
	K(I+1,I)	0.3490	0.3600

as the "maximum permissible time between measurement scans" the trapezoidal integration scheme can tolerate and still give reasonable estimates. In the following simulation, unless stated, the level of canal discretization is N = 3.

10.8.3.1 Simulation 1 ($\psi = 1.0$). Consider simulating the flow dynamics as described by problem 1. Initially the water level is horizontal, with no flow, and after t = 0 sec the flow linearly increases to t = 120 sec, when the flow is rated at 40 m^3/sec.

The initial conditions of the flow are:

$$Q_i = 0 \text{ m}^3/\text{sec} \qquad y_i = 2.63 \text{ m}$$

However, the Kalman filter starts with the initial guess

$$Q_i = 3.0 \text{ m}^3/\text{sec} \quad \text{and} \quad y_i = 0.5 \text{ m}$$

All measurements are assumed monitored:

$$\{ y_1', Q_1', y_2', Q_2', y_3', Q_3', y_4' \}$$

and the Kalman gain found in 10.8.2.4, (i), is used in the state estimator.

Since

$$\text{diag } \underline{Q} = 0.00001$$

and

$$\text{diag } \underline{R} = 0.00001$$

the "measurements" to the Kalman filter are found by observing the true dynamic state and corrupting the result by a weighted random number, W, where

$$W = 0.00316 \times RN$$

and where RN is a gaussian random number lying between + 3.0 and - 3.0.

Results of the tracking estimation are shown in Table 10.10 for a 2.33 minute (140 second) simulation. The integration step length of the Kalman filter is TTT = 0.10 seconds.

A comparison of the difference between the true state, $\underline{x}_t$, the estimate, $\hat{\underline{x}}$, and corrupted measurement $\underline{z}$ is shown at T = 140 seconds. It can be seen that $|\hat{\underline{x}} - \underline{x}_t|$ is less than $|\underline{y} - \underline{x}_t|$, thus indicating that filtering is occurring.

10.8.3.2. Simulation 2 ($\psi = 1.0$). The same problem as in (10.8.3.1) is simulated, however in order to reduce storage, only the diagonal of the gain $\underline{K}$ is used in the dynamic Kalman filter simulation when the 7×7 measurement set is processed.

Results of the tracking estimation are shown in Table 10.10 for a 2.33 minute (140 seconds) simulation. The integration step length of the Kalman filter is TTT = 0.10 sec.

Good agreement between the actual system state, $\underline{x}_t$, and the estimate still holds.

Table 10.10 Open channel flow estimate using problem 1 when the Kalman gain is modified.

Time (sec)		y_1	Q_1	y_2	Q_2	y_3	Q_3	y_4
0.0	x_t	2.7820	0.0000	2.8120	0.0000	2.8420	0.0000	2.8720
	$\hat{x}_{s1}$	0.5000	3.0000	0.5000	3.0000	0.5000	3.0000	0.5000
	$\hat{x}_{s2}$	0.5000	3.0000	0.5000	3.0000	0.5000	3.0000	0.5000
20.0	x_t	2.7820	0.0002	2.8120	0.0205	2.8396	0.9138	2.8073
	$\hat{x}_{s1}$	2.7817	0.0030	2.8103	0.0189	2.8390	0.9191	2.8065
	$\hat{x}_{s2}$	2.7816	0.0030	2.8104	0.0186	2.8391	0.9192	2.8068
40.0	x_t	2.7819	0.0231	2.8101	0.5427	2.8106	5.7705	2.6600
	$\hat{x}_{s1}$	2.7819	0.0244	2.8100	0.5445	2.8107	5.7874	2.6600
	$\hat{x}_{s2}$	2.7823	0.0247	2.8096	0.5448	2.8106	5.7868	2.6599
60.0	x_t	2.7791	0.1965	2.7951	3.0024	2.7268	13.5578	2.5092
	$\hat{x}_{s1}$	2.7792	0.2968	2.7961	3.0143	2.7262	13.5780	2.5089
	$\hat{x}_{s2}$	2.7793	0.2970	2.7964	3.0137	2.7261	13.5787	2.5090
80.0	x_t	2.7633	1.4567	2.7470	8.1690	2.6013	20.7581	2.3798
	$\hat{x}_{s1}$	2.7628	1.4625	2.7458	8.1839	2.6000	20.7722	2.3795
	$\hat{x}_{s2}$	2.7629	1.4629	2.7455	8.1832	2.6009	20.7732	2.3793
100.0	x_t	2.7089	3.9419	2.6546	14.6336	2.4719	26.1131	2.2400
	$\hat{x}_{s1}$	2.7087	3.9510	2.6538	14.6487	2.4710	26.1228	2.2398
	$\hat{x}_{s2}$	2.7088	3.9510	2.6541	14.6486	2.4711	26.1233	2.2394
120.0	x_t	2.5935	6.9606	2.5270	20.1011	2.3553	30.5875	2.0577
	$\hat{x}_{s1}$	2.5935	6.9668	2.5266	20.1099	2.3560	30.5999	2.0573
	$\hat{x}_{s2}$	2.5938	6.9664	2.5263	20.1103	2.3557	30.5999	2.0575
140.0	x_t	2.4211	8.9339	2.3792	23.2700	2.2371	34.8978	1.8973
	z	2.4199	8.9378	2.3763	23.2654	2.2396	34.8930	1.8955
	$\hat{x}_{s1}$	2.4201	8.9376	2.3773	23.2736	2.2361	34.9063	1.8972
	$\hat{x}_{s2}$	2.4201	8.9374	2.3777	23.2739	2.2364	34.9065	1.8971

Flow in m^3/sec.

Height in metres.

10.8.3.3. Simulation 3 ($\psi = 1.0$). The flow dynamics described by problem 2 are now simulated. Initially the flow is constant at $Q_i = 40$ m^3/sec, at $t = 0$, and then the flow is linearly decreased to 30 m^3/sec, at $t = 120$ seconds.

The initial conditions of the flow are:

$$Q_i = 40 \text{ m}^3/\text{sec} \qquad y_i = 2.63 \text{ m}$$

However the Kalman filter starts with the initial guess

$$Q_i = 43.0 \text{ m}^3/\text{sec} \quad \text{and} \quad y_i = 2.0 \text{ m}.$$

All measurements are assumed monitored

$$\{y_1', Q_1', y_2', Q_2', y_3', Q_3', y_4', Q_4'\}$$

and the Kalman gain found in 10.8.2.4 (ii) is used in the state estimator. Since

$$\text{diag } \underline{Q} = 0.00001$$

$$\text{diag } \underline{R} = 0.00001$$

the measurements to the Kalman filter are formed by observing the true dynamic state and corrupting the result by a weighted random number, as described in 10.8.3.1. Results of the tracking estimation are shown in Table 10.11 for a 2.33 minute (140 second) simulation. The integration step length of the Kalman filter is TTT = 0.10 sec.

A comparison of the difference between the true state $\underline{x}_t$, the estimate $\hat{\underline{x}}$ and the corrupted measurement $\underline{z}$ is shown for T = 140 seconds. It can be seen that $|\hat{\underline{x}} - \underline{x}_t|$ is less than $|\underline{y} - \underline{x}_t|$, thus showing that filtering has occurred.

10.8.3.4. Simulation 4 ($\psi = 1.0$). The same problem as in 10.8.3.3 is simulated, however in order to reduce storage, only the diagonal of $\underline{K}$ is used in the dynamic Kalman filter, when the 7×7 measurement set is processed. Results of the tracking estimation are shown in

Table 10.11 Open channel flow estimates using problem 2 when the Kalman gain or number of measurements present is modified.

Time (sec)		y_1	Q_1	y_2	Q_2	y_3	Q_3	y_4
0.00	x_t	2.6300	40.0000	2.6300	40.0000	2.6300	40.0000	2.6300
	$\hat{x}_{s_3}$	2.0000	43.0000	2.0000	43.0000	2.0000	43.0000	2.0000
	$\hat{x}_{s_4}$	2.0000	43.0000	2.0000	43.0000	2.0000	43.0000	2.0000
	$\hat{x}_{s_5}$	2.0000	43.0000	2.0000	43.0000	2.0000	43.0000	2.0000
	$\hat{x}_{s_6}$	2.0000	43.0000	2.0000	43.0000	2.0000	43.0000	2.0000
	$\hat{x}_{s_7}$	2.0000	43.0000	2.0000	43.0000	2.0000	43.0000	2.0000
	$\hat{x}_{s_8}$	2.6300	40.0000	2.6300	40.0000	2.6300	40.0000	2.6300
20.00	x_t	2.6306	39.9846	2.6301	39.9684	2.6299	39.9554	2.6472
	$\hat{x}_{s_3}$	2.6303	39.9873	2.6284	39.9667	2.6293	39.9536	2.6469
	$\hat{x}_{s_4}$	2.6302	39.9872	2.6285	39.9665	2.6294	39.9538	2.6471
	$\hat{x}_{s_5}$	2.6302	39.9873	2.6281	39.9676	2.6288	39.9529	2.6475
	$\hat{x}_{s_6}$	2.6269	40.9334	2.6286	42.5994	2.6282	44.6882	2.6519
	$\hat{x}_{s_7}$	2.6303	39.9874	2.6284	39.9667	2.6293	39.9537	2.6468
	$\hat{x}_{s_8}$	2.6301	39.9937	2.6284	39.9984	2.6293	39.9890	2.6471
40.00	x_t	2.6306	40.0052	2.6302	40.0031	2.6331	39.2115	2.6931
	$\hat{x}_{s_3}$	2.6307	40.0064	2.6300	40.0019	2.6335	39.2078	2.6935
	$\hat{x}_{s_4}$	2.6311	40.0067	2.6297	40.0023	2.6332	39.2071	2.6937
	$\hat{x}_{s_5}$	2.6305	40.0070	2.6294	40.0038	2.6316	39.2082	2.6930
	$\hat{x}_{s_6}$	2.6299	41.8085	2.6295	41.9255	2.6311	45.3314	2.7000
	$\hat{x}_{s_7}$	2.6307	40.0063	2.6300	40.0019	2.6335	39.2078	2.6935
	$\hat{x}_{s_8}$	2.6310	40.0251	2.6296	40.0198	2.6332	39.2511	2.6937
60.00	x_t	2.6304	40.0157	2.6303	39.9489	2.6504	37.3413	2.7461
	$\hat{x}_{s_3}$	2.6304	40.0146	2.6314	39.9505	2.6501	37.3358	2.7463
	$\hat{x}_{s_4}$	2.6302	40.0149	2.6317	39.9499	2.6500	37.3366	2.7464
	$\hat{x}_{s_5}$	2.6305	40.0142	2.6321	39.9482	2.6529	37.3354	2.7459
	$\hat{x}_{s_6}$	2.6289	41.1155	2.6320	40.8340	2.6463	44.8562	2.7542
	$\hat{x}_{s_7}$	2.6304	40.0147	2.6314	39.9504	2.6501	37.3358	2.7463
	$\hat{x}_{s_8}$	2.6301	40.0147	2.6319	39.9554	2.6497	37.3930	2.7465
80.00	x_t	2.6299	40.0366	2.6336	39.3599	2.6879	34.9869	2.7879
	$\hat{x}_{s_3}$	2.6295	40.0377	2.6326	39.3566	2.6871	34.9800	2.7880
	$\hat{x}_{s_4}$	2.6296	40.0381	2.6323	39.3561	2.6879	34.9810	2.7877
	$\hat{x}_{s_5}$	2.6296	40.0370	2.6333	39.3534	2.6903	34.9798	2.7885
	$\hat{x}_{s_6}$	2.6287	40.8460	2.6327	39.0122	2.6830	43.7934	2.7968
	$\hat{x}_{s_7}$	2.6295	40.0378	2.6326	39.3567	2.6871	34.9799	2.7880
	$\hat{x}_{s_8}$	2.6295	40.0219	2.6321	39.3511	2.6877	35.0702	2.7878
100.00	x_t	2.6292	39.9999	2.6478	37.8329	2.7372	33.0766	2.8186
	$\hat{x}_{s_3}$	2.6292	40.0011	2.6474	37.8273	2.7368	33.0707	2.8189
	$\hat{x}_{s_4}$	2.6293	40.0011	2.6476	37.8272	2.7369	33.0713	2.8185
	$\hat{x}_{s_5}$	2.6295	40.0005	2.6481	37.8250	2.7392	33.0716	2.8184
	$\hat{x}_{s_6}$	2.6283	40.8802	2.6488	36.2081	2.7309	42.9027	2.8288
	$\hat{x}_{s_7}$	2.6292	40.0011	2.6474	37.8273	2.7368	33.0707	2.8189
	$\hat{x}_{s_8}$	2.6293	39.9989	2.6476	37.8217	2.7368	33.1568	2.8187
120.00	x_t	2.6323	39.6234	2.6807	35.5835	2.7826	31.7889	2.8513
	$\hat{x}_{s_3}$	2.6327	39.6212	2.6808	35.5755	2.7837	31.7874	2.8514
	$\hat{x}_{s_4}$	2.6330	39.6208	2.6804	35.5760	2.7833	31.7874	2.8516
	$\hat{x}_{s_5}$	2.6326	39.6221	2.6798	35.5787	2.7806	31.7862	2.8518
	$\hat{x}_{s_6}$	2.6318	40.8189	2.6824	32.7402	2.7765	42.3172	2.8625
	$\hat{x}_{s_7}$	2.6327	39.6211	2.6808	35.5755	2.7837	31.7875	2.8513
	$\hat{x}_{s_8}$	2.6325	39.6221	2.6810	35.5762	2.7830	31.7871	2.8520
140.00	x_t	2.6498	38.5999	2.7299	33.4582	2.8169	30.5707	2.8757
	$\hat{x}_{s_3}$	2.6493	38.5976	2.7285	33.4526	2.8163	30.5668	2.8759
	$\hat{x}_{s_4}$	2.6494	38.5973	2.7290	33.4527	2.8165	30.5672	2.8757
	$\hat{x}_{s_5}$	2.6496	38.5966	2.7295	33.4487	2.8201	30.5683	2.8753
	$\hat{x}_{s_6}$	2.6475	40.2860	2.7316	29.5690	2.8087	41.4429	2.8870
	$\hat{x}_{s_7}$	2.6493	38.5976	2.7285	33.4525	2.8163	30.5668	2.8759
	$\hat{x}_{s_8}$	2.6493	38.5924	2.7287	33.4166	2.8163	30.6869	2.8758
	z	2.6486	38.6038	2.7271	33.4536	2.8194	30.5658	2.8739

Flow in m^3/sec.
Height in metres.

Table 10.11 over the 2.33 minute (140 second) simulation. Use of the diagonalised K appears to cause little degradation in the quality of the estimate.

10.8.3.5. Simulation 5 ($\psi = 1.0$). The same problem as in (10.8.3.3) is simulated. However the wrong value of $\underline{K}$ is used, valid for the starting conditions of problem 2 but evaluated with $\psi = 0.6$, not $\psi = 1.0$ (i.e. case 10.8.2.1(i)). All measurements are processed (7×7). Results of the 140 second "track are shown in Table 10.11. Use of the wrong value of $\underline{K}$ again caused little degradation in the estimate quality.

10.8.3.6. Simulation 6 ($\psi = 1.0$). The same problem as in (10.8.3.3) is simulated. However, only four measurements are made along the canal and the gain from 10.8.2.4.(iii) is used in the tests when the 7×4 measurement set is processed

$$\{y_1', y_2', y_3', y_4'\}$$

Results of the tracking estimation are shown in Table 10.11 over a 2.33 minute (140 second) time scan. The integration step length of the filter is 0.10 seconds. The results show little agreement between estimates and the known dynamics, particularly of locations which have not been monitored. However, running the state estimator for 4000 seconds showed all the estimates and known dynamics to be in agreement after 800 seconds. Filtering was shown to take place at y_1, y_2, y_3 and y_4 once the Kalman filter had "stabilized" or initialised from the close start of $Q_{INITIAL} = 43.0\ m^3/sec$ and $y_{INITIAL} = 2.0\ m$.

10.8.3.7. Simulation 7 ($\psi = 1.0$). The same problem as in (10.8.3.3) is simulated. However, the wrong value of $\underline{K}$ is used, given by 10.8.2.4.(i), which is valid for the starting conditions of problem 1 rather than

problem 2, when the 7×7 measurement set is processed. Results of the 140 second "track" are shown in Table 10.11. Use of the wrong value of $\underline{K}$ causes little degradation in the quality of the estimates and implies that $\underline{K}$ will rarely need re-evaluating when flow changes, if all measurements are present.

10.8.3.8. Simulation 8 ($\psi = 1.0$). The same problem as in (10.8.3.7) is simulated, however the state estimator starts with an exact guess. Results of the tracking estimation are shown in Table 10.11 over a 2.33 minute (140 second) time scan. Close agreement between estimates and the known dynamics results, particularly at locations where measurements are monitored. Thus, once the filter settles, after initialization, to the correct estimate it faithfully tracks the changing dynamics when only four out of seven measurements are present.

10.8.3.9. Simulation 8 ($\psi = 1.0$). In the previous simulations the integration step length of the Kalman filter has been held constant at TTT = 0.1 seconds. This means the canal measurements must be updated at 0.1 second intervals. Tests will now be carried out to find the maximum "permissible overall step length" which is possible without degrading the estimates. The step length is now changed and the same problem as in (10.8.3.3) is simulated when all measurements are present, with TTT = 0.5 seconds. Results of the 140 second "track" are shown in Table 10.12. Little or no degradation is caused by using the larger step length. Each trapezoidal integration step also takes less than 25 iterations (i.e. usually 3-6 iterations).

10.8.3.10. Simulation 9 ($\psi = 1.0$). The same problem as in (10.8.3.9) is solved, but the integration step length is increased to TTT = 1.0 second. Results of the 140 second simulation are shown in Table 10.12. However, after 100 seconds the simulation stopped because the integration

Table 10.12 Open channel flow estimates using problem 2 when the integration step length is modified.

Time (sec)		y_1	Q_1	y_2	Q_2	y_3	Q_3	y_4
0.00	x_t	2.6300	40.0000	2.6300	40.0000	2.6300	40.0000	2.6300
	$\hat{x}_{s_9}$	2.0000	43.0000	2.0000	43.0000	2.0000	43.0000	2.0000
	$\hat{x}_{s_{10}}$	2.0000	43.0000	2.0000	43.0000	2.0000	43.0000	2.0000
	$\hat{x}_{s_{11}}$	2.0000	43.0000	2.0000	43.0000	2.0000	43.0000	2.0000
	$\hat{x}_{s_{12}}$	2.0000	43.0000	2.0000	43.0000	2.0000	43.0000	2.0000
	$\hat{x}_{s_{13}}$	2.0000	43.0000	2.0000	43.0000	2.0000	43.0000	2.0000
20.00	x_t	2.6306	39.9846	2.6301	39.9684	2.6299	39.9554	2.6472
	$\hat{x}_{s_9}$	2.6298	39.9874	2.6292	39.9636	2.6311	39.9482	2.6495
	$\hat{x}_{s_{10}}$	2.6327	39.9940	2.6274	39.9682	2.6291	39.9386	2.6483
	$\hat{x}_{s_{11}}$	2.6321	39.9927	2.6283	39.9688	2.6292	39.9398	2.6480
	$\hat{x}_{s_{12}}$	2.6328	39.9904	2.6320	39.9727	2.6339	39.8678	2.6549
	$\hat{x}_{s_{13}}$	2.6314	40.0050	2.6302	39.9788	2.6343	39.7203	2.6612
40.00	x_t	2.6306	40.0052	2.6302	40.0031	2.6331	39.2115	2.6931
	$\hat{x}_{s_9}$	2.6316	40.0069	2.6305	40.0025	2.6343	39.1644	2.6956
	$\hat{x}_{s_{10}}$	2.6295	40.0075	2.6288	39.9982	2.6360	39.1171	2.6978
	$\hat{x}_{s_{11}}$	2.6297	40.0074	2.6293	39.9968	2.6373	39.1251	2.6956
	$\hat{x}_{s_{12}}$	2.6307	40.0026	2.6344	39.9992	2.6456	38.8221	2.6927
	$\hat{x}_{s_{13}}$	2.6358	40.0073	2.6368	39.9996	2.6518	38.3774	2.7037
60.00	x_t	2.6304	40.0157	2.6303	39.9489	2.6509	37.3413	2.7461
	$\hat{x}_{s_9}$	2.6311	40.0174	2.6304	39.9428	2.6505	37.2678	2.7460
	$\hat{x}_{s_{10}}$	2.6310	40.0164	2.6298	39.9369	2.6498	37.1801	2.7486
	$\hat{x}_{s_{11}}$	2.6310	40.0156	2.6306	39.9358	2.6527	37.1939	2.7446
	$\hat{x}_{s_{12}}$	2.6366	40.0153	2.6408	39.8586	2.6677	36.7247	2.7338
	$\hat{x}_{s_{13}}$	2.6365	40.0165	2.6444	39.7372	2.6782	36.1328	2.7442
80.00	x_t	2.6299	40.0366	2.6336	39.3599	2.6879	34.9869	2.7879
	$\hat{x}_{s_9}$	2.6293	40.0387	2.6318	39.3274	2.6882	34.9142	2.7880
	$\hat{x}_{s_{10}}$	2.6314	40.0393	2.6351	39.2834	2.6921	34.8300	2.7907
	$\hat{x}_{s_{11}}$	2.6318	40.0378	2.6370	39.2880	2.6931	34.8417	2.7869
	$\hat{x}_{s_{12}}$	2.6391	40.0317	2.6537	39.0433	2.7044	34.4161	2.7714
	$\hat{x}_{s_{13}}$	2.6374	40.0241	2.6561	38.6879	2.7124	33.9129	2.7797
100.00	x_t	2.6292	39.9999	2.6478	37.8329	2.7372	33.0766	2.8186
	$\hat{x}_{s_9}$	2.6289	39.9998	2.6464	37.7658	2.7373	33.0285	2.8164
	$\hat{x}_{s_{10}}$	2.6309	39.9887	2.6503	37.6872	2.7445	32.9704	2.8230
	$\hat{x}_{s_{11}}$	2.6319	39.9879	2.6531	37.6978	2.7431	32.9773	2.8199
	$\hat{x}_{s_{12}}$	2.6449	39.9426	2.6747	37.2785	2.7400	32.6889	2.8011
	$\hat{x}_{s_{13}}$	2.6442	39.8659	2.6785	36.7103	2.7498	32.3520	2.8115
120.00	x_t	2.6323	39.6234	2.6807	35.5838	2.7826	31.7889	2.8513
	$\hat{x}_{s_9}$	2.6325	39.6039	2.6801	35.5064	2.7807	31.7492	2.8532
	$\hat{x}_{s_{10}}$	-	-	-	-	-	-	-
	$\hat{x}_{s_{11}}$	2.6354	39.5792	2.6863	35.4339	2.7833	31.7138	2.8485
	$\hat{x}_{s_{12}}$	2.6630	39.4153	2.7106	34.9663	2.7806	31.4655	2.8347
	$\hat{x}_{s_{13}}$	2.6624	39.1773	2.7196	34.4153	2.7878	31.1443	2.8441
140.00	x_t	2.6498	38.5999	2.7299	33.4582	2.8169	30.5707	2.8757
	z	2.6513	38.5385	2.7309	33.3787	2.8127	30.5238	2.8803
	$\hat{x}_{s_9}$	2.6533	38.5584	2.7325	33.4001	2.8190	30.5328	2.8780
	$\hat{x}_{s_{10}}$	-	-	-	-	-	-	-
	$\hat{x}_{s_{11}}$	2.6544	38.5110	2.7336	33.3431	2.8157	30.4972	2.8747
	$\hat{x}_{s_{12}}$	2.6843	38.2332	2.7507	33.0097	2.8122	30.2877	2.8544
	$\hat{x}_{s_{13}}$	2.6926	37.8559	2.7610	32.6579	2.8204	30.0633	2.8618

Flow in m^3/sec.

Depth in metres.

step took more than 100 iterations to converge. Agreement between estimates and dynamics seems reasonable.

10.8.3.11. Simulation 10 ($\psi = 1.0$). In the previous two problems a "single step" integration process was used in the Kalman filter. However a multi-step process, where the step length is $n = 0.5$ and the process is repeated $m = 2$ times to give an overall step length (or "time between measurement scans") of $TTT = 2 \times 0.5 = 1.0$, the same as in 10.8.3.10. Results of the 140 second simulation are shown in Table 10.12. Each integration step length now takes less than 25 iterations to converge, and better agreement than in 10.8.3.9 exists between the estimate and the dynamics.

10.8.3.12. Simulation 11 ($\psi = 1.0$). The simulation (10.8.3.11) is repeated with $n = 0.5$ and $m = 10$, to give an overall step length of $TTT = 5.0$ seconds. Results of the 140 second simulation are shown in Table 10.12. Each "trapezoidal" integration step length takes less than 25 iterations to converge, and reasonable agreement exists between the estimates and the true system dynamics.

10.8.3.13. Simulation 12 ($\psi = 1.0$). The simulation (10.8.3.11) is repeated with $n = 0.5$ and $m = 20$, to give an overall step length, or time between successive scans, of $TTT = 10.0$ seconds. Results of the 140 second simulation are shown in Table 10.12. Each trapezoidal integration step length takes less than 25 iterations to converge, and reasonable agreement to within less than 1% exists between the dynamics and the estimates.

10.8.3.14. Large system Kalman filter tracking results. Using the approximate diagonalised Kalman gains, suggested in section 10.8.2.5, problems 1 and 2 were simulated, when all measurements are present, over a 140 second time scan. The step length was set at $TTT = 0.1$

Table 10.13 Open channel flow estimates for problem 1 when a 20 cell resolution is used.

TIME (SEC)		y_4	Q_4	y_{12}	Q_{12}	y_{20}
0.00	x_t	2.8420	0.0000	3.0820	0.0000	3.3220
	$\hat{x}$	0.5000	3.0000	0.5000	3.0000	0.5000
20.00	x_t	2.8420	0.0000	3.0820	0.0000	3.2607
	$\hat{x}$	2.8422	0.0003	3.0829	0.0009	3.2594
40.00	x_t	2.8420	0.0000	3.0820	0.0000	3.1250
	$\hat{x}$	2.8413	-0.0009	3.0828	0.0015	3.1242
60.00	x_t	2.8420	0.0000	3.0820	0.0000	2.9979
	x	2.8416	-0.0004	3.0832	-0.0027	2.9973
80.00	x_t	2.8420	0.0000	3.0820	0.0000	2.8955
	x	2.8410	0.0031	3.0824	-0.0030	2.8942
100.00	x_t	2.8420	0.0000	3.0820	0.0000	2.7811
	x	2.8416	-0.0013	3.0822	0.0004	2.7809
120.00	x_t	2.8420	0.0000	3.0820	0.0009	2.6319
	x	2.8424	0.0022	3.0823	0.0008	2.6310
140.00	x_t	2.8420	0.0000	3.0820	0.0080	2.5275
	x	2.8420	-0.0013	3.0812	0.0056	2.5279

* Flow in m^3/sec

Height in metres.

Table 10.14 Open channel flow estimates for problem 2 when a 20 cell resolution is used.

Time (sec)		y_4	Q_4	y_{12}	Q_{12}	y_{20}
0.0	x_t	2.6300	39.9954	2.6300	39.9954	2.6300
	$\hat{x}$	2.0000	43.0000	2.0000	43.0000	2.0000
20.00	x_t	2.6300	39.9944	2.6300	39.9944	2.6478
	$\hat{x}$	2.6301	39.9947	2.6310	39.9949	2.6473
40.00	x_t	2.6300	39.9935	2.6300	39.9935	2.6941
	$\hat{x}$	2.6292	39.9928	2.6308	39.9950	2.6938
60.00	x_t	2.6300	39.9927	2.6300	39.9926	2.7468
	$\hat{x}$	2.6296	39.9922	2.6311	39.9899	2.7465
80.00	x_t	2.6300	39.9921	2.6300	39.9918	2.7879
	$\hat{x}$	2.6292	39.9951	2.6303	39.9894	2.7869
100.00	x_t	2.6300	39.9920	2.6300	39.9911	2.8181
	$\hat{x}$	2.6297	39.9909	2.6302	39.9913	2.8182
120.00	x_t	2.6301	39.9928	2.6300	39.9903	2.8504
	$\hat{x}$	2.6305	39.9947	2.6302	39.9903	2.8500
140.00	x_t	2.6301	39.9942	2.6300	39.9897	2.8744
	$\hat{x}$	2.6300	39.9928	2.6292	39.9874	2.8749

Flow in $m^3/sec.$

Height in metres.

and $\psi = 1.0$, and the number of cells in the canal was set at 20, resulting in 41 states and 41 measurements being available. Results of the tracking simulation are shown in Tables 10.13 and 10.14. Reasonable agreement to within less than 1% exists between the dynamics and the Kalman filter estimates. The "approximate" large scale Kalman gain causes little degradation in the estimates.

The simulations have shown:

- Estimates are relatively insensitive to Kalman gains which are valid for "different" flow conditions.
- When fewer measurements than states are present, initialization from a close start takes longer than when all measurements are present.
- Time between measurement scans to the Kalman filter can be 10 seconds or less, before any degradation in estimates results from the numerical trapezoidal scheme.
- Eigenvalue calculations have shown that some of the open loop eigenvalues of the Kalman filter are positive. However, it appears that fixing the input and output Q_{IN} and Q_{OUT} suppresses these unstable eigenvalues. If only y_{IN} and Q_{IN} were fixed, the dynamic hydrocanal representation becomes unstable.
- Large scale Kalman filter estimation of open channel flow seems feasible.

10.9 CONCLUSION

Hierarchical state estimation using local dynamic estimators for hydroturbine and hydrocanal estimation has been shown to be feasible in tracking the state of the combined energy systems. Simulations have shown the "hydroturbine and generator" Kalman filter to give an

acceptable performance, generating similar results to Handschin and Galiana's (1973) "thermal turbine and generator" Kalman filter profiles.

Simulations have shown the "discretized" representation of the distributed parameter hydrocanal system to be stable, and a Kalman filter can be built using this gradually varied, unsteady flow model. It has been shown that the resulting estimates are relatively insensitive to changes in gain, as the flow conditions vary, and thus the linearized Kalman filter approach appears to be a good one. The filter has also been shown to faithfully track the changing state of the hydrocanal system when less measurements than states are present. Large scale open channel Kalman filter "implementation", where the level of discretization is 20 or so, will require better methods of calculating the Kalman gain than those used in the study. However it has been shown that when an "approximate-band structured" Kalman gain was used, the estimates were accurate to within 1% of the true dynamics. Thus it appears that combined hydrogenerator-canal dynamic estimation is feasible and worthy of further study.

CHAPTER 11

STATISTICAL TECHNIQUES IN LOADFLOW STUDIES

11.1 SUMMARY OF STATISTICAL TECHNIQUES IN LOADFLOW STUDIES

Stochastic and probabilistic loadflows can account for the variation or "spread" of nodal generation and loads over a long time period. These statistical loadflows are useful in evaluating expected power flows and their variance or "spread" down existing or planned a.c. transmission lines. Such loadflows are useful during the planning of network expansions. Planning of network expansions can be carried out by performing a series of deterministic loadflows (DFL) in the hope of highlighting extreme conditions of transmission line power flow. However there is no guarantee that any one of the postulated nodal generation-load conditions, selected for the DFL, will cause an extreme power flow condition down the transmission line or lines of interest. One statistical loadflow can replace the large number of DFL required to cover every possible contingency in the long-term planning of network expansions.

Two different approaches have been advocated to represent statistical effects in loadflow studies. These are the probabilistic loadflow (PLF) and the stochastic loadflow (SLF). The PLF approach was first suggested by Borkowska (1973) and allows the representation of gaussian, discrete or binomial nodal probability distribution function (p.d.f.). Initially only a d.c. loadflow representation was used, together with sensitivity co-efficients and probabilistic convolution

techniques (Borkowska, 1973; Allan *et al.*, 1974; Allan, Gregg and Al-Shakarchi, 1976). Later the technique was extended to a.c. loadflow analysis by Allen *et al.* (1976) and the accuracy improved by linearizing about estimates obtained from a deterministic loadflow and treating these estimates as the expected values of the P.L.F. (Allan and Al-Shakarchi, 1976, 1977). The a.c. P.L.F. can also be P-θ, Q-v decoupled in order to reduce the computation burden (Allan and Al-Shakarchi, 1977). P.L.F. techniques have been extended to represent linear nodal dependence and correlated data, and the loadflow results are used in operational decision making and expected network outage calculations (Allan *et al.*, Dec. 1976; Allan *et al.*, June 1977; Allan *et al.*, 1979). Other authors have used different approaches to represent the gaussian, discrete or binomial p.d.f.'s (Heydt, 1975; Heydt and Sauer, 1976; Jottrand, 1978). Sauer and Heydt (1978) use the method of moments to represent the different types of p.d.f.'s.

The S.L.F. approach for representing statistical effects in loadflow studies was first suggested by Dopazo *et al.* (Dopazo *et al.*, 1975; Van Slyck *et al.*, 1973). The method uses the same algorithm as state estimation, but with the problem redefined. The uncertainty of the input data to the W.L.S. state estimation algorithm can be considered from two points of view: "aposteriori", uncertainty of the past or present state of the system; and "apriori", uncertainty in specifying the future state of the power system (Dopazo *et al.*, 1975). The aposteriori uncertainty is treated by state estimation methods while apriori uncertainty is treated by a S.L.F. The S.L.F. method is fast when compared with the P.L.F. and can easily be performed by utilities that already have a state estimation algorithm. However the disadvantage of the S.L.F. is that it can only process gaussian p.d.f.'s, and non-gaussian p.d.f.'s such as the discrete or binomial

p.d.f. must be "approximated" by a gaussian p.d.f.

The concept of the S.L.F. has been extended to represent correlated nodal data (Aboyles and Cory, 1975) and P-θ, Q-v decoupling (Flann and Sasson, 1977; Hayes, 1977). Optimal S.L.F. techniques have also been investigated (Kothari and Gupta, 1978; Sobierajski, 1979).

11.2 REVIEW OF STOCHASTIC LOADFLOW CONCEPTS

The long-term nodal generation or load is assumed to vary about an expected value, $\underline{z}$. At any operating point, the expected generation or load is related to the state of the power system, $\underline{x}$ (n×1), at that operating point, via (Dopazo *et al.*, 1975)

$$\underline{z} = \underline{h}(\underline{x}) + \underline{\eta} \tag{11.1}$$

The vector $\underline{\eta}$ (m×1) represents the error between $\underline{z}$ (m×1) and $\underline{h}(\underline{x})$ (m×1). The vector $\underline{\eta}$ can be described statistically as a random variable with a mean and a variance, σ. The variance reflects the likely spread of generation over a long period of time, about its mean value, $\underline{z}$. For the S.L.F., the expected value of error is assumed zero.

$$E(\underline{\eta}) = 0 \tag{11.2}$$

and

$$E(\underline{\eta}\ \underline{\eta}^T) = \underline{R} \tag{11.3}$$

where $\underline{R}$ is an (m×m) matrix of gaussian variances, σ, and E is the expectation operator. When $\underline{R}$ is a diagonal matrix, the expected long-term nodal generation and load data is uncorrelated. The weighted least squares (WLS) criterion is to minimize

$$\underline{J}(\underline{x}) = \left(\underline{z} - \underline{h}(\underline{x})\right)^T \underline{R}^{-1} \left(\underline{z} - \underline{h}(\underline{x})\right) \tag{11.4}$$

It was shown, in section 2.3, that the solution to (11.4) is to iteratively solve

$$(\underline{H}^T(\underline{x}_k)\ \underline{R}^{-1}\ \underline{H}(\underline{x}_k))\Delta\underline{x}_{k+1} = \underline{H}^T(\underline{x}_k)\ \underline{R}^{-1}\ (\underline{z} - \underline{h}(\underline{x}_k)) \qquad (11.5)$$

until convergence.

Nominally the loadflow problem is singular, with the dimension of $\underline{z}$ being the same as that of $\underline{x}$, i.e. $m = n$. Nodal data contained in $\underline{z}$ is of two types: either "Pv" generation data or "PQ" load data. In a deterministic loadflow, one of the generation busbars is selected to be the slack or reference busbar, where the voltage phase angle is specified as zero. However in the S.L.F., constraints on the total system load are required to avoid large uncertaintites; variations in power flow about the expected values appear on lines in the vicinity of the slack busbar. A constraint on the total system load is enforced by specifying the active slack bus power, P_s, as well as the voltage, v_s. Also, the loadflow estimate for slack bus nodal voltage is kept fixed to its actual value, v_s, as the loadflow iterates. The uncertainty in forecasting the "total system load plus losses" is then distributed among the variances of the generation active power equations, thus making all generators compensate for forecasting errors rather than solely the slack bus generator. 2N measurement equations and (2N-1) states now define the S.L.F. The presence of an overdetermined measurement set has been shown to cause negligible filtering of the S.L.F. estimates.

The S.L.F., given by (11.5), converges to $\hat{\underline{x}}$, the long-term expected value of the state. The variation about this expected state can be found by evaluating the co-variance matrix about $\hat{\underline{x}}$, i.e.

$$\text{cov}(\hat{\underline{x}}) = (\underline{H}^T(\hat{\underline{x}})\ \underline{R}^{-1}\ \underline{H}(\hat{\underline{x}}))^{-1} \qquad (11.6)$$

where the co-variance of state $x_1 = \text{diag}_{ii}(\text{cov}(\hat{x}))$ (11.7)

The expected long-term uncertainty about "quantities of interest", $\underline{s}$, such as real and reactive line power flows, nodal voltages and some power injection, can be found by evaluating (Dopazo *et al.*, 1975),

$$\text{cov}(\underline{s}) = \underline{K}(\hat{\underline{x}}) \left(\underline{H}^T(\underline{x}) \, \underline{R}^{-1} \, \underline{H}(\hat{\underline{x}})\right)^{-1} \underline{K}^T(\hat{\underline{x}}) \tag{11.8}$$

where the quantities of interest, $\underline{s}$, and the long-term expected values of the states are related via the non-linear measurement equations.

$$\underline{s} = \underline{k}(\hat{\underline{x}}) \tag{11.9}$$

and where

$$\underline{K}(\hat{\underline{x}}) = \partial \underline{k}(\hat{\underline{x}}) / \partial \hat{\underline{x}} \tag{11.10}$$

11.3 CONCLUSION

In this chapter, statistical loadflow methods have been summarised. The two methods of statistical loadflow analysis are the S.L.F. and the P.L.F. The S.L.F. only handles gaussian p.d.f.'s while the P.L.F. handles all kinds of p.d.f. distributions. The statistical properties of the S.L.F. have been reviewed and it has been shown that the S.L.F. is merely a "redefinition" of the state estimation problem, and the same algorithm as outlined in Chapter 2 can be used.

CHAPTER 12

REPRESENTATION OF NON-GAUSSIAN PROBABILITY DISTRIBUTIONS IN STOCHASTIC LOADFLOW STUDIES BY GAUSSIAN SUM APPROXIMATIONS

12.1 INTRODUCTION

In the previous chapter it was noted that the S.L.F. can only model gaussian p.d.f's whereas the P.L.F. can model all types of p.d.f's; gaussian, discrete and binomial. Long-term p.d.f's that are gaussian occur at nodes of domestic loading where demand is dependent on weather conditions, etc. Large, continuous loads like smelters or other industrial plant can give rise to discrete p.d.f's. Binomial and non-gaussian p.d.f's result from outage effects at generation busbars which contain more than one generator of a similar rating. It is thus a disadvantage of the S.L.F. that it cannot model non-gaussian p.d.f. long-term nodal variations. Borkowska (1973) points out that approximating a non-gaussian p.d.f. by a single gaussian, in order to perform a S.L.F., can result in overdesign in the long-term planning of transmission lines by quite a significant amount.

A gaussian sum approximation technique is advocated in this chapter to include non-gaussian p.d.f's in S.L.F. studies and thus make the S.L.F. capable of performing a P.L.F. The benefit of this approach is that the state estimator-type S.L.F. algorithm which can be used is readily available to a number of utilities having state estimation programs. The results of the gaussian-sum approximation S.L.F. study can be as accurate as required; in the limit achieving the same or better

results as the P.L.F. Such accuracy is likely to be required when expanding the transmission line capability in a sensitive location or when generating reliability outage data.

12.2 GAUSSIAN SUM APPROXIMATION

A non-gaussian distribution P(y) can be approximated by a n^{th} order gaussian summation, $P_n(y)$, where (Sorenson and Alspach, 1971; Alspach and Sorenson, 1972; Alspach, 1978; Anderson and Moore, 1979):

$$P_n(y) = \sum_{i=1}^{n} \alpha_i \, N_{\sigma_i}(y - \mu_i) \qquad (12.1)$$

where $N_{\sigma_i}(y - \mu_i)$ is the ith component normal distribution of the summation, having variance σ_i and expectation μ_i; and

α_i is the weighting of the i^{th} normal distribution.

$$\sum_{i=1}^{n} \alpha_i = 1 \quad \text{and} \quad \alpha_i \geq 0 \quad \text{for all } i \qquad (12.2)$$

When gaussian sum approximations are used to represent non-gaussian nodal p.d.f's in the S.L.F.; all convolutions of the individual gaussian sum components, with those of other nodes, must be taken into account with the correct weighting factors.

Consider a two node example where the non-gaussian nodal p.d.f's, at each node, are replaced by a two component gaussian sum approximation. At node 1, the non-gaussian p.d.f., s_1, is replaced by

$$s_1 \rightarrow \alpha_{11} N_{\sigma_{11}}(y - \mu_{11}) \; , \; \alpha_{12} N_{\sigma_{12}}(y - \mu_{12})$$

while at node 2 the non-gaussian p.d.f., s_2, is replaced by

$$s_2 \rightarrow \alpha_{21} N_{\sigma_{21}}(y - \mu_{21}) \; , \; \alpha_{22} N_{\sigma_{22}}(y - \mu_{22})$$

where $\alpha_{11} = 1 - \alpha_{12}$; and

$\alpha_{21} = 1 - \alpha_{22}$.

All gaussian sum approximation convolution components are shown in Table 12.1, together with their respective weightings. When using the S.L.F. to perform a P.L.F., s_1 and s_2 must be replaced, sequentially, by a combination from columns 1 and 2 until all combinations have been evaluated, in the S.L.F., and the results added, together with the weighting shown in column 3 of Table 12.1, to give the non-gaussian p.d.f. results.

Table 12.1 Convolution components and their weightings

CONVOLUTION COMBINATION	s_1	s_2	TOTAL WEIGHTING α_i
1	s_{11}	s_{21}	$\alpha_1 = (\alpha_{11})\ (\alpha_{21})$
2	s_{11}	s_{22}	$\alpha_2 = (\alpha_{11})\ (\alpha_{22})$
3	s_{21}	s_{21}	$\alpha_3 = (\alpha_{12})\ (\alpha_{21})$
4	s_{12}	s_{22}	$\alpha_4 = (\alpha_{12})\ (\alpha_{22})$

Thus for the 2 bus example the S.L.F. must be evaluated (2)(2) = 4 times, each time with a different gaussian sum combination from Table 12.1. The individual results are then recombined with the correct weightings to give the non-gaussian p.d.f's.

For a P.L.F. study containing N busbars, the number of repeat evaluations of the S.L.F. required to evaluate all gaussian sum approximation-convolution components is given by

$$\pi_{i=1}^{N}(r_i)\ (q_i) \qquad (12.3)$$

where r_i is the number of gaussian components which sum to represent the real power p.d.f. at bus i ; and

q_i is the number of gaussian components which sum to represent the reactive power or voltage p.d.f. at bus i.

If P_i, Q_i are completely correlated, (12.3) reduces to $\pi_{i=1}^{N} r_i$.

12.3 TEST SYSTEM ANALYSIS

The I.E.E.E. 14 bus - 20 line test system is used. The same test system and probabilistic data were used by Allan and Al-Shakarchi (1976, 1977) to evaluate the performance of the P.L.F. All of the generator "PV" busbars in Allan and Al-Shakarchi's example have nodal real and reactive injected power data as well as the nodal voltage magnitude. In order to handle such combined "PV" and "PQ" generation data in the S.L.F., the generation busbars, 2, 3, 6 and 8, are split by connecting them to fictitious busbars, 15, 16, 17 and 18, respectively, by near-zero impedance lines.

The creation of these fictitious busbars enables the combined "PV and PQ" generation characteristics to be separated into "PV" characteristics at nodes 2, 3, 6 and 8 and "PQ" characteristics at nodes 15, 16, 17 and 18. Thus for generation node 2,

$$P_2 = P_{2_{old}}$$

$$v_2 = v_{2_{old}}$$

$$P_{15} = 0.0 \text{ p.u.}$$

$$Q_{15} = Q_{2_{old}}$$

and similar partitioning occurs at 3-16, 6-17 and 8-18. Line and nodal data for the expanded 18 bus test system is shown in Table 12.2, and nodal probabilistic data used in the evaluation is shown in Table 12.3.

Table 12.2 Deterministic data for the expanded IEEE 14 bus test system

DETERMINISTIC DATA FOR IEEE 14 BUS SYSTEM					
Busbar		Voltage p.u.	Active powers (MW)		Load reactive powers MVARr
Number	Type		Generation	Load	
1	slack	1.0600	230.00		
2	PV	1.0450	40.04		
3	PV	1.0100	0.00		
4	PQ			47.80	-3.90
5	PQ			7.60	1.60
6	PV	1.0700	0.00		
7	PQ			0.00	0.00
8	PV	1.0900	0.00		
9	PQ			29.50	16.60
10	PQ			9.00	5.80
11	PQ			3.50	1.80
12	PQ			6.10	1.60
13	PQ			13.50	5.80
14	PQ			14.90	5.00
15	PQ			21.74	12.70
16	PQ			94.20	19.00
17	PQ			11.20	7.50
18	PQ			0.00	0.00

LINE DATA FOR IEEE 14 BUS SYSTEM					
Busbar		Resistance p.u.	Reactance p.u.	Susceptance p.u.	Transformer tap
Sending	Receiving				
1	2	0.01938	0.05917	0.02640	90
1	5	0.05403	0.22304	0.02640	
2	3	0.04699	0.19797	0.02190	
2	4	0.05811	0.17632	0.01870	
2	5	0.05695	0.17388	0.01700	
3	4	0.06701	0.17103	0.01730	
4	5	0.01335	0.04211	0.00640	
4	7	-	0.20912	-	-2.2
4	9	-	0.55616	-	-3.1
5	6	-	0.25202	-	-6.8
6	11	0.09498	0.19890	-	
6	12	0.12291	0.25581	-	
6	13	0.06615	0.13027	-	
7	8	-	0.17615	-	
7	9	-	0.11001	-	
9	10	0.03181	0.08450	-	
9	14	0.12711	0.27038	-	
10	11	0.08205	0.19207	-	
12	13	0.22092	0.19988	-	
13	14	0.17093	0.34802	-	
9	9	-	-5.26000	-	
1	15	0.00100	0.00100	-	
2	16	0.00100	0.00100	-	
3	17	0.00100	0.00100	-	
4	18	0.00100	0.00100	-	

Table 12.3 Probabilistic data for the expanded IEEE 14 bus test system

1. Normal distributions

Busbar		Voltage	Active power		Reactive power	
Number	Type	p.u.	μ MW	σ %	μ MVAR	σ %
3	PV	1.010	0.00	0.00	-	-
4	PQ	-	-47.80	11.00	3.90	9.7
5	PQ	-	-7.60	5.00	-1.60	5.0
6	PV	1.070	-11.20	6.00	-	-
7	PQ	-	0.00	0.00	0.00	0.0
8	PV	1.090	0.00	0.00	-	-
10	PQ	-	-9.00	10.00	-5.80	10.0
11	PQ	-	-3.50	9.50	-1.80	9.5
12	PQ	-	-6.10	7.60	-1.60	8.6
13	PQ	-	-13.50	10.50	-5.80	9.5
14	PQ	-	-14.90	8.60	-5.00	8.6
15	PQ	-	-21.74	9.00	-12.70	9.2
16	PQ	-	-94.20	10.00	-19.00	10.5
17	PQ	-	-11.20	6.00	-7.50	6.3
18	PQ	-	0.00	0.00	0.00	0.0

2. Binomial distributions

Busbar		Voltage	Unit rating	Forced	No. of	μ	σ
Number	Type	p.u.	(MW)	outage rate	units	MW	MW
1	Slack	1.060	25.0	0.08	10	230.00	21.450
2	PV	1.045	22.0	0.09	2	40.04	8.903

3. Any discrete distribution

Busbar		Voltage	Active power		Reactive power	
Number	Type	p.u.	MW	prob.	MVAR	prob.
9	PQ	-	-13.4	0.10	-7.5	0.10
			-19.6	0.15	-11.0	0.15
			-30.2	0.30	-17.0	0.30
			-34.8	0.25	-19.6	0.25
			-37.3	0.20	-21.0	0.30
			μ (MW)	σ (MW)	μ (MVAR)	σ (MVAR)
			-29.50	7.74	-16.60	4.38

Most of the nodal p.d.f's are gaussian and can be handled by the S.L.F. without any sum approximations. The binomial distributions at nodes 1 and 2, expanded into their individual components, are shown in Table 12.4.

The binomial distribution for the active power generated at node 1 has 11 discrete components. The mean and standard deviation for this distribution is

$$\mu = np = 230 \text{ MW} \tag{12.4}$$

and

$$\sigma = \sqrt{npq} = 21.45 \text{ MW} \tag{12.5}$$

However if only the four largest components are included

$$\mu' = \sum_{i=1}^{4} p_i x_i = 229.15 \text{ MW} \tag{12.6}$$

and

$$\sigma' = \left(\sum_{i=1}^{4} p_i (x_i - \mu')^2 \right)^{\frac{1}{2}} = 20.53 \text{ MW} \tag{12.7}$$

If the 11 component binomial p.d.f. is replaced by only the four largest components, the error in the expected value is less than 0.4% while the error in the standard deviation is less than 4.5%. Thus an accurate gaussian sum approximation to the binomial can be made about the four largest discrete components by replacing each component with a gaussian type delta function where σ_{N_i}, the standard deviation of the gaussian, is very small and the weighting factor, α, equal to the probability of the generation occurring at that point. Each gaussian delta function is centred with μ_i on one of the four largest discrete components; $r_1 = 4$. Note that the order of a discrete distribution is the number of discrete components present. As long as the order is unchanged when the non-gaussian p.d.f. is replaced by gaussian type delta functions, no loss in accuracy will occur.

Table 12.4 Individual components of the binomial probability distributions

NO. OF UNITS OPERATIONAL		GENERATION (MW)	AVAILABILITY OF OCCURRENCE
Active generation @ node 1		10 units, rating = 25 MW, forced outage rate = 0.08	
1	10 out of 10	250.0	0.43439
2	9 out of 10	225.0	0.37773
3	8 out of 10	200.0	0.14781
4	7 out of 10	175.0	0.03427
5	6 out of 10	150.0	0.00522
6	5 out of 10	125.0	0.00054
7	4 out of 10	100.0	0.0000394
8	3 out of 10	75.0	0.0000020
9	2 out of 10	60.0	0.000000064
10	1 out of 10	25.0	0.000000001
11	0 out of 10	0.0	0.0
Active generation @ node 2		2 units, rating = 22 MW, forced outage rate = 0.09	
1	2 out of 2	44.0	0.8281
2	1 out of 2	22.0	0.1638
3	0 out of 2	0.0	0.0081

The binomial distribution for the active power generation at node 2 contains only three states. The mean and standard deviations for this binomial distribution are 40.04 MW and 8.904 MW respectively. It is easily shown, using (12.6) and (12.7), that all components of the binomial must be retained in order to preserve accuracy. The three discrete components of the binomial distribution at node 2 can be replaced by three gaussian type delta functions with near zero variance and with μ_i, σ_i and α_{N_i} selected in a similar manner to those variables used in the gaussian sum approximation of the active power p.d.f. at node 1, $r_2 = 3$.

The discrete p.d.f. at node 9, for real and reactive power, contains five states respectively. The mean and standard deviations for the discrete real and reactive power distribution are -29.50 MW and -16.60 MVAR, and 7.74 MW and 3.38 MVAR, respectively. All five components of the discrete distributions must be retained in order to preserve accuracy. The five component discrete p.d.f. for both real and reactive power can be replaced by five gaussian type delta functions, respectively, each with μ_i centred on one of the discrete components $\sigma_i \simeq 0$ and with the weighting factor, α_i, equal to the probability that particular generation level occurs. Thus $r_9 = 5$ and $q_9 = 5$.

The specification of voltage magnitude at generator busbars 2, 3, 6 and 8 can be regarded as a single component discrete distribution and replaced by a single gaussian delta function, centred on the specified value of voltage; with $\sigma_i = 0$ and $\alpha_i = 1$. Thus q_1, q_2, q_6 and $q_8 = 1$.

The number of repeat evaluations of the S.L.F. required to evaluate all convolution combination terms and generate P.L.F.'s is

$$\prod_{i=1}^{18} (r_i)(q_i) = \underset{r_1}{(4)}\ \underset{q_1}{(1)}\ \underset{r_2}{(3)}\ \underset{q_2}{(1)}\ \ldots\ \underset{q_8}{(1)}\ \underset{r_q}{(5)}\ \underset{q_9}{(5)}\ \underset{r_{10}}{(1)}\ \ldots\ \underset{q_{18}}{(1)}$$

$$= \text{300 separate evaluations.}$$

The revised probability data to be used in the series of stochastic loadflows is shown in Table 12.5. A summary of the data required for the nodes at which gaussian sum approximations are present is given in Table 12.6. Note also that for the test purposes, Dopazo's percentage total load constraint is set to zero.

After all 300 of the convolution components have been evaluated the results are recombined, for any quantity of interest, such as a nodal voltage, injected reactive power or the reactive and active power flows down a transmission line. Summing the 300 individual contribution gaussian p.d.f's, taking account of each mean, μ_n, variance σ_m and weighting factor α_m, at the point of interest, results in reconstructing the non-gaussian p.d.f. statistics for the point of interest. That is,

$$\text{Non-gaussian p.d.f.}_{\text{Point of interest}} = \sum_{m=1}^{300} \alpha_m N_{\sigma_m}(x-\mu_m)_{\text{Point of interest}} \tag{12.8}$$

Gaussian sum p.d.f. reconstructions for v_4, p_{5-6}, Q_{7-9} and Q_3 are shown in Figures 12.1 to 12.4, together with Allan and Al-Shakarchi's (1977) results for the P.L.F. Very close agreement between the gaussian sum approximation S.L.F. and the P.L.F. reconstructions for p_{5-6} and Q_{7-9} is evident. The gaussian-sum reconstruction for Q_3 cannot be compared with Allan and Al-Shakarchi's result because bus Q_3 was split into generation, at bus 3, and load at bus 17. Very crudely, the form of the curve can be compared by finding Q_3', where

$$\mu_{Q_3'} = \mu_{Q_3} + \mu_{Q_{17}} \tag{12.9}$$

$$\sigma^2_{Q_3'} = \sigma^2_{Q_3} + \sigma^2_{Q_{17}} \tag{12.10}$$

Table 12.5 Probabilistic data for the S.L.F.: Expected values and variances

BUSBAR		VOLTAGE		ACTIVE POWER		REACTIVE POWER	
NUMBER	TYPE	μ (p.u.)	σ (p.u.)	μ (MW)	σ %	μ (MVAR)	σ %
1	PV	1.060	0.0001	*	0.01	-	-
2	PV	1.045	0.0001	*	0.01	-	-
3	PV	1.010	0.0001	0.0	0.01	-	-
4	PQ	-	-	-47.80	11.00	3.90	9.70
5	PQ	-	-	-7.60	5.00	-1.60	5.00
6	PV	1.070	0.0001	-11.20	6.00	-	-
7	PQ	-	-	0.00	0.01	0.00	0.01
8	PV	1.090	0.0001	0.00	0.01	-	-
9	PQ	-	-	*	0.01	*	0.01
10	PQ	-	-	-9.00	10.00	-5.80	10.00
11	PQ	-	-	-3.50	9.50	-1.80	9.50
12	PQ	-	-	-6.10	7.60	-1.60	8.60
13	PQ	-	-	-13.50	10.50	-5.80	9.50
14	PQ	-	-	-14.90	8.60	-5.00	8.60
15	PQ	-	-	-21.74	9.00	-12.70	9.20
16	PQ	-	-	-94.20	10.00	-19.00	10.50
17	PQ	-	-	-11.20	6.00	-7.50	6.30
18	PQ	-	-	0.00	0.01	0.00	0.01

* For value of the gaussian sum approximation, see Table 12.6.
All values above, except at *, have weighting factors, $\alpha_i = 1$.

Table 12.6 Gaussian sum approximation component values and their weightings

NODE AND TYPE			GAUSSIAN SUM DELTA FUNCTION APPROXIMATION COMPONENTS		
			μ_i	σ_i	α_i
1	P_1 (Binomial)	1	250.00 MW	0.01 MW	0.43439
		2	225.00 MW	0.01 MW	0.37773
		3	200.00 MW	0.01 MW	0.14781
		4	175.00 MW	0.01 MW	0.03427
2	P_2 (Binomial)	1	44.00 MW	0.01 MW	0.82810
		2	22.00 MW	0.01 MW	0.16380
		3	0.00 MW	0.01 MW	0.00810
3	P_9 (Discrete)	1	-13.40 MW	0.01 MW	0.10
		2	-19.60 MW	0.01 MW	0.15
		3	-30.20 MW	0.01 MW	0.30
		4	-34.80 MW	0.01 MW	0.25
		5	-37.30 MW	0.01 MW	0.20
4	Q_9 (Discrete)	1	-7.50 MVAR	0.01 MVAR	0.10
		2	-11.00 MVAR	0.01 MVAR	0.15
		3	-17.00 MVAR	0.01 MVAR	0.30
		4	-19.60 MVAR	0.01 MVAR	0.25
		5	-21.00 MVAR	0.01 MVAR	0.20

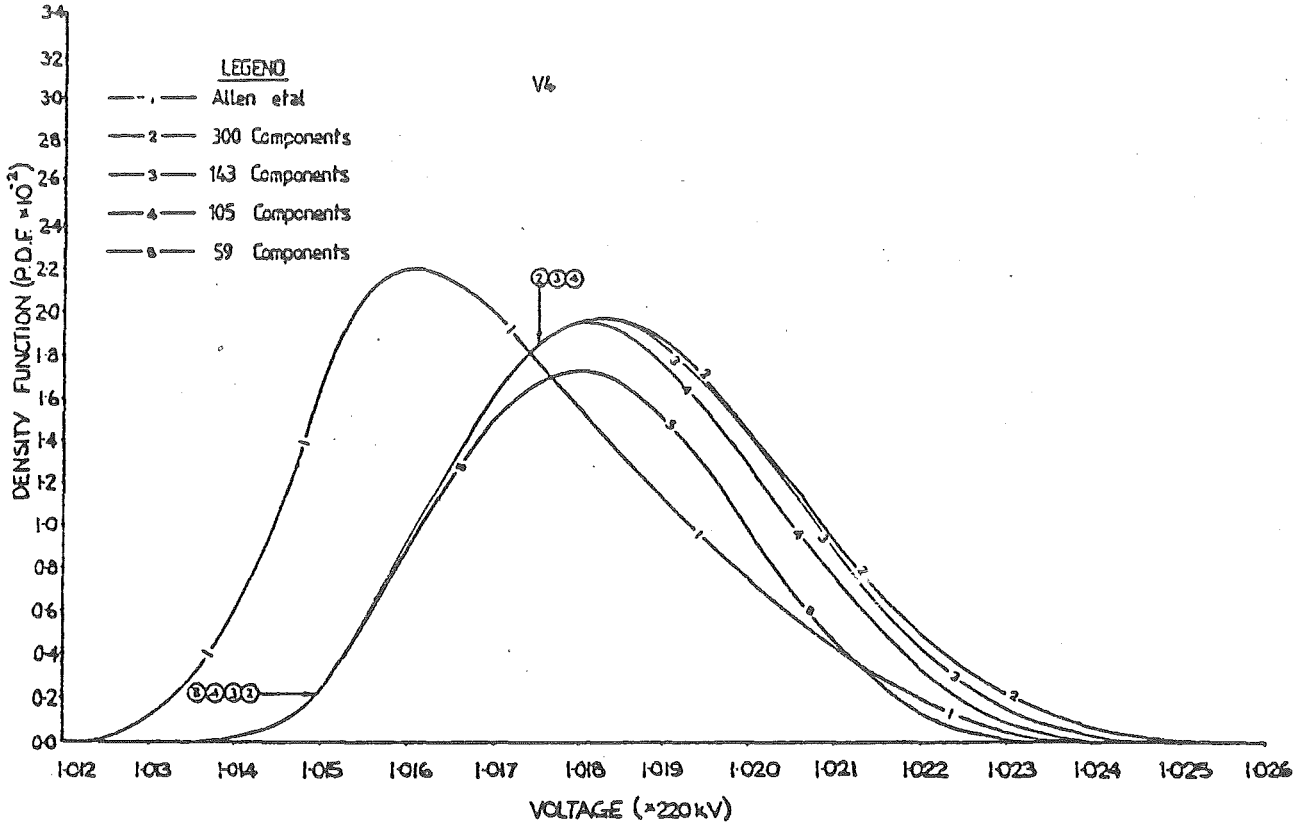

Figure 12.1 Gaussian sum reconstruction for v_4

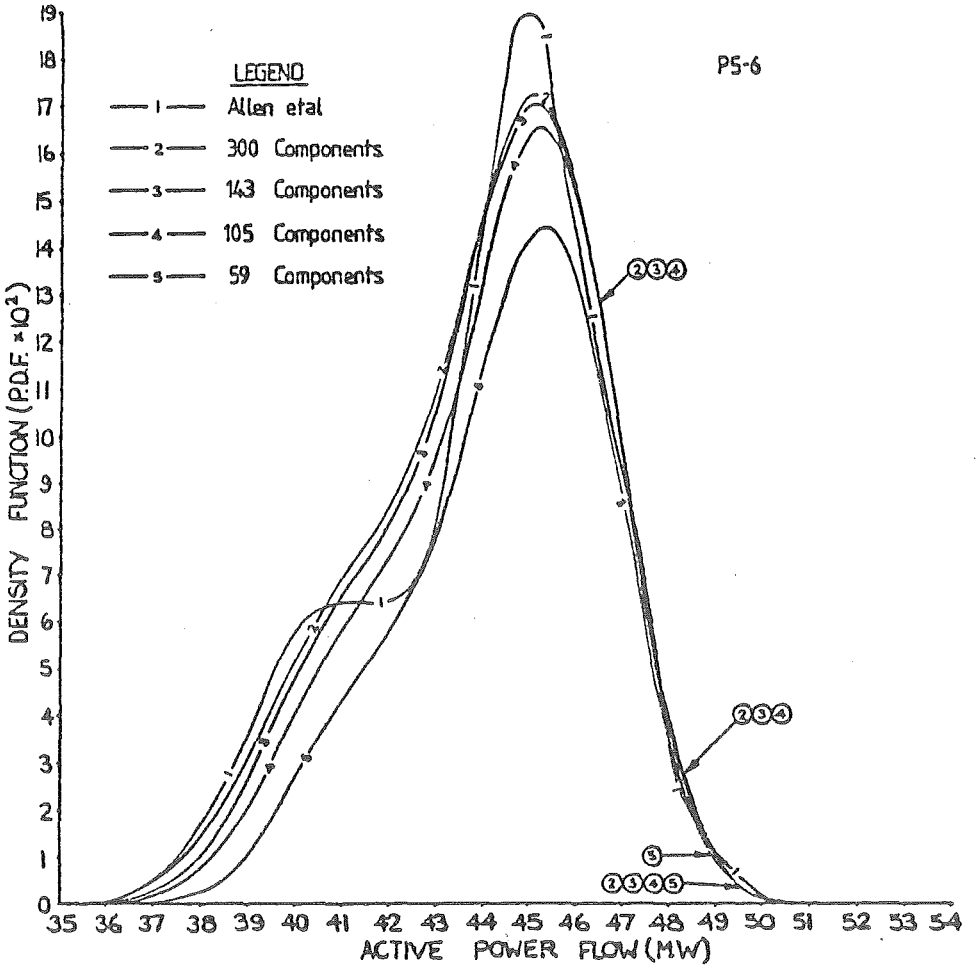

Figure 12.2 Gaussian sum reconstruction for P_{5-6}.

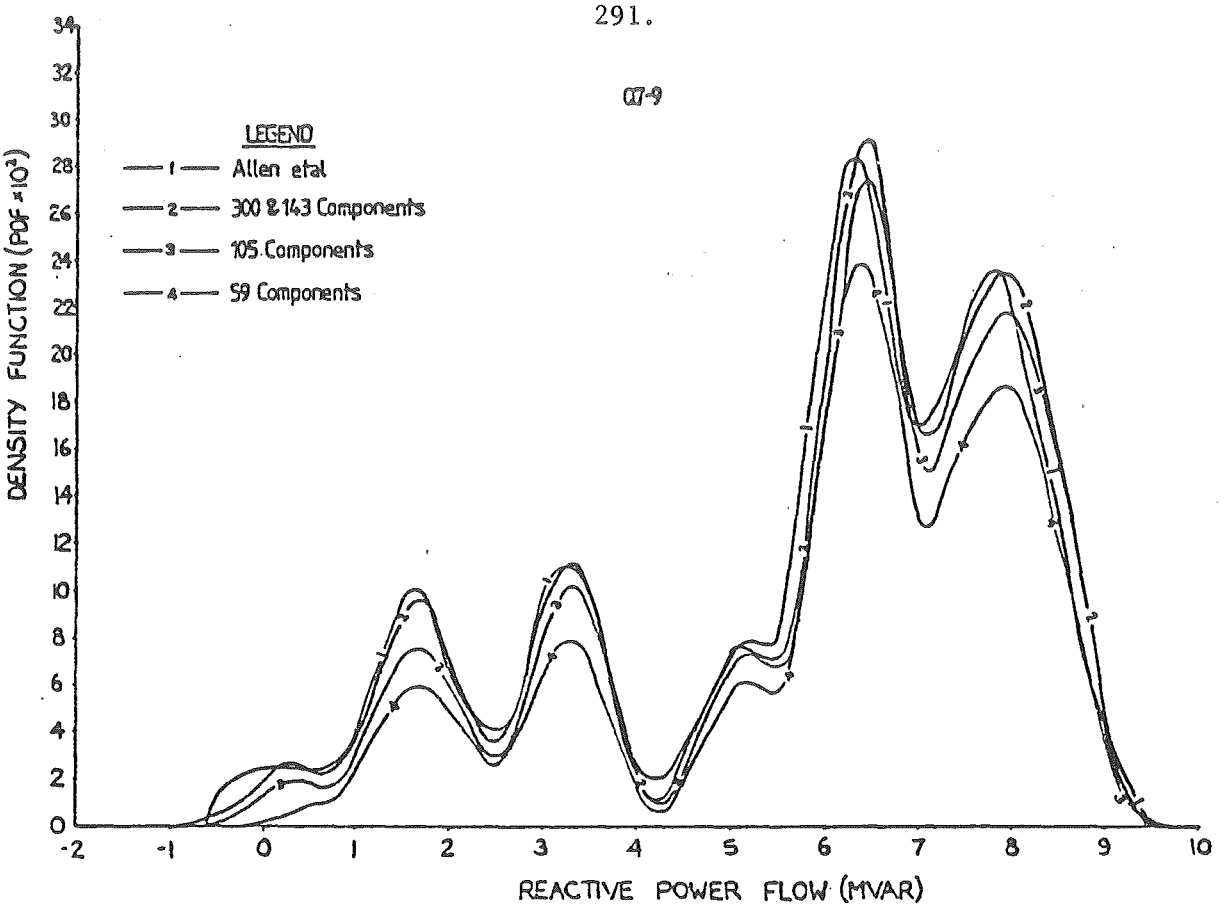

Figure 12.3 Gaussian sum reconstruction for P_{5-6}.

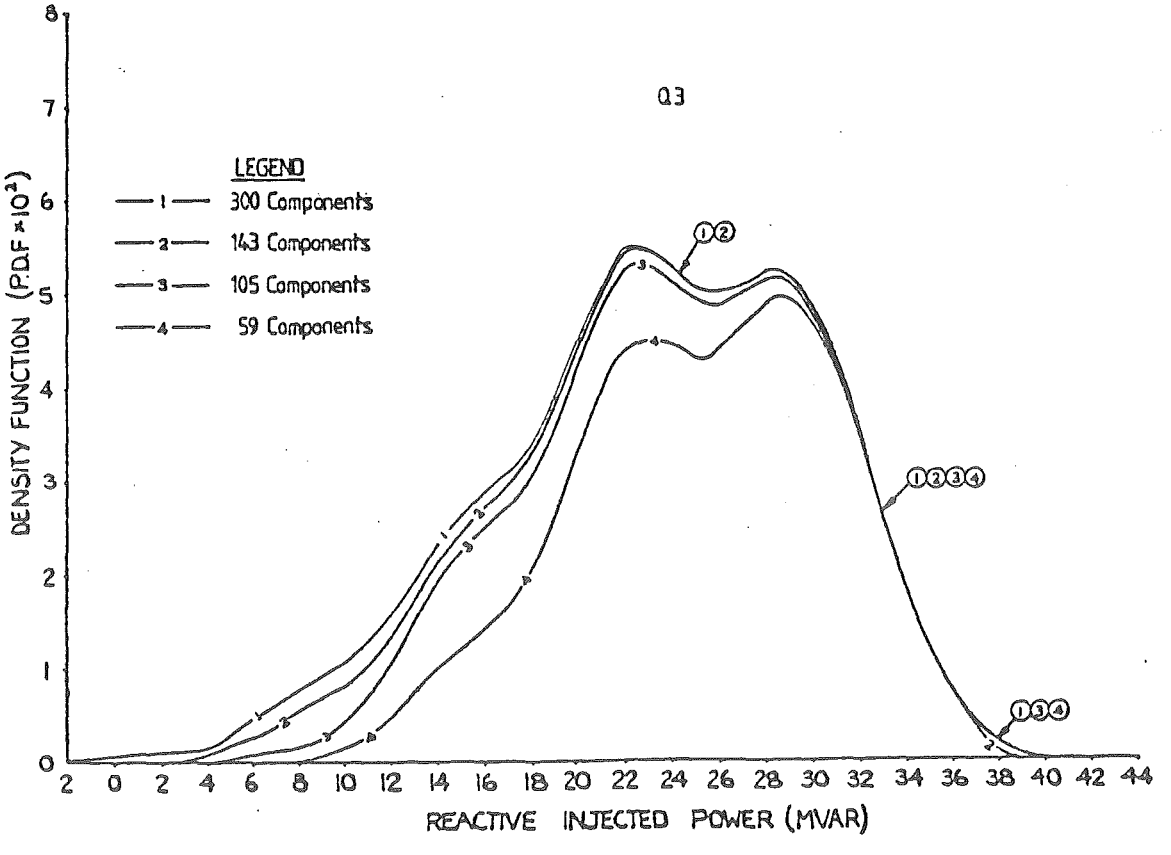

Figure 12.4 Gaussian sum reconstruction for Q_3.

and comparing the profile with that of Allan and Al-Shakarchi's for Q_3 (see Figure 12.5). Both curves have a similar profile. Q_3' may have greater spread than Allan and Al-Shakarchi's Q_3 because (12.10) assumes Q_3 and Q_{17} are independent. If not, then

$$\sigma_{Q_3'}^2 = \sigma_{Q_3}^2 + \sigma_{Q_{17}}^2 + 2 \text{ Cov } (Q_3, Q_{17}) \qquad (12.11)$$

Gaussian sum approximation S.L.F. and the P.L.F. reconstruction for v_4 have a similar shape and spread (variance), but are centred at slightly different mean values. Allan and Al-Shakarchi "linearize" the P.L.F. about the solution of the conventional loadflow, then compute non-gaussian profiles using probabilistic convolution and using the redundant loadflow data of Table 12.3. However the method used above, involving a series of gaussian sum approximation S.L.F.'s, involves 300 separate linearizations, using the redundant measurement data of Table 12.3 at different operating points. As a result, the effect of linearization error, mentioned by Sauer and Heydt (1978), is likely to be random and the error will disappear. The only linearization error effects will appear during the recombination of the gaussian sum components using (12.8). As a result the gaussian sum approximation - S.L.F. method of performing the P.L.F. will likely to be more accurate than Allan and Al-Shakarchi's. If redundant, long-term nodal data is present and available, as in Table 12.3 with the binomial probability distribution specified for p_1, the slack bus, as well as v_1, then use this "extra" information and linearize about this point rather than requiring a loadflow solution point. Redundancy in such future planning data will generate better long-term estimates and there is no reason to remain with a non-redundant loadflow solution.

The majority of the 300 convolution-combination S.L.F. terms have extremely low probabilities of occurrence. In fact, the majority

of the terms can be discarded without affecting the accuracy of the reconstruction. Figures 12.1 to 12.4 show gaussian-sum p.d.f. reconstructions for v_4, p_{5-6}, Q_{7-9} and Q_3 for the following.

(i) All components of the convolution having weighting factors $\alpha_i < 0.001$ are discarded from the summation. 143 components out of the 300 possible are used in the reconstruction.

(ii) All components of the convolution having weighting factors $\alpha_i < 0.002$ are discarded from the summation. 105 components out of the 300 possible are used in the reconstruction.

(iii) All components of the convolution having weighting factors $\alpha_i < 0.005$ are discarded from the summation. 59 components out of the 300 possible are used in the reconstruction.

It can be seen from the figures that generally when one third to one half of the 300 convolution components are present, no loss of accuracy occurs. This is particularly true of the upper and lower bounds of the distribution which may be used in assessing the maximum long-term flow through a proposed transmission line. This is an advantage of the gaussian delta function sum approximation approach to the P.L.F.; the weighting factors can be evaluated before carrying out the series of S.L.F.'s, and convolution combinations having a low weighting which are not among the third largest do not need evaluating.

The execution time for each S.L.F. run is 21.5 seconds on a Burroughs B6700 time-shared computer, and performance would improve dramatically if the program was run on a more powerful computer. The execution time includes computing (11.8) for 154 different quantities, $18\ v_i + 18\ p_i + 18\ Q_i + 50\ p_{ij} + 50\ Q_{ij}$. Note also that the program used and evaluated all of the elements of the covariance matrix for quantities of interest, i.e. (154×154) elements in this case.

Computation time could thus be improved greatly by only evaluating the trace of the covariance matrix for quantities of interest, given by (11.8), and only evaluating selected quantities of interest rather than all 154 possibilities, as was done in this study.

Total execution time to evaluate all 300 convolution components of the gaussian-sum approximation based S.L.F. took approximately 6450 seconds. When only 105 components were used in the non-gaussian p.d.f. reconstruction, total execution time decreases to 2257 seconds. However the P.L.F. is only required to run off line, and most utilities with their own computers could run it overnight when the machine would otherwise be idle. As a general rule of thumb for utilities who have state estimation algorithms, each S.L.F. run will take approximately $1\frac{1}{2} - 2$ times the execution time of a single state estimation.

12.3.1 Comparison between probabilistic and stochastic loadflow results

The above results show that the P.L.F. can be carried out by a series of gaussian-sum approximation S.L.F.'s. However the original idea behind Dopazo et al.'s (1975) S.L.F. was to replace a non-gaussian p.d.f. by a single gaussian p.d.f. approximation. The data from the S.L.F. would then be used in the design and long-term planning of a new transmission line. Of particular importance was the expected maximum long-term power flow through the proposed transmission line. Once this has been found, ratings can be established for the circuit breaker equipment and the transmission line loading. The best method of choosing the single gaussian approximation to the non-gaussian p.d.f. is to match the spread, determining the upper and lower bounds, and to match the central value. That is, match

$$\begin{aligned} \mu_G &= \mu_{NG} \\ \sigma_G &= \sigma_{NG} \end{aligned} \qquad (12.12)$$

where G stands for gaussian p.d.f.; and

NG stands for non-gaussian p.d.f.

When applied to P_1, P_2, P_9 and Q_9 in order to match the non-gaussian p.d.f's of the test system at these nodes, the resulting gaussian S.L.F. results are shown in Table 12.7.

Table 12.7 Comparison of upper and lower limits of S.L.F. and P.L.F. results

	NON-GAUSSIAN P.D.F.		SINGLE GAUSSIAN P.D.F.	
LOCATION	LOWER LIMIT	UPPER LIMIT	LOWER LIMIT (3σ)	UPPER LIMIT (3σ)
P_{5-6}	35.57 MW	50.27 MW	36.52 MW	51.44 MW
P_{4-7}	18.47 MW	33.88 MW	17.69 MW	38.29 MW
P_{3-4}	-42.80 MW	0.65 MW	-36.17 MW	-10.38 MW
V_4	1.0138 p.u.	1.0262 p.u.	1.0132 p.u.	1.0243 p.u.
Q_{7-4}	8.98 MVAR	13.75 MVAR	8.47 MVAR	13.71 MVAR
Q_3	-1.00 MVAR	40.00 MVAR	11.08 MVAR	35.56 MVAR
Q_{7-9}	-0.54 MVAR	9.42 MVAR	-0.88 MVAR	12.45 MVAR

Clearly, from Table 12.7, upper and lower bounds for voltage and power flow can be 20-25% greater than the non-gaussian P.L.F. upper and lower bounds (see also Figures 12.6 and 12.7 for a comparison of non-gaussian P.L.F. p.d.f. and the single gaussian p.d.f resulting from the S.L.F. for P_{4-7} and P_{3-4}). Application of the S.L.F. using only a single gaussian approximation leads to about 20% over-design of the maximum expected power flow in the case of P_{4-7}, and under-design by about 15% in the maximum expected absolute power flow, $|P|_{3-4}$. Benefits appear to be gained by carrying out a P.L.F. study, using a series of S.L.F.'s rather than a single S.L.F. study.

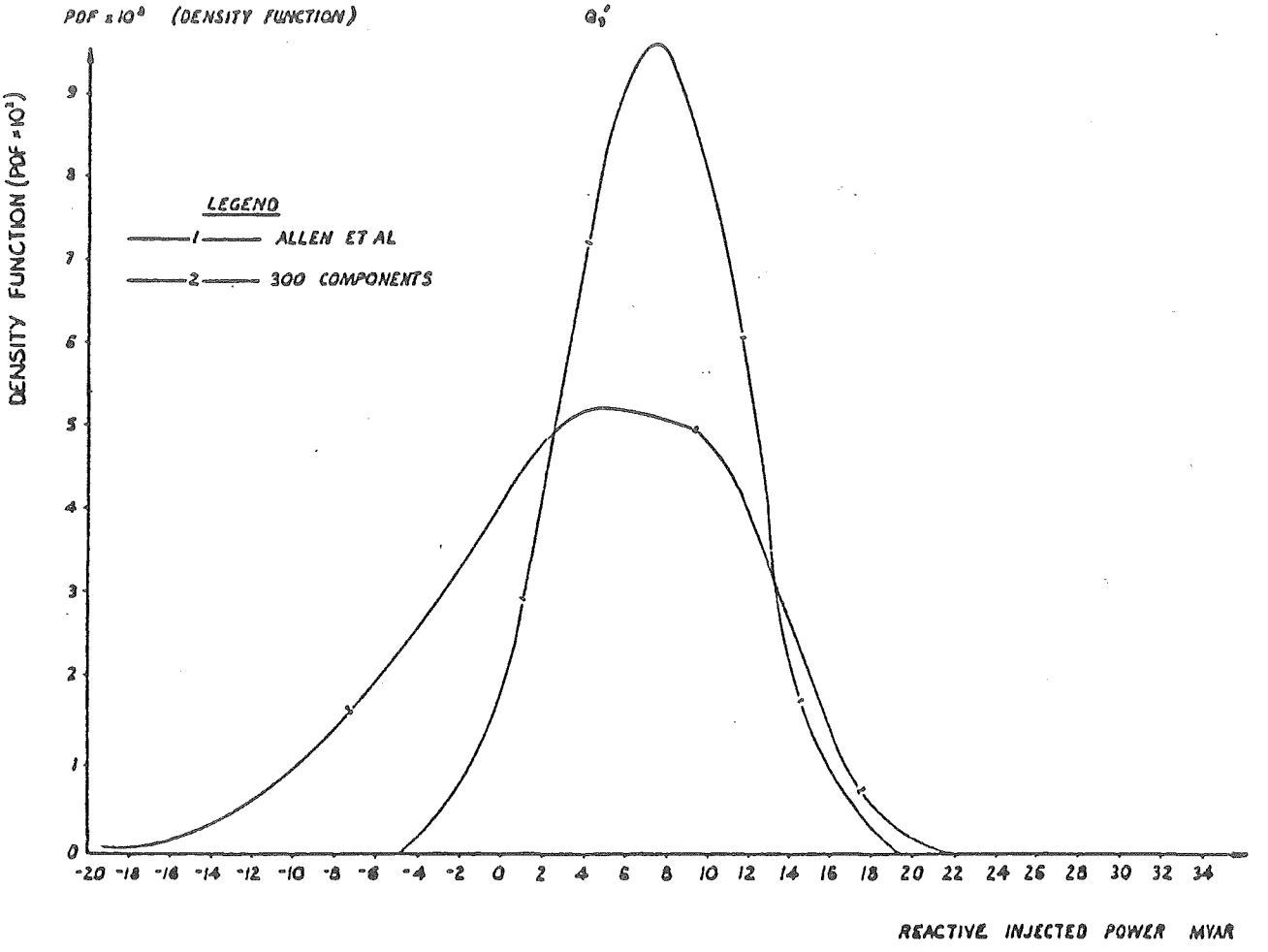

Figure 12.5 Gaussian sum reconstruction for $Q_3' = (Q_3 + Q_{17})$.

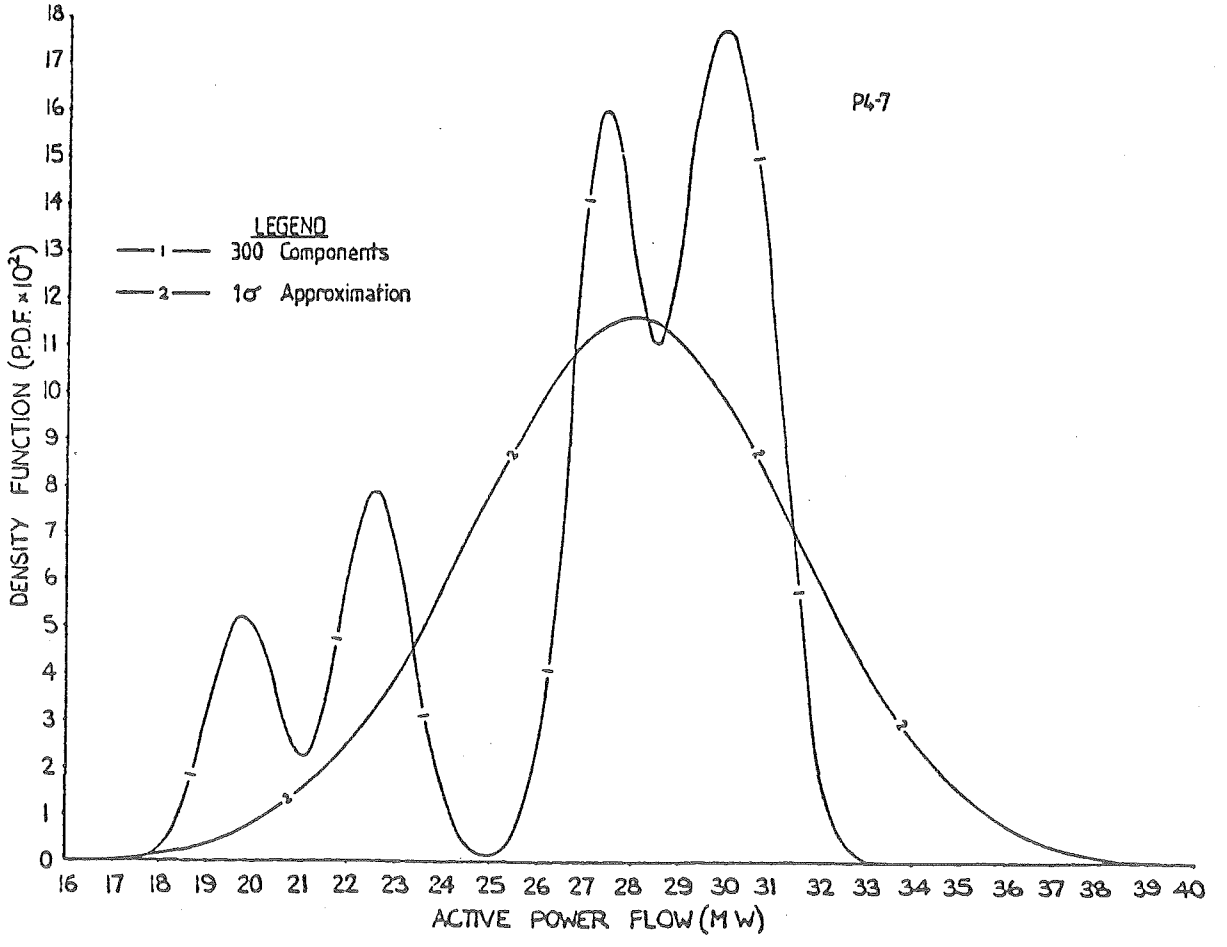

Figure 12.6 Gaussian p.d.f. "stochastic loadflow" for P_{4-7}.

12.3.2 P-θ, Q-v decoupling

Allan and Al-Shakarchi (1977) P-θ, Q-v decoupled the P.L.F.. P-θ, Q-v decoupling can be applied to the convolution-combinations of the S.L.F. when processing gaussian sum approximation data for non-gaussian p.d.f.'s. The convolution process is partitioned into a separate P.L.F. evaluation only involving uncertainty in the active injected powers (P-θ), and a separate P.L.F. evaluation only involving uncertainty in the reactive injected powers or the terminal voltages (Q-v). The S.L.F. algorithm is not affected when the decoupling occurs; only the convolution-combinations that require evaluation are decoupled.

When analysing the P-θ decoupled P.L.F., all terminal voltage and reactive power loadflow nodal data is set to its expected value and its variance set to near zero. Thus, each such nodal reactive power or voltage distribution is replaced by a single gaussian delta function distribution, centred on the mean value of the p.d.f. As a result, the series of S.L.F. only takes into account the uncertainty in active power nodal p.d.f.'s when computing the expected active line-flow power and its variance, for transmission lines of interest. The number of decoupled convolution component S.L.F. runs required in the evaluation of the P-θ decoupled P.L.F. is given by

$$\pi_{i=1}^{N} (r_i) \qquad (12.13)$$

For the expanded 14 bus test system, the value of Q_9 is replaced by $Q_{9_{AV}} = -16.60$ MVAR, and all nodal voltage and injected reactive power variance data is reset to 0.0001 in Tables 12.5 and 12.6. The number of P-θ decoupled convolution combinations requiring evaluating using the S.L.F. are

$$(4)_1 \ (3)_2 \ (1)_3 \ \ldots \ (1)_8 \ (5)_9 \ (1)_{10} \ \ldots \ = \ 60$$

Results of the P-θ decoupled P.L.F. for line power flows P_{5-6} and P_{4-7} are shown in Figures 12.8 and 12.9. No appreciable degradation in the non-gaussian p.d.f. profiles occurs when P-θ, Q-v is used for the active line power flow estimation. Note also when all components of the convolution, having weighting factors $\alpha_i < 0.01$, are discarded, leaving only 22 out of the 60 possible decoupled components to be used in the p.d.f. reconstruction, no degradation in profile occurs. A similar decoupling can be applied to the Q-v uncertainty data shown in Tables 12.5 and 12.6. All active power injection data is replaced by a single gaussian type delta function centred on the expected value of the nodal active power p.d.f. As a result the series of decoupled S.L.F.'s only accounts for the long-term uncertainty in the reactive power and voltage nodal p.d.f's when computing the expected nodal voltage and reactive power and line-flow reactive power, and their variance, at points of interest. The number of decoupled convolution component - S.L.F. runs required to evaluate terms in the Q-v decoupled P.L.F. is given by

$$\pi_{i=1}^{N} (q_i) \tag{12.14}$$

For the expanded 14 bus test system, the values of P_1, P_2 and P_9 are replaced by $P_{1_{AV}} = 230$ MW, $P_{2_{AV}} = 40.04$ MW and $P_{q_{AV}} = -29.50$ MW, and the active injected power variances are all reset to near zero, i.e. 0.00001 p.u. in Tables 12.5 and 12.6. The number of Q-v decoupled convolution combinations requiring evaluation using the S.L.F. are

$$(1)_1 \ldots (1)_8 (5)_9 (1)_{10} \ldots = 5$$

Results of the Q-v decoupled P.L.F. for the reactive power flow Q_{7-9} and nodal voltage v_4 are shown in Figures 12.10 and 12.11. Decoupling of reactive and voltage nodal data (Q-v) produces different p.d.f. profiles. However the bounds of the distribution, the upper

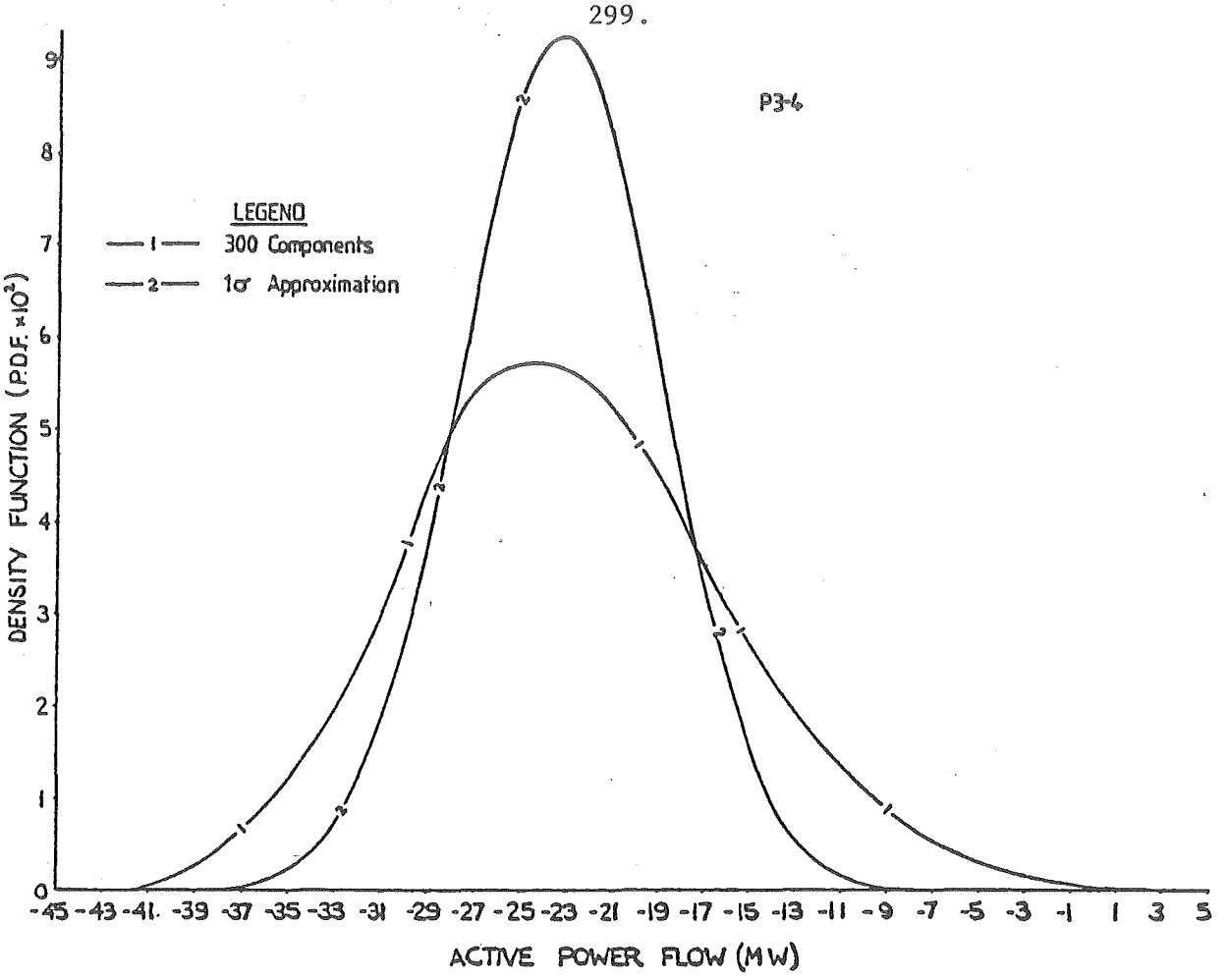

Figure 12.7 Gaussian p.d.f. "stochastic loadflow" for P_{3-4}.

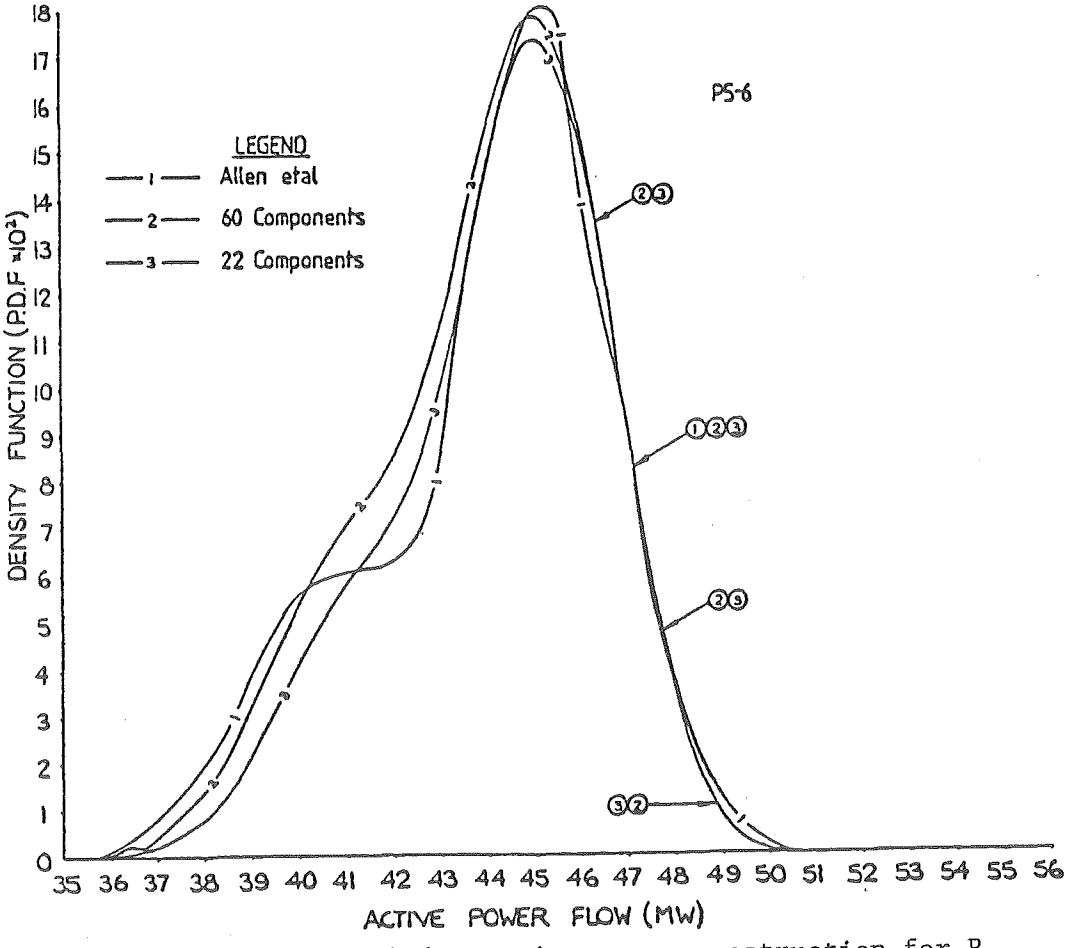

Figure 12.8 Decoupled gaussian sum reconstruction for P_{5-6}.

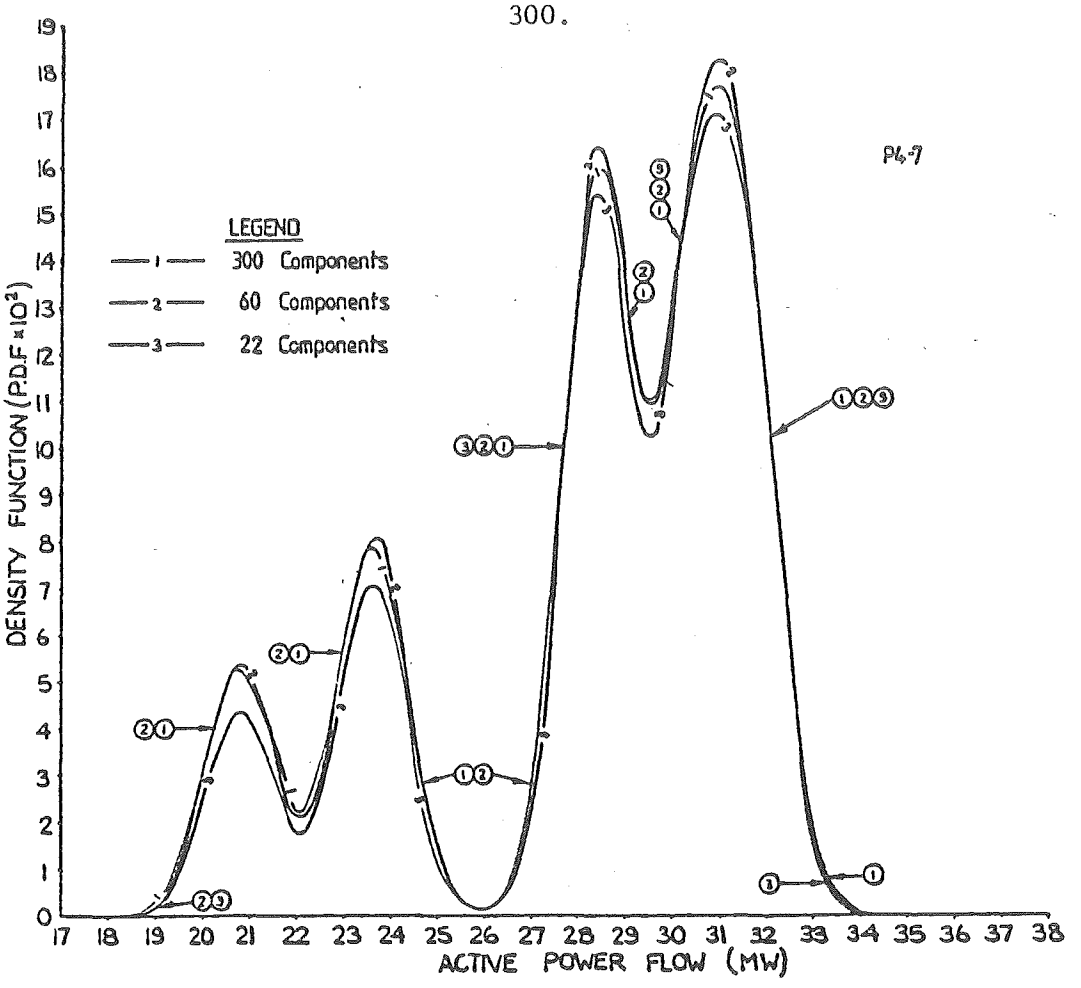

Figure 12.9 Decoupled gaussian sum reconstruction for P_{4-7}.

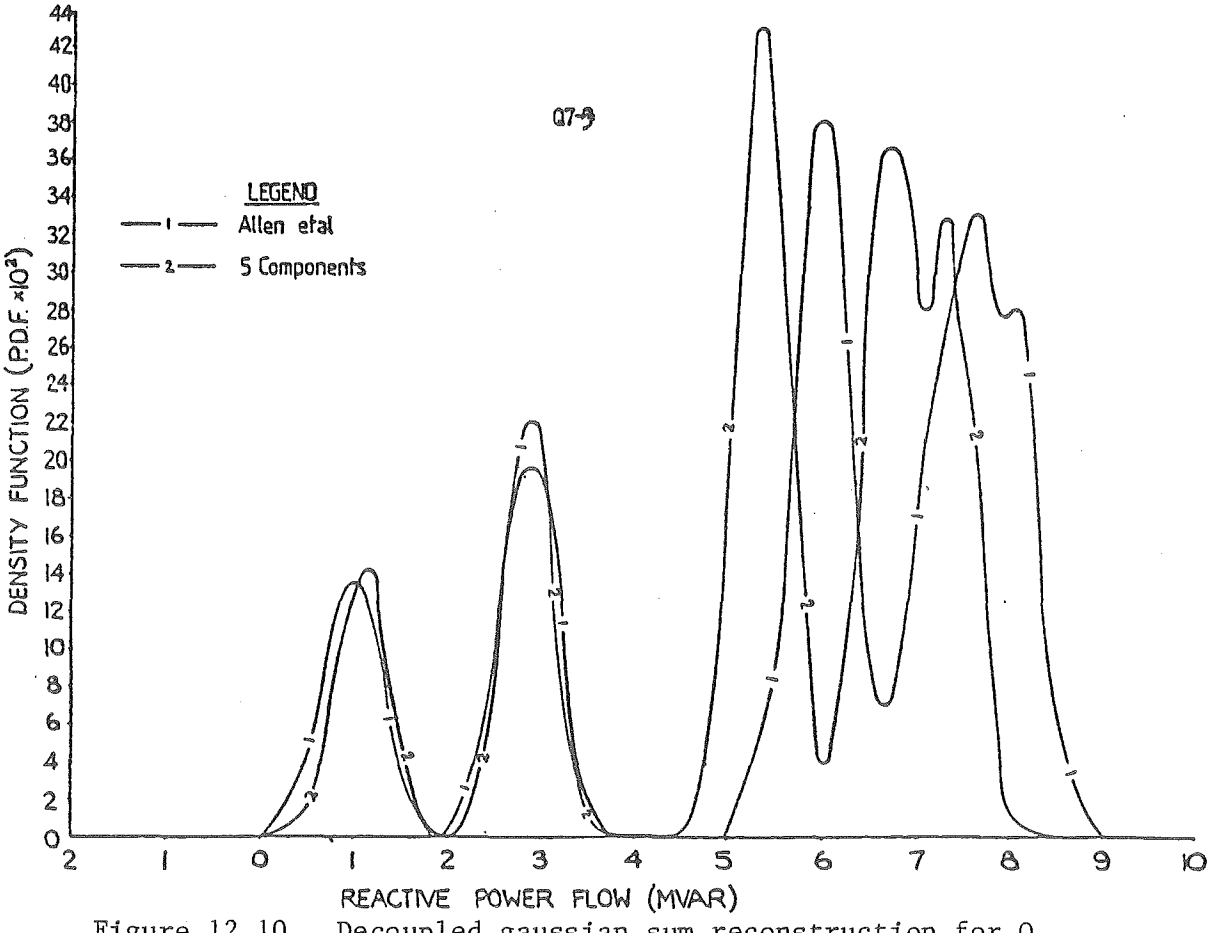

Figure 12.10 Decoupled gaussian sum reconstruction for Q_{7-9}.

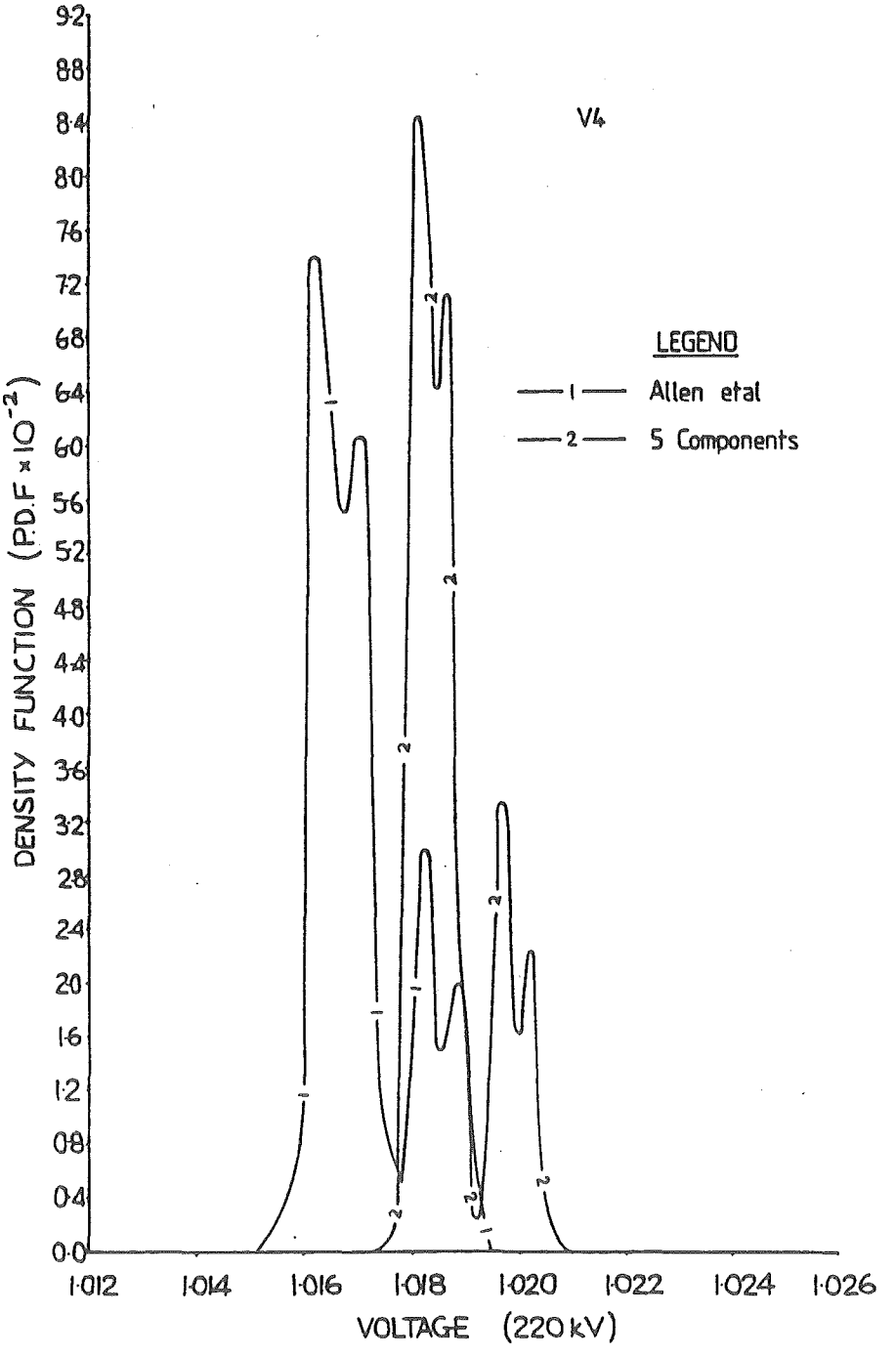

Figure 12.11 Decoupled gaussian sum reconstruction for V_4.

and lower limits, are still similar. Upper bounds of the p.d.f. are used in designing ratings for planned transmission lines, etc.

Note, however, that the Q-v decoupled non-gaussian profiles for v_4 and Q_{7-9} are different from the decoupled versions that result from Allan and Al-Shakarchi's method of decoupling. This may be due to the following.

(i) Allan and Al-Shakarchi fully decouple their P.L.F. algorithm, whereas the decoupling applied to the series of gaussian sum approximation - S.L.F.'s only affects the component selection, not the S.L.F.

(ii) Allan and Al-Shakarchi linearize around the conventional loadflow solution and then use redundant data to compute the non-gaussian p.d.f. profiles. The technique, based on a series of gaussian sum approximation - S.L.F.'s, on the other hand linearizes about the redundant data set randomly, at five different points.

When the expected value resulting from each Q-v decoupled gaussian sum approximation S.L.F. convolution component is replaced by a value resulting from a non-redundant loadflow at the same point (but excluding P_1) and summed together with the variance, this yields the same profile, for Q_{7-9}, as the P.L.F. of Allan and Al-Shakarchi (see Figure 12.12).

12.3.3 Effect of nodally dependent real and reactive injection non-gaussian p.d.f.'s

Both the real and reactive power discrete distributions at node 9 have a similar appearance. In the analysis of 12.3.1 it was assumed that the possible variation of P_9 was totally independent of Q_9. However the variations could be modelled as being dependent so that P_9 and Q_9 occur, together with the probabilities, as shown in Table 12.8.

Table 12.8 Dependent combinations of P_9 and Q_9

NO.	DEPENDENT VALUES OF P_9 AND Q_9		PROBABILITY
1	-13.0 MW	-7.5 MVAR	0.10
2	-19.6 MW	-11.0 MVAR	0.15
3	-30.2 MW	-17.0 MVAR	0.30
4	-34.8 MW	-19.6 MVAR	0.25
5	-37.3 MW	-21.0 MVAR	0.20

The number of nodally dependent convolution component S.L.F. runs required to evaluate terms of the nodally dependent P.L.F. is given by

$$\pi_{i=1}^{N} (m_i) \tag{12.15}$$

where m_i is the number of nodally dependent gaussian components which sum to represent the p.d.f. at bus i, where $m_i = r_i q_i$ if the real and reactive nodal data is uncorrelated and $m_i = r_i$ when correlations exist.

Thus, for the expanded 14 bus test system the number of convolution combinations requiring evaluation using the S.L.F. are

$$(4)_1 (1)_1 (2)_2 (1)_2 \ldots (1)_8 (1)_8 (5)_9 (1)_{10} (1)_{10} = 60$$

Results of the nodally dependent P.L.F. for V_4, P_{5-6}, Q_{7-9} and Q_3 are shown in Figures 12.13 to 12.16, together with the more exact results from section 12.3.1 which assume no dependence. It can be seen from the figures, that provided the node or line in question is not a part of or attached to a "dependent" node, like node 9, no degradation in the profile of the p.d.f results. The absence of the cross-coupling terms in the profile for the p.d.f. of Q_{7-9} can be seen

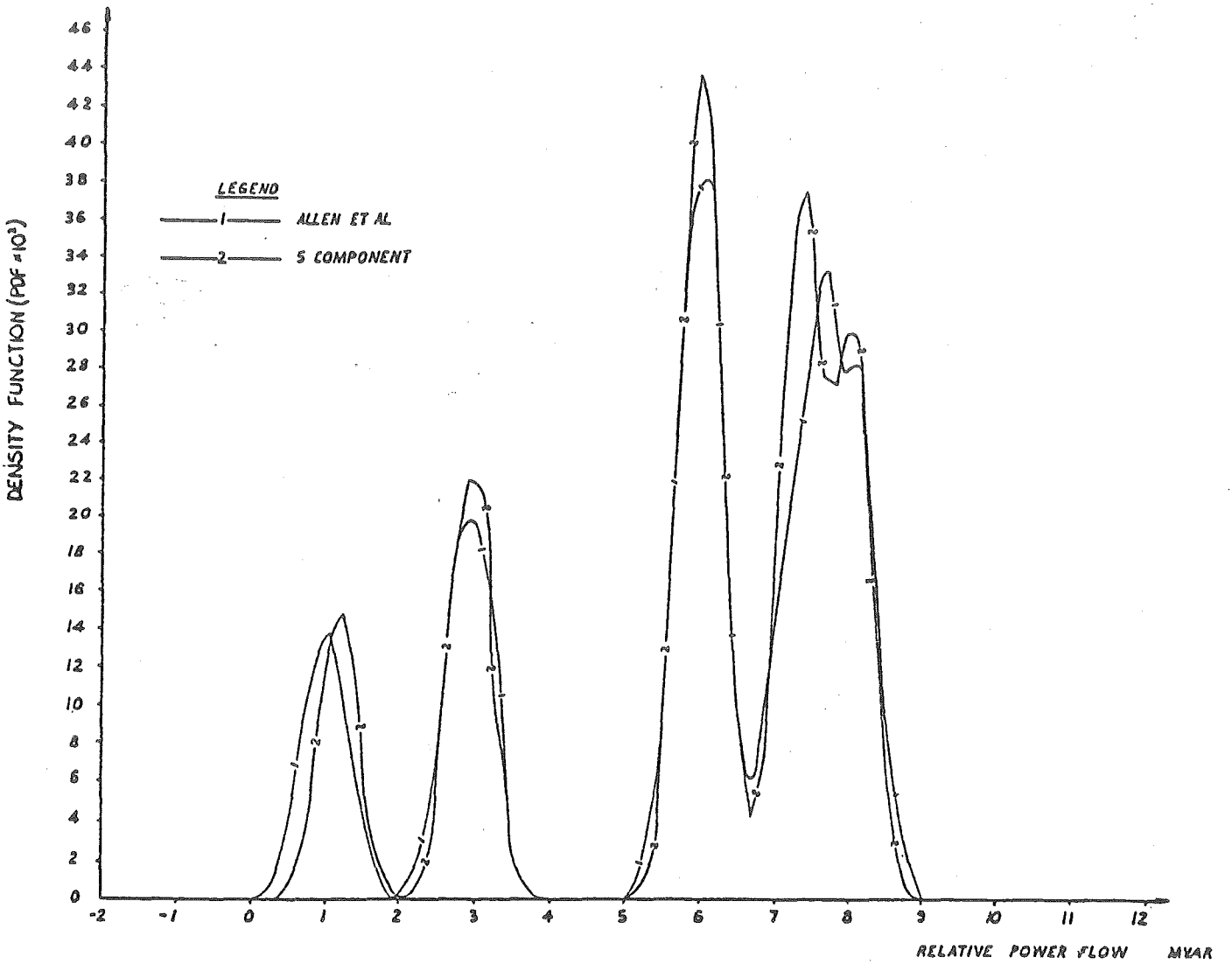

Figure 12.12 Detailed decoupled gaussian sum reconstruction for Q_{7-9}.

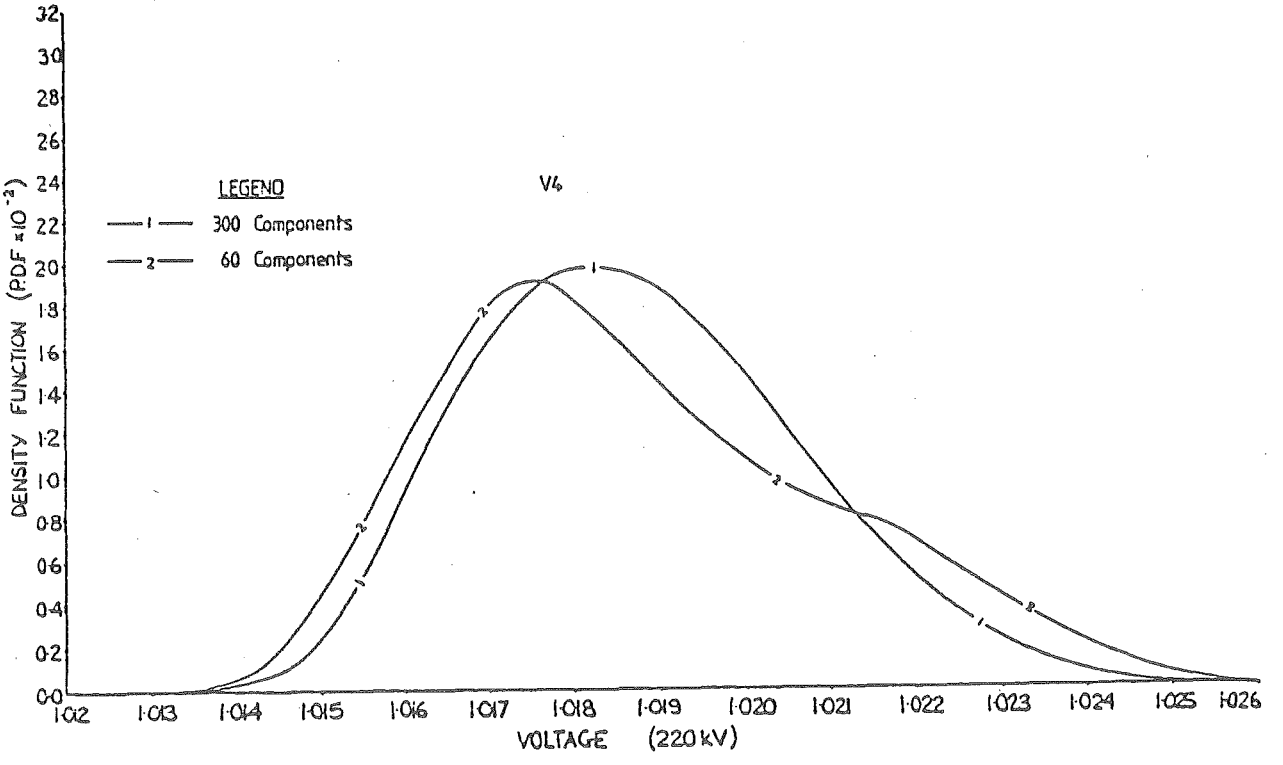

Figure 12.13 Nodal-dependent gaussian sum reconstruction for V_4.

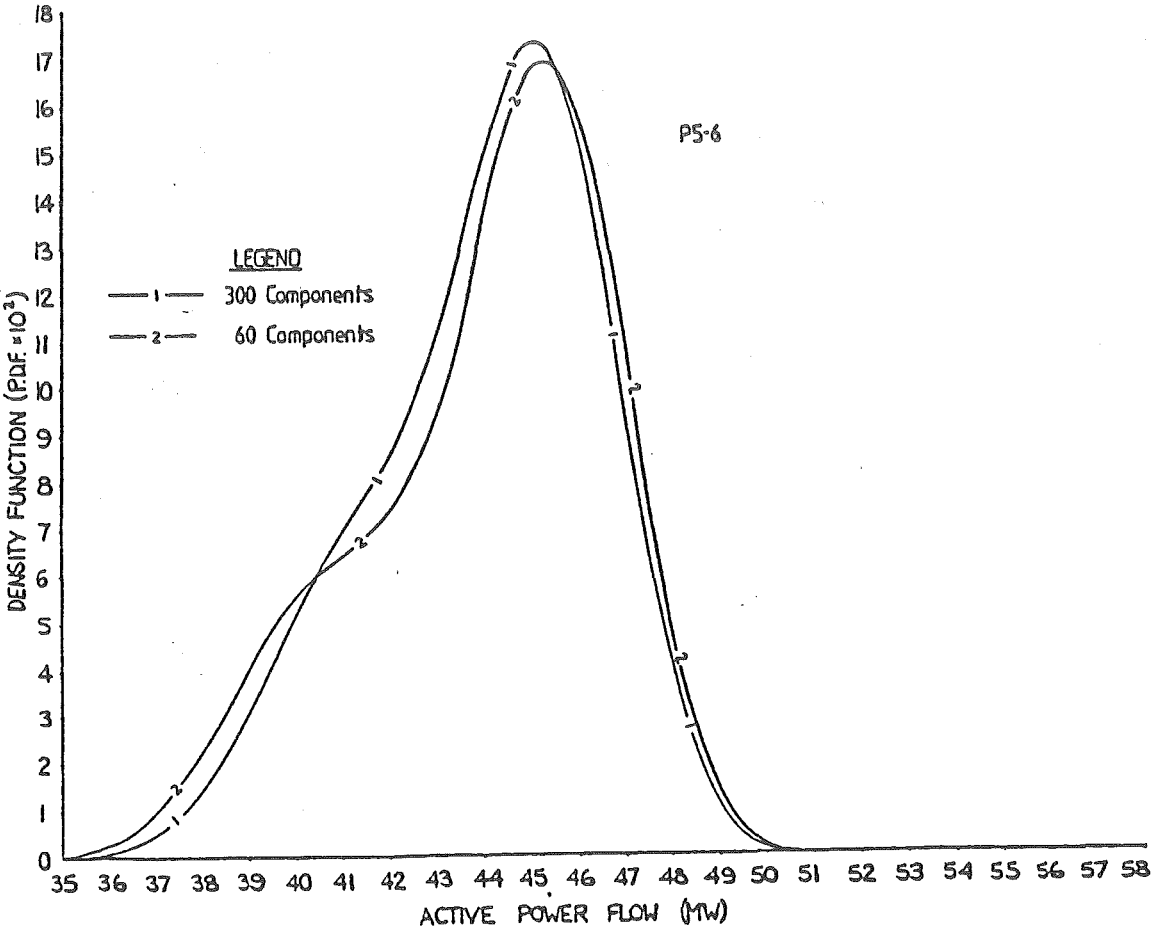

Figure 12.14 Nodal-dependent gaussian sum reconstruction for P_{5-6}.

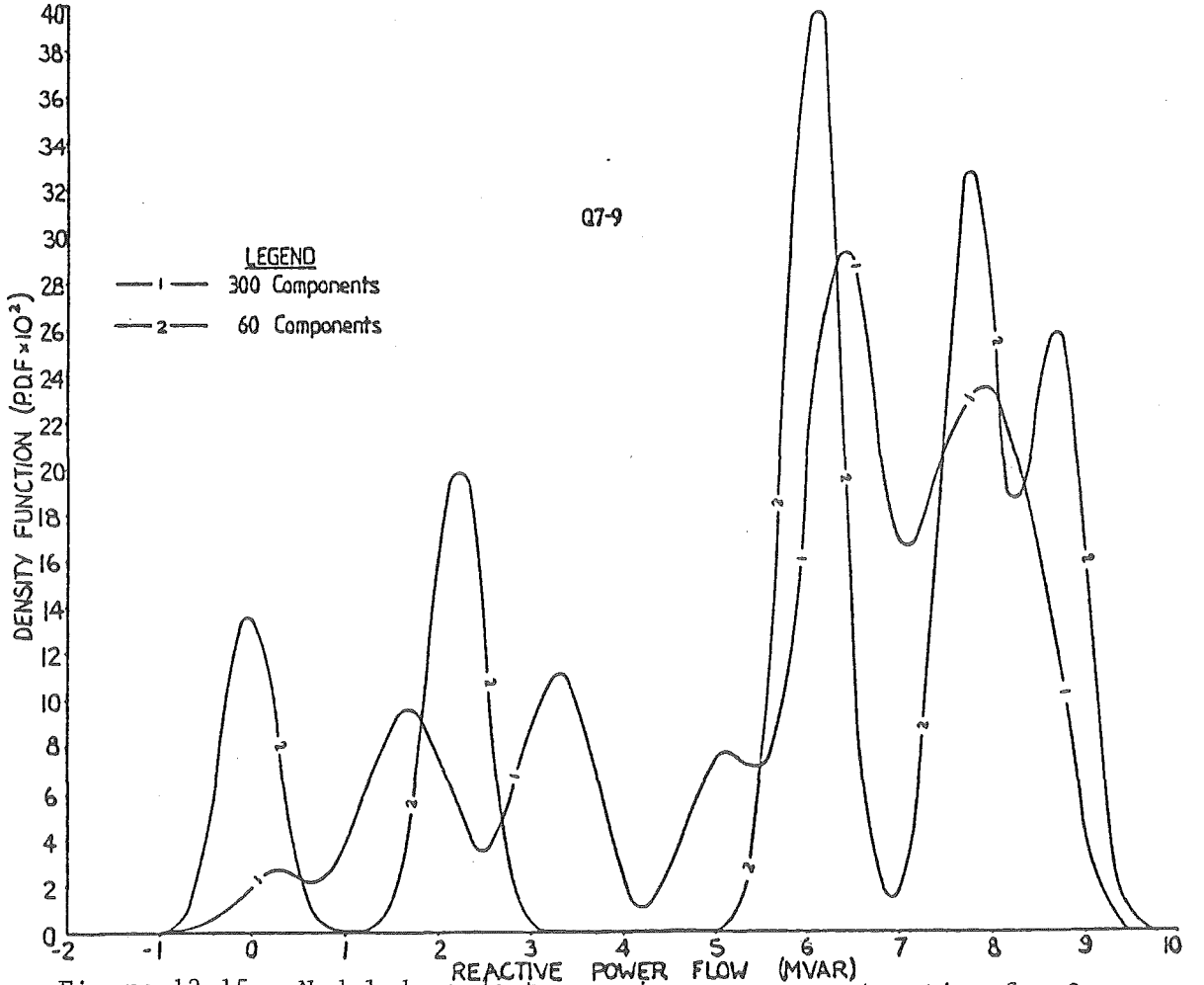

Figure 12.15 Nodal-dependent gaussian sum reconstruction for Q_{7-9}.

in Figure 12.16 since the troughs between the "peaks"; discrete states of Q_9, are no longer filled in.

12.4 LOWER ORDER GAUSSIAN SUM APPROXIMATIONS

In section 12.3.1 the non-gaussian distribution was replaced by a gaussian delta function approximation of the same order. Thus if the discrete distribution has three components, three gaussion delta functions were specified to model the discrete p.d.f. accurately. In order to reduce the amount of computation, lower order gaussian sum approximations could be used. Thus instead of, say, the three gaussian delta functions, two gaussian sum components could be used. The problem is to choose the "best fit" of these two gaussian components, with regard to their location, variance and weighting factors. Selection by trial and error is unreliable and can take some time. It is also better to fit the expected values and higher moments of variance about this expected value, because the limits of the p.d.f. are of interest in the design of new transmission lines. Thus the best way of selecting the parameters of the gaussian sum approximation is to match these to moments of the non-gaussian p.d.f. The number of independent variables that need matching, for the 2-gaussian sum approximation to the non-gaussian nodal data are the two means, u_1, u_2, the two variances, σ_1 and σ_2, and one of the weightings, α_1, since $\alpha_2 = 1 - \alpha_1$. Thus if a n-gaussian sum approximation to the non-gaussian nodal data is used, then the number of independent parameters to be matched are equal to $k = 3n - 1$.

These independent parameters can be found by matching the first $k = 5$ moments of the non-gaussian distribution to the gaussian sum approximation having two components.

Thus for the expanded 14 bus test system, the non-gaussian p.d.f's at nodes 1, 2 and 9 are replaced by a 2-gaussian sum approximation for P_1, P_2, P_9 and Q_9, and hence the number of convolution combinations requiring evaluation using the S.L.F. are

$$(2)_1(1)_1(2)_2(1)_2 \ldots (1)_8(2)_9(2)_9(1)_{10} \ldots = 16 \text{ combinations}$$

For each 2-gaussian sum approximation the first five moments, $m_1 \ldots m_5$, require matching. The first moment of the non-gaussian p.d.f. can be found by evaluating

$$\mu = m_{NG_1} = \sum_{i=1}^{N} x_i P_i \tag{12.16}$$

and the 2nd .... 5th order moments can be found from

$$[m_{NG_j} = \sum_{i=1}^{N} (x_i - \mu)^j P_i]_{j=2, \ldots 5} \tag{12.17}$$

These non-central non-gaussian moments, $m_{NG_1} \ldots m_{NG_5}$, are found analytically and matched to the non-central non-gaussian moments of each of the 2-gaussian approximations for P_1, P_2, P_9 and Q_9. Normalized non-central moments $m_1 \ldots m_5$ for the binomial and discrete probability distributions at P_1, P_2, P_9 and Q_9, from Table 12.3, are summarized in Table 12.9.

Table 12.9 Normalized non-central moments for non-gaussian distributions for P_1, P_2, P_9 and Q_9

LOCATION	NORMAL-ISATION FACTOR	m_{NG_1}	m_{NG_2}	m_{NG_3}	m_{NG_4}	m_{NG_5}
P_1	100 MW	2.3	5.331017	13.120176	30.815459	72.803736
P_2	10 MW	4.004	16.824808	72.285012	314.216943	1374.112091
P_9	10 MW	-2.95	9.302100	-30.548193	102.869815	-352.131548
Q_9	10 MVAR	-1.66	2.947150	-5.450322	10.335979	-19.924446

A 2-gaussian sum approximation is represented by

$$pdf_2 = \alpha_1 N_{\sigma_1}(x - \mu_1) + (1-\alpha_1) N_{\sigma_2}(x-\mu_2) \tag{12.18}$$

Non-central moments are found by solving

$$\underline{m}_{N.G} = \underline{m}_{GA} \tag{12.19}$$

where

$$\begin{aligned}
m_{GA_1} &= \alpha_1 (\mu_1) + (1 - \alpha_1) (\mu_2) \\
m_{GA_2} &= \alpha_1 (\mu_1^2 + \sigma_1^2) + (1 - \alpha_1) (\mu_2^2 + \sigma_2^2) \\
m_{GA_3} &= \alpha_1 (u_1^3 + 3\sigma_1^2 \mu_1) + (1-\alpha_1) (\mu_2^3 + 3\sigma_2^2 \mu_2) \\
m_{GA_4} &= \alpha_1 (\mu_1^4 + 6\sigma_1^2 \mu_1^2 + 3\sigma_1^4) + (1-\alpha_1)(\mu_2^4 + 6\sigma_2^2 \mu_2^2 + 3\sigma_2^4) \\
m_{GA_5} &= \alpha_1(\mu_1^5 + 10\mu_1^3 \sigma_1^2 + 5\mu_1(3\sigma_1^4)) + (1-\alpha_1)(\mu_2^5 + 10\mu_2^3 \sigma_2^2 + 5\mu_2(3\sigma_2^4))
\end{aligned} \tag{12.20}$$

Originally it was intended to solve (12.19) using a Newton-Ralphson iterative formulae, but the method was found to be highly unstable. Conversion of $\underline{m}_{NG}$ and $\underline{m}_{GA}$ to centralised moment data did not stabilize the convergence either.

A simulation was carried out, altering α_1, μ_1, σ_2, μ_2 and σ_2 computing the error

$$E_r = \left[\left(\frac{m_{NG_1} - m_{GA_1}}{m_{NG_1}} \right)^2 + \left(\frac{m_{NG_2} - m_{GA_2}}{m_{NG_2}} \right)^2 + \left(\frac{m_{NG_3} - m_{GA_3}}{m_{NG_3}} \right)^2 + \left(\frac{m_{NG_4} - m_{GA_4}}{m_{NG_4}} \right)^2 + \left(\frac{m_{NG_5} - m_{GA_5}}{m_{NG_5}} \right)^2 \right]^{\frac{1}{2}} \tag{12.21}$$

and identifying regions of probability space which minimize (12.21). Minimum values identified for α_1, μ_1, σ_1, μ_2 and σ_2, at P_1, P_2, P_9 and Q_9, and their errors are shown in Table 12.10. These values were used

as the two component-gaussian sum approximations to P_1, P_2, P_9 and Q_9.

Table 12.10 Minimum values of α_1, μ_1, σ_1, μ_2 and σ_2 (normalized)

LOCATION	NORMALIZATION FACTOR	α_1	μ_1	σ_1	μ_2	σ_2	ERROR E_r
P_1	100 MW	0.71	2.31	0.20	2.35	0.25	0.0321071
P_2	10 MW	0.31	2.95	0.66	4.50	0.00001	0.0070031
P_9	10 MW	0.59	-3.50	0.14	-2.15	0.63	0.0014350
Q_9	10 MVAR	0.92	-1.75	0.30	-0.60	0.65	0.0067348

Results of the lower order gaussian sum approximation S.L.F. for P_{3-4}, P_{4-7}, P_{5-6}, Q_{7-9}, V_4 and Q_3 are shown in Figures 12.17 to 12.22. Very good agreement is obtained with the 300 component reconstructs of section 12.3 and the 16 component lower order gaussian sum approximation S.L.F. for V_4, Q_3, P_{5-6} and P_{4-7}. The lower order gaussian sum approximation for P_{3-4} is slightly more accurate than the single gaussian approximation, section 12.3.1, but the reconstruct for Q_{7-9} does not have very good agreement. It appears that a 3rd order gaussian sum approximation may be required to approximate P_9 and Q_9.

12.5 SELECTION OF NON-GAUSSIAN LONG-TERM PROBABILITY GENERATION DATA

The specification of normal and discrete p.d.f's for domestic and large industrial loads follows patterns observed in practice. However the specification of long-term generation patterns using unit ratings and availability data appears rather dubious, particularly when applied to the slack bus which is designed to absorb line losses in the loadflow problem.

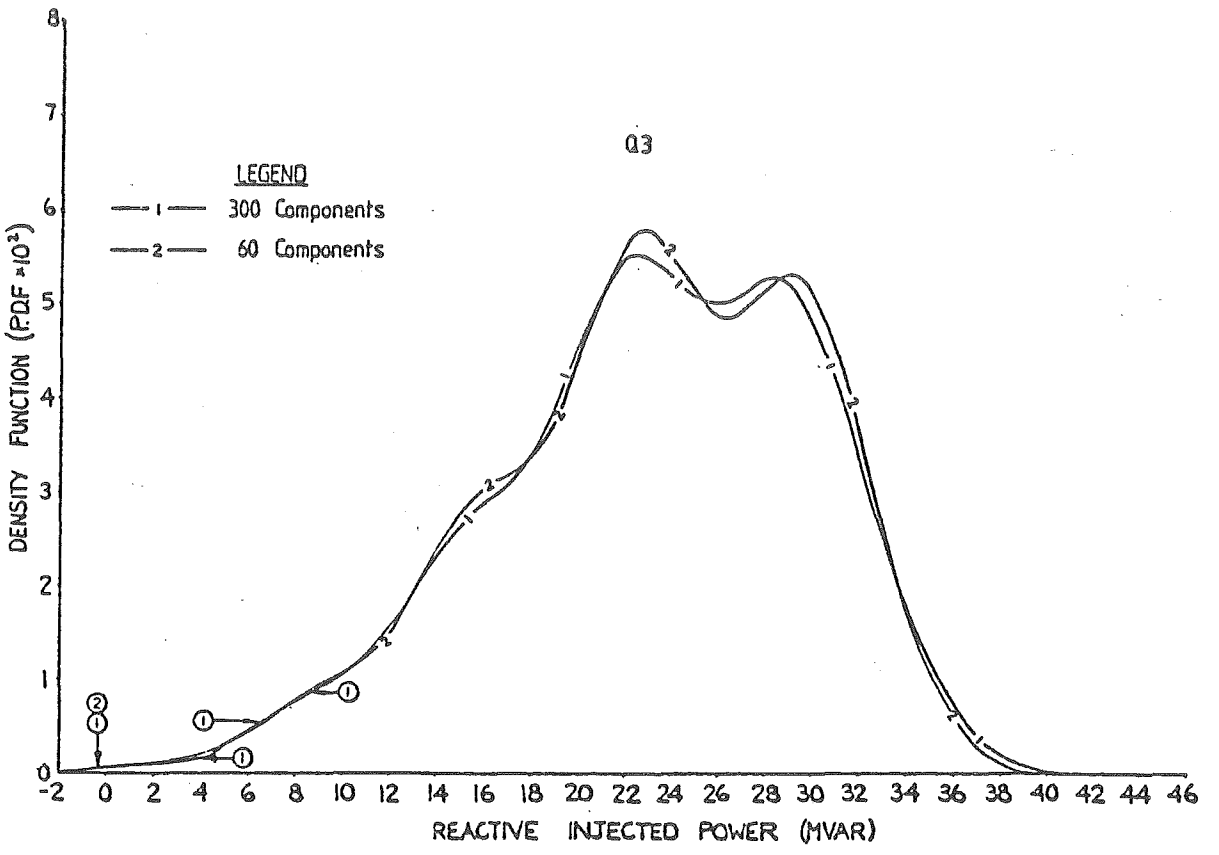

Figure 12.16 Nodal dependent gaussian sum reconstruction for Q_3.

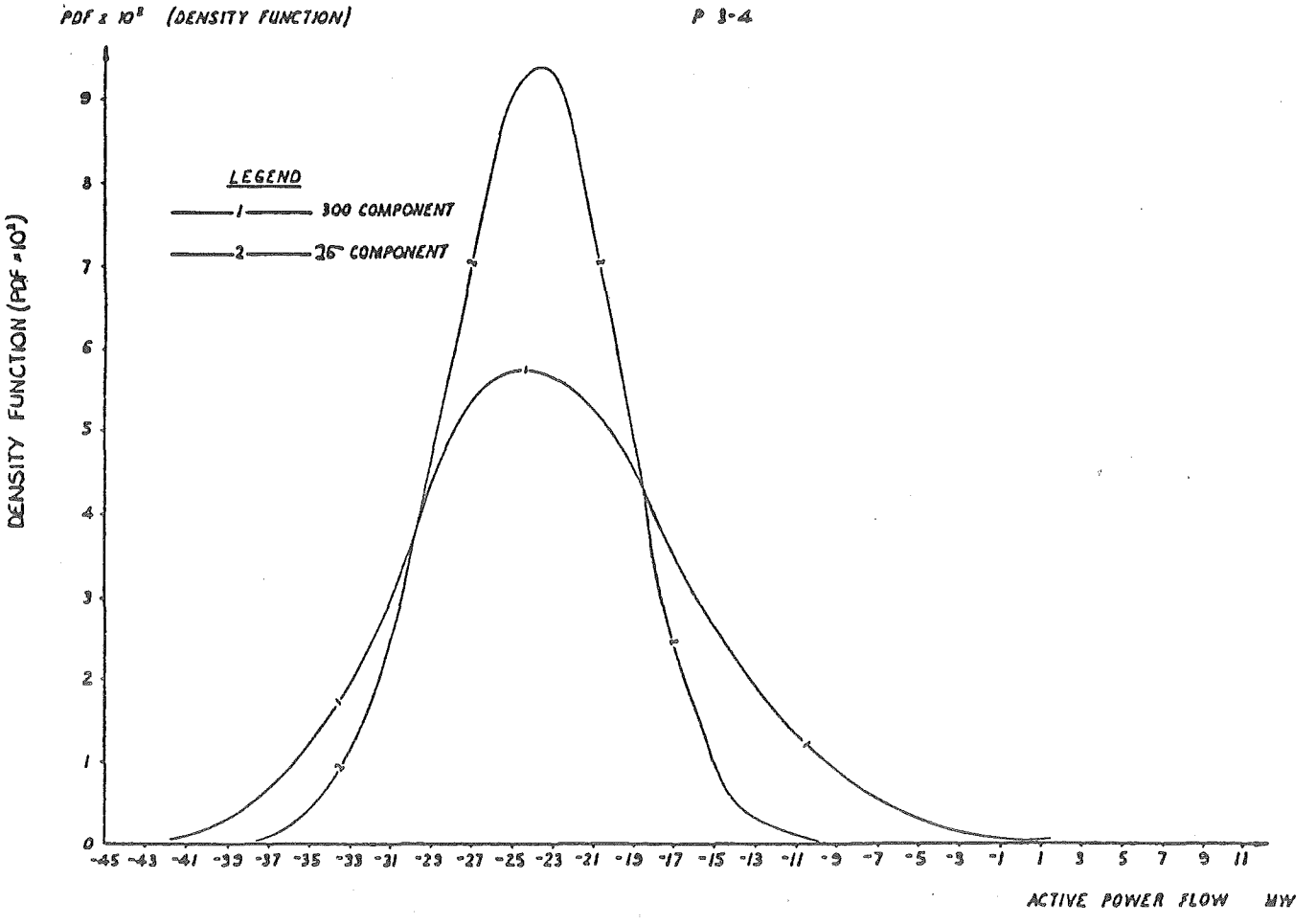

Figure 12.17 Lower order gaussian sum reconstruction for P_{3-4}.

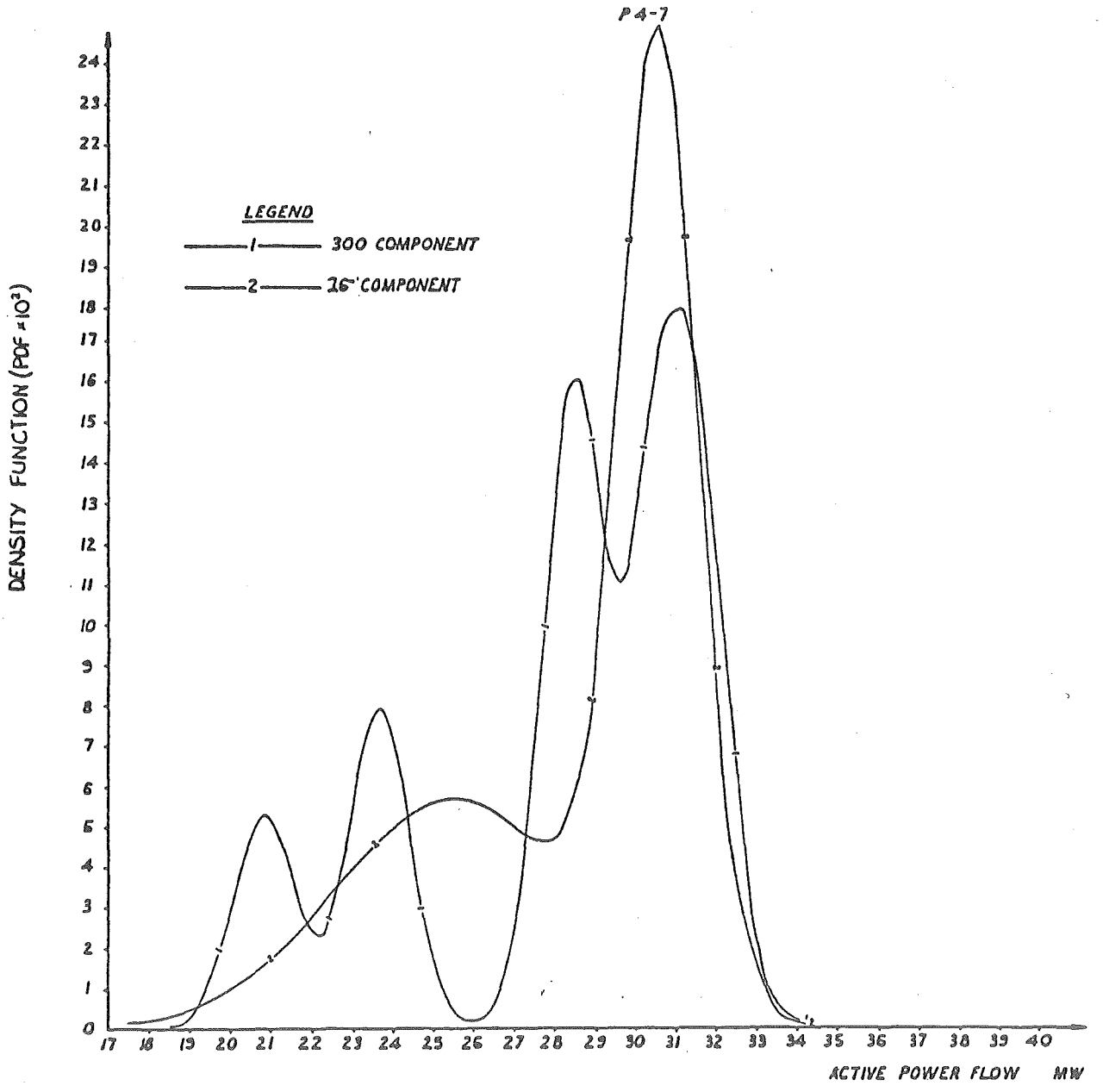

Figure 12.18 Lower order gaussian sum reconstruction for P_{4-7}.

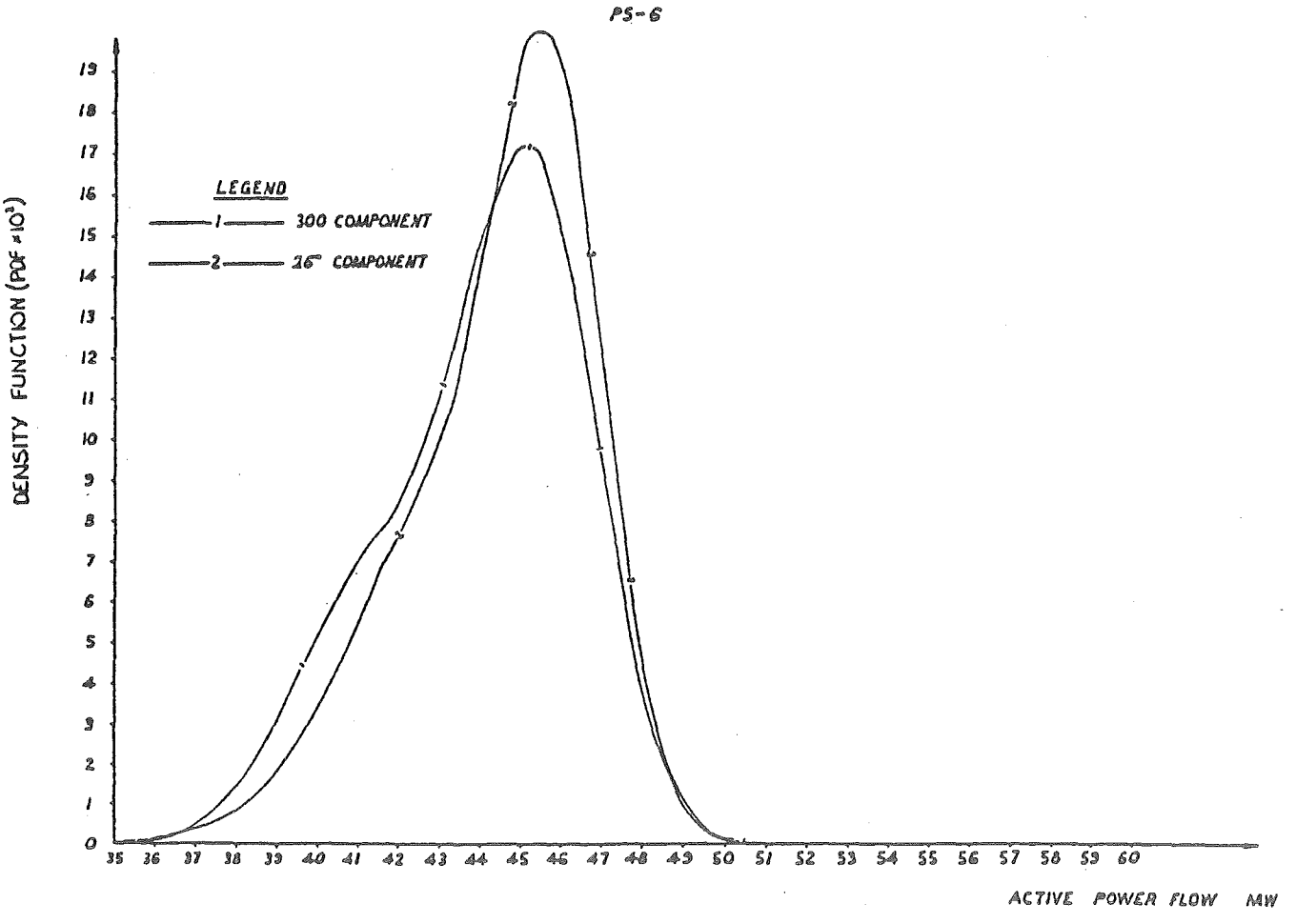

Figure 12.19 Lower order gaussian sum reconstruction for P_{5-6}.

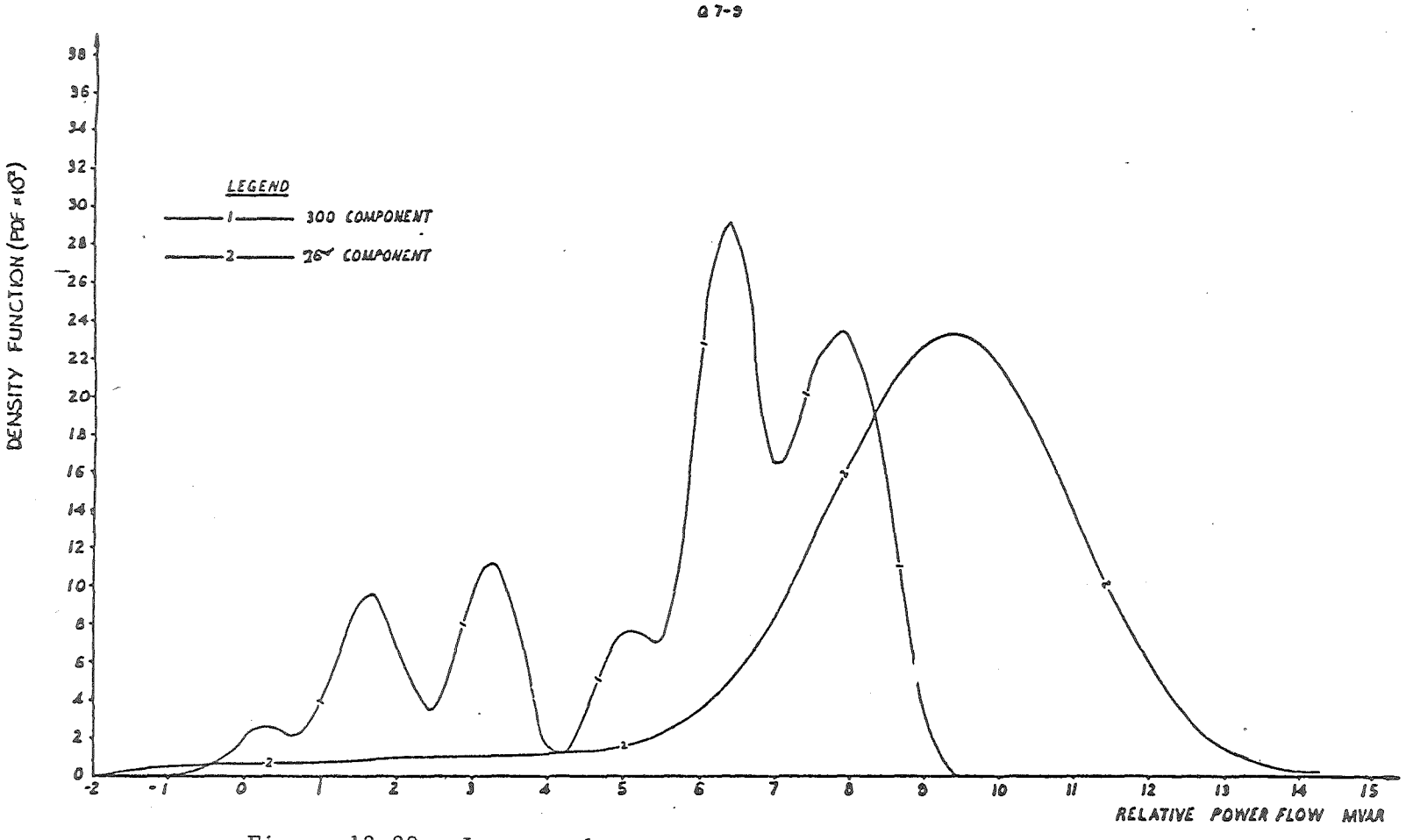

Figure 12.20 Lower order gaussian sum reconstruction for Q_{7-9}.

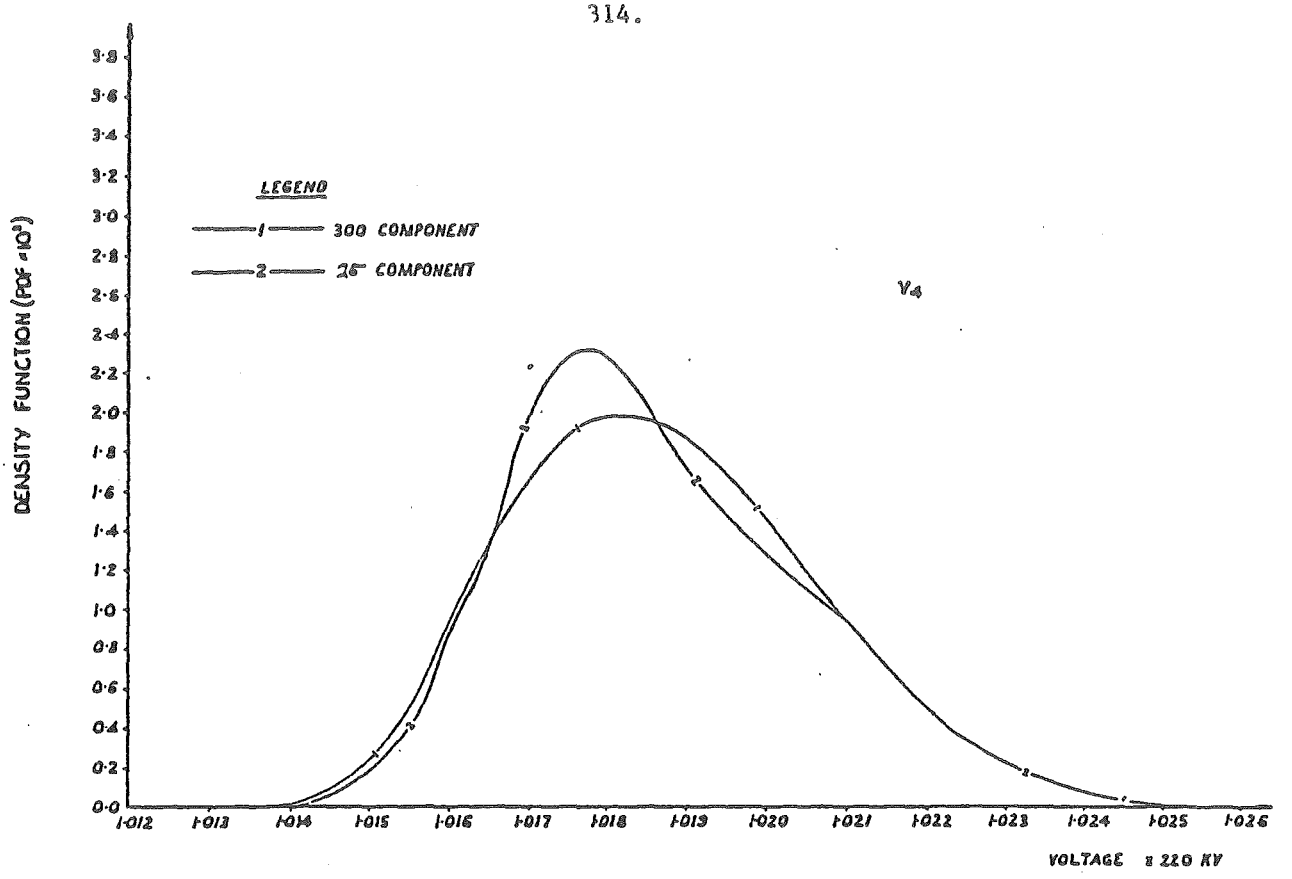

Figure 12.21 Lower order gaussian sum reconstruction for V_4.

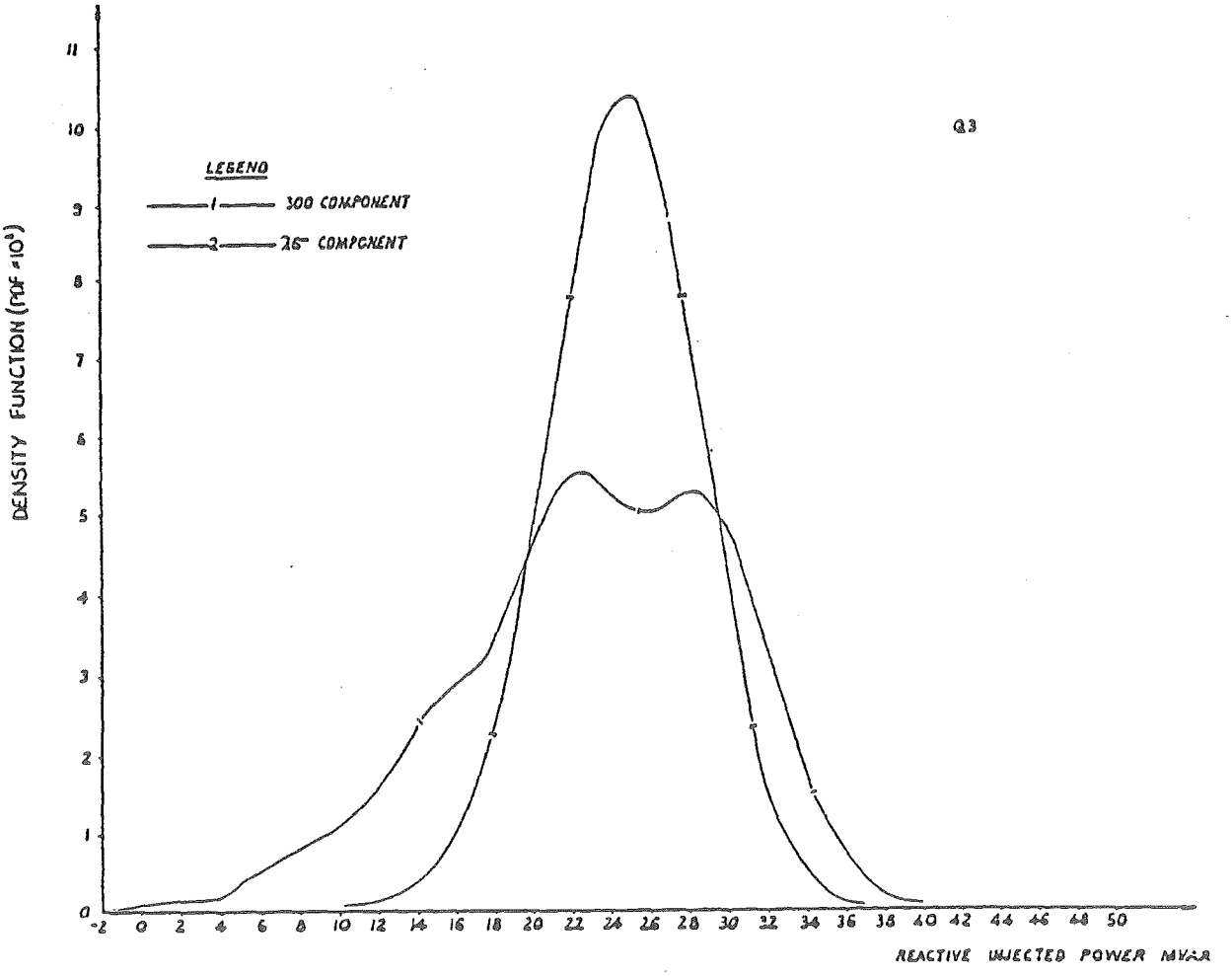

Figure 12.22 Lower order gaussian sum reconstruction for Q_3.

The 11 component discrete-component binomial distribution for generation at node 1 actually represents the continuous curve p.d.f. profile equivalent, shown in Figure 12.23. This continuous distribution may be easily represented by lower order gaussian sum approximations, as described in section 12.4.

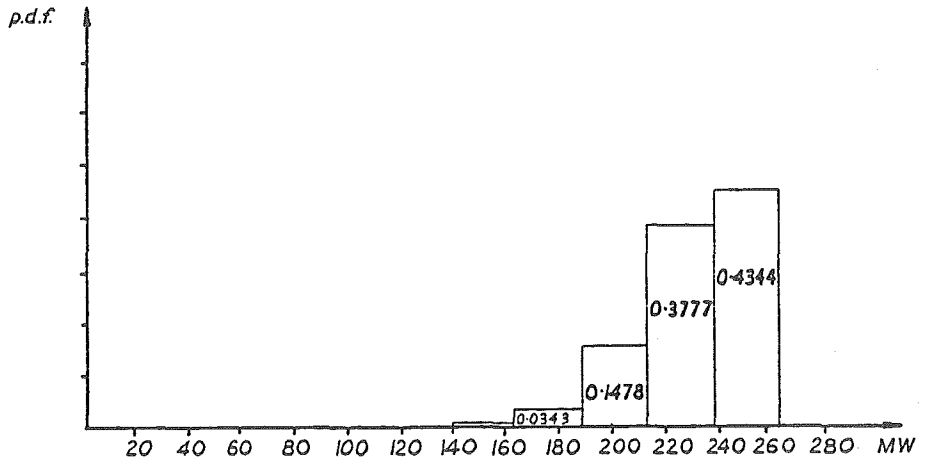

Figure 12.23 "Continuous equivalent" of a discrete binomial p.d.f.

For a power system which has been operational for many years, the long-term expected nodal generation data can be found by examining past records of generation. It is unlikely, however, that such generation will have the same characteristics as the "availability data based binomial distribution" used by Allan and Al-Shakarchi. Although large amounts of generation may be available, it does not mean in fact that all units will be used. In extreme cases the

generation from some stations may be expensive, due to transmission loss and/or high maintenance costs, and as a result such generation will be used sparingly, never exceeding 50 MW, although according to the binomial distribution describing its availability, the station has the expected "potential" of producing 230 MW. Such arguments are particularly true when considering the slack bus, which in the problem postulated by Allan and Al-Shakarchi and analysed here, takes up the long-term expected losses in the system. In such cases, having the generation equal to the generation "availability" at the slack busbar is impossible in practice. Thus when postulating generation statistics, past records rather than availability statistics should be used. The use of past records will also mean that smoother generation curves that can easily be approximated by lower order gaussian sums will likely be present if past record generation data is used. Thus it appears that the advantages of the lower order gaussian sum approximation will be greater when the data used in the P.L.F. becomes more realistic.

Another approach to accurately modelling the generation would be to formulate the W.L.S. minimization problem, which is the basis of the S.L.F., as an inequality constrained minimization where p.d.f. distributions are specified for the loads, either discrete, gaussian or binomial, and the generation is specified as an inequality constraint, less than or equal to the maximum possible value. Such a stochastic inequality constrained minimization would be difficult to solve in practice however.

12.6 CONCLUSION

It has been demonstrated that a series of gaussian sum approximation S.L.F. runs can reproduce the results of the P.L.F. It also has been shown that for certain nodal or line-flow p.d.f's a single gaussian approximated S.L.F. can cause over- or under-design of the expected long-term maximum power flow through a planned transmission line by about 20-25%. Thus it is advantageous to have in some cases the more accurate P.L.F. results for long-term planning or design. The P.L.F. technique using the series of gaussian sum approximated S.L.F.'s can easily be adopted by utilities that have existing state estimation algorithms with very little modification. Tests have shown that only a third of the convolution combination, having the highest weighting factors, needs evaluating when reconstructing the non-gaussian p.d.f. nodal or line-flow data.

Decoupling of the convolution-combination process has been investigated and tested and shown to produce near identical results to those of the decoupled P.L.F. No decoupling of the S.L.F. algorithm occurs, only of the convolution-combination process. Decoupling does not degrade the p.d.f. profiles for active line-flow pairs. Other methods to reduce the burden of computation, nodally coupling similar real and reactive power distributions, have been shown not to degrade p.d.f. profiles except on lines allowed to the dependent nodes.

Reduced order gaussian sum approximations that had a lower order sum than the number of discrete components of the p.d.f. were investigated, and ways for selecting the best reduced order approximation via the method of moments outlined. Using a 2 order gaussian sum approximation for non-gaussian nodal data, 16 convolution components can replace the 300 components required for an "exact"

study. In most cases the curve reconstructions are reasonably accurate for determining the upper load limits of a proposed transmission line.

The computational burden required to carry out P.L.F. studies using a series of gaussian sum approximation S.L.F.'s will reduce when the nodal generation data is realistically defined in terms of past yearly records rather than discrete binomial availability statistics. The use of availability statistics, particularly to specify generation profiles at the slack busbar can only be regarded as an extremely bad long-term forecast.

The formulation of the long-term planning study does not have to be non-redundant. Indeed, if any long-term predictions on line power flow or slack bus generation are available from past records, these should be used and the algorithm linearized about such redundant data. On the other hand, in cases where a new transmission line is being planned, long-term expected line-flow data or slack generation based on previous years' data may not be very accurate since inserting the "proposed" transmission line will change the slack generation and line power flows.

CHAPTER 13

INCLUSION OF H.V.D.C. LINKS IN A.C. STOCHASTIC LOADFLOW STUDIES

13.1 INTRODUCTION

H.v.d.c. links have been included in a.c. loadflows and in a.c. state estimation in Chapters 7 and 8. The h.v.d.c. link can also be included in a.c. S.L.F. studies. The h.v.d.c. link representation that was used to model converter operation in Chapter 8 can be used as the basis for the multi a.c.-h.v.d.c. stochastic loadflow study.

Converter relationships and measurement equations from Chapters 7 and 8 can be reformated to describe loadflow conditions.

13.2 SPECIFICATION OF A MULTI A.C. - H.V.D.C. STOCHASTIC LOADFLOW

The approximate h.v.d.c. link representation with exact residuals, outlined in section 8.5, can be used to model the h.v.d.c. link in the multi a.c.-h.v.d.c. S.L.F. A.c. nodal data is specified according to whether the node is a load, "PQ", or a generation busbar, "Pv or slack" busbar, as outlined in section 11.2.

The h.v.d.c. link part of the multi a.c. - h.v.d.c. power system becomes non-redundant when the seven converter relationships, $s_1 - s_7$, are included together with four additional variables that act as control specifications, $s_8 - s_{10}$. The non-redundant h.v.d.c. link loadflow specifications are summarized in Table 13.1, where

$$\{s_a, s_b, s_c, s_d\} \in \{\cos\alpha_m, \cos\delta_n, p_{dm}, V_{dn}, I_{dc}, a_m, a_n\} \qquad (13.1)$$

Table 13.1 H.v.d.c. link loadflow specifications

H.V.D.C. LINK LOADFLOW SPECIFICATIONS

For the rectifier

$$s_1 \quad 0 = I_{1-2} - a_m K_1 I_{dc}$$

$$s_2 \quad 0 = V_{dm} - a_m K_1 V_m \cos\psi_m$$

$$s_3 \quad 0 = V_{dm} - a_m K_1 \cos\psi_m - K_2 X_m I_{dc}$$

and for the inverter

$$s_4 \quad 0 = I_{5-6} - a_n K_1 I_{dc}$$

$$s_5 \quad 0 = V_{dn} - a_n K_1 V_n \cos\psi_n$$

$$s_6 \quad 0 = V_{dn} - a_n K_1 \cos\delta_n + K_2 X_n I_{dc}$$

Across the h.v.d.c. link

$$s_7 \quad 0 = V_{dm} - V_{dn} + R_{dc} I_{dc}$$

Together with control specifications

$$s_8 \quad 0 = S_a^p - s_a$$

$$s_9 \quad 0 = s_b^p - s_b$$

$$s_{10} \quad 0 = s_c^p - s_c$$

$$s_{11} \quad 0 = s_d^p - s_d$$

Eight possible combinations of the control specifications are shown in Table 13.2.

Table 13.2 Possible combinations of h.v.d.c. link control specifications.

CONTROL SPECIFICATION COMBINATION	s_1^p	s_2^p	s_3^p	s_4^p
1	P_{dm}	$\cos\psi_m$	V_{dn}	$\cos\delta_n$
2	P_{dm}	$\cos\psi_m$	V_{dn}	a_n
3	P_{dm}	a_m	V_{dn}	a_n
4	P_{dm}	a_m	V_{dn}	$\cos\delta_n$
5	P_{dm}	a_m	a_n	$\cos\delta_n$
6	P_{dm}	a_m	$\cos\alpha_m$	$\cos\delta_n$
7	I_{dc}	a_m	V_{dn}	$\cos\delta_n$
8	V_{dm}	a_m	P_{dn}	$\cos\delta_n$

The long-term expectation and variance for possible h.v.d.c. quantities of interest, $\underline{s}_{hvdc}$, can be found after the convergence of the multi a.c. - h.v.d.c. S.L.F. to its expected long-term state, $\hat{\underline{x}}$, where

$$\hat{\underline{x}}_{hvdc} = \{I_{1-2}, V_{dm}, a_m, \cos\alpha_m, \psi_m, I_{5-6}, V_{dn}, a_n, \cos\delta_n, \psi_n, I_{dc}\} \quad (13.2)$$

Quantities of interest include

$$\underline{s}_{hvdc} = \begin{bmatrix} |I|_{fm}, Q_{fm}, P_{1-2}, Q_{1-2}, E_m, P_{2-3}, Q_{2-3}, |I|_{2-3}, P_{dm} \\ |I|_{fn}, Q_{fn}, P_{5-6}, Q_{5-6}, E_n, P_{4-5}, Q_{4-5}, |I|_{4-5}, P_{dn} \end{bmatrix} \quad (13.3)$$

where $\underline{s}$ is defined by equation (11.9), and the variation of "spread" about the expected value, for quantities of interest, is given by equation (11.8).

13.3 USES FOR THE MULTI A.C. - H.V.D.C. STOCHASTIC LOADFLOW.

Multi a.c. - h.v.d.c. stochastic loadflows can be used in the following:

(i) When planning or designing an h.v.d.c. link between a.c. system/s. The multi a.c. - h.v.d.c. S.L.F. allows the designer to establish what effect the expected long-term a.c. power generation or loads, and their variances, together with the expected long-term values of the h.v.d.c. control specifications and their variances, have on the variance and expected value of h.v.d.c. quantities of interest given by either (13.2) or (13.3).

(ii) When planning a new a.c. transmission line/s in the vicinity of an existing h.v.d.c. link. The long-term expected variations in h.v.d.c. link operation, together with the expected nodal a.c. generation or load long-term fluctuations, can be accounted for in the prediction of maximum power flow conditions down the proposed transmission line.

The multi a.c. - h.v.d.c. stochastic loadflow can also be used as an "operations" tool to set upper and lower limits of variation for the control specifications. For a given set of postulated h.v.d.c. control specification "operating limits", and with the expected a.c. nodal generation and load variation; the multi a.c. - h.v.d.c. S.L.F. estimates and quantities of interest can be found. If the resulting variation in the h.v.d.c. quantities of interest, $\underline{s}_{hvdc}$, is too great, the allowed variation about the control specifications can be reduced and the multi a.c. - h.v.d.c. S.L.F. re-evaluated until suitable bounds of uncertainty are obtained about the "quantities of interest". Thus the multi a.c. - h.v.d.c. S.L.F. can be used to obtain suitable long-term limits on the uncertainty of the operating constraints.

13.4 MULTI A.C. - H.V.D.C. STOCHASTIC LOADFLOW TEST RESULTS

13.4.1 Uncorrelated multi a.c. - h.v.d.c. loadflow data

For the purposes of this section, all loadflow data is treated as uncorrelated, i.e. independent. When the S.L.F. data is uncorrelated, the $\underset{\sim}{R}$ matrix, shown in (11.5), becomes diagonal and the W.L.S. type S.L.F. algorithm can be easily implemented using sparsity techniques.

The multi a.c. - h.v.d.c. test power system consists of two identical 5 bus a.c. systems connected by a single h.v.d.c. link, as shown in Figure 13.1. Parameters for the a.c. and h.v.d.c. test systems are summarised in Table 7.5. A.c. nodal S.L.F. data and expected possible h.v.d.c. control specificiations are given in Table 13.3.

Table 13.3 Expected values of a.c. and h.v.d.c. long-term operating data.

A.C. SYSTEM 1		A.C. SYSTEM 2		H.V.D.C. LINK CONTROL SPECIFICATIONS	
LOCATION	VALUE (p.u.)	LOCATION	VALUE (p.u.)	LOCATION	VALUE (p.u.)
V_{11}	1.06000	V_{16}	1.06000	$\cos\alpha_m$	0.99260
P_{11}	1.92767	P_{16}	0.69718	P_{dm}	0.58600
P_{12}	0.20000	P_{17}	0.20000	$\cos\delta_n$	-0.98481
Q_{12}	0.22080	Q_{17}	-0.54150	V_{dn}	-1.27668
V_{13}	1.02300	V_{18}	1.02400	a_n	0.93974
P_{13}	-0.45000	P_{18}	-0.45000	a_m	0.97220
P_{14}	-0.40000	P_{19}	-0.40000	I_{dc}	0.45850
Q_{14}	-0.05000	Q_{19}	-0.05000	P_{dn}	-0.58526
P_{15}	-0.58600	P_{20}	-0.60000		
Q_{15}	-0.10000	Q_{20}	-0.10000		

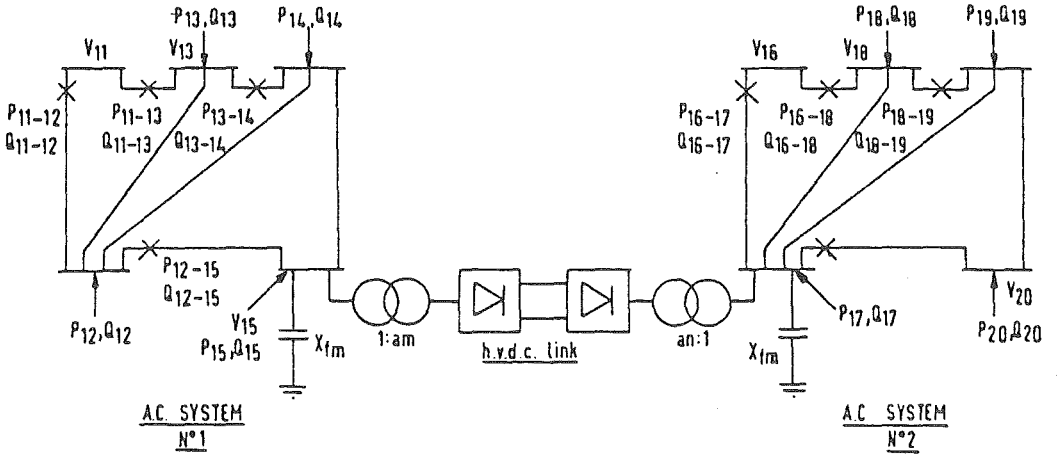

Figure 13.1 Multi a.c. - h.v.d.c. stochastic loadflow test system.

- 2 a.c. systems
- 1 h.v.d.c. link.

Note that for the test purposes, the percentage total load constraint uncertainty is assumed to be zero. Long-term uncertainties about the nodal a.c. voltage data are considered small, with $\sigma_{v_{ac}} = 0.0001$ p.u., while the uncertainty in the a.c. nodal real and reactive power injections is considered to be greater, with $\sigma_{s_{ac}} = 0.01$ p.u. The seven h.v.d.c. convertor relationships, $s_1 - s_9$, are treated as being near exact, with $\sigma_c = 0.00001$ p.u., while the expected deviation of the h.v.d.c. link constraints around the specified values is more uncertain, having a variance of $\sigma_s = 0.01$ p.u. The effect of choosing different sets of h.v.d.c. link operating constraints on the multi a.c. - h.v.d.c. stochastic loadflow results is shown in Table 13.4. Uncertainties in the power flows connecting the a.c. terminal busbars of the h.v.d.c. link are invariant to the choice of the h.v.d.c. link constraint set. On and around the h.v.d.c. link, however, uncertainty depends on the initial uncertainty and nature of the control specifications chosen. Since the multi a.c. - h.v.d.c. S.L.F. is used for long-term planning or design, if highly accurate results are required, each of the operating specification combinations given by Table 13.1 should be used in the S.L.F. study and the S.L.F. evaluated eight times. This is because all of the operating constraint combinations in Table 13.1 are likely to be enforced at some stage during the long time scale of the S.L.F. study.

Table 13.5 summarises the uncertainties which occur at a.c. terminal busbars and on the h.v.d.c. link when:

(i) The uncertainty associated with the h.v.d.c. link control specification is reduced to $\sigma_s = 0.00001$ p.u. while other variance data remains the same as in Table 13.4. Test results are shown in the first four columns of Table 13.5.

As expected, the overall uncertainty associated with quantities of interest on the h.v.d.c. link is greatly reduced. This drop in uncertainty is also felt in the neighbouring a.c. systems.

(ii) Uncertainty conditions are the same as in (i), however, the uncertainty associated with the expected a.c. nodal voltages is increased to $\sigma_{V_{a.c.}} = 0.01$ p.u. Increasing the uncertainty associated with the nodal a.c. voltage data causes a sharp increase in the uncertainty of the S.L.F. quantities of interest, both on the a.c. systems and on the h.v.d.c. link (see Table 13.5).

(iii) Uncertainty conditions are maintained the same as in (ii), with the exception that the uncertainty associated with the expected value of the h.v.d.c. control specifications is increased to $\sigma_i = 0.01$ p.u. An even greater degree of uncertainty appears in both the h.v.d.c. link and a.c. system S.L.F. estimates (see Table 13.5).

(iv) Uncertainty conditions are kept the same as in (i), with the exception that the uncertainty associated with the expected value of the h.v.d.c. link control specification and converter relations is increased to $\sigma_i = 0.01$ p.u. and $\sigma_s = 0.01$ p.u. The uncertainty increases in the S.L.F. results but the rise is not as great as that in (ii) or (iii) (see Table 13.5).

13.4.2 Correlated multi a.c. - h.v.d.c. loadflow data

Correlation between different nodes in the a.c. system can occur, for example, due to:

(i) Hydro generating stations being fed by the same river. Any increase in flow rate, due to rain run-off or snow melting, may cause an increased generation output from all stations along the

Table 13.4 S.L.F. results (uncorrelated data and different h.v.d.c. link control specifications).

CORRELATED DATA	MEAN (μ)	CONTROL SPECIFICATION SET 1	2	3	4	5	6	7	8
AC 1 (TERMINAL)									
θ_{15}	-0.18979	0.00114	0.00114	0.00117	0.00117	0.00126	0.00116	0.00127	0.00118
V_{15}	1.02366	0.00262	0.00262	0.00257	0.00257	0.00361	0.00285	0.00249	0.00257
P_{15}	-0.58598	0.01213	0.01213	0.01202	0.01202	0.01215	0.01217	0.01306	0.01203
Q_{15}	-0.10000	0.02360	0.02360	0.02390	0.02390	0.03380	0.02580	0.02340	0.02390
P_{15-12}	-0.93801	0.00703	0.00703	0.00705	0.00705	0.00705	0.00703	0.00763	0.00705
Q_{15-12}	0.15355	0.01633	0.01633	0.01625	0.01625	0.02311	0.01783	0.01593	0.01626
P_{15-14}	-0.23395	0.00439	0.00439	0.00436	0.00436	0.00438	0.00440	0.00465	0.00436
Q_{15-14}	0.06301	0.00931	0.00931	0.00923	0.00923	0.01310	0.01016	0.00902	0.00923
RECTIFIER									
I_{1-2}	0.59954	0.01203	0.01203	0.01163	0.01163	0.01454	0.01263	0.01203	0.01165
I_{dc}	0.45845	0.00748	0.00748	0.00749	0.00749	0.01000	0.01094	0.00785	0.00751
V_{dm}	1.27819	0.00999	0.00999	0.00999	0.00999	0.02052	0.02293	0.00974	0.00999
a_m	0.97174	0.01387	0.01387	0.01000	0.01000	0.01000	0.01000	0.01000	0.01000
$\cos\alpha_m$	0.99255	0.00999	0.00999	0.01024	0.01024	0.01447	0.01000	0.01036	0.01024
ψ_m	0.30182	0.03248	0.03248	0.03399	0.03399	0.04996	0.03605	0.03397	0.03401
P_{1-2}	0.58599	0.00845	0.00845	0.00844	0.00844	0.00845	0.00845	0.01025	0.00845
Q_{1-2}	0.18244	0.02122	0.02122	0.02193	0.02193	0.03227	0.02352	0.02145	0.02195
E_m	0.97446	0.01059	0.01059	0.00712	0.00712	0.00898	0.01219	0.00702	0.00712
P_{2-3}	0.58599	0.00845	0.00845	0.00844	0.00844	0.00845	0.00845	0.01025	0.00845
Q_{2-3}	0.13447	0.02097	0.02097	0.02142	0.02142	0.03090	0.02191	0.02119	0.02143
I_{2-3}	0.61698	0.01010	0.01010	0.01011	0.01011	0.01352	0.01477	0.01059	0.01014
P_{dm}	0.58598	0.00841	0.00841	0.00841	0.00841	0.00841	0.00841	0.01022	0.00842
Q_{fm}	-0.49899	0.00256	0.00256	0.00250	0.00250	0.00352	0.00278	0.00242	0.00250
I_{fm}	0.48746	0.00125	0.00125	0.00122	0.00122	0.00172	0.00136	0.00118	0.00122
INVERTER									
I_{5-6}	0.58101	0.01068	0.01134	0.01134	0.01067	0.01090	0.01072	0.01216	0.01068
V_{dn}	-1.27668	0.01000	0.01000	0.01000	0.01000	0.02055	0.02295	0.00974	0.01001
a_n	0.93969	0.01241	0.01000	0.01000	0.01241	0.01000	0.01899	0.01238	0.01242
$\cos\delta_n$	-0.98481	0.01000	0.01191	0.01191	0.01000	0.01000	0.01000	0.01000	0.01000
ψ_n	2.86544	0.03588	0.04337	0.04337	0.03588	0.03783	0.03599	0.03587	0.03588
P_{5-6}	-0.58529	0.00840	0.00840	0.00840	0.00840	0.00840	0.00840	0.01021	0.00841
Q_{5-6}	0.16587	0.02290	0.02753	0.02754	0.02289	0.02413	0.02299	0.02297	0.02289
E_n	0.97259	0.01126	0.00842	0.00842	0.01127	0.00110	0.01908	0.01117	0.01128
P_{4-5}	-0.58529	0.00840	0.00840	0.00840	0.00840	0.00840	0.00840	0.01021	0.00841
Q_{4-5}	0.13804	0.02279	0.02722	0.02722	0.02279	0.02337	0.02282	0.02284	0.02279
I_{4-5}	0.61829	0.01010	0.01011	0.01011	0.01011	0.01352	0.01476	0.01059	0.01014
P_{dn}	-0.58529	0.00839	0.00839	0.00839	0.00839	0.00839	0.00839	0.01019	0.00840
Q_{fn}	-0.68950	0.00115	0.00132	0.00132	0.00116	0.00120	0.00116	0.00116	0.00116
I_{fn}	0.65852	0.00055	0.00063	0.00063	0.00055	0.00058	0.00055	0.00055	0.00055
AC 2 (TERMINAL)									
θ_{17}	-0.01883	0.00050	0.00052	0.00052	0.00050	0.00050	0.00050	0.00051	0.00050
V_{17}	1.04705	0.00088	0.00100	0.00100	0.00088	0.00091	0.00088	0.00088	0.00088
P_{17}	0.20000	0.01186	0.01186	0.01186	0.01186	0.01187	0.01187	0.01302	0.01187
Q_{17}	-0.54150	0.02300	0.02760	0.02760	0.02300	0.02420	0.02310	0.02300	0.02300
P_{17-16}	-0.38030	0.00704	0.00705	0.00705	0.00704	0.00705	0.00705	0.00720	0.00705
Q_{17-16}	-0.12886	0.01533	0.01752	0.01752	0.01534	0.01597	0.01538	0.01537	0.01534
P_{17-28}	0.28841	0.00339	0.00339	0.00339	0.00339	0.00339	0.00339	0.00353	0.00339
Q_{17-18}	0.02228	0.00518	0.00589	0.00589	0.00518	0.00539	0.00519	0.00519	0.00518
P_{17-19}	0.31251	0.00342	0.00342	0.00342	0.00342	0.00342	0.00342	0.00356	0.00342
Q_{17-19}	0.01947	0.00409	0.00467	0.00467	0.00409	0.00426	0.00410	0.00410	0.00409
P_{17-20}	0.56467	0.00634	0.00635	0.00635	0.00634	0.00634	0.00634	0.00648	0.00635
Q_{17-20}	0.06924	0.00673	0.00684	0.00684	0.00673	0.00674	0.00673	0.00673	0.00673

The mean values from the eight different sets of constraints are accurate to within 0.001 p.u.

river.

(ii) Domestic loads in the same geographical area may be correlated due to weather. All loads in the same area will experience similar temperature fluctuations.

Normally, correlations are not included in a.c. S.L.F.'s because the diagonal R matrix, shown in (11.5), will become square, complicating the implementation of the W.L.S. type - S.L.F. algorithm. However, the "integrity" of the S.L.F. study will increase if a.c. loadflow nodal correlation effects are included.

Correlations on the h.v.d.c. link clearly exist and must be accounted for. In normal operation, the h.v.d.c. link (a controllable transmission line) is highly correlated. During normal h.v.d.c. link operation, the total active power flowing into the link is much the same as that flowing out the inverter.

Consider the multi a.c. - h.v.d.c. test system shown in Figure 13.1. A.c. nodal correlations are assumed to exist between:

(i) All generators in the same a.c. system, i.e. between nodes 11 and 13 in a.c. system 1 and between nodes 16 and 18 in a.c. system 2.

(ii) All loads in the same a.c. system, i.e. between nodes 12, 14 and 15 in a.c. system 1 and between nodes 17, 19 and 20 in a.c. system 2.

The percentage "total load" constraint forecasting uncertainty, to be spread amongst all the generators, is set to zero. Consider a multi a.c. - h.v.d.c. S.L.F. when the h.v.d.c. link control specifications selected are P_{dm}, $\cos\alpha_m$, V_{dn} and $\cos\delta_n$. The physical correlations between these variables are:

Table 13.5 S.L.F. test results (uncorrelated data and different initial loadflow data uncertainties).

UNCERTAINTY SIZE		$\sigma_{V_{AC}} = 0.0001$ $\sigma_{\theta_{AC}} = 0.01$ $\sigma_c = 0.00001$ $\sigma_a = 0.00001$	$\sigma_{V_{AC}} = 0.0001$ $\sigma_{\theta_{AC}} = 0.01$ $\sigma_c = 0.00001$ $\sigma_a = 0.00001$	$\sigma_{V_{AC}} = 0.0001$ $\sigma_{\theta_{AC}} = 0.01$ $\sigma_c = 0.00001$ $\sigma_a = 0.00001$	$\sigma_{V_{AC}} = 0.0001$ $\sigma_{\theta_{AC}} = 0.01$ $\sigma_c = 0.00001$ $\sigma_a = 0.00001$	$\sigma_{V_{AC}} = 0.01$ $\sigma_{\theta_{AC}} = 0.01$ $\sigma_c = 0.00001$ $\sigma_a = 0.00001$	$\sigma_{V_{AC}} = 0.01$ $\sigma_{\theta_{AC}} = 0.01$ $\sigma_c = 0.01$ $\sigma_a = 0.00001$	$\sigma_{V_{AC}} = 0.0$ $\sigma_{\theta_{AC}} = 0.0$ $\sigma_c = 0.0$ $\sigma_a = 0.0$
	MEAN (μ)	CONTROL SPECIFICATION SET 1	6	7	8	1	1	1
AC 1 (TERMINAL)								
θ_{15}	-0.18979	0.00093	0.00093	0.00094	0.00094	0.00390	0.00390	0.00139
V_{15}	1.02366	0.00119	0.00121	0.00097	0.00098	0.00815	0.00847	0.00347
P_{15}	-0.58598	0.00895	0.00895	0.00892	0.00892	0.01024	0.01305	0.01433
Q_{15}	-0.10000	0.00990	0.01000	0.00911	0.00921	0.01011	0.02370	0.03220
P_{15-12}	-0.93802	0.00572	0.00572	0.00573	0.00573	0.00601	0.00726	0.00814
Q_{15-12}	0.15355	0.00701	0.00714	0.00581	0.00584	0.02077	0.02547	0.02219
P_{15-14}	-0.23396	0.00359	0.00359	0.00358	0.00358	0.00399	0.00471	0.00499
Q_{15-14}	0.06300	0.00408	0.00416	0.00337	0.00338	0.01864	0.02042	0.01258
RECTIFIER								
I_{1-2}	0.59956	0.000715	0.000795	0.000018	0.000017	0.004904	0.012887	0.015705
I_d	0.45846	0.000009	0.000605	0.000010	0.000009	0.000009	0.007488	0.008271
V_{dm}	1.27819	0.000014	0.001689	0.000014	0.000010	0.000014	0.009988	0.014027
a_m	0.97174	0.001155	0.000010	0.000010	0.000010	0.007920	0.015922	0.017903
$\cos\alpha_m$	0.99255	0.000010	0.000010	0.000967	0.000973	0.000010	0.009999	0.009999
ψ_m	0.30182	0.000048	0.000340	0.003116	0.003039	0.000048	0.032483	0.047419
P_{1-2}	0.58600	0.000024	0.000026	0.000022	0.000020	0.000128	0.008454	0.011853
Q_{1-2}	0.18244	0.000031	0.000225	0.002001	0.001962	0.000050	0.021222	0.030315
E_m	0.97446	0.000031	0.001223	0.000709	0.000720	0.000187	0.010601	0.014179
P_{2-3}	0.58600	0.000024	0.000026	0.000027	0.000020	0.000128	0.008454	0.011853
Q_{2-3}	0.13449	0.000031	0.000101	0.002001	0.001962	0.000048	0.020975	0.029947
I_{2-3}	0.61699	0.000016	0.000816	0.000017	0.000016	0.000024	0.010107	0.013704
P_{dm}	0.58600	0.000010	0.000010	0.000014	0.000011	0.000010	0.008414	0.008682
Q_{fm}	-0.49899	0.001158	0.001181	0.000950	0.000955	0.007946	0.008254	0.003388
I_{fm}	0.48745	0.000566	0.000577	0.000464	0.000467	0.003881	0.004032	0.001655
INVERTER								
I_{5-6}	0.58102	0.000258	0.000261	0.000258	0.000258	0.004213	0.011479	0.014716
V_{dn}	-1.27668	0.000010	0.001691	0.000010	0.000014	0.000010	0.010000	0.010000
a_n	0.93969	0.000416	0.001251	0.000416	0.000416	0.006805	0.014150	0.014627
$\cos\delta_n$	-0.98481	0.000010	0.000010	0.000010	0.000010	0.000010	0.010000	0.010000
ψ_n	2.86544	0.000053	0.000227	0.000053	0.000052	0.000053	0.035876	0.052539
P_{5-6}	-0.58531	0.000019	0.000020	0.000021	0.000019	0.000197	0.008409	0.012591
Q_{5-6}	0.16587	0.000033	0.000143	0.000258	0.000033	0.000065	0.022899	0.033008
E_n	0.97259	0.000024	0.001262	0.000024	0.000025	0.000320	0.011274	0.012992
P_{4-5}	-0.58531	0.000020	0.000020	0.000021	0.000019	0.000197	0.008409	0.012591
Q_{4-5}	0.13804	0.000033	0.000074	0.000033	0.000033	0.000064	0.022789	0.032817
I_{4-5}	0.61831	0.000017	0.000816	0.000017	0.000017	0.000018	0.010109	0.013805
P_{dn}	-0.58531	0.000011	0.000011	0.000014	0.000016	0.000011	0.008394	0.009518
Q_{fn}	-0.68950	0.000583	0.000583	0.000583	0.000583	0.009538	0.009589	0.001565
I_{fn}	0.65852	0.000278	0.000278	0.000278	0.000278	0.004555	0.004579	0.000747
AC 2 (TERMINAL)								
θ_{17}	-0.01883	0.00041	0.00041	0.00041	0.00041	0.00207	0.00207	0.00057
V_{17}	1.04705	0.00044	0.00044	0.00044	0.00044	0.00729	0.00728	0.00119
P_{17}	0.20000	0.00894	0.00894	0.00894	0.00894	0.01018	0.01284	0.01462
Q_{17}	-0.54150	0.00004	0.00010	0.00004	0.00004	0.00121	0.02301	0.03311
P_{17-16}	-0.38029	0.00670	0.00670	0.00670	0.00670	0.00707	0.00741	0.00741
Q_{17-16}	-0.12887	0.00760	0.00760	0.00760	0.00760	0.09823	0.09919	0.02066
P_{17-18}	0.28841	0.00309	0.00309	0.00309	0.00309	0.00327	0.00355	0.00373
Q_{17-18}	0.02228	0.00262	0.00262	0.00262	0.00262	0.04663	0.04684	0.00692
P_{17-19}	0.31251	0.00311	0.00311	0.00311	0.00311	0.00317	0.00347	0.00377
Q_{17-19}	0.01947	0.00208	0.00208	0.00208	0.00208	0.03725	0.03741	0.00547
P_{17-20}	0.56468	0.00606	0.00606	0.00606	0.00606	0.00613	0.00642	0.00668
Q_{17-20}	0.06924	0.00655	0.00655	0.00655	0.00655	0.01958	0.01964	0.00692

The mean values of the eight different constraint sets are identical to within 0.001 p.u.

(1) "$\cos\alpha_m - P_{dm}$". Sign (+). As $\cos\alpha_m$ increases, α_m tends to zero and the average d.c. voltage, V_{dn}, increases, causing an increase in P_{dm}.

(2) "$P_{dm} - V_{dn}$". Sign (-). As P_{dm} increases, P_{dn} increases in magnitude and the value of V_{dn} becomes more negative.

(3) "$P_{dm} - \cos\delta_n$". Sign (-). As P_{dm} increases, P_{dn} increases in magnitude, causing δ_m to tend toward 180^o and thus making $\cos\delta_n$ more negative.

(4) "$\cos\alpha_m - V_{dn}$". Sign (-). Because of the arguments given in (1) and (2).

(5) "$\cos\alpha_m - \cos\delta_n$". Sign (-). Because of the arguments given in (1) and (3).

(6) "$\cos\delta_n - V_{dn}$". Sign (+). As δ_n tends toward 180^o, $\cos\delta_n$ becomes more negative, causing the average d.c. voltage, V_{dn}, to become more negative.

All correlations are symmetric so that the correlation data for "$\cos\alpha_m - P_{dm}$" is the same as that for "$P_{dm} - \cos\alpha_m$". The converter relationships, $s_1 - s_7$, are treated as uncorrelated and highly accurate, by making $\sigma_s = 0.00001$ p.u.

Weightings given to the correlations between a.c. system variables are shown in Table 13.6, while the weightings given to the h.v.d.c. link control specification correlations are shown in Table 13.7. Two classes of a.c. correlation are considered, those that are "decoupled", i.e. real and reactive nodal quantiles are not correlated, and those which are fully correlated. H.v.d.c. link correlations are considered to be either all positive (magnitude-only) or signed according to the previous discussion.

Table 13.6 A.c. correlation weightings ($\underline{R}_{ij}$).

	A.C. CORRELATION	
	P-θ, Q-v DECOUPLED A.C. CORRELATION DATA	A.C. CORRELATION DATA
GENERATOR P-v	$\underline{R}_{ij}$	$\underline{R}_{ij}$
$v_{11} - v_{11}$	0.000000010	0.000000010
$v_{11} - v_{13}$	0.000000005	0.000000005
$v_{13} - v_{13}$	0.000000010	0.000000010
$v_{11} - P_{11}$	-	0.000000002
$v_{13} - P_{11}$	-	0.00001
$v_{11} - P_{13}$	-	0.000000001
$v_{13} - P_{13}$	-	0.000000002
$P_{11} - P_{11}$	0.00010	0.00010
$P_{11} - P_{13}$	0.00005	0.00005
$P_{13} - P_{13}$	0.00010	0.00010
LOAD P-θ CORRELATIONS		
$P_{12} - P_{12}$	0.00010	0.00010
$P_{12} - P_{14}$	0.00008	0.00008
$P_{12} - P_{15}$	0.00006	0.00006
$P_{14} - P_{14}$	0.00010	0.00010
$P_{14} - P_{15}$	0.00007	0.00007
$P_{15} - P_{15}$	0.00010	0.00010
$P_{12} - Q_{12}$	-	0.00003
$P_{12} - Q_{14}$	-	0.00002
$P_{12} - Q_{15}$	-	0.00001
$P_{14} - Q_{14}$	-	0.00003
$P_{14} - Q_{15}$	-	0.00002
$P_{15} - Q_{15}$	-	0.00003
$Q_{12} - Q_{12}$	0.00010	0.00010
$Q_{12} - Q_{14}$	0.00008	0.00008
$Q_{12} - Q_{15}$	0.00006	0.00006
$Q_{14} - Q_{14}$	0.00010	0.00010
$Q_{14} - Q_{15}$	0.00007	0.00007
$Q_{15} - Q_{15}$	0.00010	0.00010
$P_{14} - Q_{12}$	-	0.00002
$P_{15} - Q_{12}$	-	0.00001
$P_{15} - Q_{14}$	-	0.00002

Correlations can be found by replacing prefix 11 by 16....15 by 20 etc.

Table 13.7 H.v.d.c. link data correlation weightings (R_{ij})

H.V.D.C. LINK CORRELATIONS	SET A R_{ij}	SET B R_{ij}
$\cos\alpha_m - \cos\alpha_m$	0.00010	0.00010
$\cos\alpha_m - P_{dm}$	0.00005	0.00005
$\cos\alpha_m - \cos\delta_n$	0.00005	-0.00005
$\cos\alpha_m - V_{dn}$	0.00005	-0.00005
$P_{dm} - P_{dm}$	0.00010	0.00010
$P_{dm} - \cos\delta_n$	0.00003	-0.00003
$P_{dm} - V_{dn}$	0.00003	-0.00003
$\cos\delta_n - \cos\delta_n$	0.00010	0.00010
$\cos\delta_n - V_{dn}$	0.00050	0.00005
$V_{dn} - V_{dn}$	0.00010	0.00010

Table 13.8 summarises the results of the correlated multi a.c. - h.v.d.c. S.L.F. for various choices and combinations of correlated data. Inclusion of correlation data generally causes only a slight decrease in the variance or "spread" of the S.L.F. results over the uncorrelated case shown in column 1 of Table 13.4. Thus, if the inclusion of correlated a.c. and h.v.d.c. link loadflow data is to be attempted, identification techniques must be employed to estimate accurately the magnitude of the off-diagonal values of R_{ij} and make the study meaningful.

Table 13.8 Multi a.c. -h.v.d.c. link S.L.F. results when correlated data is present.

		CORRELATED DATA							
	MEAN (μ)	H.V.D.C. LINK (SET A)	H.V.D.C. LINK (SET A)	A.C. DECOUPLED 12,14,15 17,19,20	A.C. 12,14,15 17,19,20	A.C. DECOUPLED 12,14,15 11,13 17,19,20 16,18	A.C. 12,14,15 11,13 17,19,20 16,18	A.C. DECOUPLED 12,14, 15,11,13,17 19,20,16,18 H.V.D.C. LINK (SET B)	A.C. 12,14,15 11,13,17 19,20,16,18 H.V.D.C. LI (SET B)
AC 1 (TERMINAL)									
θ_{15}	-0.18979	0.00121	0.00122	0.00106	0.00103	0.00112	0.00111	0.00120	0.00120
v_{15}	1.02366	0.00222	0.00232	0.00274	0.00272	0.00275	0.00266	0.00245	0.00242
P_{15}	-0.58598	0.01176	0.01174	0.01084	0.01083	0.01121	0.01113	0.01072	0.01065
Q_{15}	-0.10000	0.02081	0.02181	0.02371	0.02352	0.02371	0.02352	0.02201	0.02200
P_{15-12}	-0.93801	0.00709	0.00709	0.00590	0.00589	0.00619	0.00612	0.00628	0.00621
Q_{15-12}	0.15355	0.01439	0.01510	0.01639	0.01625	0.01639	0.01622	0.01521	0.01528
P_{15-14}	-0.23395	0.00431	0.00430	0.00355	0.00356	0.00368	0.00370	0.00356	0.00359
Q_{15-14}	0.06301	0.00816	0.00855	0.00937	0.00931	0.00937	0.00940	0.00863	0.00873
RECTIFIER									
I_{1-2}	0.59954	0.00899	0.00909	0.01258	0.01253	0.01265	0.01258	0.00946	0.00939
I_d	0.45845	0.00821	0.00661	0.00792	0.00792	0.00798	0.00798	0.00703	0.00703
V_{dm}	1.27819	0.00985	0.00986	0.00999	0.00999	0.00999	0.00999	0.00992	0.00992
a_m	0.97174	0.01541	0.00988	0.01389	0.01389	0.01390	0.01388	0.00995	0.00997
$\cos\alpha_m$	0.99255	0.00961	0.00961	0.00999	0.00999	0.00999	0.00999	0.00978	0.00978
ψ_m	0.30182	0.02945	0.03132	0.03249	0.03249	0.03249	0.03249	0.03175	0.03175
P_{1-2}	0.58599	0.00842	0.00841	0.00909	0.00908	0.00917	0.00916	0.00913	0.00912
Q_{1-2}	0.18244	0.01812	0.01929	0.02127	0.02127	0.02128	0.02128	0.01942	0.01942
E_m	0.97446	0.01246	0.00741	0.01060	0.01060	0.01060	0.01060	0.00742	0.00742
P_{2-3}	0.58598	0.00842	0.00841	0.00909	0.00908	0.00917	0.00916	0.00913	0.00912
Q_{2-3}	0.13447	0.01883	0.01932	0.02099	0.02099	0.02099	0.02099	0.01952	0.01950
I_{2-3}	0.61698	0.01106	0.00893	0.01069	0.01069	0.01077	0.01077	0.00949	0.00948
P_{dm}	0.58599	0.00839	0.00839	0.00904	0.00904	0.00912	0.00912	0.00911	0.00911
Q_{fm}	-0.49899	0.00217	0.00227	0.00267	0.00265	0.00268	0.00260	0.00239	0.00236
I_{fm}	0.48746	0.00106	0.00111	0.00130	0.00130	0.00131	0.00127	0.00117	0.00115
INVERTER									
I_{5-6}	0.58101	0.01193	0.00926	0.01121	0.01122	0.01127	0.01130	0.00971	0.00974
V_{dn}	-1.27668	0.00986	0.00986	0.01000	0.01000	0.01000	0.01000	0.00992	0.00992
a_n	0.93969	0.00911	0.00904	0.01242	0.01242	0.01242	0.01242	0.00905	0.00904
$\cos\delta_n$	-0.98481	0.00986	0.00986	0.00999	0.00999	0.00999	0.00999	0.00992	0.00992
ψ_n	2.86544	0.03633	0.03569	0.03588	0.03588	0.03588	0.03588	0.03586	0.03586
P_{5-6}	-0.58529	0.00839	0.00839	0.00904	0.00903	0.00911	0.00911	0.00910	0.00910
Q_{5-6}	0.16587	0.02378	0.02216	0.02293	0.02293	0.02294	0.02294	0.02219	0.02219
E_n	0.97259	0.00800	0.00799	0.01127	0.01127	0.01127	0.01127	0.00799	0.00799
P_{4-5}	-0.58529	0.00839	0.00839	0.00904	0.00903	0.00911	0.00911	0.00910	0.00910
Q_{4-5}	0.13804	0.02326	0.02206	0.02281	0.02281	0.02281	0.02281	0.02211	0.02211
I_{4-5}	0.61829	0.01108	0.00893	0.01069	0.01069	0.01077	0.01077	0.00949	0.00949
P_{dn}	-0.58529	0.00838	0.00838	0.00902	0.00902	0.00910	0.00910	0.00910	0.00910
Q_{fn}	-0.68950	0.00118	0.00114	0.00127	0.00127	0.00128	0.00121	0.00126	0.00117
I_{fn}	0.65852	0.00056	0.00055	0.00061	0.00061	0.00061	0.00058	0.00060	0.00056
AC 2 (TERMINAL)									
θ_{17}	-0.01883	0.00052	0.00048	0.00052	0.00051	0.00053	0.00060	0.00051	0.00058
V_{17}	1.04705	0.00089	0.00087	0.00097	0.00097	0.00097	0.00092	0.00096	0.00089
P_{17}	0.20000	0.01195	0.01176	0.01022	0.01021	0.01060	0.01066	0.01048	0.01053
Q_{17}	-0.54150	0.02391	0.02221	0.02302	0.02302	0.02302	0.02302	0.02231	0.02233
P_{17-16}	-0.38029	0.00708	0.00701	0.00729	0.00727	0.00748	0.00755	0.00745	0.00752
Q_{17-16}	-0.12886	0.01577	0.00339	0.01686	0.01675	0.01682	0.01686	0.01649	0.01625
P_{17-18}	0.28841	0.00340	0.01497	0.00284	0.00284	0.00256	0.00257	0.00255	0.00256
Q_{17-18}	0.02228	0.00535	0.00342	0.00569	0.00568	0.00566	0.00600	0.00551	0.00588
P_{17-19}	0.31251	0.00342	0.00503	0.00251	0.00250	0.00223	0.00223	0.00223	0.00223
Q_{17-19}	0.01947	0.00422	0.00398	0.00382	0.00382	0.00380	0.00403	0.00367	0.00395
P_{17-20}	0.56468	0.00634	0.00635	0.00505	0.00502	0.00522	0.00516	0.00522	0.00516
Q_{17-20}	0.06924	0.00673	0.00627	0.00663	0.00660	0.00663	0.00653	0.00663	0.00656

The mean values of the sets above agree with those in column 1 to within 0.001 p.u.
Unless mentioned otherwise, all other data is assumed uncorrelated.

13.5 CONCLUSION

A multi a.c. - h.v.d.c. S.L.F. has been formulated and tested, both with and without correlated a.c. and h.v.d.c. link loadflow data. The technique advocated in Chapter 12 for including non-gaussian p.d.f.'s in S.L.F.'s can be used with the multi a.c. - h.v.d.c. S.L.F. to generate multi a.c. - h.v.d.c. P.L.F.'s. The multi a.c. - h.v.d.c. S.L.F. can be used as a tool in long-term planning or design of h.v.d.c. links, or expansion of a.c. transmission line capability in the vicinity of existing h.v.d.c. links. The results of the multi a.c. - h.v.d.c. S.L.F. gives upper and lower bounds on the long-term likely values of quantities of interest, such as line power flows. The inclusion of a.c. and h.v.d.c. link data correlation has been shown to slightly reduce the long-term uncertainties in the S.L.F. study. However, identification techniques will need to be employed to identify the size of any correlations before undertaking a study using correlated data.

CHAPTER 14

CONCLUSIONS

The introduction of automated data acquisition and computerised data storage is a trend in power systems which will rapidly increase. State estimators can be used to buffer a data base from raw measurements made on the power system. These raw measurements may contain bad data. The state estimation algorithm is designed to detect and locate any bad data present in the measurement set. The weighted least squares approach to state estimation was used in the study because it is extremely versatile, being able to handle all types of measurements including zero injection pseudomeasurements. In practice, however, W.L.S. state estimation had proved to be computationally "slow" from an on-line, tracking point of view. Indeed many utilities have implemented the less versatile A.E.P. state estimation algorithm which processes only line-flow measurements. Zero-injection pseudomeasurements which have 100% availability, high accuracy and involve no monitoring costs, were not included in the original A.E.P. formulation. Yet it is uneconomic to neglect these pseudomeasurements. Two factors can improve the speed of W.L.S.:

(1) A pseudo line-flow creation technique was advocated, which makes the density of non-zero elements in the information matrix constant, with an admittance-like structure similar to the A.E.P. algorithm, when processing injection measurement mixes. When pseudo line-flow creation from injection measurements is included in W.L.S., speed improvements by a factor of 3-4 can result and optimality can be

retained if required.

(2) Fast decoupling can be applied to make the Jacobian matrix in W.L.S. state independent, with only half the number of non-zero elements remaining that were originally present. A theoretical eigenvalue-convergence analysis technique was presented and used to identify potentially unstable decoupling and fast decoupling schemes which, when coupled with test simulations, identified the sequential fast decoupling scheme advocated by Bermundez and Brameller (1978) as being most promising for implementation. The degradation in the optimality of the state estimates was shown to be less than 0.001 p.u. when this sub-optimal method was used.

When pseudo line-flow creation from injection measurement data was used in fast decoupled W.L.S., an extremely fast, stable, sparse, constant-matrix state estimator was realized with a similar structure to the A.E.P. algorithm. This hybrid algorithm is recommended for rapid on-line state estimation because it generates near-optimal estimates and handles all types of measurement data.

Bad data detection and identification concepts were discussed with reference to their suitability for use in an on-line manner. A method was proposed to mathematically remove the presence of suspect measurements in the estimator, by setting the residuals at the suspect measurements to zero. Mathematical removal of bad data was shown to generate the same estimate as the physical removal of the suspect bad data from the measurement set. Mathematical removal, however, does not change the dimension of matrices in the state estimator while physical removal does. Consequently, the physical removal of suspect bad data, and re-estimation, a traditional method of identifying the bad data, requires all matrix terms to be re-numbered and re-calculated, while mathematical removal does not. As a result, the use of mathematical

removal of suspect bad data, coupled with the weighted residual method of detecting bad data, results in an extremely fast state estimation bad data detection and identification scheme, suitable for on-time purposes.

The inclusion of h.v.d.c. link representations in a.c. state estimation was also considered and shown to be a practical possibility. Both multi a.c. -h.v.d.c. state estimators and fast decoupled multi a.c. -h.v.d.c. state estimators were tested and found to cause little increased burden in the computation. Two, general h.v.d.c. link representations were analysed: an "approximate" h.v.d.c. link model, without the effect of the commutation angle overlap which occurs after convertor switching; and the other an "exact" h.v.d.c. link model which includes the effect of commutation angle overlap. The "exact" h.v.d.c. link model was shown to have highly non-linear measurement equations and an unstable convergence of minimum observability. A method was advocated to generate exact h.v.d.c. link model estimates from the stable, "approximate" h.v.d.c. link model by enforcing exact residuals in the approximate model estimator, at each iteration. This method for obtaining "exact" estimates was shown to be stable and applicable to both multi a.c. -h.v.d.c. state estimation and loadflow analysis.

Optimal meter placement design techniques for selecting the "best" metering pattern, with regard to the individual meter type, location and accuracy, were reviewed and a new approach using time dependent availability analysis presented. Inclusion of availability factors in the design and operation of state estimation allows the expected long-term metering pattern, in the presence of measurement failure and repair, to be considered rather than just including all meters, valid only when the state estimator data acquisition system is commissioned. During operations, sensitive meter-failure locations

can be identified and maintenance repair policies modified in the vicinity to maintain the required nodal estimate availabilities. The availability based meter placement design was shown to be a "necessary but not sufficient" test to detect and identify single and multiple bad data and therefore needs to be used in conjunction with the Handschin *et al.*'s (1975) "Power of the J(x) test" which accurately models only the detection of single and multiple non-interacting bad data but assumes all measurements are always available, and cannot handle multiple interacting bad data.

The structure of small, regional state estimators to process measurements from a combined electrical hydrogenerator and hydrocanal system were considered and discrete Kalman filtering techniques were used to track the changes in the hydraulic turbine and water flow in the canal. Co-ordination to the local, dynamic hydroturbine and hydrocanal estimators is from a central static tracking state estimator which estimates the electrical status of the power system. It was found that the input and output flow of the hydrocanal must be specified before a stable dynamic model could be realized. Fixing only the input causes the dynamics of the hydrocanal to diverge. Hydrocanal dynamic state estimation was shown to be feasible, but its "real time performance" needs evaluating.

Long-term planning and design of new transmission lines has also been considered. It was shown that the W.L.S. state estimation algorithm, which accounts for present "apostiori" measurement uncertainties, can be redefined to account for future "apriori" generation-load prediction uncertainties in future planning, and perform a stochastic loadflow. Present statistical loadflow methods used in long-term planning were reviewed, comprising either a

probabilistic loadflow or a stochastic loadflow study. In a statistical loadflow, the long-term expected nodal generation-voltage or load is specified, together with the long-term variations about these mean values. The statistical loadflow is then solved, generating the long-term expected power flow, and variation or "spread" about these expected values, for transmission lines of interest. Stochastic loadflows only handle gaussian nodal probability distributions while probabilistic loadflows can handle any type of nodal probability distribution; discrete binomial or gaussian, and therefore result in a more accurate study. Any discrete or binomial probability distributions present must be replaced by a single gaussian distribution and an approximate study using the S.L.F. attempted. Errors in the maximum values of some of the line-flow probability distributions can exceed 20%. As a result, the expected long-term ratings for proposed transmission lines can be over or underdesigned by as much as 20%.

A gaussian sum approximation technique was proposed to model non-gaussian nodal probability distributions and handle them by a series of stochastic loadflows. The computed results were shown to be near identical in most cases to Allan *et al.*'s (1976) probabilistic loadflow results for the I.E.E.E. 14 bus test system. Methods of approximating the probability distribution profile to lower the computational burden were also investigated and it was found that only half to one third of the most significant convolution-combination components usually need evaluating in the study. $P-\theta$, $Q-v$ decoupling was also applied to reduce the computational burden. The use of gaussian sum approximations in a series of stochastic loadflows means that the more accurate probabilistic loadflow can be performed by utilities already possessing state estimation programs, with little or no modification.

Probabilistic loadflow results are very useful for assessing long-term reliability margins and operating decisions.

The inclusion of h.v.d.c. links into a.c. stochastic loadflow studies, using both correlated and uncorrelated data, was also considered. Multi a.c. - h.v.d.c. stochastic loadflows can be useful in the planning and design of new h.v.d.c. links or new a.c. transmission lines near existing h.v.d.c. links.

Further works needs to be spent in finding "equivalents" for remote parts of a.c. systems to allow stochastic or probabilistic loadflow assessment for lines or nodes of interest in large power systems. Nodal loadflow uncertainty data, remote from the transmission line of interest, may be able to be replaced by an "equivalent". Work could also be spent interfacing the local dynamic hydroturbine-canal state estimator to an "actual" small regional control centre computer such as the one described at Twizel. A program that allows large scale computation of Kalman gain also needs to be written to interface to measurements and the hydrodynamics of the canal system.

A study also needs to be carried out to assess if any benefits can be gained from using a three phase a.c. state estimation program. Like all state estimators that have been advocated, the present work is a single-phase representation. In the South Island a.c. system of the New Zealand Electricity, over half the total power generated is rectified and this proportion is likely to increase as new aluminium smelters are built. Transposition of a.c. transmission lines is not used in New Zealand. As a result, the South Island a.c. system has some degree of imbalance and a higher than normal harmonic content.

REFERENCES

ABOYTES, F., and CORY, B.J.: "An alternative formulation of the stochastic load flow method", 1975 Power Industry Computer Applications Conference, 9th, pp. 209-215.

ABOYTES, F., and MOLINA, S.A.: "An efficient state estimation method through transformations", 1979 Power Industry Computer Applications Conference, pp. 12-18.

ALLAM, M., and LAUGHTON, M.A.: "A general algorithm for estimating power system variables and network parameters", I.E.E.E. PES Summer Meeting, Anaheim, Cal, July 14-19, 1974, Paper C74 331-5.

ALLAN, R.N., BORKOWSKA, B., and GRIGG, C.H.: "Probabilistic analysis of power flows", Proc. I.E.E., Vol. 121, No. 12, Dec. 1974, pp. 1551-1556.

ALLAN, R.N., and AL-SHAKARCHI, M.R.G.: "Probabilistic a.c. load flow", Proc. I.E.E., Vol. 123, No. 6, June 1976, pp. 531-535.

ALLAN, R.N., GRIGG, C.H., and AL-SHAKARCHI, M.R.G.: "Numerical techniques in probabilistic load flow problems", Int. Journal for Numerical Methods in Engineering, Vol. 10, 1976, pp. 853-860.

ALLAN, R.N., GRIGG, C.H., NEWEY, D.A., and SIMMONS, R.F.: "Probabilistic power-flow techniques extended and applied to operational decision making", Proc. I.E.E., Vol. 123, No. 12, Dec. 1976, pp. 1317-1324.

ALLAN, R.N., and AL-SHAKARCHI, M.R.G.: "Probabilistic techniques in a.c. loadflow analysis", Proc. I.E.E., Vol. 124, No. 2, Feb. 1977, pp. 154-160.

ALLAN, R.N., and AL-SHAKARCHI, M.R.G.: "Linear dependance between nodal powers in probabilistic a.c. load flows", Proc. I.E.E., Vol. 124, No. 6, June 1977.

ALLAN, R.N., GRIGG, C.H., and PRATO-GARCIA, J.A.: "Effect of network outages in probabilistic load flow analysis", 1979 I.E.E.E. Power Engineering Society Winter Meeting, New York, Feb., Paper A79 032-4.

ALSPACH, D.L.: "Gaussian sum approximations in nonlinear filtering and control", pp. 81-100 in "Estimation theory", (ed.) D.G. Lainiotis, American Elsevier, 1974.

ALSPACH, D.L., and SORENSON, H.W.: "Nonlinear Baysian estimation using gaussian sum approximations", I.E.E.E. Trans. Automatic Control, Vol. AC-17, No. 4, August 1972, pp. 439-448.

ANDERSON, B.D.O., and MORE, J.B.: "Optimal filtering", Prentice Hall, 1979.

ARIATTI, F.: "System telemetry and estimation of state variables - Review of practices and proposals", Cigŕe 1976 Session, Cigŕe Paper 32-14.

ARIATTI, F., MARZIO, L., and RICCI, P.: "Designing state estimation in view of reliability", 5th Power Systems Computations Conference, Vol. 1, Cambridge, 1975, Paper 2.3/8.

ARRILLAGA, J., and BODGER, P.: "Integration of h.v.d.c. links with fast decoupled loadflow solutions", Proc. I.E.E., Vol. 124, No. 5, May 1977, pp. 463-468.

ARRILLAGA, J., HARKER, B.J., and BODGER, P.: "Unified and sequential load flows for a.c. systems containing static convertors", 6th Power Systems Computations Conference, Darmstartd, West Germany, 21-25 August 1978.

ARRILLAGA, J., HARKER, B.J., and BODGER, P.: "Fast decoupled loadflow algorithm for a.c./d.c. systems", 1978 I.E.E.E. Power Engineering Society Summer Meeting, Los Angeles, U.S.A, Paper A78 555-5.

ARRILLAGA, J., HEFFERNAN, M.D., LAKE, C.B., and ARNOLD, C.P.: "Fault atudies in a.c. systems interconnected by h.v.d.c. links", Proc. I.E.E., Vol. 127, Pt. C, No. 1, January 1980.

ARRILLAGA, J., HARKER, B.J., and TURNER, K.S. "Clarifying an ambiguity in recent a.c.-d.c. load flow formulations", Technical Note, Proc. I.E.E., Vol. 127, Pt. C, No. 5, September 1980, pp. 324-325.

ASCHMONEIT, F.C.: "Optimal power system static state estimation", 5th Power Systems Computations Conference, Cambridge, September 1975, Paper 2.3/9.

ASCHMONEIT, F., DENZEL, D., GRAF, R., and SCHELLSTEDE, G.: "Development of an optimal state estimator and implementation in a real-time computer system", Cigŕe 1976 Session, Cigŕe Paper 32-16.

ASCHMONEIT, F.C., PETERSON, N.M., and ADRIAN, E.C.: "State estimation with equality constraints", 1977 Power Industry Computer Applications Conference, pp. 427-432.

BANERJEE, S.K., and RAJAMANI, K.: "Cyclic sequential state estimator - a new approach to power system state estimation", IFAC Symposium 1977 on Automatic Control and Protection of Electric Power Systems, Melbourne, Australia, 21-25 Feb. 1977, pp. 130-134.

BARTELS, R.H., and STEWART, G.W.: Algorithm 432 "Solution of the matrix equation AX + XB = C", Communications of the ACM, Sept., 1972, Vol. 15, No. 9, pp. 820-826.

BERMUNDEZ, J.F.: "Efficient static power system state estimation", Ph.D. Thesis, University of Manchester, 1977.

BERMUNDEZ, J.F., and BRAMELLER, A.: "State estimation in power systems: a comparison of methods", 6th Power Systems Computation Conference, Darmstartd, West Germany, 21-25 August 1978.

BORKOWSKA, B.: "Probabilistic load flow", 1973 I.E.E.E. Power Engineering Society Summer Meeting, Vancouver, B.C., Canada, July, Paper T-73 485-0.

BRAMELLER, H., and KORAKI, S.H.: "Comments on 'Power System State Estimation using Linear Programming' and reply by Irving, M.R., Owen, R.C., and Sterling, M.J.H.", Proc. I.E.E.E, Vol. 126, No. 3, March 1979, pp. 246-247.

BREKKE, H.: "Stability studies for a governed turbine operating under isolated load conditions", Water Power, September 1974, pp. 333-341.

BROUSSOLLE, F.: "State estimation in power systems: detecting bad data through the sparse inverse matrix method", 1977 I.E.E.E. Power Engineering Society Summer Meeting, Mexico City, July 17-22, 1977, Paper F77 579-6.

BROWN, E.P.M., and SIRISENA, H.R.: "Treatment of uncertainty in power systems on-line monitoring and long-term planning: state estimation and stochastic load flow studies", N.Z. Institute of Engineers, Proc. Technical Groups, Vol. 7, Issue 1 (ETG) 1981.

CHAUDRY, M.H.: "Governing stability of a hydroelectric power plant", Water Power, April 1970, pp. 131-136.

CHIU, C.L., and ISU, E.O.: "Kalman filter in open channel flow estimation", Journal of the Hydraulics Division, Proc. of American Society of Civil Engineers, August 1978, pp. 1137-1152.

CHOW, Wen-le: "Open channel hydraulics", McGraw Hill, 1959.

CLEMENTS, K.A. and RINGLEE, R.J.: "Treatment of parameter uncertainty in power system state estimation", 1974 I.E.E.E. Power Engineering Society Summer Meeting, Anaheim, Cal, July 14-19, Paper C74 311-7.

CLEMENTS, K.A., and WOLLENBERG, B.F.: "Observability determination for networks containing bus injections and line flow measurements", 1975 I.E.E.E. Power Engineering Society Summer Meeting, San Francisco, California, July 20-25, 1979, Paper A75 447-3.

COUCH, G.H.: "Improved power system state estimation with constant gain matrices", I.E.E.E. Proceedings, November 1976, pp. 1641-1643.

COUCH, G.H., and MORRISON, I.F.: "Data validation and topology determination for power system monitoring and control", 1974 I.E.E.E. Power Engineering Society Summer Meeting, Anaheim, Cal, July 14-19, Paper C74 361-2.

COUCH, G.H., SULLIVAN, A.C., and DEMBECKI, J.A.: "A state estimator oriented to a semi-isolated 5GW power system", 1974 I.E.E.E. Power Engineering Society Summer Meeting, Anaheim, California, July 14-19, Paper C74 346-3.

COUCH, G.H., SULLIVAN, A.C., and DEMBECKI, J.A.: "Results from a decoupled state estimator with transformer ratio estimation for a 5 GW power system in the presence of bad data", 5th Power Systems Computations Conference, Proceedings, Cambridge, Sept. 1975, Paper 2.3/3, pp. 1-9.

DEBS, A.S.: "Parameter estimation for power systems in the steady state", I.E.E.E. Trans. on Automatic Control, Vol. AC-19, No. 6, Dec. 1974, pp. 882-886.

DEBS, A.S., and LARSON, R.E.: "A dynamic estimator for tracking the state of a power system", I.E.E.E. Trans. Power Apparatus and Systems, Vol. PAS-89, No. 7, Sept./Oct. 1970, pp. 1670-1678.

DEBS, A.S., and LITZENBERGER, W.H.: "Experimental evaluation of tracking state estimation", Power Industry Computer Applications (PICA) Conference Proceedings, Boston, Mass., 1971, pp. 348-355.

DEBS, A.S., and LITZENBERGER, W.H.: "The BPA state estimator project: tuning of the network model", 1975 I.E.E.E. Power Engineering Society Summer Meeting, San Francisco, California, July 1975, Paper A75 448-1.

DHALIWAL, N.S., and WICHERT, H.E.: "Analysis of PID governors in multimachine systems", I.E.E.E. Trans. Power Apparatus and Systems, Vol. PAS-97, No. 2, March/April 1978, pp. 456-468.

DOPAZO, J.F., KLITIN, O.A., STAGG, G.W., and VAN SLYCK, L.S.: "State calculation of power systems from line flow measurements", I.E.E.E. Trans. Power Apparatus and Systems, Vol. PAS-89, No. 7, Sept./Oct. 1970, pp. 1693-1708.

DOPAZO, J.F., KLITIN, O.A., and VAN SLYCK, L.S.: "State calculation of power systems from line flow measurements, Part II", I.E.E.E. Trans. Power Apparatus and Systems, Vol. PAS-91, Jan./Feb. 1972, pp. 145-151.

DOPAZO, J.F., KLITIN, O.A., and SASSON, A.M.: "State estimation for power systems: detection and identification of gross measurement errors", PICA Conference 1973, pp. 313-318.

DOPAZO, J.F., KLITIN, O.A., and SASSON, A.M.: "Stochastic load flows", I.E.E.E. Trans. Power Apparatus and Systems, Vol. PAS-94, No. 2, March/April 1975, pp. 299-309.

DOPAZO, J.F., EHRMANN, S.T., KLITIN, O.A., SASSON, A.M., and VAN SLYCK, L.S.: "Implementation of the A.E.P. real-time monitoring system", I.E.E.E. Trans. Power Apparatus and Systems, Vol. PAS-95, Oct. 1976, pp. 1618-1629.

DURAN, H.: "Surrogate measurements make faster state estimation optimal and general", 1977 I.E.E.E. Power Engineering Society Summer Meeting, Mexico City, July 17-22, 1977, Paper A77 598-6.

DY LIACCO, T.E.: "System security: the computers role", I.E.E.E. Spectrum, Vol. 15, No. 6, June 1978, pp. 43-50.

EDELMANN, H.: "A universal assessment for the superior quality of distribution of measuring points for the state estimation of h.v. networks", 5th Power Systems Computations Conference, Cambridge, 1975, Vol. 1, Paper 2.3/7.

EL-AMIN, I.M., YACAMINI, R., and BRAMELLER, A.: "A.c.-h.v.d.c. solution and security assessment using a diakoptical method", Electrical Power and Energy Systems, Vol. 1, No. 3, October 1979, pp. 175-179.

EL-TABLAWI, T.A., and EL-HAGRY, M.T.: "State estimation of power systems - 1. Optimal meter placement", M.T. Conference of Power Systems Conference Expo., Texas, A. and M. University, College Station, March 19-21, 1979. (Published by I.E.E.E.) pp. 35-39.

FETZER, E.E. and ANDERSON, P.M.: "Observability in the state estimation of power systems", I.E.E.E. Trans. Power Apparatus and Systems, Vol. 94, Nov./Dec. 1975, pp. 1981-1988.

FLANN, M., and SASSON, A.M. "Stochastic load flow decoupled implementation", 1977 I.E.E.E. Power Engineering Society Summer Meeting, Mexico City, Mexico, July 1977, Paper A77 515-0/8.

GALIANA, F.D., and HANDSCHIN, E.: "Combined network and power station dynamic state estimation", Fourth Power Systems Computation Conference (P.S.S.C.) Proceedings, Grenoble, France, Sept. 1972, Paper 3.3/4.

GARCIA, A., MONTICELLI, A., and ABREU, P.: "Fast decoupled state estimation and bad data processing", I.E.E.E. Trans. Power Apparatus and Systems, Vol. 98, No. 5, Sept./Oct. 1979, pp. 1645-1652.

HAGIHARA, S., YOKOTA, H., GODA, K., and ISOBE, K.: "Stability of a hydraulic turbine generating unit controlled by P.I.D. governor", I.E.E.E. Trans. Power Apparatus and Systems, Vol. PAS-98, No. 6, Nov./Dec. 1979, pp. 2294-2298.

HANDSCHIN, E.: "Real time data processing using state estimation in electric power systems", in "Real time control of electric power systems", (ed.) E. Handschin, Proc. of Brown Boveri Symposium, Baden, Switzerland, 1971. Published by Elsevier, Amsterdam 1972.

HANDSCHIN, E., and GALIANA, F.D.: "Hierarchical state estimation for real-time monitoring of electric power systems", Power Industry Computer Applications (PICA) Conference Proceedings, Minneapolis, U.S.A., June 1973, pp. 304-312.

HANDSCHIN, E.J., and SCHWEPPE, F.C.: "Comments on S.L. Johnsson: An algorithm for state estimation in power systems", I.E.E.E. Trans. Power Apparatus and Systems, Vol. PAS-93, Jan./Feb. 1974, pp. 23-24.

HANDSCHIN, E.J., and BONGERS, C.: "Theoretical and practical considerations in the design of state estimators for electric power systems", Int. Symp. on "Computerized operation of power systems", 3rd, San Carlos, Brazil, 1975.

HANDSCHIN, E., SCHWEPPE, F.C., KOHLAS, J., and FIECHTER, A.: "Bad data analysis for power system state estimation", I.E.E.E. Trans. Power Apparatus and Systems, Vol. PAS-94, No. 2, March/April 1975, pp. 329-337.

HAYES, T.: "Stochastic load flow using partially-coupled equations", Control of Power Systems Conference and Exposition, College Station, Texas, U.S.A., 14-16 March 1977, pp. 135-138.

HEFFERNAN, M.D.: "Analysis of a.c./d.c. system disturbances", University of Canterbury, Christchurch, New Zealand, 1980, 315 pp. (Thesis: Ph.D.: Engineering).

HEFFERNAN, M.D., ARRILLAGA, J., TURNER, K.S., and ARNOLD, C.P.: "Recovery from temporary h.v.d.c. line faults", 1980 I.E.E.E. Power Engineering Society Summer Meeting, Minneapolis, Minnesota, July 13-18, 1980, Paper 80 SM 675-9.

HEYDT, G.T.: "Stochastic power flow calculations", 19755 I.E.E.E. Power Engineering Society Summer Meeting, San Francisco, Calif., July, 1975, Paper A75 530-6.

HEYDT, G.T., and SAUER, P.W.: "Stochastic power flow study methods", Allerton Conference on Circuit and Systems Theory, 14th, October 1976, pp. 253-260.

HORISBERGER, H.P., RICHARD, J.C., and ROSSIER, G.: "A fast decoupled static state estimator for electric power systems", I.E.E.E. Trans. Power Apparatus and Systems, Vol. PAS-95, No. 1, Jan./Feb. 1976.

HOVEY, L.M.: "Optimum adjustment of hydrogovernors on Manitoba hydro system", A.I.E.E. Trans. Power Apparatus and Systems, Vol. 81, Dec. 1962, pp. 581-587.

IONESCU, S., and RADU, L. "State estimation from line flow measurements and zero injection pseudo measurements", Seminar on Computer Methods of Power System Analysis and Control, Bucharest, Romania, June 1974.

IRVING, M.R.: "Power system state estimation using linear programming", Proc. Inst. Electr. Eng. (G.B.), Vol. 125, No. 9, Sept. 1978, pp. 879-885.

JOHNSSON, S.L.: "An algorithm for state estimation in power systems", Power Industry and Computer Applications Conference, Minneapolis, June 1973, pp. 319-326.

JOTTRAND, G.E.: "Probabilistic load flow analysis applicable to large sized meshed networks", 1978 Cigŕe Conference, 1978, Paris, Paper 31-04.

KIMBARK, E.W.: "Direct current transmission - Vol. 1", Wiley, 1971.

KLEINMAN, D.L.: "On an iterative technique for Riccati equation computations", I.E.E.E. Trans. Automatic Control, Feb. 1968, p. 114.

KATO, K., and HAMMERLUND, A.C.: "Real time network topology determination", I.E.E.E. Power Engineering Society Summer Meeting, Mexico City, Mexico, July 17-22, 1977, Paper A77 517-6/7.

KOENIG, D.F., and O'MALLEY, J.P.: "State estimation: an on-line luxury for the electric utilities industry?", I.E.E.E. Power Engineering Society Summer Meeting, San Francisco, Calif., July 9-14, 1972, Paper C72 463-8.

KOGLIN, H.J.: "Optimal measuring system for state estimation", 5th Power Systems Computations Conference, Cambridge, 1975, Vol. 1, Paper 2.3/12.

KOTHARI, D.P., and GUPTA, R.K.: "Optimal stochastic loadflow studies", Institution of Engineers (India) Journal, Vol. 59, EL-1, August 1978, pp. 34-37.

LARSON, R.E., TINNEY, W.F., and PESCHON, J.: "State estimation in power systems. Part 1: theory and feasibility", I.E.E.E. Trans. Power Apparatus and Systems, Vol. PAS-89, No. 3, March 1970, pp. 345-352.

LARSON, R.E., TINNEY, W.F., HAJOU, L.P., and PIERCY, D.S.: "State estimation in power systems. Part II: Implementation and applications", I.E.E.E. Trans Power Apparatus and Systems, Vol. PAS-89, No. 3, March 1970, pp. 353-363.

LAW, C.K.: "A fast transient stability program", University of Manchester, Institute of Science and Technology, 1972, 71 pp. (Thesis: M.Sc.: Engineering).

LE, H.Q., and OUTHRED, H.R.: "Identification and elimination of bad data and line errors from power system state estimators", IFAC Symposium 1977, Melbourne, February 21-25, 1977.

LE ROY, A., and VILLARD, P.: "Application of state estimation methods to evaluation of a telemeasurement configuration for energy power systems", Int. Symp. on "Computerized operation of power systems", 3rd, San Carlos, Brazil, 1975, Procs, (ed.) Savu Crivat Savulescu.

LIPSCHUTZ, S.: "Theory and problems of probability", Schaum's outline series, McGraw-Hill, 1965.

LJUBOJEVIC, M.: "Recursive hierarchical estimation of the states of an electrical power system", Comput. Elect. Engng, Vol. 6, Sept. 1979, pp. 205-220.

LONGHAM, E.J.: "New approach to hydrology data acquisition", Journal of the Hydraulics Division, Proc. of American Society of Civil Engineers, Dec. 1971, pp. 1965-1978.

LU, K.V., and RAD, N.D.: "Detection, estimation and correction of bad data in power system state estimation through SRIF", I.E.E.E. Power Engineering Society Summer Meeting, Los Angeles, CA, U.S.A., 16-21 July 1978, Paper A78 500-1, pp. 1-9.

MAFAAKHER, F., BRAMELLER, A., and BERMUNDEZ, J.F.: "Optimum metering design using a fast decoupled state estimator", Proc. I.E.E., Vol. 126, No. 1, Jan. 1979, pp. 62-68.

MAHALANABIS, A.K., BISWAS, K.K., and SINGH, G.: "An algorithm for decoupled dynamic state estimation of power systems", I.E.E.E. Power Engineering Society Summer Meeting, Los Angeles, CA, July 16-21, 1978, Paper A78 573-8.

MASIELLO, R.D., and HORTON, J.S.: "On-line decoupled observability processing", 1977 Power Industry Computer Applications Conference, pp. 420-426.

MERLIN, A., and BROUSSOLLE, F.: "Fast method of bad data identification in power system state estimation", IFAC Symposium 1977 on "Automatic Control and Protection of Electric Power Systems", Melbourne, Australia, Feb. 21-25, 1977.

MERRILL, H.M., and SCHWEPPE, F.C.: "Bad data suppression in power system static state estimation", I.E.E.E. Trans. Power Apparatus and Systems, Vol. 90, March/April 1971, pp. 1025-1033.

MILLER, W.L., and LEWIS, J.B.: "Dynamic state estimation in power systems", I.E.E.E. Trans. on Automatic Control, Vol. AC-16, No. 6, Dec. 1971, pp. 841-846.

MOORE, S.F.: "Estimation theory applications to design of water quality monitoring systems", Journal of the Hydraulics Division, Proc. of American Society of Civil Engineers, May 1973, pp. 815-831.

OGAWA, T., and MO-SHING, CHEN.: "A disposition method for data acquisition points in power system state estimation", 1978 I.E.E.E. Power Engineering Society Summer Meeting, Los Angeles, CA, U.S.A., July 16-21, 1978, A78-501-9/1-7.

PETERSON, N.M.: "State estimator application to the energy management system", 1977 Control of Power Systems Conference on Exposition, College Station, Texas, U.S.A., 14-16 March, pp. 83-87.

PHUA, K., and DILLON, T.: "Optimal choice of measurements for state estimation", 1977 Power Industry Computer Applications Conference, pp. 431-441.

PURIPANJAVANANT, C.: "Optimal and suboptimal load frequency control of two interconnected power areas", University of Canterbury, Christchurch, New Zealand, 1980. (Thesis: M.E.: Engineering).

RAMEY, D.G., and SKOOGLUND, J.W.: "Detailed hydrogovernor representation for system stability studies", I.E.E.E. Trans. Power Apparatus and Systems, Vol. PAS-89, No. 1, Jan. 1970, pp. 106-112.

RAO, N.D., and TRIPATHY, S.C.: "Variable step size decoupled estimator", 1978 I.E.E.E. Power Engineering Society Winter Meeting, New York, Jan./Feb. 1978, Paper F78 264-4.

REICHERT, K., and SULLIVAN, A.C.: "A systematic study of state estimation in electric power systems", IFAC Symposium 1977, Melbourne, Australia, 21-25 Feb. 1977, pp. 434-440.

SANDELL, N.R., and ATHANS, M.: "Modern control theory: A self study subject - Manual for FORTRAN computer subroutine for linear, quadratic and gaussian designs", Center for Advanced Engineering Study. Massachusetts Institute of Technology. 1972.

SASSON, A.M., EHRMANN, S.T., LYNCH, P., and VAN SLYCK, L.S.: "Automatic power system network topology determination", I.E.E.E. Trans. Power Apparatus and Systems, Vol. PAS-92, March/April 1973, pp. 610-618.

SAUER, P.W, and HEYDT, G.T.: "A generalized stochastic power flow algorithm", 1978 I.E.E.E. Power Engineering Society Summer Meeting, Los Angeles, CA, Calif., July 1978, Paper A78 544-9.

SCHLEIF, F.R., and WILBUR, A.B.: "The co-ordination of hydraulic turbine governors for power system operation", I.E.E.E. Trans. Power Apparatus and Systems, Vol. PAS-85, No. 7, July 1966, pp. 750-758.

SCHWEPPE, F.C., WILDES, J., and ROM, D.B.: "Power system static state estimation, Parts I-III", I.E.E.E. Trans. Power Apparatus and Systems, Vol. PAS-89, Jan. 1970, pp. 120-135.

SCHWEPPE, F.C., and MASIELLO, R.D.: "A tracking static state estimator", I.E.E.E. Power Apparatus and Systems, Vol. PAS-90, March/April 1971, pp. 1025-1033.

SCHWEPPE, F.C., and HANDSCHIN, E.J.: "Static state estimation in electric power systems", I.E.E. Proceedings, Vol. 62, July 1974, pp. 972-982.

SHOOMAN, M.L.: "Probabilistic reliability; an engineering approach", McGraw-Hill, 1968.

SIMPSON, R.J.: "Power system loading dynamics", University of Canterbury, Christchurch, New Zealand, 1975. (Thesis: M.E.: Engineering).

SINGH, G., BISWAS, K.K., and MAHALANABIS, A.K.: "Tracking state estimators for power systems", Int. Conf. on Information, Sciences and Systems, Patras, Greece, April 19-24, 1976.

SINGH, G., BISWAS, K.K., and MAHALANABIS, A.K.: "Dynamic estimation of complex node voltage in power systems", Journal of Institution of Engineers (India), Electrical Engineering Division, Vol. 58, ELS April 1978, pp. 252-255.

SOBIERAJSKI, M.: "Optimal stochastic load flows", Journal of Electric Power Systems Research, Vol. 2, 1979, pp. 71-75.

SORENSON, H.W., and ALSPACH, D.L.: "Recursive Baysian estimation using gaussian sums", Automatica, Vol. 7, pp. 465-479, Pergamon Press, 1971.

SRINVASAN, K.V.: "State estimation from line flows and bus injections in the absence of a reference voltage", 1976 I.E.E.E. Power Engineering Society Summer Meeting, 18-23 July 1976, Paper A76 414-3.

SRINVASAN, K.V., and ROBICHAUD, Y.: "A dynamic estimator for complex bus voltage determination", I.E.E.E. Trans. Power Apparatus and Systems, Vol. PAS-93, Sept./Oct. 1974, pp. 1581-1588.

STADLIN, W.O.: "Comments on H.P. Horsberger, J.C. Richard, C. Rossier: a fast decoupled static state-estimator for electric power systems", I.E.E.E. Trans. Power Apparatus and Systems, Vol. PAS-95, No. 1, Jan./Feb. 1976, pp. 212-215.

STAGG, G.W., and EL-ABIAD, A.H.: "Computer methods in power systems analysis", McGraw-Hill, 1968.

STERLING, M.J.H.: "Power system control", Institute of Electrical Engineering, IEE Control Engineering Series 6, 1978.

STOTT, B.: "Loadflows for a.c. and integrated a.c./d.c. systems", Ph.D. Thesis, University of Manchester, England, 1971.

STOTT, B., and ALSAC, D.: "Fast decoupled load flow", I.E.E.E. Power Apparatus and Systems, Vol. PAS-93, May/June 1974, pp. 859-867.

SUGARMAN, R.: "Superpower computers", I.E.E.E. Spectrum, Vol. 17, No. 4, April 1980, pp. 28-64.

THORNE, L.M., and HILL, E.F.: "Extensions of stability boundaries of a hydraulic turbine generating unit", I.E.E.E. Trans. Power Apparatus and Systems, Vol. PAS-94, No. 4, July/August 1975, pp. 1401-1409.

TRIPATHY, S.C., DURGAPRASAD, S., and RAO, N.D.: "Fast decoupled state estimation with adaptive step size adjustment", I.F.A.C. Symposium, New Delhi, India, 1979, pp. 89-96.

TURNER, K.S.: "Transient stability analysis of integrated a.c. and d.c. power systems", University of Canterbury, Christchurch, New Zealand, 1980, 261 pp. (Thesis: Ph.D.: Engineering).

UEMURA, K.: "State estimation of large scale electric power systems by decomposition methods", in Proc. 5th I.F.A.C. World Congress, Paris, France, 1972, Paper C72 465-3.

VAN MEETEREN, H.P.: "Fast decoupled state estimator with linear models", Journal of Electric Power and Energy Systems, Vol. 1, No. 3, Oct. 1979, pp. 187-192.

VAN MEETEREN, H.P., FEIGERS, A.R., and MICHELIS, E.J.: "Comparative study of two different types of state estimation including bad data identification methods", Proc. 5th Power Syst. Comp. Conf., Cambridge, Sept. 1975, Paper 2.3/4.

VAN MEETEREN, H.P., and MICHELIS, E.J.: "Fast decoupled state-estimator using linear models", Proc. 6th Power Syst. Comp. Conf., Dramstard, West Germany, 1978, pp. 760-765.

VAN SLYCK, L.S., and DOPAZO, J.F.: "Conventional load flow not suited for real-time power system monitoring", 1973 Power Industry Computer Applications Conference, pp. 427-432.

WOGNAR, A.: "A method of fast state estimation of a power system", Energetyka (Poland), Vol. 31, Part 12, 1977, pp. 312-313.

WYLIE, E.B., and STREETER, V.L.: "Fluid Transients", McGraw Hill, 1978.

YEH, W.G., and BECKER, L.: "Linear programming and channel flow identification", Journal of the Hydraulics Division, Proc. of American Society of Civil Engineers, Nov. 1973, pp. 2013-2022.

APPENDIX A.1

OPTIMALITY OF ESTIMATES OBTAINED FROM PSEUDO LINE-FLOW CREATION

To show that no degradation in the optimality of the estimates occurs when pseudo line-flows are created from injection measurements, consider a single injection measurement at node i. Node i is connected to only nodes j and k via transmission lines. For simplicity, assume a linear system model. Thus:

$$h_{p_i} \cdot \underline{x} = \sum_{n=1}^{2} h_{p_{ij}} \cdot \underline{x} = h_{p_{ij}} \cdot \underline{x} + h_{p_{ik}} \cdot \underline{x} \tag{A1.1}$$

$$z_{p_i} = h_{p_i} \cdot \underline{x} + \eta \tag{A1.2}$$

where $E\{\eta\eta^T\} = R$.

Pseudo line-flows created from the injection measurement are:

$$\begin{aligned} z_{p_{ij}}' &= z_{p_i} - h_{p_i} \cdot \underline{x} + h_{p_{ij}} \cdot \underline{x} \\ z_{p_{i\ell}}' &= z_{p_i} - h_{p_i} \cdot \underline{x} + h_{p_{i\ell}} \cdot \underline{x} \end{aligned} \tag{A1.3}$$

The condition for a minimum using the pseudo line-flow injections is given by the R.H.S. of equation (3.10), i.e.

$$[h_{p_{ij}} \cdot \underline{x} \ , \ h_{p_{ik}} \cdot \underline{x}]^T \begin{vmatrix} R_1^{-1} & 0 \\ 0 & R_2^{-1} \end{vmatrix} \begin{vmatrix} z_{ij}' - h_{ij} \cdot \underline{x} \\ z_{ik}' - h_{ik} \cdot \underline{x} \end{vmatrix} = 0 \tag{A1.4}$$

Using the relationships for $z_{p_{ij}}'$ and $z_{p_{ik}}'$, in equation (A1.3), (A1.4)→

$$= [(h_{p_{ij}} \cdot \underline{x})^T, (h_{p_{ik}} \cdot \underline{x})^T] \begin{vmatrix} R_1^{-1} & 0 \\ 0 & R_2^{-1} \end{vmatrix} \begin{vmatrix} z_i - h_i \cdot \underline{x} \\ z_i - h_i \cdot \underline{x} \end{vmatrix} = 0 \tag{A1.5}$$

$$= [(h_{p_{ij}} \cdot \underline{x})^T R_1^{-1}(z_i - h_i \cdot \underline{x}) + (h_{p_{ik}} \cdot \underline{x})^T R_2^{-1}(z_i - h_i \cdot \underline{x})] = 0 \qquad \text{(A1.6)}$$

$$= [(h_{p_{ij}} \cdot \underline{x})^T R_1^{-1} + (h_{p_{ik}} \cdot \underline{x})^T R_2^{-1}] \cdot (z_i - h_i \cdot \underline{x}) = 0 \qquad \text{(A1.7)}$$

If $R_1 = R_2 = R$, then equation (A1.7) becomes

$$[(h_{p_{ij}} \cdot \underline{x} + h_{p_{ik}} \cdot x)^T R^{-1} (z - h_i \cdot \underline{x})] = 0 \qquad \text{(A1.8)}$$

Using equation (A1.3) above, this becomes

$$= [(h_i \cdot \underline{x})^T R^{-1} (z - h_i \cdot \underline{x})] = 0 \qquad \text{(A1.9)}$$

This is the same condition for the minimum as given by W.L.S. without pseudo line-flow creation. Pseudo line-flow creation therefore does not modify the minimum variance properties of W.L.S. estimates.

APPENDIX A.2

PROPERTIES OF ESTIMATES RESULTING FROM PSEUDO LINE-FLOW CREATION USING METHOD (2)

The estimation algorithm is

$$(\underline{H}_a^T(\hat{\underline{x}}_i)^T \underline{R}_a^{-1} \underline{H}_a(\hat{\underline{x}}_i))\Delta\underline{x}_i = \underline{H}_a^T(\hat{\underline{x}}_i)\ \underline{R}_a^{-1}\ [z' - h_a(\hat{\underline{x}}_i)] \tag{A2.1}$$

The requirement for a minimum is that

$$\underline{H}_a^T(\hat{\underline{x}})\ \underline{R}_a^{-1}\ [\underline{z}' - \underline{h}_a(\hat{\underline{x}})] = \underline{0} \tag{A2.2}$$

A2.1 Estimation error, $\hat{\delta}_x = \underline{x} - \hat{\underline{x}}$

Since

$$\begin{aligned} z_{p_{ij}}' &= z_{p_i} \frac{h(\underline{x})_{p_{ij}}}{h(\underline{x})_{p_i}} \\ z_{p_{i\ell}}' &= z_{p_i} \frac{h(\underline{x})_{p_{i\ell}}}{h(\underline{x})_{p_i}} \\ &\vdots \qquad\qquad \vdots \\ z_{p_{ik}}' &= z_{p_i} \frac{h(\underline{x})_{p_{ik}}}{h(\underline{x})_{p_i}} \end{aligned} \tag{A2.3}$$

and consider injection measurements only in the state estimation

$$\underline{z}' = \underline{z} \circ \underline{h}_p^{-1}(\underline{x}) \circ \underline{h}_a(\underline{x}) \tag{A2.4}$$

and

$$\underline{z} = \underline{h}(\underline{x}) + \underline{\eta} \tag{A2.5}$$

Substituting (A2.5) into (A2.4) gives

$$\underline{z}' = (\underline{h}(\underline{x}) + \underline{\eta})\ \underline{h}_p^{-1}(\underline{x})\underline{h}_a(\underline{x}) \tag{A2.6}$$

Substitute (A2.6) into (A2.2)

$$\underline{H}_a^T(\underline{x})\ \underline{R}_a^{-1}[h(\underline{x})\ \underline{h}_p^{-1}(\underline{x})\ \underline{h}_a(\underline{x}) + \underline{h}_p^{-1}(\underline{x})\ \underline{h}_a(\underline{x})\ \underline{\eta} - \underline{h}_a(\hat{\underline{x}})] = \underline{0}$$

Assume that $\delta\underline{x}$ is small, and set

$$\underline{h}_a(\underline{x}) = \underline{h}_a(\hat{\underline{x}}) + \underline{H}_a(\underline{x})\ \delta\underline{x}$$

$$\rightarrow \underline{H}_a^T(\underline{x})\ \underline{R}_a^{-1}\ [\underline{h}(\underline{x})\ \underline{h}_p^{-1}(\underline{x})\ \underline{h}_a(\underline{x}) + \underline{h}_p^{-1}(\underline{x})\ \underline{h}_a(\underline{x})\cdot\underline{\eta} - \underline{h}_a(\underline{x}) + \underline{H}_a(\underline{x})\delta\underline{x}] = \underline{0}$$

i.e.

$$(\underline{H}_a^T(\underline{x})\underline{R}_a^{-1}\underline{H}_a(\underline{x}))\delta\underline{x} = \underline{H}_a^T(\underline{x})\ \underline{R}_a^{-1}[\underline{h}(\underline{x})\underline{h}_p^{-1}(\underline{x})\underline{h}_a(\underline{x}) - \underline{h}_a(\underline{x})) + \underline{h}_p^{-1}(\underline{x})\underline{h}_a(\underline{x})\cdot\underline{\eta}]$$

i.e.

$$\delta\underline{x} = (\underline{H}_a^T(\underline{x})\underline{R}_a^{-1}\underline{H}_a(\underline{x}))^{-1}\underline{H}_a^T(\underline{x})\ \underline{R}_a^{-1}\underline{h}_a(\underline{x})\ [(\underline{h}(\underline{x})\ \underline{h}_p^{-1}(\underline{x}) - \underline{I}) + \underline{h}_p^{-1}(\underline{x})\cdot\underline{\eta}] \tag{A2.7}$$

Thus the estimation error clearly depends on both state and measurement uncertainties in a complicated manner.

Compare for exact W.L.S.,

$$\delta\underline{x} = (\underline{H}^T(\underline{x})\ \underline{R}^{-1}\ \underline{H}(\underline{x}))^{-1}$$

A2.2 Variance of $\hat{\underline{x}}$

Clearly from (A2.7)

$$E\{\delta\underline{x}\delta\underline{x}^T\} = \underline{M}(\underline{x})E\{(\underline{h}(\underline{x})\underline{h}_p^{-1}(\underline{x}) - \underline{I}) + \underline{h}_p^{-1}(\underline{x})\underline{\eta}\}\{(\underline{h}(\underline{x})\underline{h}_p^{-1}(\underline{x}) - \underline{I}) + \underline{h}_p(\underline{x})\underline{\eta}\}^T\underline{M}(\underline{x})$$

where $$\underline{M}(\underline{x}) = (\underline{H}_a^T(\underline{x})\underline{R}_a^{-1}\ \underline{H}_a(\underline{x}))^{-1}\ \underline{H}_a^T(\underline{x})\ \underline{R}_a^{-1}\ \underline{h}_a(\underline{x})$$

Thus $E\{\delta\underline{x}\ \delta\underline{x}^T\} = \underline{M}(\underline{x})\ \underline{h}_p^{-1}(\underline{x})\ E\{\underline{\eta}\ \underline{\eta}^T\}\ (\underline{h}_p^{-1}(\underline{x}))^T\ \underline{M}^T(\underline{x})$

Since $E\{\delta\underline{x}\ \delta\underline{x}^T\} = \underline{R}^{-1}$

$$E\{\delta\underline{x}\ \delta\underline{x}^T\} = \underline{M}(\underline{x})\ \underline{h}_p^{-1}(\underline{x})\ \underline{R}^{-1}\ (\underline{h}_p^{-1}(\underline{x}))^T\ \underline{M}^T(\underline{x}) \tag{A2.8}$$

A2.3 Expectation of $\hat{\underline{x}}$

From (A2.7)

$$E\{\delta\underline{x}\} = E\{\underline{M}(\underline{x}) \quad [\underline{h}(\underline{x})\underline{h}_p^T(\underline{x}) - \underline{I}) + \underline{h}_p^{-1}(\underline{x})\underline{\eta}]$$

$$= \underline{M}(\underline{x}) \left(\underline{h}(\underline{x}) \, \underline{h}_p^{-1}(\underline{x}) - \underline{I}\right) \qquad \text{(A2.9)}$$

That is, $E\{\delta\underline{x}\} \neq 0$, thus estimator is biased. This fact can also be shown from a "linearized analysis", i.e.

$$\underline{H}_a(\underline{x}) \rightarrow \underline{H}_a$$

and

$$\underline{h}_a(\underline{x}) \rightarrow \underline{H}_a \cdot \underline{x}$$

$$\text{(A2.2)} \xrightarrow{\text{linearize}} \quad \underline{H}_a^T \underline{R}_a^{-1}(\underline{z}' - \underline{H}_a \, \underline{x}) = \underline{0} \qquad \text{(A2.10)}$$

$$\text{(A2.4)} \xrightarrow{\text{linearize}} \quad \underline{z}' = \underline{z}(\underline{K} \cdot \underline{x} \cdot \underline{H}_a \cdot \underline{x})$$

where $\underline{K}(\underline{x}) = \underline{h}_p^{-1}(\underline{x})$

and since $\underline{z} = \underline{H} \cdot \underline{x} + \underline{\eta}$

$$\underline{z}' = (\underline{H} \cdot \underline{x} + \underline{\eta}) \; \underline{K} \cdot \underline{x} \; \underline{H}_a \cdot \underline{x} \qquad \text{(A2.11)}$$

Re-arrange (A2.10) results in

$$\hat{\underline{x}} = (\underline{H}_a^T \underline{R}_a^{-1} \underline{H}_a)^{-1} \; \underline{H}_a \; \underline{R}_a^{-1} \; \underline{z}' = \underline{0}$$

$$\hat{\underline{x}} = (\underline{H}_a^T \underline{R}_a^{-1} \; \underline{H}_a)^{-1} \; \underline{H}_a^T \underline{R}_a^{-1} \; (\underline{H} \cdot \underline{x} \; \underline{K} \cdot \underline{x} \; \underline{H}_a \cdot \underline{x} + \underline{\eta} \cdot \underline{K} \cdot \underline{x} \; \underline{H}_a \cdot \underline{x})$$

i.e.

$$E\{\hat{\underline{x}}\} = (\underline{H}_a^T \underline{R}_a^{-1} \; \underline{H}_a)^{-1} \; \underline{H}_a^T \underline{R}_a^{-1} \; (\underline{H} \cdot \underline{x} \; \underline{K} \cdot \underline{x} \; \underline{H}_a \cdot \underline{x})$$

since $E\{\underline{\eta}\} = \underline{0}$ (A2.12)

$E\{\hat{\underline{x}}\} \neq \underline{x}$, so estimator is biased.

APPENDIX A.3

CONVERGENCE ANALYSIS

The following analysis is similar to Schweppe and Masiello's (1971) analysis for conditions on stability, based on the Σ gain. Schweppe and Masiello's stability concepts are extended to allow convergence analysis.

Consider the general form of the state estimator

$$\underline{L}(\underline{x}_k)\ (\underline{x}_{k+1} - \underline{x}_k) = \underline{G}(\underline{x}_k)\ (\underline{z} - \underline{h}(\underline{x}_k)) \tag{A3.1}$$

thus

$$\underline{x}_{k+1} = \underline{x}_k + \underline{L}^{-1}(\underline{x}_k)\ \underline{G}(\underline{x}_k)\ (\underline{z} - \underline{h}(\underline{x}_k)) \tag{A3.2}$$

$$= \underline{x}_k + \underline{L}^{-1}(\underline{x}_k)\ \underline{c}(\underline{x}_k) \tag{A3.3}$$

where

$$\underline{c}(\underline{x}_k) = -\tfrac{1}{2}\frac{\partial J(\underline{x}_k)}{\partial \underline{x}} = \underline{G}(\underline{x}_k)\ [\underline{z} - \underline{h}(\underline{x}_k)] \tag{A3.4}$$

Let $\hat{\underline{x}}$ be the value of $\underline{x}$ which minimizes $J(\underline{x})$ so

$$\underline{c}(\hat{\underline{x}}) = \underline{0} \tag{A3.5}$$

Define

$$\underline{\delta}_k = \underline{x}_k - \hat{\underline{x}} \tag{A3.6}$$

A Taylor series about $\underline{c}(\underline{x})$ about $\underline{x}$, yields

$$\underline{c}(\underline{x}) = \underline{c}(\hat{\underline{x}}) + \underline{C}(\hat{\underline{x}})\ [\underline{x}_k - \hat{\underline{x}}] + \ldots \tag{A3.7}$$

That is,

$$\underline{c}(\underline{x}) = \underline{C}(\hat{\underline{x}})\ [\underline{x}_k - \hat{\underline{x}}] + \ldots \tag{A3.8}$$

since $\underline{c}(\hat{\underline{x}}) = \underline{0}$

$$\underline{x}_{k+1} = \underline{x}_k + \underline{L}^{-1}(\underline{x}_k)\ \underline{C}(\underline{x}_k)$$

$$= \underline{x}_k + \underline{L}^{-1}(\underline{x}_k)\ \underline{C}(\hat{\underline{x}})\ [\underline{x}_i - \hat{\underline{x}}] + \ldots \tag{A3.9}$$

$$\therefore \quad \underline{x}_{k+1} - \hat{\underline{x}} = \underline{x}_k - \hat{\underline{x}} + \underline{L}^{-1}(\underline{x}_k)\ \underline{C}(\hat{\underline{x}})\ [\underline{x}_i - \hat{\underline{x}}] + \ldots \tag{A3.10}$$

$$\underline{\delta}_{i+1} = [\underline{I} + \underline{L}^{-1}(\underline{x}_k)\ \underline{C}(\hat{\underline{x}})]\underline{\delta}_i + \text{higher terms} \tag{A3.11}$$

$$\simeq [\underline{I} + \underline{L}^{-1}(\underline{x}_k)\ \underline{C}(\underline{x}_k)]\underline{\delta}_i + \text{higher terms} \tag{A3.12}$$

Note from (A3.3)

$$\underline{C}(\underline{x}_k) = \frac{\partial}{\partial \underline{x}}\ [-\underline{G}(\underline{x}_k)\ \underline{h}(\underline{x}_k) + \underline{G}(\underline{x}_k)\ \underline{z}\ ] \tag{A3.13}$$

$$= -\left(\frac{\partial}{\partial \underline{x}}\ \underline{G}(\underline{x}_k)\right)\ \underline{h}(\underline{x}_k) - \underline{G}(\underline{x}_k)\ \underline{H}(\underline{x}_k) + \left(\frac{\partial}{\partial \underline{x}}\ \underline{G}(\underline{x}_k)\right)\underline{z} \tag{A3.14}$$

$$= -\underline{G}(\underline{x}_k)\ \underline{H}(\underline{x}_k) + \left(\frac{\partial}{\partial \underline{x}}\ \underline{G}(\underline{x}_k)\right)\ (\underline{z} - \underline{h}(\underline{x}_k)) \tag{A3.15}$$

$$\simeq -G(\underline{x}_k)\ \underline{H}(\underline{x}_k)$$

since $(\underline{z} - h(\underline{x}_k))$ will tend to zero at the minimum. Thus (A3.12) becomes

$$\underline{\delta}_{i+1} \simeq \underline{I} - \underline{h}^{-1}(\underline{x}_k)\ \underline{G}(\underline{x}_k)\ \underline{H}(\underline{x}_k)\ \underline{\delta}_i + \text{higher terms} \tag{A3.16}$$

Ignoring higher order terms of the Taylor series expansion, (A3.7); the rate of convergence, for the general form of the state estimator, is given by the eigenvalues of $(\underline{I} - \underline{L}^{-1}(\underline{x}_k)\ \underline{G}(\underline{x}_k)\ \underline{H}(\underline{x}_k))$. Fast convergence occurs as the eigenvalues approach zero, while instability occurs when the eigenvalues exceed unity.

APPENDIX A4

CONVERGENCE ANALYSIS OF W.L.S. WITH AND WITHOUT PSEUDO LINE-FLOW CREATION OR INFORMATION MATRIX MODIFICATION

A4.1 W.L.S. STATE ESTIMATION

Consider W.L.S. estimation without pseudo line-flow creation or information matrix modification. The form of the algorithm is

$$(\underline{H}^T(\underline{x}_k)\ \underline{R}^{-1}\ \underline{H}(\underline{x}_k))\Delta\underline{x}_{k+1} = \underline{H}^T(\underline{x}_k)\ \underline{R}^{-1}(\underline{z} - \underline{h}(\underline{x}_k)) \qquad \text{(A4.1)}$$

Using the convergence-eigenvalue expression, (A3.16), the convergence rate for W.L.S. depends on the eigenvalues of

$$[\underline{I} - (\underline{H}^T(\underline{x}_k)\ \underline{R}^{-1}\underline{H}(\underline{x})_k)^{-1}\ (\underline{H}^T(\underline{x}_k)\underline{R}^{-1}\underline{H}(\underline{x}_k))] \qquad \text{(A4.2)}$$

$$= [\ \underline{I} - \underline{I}\ ] \qquad \text{(A4.3)}$$

That is, the eigenvalues are $\underline{0}$, $\underline{0}$.

Convergence is thus very rapid. In practice, "line-flow only" measurement sets in W.L.S. converge in three iterations to a tolerance of 0.00001 p.u. while "injection-only" measurement sets converge in four iterations to within 0.00001 p.u. The slight difference in convergence is due to higher order effects in the Taylor series expansion which were ignored. For most purposes however such discrimination, involving the higher order terms, is unnecessary.

A4.2 METHOD 1

Consider W.L.S. state estimation when pseudo line-flow creation is used via method 1. The form of the algorithm is

$$(\underline{H}_a^T(\underline{x}_k)\ \underline{R}_{a_L}^{-1}\ \underline{H}_a(\underline{x}_k))\Delta\underline{x}_{k+1} = \underline{H}_a^T(\underline{x}_k)\ \underline{R}_{a_R}^{-1}(\underline{z}_a - \underline{h}_a(\underline{x})) \tag{A4.4}$$

The rate of convergence depends on the eigenvalues of

$$[\ \underline{I} - (\underline{H}_a^T(\underline{x}_k)\ \underline{R}_{a_L}^{-1}\ \underline{H}_a(\underline{x}_k))^{-1}\ (\underline{H}_a(\underline{x}_k)\ \underline{R}_{a_R}^{-1}\ \underline{H}_p(\underline{x}_k))] \tag{A4.5}$$

These eignevalues are not zero.

A4.3 METHOD 2

Consider W.L.S. state estimation when pseudo line-flow creation is used via method 2. The form of the algorithm is the same as method 1. However in the calculation of the convergence eigenvalues, from Appendix A3,

$$\underline{C}(\underline{x}_k) = \frac{\partial}{\partial \underline{x}}\ [-\ \underline{H}_a^T\ (\underline{x}_k)\ \underline{R}_{a_R}^{-1}\ \underline{h}(\underline{x}_k) + \underline{H}_a^T\ (\underline{x}_k)\ \underline{R}_{a_R}^{-1}\ \underline{z}_a] \tag{A4.6}$$

where $$z_a = z_a(\underline{x}_k) = \underline{z} \cdot \underline{h}_p^{-1}(\underline{x}_k)\ \underline{h}_a(\underline{x}_k) \tag{A4.7}$$

Clearly the convergence eigenvalue expressions will now depend on the measurement properties, $\underline{z}$, as well as on the state $\underline{x}_k$. That is,

$$\begin{aligned}\underline{C}(\underline{x}_k) = &- \left(\frac{\partial}{\partial \underline{x}}\ \underline{H}_a^T(\underline{x}_k)\right)\underline{R}_{a_R}^{-1}\ \underline{h}_p(\underline{x}_k) - \underline{H}_a^T(\underline{x}_k)\ \underline{R}_{a_R}^{-1}\ \underline{H}_p(\underline{x}_k) \\ &+ \left(\frac{\partial}{\partial \underline{x}}\ \underline{H}_a^T(\underline{x}_k)\right)\ \underline{R}_{a_R}^{-1}\ \underline{z}\ \underline{h}_p^{-1}(\underline{x}_k)\ \ \underline{h}_a(\underline{x}_k) \\ &+ \underline{H}_a^T(\underline{x}_k)\ \underline{R}_{a_R}^{-1}\ \underline{z}\left[\frac{\partial}{\partial \underline{x}}\ \underline{h}_p^{-1}(\underline{x}_k)\right]\underline{h}_a(\underline{x}_k) \\ &+ \underline{H}_a^T(\underline{x}_k)\ \underline{R}_{a_R}^{-1}\underline{z}\ \underline{h}_p^{-1}(\underline{x}_k)\ \underline{H}_a(\underline{x}_k)\end{aligned} \tag{A4.8}$$

and the convergence is given by the eigenvalues of

$$\underline{\delta}_{i+1}\quad [\underline{I} - (\underline{H}_a^T(\underline{x}_k)\ \underline{R}_{a_L}^{-1}\ \underline{H}_a(\underline{x}_k))^{-1}\ \underline{C}(\underline{x}_k)] \tag{A4.9}$$

A4.4 METHOD 3

Consider W.L.S. state estimation when method 3 is used to form the information matrix. The form of the algorithm is

$$(\underline{H}_a^T(\underline{x}_k)\ \underline{R}_a^{-1}\ \underline{H}_a(\underline{x}_k))\Delta\underline{x}_k = \underline{H}^T(\underline{x}_k)\ \underline{R}^{-1}\ (\underline{z} - \underline{h}(\underline{x})) \tag{A4.10}$$

The rate of convergence for this method depends on the eigenvalues of

$$[\ \underline{I} - \underline{H}_a^T(\underline{x}_k)\ \underline{R}_a^{-1}\ \underline{H}_a(\underline{x}_k))^{-1}(\underline{H}^T(\underline{x}_k)\ \underline{R}^{-1}\ \underline{H}(\underline{x}_k))] \tag{A4.11}$$

Using the identity that

$$[\ \underline{I} - \underline{A}^{-1}\ \underline{B}\ ] \equiv \underline{A}^{-1}\ [\ -\underline{A} + \underline{B}\ ] \tag{A4.12}$$

(A4.11) can be rewritten as

$$(\underline{H}_a^T(\underline{x}_k)\ \underline{R}_a^{-1}\ \underline{H}_a(\underline{x}_k))^{-1}[(\underline{H}^T(\underline{x}_k)\ \underline{R}^{-1}\ \underline{H}(\underline{x}_k)) - (\underline{H}_a^T(\underline{x}_k)\ \underline{R}_a^{-1}\underline{H}_a(\underline{x}_k))] \tag{A4.13}$$

These eigenvalues are not zero.

A4.5 METHOD 4

Consider W.L.S. state estimation when method 4 is used to modify the information matrix

$$\left(\underline{H}^T(\underline{x}_k)\ \underline{R}^{-1}\ \underline{H}(\underline{x}_k)\right)^{op}\ \Delta\underline{x}_{k+1} = \underline{H}^T(\underline{x}_k)\underline{R}^{-1}(\underline{z} - \underline{h}(\underline{x})) \tag{A4.14}$$

where $$\left[\underline{H}^T(\underline{x}_k)\ \underline{R}^{-1}\ \underline{H}(\underline{x}_k)\right]^{op} = \underline{H}^T(\underline{x}_k)\underline{R}^{-1}\underline{H}(\underline{x}_k) \quad \text{if } Y_{ij} \neq 0$$

$$= 0 \quad \text{otherwise.}$$

The rate of convergence for this method depends on the eigenvalues of

$$[\underline{I} - (\underline{H}^T(\underline{x}_k)\ \underline{R}^{-1}\ \underline{H}(\underline{x}_k))^{op}\ (\underline{H}^T(\underline{x}_k)\ \underline{R}^{-1}\ \underline{H}(\underline{x}_k))] \tag{A4.15}$$

or using the matrix identity, (A4.12); (A4.15) can be rewritten as

$$\left((\underline{H}^T(\underline{x}_k)\ \underline{R}^{-1}\underline{H}(\underline{x}_k))^{op}\right)^{-1}[(\underline{H}^T(\underline{x}_k)\ \underline{R}^{-1}\ \underline{H}(\underline{x}_k)) - (\underline{H}^T(\underline{x}_k)\ \underline{R}^{-1}\underline{H}(\underline{x}_k))] \tag{A4.16}$$

APPENDIX A.5

INVARIANCE OF COUCH ET AL. SIMULTANEOUS UPDATE (1.4.1) DECOUPLING WITH RESPECT TO VARIATIONS IN THE RATIO OF $\underline{R}_p^{-1}$ TO $\underline{R}_q^{-1}$

The convergence eigenvalues for Couch et al. simultaneous update, (1.4.1) are given by

$$\begin{bmatrix} \underline{0} & -(\underline{h}_{11}^T \underline{R}_p^{-1} \underline{h}_{11})^{-1}(\underline{h}_{11}^T \underline{R}_p^{-1} \underline{h}_{21}) \\ -(\underline{h}_{22}^T \underline{R}_q^{-1} \underline{h}_{22})^{-1}(\underline{h}_{22}^T \underline{R}_q^{-1} \underline{h}_{12}) & \underline{0} \end{bmatrix} \tag{A5.1}$$

It remains to show that when the R/X ratio of all lines within the power system are constant, equal to α,

$$\underline{h}_{11} = \alpha \, \underline{h}_{21}$$

and (A5.2)

$$\underline{h}_{22} = \alpha \, \underline{h}_{12}$$

and so (A5.1) becomes invariant of the ratio of $\underline{R}_p^{-1} : \underline{R}_q^{-1}$.

Consider P_{ij}

$$P_{ij} = v_i^2 \, G_{ii} + c_{ij} \tag{A5.3}$$

Diagonal elements ($\underline{h}_{11}$)

$$\frac{\partial P_{ij}}{\partial \theta_i} = d_{ij} \tag{A5.4}$$

$$\frac{\partial P_{ij}}{\partial \theta_k} = - d_{ij} \tag{A5.5}$$

off-diagonal elements ($\underline{h}_{21}$)

$$v_i \frac{\partial P_{ij}}{\partial v_i} = 2 \, v_i^2 \, G_{ij} + c_{ij} \tag{A5.6}$$

$$v_i \frac{\partial P_{ij}}{\partial v_j} = c_{ij} \tag{A5.7}$$

where in cartesian components, $\underline{v} = e_i + jf = v_i \angle \theta_i$

$$c_{ij} = - e_i a_{ij} - f_i b_{ij} \tag{A5.8}$$

$$d_{ij} = e_i b_{ij} - f_i a_{ij} \tag{A5.9}$$

$$a_{ij} = e_j G_{ij} - f_j B_{ij} \tag{A5.10}$$

$$b_{ij} = e_j B_{ij} + f_j G_{ij} \tag{A5.11}$$

When all lines have the same R/X ratio, α,

$$B_{ij} = - \alpha G_{ij} \tag{A5.12}$$

$\therefore$ (A5.10) and (A5.11) become

$$c_{ij} = e_j G_{ij} + f_j \alpha G_{ij} \tag{A5.13}$$

$$b_{ij} = - \alpha e_j G_{ij} + f_j G_{ij} \tag{A5.14}$$

while (A5.8) and (A5.9)

$$\therefore \; c_{ij} = - e_i e_j G_{ij} - e_i f_j \alpha G_{ij} + f_i e_j \alpha G_{ij} - f_i f_j G_{ij} \tag{A5.15}$$

and

$$d_{ij} = - e_i e_j \alpha G_{ij} + e_i f_j G_{ij} - f_i e_j G_{ij} - f_i f_j \alpha G_{ij} \tag{A5.16}$$

$$= \alpha c_{ij} + (e_i f_j - f_i e_j)(1 + \alpha^2) G_{ij} \tag{A5.17}$$

Consider Q_{ij}

$$Q_{ij} = - 2 v_i^2 B_{ii} + d_{ij} \tag{A5.18}$$

where $$B_{ii} = B_{ij} + B_{ish} = - \alpha G_{ij} + B_{ish} \tag{A5.19}$$

Diagonal elements ($\underline{h}_{22}$)

$$v_i \frac{\partial Q_{ij}}{\partial v_i} = -2 v_i^2 B_{ii} + d_{ij} \tag{A5.20}$$

$$v_j \frac{\partial Q_{ij}}{\partial v_j} = d_{ij} \tag{A5.21}$$

Off-diagonal elements ($\underline{h}_{12}$)

$$\frac{\partial Q_{ij}}{\partial \theta_i} = c_{ij} \tag{A5.22}$$

$$\frac{\partial Q_{ij}}{\partial \theta_j} = - c_{ij} \tag{A5.23}$$

Thus the condition that

$$\underline{h}_{11} \simeq \alpha \underline{h}_{21}$$

and (A5.24)

$$\underline{h}_{22} \simeq \alpha \underline{h}_{12}$$

occur when:

(i) $$d_{ij} = \alpha c_{ij} \tag{A5.25}$$

This requires that $(e_i f_j - f_i e_j)(1+\alpha^2) G_{ij}$ be small, and

(ii) $- 2v_i^2 B_{ii} \ll d_{ij}$ in (A5.20) and

(iii) $2v_i^2 G_{ij} \ll c_{ij}$ in (A5.6)

when conditions (i) - (iii) hold for P_{ij} and Q_{ij} they also hold for P_i and Q_i since

$$P_i = \sum_{j \varepsilon \{\alpha\}} P_{ij} \tag{A5.26}$$

and

$$Q_i = \sum_{j \varepsilon \{\alpha\}} Q_{ij} \tag{A5.27}$$

When not all lines have the same R/X ratio, the convergence-eigenvalues given by (A5.1) are bounded by the smallest R/X ratio of the test power system, i.e.

$$\underline{h}_{11} = \underline{\alpha}\, \underline{h}_{21} \tag{A5.28}$$

$$\underline{h}_{22} = \underline{\alpha}\, \underline{h}_{12} \tag{A5.29}$$

where $\underline{\alpha}$ is a vector of R/X ratios, then

$$\underline{h}_{11} \leq \alpha_{min} |\underline{I}| \underline{h}_{21} \tag{A5.30}$$

and

$$\underline{h}_{22} \leq \alpha_{min} |\underline{I}| \underline{h}_{12} \tag{A5.31}$$

since

$$\alpha_{min} |\underline{I}| < \underline{\alpha} \tag{A5.32}$$

APPENDIX A6

EFFECT OF MULTIPLE BAD DATA ON THE r_W AND r_N TESTS

6.1 SINGLE BAD DATA

Consider a single bad data point, present in the i^{th} measurement.

$$\underline{v} = \underline{v}_z + \underline{e}_i \alpha \qquad \text{where} \quad \underline{e}_i \alpha = \begin{vmatrix} 0 \\ 0 \\ 1 \\ 0 \end{vmatrix} \alpha \quad \text{say} \tag{A6.1}$$

The value of $J(\hat{\underline{x}})$ is given by

$$\begin{aligned} J(\hat{\underline{x}}) &= \hat{\underline{r}}^T \underline{R}^{-1} \hat{\underline{r}} = \underline{v}^T \underline{R}^{-1} \underline{W} \underline{v} \\ &= \underline{v}_z^T \underline{R}^{-1} \underline{W} \underline{v}_z + 2\alpha \underline{e}_i^T \underline{R}^{-1} \underline{W} \underline{v}_z + \alpha^2 \underline{e}_i^T \underline{R}^{-1} \underline{W} \underline{e}_i \end{aligned} \tag{A6.2}$$

where $\underline{v}_z$ is the normal component of measurement error ($<3\sigma_i$);

$\hat{\underline{r}}$ is the residual vector, $\underline{r} = \underline{z} - \underline{h}(\hat{\underline{x}})$; and

$\underline{W}$ is the residual sensitivity matrix.

As the number of measurements present, K, become large, it can be shown (Handschin *et al.*, 1975) that $J(\hat{x})$ approaches a normal distribution with mean μ_J and variance σ_J^2

$$\mu_J = K + \frac{\alpha^2}{\sigma_i^2} W_{ii} \quad \text{and} \quad \sigma_J^2 = 2K + \frac{4\alpha^2}{\sigma_i^2} W_{ii} \tag{A6.3}$$

The distortion, $\frac{\alpha^2}{\sigma_i^2} W_{ii}$ comes from the multiplication of $\alpha^2 \underline{e}_i^T \underline{R}^{-1} \underline{W} \underline{e}_i$, i.e.

$$\alpha^2 \begin{bmatrix} 0 \\ 0 \\ 1 \\ 0 \end{bmatrix}^T \begin{bmatrix} R_1^{-1} & 0 & 0 & 0 \\ 0 & R_2^{-1} & 0 & 0 \\ 0 & 0 & R_3^{-1} & 0 \\ 0 & 0 & 0 & R_4^{-1} \end{bmatrix} \begin{bmatrix} w_{11} & w_{12} & w_{13} & w_{14} \\ w_{21} & w_{22} & w_{23} & w_{24} \\ w_{31} & w_{32} & w_{33} & w_{34} \\ w_{41} & w_{42} & w_{43} & w_{44} \end{bmatrix} \begin{bmatrix} 0 \\ 0 \\ 1 \\ 0 \end{bmatrix} = \frac{\alpha^2}{\sigma_3^2} W_{33} \tag{A6.4}$$

Standardized variables, Σ_1 and Σ_2, are calculated from μ_J and σ_J, where

$$\Sigma_1 = N\left[\frac{\mu_J - K}{2\sqrt{K}}, \quad \frac{\sigma_J^2}{2K}\right]$$

and (A6.5)

$$\Sigma_2 = N\left[\sqrt{2\mu_J} - \sqrt{2K}, \frac{\sigma_J^2}{2\mu_J}\right]$$

Σ_1 and Σ_2 are used in calculating the power of the $J(\hat{\underline{x}})$, which reflects the capability of the $\underline{r}_N$ test. This test accurately detects and identifies single bad data because it can be shown that for single bad data present in measurement i,

$$|W_{ii}| > |W_{ij}| \tag{A6.6}$$

6.2 MULTIPLE NON-INTERACTING BAD DATA

Consider multiple non-interacting bad data present (at i = 1,2 and 3)

$$\underline{v} = \underline{v}_z + \sum_{i=1}^{k} \underline{e}_i \, \underline{\alpha}_i$$

where $$\sum_{i=1}^{k} \underline{e}_i \, \underline{\alpha}_i = \alpha_1 \begin{vmatrix} 1 \\ 0 \\ 0 \\ 0 \end{vmatrix} + \alpha_2 \begin{vmatrix} 0 \\ 1 \\ 0 \\ 0 \end{vmatrix} + \alpha_3 \begin{vmatrix} 0 \\ 0 \\ 1 \\ 0 \end{vmatrix} \quad \text{say} \tag{A6.7}$$

The product $(\alpha \, \underline{e}_i)^T \, \underline{R}^{-1} \, \underline{W}(\alpha \, \underline{e}_i)$ now becomes

$$\left(\frac{\alpha_1^2}{\sigma_1^2} W_{11} + \frac{\alpha_2^2}{\sigma_2^2} W_{22} + \frac{\alpha_3^2}{\sigma_3^2} W_{33} \right) \tag{A6.8}$$

Provided the bad data locations are not clustered around any one node, the power of the $J(\hat{\underline{x}})$ test will still accurately reflect the distortion in the estimates because it will hold at the individual bad data locations, and the $\underline{r}_N$ test will locate such bad data.

6.3 MULTIPLE INTERACTING BAD DATA (at i = 1, 2 and 3)

Bongers does not represent the detection of multiple interacting bad data. Multiple interacting bad data represents a worse-case failure and can happen when all the measurements from one switchyard are transmitted over the same communication channel, or when several power flow meters use a common potential transformer (Handschin *et al.*, 1975). Also, due to the random nature of bad data, multiple interacting bad data can be represented by

$$\underline{v} = \underline{v}_z + \underline{e\alpha}_i \tag{A6.9}$$

where $\underline{e\alpha}_i = \begin{bmatrix} \alpha_1 \\ \alpha_2 \\ \alpha_3 \\ 0 \end{bmatrix}$

The produce $(\underline{e\alpha}_i)^T \underline{R}^{-1} \underline{W}(\underline{\alpha e}_i)$ now becomes

$$\alpha_1 R_1^{-1}(W_{11}\alpha_1 + W_{12}\alpha_2 + W_{13}\alpha_3) + \alpha_2 R_2^{-1}(W_{21}\alpha_1 + W_{22}\alpha_2 + W_{23}\alpha_3)$$
$$+ \alpha_3 R_3^{-1}(W_{31}\alpha_1 + W_{32}\alpha_2 + W_{33}\alpha_3) \tag{A6.10}$$

When multiple interacting bad data is present, off-diagonal values of $\underline{W}$ may become negative and can be of greater magnitude than diagonal values, and the r_n test no longer holds

6.4 EXAMPLE INVOLVING THE $\underline{r}_N$ AND $\underline{r}_W$ TESTS

Tests were performed on the 5 bus 7 line system (Stagg and El-Abiad, 1968), shown in Figure 3.5, to evaluate the effectiveness of $\underline{r}_W$ and $\underline{r}_N$ tests in the presence of single and multiple bad data. Measurement system 2, outlined in section 6.3, having 1 voltage magnitude, 2 real and reactive line-flow measurements, and 5 real

and reactive injection measurements was used as the basis for the tests. Table A6.1 shows the normalized and weighted residuals that result with and without the bad data present. A portion of the residual sensitivity matrix, with and without the bad data present, is shown in Table A6.2. The inclusion of a single bad data point, of size 10σ, at P_{11}, is easily identified by both $\underline{r}_W$ and $\underline{r}_N$ tests. Little change occurs in the values of the residual sensitivity matrix when a single bad data is present. However the inclusion of multiple bad data of size 10σ, at Q_1, Q_{1-2} and Q_{1-3}, distorts the residual sensitivity matrix. Terms differ and off-diagonal terms may exceed diagonal values, e.g. $W_{Q_1,Q_2} > W_{Q_1,Q_1}$. In such cases the residual sensitivity matrix cannot be calculated off-line and stored, ready to be used to calculate $\underline{r}_N$. Both the $\underline{r}_N$ test and the $\underline{r}_W$ test identify the same measurements as being bad data. Some of these measurements contain bad data, while others do not (i.e., Q_2). If suspect measurements are ordered according to the size of their normalised or weighted residuals, the $\underline{r}_W$ test gives a more correct ranking (Q_{1-3}, Q_{1-2}, Q_2, Q_1) than the ranking (Q_{1-3}, Q_2, Q_{1-2}, Q_1) given by the $\underline{r}_N$ test.

Table A6.1 Comparison of r_N and r_W values for single and multiple bad data present.

MEASUREMENT LOCATION	NO BAD DATA PRESENT		SINGLE BAD DATA, SIZE 10σ AT P_1		MULTIPLE BAD DATA, SIZE 10σ, AT Q_{1-2}, Q_{1-3} AND Q_1	
	r_N	r_W	r_N	r_W	r_N	r_W
V_1	0.000	0.000	0.26835	0.11421	2.08139	1.16191
P_{1-2}	"	"	-4.52873	3.79133	0.12774	0.10554
P_{1-3}	"	"	1.47011	1.42289	0.07689	0.07477
P_{2-3}	"	"	0.65543	0.63072	0.03248	0.03146
P_{2-5}	"	"	1.01767	0.88631	0.11300	0.10002
P_{3-4}	"	"	0.43413	0.36726	0.06699	0.07066
P_{4-2}	"	"	0.69999	0.67493	0.03863	0.03742
P_{5-4}	"	"	0.07926	0.07563	0.08864	0.08426
Q_{1-2}	"	"	0.11349	0.09482	5.49278	3.95224
Q_{1-3}	"	"	0.08225	0.07937	12.11488	11.68607
Q_{2-3}	"	"	0.03464	0.03332	0.19929	0.19176
Q_{2-5}	"	"	0.05997	0.05206	1.68754	1.48558
Q_{3-4}	"	"	0.08173	0.06878	0.87264	0.87790
Q_{4-2}	"	"	0.12164	0.11675	0.14783	0.14328
Q_{5-4}	"	"	0.00000	0.00000	0.39626	0.37975
P_1	"	"	6.91334	4.78683	0.26525	0.18127
P_2	"	"	2.50025	1.45855	0.05651	0.03755
P_3	"	"	2.42499	1.58813	0.07635	0.07848
P_4	"	"	1.71941	1.11780	0.06375	0.05431
P_5	"	"	1.12293	0.77643	0.10659	0.13657
Q_1	"	"	0.25372	0.17216	4.79384	2.26417
Q_2	"	"	0.45191	0.24513	8.58860	3.75687
Q_3	"	"	0.43163	0.26610	0.63651	0.50765
Q_4	"	"	0.30114	0.18449	0.36434	0.37599
Q_5	"	"	0.27771	0.18406	2.26939	1.56496

Table A6.2 Selected segments of the residual sensitivity matrix with and without single and multiple bad data present.

J \ K	SAMPLE ELEMENTS OF THE RESIDUAL SENSITIVITY MATRIX $w_{J,K}$						
	P_1	P_2	P_3	P_4	P_5	Q_1	Q_2
(1) No Bad Data Present							
P_1	0.47802	0.14390	0.15771	0.13084	0.07859	-0.01676	-0.02495
P_2	0.14390	0.34313	0.17709	0.16148	0.16132	-0.00797	-0.00920
Q_1	-0.01676	-0.00799	0.00651	0.00511	-0.00117	0.45923	0.12168
Q_2	-0.24466	-0.00919	0.00049	0.00927	0.00371	0.12168	0.29459
(2) Single Bad Data, size 10σ and P_1							
P_1	0.47942	0.14394	0.15813	0.11284	0.07796	-0.01663	-0.02505
P_2	0.14394	0.34031	0.17611	0.16268	0.16349	-0.01099	-0.00844
Q_1	-0.01663	-0.01098	0.00550	0.00816	-0.00121	0.46045	0.11774
Q_2	-0.02505	-0.00844	0.00283	0.00499	0.00477	0.11774	0.29423
(3) Multiple Bad Data, size 10σ and Q_{1-2}, Q_{1-3}, Q_1							
P_1	0.46762	0.16591	0.00379	0.23375	0.10294	-0.28613	0.37148
P_2	0.16591	0.44157	0.34344	-0.06913	0.10436	0.56924	-0.68220
Q_1	-0.28613	0.56924	-0.03442	-0.18928	-0.06934	0.22308	0.37496
Q_2	0.37148	-0.68220	-0.27712	0.54052	0.02995	0.37496	0.19133

APPENDIX A.7

MATHEMATICAL "REMOVAL" OF MEASUREMENT DATA

Mathematical "removal" is equivalent to physical "removal" of suspect bad data. The mechanism behind the mathematical removal of measurement data can be explained by reference to the 4×2 matrix $\underline{H}$ and the 4×1 column vector, $\underline{D}$, shown below, where

$$\underline{D} = \underline{R}^{-1}(\underline{z} - \underline{h}(\underline{x}))$$

$$\underline{H} = \begin{vmatrix} h_{11} & h_{12} \\ h_{21} & h_{22} \\ h_{31} & h_{32} \\ h_{41} & h_{42} \end{vmatrix} \qquad \underline{D} = \begin{vmatrix} D_1 \\ D_2 \\ D_3 \\ D_4 \end{vmatrix} \tag{A7.1}$$

Enforcing equation (6.10) at each iteration amounts to setting an element, i, of vector $\underline{z} - \underline{h}(\underline{x})$ equal to zero. Consider when D_3 equals zero, mathematical "removal" of D_3 corresponds to

$$\underline{H}^T\underline{D} = \begin{vmatrix} h_{11} & h_{21} & h_{31} & h_{41} \\ h_{12} & h_{22} & h_{32} & h_{42} \end{vmatrix} \begin{vmatrix} D_1 \\ D_2 \\ 0 \\ D_4 \end{vmatrix} = \begin{vmatrix} h_{11}\,D_1 + h_{21}\,D_2 + h_{41}\,D_4 \\ h_{21}\,D_1 + h_{22}\,D_2 + h_{42}\,D_4 \end{vmatrix} \tag{A7.2}$$

Physical removal of D_3 corresponds to

$$\underline{H}^T\underline{D} = \begin{vmatrix} h_{11} & h_{21} & h_{41} \\ h_{12} & h_{22} & h_{42} \end{vmatrix} \begin{vmatrix} D_1 \\ D_2 \\ D_4 \end{vmatrix} = \begin{vmatrix} h_{11}\,D_1 + h_{21}\,D_2 + h_{41}\,D_4 \\ h_{12}\,D_1 + h_{22}\,D_2 + h_{42}\,D_4 \end{vmatrix} \tag{A7.3}$$

Both "removal" methods generate the same R.H.S. in the state estimator equation. As a result they both converge to the same solution. This is because the matrices on the L.H.S. of the state estimator equation, equation (2.22), act only as a gain (Schweppe *et al.*, 1970). Extensive simulation shows that convergence is unaffected by "mathematical" removal of bad data.

A consequence of the mathematical "removal" technique is that the structure of lists and pointers in the state estimation algorithm can initially be set up to contain all the measurements that are available to the estimator. During operation, some pseudomeasurement will be unavailable due to presence of bad data, failure and/or maintenance. The presence of these "absent" measurements can be suspended from the state estimator simply by invoking the relationship in (6.10). No "dynamic" updating or re-ordering of lists is necessary to reduce the order of the system. The information matrix remains unchanged. When measurements become available the suspension can be lifted.

APPENDIX A.8

DERIVATION OF MEASUREMENT EQUATIONS FOR E_m, P_{2-3}, Q_{2-3} AND $|I|_{2-3}$

Consider the lossless, purely reactive tap transformer representation shown in Figure 7.1. For this representation

$$\begin{vmatrix} \underline{I}_{p_r} \\ \underline{I}_{sec} \end{vmatrix} = \begin{vmatrix} ja^2B & -jaB \\ -jaB & jB \end{vmatrix} \cdot \begin{vmatrix} \underline{V}_{p_r} \\ \underline{V}_{sec} \end{vmatrix} \tag{A8.1}$$

where the subscripts p_r and sec refer to the transformer primary and secondary windings respectively.

For the h.v.d.c. link shown, $\underline{I}_{pr} = I_{1-2}\angle 0$ and $\underline{I}_{sec} = I_{2-3}\angle 0$. This is due to the fact that the phase angle of the convertor current is defined to be zero. Also,

$$\underline{V}_{p_r} = V_m \angle \psi_m \quad \text{and} \quad \underline{V}_{sec} = E_m \angle \Phi_m$$

From equation (A8.1)

$$I_{2-3_I} = 0 = - a_m V_m \cos\psi_m + E_m \cos\Phi_m \tag{A8.2}$$

$$\therefore \quad \underline{E}_{m_r} = - a_m \underline{V}_{m_r} \tag{A8.3}$$

From equation (A8.1)

$$I_{2-3_r} = - a_m^2 B_m V_m \sin\psi_m + a_m B_m E_m \sin\Phi_m \tag{A8.4}$$

$$\therefore \quad \underline{E}_{m_I} = \frac{\underline{I}_{1-2_r} + a_m^2 B_m \underline{V}_{m_I}}{a_m} \tag{A8.5}$$

Since the transformer is lossless and $\underline{I}_{2-3}$ has a phase angle of zero, $I_{2-3}\angle 0$, $\underline{I}_{1-2}$ also has a phase angle of zero.

$$\therefore \quad \underline{I}_{1-2_r} = I_{1-2}$$

and
$$E_m = (\underline{E}_{m_r}^2 + \underline{E}_{m_I}^2)^{\frac{1}{2}} \tag{A8.6}$$

$$\therefore \quad E_m = \frac{a_m^4 B_m^2 V_m^2 + I_{1-2}^2 + 2 a_m^2 B_m I_{1-2} V_m \sin\psi_m}{a_m^2 B_m^2} \tag{A8.7}$$

Also

$$\underline{I}_{2-3_r} = I_{2-3} = a_m B_m V_m \sin\psi_m - B_m E_m \sin\Phi_m \tag{A8.8}$$

$$= a_m B_m \underline{V}_{m_I} - B_m \underline{E}_{m_I} \tag{A8.9}$$

Substitute (A8.5) for $\underline{E}_{m_I}$

$$\therefore \quad I_{2-3} = \frac{I_{1-2}}{a_m} \tag{A8.10}$$

and hence

$$P_{2-3} = \sqrt{3}\, I_{2-3}\, \underline{E}_{m_r} = \sqrt{3}\, I_{1-2}\, V_m \cos\psi_m \tag{A8.11}$$

$$Q_{2-3} = \sqrt{3}\, I_{2-3}\, \underline{E}_{m_I} = \sqrt{3}\, I_{1-2}\, V_m \sin\psi_m \tag{A8.12}$$

APPENDIX A.9

DERIVATION OF H.V.D.C. LINK "MINIMAL-STATE" REALIZATION MEASUREMENT EQUATIONS

The "minimal state" - space is given by

$$[\psi_m,\ a_m,\ \psi_n,\ a_n]$$

These states are in addition to the a.c. terminal bus magnitude states V_m and V_n.

The "minimal approximation error" h.v.d.c. link measurement equations are modified by re-arranging (7.2) and (7.5)

$$V_{dm} = K_1\ a_m\ V_m\ \cos\psi_m \tag{A9.1}$$

$$V_{dn} = K_1\ a_n\ V_n\ \cos\psi_n \tag{A9.2}$$

Re-arrange (7.7)

$$I_{dc} = (V_{dm} + V_{dn})/R_{dc}$$

and substitute (A9.1) and (A9.2) for V_{dm} and V_{dn}

$$I_{dc} = K_1\ (a_m\ V_m\ \cos\psi_m + a_n\ V_n\ \cos\psi_n)\ /\ R_{dc} \tag{A9.3}$$

Re-arrange (7.3)

$$\cos\alpha_m = (V_{dm} + K_2\ X_m\ I_{dc})\ /\ K_1\ a_m\ V_m$$

and substitute (A9.1) and (A9.3) for V_{dm} and I_{dc}

$$\cos\alpha_m = (R_{dc}\ a_m\ V_m\ \cos\psi_m + K_2\ X_m\ (a_m\ V_m\ \cos\psi_m + a_n\ V_n\ \cos\psi_n))\ /\ a_n\ V_n \tag{A9.4}$$

Re-arrange (7.1) and substitute

$$I_{1-2} = a_m K_1 (V_{dm} + V_{dn}) / R_{dc}$$

and substitute (A9.1) and (A9.2) for V_{dm} and V_{dn}

$$I_{1-2} = a_m K_1^2 (a_m V_m \cos\psi_m + a_n V_n \cos\psi_n) / R_{dc} \qquad (A9.5)$$

Substituting (A9.5) in (7.10), (7.12), (7.13), (7.14), (7.15) and (7.16) gives the entries of Table 7.3 for P_{1-2}, Q_{1-2}, E_m, P_{2-3}, Q_{2-3} and I_{2-3}. Finally, substitute (A9.1) and (A9.3) for V_{dm} and I_{dm} in (7.17), which gives the expression for P_{dm} in Table 7.3.

Inverter measurement equations can be derived in a similar fashion by replacing prefixes m by n, 1-2 by 5-6, 2-3 by 4-5, $\cos\alpha_m$ by $\cos\delta_n$ and X_m by $-X_n$. The four pseudomeasurements which contain the approximation error are now fully merged in the measurement set. Only the measurement equation for a_m and a_n do not contain approximation error effects. In some cases, approximation error equations have been used four times in reducing the original measurement equation to the form above, i.e. (A9.4).

APPENDIX A10

TO SHOW THE EXACT RELATIONSHIP BETWEEN α ψ AND δ IS MONOTONICALLY INCREASING FOR $\alpha < x < \pi - \alpha$

The exact relationship between α , ψ and δ is given by

$$f(x) = -\tan\psi + \frac{2x - 2\alpha + \sin 2\alpha - \sin 2x}{\cos 2\alpha - \cos 2x} \qquad \text{(A10.1)}$$

Thus

$$f'(x) = \frac{(\cos 2\alpha - \cos 2x)[2 - 2\cos 2x] - (2x - 2\alpha + \sin 2\alpha - \sin 2x)(2\sin 2x)}{(\cos 2\alpha - \cos 2x)^2} \qquad \text{(A10.2)}$$

substituting $\quad 2 - 2\cos 2x = 4\sin^2 x$

and $\quad 2\sin 2x = 4 \sin x \cos x$

results in

$$f'(x) = \left[\frac{4\sin x}{(\cos 2\alpha - \cos 2x)^2}\right](\cos 2\alpha \sin x - \cos 2\alpha \sin x - (2x - 2\alpha)\cos x - (2x - 2\alpha)\cos x + 2\cos(\alpha + x)\sin(x - \alpha)\cos x) \qquad \text{(A10.3)}$$

$$= \left[\frac{4\sin x}{(\cos 2\alpha - \cos 2x)^2}\right](2\sin(\alpha + x)\sin(x - \alpha)\sin x - 2 - (2x - 2\alpha)\cos x + 2\cos x(\alpha + x)\sin(x - \alpha)\cos x) \qquad \text{(A10.4)}$$

$$= \left[\frac{4\sin x}{(\cos 2\alpha - \cos 2x)^2}\right][(2\sin(x - \alpha)\cos(2x + \alpha) - 2(x - \alpha)\cos x)] \qquad \text{(A10.5)}$$

$$= \left[\frac{4\sin x}{(\cos 2\alpha - \cos 2x)^2}\right](2\cos\alpha \sin(x - \alpha) - 2(x - \alpha)\cos x) \qquad \text{(A10.6)}$$

$\dfrac{4\sin x}{(\cos 2\alpha - \cos 2x)^2}$ is positive for $0 < x < \pi$

and $(2\cos\alpha \sin(x-\alpha) - 2(x-\alpha)\cos x)$ can be shown to be positive for $\alpha < x < \pi - \alpha$. That is, since $\alpha > 0$, both terms in

$$2\cos\alpha \sin(x-\alpha) - 2(x-\alpha) \cos x \qquad \text{(A10.7)}$$

are >0 for $\frac{\pi}{2} < x < \pi$.

Equation (A10.7) can be rewritten as

$$2\cos\alpha \cos(x-\alpha) \tan(x-\alpha) - 2(x-\alpha) \cos x$$
$$= (\cos x + \cos(x-2\alpha)) \tan(x-\alpha) - 2(x-\alpha) \cos x.$$

Now $\tan(x-\alpha) > (x-\alpha)$ in the interval $0 < (x-\alpha) < \frac{\pi}{2}$ and $\cos(x-2\alpha) > \cos x > 0$ for $\alpha < x < \frac{\pi}{2}$. Hence, expression (A10.7) is greater than 0 for $\alpha < x < \frac{\pi}{2}$. Thus $f'(x) > 0$ for $\alpha < x < \frac{\pi}{2}$.

The function can be shown to be monotonically increasing by noting that

(i) At $x = \alpha$, and applying L'Hospitals rule

$$f(\alpha) = \frac{2 - 2\cos 2\alpha}{2\sin 2\alpha} = \tan\alpha - \tan\psi$$

Since for $\alpha < \frac{\pi}{2}$, $\alpha < \psi$ as the iteration scheme proceeds (since physically ψ is always greater than α).

Thus $f(\alpha) < 0$

(ii) At $x = \pi - \alpha$, from (A10.1),

$$f(\pi - \alpha) \to \infty$$

Thus the function is monotonically increasing since $f'(x)$ is greater than zero. The probable profile of the function, $f(x)$, is shown in Figure A10.1.

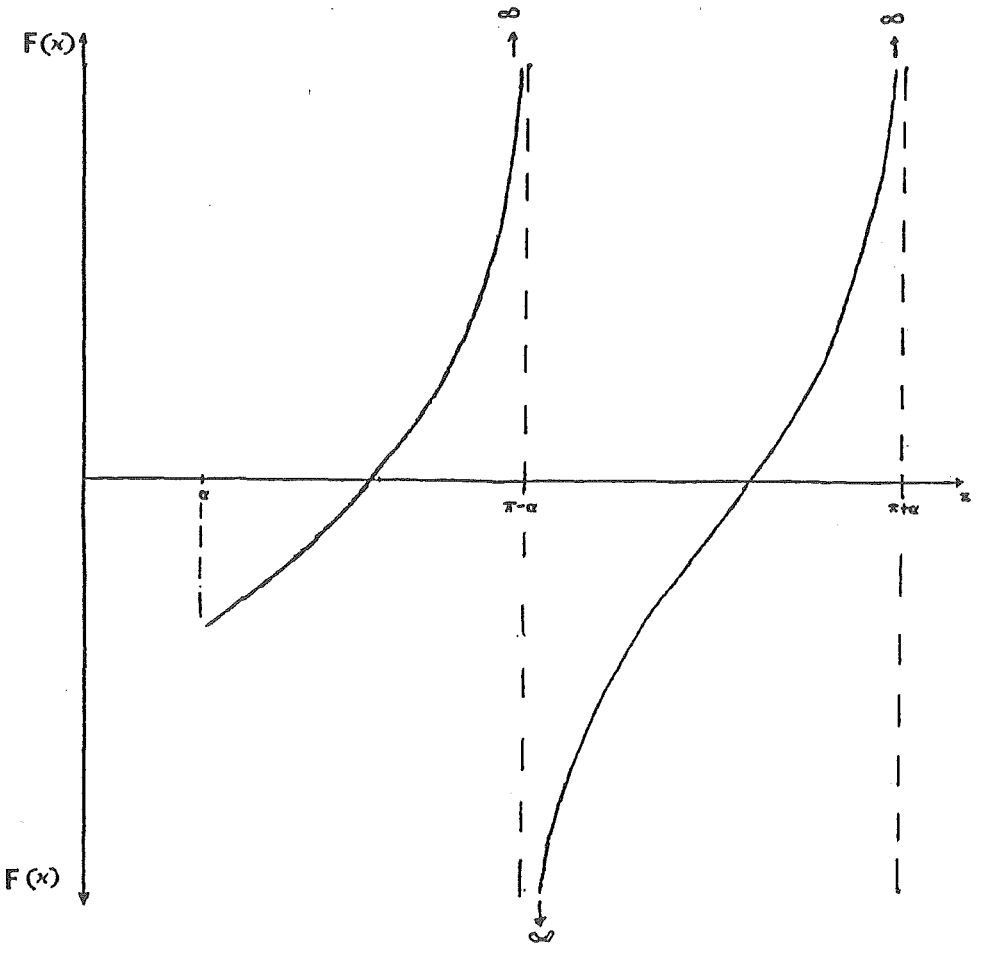

Figure A10.1 "Monotonic increasing" profile of f(x).

APPENDIX A11

APPROXIMATE NODAL ESTIMATE UNAVAILABILITY, $\bar{A}_i$

Consider the a.c. system shown in Figure A11.1 and the availability of node 12 being observable. Node 12 and its nearest neighbours, isolated from the rest of the a.c. system, are shown in Figure A11.2. Table A11.1 details the effect that measurement loss within the a.c. system has on the observability of node 12. The smallest combination of measurements that must be simultaneously unavailable to render node 12 unobservable is two, when measurement of s_{13-12} and s_6 is lost from the state estimator. It remains to show that the approximate unavailability for node 12, given by

$$\bar{A} \text{ (node 12 observable)} = \bar{A}_{s_{13-12}} \cdot \bar{A}_{s_6} \qquad \text{(A11.1)}$$

is sufficiently accurate.

Measurement unavailability combinations which cause a loss of observability to node 12 and contain $\bar{A}_{s_{13-12}}, \bar{A}_{s_6}$ are marked with a "*" in Table A11.1. Measurement combinations which cause a loss of observability to node 12, as a result of the loss of voltage reference, $\bar{A}_{v_{13}} \cdot \bar{A}_{v_6} \cdot \bar{A}_{v_{14}}$, are marked with a "+". No other measurement/loss of measurement combinations can cause a loss of observability to node 12.

From Table A11.1, $\bar{A}$(node 12 observable),

$$= \bar{A}_{s_{13-12}} \cdot \bar{A}_{s_6} (\text{all combinations involving } v_{13},\ v_6,\ v_{14} \text{ and } s_{14})$$
$$\longleftarrow\!\!\!

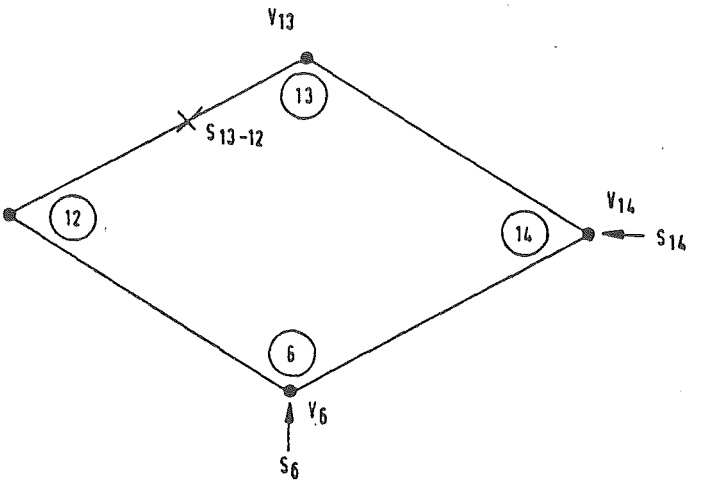

Figure A11.1 Sample a.c. system.

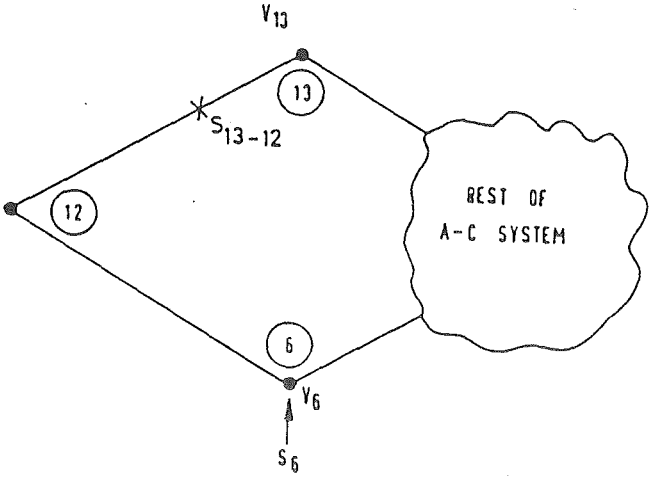

Figure A11.2 Node 12 and its nearest neighbours isolated from the a.c. system.

Table A11.1 Effect of measurement unavailability on the observability of node 12.

MEASUREMENTS UNAVAILABLE		IS NODE 12 OBSERVABLE?
0 order (1)	No measurements lost	Yes
1st order (6)	v_{13} lost	Yes
	s_{13-12} lost	Yes
	v_6 "	Yes
	s_6 "	Yes
	s_{14} "	Yes
	v_{14} "	Yes
2nd order (15)	v_{13} and s_{13-12} lost	Yes
	v_{13}, v_6 lost	Yes
	v_{13}, s_6 "	Yes
	v_{13}, s_{14} "	Yes
	v_{13}, v_{14} "	Yes
	s_{13-12}, v_6 lost	Yes
	s_{13-12}, s_6 "	No *
	s_{13-12}, s_{14}	Yes
	s_{13-12}, v_{14}	Yes
	v_6, s_6 lost	Yes
	v_6, s_{14} "	Yes
	v_6, v_{14} "	Yes
	s_6, s_{14} "	Yes
	s_6, v_{14} "	Yes
	s_{14}, v_{14} "	Yes
3rd order (20)	v_{13}, s_{13-12} and v_6 lost	Yes
	v_{13}, s_{13-12}, s_6 lost	No*
	$v_{13}, s_{13-12}, s_{14}$ "	Yes
	$v_{13}, s_{13-12}, v_{14}$ "	Yes
	v_{13}, v_6, s_6 lost	Yes
	v_{13}, v_6, s_4 "	Yes
	v_{13}, v_6, v_{14} "	No+
	v_{13}, s_6, s_{14} "	Yes
	v_{13}, s_6, v_{14} "	Yes
	v_{13}, s_{14}, v_{14} "	Yes
	s_{13-12}, v_6, s_6 lost	No*
	s_{13-12}, v_6, s_{14} "	Yes
	s_{13-12}, v_6, v_{14} "	Yes
	s_{13-12}, s_6, s_{14} "	No*
	s_{13-12}, s_6, v_{14} "	No*
	$s_{13-12}, s_{14}, v_{14}$ lost	Yes
	v_6, s_6, s_{14} lost	Yes
	v_6, s_6, v_{14} "	Yes
	v_6, s_{14}, v_{14} lost	Yes
	s_6, s_{14}, v_{14} "	Yes
4th order (15)	$v_{13}, s_{13-12}, v_6, s_6$ lost	No*
	$v_{13}, s_{13-12}, v_6, s_{14}$ "	Yes
	$v_{13}, s_{13-12}, v_6, v_{14}$ "	No +
	$v_{13}, s_{13-12}, s_6, s_{14}$ "	No*
	$v_{13}, s_{13-12}, s_6, v_{14}$ "	No*
	$v_{13}, s_{13-12}, s_{14}, v_{14}$ lost	Yes
	v_{13}, v_6, s_6, s_{14} lost	Yes
	v_{13}, v_6, s_6, v_{14} "	No +
	$v_{13}, v_6, s_{14}, v_{14}$ "	No +
	$v_{13}, s_6, s_{14}, v_{14}$ "	Yes
	$s_{13-12}, v_6, s_6, s_{14}$ lost	No*
	$s_{13-12}, v_6, s_6, v_{14}$ "	No*
	$s_{13-12}, v_6, s_{14}, v_{14}$ "	Yes
	$s_{13-12}, s_6, s_{14}, v_{14}$ "	No*
	v_6, s_6, s_{14}, v_{14}	Yes
5th order (6)	$v_{13}, s_{13-12}, v_6, s_6, s_{14}$ lost	No*
	$v_{13}, s_{13-12}, v_6, s_6, v_{14}$ "	No* +
	$v_{13}, s_{13-12}, v_6, s_{14}, v_{14}$ "	No+
	$v_{13}, s_{13-12}, s_6, s_{14}, v_{14}$ "	No*
	$v_{13}, v_6, s_6, s_{14}, v_{14}$ lost	No+
	$s_{13-12}, v_6, s_6, s_{14}, v_{14}$ lost	No*
6th order (1)	$v_{13}, s_{13-12}, v_6, s_6, s_{14}, v_{14}$ lost	No* +

It is easily shown that

$$\bar{A}_{s_{13-12}} \cdot \bar{A}_{s_6} (\text{all combinations involving } v_{13}, v_6, v_{14} \text{ and } s_{14}) = \bar{A}_{s_{13-12}} \cdot \bar{A}_{s_6}$$

$$\bar{A}_{v_{13}} \cdot \bar{A}_{v_6} \cdot \bar{A}_{v_{14}} (\text{all combinations involving } s_{13}, s_6 \text{ and } s_{14}) = \bar{A}_{v_{13}} \cdot \bar{A}_{v_6} \cdot \bar{A}_{v_{14}}$$

and from Table A11.1, (all combinations occurring in both (i) and (ii))

$$= \bar{A}_{v_{13}} \bar{A}_{s_{13-12}} \bar{A}_{v_6} \bar{A}_{s_6} \bar{A}_{v_{14}} (A_{s_{14}} + \bar{A}_{s_{14}})$$

$$= \bar{A}_{v_{13}} \bar{A}_{s_{13-12}} \bar{A}_{v_6} \bar{A}_{s_6} \bar{A}_{v_{14}}$$

Thus (A11.2) becomes

$$\bar{A} \text{ (node 12 observable)} = \bar{A}_{s_{13-12}} \bar{A}_{s_6} + \bar{A}_{v_{13}} \bar{A}_{v_6} \bar{A}_{v_{14}} - \bar{A}_{v_{13}} \bar{A}_{s_{13-12}} \bar{A}_{v_6} \bar{A}_{s_6} \bar{A}_{v_{14}} \qquad \text{(A11.3)}$$

The terms appearing due to the loss of voltage reference, $\bar{A}_{v_{13}} \bar{A}_{v_6} \bar{A}_{v_{14}}$, are third order and above in availability. Since availabilities of $A_v = 0.97 - 0.999$ are usually present (Arriatti *et al.*, 1975), $\bar{A}_v \leq 0.03$ and the third order terms can be neglected and

$$\bar{A} \text{ (node 12 observable)} = \bar{A}_{s_{13-12}} \bar{A}_{s_6} \qquad \text{(A11.4)}$$

is a good approximation.

For larger systems, such as the 14 bus test system, seven voltage measurements must be simultaneously lost before the voltage reference of the state estimator is lost. Terms appearing due to the loss of voltage reference would be seventh order and higher, rather than third order as in the example above. Consequently the error in neglecting the unavailability due to the "loss of voltage reference" would be even smaller.

Note also that the assumption of independence made above, i.e.

$$\bar{A}\ (\text{all voltage measurements}) = \bar{A}_{v_{13}}\ \bar{A}_{v_6}\ \bar{A}_{v_{14}}$$
$$v_{13},\ v_6 \text{ and } v_{14}$$

and

$$\bar{A}\ (\text{link measurements}) = \bar{A}_{s_{13-12}}\ \bar{A}_{s_6}$$
$$s_{13-12} \text{ and } s_6$$

is, in practice, valid only for voltage measurements. This is because voltage measurements are scattered around the system, and their multiple failure would likely be caused by a series of independent events, whereas the link measurements are all made in the neighbourhood of node 12 and may be correlated, particularly if all link measurements use the same communication path.

Thus

$$\bar{A}\ (\text{link measurements}) = \bar{A}_{s_{13-12}} \cdot \left(s_6 \text{ unavailable given } s_{13-12} \text{ is unavailable}\right)$$
$$\text{s and s}$$
$$= \bar{A}_{s_{13-12}}\ \bar{A}\ \left(s_6 | s_{13-12}\right) \qquad \text{(A11.5)}$$

If measurements s_6 and s_{13-12} are completely correlated, then

$$\bar{A}\ (s_6 | s_{13-12}) = 1$$

and

$$\bar{A}\ (\text{link measurements}) = A_{s_{13-12}} = A_{s_6}$$
$$s_{13-12} \text{ and } s_6$$

If measurements s_6 and s_{13-12} are uncorrelated

$$\bar{A}\ (s_6 \mid s_{13-12}) = \bar{A}_{s_6}$$

Thus in practice the unavailability of n link measurements should be higher than the unavailability of n voltage measurements, if the link measurement correlation effects are included. As a result, discarding the loss of voltage terms is even more realistic and the approximation, given by (A11.4), can be re-written to include correlations if they are assumed to exist.

$$\bar{A} \text{ (node 12 observable)} = \bar{A} \underset{s_{13-12} \text{ and } s_6}{\text{(link measurements)}} \qquad \text{(A11.6)}$$

APPENDIX A12

ROTOR ANGLE ESTIMATION

The following rotor angle estimator-derivation follows that of Handschin and Galiana (1973). A rotor angle estimator can be designed for the dynamic equation (10.20) and the observation equation (10.21).

The difference $\underline{e}(t)$ between actual $(\underline{x}_{HG}(t))$ and estimated $(\hat{\underline{x}}_{HG}(t))$ state vectors, i.e.

$$\underline{e}(t) = \underline{x}_{HG}(t) - \hat{\underline{x}}_{HG}(t) \tag{A12.1}$$

is a white noise process

$$E\{\underline{e}(t)\} = 0 \tag{A12.2}$$

and

$$E\{\underline{e}(t)\ \underline{e}^{T}(t+\tau)\} = \underline{\Sigma}\ \delta(\tau) \tag{A12.3}$$

where the numerical value of (A12.3) can be found from the steady state solution of the Ricatti equation (as in section 10.4.1). Since $\underline{\Sigma}$ is known, the actual frequency deviation f(t) in the generator is

$$f(t) = \hat{f}(t) + e_f(t) \tag{A12.4}$$

where $e_f(t)$ is the sixth element of (A12.1).

Assuming the frequency deviation $f_{ref}(t)$ is measured

$$z_f(t) = f_{ref}(t) + v_f(t) \tag{A12.5}$$

$$\therefore\quad f_{ref}(t) = z_f(t) - v_f(t) \tag{A12.6}$$

Substituting (A12.6) and (A12.4) into (10.20) yields the following differential equation for the rotor angle $\delta(t)$

$$\dot{\delta}(t) = 2\pi f_o\ [\hat{f}(t) + e_f(t) - z_f(t) + v_f(t)] \tag{A12.7}$$

$$= 2\pi f_o\ [\hat{f}(t) - z_f(t)] + \omega_f(t) \tag{A12.8}$$

where $\omega_f(t) : E\{\omega_f(t)\} = 0$

and $$E\{\omega_f(t)\ \omega_f^T\ (t+\tau)\} = \sigma_{wf}^2\ \delta(\tau) \tag{A12.9}$$

$$\text{where}\quad \sigma_{wf}^2 = \sigma_f^2\ \delta(\tau) + \text{cov}\ (e_f(t)) \tag{A12.10}$$

since $v_f(t)$ and $e_f(t)$ are independent gaussian white noise processes.

The estimator for rotor angle $\delta(t)$ is based on the dynamic equation (A12.8) and the observation equation

$$z_p(t) = \frac{E'v(t)}{x_d'}\ \sin\ [\delta(t) - \theta(t)] + v_p(t) \tag{A12.11}$$

and takes the form

$$\dot{\hat{\delta}}(t) = 2\pi f_o[\hat{f}(t) - z_f(t)] + K_\sigma[z_p(t) - \frac{E'v(t)}{x_d'}\ \sin(\hat{\delta}(t) - \theta(t_k))]$$

In order to compute the Kalman gain, K_σ, linearize the observation equation (A12.11) according to

$$z_p(t) \simeq \frac{E'}{x_d'}\ [\delta(t) - \theta(t_k)] + v_p(t) \tag{A12.13}$$

and together with (A12.8) the optimal "linearised" filter gain, K_σ, is obtained as

$$K_\sigma = \sigma_{wf} / \sigma_p \tag{A12.14}$$

Note that the only linearization that is involved is when finding the Kalman gain, K_σ.

APPENDIX A13

DERIVATION OF UNSTEADY OPEN CHANNEL FLOW MOMENTUM AND CONTINUITY EQUATIONS

The following derivation is taken from Wylie and Streeter (1978). In the derivation, the assumption is made that $\cos\alpha \simeq 1$. This condition is usually met in power channels serving hydroturbines. A further assumption is made in that hydrostatic conditions prevail along any vertical line in the fluid (i.e. vertical accelerations are not considered). Figure A13.1 shows a control volume enclosing an elemental strip of liquid, the x-direction of which is taken along the channel bottom while the y direction is measured normal to the bottom.

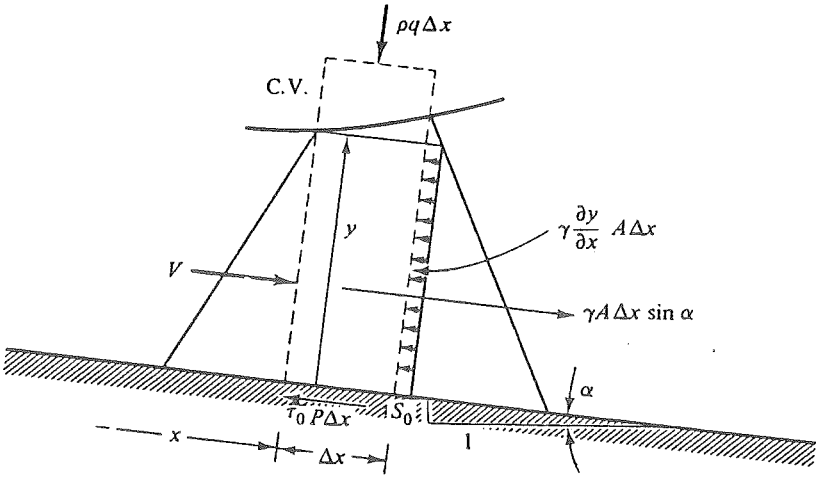

Figure A13.1 Control volume for unsteady-momentum equation (Wylie and Streeter, 1978).

In the application of the unsteady momentum equation, the nett hydrostatic force on the two faces is

$$-\nu\left(\frac{\partial y}{\partial x}\right)\Delta x\, A \qquad \text{(A13.1)}$$

when $\cos\alpha = 1$, and

where ν = unit weight of fluid or shear strain $\frac{\partial u}{\partial z}$

A = cross-sectional area of the flow.

The shear force on the wetted area is given by

$$-\tau_o\, P\, \Delta x \qquad \text{(A13.2)}$$

where P is the wetted perimeter of the trapezoidal canal; and

τ_o is the shear stress.

The gravity force in the x-direction is given by

$$\nu\, A\, \Delta x \sin\alpha = \nu\, A\, \Delta x\, s_o \qquad \text{(A13.3)}$$

where α is the channel slope; and

s_o is the slope of the hydraulic grade line.

The net efflux of momentum in the (+)x direction is

$$\frac{\partial}{\partial x}(\rho\, V^2\, A)\cdot\Delta x \qquad \text{(A13.4)}$$

where ρ is the mass density; and

V is the instantaneous relativity of the fluid.

The time rate of increase of x momentum within the control volume is

$$\frac{\partial}{\partial t}\ (\rho\, A\, V\, \Delta x) \qquad \text{(A13.5)}$$

Assembling the terms results in

$$-\nu\frac{\partial y}{\partial x}\Delta x\, A - \tau_o\, P\, \Delta x + \nu A\, \Delta x \sin\alpha = \frac{\partial}{\partial x}(\rho\, V^2\, A) + \frac{\partial}{\partial t}(\rho\, A\, V\, \Delta x) \qquad \text{(A13.6)}$$

and after expanding and dividing through, by the mass of the element $\rho\, A\, \Delta x$,

$$\frac{g\partial y}{\partial x} + \frac{\tau_o}{\rho R} - g \sin\alpha + 2V \frac{\partial v}{\partial x} + \frac{V^2}{A} \frac{\partial A}{\partial x} + \frac{V}{A} \frac{\partial A}{\partial t} + \frac{\partial V}{\partial t} = 0 \qquad \text{(A13.7)}$$

where g is the gravitational constant; and

R is the hydraulic radius

$$R = \frac{A}{P} \qquad \text{(A13.8)}$$

The continuity equation can also be applied to the control volume, and yields

$$\rho\, q\, \Delta x - \frac{\partial}{\partial x} (\rho\, A\, V)\, \Delta x = \frac{\partial}{\partial t} (\rho\, A\, \Delta x) \qquad \text{(A13.9)}$$

where q is the lateral inflow per unit length of channel.

By expanding and dividing by $\rho\, \Delta x$

$$V \frac{\partial A}{\partial x} + \frac{\partial A}{\partial t} + A \frac{\partial v}{\partial x} = q \qquad \text{(A13.10)}$$

Equation (A12.7) can be simplified by subtracting (A13.10), when multiplied by $\frac{V}{A}$, from it. The Manning equation can also be used to express

$$\frac{\tau_o}{\rho R} = g\, S \qquad \text{(A13.11)}$$

where $S = \dfrac{n^2\, V^2}{c_m^{\,2} R^{\,4/3}}$ (A13.12)

where n is the Manning roughness factor; and

c_m is an empirical constant equal to 1.0 in SI units.

Then

$$g \frac{\partial y}{\partial x} + g\, S - g \sin\alpha + V \frac{\partial V}{\partial x} + \frac{\partial V}{\partial t} + \frac{V}{A} q = 0 \qquad \text{(A13.13)}$$

and equation (A13.10) can be written

$$V\, T \frac{\partial y}{\partial x} + T \frac{\partial y}{\partial t} + A \frac{\partial v}{\partial x} - q = 0 \qquad \text{(A13.14)}$$

since $\frac{\partial A}{\partial x} = \frac{\partial A}{\partial y}\frac{\partial y}{\partial x} = T\frac{\partial y}{\partial x}$

and $\frac{\partial A}{\partial t} = \frac{\partial A}{\partial y}\frac{\partial y}{\partial t} = T\frac{\partial y}{\partial t}$

when (A12.7) and (A12.10) are written in terms of discharge and depth as the dependent variables, the equations become

$$\left(1 - \frac{Q^2T}{g\,A^3}\right)\frac{\partial y}{\partial x} + \frac{2Q}{g\,A^2}\frac{\partial Q}{\partial x} + \frac{1}{g\,A}\frac{\partial Q}{\partial t} + s - s_o = 0 \qquad \text{(A13.15)}$$

$$T\frac{\partial y}{\partial t} + \frac{\partial Q}{\partial x} = 0 \qquad \text{(A13.16)}$$

APPENDIX A14

IMPLICIT TRAPEZOIDAL NUMERICAL INTEGRATION

Implicit integration using the trapezoidal rule allows differential equations to be algebaized, has been shown to be numerically stable and can be used with step lengths greater than the smallest time constant of the dynamic model, without instability or excessive error resulting (Law, 1972).

A14.1 SINGLE STEP INTEGRATION

Consider integrating the area under the curve, shown in Figure A14.1, between t_1 and t_2. The integration step length is $TTT = t_2 - t_1$, and the trapezoidal integration scheme is

$$x(t_2) = x(t_1) + \frac{TTT}{2}\left(h(t_1) + h(t_2)\right) \qquad \text{(A14.1)}$$

where

$$h(t) = \frac{\partial x(t)}{\partial t} \qquad \text{(A14.2)}$$

However, since in our case $x(t_2)$ is unknown, initially put

$$h(t_2) = h(t_1)$$

and iterate (A14.1) until the algorithm converges, when

$$\left|x(t_2)_{k+1} - x(t_2)_k\right| < \text{tolerance} \qquad \text{(A14.3)}$$

A14.2 MULTI STEP INTEGRATION

In the single step integration case above, the integration is done in one "shot". However the same interval can be integrated in a

series of small steps, repeated until the interval $t_2 - t_1$ is spanned (see Figure A14.2). The same technique as in (A14.1) is used to integrate each small interval. The step length chosen is such that

$$m \times n = TTT = t_2 - t_1 \qquad \text{(A14.4)}$$

where m is the number of sub-integrations; and

n is the step length of each sub-integration.

Generally, multi-step integration is preferred for large step lengths because it gives a more accurate result.

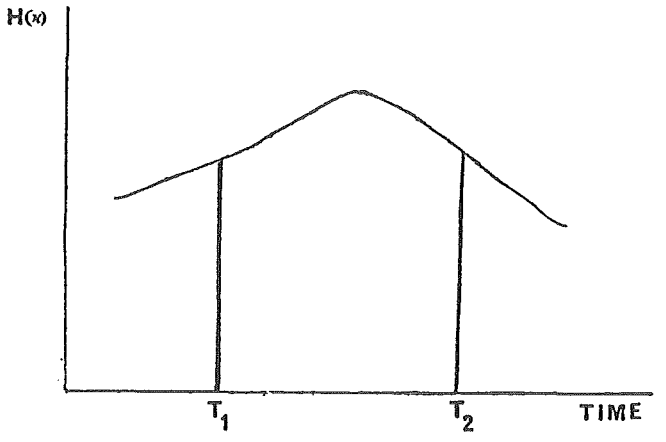

Figure A14.1 Single step trapezoidal integration.

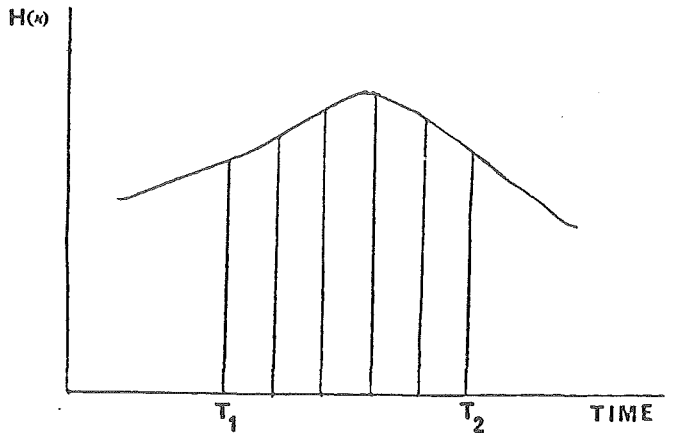

Figure A14.2 Multi step trapezoidal integration.